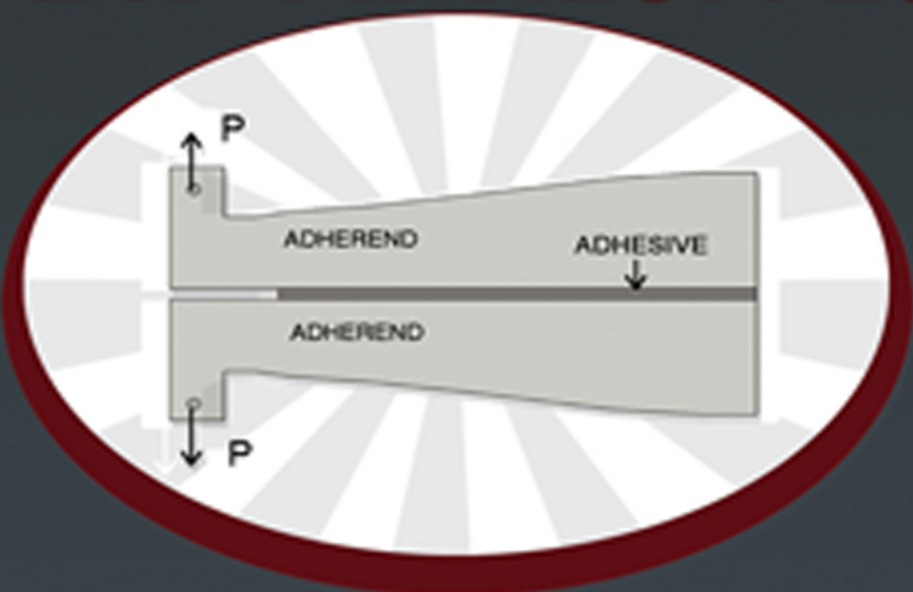


PROGRESS IN ADHESION AND ADHESIVES



Edited by K.L. Mittal

 Scrivener
Publishing

WILEY

Progress in Adhesion and Adhesives

Scrivener Publishing

100 Cummings Center, Suite 541J
Beverly, MA 01915-6106

Publishers at Scrivener

Martin Scrivener(martin@scrivenerpublishing.com)
Phillip Carmical (pcarmical@scrivenerpublishing.com)

Progress in Adhesion and Adhesives

Edited by

K.L. Mittal



WILEY

Copyright © 2015 by Scrivener Publishing LLC. All rights reserved.

Co-published by John Wiley & Sons, Inc. Hoboken, New Jersey, and Scrivener Publishing LLC, Salem, Massachusetts.
Published simultaneously in Canada.

No part of this publication may be reproduced, stored in a retrieval system, or transmitted in any form or by any means, electronic, mechanical, photocopying, recording, scanning, or otherwise, except as permitted under Section 107 or 108 of the 1976 United States Copyright Act, without either the prior written permission of the Publisher, or authorization through payment of the appropriate per-copy fee to the Copyright Clearance Center, Inc., 222 Rosewood Drive, Danvers, MA 01923, (978) 750-8400, fax (978) 750-4470, or on the web at www.copyright.com. Requests to the Publisher for permission should be addressed to the Permissions Department, John Wiley & Sons, Inc., 111 River Street, Hoboken, NJ 07030, (201) 748-6011, fax (201) 748-6008, or online at <http://www.wiley.com/go/permission>.

Limit of Liability/Disclaimer of Warranty: While the publisher and author have used their best efforts in preparing this book, they make no representations or warranties with respect to the accuracy or completeness of the contents of this book and specifically disclaim any implied warranties of merchantability or fitness for a particular purpose. No warranty may be created or extended by sales representatives or written sales materials. The advice and strategies contained herein may not be suitable for your situation. You should consult with a professional where appropriate. Neither the publisher nor author shall be liable for any loss of profit or any other commercial damages, including but not limited to special, incidental, consequential, or other damages.

For general information on our other products and services or for technical support, please contact our Customer Care Department within the United States at (800) 762-2974, outside the United States at (317) 572-3993 or fax (317) 572-4002.

Wiley also publishes its books in a variety of electronic formats. Some content that appears in print may not be available in electronic formats. For more information about Wiley products, visit our web site at www.wiley.com.

For more information about Scrivener products please visit www.scrivenerpublishing.com.

Cover design by Russell Richardson

Library of Congress Cataloging-in-Publication Data:

ISBN 978-1-119-16219-3

Printed in the United States of America

10 9 8 7 6 5 4 3 2 1

Contents

Preface	xv
1 Adhesion of Condensed Bodies at Microscale: Variation with Movable Boundary Conditions	1
<i>Jian-Lin Liu, Jing Sun, Runni Wu and Re Xia</i>	
1.1 Introduction	1
1.2 Kinematics: Energy Variation with Movable Boundary Conditions	3
1.3 Microbeam/plate Adhesion	9
1.4 Droplet Adhesion to a Solid	13
1.5 Elastica Model of CNT Adhesion	17
1.6 Cell Adhesion	20
1.7 Summary and Prospects	23
Acknowledgements	24
References	24
2 Imparting Adhesion Property to Silicone Materials: Challenges and Solutions	31
<i>R. Kalinova, R. Mincheva and Ph. Dubois</i>	
2.1 Introduction	32
2.2 Cured PDMS	32
2.2.1 Curing Reactions	32
2.2.1.1 Free-Radical Curing	33
2.2.1.2 Condensation Curing	33
2.2.1.3 Hydrosilylation (Addition) Curing	35
2.2.2 Surface Properties	36
2.2.3 Adhesion Property	37
2.3 Methods for Cross-Linked PDMS Surface Modification	37
2.3.1 Physical Techniques	37
2.3.1.1 Plasma Treatment	37
2.3.1.2 Corona Treatment	39
2.3.1.3 UV/O ₃ Treatment	40

2.3.1.4	Laser Treatment	41
2.3.1.5	Physical Adsorption	41
2.3.2	Wet Chemical Techniques	42
2.3.2.1	LbL Deposition	42
2.3.2.2	Sol-Gel Method	43
2.3.2.3	Other Wet Chemical Treatments	43
2.3.3	Combination of Physical and Chemical Techniques	43
2.3.3.1	Covalent Surface Grafting	44
2.3.3.2	Modification by Amphiphilic Block Copolymers	46
2.3.3.3	Other Combination of Physical and Chemical Techniques	48
2.4	Summary and Prospects	48
	Acknowledgements	48
	References	50
3	Functionally Graded Adhesively Bonded Joints	57
	<i>M. Kemal Apalak</i>	
3.1	Introduction	57
3.2	Functionally Graded Materials	61
3.3	Constitutive Relations	63
3.4	Joints with Functionally Graded Adherends	67
3.5	Functionally Graded Adhesives	73
3.6	Conclusions	77
	References	78
4	Synthetic Adhesives for Wood Panels: Chemistry and Technology	85
	<i>A. Pizzi</i>	
4.1	Introduction	85
4.2	Urea-formaldehyde (UF) Adhesives	87
4.3	Melamine-formaldehyde (MF) and Melamine-urea-formaldehyde (MUF) Adhesives	93
4.4	Phenolic Resins	99
4.4.1	Reactivity and Hardening Reactions of PF Adhesive Resins	103
4.4.2	Modification of Phenolic Resins	104
4.4.2.1	Post-addition of Urea	104
4.4.2.2	Co-condensation Between Phenol and Urea	105
4.4.2.3	Addition of Tannins, Lignins and Isocyanates	105

4.5	Isocyanate Wood Adhesives	106
4.5.1	Chemistry of Isocyanate Wood Adhesives	107
4.5.2	Technology of Isocyanate as Adhesives	109
4.5.3	Emulsified/emulsifiable Water-dispersed PMDI	112
4.5.4	PF/pMDI and UF/pMDI Hybrid Adhesives	112
4.5.5	Conditions for Application of Isocyanate Adhesives for Wood	114
4.6	Summary	116
	References	116
5	Adhesion Theories in Wood Adhesive Bonding	125
	<i>Douglas J. Gardner, Melanie Blumentritt, Lu Wang and Nadir Yildirim</i>	
5.1	Introduction	125
5.1.1	Wood Material Properties Relevant to Adhesion	126
5.1.2	Objectives	129
5.2	Mechanical Interlocking and Mechanics of Adhesive-Wood Interactions	129
5.2.1	Atomic Force Microscopy (AFM) & Nanoindentation	132
5.3	Electrostatic Adhesion	135
5.4	Wettability, Surface Energy, Thermodynamic Adhesion	137
5.4.1	Wood Anatomy Impact on Wetting	140
5.4.2	Extractives	141
5.4.3	Adhesive Wettability	141
5.4.4	Wood Modification	141
	5.4.4.1 Acetylation	142
	5.4.4.2 Grafting	142
	5.4.4.3 Fire Retardants, Preservatives and Adhesion Promotion	142
5.4.5	Test Methods	143
5.5	Diffusion Theory of Adhesion	145
5.6	Covalent Bonding	148
5.7	Acid-base Theory	149
5.8	Weak Boundary Layer	150
5.8.1	Extractives	151
5.8.2	Heat Treatment	152
5.8.3	Wood Impregnation and Densification	153
5.8.4	Machining Processes	153
5.8.5	Surface Degradation	154
5.8.6	Surface Activation	154

5.9	Discussion and Future Research Prospects	155
5.10	Summary	157
	References	158
6	Adhesion and Surface Issues in Biocomposites and Bionanocomposites	169
	<i>Cintil Jose, Merin Sara Thomas, B. Deepa, Laly A. Pothan and Sabu Thomas</i>	
6.1	Introduction	170
6.2	Biopolymers	170
6.2.1	Cellulose	170
6.2.2	Chitin	171
6.2.3	Starch	173
6.3	Chemical Modification of Cellulose, Chitin and Starch	174
6.4	Bio-based Matrices	177
6.4.1	Poly(lactic acid) (PLA)	177
6.4.2	Polyhydroxybutyrate (PHB)	178
6.4.3	Cellulose	179
6.4.4	Chitosan	180
6.4.5	Starch	181
6.4.6	Natural Rubber	182
6.5	Processing Techniques	184
6.6	Interfacial Adhesion Issues	185
6.6.1	Challenges of Interfacial Adhesion of Natural Fibres in Polymer Matrix	185
6.6.1.1	Challenges of Dispersion of Cellulose Nanofibres	186
6.6.2	Strategies for Improving Interfacial Adhesion	186
6.6.3	New Challenges and Future Trends in Fibre/Matrix Interfacial Adhesion	188
6.7	Interface Characterization Techniques	189
6.7.1	Morphological Characterization	189
6.7.1.1	Scanning Electron Microscopy (SEM)	190
6.7.1.2	Atomic Force Microscopy (AFM)	194
6.7.2	Thermal Analysis	196
6.7.2.1	Thermogravimetric Analysis (TGA)	196
6.7.2.2	Differential Scanning Calorimetry (DSC)	199
6.7.2.3	Dynamic Mechanical Thermal Analysis (DMTA)	199

6.7.3	Spectroscopic Techniques	203
6.7.3.1	Fourier Transform Infrared (FTIR) and Raman Spectroscopies	203
6.7.3.2	Attenuated Total Reflectance Infrared Spectroscopy (ATR-IR)	205
6.7.3.3	Nuclear Magnetic Resonance (NMR) Spectroscopy	206
6.8	Summary and Conclusions	207
	References	207
7	Adhesion Phenomena in Pharmaceutical Products and Applications of AFM	219
	<i>Emily Callard Preedy, Stefano Perni and Polina Prokopovich</i>	
7.1	Introduction	220
7.2	Adhesion in Pharmaceuticals	222
7.2.1	Adhesion Interactions	223
	7.2.1.1 Drug-Drug/Carrier Interactions	223
	7.2.1.2 Drug-Device/Packaging Interactions	224
7.2.2	Factors Influencing Adhesion	225
	7.2.2.1 Monitoring and Controlling Influential Factors	229
7.3	Atomic Force Microscopy	232
	7.3.1 AFM and Pharmaceutical Formulations	233
	7.3.2 Advantages of AFM	234
7.4	Prospects	236
7.5	Summary	237
	Acknowledgments	237
	References	237
8	Cyanoacrylate Adhesives in Surgical Applications	245
	<i>Edward M. Petrie</i>	
8.1	Introduction	245
	8.1.1 Basic Requirements of Surgical Adhesives	246
	8.1.2 Surgical Substrates	248
	8.1.3 Scope and Objectives of this Review	249
8.2	Types of Surgical Adhesives	249
	8.2.1 Full Scope of Surgical Adhesives	249
	8.2.2 The Surgeon's Toolbox	252
	8.2.2.1 Fibrin Sealants	252
	8.2.2.2 Cyanoacrylates	254

	8.2.2.3	Collagen-Based Adhesives	255
	8.2.2.4	Poly(ethylene glycol) Polymers	255
	8.2.2.5	Albumin and Glutaraldehyde Products	256
	8.2.2.6	Others	256
	8.2.3	Comparison of Adhesive Types	257
8.3		History of Cyanoacrylate Surgical Adhesives	257
	8.3.1	Development of Cyanoacrylates as Industrial Adhesives	257
	8.3.2	Development of Cyanoacrylate Tissue Adhesives	263
	8.3.2.1	n-Butyl-2-Cyanoacrylate	264
	8.3.2.2	2-Octyl-Cyanoacrylate	267
	8.3.2.3	Newer Cyanoacrylate Surgical Adhesives	269
8.4		Formulation Development	269
	8.4.1	Monomeric Derivatives	270
	8.4.2	Optimal Formulation Development	272
	8.4.2.1	Inhibitors	273
	8.4.2.2	Stabilizers Added Depending on the Surgical Procedure	274
	8.4.2.3	Accelerators	276
	8.4.2.4	Thickeners	277
	8.4.2.5	Plasticizers	277
8.5		Properties	278
	8.5.1	Curing Mechanism	278
	8.5.1.1	Comparative Shelf-Life	279
	8.5.1.2	Container Materials for Packaging	279
	8.5.2	Bond Strength	282
	8.5.3	Toxicity	283
	8.5.4	Biocompatibility	284
8.6		Clinical History	285
	8.6.1	Closure of Skin Wounds and Superficial Incision Closure	288
	8.6.2	Other Surgical Procedures and Future Uses	289
	8.6.3	Graft Fixation	289
8.7		Future Potential	290
	8.7.1	Development Path	290
	8.7.1.1	Light Curing Cyanoacrylates	291
	8.7.1.2	Solid Cyanoacrylate	291
	8.7.2	Drivers for Increased Demand	292
8.8		Summary	292
		References	293

9	Ways to Generate Monosort Functionalized Polyolefin Surfaces	299
	<i>J. Friedrich, R. Mix and G. Hidde</i>	
9.1	Introduction	300
9.1.1	General Principles	300
9.1.2	Formation of Functional Groups at Polyolefin Surfaces by Plasma Exposure	304
9.1.3	Polymer Degradation Caused by Plasma Exposure	310
9.1.4	Possible Strategies to Produce Monosort Functional Groups on Polyolefin Surfaces	311
9.2	Production of Monotype Functional Groups	312
9.2.1	OH Group Formation by Exposure to Oxygen Plasma	312
9.2.2	Formation of COOH Groups by Exposure to Carbon Dioxide Plasma	315
9.2.3	Formation of Amino Groups by Exposure to Ammonia or Nitrogen Plasmas	318
9.2.3.1	Significance of Primary Amino Groups in Life Sciences	318
9.2.3.2	Ammonia Plasma Treatment of Polymers and Graphitic Materials	319
9.2.3.3	Undesired Oxygen Introduction on Exposure to Ammonia Plasma	320
9.2.3.4	Additional Side Reactions on Exposure to Ammonia Plasma	322
9.2.4	Surface Bromination	325
9.2.4.1	Kinetics, Thermodynamics and Mechanism	325
9.2.4.2	Parameter Dependence	327
9.2.4.3	Conversion of C-Br into Other Monotype Functional Groups	327
9.3	Other Methods for Introduction of Monotype Functional Groups onto the Polyolefin Surface (Plasma Polymerization, Underwater Plasma, ElectroSpray Ionization Deposition, Atmospheric-Pressure Chemical Ionization, Chemical Pretreatment)	329
9.3.1	Plasma Polymerization	329
9.3.2	Underwater Plasma	331
9.3.3	ElectroSpray Ionization (ESI) Deposition	332
9.3.4	Chemical Pretreatment	333

9.4	Hydrophobic Recovery	335
9.5	Grafting onto Functionalized Polyolefin Surfaces	336
9.5.1	Direct Grafting onto Radical Sites	336
9.5.2	Grafting onto Peroxy Radicals/Hydroperoxides	337
9.5.3	Grafting onto Monosort Functional Groups by Nucleophilic Substitution	339
9.5.3.1	Wet-Chemical Chain Extension at Amino Groups	339
9.5.3.2	Spacer Grafting onto OH-Groups at Polymer Surface	340
9.5.3.3	Spacer Anchoring onto C-Br Groups	340
9.5.3.4	Silane Attachment	341
9.6	Summary and Conclusions	342
	References	344
10	Nano-Enhanced Adhesives	357
	<i>Shahin Shadlou, Babak Ahmadi-Moghadam and Farid Taheri</i>	
10.1	Introduction	357
10.2	Why Nanostructured Reinforcements?	358
10.2.1	Carbon-based NPs	359
10.2.2	Metal-based NPs	359
10.2.3	POSS	360
10.2.4	Other Nanomaterials	360
10.2.4.1	Nanoclays	360
10.2.4.2	Nanosilicas (SiO ₂)	360
10.3	Development of Polymer-based Nanocomposites	360
10.3.1	Sonication	361
10.3.2	Three-roll Milling (Calendering)	363
10.3.3	High-Shear Mixing	364
10.4	Mechanical Properties of Nano-reinforced Adhesives	364
10.4.1	Effect of Adhesive Stiffness	365
10.4.2	Effect of Fracture Toughness	374
10.4.3	Effect of Surface Wettability	377
10.4.4	Effects of Residual Stresses	380
10.4.5	Effect of Durability of Adhesives	382
10.5	Other Advantages of Nano-Reinforced Adhesives	383
10.5.1	Electrical Properties	384
10.5.2	Thermal Properties	385
10.5.3	Gas Permeation Barrier Properties	386
10.5.4	Bio-Adhesives	387

10.6	Conclusion	389
10.7	Acknowledgements	390
	References	390
11	Bonding Dissimilar Materials in Dentistry	397
	<i>Muhammad Zakir, James Kit-Hon Tsoi, Chun Hung Chu, Christie Ying Kei Lung and Jukka Pekka Matinlinna</i>	
11.1	Introduction	398
11.2	Silane Coupling Agents	399
11.3	Zirconate Coupling Agents	403
11.4	Phosphate Coupling Agents	404
11.5	Thione/thiol Coupling Agents	405
11.6	Titanate Coupling Agents	406
11.7	Zircoaluminate Coupling Agents	408
11.8	Other Coupling Agents	408
11.9	Conclusion	410
	References	411
12	Flame Treatment of Polymeric Materials: Relevance to Adhesion	417
	<i>L. Mazzola and A. Cusma</i>	
12.1	Introduction	418
12.2	Flame Treatment Equipment	418
	12.2.1 Process Parameters	421
	12.2.1.1 Combustion Conditions – Air/Gas Ratio	421
	12.2.1.2 Flame Energy	422
	12.2.1.3 Burner to Substrate Gap	422
	12.2.1.4 System Layout	422
	12.2.1.5 Valve Train	422
	12.2.1.6 Control Instrumentation	423
	12.2.1.7 Gas Saving	423
	12.2.2 Flame Chemistry	423
	12.2.2.1 Pre-reaction Zone	423
	12.2.2.2 Main Reaction Zone	424
	12.2.2.3 Post-combustion Zone	425
12.3	Effects of Flame Treatment on Plastics	426
	12.3.1 Flame Treatment of Polypropylene	426
	12.3.2 Flame Treatment on Polyethylene	441
12.4	Conclusion	445
	References	447

13 Mucoadhesive Polymers for Enhancing Retention in Ocular Drug Delivery	451
<i>Anubha Khare, Kanchan Grover, Pravin Pawar and Inderbir Singh</i>	
13.1 Introduction	451
13.2 Composition of Mucus Layer	453
13.2.1 Expression of Human Mucin Genes	453
13.3 Natural Mucoadhesive Polymers	454
13.3.1 Chitosan	454
13.3.1.1 Chitosan-based Formulations	460
13.3.2 Human Serum Albumin (HSA)	461
13.3.3 Alginate	462
13.3.4 Gellan gum	463
13.3.5 Xanthan gum	463
13.3.6 Guar gum	464
13.3.7 Sodium Hyaluronate	465
13.3.8 Carrageenan	465
13.3.9 Tamarind Gum Polysaccharide (TGP)	466
13.3.10 Arabinogalactan	467
13.4 Synthetic Polymers	467
13.4.1 Poly (acrylic acid) PAA or Carbomer	467
13.4.2 Eudragit	468
13.4.3 Cellulose Derivatives	469
13.4.4 Poly (D, L-Lactic acid) and poly (D, L-Lactide-co-glycolide)	470
13.4.5 Poloxamers	471
13.5 Gene Delivery	472
13.6 Patented Formulations	472
13.7 Future Prospects	472
13.8 Conclusion	473
Acknowledgement	474
References	474
Index	485

Preface

This book is based on the 13 (a lucky number) review articles published in 2014 in the journal *Reviews of Adhesion and Adhesives* (RAA). The sole purpose of RAA is to publish concise, critical, illuminating and thought-provoking review articles on any topic within the broad purview of adhesion science and adhesive technology.

With the voluminous research being published, it is difficult, if not impossible, to stay abreast of current developments in a given area. So the review articles consolidating the information provide an alternative way to follow the latest research activity and developments in a particular subject area. It should be recorded that all these review articles were rigorously reviewed to maintain the highest standards of publication.

The rationale for publication of this book is that currently the RAA has limited circulation, so this book was conceived to provide broad exposure and dissemination of information published in RAA. Apropos, the authors of the articles published in RAA were consulted and they all enthusiastically endorsed the idea of this book.

Although the book is not formally divided into different sections, it essentially addresses the following four areas in the wide domain of adhesion and adhesives.

1. General adhesion aspects
2. Polymer surface modification and relevance to adhesion
3. Adhesion and adhesives in biomedical, pharmaceutical and dental fields
4. Adhesives and adhesive joints

The topics covered include: Adhesion of condensed bodies at microscale; imparting adhesion property to silicone materials; functionally graded adhesively bonded joints; synthetic adhesives for wood panels; adhesion theories in wood adhesive bonding; adhesion and surface issues in bio-composites and bionanocomposites; adhesion phenomena in pharmaceutical products and applications of AFM; cyanoacrylate adhesives in surgical

applications; ways to generate monosort functionalized polyolefin surfaces; nano-enhanced adhesives; bonding dissimilar materials in dentistry; flame treatment of polymeric materials with relevance to adhesion; and mucoadhesive polymers for enhancing retention in ocular drug delivery.

This book containing bountiful information on certain topics of contemporary interest should be valuable and useful to researchers and technologists in academia, industry, various research institutes and other organizations. Yours truly sincerely hopes that this book will be warmly received by the materials science community in general and the adhesion and adhesives community in particular.

Kash Mittal
P.O. Box 1280
Hopewell Jct., NY 12533
E-mail: usharmittal@gmail.com
June 3, 2015

Adhesion of Condensed Bodies at Microscale: Variation with Movable Boundary Conditions

Jian-Lin Liu^{1,*}, Jing Sun¹, Runni Wu² and Re Xia²

¹*Department of Engineering Mechanics, China University of Petroleum, Qingdao, China*

²*School of Power and Mechanical Engineering, Wuhan University, Wuhan, China*

Abstract

We review here the recent developments on the adhesion of condensed bodies at microscale, spanning from droplets, microbeams, CNTs (carbon nanotubes) to cells. We first introduce a general method to completely tackle the adhesion problem with movable boundary conditions, from the viewpoint of energy variation. Based on this theoretical framework, we then use the developed line of reasoning to investigate the adhesion behaviors of several condensed systems. According to the variation with movable boundary conditions, the governing equations and transversality conditions of these systems are derived, leading to closed-form problems. The presented method is verified via the concept of energy release rate or J -integral in fracture mechanics. This analysis provides a new approach to explore the mechanism of different systems with similarities as well as to better understand the unification of nature. The analysis results may be beneficial to the design of micro-machined MEMS (micro-electro-mechanical systems) structures, super-hydrophobic materials, nano-structured materials, and hold potential for predicting the adhesion behavior of cells or vesicles.

Keywords: Variational theory, transversality condition, beam adhesion, droplet adhesion, CNT adhesion, cell adhesion

1.1 Introduction

A plethora of adhesion phenomena exist widely at micro/nanoscale in nature, which are caused by van der Waals force, Casimir force, capillary force, or some other interaction forces. In these low-dimensional systems with considerable surface-to-volume ratio, the surface

*Corresponding author: liujianlin@upc.edu.cn

interaction dominates over the volume force as the scale reduces to micro/nano-meters, and this feature leads to many novel behaviors distinct from those of macroscopic systems [1]. An interesting example is the striking adhesion ability of geckos, which is primarily attributed to the van der Waals force between their feet and the contact surfaces [2, 3]. Besides, the adhesion of liquid drops plays a critical role in the famous “lotus effect” [4–6], water-walking capability of aquatic creatures like water strider, water spider [7–9], mosquito [10] and ant [11], and the ability of collecting dew by Namibia desert beetle *Stenocara* [12]. These magical phenomena inspired the spirit of “learning from nature”, and one of the challenging subjects is to mimic the microstructures of biological materials to achieve ultrahydrophobic properties of materials with microstructured surfaces [13]. Therefore, the core issue dealing with droplet adhesion is how to predict the macroscopic contact angle appropriately, which has spurred great interest in both fundamental science and engineering applications [14–18]. It has been further shown that the contact angle of a liquid drop can be derived from the energy variation on its energy functional [19–21], and this conclusion provides a new perspective on considering the adhesion of a droplet on a substrate.

Adhesion can also cause the failure of such slender structures as beams, fibers and plates in micro/nano systems. For instance, in micro-contact printing technology, adhesion associated with van der Waals force often produces stamp deformation because of small spacings [22], and the micro-machined MEMS structures will spontaneously come into contact with the substrate under the influence of solid surface energy or capillary force of liquid [23–27]. Similar problem has become a crucial bottleneck in the bottom-up approach, in which nanowires and nanobelts are widely used as building blocks of micro/nano-devices, typically, the micro-sensors, resonators, probes, transistors and actuators in micro/nano-electro-mechanical systems (M/NEMS) [27, 28]. This sort of failure mode has proved to be a major limitation to push further application of these novel engineering devices, and it has been highlighted as a hot research topic in the past decades.

Another topic is the deformation of CNT (carbon nanotube) induced by adhesion, holding great potential in a number of applications such as flexible and stretchable load-bearing structural components in nanoscale systems [29]. There are mainly two aspects of the CNT deformation, i.e. the adhesion and cross section collapse, which are due to the fact that CNTs are one of the strongest and most flexible materials with the C-C covalent bonding and the seamless hexagonal network architecture. In the pursuit of engineering applications, it is imperative to exploit this elastic behavior and mechanism of CNT adhesion. Among others, for a CNT ring adhered to a flat substrate, Zheng and Ke [30] established an elastica model for numerical simulation, and then experimentally characterized the CNT deformation under both compressive and tensile loadings. Like a microtubule inside a vesicle buckling into a racket-like shape [31], CNTs with a similar shape were also observed in a sample of HiPCo single-walled nanotubes after 30-minute of sonication in dichloroethane [32]. This behavior is termed as “self-folding”, and its occurrence in such small-scale materials such as nanowires, microtubules and nanotubes is mainly attributed to the high aspect ratio. In this situation, the maximal size (e.g., the length of nanowire) is much larger than its persistence length [33, 34]. As a consequence, a CNT can be easily bent into an arc shape with significant curvature [35]. This form of adhesion or self-folding

of CNT is actually an energetically favorable state, with the interplay of elastic deformation and van der Waals attraction between different parts of CNT. The second aspect of the CNT deformation is cross section collapse, in which its initially circular cross section will jump to a flat ribbon-like shape. The reason lies in that CNTs capture the characteristic of hollow cylindrical structures, which renders them susceptible to lateral deformation. In reality, this morphology was first observed and explored by TEM (Transmission Electron Microscopy) [36, 37] and then by AFM (Atomic Force Microscopy) [38–40]. From the viewpoint of elastic stability, the collapse of CNTs is essentially a buckling process, which has been one of the recent topics of considerable interest. A number of shell, tube and elastica models have been developed to investigate the buckling of CNTs, with the adoption of continuum mechanics, finite element, and molecular simulations [41–45].

The last related problem is cell or vesicle adhesion, which has profound implications in the forming of biological tissues and organs [46]. It also involves many physiological activities, which contribute to cellular organization and structure, proliferation and survival, phagocytosis and exocytosis, metabolism, and gene expression [47]. Appropriate cell adhesion can induce such diseases as thrombosis, inflammation, and cancer. Excessive adhesion can even cause monocytes to bond to the aorta wall and eventually leads to atherosclerotic plaques [48], and conversely the lack of adhesion can result in the loss of synaptic contact and induce Alzheimer disease [49]. Especially, the adhesion of a vesicle or a cell to a solid substrate is of great significance in many application fields, such as the adhesion between the target tumor cells and drug membrane in drug delivery [50, 51], the surface-sensitive technique based on lipid-protein bilayers [52, 53], and stem cell division modulated by the substrate rigidity [54]. Much effort in the areas of molecular and cellular biomechanics, both theoretically and experimentally, has been devoted to exploring this adhesion behavior [55].

This review article is organized as follows. In Section 2, we introduce a general framework to deal with adhesion problem with movable boundary conditions, i.e., the transversality condition method, which can be verified with the energy release rate method. In Sections 3, 4, 5 and 6, we apply the developed approach to study the adhesion of a microbeam, droplet, CNT and cell, respectively. Through the transversality conditions and governing equations originating from the energy variation, we can completely solve the critical adhesion length and deflection of a microbeam, the morphology of a droplet, and the configuration of a CNT or cell. Then the conclusion and discussion follow in the last section.

1.2 Kinematics: Energy Variation with Movable Boundary Conditions

We start from a generalized condensed system represented as a continuous and smooth curve, where only a portion of the curve is adhered by interfacial forces. As schematized by the anti-clockwise arc length s in Figure 1.1, the total length of the curve is L . We assume that the “generalized elastic deformation” only happens on the segment from $s = 0$ to $s = a$. The “elastic deformation” is a more general terminology, referring to the strain energy or some other energies (such as the liquid/vapor interfacial energy which appears in Section 4) related with this segment. It is noticeable that this model is similar to the famous JKR model in contact mechanics [56]. The total potential energy of the system originates from three

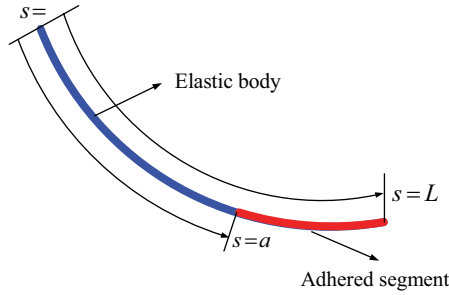


Figure 1.1 Schematic of a general system incorporating two sections with elastic energy and interfacial energy, respectively.

sources, namely, elastic strain energy, interfacial energy, and potential energy of gravity. If the typical length of the structure is denoted as L_c , the scaling laws for a planar system are set forth as follows: the interfacial or surface energy $U_s \propto L_c$, the elastic strain energy $U_E \propto L_c^2$, and the potential energy of gravity $U_G \propto L_c^3$ [57]. Consequently, as the dimension of a macroscopic structure reduces to micro/nanometers, the effect of surface energy becomes significant and that of the gravitational energy becomes negligible. Hence, the interplay between the surface energy and elasticity is predominant in the current micro/nano-systems.

Point $s = a$ is a key point, as its value is an unknown and should be determined by calculation, so the total potential energy of the system Π is viewed as a function of the parameter a :

$$\Pi[a] = U(a) + \Gamma(a), \tag{1.1}$$

where $\Gamma(a)$ is the interfacial energy, $U(a)$ is the strain energy stored in the system which is often expressed as $U = \int_0^a F[s, y(s, a), y'(s, a), y''(s, a)] ds$, and y is a function with two variables, i.e. $y = y(s, a)$.

If the segment from $s = 0$ to $s = a$ is regarded as a crack, then according to the extreme condition of $\frac{d\Pi[a]}{da} = 0$, one can arrive at the definition of the energy release rate G in classical fracture mechanics:

$$G = - \left. \frac{\partial U(a)}{\partial a} \right|_{\Delta} = \frac{\partial \Gamma(a)}{\partial a} = W. \tag{1.2}$$

For elastic materials under displacement loading, the energy release rate is equal to the J -integral named after James Rice [58].

The parameter W in Eq. (1.2) is the interfacial energy per unit area or the work of adhesion at the interface. The work of adhesion between two surfaces is normally expressed as

$$W = \gamma_1 + \gamma_2 - \gamma_{12}, \quad (1.3)$$

where γ_1 and γ_2 are the surface energies per unit area of the two different phases, and γ_{12} is the interfacial energy per unit area. In the conventional definition, the work of adhesion is actually the work per unit area which is necessary to create two new surfaces from a unit area of an adhered interface, which is a positive constant for any two homogeneous materials binding at an interface at a fixed temperature [59]. If the two materials are the same, the work of adhesion reduces to the work of cohesion:

$$W = 2\gamma_1. \quad (1.4)$$

At micro and nanoscales, the work is normally termed as the binding energy E_b [60]. For a droplet on a substrate, the work of adhesion becomes

$$W = \gamma_{SV} + \gamma_{LV} - \gamma_{SL} = \gamma_{LV} (1 + \cos\theta_Y), \quad (1.5)$$

where γ_{SV} , γ_{SL} and γ_{LV} are the interfacial tensions of the solid/vapor, solid/liquid and liquid/vapor interfaces, respectively, with θ_Y being the Young's contact angle of the liquid. In the above derivation, the Young's equation $\gamma_{SV} - \gamma_{SL} = \gamma_{LV} \cos\theta_Y$ has been used.

Considering the movable boundary of the integrand and using Eqs. (1.1) and (1.2), the energy release rate G can be expressed as:

$$G = -\left. \frac{\partial U(a)}{\partial a} \right|_{\Delta} = F(a) + \int_0^a \left(F_y \frac{\partial y}{\partial a} + F_{y'} \frac{\partial y'}{\partial a} + F_{y''} \frac{\partial y''}{\partial a} \right) ds = W, \quad (1.6)$$

where the partial derivative symbols are designated as $(\)' = \frac{\partial(\)}{\partial s}$, $(\)'' = \frac{\partial^2(\)}{\partial s^2}$,

$F_{(\)} = \frac{\partial F}{\partial(\)}$. Equation (1.6) indicates that the energy release rate is compensated by a gain in the interfacial energy in the process of interface enlargement. Applying this line of reasoning to the current problem, it is straightforward to solve the unknown parameter a in use of this energy balance relation. However, in many situations, the analytical expressions for the energy release rate and the function F are not available, because they are dependent on the governing equation. Thus, we have to seek another route to obtain the governing differential equation and then tackle this problem. Since the value of a needs to be determined when the system achieves an equilibrium state, the point $s = a$ can be considered as a moving boundary from the viewpoint of mathematics [61].

The functional of the total potential energy about the system schematized in Figure 1.1 is normally written as:

$$\Pi[y(s, a)] = \int_0^a F[s, y(s, a), y'(s, a), y''(s, a)] ds - \int_a^L W ds. \quad (1.7)$$

In fact, the energy functional of Eq. (1.7) is unique in that it deals with two variables, i.e. the function y and the length a . This fact results in an intractable problem, because the undetermined variable a causes the boundary movement of the system, which will create an additional term during the variational process.

Generally, the forced or fixed boundary conditions are prescribed as:

$$y(0) = y_0, \quad y'(0) = y'_0; \quad y(a) = y_a, \quad y'(a) = y'_a. \quad (1.8)$$

The governing equation and additional boundary conditions can then be derived according to the definition of variation with movable boundary condition. Let

$$y(s) = y_0(s) + \varepsilon Y(s), \quad (1.9)$$

where $y_0(s)$ denotes the extreme solution to be found [62]. According to the prescribed boundary condition of Eq. (1.8), the extreme and varied solutions must fulfill

$$y_0(a_0) = y_a, \quad y'_0(a_0) = y'_a; \quad y(a) = y_a, \quad y'(a) = y'_a; \quad Y(0) = Y'(0) = 0. \quad (1.10)$$

The unknown a can be expanded as

$$a(\varepsilon) = a_0 + \varepsilon \left. \frac{da}{d\varepsilon} \right|_{\varepsilon=0} + O(\varepsilon^2). \quad (1.11)$$

The boundary value in Eq. (1.9) can also be expanded as

$$y(a) = y_0(a_0) + \varepsilon y'(a_0) \left. \frac{da}{d\varepsilon} \right|_{\varepsilon=0} + \varepsilon Y(a_0) + O(\varepsilon^2), \quad (1.12)$$

$$y'(a) = y'_0(a_0) + \varepsilon y''(a_0) \left. \frac{da}{d\varepsilon} \right|_{\varepsilon=0} + \varepsilon Y'(a_0) + O(\varepsilon^2). \quad (1.13)$$

Comparing Eqs. (1.9), (1.12) and (1.13), one arrives at

$$Y(a_0) = -y'(a_0) \left. \frac{da}{d\varepsilon} \right|_{\varepsilon=0}, \quad (1.14)$$

$$Y'(a_0) = -y''(a_0) \left. \frac{da}{d\varepsilon} \right|_{\varepsilon=0}. \quad (1.15)$$

Eqs. (1.14) and (1.15) give the variation of the “new” end-point $a(\varepsilon)$ as a function of the variation in y and the derivatives y' and y'' at the “old” end-point a_0 .

Before proceeding further, we first revisit the definition of derivative about an integration including a parameter a . Let

$$\phi(a) = \int_{a(a)}^{b(a)} F(x, a) dx, \quad (1.16)$$

and then we have its derivative

$$\phi'(a) = \int_{a(a)}^{b(a)} F_a(x, a) dx + F[b(a), a]b'(a) - F[a(a), a]a'(a). \quad (1.17)$$

Now let us return to the variation of the energy functional in Eq. (1.7). Substituting Eqs. (1.8), (1.9), (1.10), (1.12) and (1.14) into Eq. (1.15), and using Eq. (1.17), one can obtain the derivative of the functional

$$\begin{aligned} \left. \frac{d\Pi}{d\varepsilon} \right|_{\varepsilon=0} &= [W + F]_{s=a_0} \left. \frac{da}{d\varepsilon} \right|_{\varepsilon=0} + \int_0^{a_0} [F_y Y + F_{y'} Y' + F_{y''} Y''] ds \\ &= [W + F]_{s=a_0} \left. \frac{da}{d\varepsilon} \right|_{\varepsilon=0} + [F_{y'} Y + F_{y''} Y']_0^{a_0} + \int_0^{a_0} \left[F_y Y - \frac{dF_{y'}}{ds} Y - \frac{dF_{y''}}{ds} Y' \right] ds \\ &= [W + F]_{s=a_0} \left. \frac{da}{d\varepsilon} \right|_{\varepsilon=0} + \left[F_{y'} Y + F_{y''} Y' - \frac{dF_{y''}}{ds} Y \right]_0^{a_0} + \int_0^{a_0} \left[F_y - \frac{dF_{y'}}{ds} + \frac{d^2 F_{y''}}{ds^2} \right] Y ds \quad (1.18) \\ &= \left[W + F - y' F_{y'} - y'' F_{y''} + y' \frac{dF_{y''}}{ds} \right]_{s=a_0} \left. \frac{da}{d\varepsilon} \right|_{\varepsilon=0} + \left[F_{y'} Y + F_{y''} Y' - \frac{dF_{y''}}{ds} Y \right]_0^{a_0} \\ &\quad + \int_0^{a_0} \left[F_y - \frac{dF_{y'}}{ds} + \frac{d^2 F_{y''}}{ds^2} \right] Y ds = 0. \end{aligned}$$

The fact that the above integral equals zero leads to the governing differential equation, i.e. the Euler-Poisson equation:

$$F_y - \frac{\partial}{\partial s} F_{y'} + \frac{\partial^2}{\partial s^2} F_{y''} = 0. \quad (1.19)$$

The remainder of Eq. (1.18) takes the following form

$$\left[W + F - y'F_{y'} - y''F_{y''} + y' \frac{dF_{y''}}{ds} \right]_{s=a_0} \frac{da}{d\varepsilon} \Big|_{\varepsilon=0} = 0. \quad (1.20)$$

This expression vanishes for arbitrary $\frac{da}{d\varepsilon} \Big|_{\varepsilon=0}$, which corresponds to arbitrary $Y(a_0)$ if the bracket is zero. Then we can obtain the additional boundary condition, which is defined as transversality boundary condition for this variation problem:

$$W = \left[y'F_{y'} + y''F_{y''} - y' \frac{dF_{y''}}{ds} - F \right]_{s=a}. \quad (1.21)$$

In fact, the transversality condition dealing with movable boundaries has already been deciphered in the book titled as “Methods of Mathematical Physics”, authored by Courant and Hilbert in 1953 [63]. In essence, this additional condition indicates the equilibrium state originating from the competition between surface energy and elastic energy at the critical point.

Therefore, based on the above fundamental deductions, utilizing the principle of least potential energy and considering the movable boundary, one can obtain the following variation result

$$\delta \Pi [y(s, a)] = \delta \Pi_1 + \delta \Pi_2 = 0, \quad (1.22)$$

where

$$\begin{aligned} \delta \Pi_1 &= \int_0^a (F_y \delta y + F_{y'} \delta y' + F_{y''} \delta y'') ds \\ &= \left[F_{y'} \delta y + F_{y''} \delta y' - \frac{\partial}{\partial x} F_{y''} \delta y \right]_0^a + \int_0^a \left(F_y - \frac{\partial}{\partial x} F_{y'} + \frac{\partial^2}{\partial x^2} F_{y''} \right) \delta y ds, \end{aligned} \quad (1.23)$$

and

$$\delta \Pi_2 = \left[F - y'F_{y'} - y''F_{y''} + y' \frac{dF_{y''}}{ds} + W \right]_{s=a} \delta a. \quad (1.24)$$

Inserting Eq. (1.23) and (1.24) into (1.22), and because of the arbitrariness of the variation, one can obtain the Euler-Poisson equation shown in Eq. (1.19), and the arbitrariness of variation about the point a leads to the transversality condition in Eq. (1.21).

The combination of Eqs. (1.6) and (1.21) yields

$$\left[y'F_{y'} + y''F_{y''} - y' \frac{dF_{y''}}{ds} - F \right]_{s=a} = W = G = F(a) + \int_0^a \left(F_y \frac{\partial y}{\partial a} + F_{y'} \frac{\partial y'}{\partial a} + F_{y''} \frac{\partial y''}{\partial a} \right) ds. \quad (1.25)$$

It is indicated from Eq. (1.25) that there are two approaches to determine the variable a , namely the energy release rate method, and the movable boundary condition method. However, in most cases when adopting the first method, the explicit expression for the integral on the right side of Eq. (1.25) is impossible to obtain, and therefore the second one is the only choice. This idea sheds a new light on solving the problem with movable boundaries.

Next, we will review some case studies, where the governing equations and transversality conditions can be easily derived from the variation viewpoint in light of energy minimization. These issues include microbeam adhesion, CNT deformation, droplet wetting, and cell adhesion. From these examples, we can see that the novel idea of movable boundary condition proves to be more challenging and fruitful.

1.3 Microbeam/plate Adhesion

Within the above framework, the first typical example is a microbeam stuck to the substrate with strong work of adhesion W , with the Young's modulus E , and the moment of inertia on the cross section I , which is schematized in a Cartesian coordinate system ($o-xy$). As shown in Figure 1.2, the gap height is h , the detached segment length is a , and the total length of the beam is L . The potential energy of the system can be expressed as

$$\Pi = \frac{1}{2} \int_0^a EIw''^2 dx - W(L-a). \quad (1.26)$$

According to the variation method of Section 2, one can arrive at the governing equation

$$w^{(4)} = 0 \quad (1.27)$$

and the transversality condition at the moving boundary

$$W = \frac{1}{2} EIw''(a)^2 = \frac{18EIh^2}{a^4}. \quad (1.28)$$

This expression is in good agreement with the former results [24, 27]. According to the above equations, one can naturally determine the detachment length and the deflection of the beam.

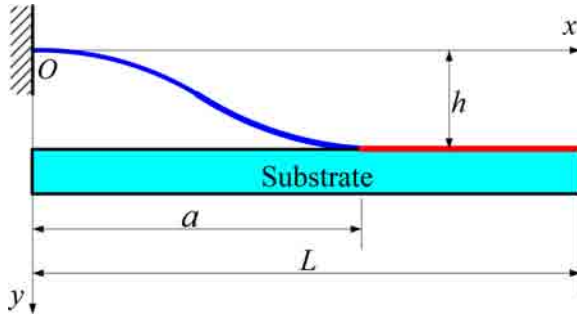


Figure 1.2 Adhesion of a microbeam to a solid substrate due to interfacial energy.

To validate the aforementioned results, we revisit this problem from the viewpoint of fracture mechanics. The detached segment of the beam is modeled as a crack, and the energy release rate G is then deduced as

$$G = -\left. \frac{\partial U}{\partial a} \right|_{\Delta} = \frac{18EIh^2}{a^4} = W, \tag{1.29}$$

which bears the same form as Eq. (1.28). This re-emphasizes the equivalence of the methods of movable boundary condition and the energy release rate.

However, for the nanobeam adhesion to a solid substrate, we must take the surface effects into account. Using the Gurtin’s theory, the potential energy of the beam-substrate system is given as [64]

$$\Pi = \frac{1}{2}(EI)^* \int_0^a (w'')^2 dx - \int_0^a q w dx - W(L - a), \tag{1.30}$$

where $(EI)^*$ is the modified bending stiffness due to surface elasticity, and q is the transversely distributed load along the longitudinal direction of the beam due to the residual surface stress. Based on the presented variation method, the nanobeam deflection with surface effects can be presented, indicating that it is not in symmetric configuration.

However, these analyses are only applicable to the case of stiff substrate, and the boundary condition at the adhesion point is assumed to be a clamped end. Following the model in Figure 1.2, Zhang and Zhao [65, 66] considered the elastic deformation of the substrate, and mentioned that the slope angle at the movable point is not zero. They derived the boundary conditions through energy variation, where they named these transversality conditions as “matching conditions”. In essence, their approach offers a more accurate model for the stuck cantilever without prescribing its deflection shape.

Besides the system consisting of a single beam adhered to a substrate, considerable attention has been paid to the capillary adhesion of multiple beams with liquid bridges. For

illustration, the adhesion of two initially parallel microbeams with a rectangular cross section is shown in Figure 1.3, where d is the initial distance between the two beams. Adopting the energy minimization method, Bico *et al.* [67] obtained the equilibrium sizes of two beams and two bundles of beams in capillary adhesion. Kim and Mahadevan [68] derived the rising height of the meniscus between two thin sheets dipped vertically in a liquid bath. In their model, the liquid bridge was first modeled as a thin liquid film and the equilibrium configuration of the static beams was determined. These theories have been verified by their experimental results respectively, but the meniscus height is found to be different from that predicted by Jurin's law. By using the energy variation with movable boundary condition, Liu *et al.* [69] presented the total potential energy of the system, where the values of the strain energy and interfacial energy are twice those of Eq. (1.26). Based on these investigations and the minimum total potential energy principle, Liu *et al.* [69] derived the analytical expressions for the critical adhesion lengths of two beams, three beams, and two bundles of beams under capillary forces. Their solutions were also validated by experiments using polyester and silicone oil.

It is worth mentioning that the aforementioned studies are mainly based on the infinitesimal deformation theory of elastic structures. However, a slender structure under the action of capillary forces may undergo large deformation, especially when its characteristic sizes are in the range of micrometers or nanometers. For instance, Journet *et al.* [70] observed that when a volatile droplet is placed on an array of aligned CNTs, it will experience large deformation and will be adhered to bundles. In light of this experiment, Liu and Feng [71] studied the finite deformation of two originally parallel CNTs stuck with each other by a thin liquid film as schematized in Figure 1.3. With the variation of the energy functional of the system, the governing equation of an elastica beam was derived as

$$EI \frac{d^2\theta}{ds^2} \mathbf{e}_z + \mathbf{t} \times \mathbf{R} = \mathbf{0}, \quad (1.31)$$

where θ denotes the angle between the horizontal and the tangential directions, \mathbf{e}_z the unit vector normal to the plane of the deformed beam, \mathbf{t} the tangential unit vector of

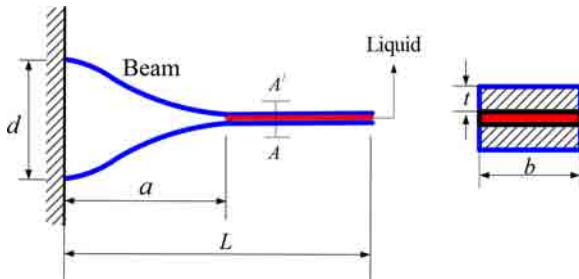


Figure 1.3 Two microbeams adhered by a thin liquid film, where left is the side view, and right is the cross section.

the beam, and \mathbf{R} the constant vectorial tension acting on the beam. The critical point of the adhesion segment is unknown and can be viewed as a movable boundary condition during the variation process. By solving the elastica equation [72] and the corresponding transversality condition, Liu and Feng [71] obtained the solutions of key parameters and deflection curve of the adhered beams. In comparison with the solution of infinitesimal deformation, the finite deformation theory shows a better agreement with relevant experimental results.

Furthermore, Liu [73] generalized the existing models of microbeams to microplates with the effects of capillary adhesion. Assume that the plate is usually adhered to the rigid substrate due to the capillary force induced by the liquid film between the stiction zone of the plate and the substrate. Therefore, the plate includes a non-adhered portion and an adhered one, denoted as D_1 and D_2 , respectively. The boundary of the adhesion zone is also assumed as a plane curve Γ_2 . The initial distance of the substrate from the plate is H , and the deflection of the plate is w . As schematized in Figure 1.4, the potential energy functional of the plate-substrate system is expressed as

$$\Pi = \iint_{D_1} \left[\frac{\kappa}{2} (\nabla^2 w)^2 + 2\gamma_{LV} \cos\theta_Y \right] dx dy - 2 \iint_{D_1+D_2} \gamma_{LV} \cos\theta_Y dx dy. \quad (1.32)$$

From the variation of the energy functional of the solid/liquid system, Liu [73] derived the governing equation of a plate adhered to a substrate and the supplementary boundary condition, i.e. the transversality condition. The latter is written as

$$\left\{ \kappa \left[l \frac{\partial}{\partial x} (\nabla^2 w) + m \frac{\partial}{\partial y} (\nabla^2 w) \right] \frac{\partial w}{\partial n_2} - \kappa \nabla^2 w \left[l \frac{\partial}{\partial x} \left(\frac{\partial w}{\partial n_2} \right) + m \frac{\partial}{\partial y} \left(\frac{\partial w}{\partial n_2} \right) \right] \right\}$$

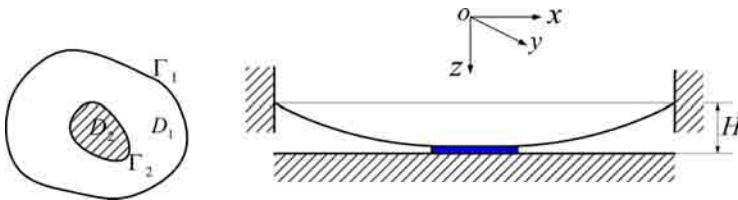


Figure 1.4 Adhesion of a microplate to the substrate by surface energy, where left is the top view, and right is the side view.

$$\left. \left. + \frac{\kappa}{2} (\nabla^2 w)^2 + 2\gamma_{LV} \cos \theta_Y \right\} \right|_{\Gamma_2} = 0. \quad (1.33)$$

$$= \left[\frac{\kappa}{2} (\nabla^2 w)^2 + 2\gamma_{LV} \cos \theta_Y + \kappa \frac{\partial}{\partial n_2} (\nabla^2 w) \frac{\partial w}{\partial n_2} - \kappa \nabla^2 w \frac{\partial^2 w}{\partial n_2^2} \right]_{\Gamma_2} = 0. \quad (1.33)$$

It was found that for a circular plate, there exists a minimum critical radius, below which no capillary adhesion will occur. This conclusion is in accord with the experimental observation of Mastrangelo and Hsu [27].

1.4 Droplet Adhesion to a Solid

As another classical example, we investigate the morphology of a liquid droplet deposited on a smooth solid substrate. As exhibited in Figure 1.5, the radius of the liquid/solid area is a , the maximum height of the droplet is h , and the mass density of the liquid is ρ . To simplify the problem, we only concentrate on two-dimensional case without loss of generality, but the presented analysis can also be extended to three-dimensional case.

The boundary condition of the semi-droplet is

$$y(0) = h, \quad y'(0) = 0; \quad y(a) = 0, \quad y'(a) = -\tan \theta_Y. \quad (1.34)$$

The energy functional of this condensed system includes the interfacial energy of the liquid/vapor interface, the potential energy due to gravity, and the surface energy of the solid substrate, which can finally be written as

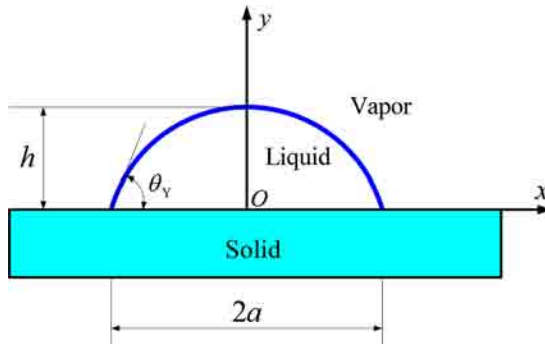


Figure 1.5 Schematic of a liquid droplet deposited on a solid substrate.

$$\Pi = 2 \int_0^a F[y(x, a)] dx + 2 \int_0^a \gamma_{LV} dx - 2 \int_0^a W dx + \lambda \int_{-a}^a y dx. \quad (1.35)$$

The symbol λ is the Lagrange multiplier, to enforce the fact of mass conservation.

In light of the variation operation with respect to Eq. (1.35) with movable boundary conditions, one can obtain the classical Laplace equation across the liquid/vapor interface:

$$\gamma_{LV} \frac{y''}{(1 + y'^2)^{3/2}} = \rho g y - \lambda, \quad (1.36)$$

where g is the gravitational acceleration and the Lagrange multiplier λ can be identified as the Laplace pressure difference at the triple contact point. The transversality condition can also be obtained as:

$$\gamma_{SV} - \gamma_{SL} = \left[\gamma_{LV} \sqrt{1 + y'^2} + \frac{1}{2} \rho g y^2 - \lambda y - \gamma_{LV} y' \frac{y'}{\sqrt{1 + y'^2}} \right]_{x=a} = \gamma_{LV} \cos \theta_Y, \quad (1.37)$$

which is just the Young's equation.

Moreover, Bormashenko [74] deduced the Young, Boruvka-Neumann, Wenzel and Cassie-Baxter equations as the transversality conditions for the variational problem of wetting. Among others, he derived the Wenzel equation [75] as

$$\cos \theta_W = r \cos \theta_Y, \quad (1.38)$$

where θ_W is the macroscopic contact angle, and r is the roughness parameter. The Cassie-Baxter equation [76] is expressed as

$$\cos \theta_{CB} = \phi \cos \theta_Y + \phi - 1, \quad (1.39)$$

where ϕ is the percentage of the solid area to the total droplet-substrate contact surface. Bormashenko and Whyman [19] further applied the variational approach to wetting problems: calculations of the shape of a sessile liquid drop deposited on a solid substrate under external field. They obtained explicit expressions describing the drop's shape with a calculation of variation for two-dimensional and three-dimensional wetting problems. This investigation may be applicable for analysis of electrowetting problems, and for the study of vibrated and centrifuged drops.

However, the actual distribution of roughness of the substrate was not considered in the analysis mentioned above. Here, we suppose that the top profile of the substrate is a continuous and smooth curve in mathematical meaning. For the sake of brevity, we only consider the symmetry case for this droplet-substrate system. The origin of the coordinate is selected

at the symmetry point of the substrate and droplet, and the corresponding right portion is schematized in Figure 1.6. The morphology of the droplet is designated as $y = y(x)$, and the shape function of the substrate is $z = z(x)$. The TCL (triple contact line) is located at the point $x = a$, where the macroscopic contact angle $\theta(a)$ is defined as the parameter in experimental measurement, i.e., the angle between the tangent line of the liquid/vapor interface and substrate [77].

All the variables which are related to the substrate surface are field functions according to continuum theory. In other words, they are all functions with respect to the coordinate of an arbitrary point, such as $\gamma_{SL} = \gamma_{SL}(x)$, $\gamma_{SV} = \gamma_{SV}(x)$ and $\theta_Y(x)$ is the Young's contact angle at any point. The Young's contact angle at any point is expressed via the classical Young's equation

$$\cos \theta_Y(x) = \frac{\gamma_{SV}(x) - \gamma_{SL}(x)}{\gamma_{LV}}. \quad (1.40)$$

To derive the expression for the macroscopic contact angle at any point, we only focus on the TCL, where the fixed boundary conditions are prescribed as

$$y(a) = z(a), \quad \dot{y}(a) = -\tan \theta(a), \quad \dot{z}(a) = \tan \phi(a). \quad (1.41)$$

Here, the dot above a character stands for the derivative of the variable with respect to the horizontal coordinate x , and the slope angle of the substrate at any point is denoted as $\phi(x)$.

Figure 1.6 is a magnified view of the area near TCL. The Gibbs free energy of the droplet-substrate system consists of potential energies from gravity and reaction force at TCL, and the interfacial energies at the liquid/vapor, solid/liquid, and solid/vapor interfaces, respectively. Applying variation about the movable boundary condition to the TCL, one can obtain the following relation

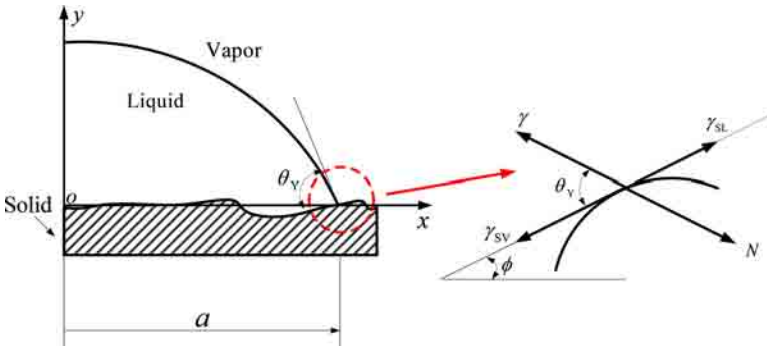


Figure 1.6 Schematic of a droplet deposited on a rough and heterogeneous substrate with the force balance at the TCL.

$$\left[\gamma_{LV} \sqrt{1 + \dot{y}^2} - \dot{y} \gamma_{LV} \frac{\dot{y}}{\sqrt{1 + \dot{y}^2}} + \gamma_{SL}(x) \sqrt{1 + \dot{z}^2} - \dot{z} \gamma_{SL}(x) \frac{\dot{z}}{\sqrt{1 + \dot{z}^2}} - \gamma_{SV}(x) \sqrt{1 + \dot{z}^2} + \dot{z} \gamma_{SV}(x) \frac{\dot{z}}{\sqrt{1 + \dot{z}^2}} - \gamma_{LV} \sin \theta_Y \sin \phi + \frac{1}{2} \rho g (y^2 - z^2) - \mu (y - z) \right]_{x=a} = 0. \quad (1.42)$$

Then the macroscopic contact angle at the TCL can be deduced as

$$\theta(a) = \theta_Y(a) - \arctan[\dot{z}(a)]. \quad (1.43)$$

It is clear that the macroscopic contact angle strongly depends on the geometrical and chemical properties of the substrate, as it is a continuum field variable at any point. This means that different positions will possess different contact angles. Finally, we again emphasize that the macroscopic contact angle is only relevant to the properties of TCL and is independent of those of the area underneath the droplet, and this conclusion violates the conventional idea. As is well known, the classical Wenzel and Cassie models are both concerned with the geometrical and chemical properties of the contact zone rather than the contact point. Moreover, using this model, one can illustrate the pinning effect of a droplet located at a sharp wedge or the interface between the two phases [77, 78].

For another typical substrate, i.e. a slender fiber as shown in Figure 1.7, Wu and Dzenis [79] solved the droplet shape in Legendre’s elliptical functions. The free energy of the droplet-fiber system reads

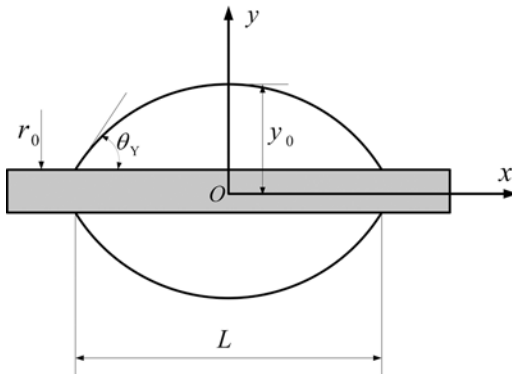


Figure 1.7 A droplet adhered to a fiber, with a barrel shape.

$$\Pi = 4\pi \int_0^{L/2} \left[(\gamma_{SL} - \gamma_{SV})r_0 + \gamma_{LV}y\sqrt{1+y'^2} \right] dx - 4\pi \int_0^{L/2} F[y(x), y'(x), \mu] dx. \quad (1.44)$$

By using the former variation method considering the movable boundary conditions, they deduced the Laplace equation and Young's equation as the governing equation and transversality boundary condition, respectively. They also proposed a novel efficient semi-analytical approach to extract the contact angle from experimental data, when the contact angle is larger than 15° .

1.5 Elastica Model of CNT Adhesion

The adhesion of a bending CNT ring to a solid substrate is also a representative case study, which is schematized in Figure 1.8. Due to the symmetry and smoothness of this configuration, only the right half of the structural portion is selected and modeled as a beam with two clamped ends. The initial radius of the carbon nanotube ring is R , and the adhered segment is a . The slope angle of the beam at an arbitrary point is Φ , which continuously changes from 0° at its lower end to 180° at its upper end.

This configuration is stabilized by the van der Waals interaction between the upper and lower portion of the CNT ring, primarily within the horizontal contact zone, because the van der Waals force decays rapidly in the non-contact areas. As a reasonable simplification, the van der Waals force between the upper and lower portion of the CNT ring in the non-contact domain is negligible. Then the total potential energy of the system mainly consists of two parts, i.e., the elastic strain energy and surface energy. Considering the symmetry of this configuration, the energy functional of the elastica in Figure 1.8 can be expressed as

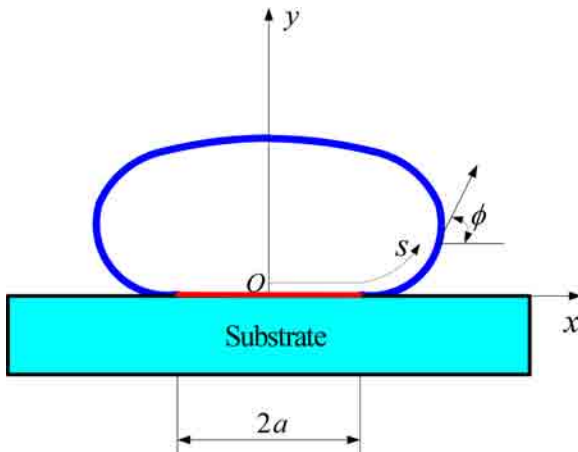


Figure 1.8 A CNT ring adhered to a solid substrate due to strong interfacial energy.

$$\Pi = \int_a^{\pi R} \left[\frac{1}{2} EI \dot{\phi}^2 + \lambda_1 (\dot{x} - \cos \phi) + \lambda_2 (\dot{y} - \sin \phi) \right] ds - Wa, \tag{1.45}$$

where λ_1 and λ_2 serve as two Lagrange multipliers. Using the aforementioned method, one can obtain the governing equation, Eq. (1.31) and the transversality condition [61, 80, 81]:

$$\frac{1}{2} EI \dot{\phi}(a)^2 + \lambda_1 = W. \tag{1.46}$$

The next problem is the self-folding of CNT, as schematized in Figure 1.9. The total length of the rod is $L/2$, and the adhered segment is l . Much effort has been directed toward understanding the physical mechanism of self-folding process. The first atomistic simulation of the single-walled CNT with very large aspect ratio subjected to compressive loading was carried out by Buehler *et al* [35]. They investigated the shell-rod-wire transition of CNTs with increasing aspect ratio. Following this work, Buehler *et al.* [82] utilized atomistic simulation to study the deformation of a highly flexible nanotube forming a thermodynamically stable self-folded structure, and presented the critical length and critical temperature for folding or unfolding. In succession, Zhou *et al.* [83] obtained the critical length of the self-folding of CNTs by MD simulations and infinitesimal deformation analysis. Mikata [84] then derived an approximate solution for the self-folding of CNTs on the assumption that the curvature at the adhesion point was zero. Moreover, Glassmaker and Hui [85] modeled the CNT as an elastica, presented the closed-form differential equation set, and gave the numerical results. Similar to CNT folding, Cranford *et al.* [86] studied the self-folding of mono- and multilayer graphene sheets, utilizing a coarse-grained hierarchical multiscale model derived directly from atomistic simulation. Although the above-mentioned studies have been devoted to self-folding problems, there is still a lack of systematic theoretical analysis on the underlying physical mechanisms, which involve very large deformation and strong geometric nonlinearity. However, adopting the above-presented variational method with movable boundary conditions, it is easy to derive the governing equation (1.31) of the racket-like CNT. The transversality condition is similar to the former result:

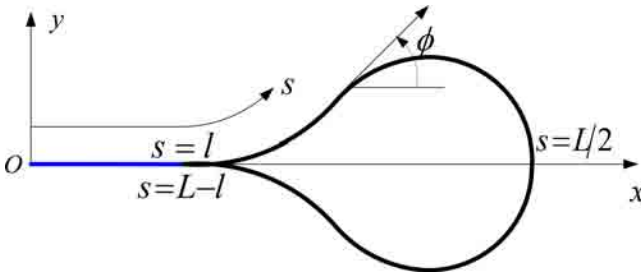


Figure 1.9 Self-folding of a slender CNT with a racket shape.

$$EI\dot{\phi}(l)^2 - W = 0. \quad (1.47)$$

The second aspect of CNT deformation is the cross section collapse of CNT. As shown in Figure 1.10, if the radius of the CNT is small, the cross section is normally circular; if the radius is large enough, the cross section is called the collapsed morphology. We consider the collapsed morphology of a single-walled CNT, which is initially circular with a radius R and an axial length L . The current configuration incorporates a flat contact zone in the middle part and two non-contact regions at the ends, as shown in Figure 1.10. As a reasonable simplification, the van der Waals force between the upper and lower portion of the CNT walls in the non-contact domain is ignored. Normally, the van der Waals force between two carbon atoms is repulsive at a very close range, so the CNT wall contact is defined by an equilibrium separation d_0 between the flat regions. The distance between the flat contact zone and the extreme point of the CNT is denoted as b . From the experimental picture, we can see that the collapsed shape of CNT is symmetrical, which was also verified by molecular simulations [87]. For the collapsed morphology, due to the symmetry and smoothness of this configuration, only a quarter of the structure is selected and then modeled as a plate or as an elastica with two clamped ends. In fact, there is another underlying assumption that the deformation along the axis of the nanotube is uniform, which has already been verified by experiments and MD simulations [39, 40, 87, 88]. As a result, we select the cross section representing the whole tube, and model the thin wall as a curvilinear abscissa. Therefore, within the presented analysis framework, similar governing equation

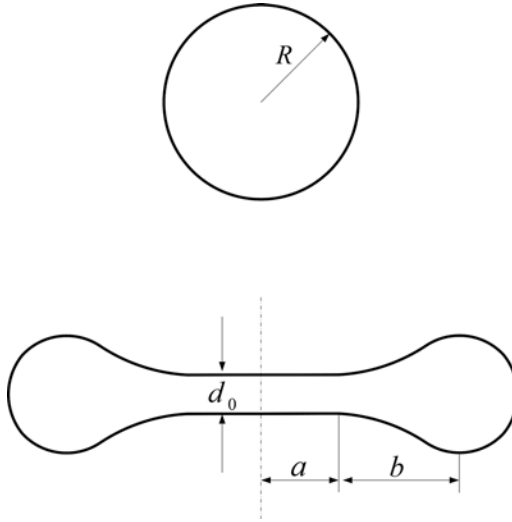


Figure 1.10 Cross section collapse of a CNT, from a circular shape to the dumbbell shape.

and transversality condition can also be derived [89]. In the analysis, we have defined a new characteristic length, i.e. the elasto-cohesive length $L_{ec} = \sqrt{EI/W}$, which is different from the elasto-capillary length L_{EC} named by Roman and Bico [57]. It can be noticed that the elasto-cohesive length is identical to another parameter, $1/\sqrt{Q}$, which is determined in [85]. For a slender structure adhered by a liquid film, the elasto-cohesive length $L_{ec} = \frac{\sqrt{2}}{2} L_{EC}$ when $\theta_Y = 0$, which is consistent with the former result [67].

In succession Zhang *et al.* [90] carried out continuum mechanics analysis and molecular mechanics simulations to study the adhesion between two identical, radially collapsed single-walled CNTs, as shown in Figure 1.11. They considered both the inter-adhesion energy between nanotubes and the intra-adhesion energy in a nanotube, and gave a closed-form solution to the adhesion configuration. Comparing the potential energy of the adhesion structures formed by two identical single-walled CNTs, three types of configurations, i.e., circular, deformed, and collapsed shape, can be formed with increasing CNT radius and separated by two critical radii of the single-walled carbon nanotube. Furthermore, they pointed out that the collapsed adhesion structure possesses the highest interfacial energy. The results demonstrate that as a potential application in carbon nanotube reinforced composites, arrays formed by collapsed carbon nanotubes will be optimal due to the strong interface strength.

1.6 Cell Adhesion

For a cell adhered to a solid substrate, Seifert [91] first gave the free energy expression for the cell membrane:

$$\Pi = \frac{\kappa}{2} \iint dA (C_1 + C_2 - C_0)^2 + P \int dV + \Sigma \iint dA - WA^*, \quad (1.48)$$

where C_1 and C_2 are two principal curvatures of any point on the membrane, C_0 is the spontaneous curvature, A is the area of the membrane, A^* is the adhered area of the membrane, V is the volume of the membrane, P is the pressure difference across the membrane interface, and Σ is the Lagrange multiplier. According to the variation with respect to the free energy, they gave the nontrivial boundary condition, i.e. the transversality condition at the adhesion point as

$$c(A^*) = \sqrt{\frac{2W}{\kappa}}, \quad (1.49)$$

which is equivalent to the former result [92]. Moreover, they presented the morphologies of a cell adhered to a smooth substrate by solving the governing equation considering the transversality condition.

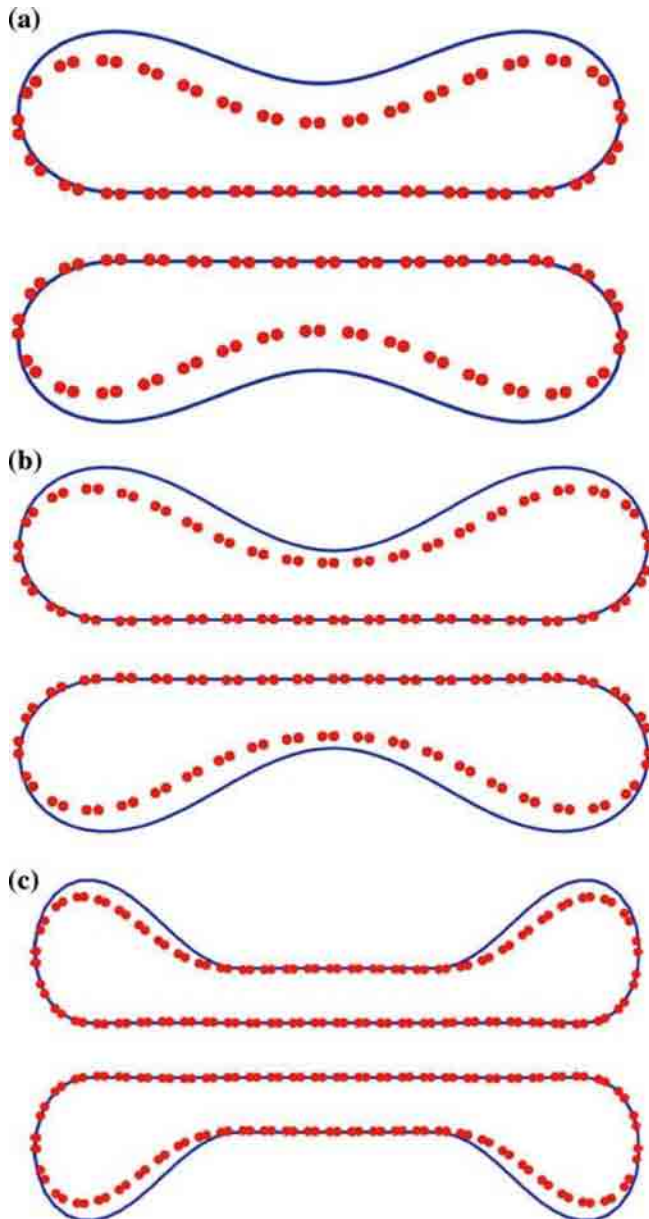


Figure 1.11 Adhesion between two radially collapsed single-walled CNTs. (a) Partial collapsed configuration (pillow-shaped) for the case with an initial radius smaller than R_{lmin} . (b) Critical collapsed configuration with an initial radius equal to R_{lmin} . (c) Collapsed configuration with an initial radius larger than R_{lmin} .

Furthermore, Yin *et al.* [93] constructed a general mathematical frame for the equilibrium theory of open or closed biomembranes. Based on the generalized potential functional, they derived the equilibrium differential equation for open biomembrane (with free edge) or closed one (without boundary). They also presented the boundary conditions, including the transversality conditions for open biomembranes. Based on this theoretical framework, they also established the shape equation of the membrane by treating the inhomogeneous biomembrane as a lipid bilayer vesicle containing inclusions or impurities [94]. After careful examination of the equation, they found that the rigidity gradient is an initial “driving force” that may destabilize the biomembrane and stimulate shape transitions, and proposed a concept termed “curvature bifurcations induced by rigidity gradients”. In succession, Lv *et al.* [95] introduced several differential operators and integral theorems to study a vesicle sitting on a curved surface from the geometrical point of view. In their analysis, the inhomogeneous property and line tension effect of the vesicle were taken into account.

Similarly, Deserno *et al.* [96] developed a geometrical framework to deduce the equilibrium shape equations and boundary conditions for both a liquid adhered to a substrate and two liquid surfaces adhered together. Recently, Das and Du [97] investigated the adhesion of a vesicle to a substrate with various geometries. The axisymmetric configuration of the vesicle, and the typical substrates with concave, convex and flat shapes were analyzed. The result shows that the transition from a free vesicle to a bound state depends significantly on the substrate shape. Following this work, Zhang *et al.* [98] established a phase field model for vesicle adhesion involving complex substrates, where an adaptive finite element method was utilized to find the solutions. The conclusion is that concave substrates favor adhesion. More recently, Yi *et al.* [99] investigated the adhesion wrapping of a soft elastic vesicle by a lipid membrane. It indicates that there exist several wrapping phases, such as full wrapping, partial wrapping, and no wrapping states. Shi *et al.* [100] further explored the pulling of a vesicle deposited on a curved substrate, and gave the relation between the external force and the displacement of the vesicle for different substrate shapes and interaction potentials. All these related works deal with the transversality boundary conditions at the adhesion edge.

In addition, recent report indicates that when cells are adhered to a substrate with a non-uniform rigidity, they will move directionally and congregate at the area where the rigidity is higher [101, 102], and this phenomenon is different from a droplet on a substrate with gradient rigidity [103]. Understanding the mechanism of the cell-substrate adhesion is beneficial to understanding the phenomenon of cell migration, embryonic development, wound healing and immune response. Zhou *et al.* [104] studied a cell or a vesicle adhered to an elastic and smooth substrate, i.e. a slender beam in two dimensions, as schematized in Figure 1.12. Due to the strong adhesion ability of the vesicle, part of the substrate will stick to the vesicle. The adhered portions of the two elastic bodies deform conformally and the un-adhered segment of the vesicle experiences large deformation. The total length of the vesicle is designated as L_0 , the non-adhesion length of the vesicle is a , and the angle at the point $s = a$ is termed as Φ_0 . The bending stiffnesses of the vesicle and the substrate are respectively denoted as κ_1 and κ_2 . They constructed the total free energy functional of vesicle-substrate system as follows:

$$\begin{aligned} \Pi = & \int_0^a \frac{1}{2} \kappa_1 (\dot{\phi} - c_0)^2 ds + \int_a^{L_0/2} \frac{1}{2} (\kappa_1 + \kappa_2) \dot{\phi}^2 ds - W \left(\frac{L_0}{2} - a \right) \\ & + \int_0^{L_0/2} \left[\lambda_1 x \sin \phi + \lambda_2 (\dot{x} - \cos \phi) \right] ds. \end{aligned} \quad (1.50)$$

In using the variation principle with movable boundary conditions, one can derive the transversality condition as

$$w = \frac{WL_0^2}{4\pi^2\kappa_1} = \phi'_{01} (\phi'_{01} - C_0) - \frac{2+\mu}{2(1+\mu)} (\phi'_{01} - C_0)^2. \quad (1.51)$$

When $\kappa_2 \rightarrow \infty$ and $C_0 = 0$, Eq. (1.51) reduces to the situation of a vesicle sitting on a rigid substrate, i.e. $\phi'^2_{01} = 2w$, and this solution is consistent with the former results [61]. In succession, they presented the morphology of the vesicle-substrate system and the phase diagram, and then pointed out that there exist different wrapping states depending on the work of adhesion and bending stiffness. They further investigated the adhesion behavior of a vesicle to a rigid substrate. These analyses are helpful to understand the mechanism of cell motility and provide a new outlook on the droplet wrapped by a membrane when the voltage is inputted.

1.7 Summary and Prospects

In this review article, we mainly concentrated on the recent work about adhesion of condensed bodies, spanning from droplets, microbeams, CNTs to cells. We first introduced the

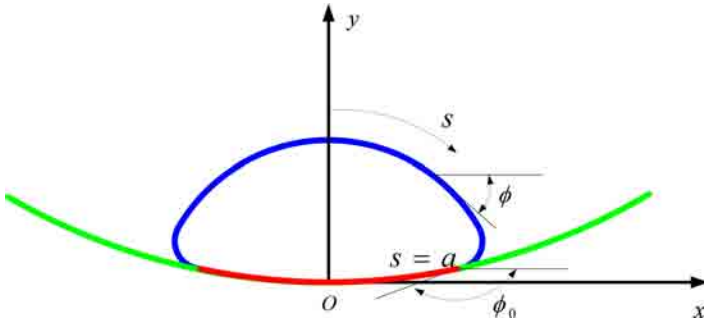


Figure 1.12 Schematic of a vesicle adhered to an elastic substrate, with the deformations of the vesicle and the interfacial segment of the substrate.

concept of unified analysis framework for the adhesion of an elastic system with movable boundaries. According to the principle of least potential energy and variational theory, we derived the governing equation, i.e. the Euler-Poisson equation, and the transversality condition at the movable boundary. The transversality condition actually represents the competition between elastic energy and interfacial energy at the critical point. This approach can be validated by the concept of energy release rate in fracture mechanics.

It is pointed out that the adhesion of microbeams, droplets, CNTs and cells can be grouped into this framework, and the developed method can be used to examine the adhesion behaviors of these systems. The detachment length and deflection of the beam, the Young's equation and morphology of the droplet, the adhesion configuration of a CNT, and the energy landscape of cell adhesion can all be acquired considering the transversality conditions. In fact, the different adhesion models presented previously can be formulated by the same governing equation and transversality condition after coordinate translation and scale transformation, and the physical parameters have correspondence relationships [105, 106]. Consequently, these conclusions would give insight into designing some analogous experiments or numerical simulation methods among different systems, such as the slender structures and droplets. These analyses open a new avenue for exploring the mechanism of different systems with similarities and the unity of nature in depth. The obtained results are beneficial to the design of nano-structured materials, and pave a new way to enhance their mechanical, chemical, optical and electronic properties.

Acknowledgements

The project was supported by the National Natural Science Foundation of China (11272357, 11320003 and 11102140), the Doctoral Fund of the Ministry of Education of China (Grant No. 20110141120024), the Opening Project of the State Key Laboratory of Nonlinear Mechanics in Chinese Academy of Sciences (LNM201319), and the Scientific Research Foundation for the Returned Overseas Chinese Scholars, State Education Ministry.

References

1. J.L. Liu and X.Q. Feng, On elastocapillarity: A review. *Acta. Mech. Sinica.* 28, 928–940 (2012).
2. A.K. Geim, S.V. Dubonos, I.V. Grigorieva, K.S. Novoselov, A.A. Zhukov and S.Yu. Shapoval, Microfabricated adhesive mimicking gecko foot-hair. *Nature Mater.* 2, 461–463 (2003).
3. H.J. Gao, X. Wang, H.M. Yao, S. Gorb and E. Arzt, Mechanics of hierarchical adhesion structures of geckos. *Mech. Mater.* 37, 275–285 (2005).
4. C. Neinhuis and W. Barthlott, Characterization and distribution of water-repellent, self-cleaning plant surfaces. *Annals Botany* 79, 667–677 (1997).
5. W. Barthlott and C. Neinhuis, Purity of the sacred lotus, or escape from contamination in biological surfaces. *Planta* 202, 1–8 (1997).
6. A. Otten and S. Herminghaus, How plants keep dry: A physicist's point of view. *Langmuir* 20, 2405–2408 (2004).

7. D.L. Hu, B. Chan and J.W. Bush, The hydrodynamics of water strider locomotion. *Nature* 424, 663–666 (2003).
8. J.L. Liu, X.Q. Feng and G.F. Wang, Buoyant force and sinking condition of a hydrophobic thin rod floating on water. *Phys. Rev. E* 76, 066103 (2007).
9. F. Shi, J. Niu, J.L. Liu, F. Liu, Z.Q. Wang, X.Q. Feng and X. Zhang, Towards understanding why a superhydrophobic coating is needed by water striders. *Adv. Mater.* 19, 2257–2261 (2007).
10. C.W. Wu, X.Q. Kong and D. Wu, Microstructures of the scales on a mosquito's legs and their role in weight support. *Phys. Rev. E* 76, 017301 (2007).
11. N.J. Mlot, C.A. Tovey and D.L. Hu, Fire ants self-assemble into waterproof rafts to survive floods. *Proc. Natl Acad. Sci. USA* 108, 76697673 (2011).
12. A.R. Parker and C.R. Lawrence, Water capture by a desert beetle. *Nature* 414, 33–34 (2001).
13. A. Carré and K.L. Mittal (Eds.) *Superhydrophobic Surfaces*, CRC Press, Boca Raton, FL (2009).
14. L. Zhai, F.C. Cebeci, R.E. Cohen and M.F. Rubner, Stable superhydrophobic coatings from polyelectrolyte multilayers. *Nano. Lett.* 4, 1349–1353 (2004).
15. E. Hosono, S. Fujihara, I. Honma and H. Zhou, Superhydrophobic perpendicular nanopin film by the bottom-up process. *J. Am. Chem. Soc.* 127, 13458–13459 (2005).
16. T. Onda, S. Shibuichi, N. Satoh and K. Tsujii, Super-water-repellent fractal surfaces. *Langmuir* 12, 2125–2127 (1996).
17. H.E. Jeong, S.H. Lee, J.K. Kim and K.Y. Suh, Nanoengineered multiscale hierarchical structures with tailored wetting properties. *Langmuir* 22, 1640–1645 (2006).
18. S. Shibuichi, T. Onda, N. Satoh and K. Tsujii, Super water-repellent surfaces resulting from fractal structure. *J. Phys. Chem.* 100, 19512–19517 (1996).
19. E. Bormashenko and G. Whyman, Variational approach to wetting problems: Calculation of a shape of sessile liquid drop deposited on a solid substrate in external field. *Chem Phys Lett* 463, 103–105 (2008).
20. A. Marmur, Contact angles in constrained wetting. *Langmuir* 12, 5704–5708 (1996).
21. P.S. Swain and R. Lipowsky, Contact angles on heterogeneous surfaces: A new look at Cassie's and Wenzel's laws. *Langmuir* 14, 6772–6780 (1998).
22. C.Y. Hui, A. Jagota, Y.Y. Lin and E.J. Kramer, Constraints on microcontact printing imposed by stamp deformation. *Langmuir* 18, 1394–1407 (2002).
23. J.A. Williams and H.R. Le, Tribology and MEMS. *J. Phys. D-Appl. Phys.* 39, R201 (2006).
24. M.P. de Boer and T.A. Michalske, Accurate method for determining adhesion of cantilever beams. *J. Appl. Phys.* 86, 817–827 (1999).
25. S.H. Kim, M.T. Dugger and K.L. Mittal (Eds.) *Adhesion Aspects in MEMS/NEMS*, CRC Press, Boca Raton, FL (2011).
26. C.H. Mastrangelo and C.H. Hsu, Mechanical stability and adhesion of microstructures under capillary forces. I. Basic theory. *J. Microelectromech. Syst.* 2, 33–43 (1993).
27. C.H. Mastrangelo and C.H. Hsu, Mechanical stability and adhesion of microstructures under capillary forces. II. Experiments. *J. Microelectromech. Syst.* 2, 44–55 (1993).
28. Y.P. Zhao, L.S. Wang and T.X. Yu, Mechanics of adhesion in MEMS—A review. *J. Adhesion Sci. Technol.* 17, 519–546 (2003).
29. R.H. Baughman, A.A. Zakhidov and W.A. de Heer, Carbon nanotubes: The route toward applications. *Science* 297, 787–792 (2002).
30. M. Zheng and C.H. Ke, Mechanical deformation of carbon nanotube nano-rings on flat substrate. *J. Appl. Phys.* 109, 074304 (2011).

31. D.K. Fygenson, J.F. Marko and A. Libchaber, Mechanics of microtubule-based membrane extension. *Phys. Rev. Lett.* 79, 4497–4500 (1997).
32. A.E. Cohen and L. Mahadevan, Kinks, rings, and rackets in filamentous structures. *Proc. Natl Acad. Sci. USA* 100, 12141–12146 (2003).
33. H.S. Lee, C.H. Yun, H.M. Kim and C.J. Lee, Persistence length of multiwalled carbon nanotubes with static bending. *J. Phys. Chem. C* 111, 18882–18887 (2007).
34. L.X. Zheng, M.J. O'Connell, S.K. Doorn, X.Z. Liao, Y.H. Zhao, E.A. Akhador, M.A. Hoffbauer, B.J. Roop, Q.X. Jia, R.C. Dye, D.E. Peterson, S.M. Huang, J. Liu and Y.T. Zhu, Ultralong single-wall carbon nanotubes. *Nature Mater.* 3, 673–676 (2004).
35. M.J. Buehler, Y. Kong and H.J. Gao, Deformation mechanisms of very long single-wall carbon nanotubes subject to compressive loading. *J. Eng. Mater. Technol.* 126, 245–249 (2004).
36. R.S. Ruoff, J. Tersoff, D.C. Lorents, S. Subramoney and B. Chan, Radial deformation of carbon nanotubes by van der Waals forces. *Nature* 364, 514–516 (1993).
37. N.G. Chopra, L.X. Benedict, V.H. Crespi, M.L. Cohen, S.G. Louie and A. Zettl, Fully collapsed carbon nanotubes. *Nature* 377, 135–138 (1995).
38. R. Martel, T. Schmidt, H.R. Shea, T. Hertel and Ph. Avouris, Single- and multi-wall carbon nanotube field-effect transistors. *Appl. Phys. Lett.* 73, 2447–2449 (1998).
39. M.F. Yu, M.J. Dyer, J. Chen, D. Qian, W.K. Liu and R.S. Ruoff, Locked twist in multiwalled carbon-nanotube ribbons. *Phys. Rev. B* 64, 241403 (2001).
40. M.F. Yu, T. Kowalewski and R.S. Ruoff, Investigation of the radial deformability of individual carbon nanotubes under controlled indentation force. *Phys. Rev. Lett.* 85, 1456–1459 (2000).
41. E.W. Wong, P.E. Sheehan and C.M. Lieber, Nanobeam mechanics: Elasticity, strength, and toughness of nanorods and nanotubes. *Science* 277, 1971–1975 (1997).
42. C.Q. Ru, Effect of van der Waals forces on axial buckling of a double-wall carbon nanotube. *J. Appl. Phys.* 87, 7227–7231 (2000).
43. C.Q. Ru, Elastic buckling of singlewalled carbon nanotube ropes under high pressure. *Phys. Rev. B* 62, 10405–10408 (2000).
44. C.Y. Wang, C.Q. Ru and A. Mioduchowski, Elastic buckling of multiwall carbon nanotubes under high pressure. *J. Nanosci. Nanotechnol.* 3, 199–208 (2003).
45. B.I. Yakobson, C.J. Brabec and J. Bernholc, Nanomechanics of carbon tubes: Instabilities beyond linear response. *Phys. Rev. Lett.* 76, 2511–2514 (1996).
46. B.M. Gumbiner, Cell adhesion: The molecular basis of tissue architecture and morphogenesis. *Cell* 84 345–357 (1996).
47. B. Alberts, A. Johnson, J. Lewis, M. Raff, K. Roberts and P. Walter, *Molecular Biology of the Cell*, 4th ed., Garland Science, New York (2002).
48. I. Joris, T. Zand, J.J. Nunnari, F.J. Krolikowski and G. Majno, Studies on the pathogenesis of atherosclerosis. I. Adhesion and emigration of mononuclear cells in the aorta of hypercholesterolemic rats. *Am. J. Pathol.* 113, 341–358 (1983).
49. N. Singh, Y. Talalayeva, M. Tsiper, V. Romanov, A. Dranovsky, D. Colflesh, G. Rudamen, M. P. Vitek, J. Shen, X. Yang, D. Goldgaber and A. L. Schwarzman, The role of Alzheimer's disease-related presenilin 1 in intercellular adhesion. *Expl. Cell. Res.* 263, 1–13 (2001).
50. K. Hosokawa, F. Arai, H. Yoshihara, H. Iwasaki, M. Hembree, T. Yin, Y. Nakamura, Y. Gomei, K. Takubo, H. Shima, S. Matsuoka, L. Li and T. Suda, Cadherin-based adhesion is a potential target for niche manipulation to protect hematopoietic stem cells in adult bone marrow. *Cell. Stem. Cell.* 6, 194–198 (2010).

51. Y. Geng, P. Dalhaimer, S. Cai, T. Richard, T. Manorama, M. Tamara and D.E. Discher, Shape effects of filaments versus spherical particles in flow and drug delivery. *Nature Nanotechnol.* 2, 249–255 (2007).
52. E. Sackmann, Supported membranes: Scientific and practical applications. *Science* 271, 43–48 (1996).
53. P.S. Swain and D. Andelman, Supported membranes on chemically structured and rough surfaces. *Phys. Rev. E* 63, 051911 (2001).
54. A.J. Engler, S. Sen, H.L. Sweeney and D.E. Discher, Matrix elasticity directs stem cell lineage specification. *Cell* 126, 677–689 (2006).
55. A. Carré and K.L. Mittal (Eds.) *Surface and Interfacial Aspects of Cell Adhesion*, CRC Press, Boca Raton, FL (2011).
56. K.L. Johnson, K. Kendall and A.D. Roberts, Surface energy and the contact of elastic solids. *Proc. Roy. Soc. London A* 324, 301–313 (1971).
57. B. Roman and J. Bico, Elasto-capillarity: Deforming an elastic structure with a liquid droplet. *J. Phys-Condens Matter.* 22, 493101 (2010).
58. J.R. Rice, A path independent integral and the approximate analysis of strain concentration by notches and cracks. *J. Appl. Mech.* 35, 379–386 (1968).
59. T. Tang, A. Jagota and C.Y. Hui, Adhesion between single-walled carbon nanotubes. *J. Appl. Phys.* 97, 074304 (2005).
60. W. Zhou, Y. Huang, B. Liu and K.C. Kwang, Self-folding of single- and multiwall carbon nanotubes. *Appl. Phys. Lett.* 90, 073107 (2007).
61. J.L. Liu and R. Xia, A unified analysis of a micro-beam, droplet and CNT ring adhered on a substrate: Calculation of variation with movable boundaries. *Acta. Mech. Sinica.* 29, 62–72 (2013).
62. U. Seifert, Adhesion of vesicles in two dimensions. *Phys. Rev. A* 43, 6803–6814 (1991).
63. R. Courant and D. Hilbert, *Methods of Mathematical Physics*, Interscience, New York (1953).
64. J.L. Liu, R. Xia and Y.T. Zhou, Stiction of a nano-beam with surface effect. *Chinese Phys. Lett.* 28, 116201 (2011).
65. Y. Zhang and Y.P. Zhao, Adhesive contact of nanowire in three-point bending test. *J. Adhesion. Sci. Technol.* 25, 1107–1129 (2011).
66. Y. Zhang and Y.P. Zhao, A precise model for the shape of an adhered microcantilever. *Sensors Actuators. A* 171, 381–390 (2011).
67. J. Bico, B. Roman, L. Moulin and A. Boudaoud, Adhesion: Elastocapillary coalescence in wet hair. *Nature* 432, 690 (2004).
68. H.Y. Kim and L. Mahadevan, Capillary rise between elastic sheets. *J. Fluid. Mech.* 548, 141–150 (2006).
69. J.L. Liu, X.Q. Feng, R. Xia and H.P. Zhao, Hierarchical capillary adhesion of microcantilevers or hairs. *J. Phys. D-Appl. Phys.* 40, 5564–5570 (2007).
70. C. Journet, S. Moulinet, C. Ybert, S.T. Purcell and L. Bocquet, Contact angle measurements on superhydrophobic carbon nanotube forest: Effect of fluid pressure. *Europhys. Lett.* 71, 104–109 (2005).
71. J.L. Liu and X.Q. Feng, Capillary adhesion of micro-beams: Finite deformation analyses. *Chinese Phys. Lett.* 24, 2349–2352 (2007).
72. K.E. Bisshopp and D.C. Drucker, Large deflection of cantilever beams. *Q Appl. Math.* 3, 272–275 (1945).
73. J.L. Liu, Theoretical analysis on capillary adhesion of microsized plates with a substrate. *Acta Mech. Sinica.* 26, 217–223 (2010).

74. E. Bormashenko, Young, Boruvka-Neumann, Wenzel and Cassie-Baxter equations as the transversality conditions for the variational problem of wetting. *Colloids Surfaces A* 345, 163–165 (2009).
75. R.N. Wenzel, Resistance of solid surfaces to wetting by water. *Ind. Eng. Chem.* 28, 988–994 (1936).
76. A.B.D. Cassie and S. Baxter, Wettability of porous surfaces. *Trans. Faraday Soc.* 40, 546–551 (1944).
77. J.L. Liu, R. Xia and X.H. Zhou, A new look on wetting models: Continuum analysis. *Sci. China Phys. Mech.* 55, 2158–2166 (2012).
78. J.L., Liu, Y. Mei and R. Xia, A new wetting mechanism based upon triple contact line pinning. *Langmuir* 27, 196–200 (2011).
79. X.F. Wu and Y.A. Dzenis, Droplet on a fiber: Geometrical shape and contact angle. *Acta. Mech.* 185, 215–225 (2006).
80. J.L. Liu and J.H. Lee, Self-folding of a slender microbeam and thin film: An elastica model. *J. Mech. Mater. Struct.* 8, 169–183 (2013)
81. C. Majidi, Remarks on formulating an adhesion problem using Euler's elastica. *Mech. Res. Commu.* 34, 85–90 (2007)
82. M.J. Buehler, Y. Kong, H.J. Gao and Y. Huang, Self-folding and unfolding of carbon nanotubes. *J. Eng. Mater. Technol.* 128, 3–10 (2006).
83. W. Zhou, Y. Huang, B. Liu, K.C. Hwang, J.M. Zuo, M.J. Buehler and H.J. Gao, Self-folding of single- and multiwall carbon nanotubes. *Appl. Phys. Lett.* 90, 073107 (2007).
84. Y. Mikata, Approximate solutions for a self-folding problem of carbon nanotubes. *J. Eng. Mater. Technol.* 132, 011013 (2010).
85. N.J. Glassmaker and C.Y. Hui, Elastica solution for a nanotube formed by self-adhesion of a folded thin film. *J. Appl. Phys.* 96, 3429–3434 (2004).
86. S. Cranford, D. Sen and M.J. Buehler, Meso-origami: Folding multilayer graphene sheets. *Appl. Phys. Lett.* 95, 123121 (2009)
87. B. Liu, M.F. Yu and Y. Huang, Role of lattice registry in the full collapse and twist formation of carbon nanotubes. *Phys. Rev. B* 70, 161402 (2004).
88. J. Xiao, B. Liu, Y. Huang, J. Zuo, K.C. Hwang and M.F. Yu, Collapse and stability of single- and multi-wall carbon nanotubes. *Nanotechnology* 18, 395703 (2007).
89. J.L. Liu, Explicit solutions for a SWCNT collapse. *Archives Appl. Mech.* 82, 767–776 (2012).
90. C. Zhang, L. Chen and S.H. Chen, Adhesion between two radially collapsed single-walled carbon nanotubes. *Acta. Mech.* 224, 2759–2770 (2013).
91. U. Seifert, Adhesion of vesicles in two dimensions. *Phys. Rev. A* 43, 6803–6814 (1991).
92. X. Oyharcabal and T. Frisch, Peeling off an elastica from a smooth attractive substrate. *Phys. Rev. E* 71, 036611 (2005)
93. Y.J. Yin, J. Yin and D. Ni, General mathematical frame for open or closed biomembranes (Part I): Equilibrium theory and geometrically constraint equation. *J. Math. Biol.* 51, 403–413 (2005).
94. Y.J. Yin, Y.Q. Chen, D. Ni, H.J. Shi and Q.S. Fan, Shape equations and curvature bifurcations induced by inhomogeneous rigidities in cell membranes. *J. Biomech.* 38, 1433–1440 (2005).
95. C. Lv, Y. Yin and J. Yin, Geometric theory for adhering lipid vesicles. *Colloids Surfaces B* 74, 380–388 (2009).
96. M. Deserno, M.M. Müller and J. Guven, Contact lines for fluid surface adhesion. *Phys. Rev. E* 76, 011605 (2007).

97. S. Das and Q. Du, Adhesion of vesicles to curved substrates. *Phys. Rev. E* 77, 011907 (2008).
98. J. Zhang, S. Das and Q. Du, A phase field model for vesicle-substrate adhesion. *J. Comput. Phys.* 228, 7837–7849 (2009).
99. X. Yi, X.H. Shi and H.J. Gao, Cellular uptake of elastic nanoparticles. *Phys. Rev. Lett.* 107, 098101 (2011).
100. W. Shi, X. Q. Feng and H.J. Gao, Two-dimensional model of vesicle adhesion on curved substrates. *Acta. Mech. Sinica.* 22, 529–535 (2006).
101. C.M. Lo, H.B. Wang, M. Dembo and Y.L. Wang, Cell movement is guided by the rigidity of the substrate. *Biophys. J.* 79, 144–152 (2000).
102. T. Yeung, P.C. Georges, L.A. Flanagan, B. Marg, M. Ortiz, M. Funaki, N. Zahir, W. Ming, V. Weaver and P.A. Janmey, Effects of substrate stiffness on cell morphology, cytoskeletal structure, and adhesion. *Cell. Motility Cytoskel.* 60, 24–34 (2005).
103. X.P. Zheng, H.P. Zhao, L.T. Gao, J.L. Liu, S.W. Yu and X.Q. Feng, Elasticity-driven droplet movement on a microbeam with gradient stiffness: A biomimetic self-propelling mechanism. *J. Colloid Interface Sci.* 323, 133–140 (2008).
104. X.H. Zhou, J.L. Liu and S.L. Zhang, Adhesion of a vesicle on an elastic substrate: 2D analysis. *Colloids Surfaces B* 110, 372–378 (2013).
105. N.M. Pugno, An analogy between the adhesion of liquid drops and single-walled nanotubes. *Scripta. Mater.* 58, 73–75 (2008).
106. J.L. Liu, Analogies between a meniscus and a cantilever. *Chinese Phys. Lett.* 26, 116803 (2009).

Imparting Adhesion Property to Silicone Materials: Challenges and Solutions

R. Kalinova^{1,2}, R. Mincheva² and Ph. Dubois^{2,*}

¹*Institute of Polymers, Bulgarian Academy of Sciences, Acad. Sofia, Bulgaria*

²*Laboratory of Polymeric and Composite Materials (LPCM), Center of Innovation and Research in Materials and Polymers (CIRMAP), University of Mons (UMONS), Mons, Belgium*

Abstract

This review summarizes the techniques used in imparting adhesion property to poly(dimethylsiloxane) (PDMS) surfaces. It is well known that the adhesion is strongly dependent on the surface free energy of the substrate, which can be controlled by tuning its hydrophobic/hydrophilic properties. PDMS has very low surface free energy and it can be of interest to alter its surface chemistry by transforming it from hydrophobic to hydrophilic. For this reason, different methods have been developed to introduce functional groups on the PDMS surface. They can reasonably be classified into three main categories: (1) physical approaches, such as plasma/corona discharge treatments, UV-ozone exposure, laser treatments, physical adsorption, (2) wet chemical approaches including layer by layer (LbL) deposition, sol-gel coating, some other wet chemical treatments, and (3) combinations of physical and chemical methods including covalent surface grafting and incorporation of amphiphilic block copolymers.

Keywords: Poly(dimethylsiloxane) (PDMS), surface modification, physical treatment, wet chemical treatment, hydrophilicity, adhesion

*Corresponding author: philippe.dubois@umons.ac.be

2.1 Introduction

As it can be easily structured or patterned, commercially available and non-expensive, poly(dimethylsiloxane) (PDMS) elastomer is one of the most suitable polymers for many conventional and advanced technologies. It is widely used in preparation of microfluidic devices [1–4] such as channels, valves, diaphragms and biosensors because of its elasticity, transparency and biocompatibility. Its good mechanical properties, high gas permeability, low toxicity, exceptionally low reactivity and long-term durability in the presence of aqueous solutions make PDMS attractive for biomaterials applications [5–12]. PDMS has also other advantages as excellent flexibility, bio-inertness [13, 14], and high thermal and oxidative stability [15, 16]. However, in spite of all these advantages one of the major drawbacks is that PDMS is naturally hydrophobic with water contact angle of $\sim 109^\circ$. For variety of applications the hydrophobic nature is disadvantageous and requires surface modification in order to improve the PDMS wettability and adhesion property. This can be achieved with increasing the surface free energy of PDMS by introducing reactive functional groups into the polymer surface. Different approaches have been used to alter the surface chemistry of PDMS. After such treatments the polymer retains its bulk properties and the resulted modified surfaces show enhanced wettability. This is a fundamental (but not sufficient) requirement for improving the adhesion ability of PDMS [17, 18].

In the last two decades, several reviews have been published describing the surface modifications of PDMS and their applications. Zhou and coworkers [1, 2], Makamba *et al.* [19] and Wong and Ho [20] focused on the progresses made in PDMS surface modification for microfluidic devices. The strategies applied for modifying the surface of PDMS polymers to enhance their biocompatibility and clinical performance have been reviewed by Abbasi *et al.* [5].

This review mainly focuses on the developments of surface modification methods used to improve PDMS surface adhesion property. These methods are divided into three main categories: physical, chemical and combination of both. Physical techniques include plasma, corona, UV-ozone, laser treatment and physical adsorption. The wet chemical methods include LbL deposition, sol-gel coating and some other wet chemical treatments. Finally, the third category - combinations of physical and chemical methods including covalent surface grafting and incorporation of amphiphilic block copolymers will be discussed. Advantages and disadvantages of each of these surface modification methods are also presented.

2.2 Cured PDMS

2.2.1 Curing Reactions

Poly(dimethylsiloxane)s are liquid at room temperature and their transformation into elastomeric materials proceeds via cross-linking reactions, i.e., formation of chemical bonds between adjacent chains. The three-dimensional networks can be obtained via a wide variety of methods but the most typical routes are: free-radical reaction (normally performed at high temperatures), condensation reaction (moisture-triggered curing) or addition reaction (hydrosilylation curing).

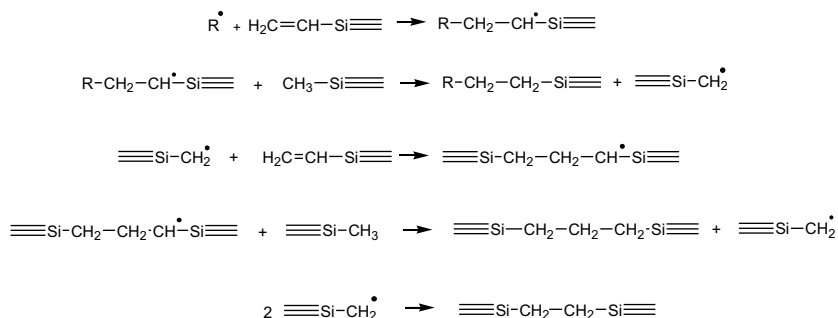


Figure 2.1 Free-radical reactions taking place in cross-linking of vinyl-functionalized PDMS. Reproduced from Ref. [21] with permission from Elsevier.

2.2.1.1 Free-Radical Curing

The reaction requires a high temperature for activation of the free-radical precursor, followed by homolytic bond cleavage. The resulting radical-containing components transfer their free-radicals to the silicone polymer bearing either alkyl or vinyl functionalities. Cross-linking occurs as the free-radicals of one polymer chain react and bond with alkyl/vinyl species of another polymer chain (Figure 2.1).

Organic peroxides (for example, benzoyl or dicumyl peroxide) are very often used as free-radical precursors due to their convenience and availability. They are relatively inert at room temperature but rapidly decompose (within a few minutes) at temperatures between 90 and 180 °C. However, peroxide curing has some drawbacks. The peroxides can attack molecules that are not part of the polymer, such as atmospheric O₂ thus reducing the quantity of active free-radicals and grafting undesired molecules to the polysiloxane backbone. Free-radical precursors are also sensitive to acidic conditions and tend to decompose into ionic species. Another drawback is the presence of residues in the cured elastomer, including acid by-products and polychlorinated biphenyls (PCBs), which are highly toxic and can act also as depolymerization catalysts at higher temperature. Therefore, rubbers obtained by this free-radical reaction pathway often require a post-curing treatment at temperature as high as 200 °C for several hours. All these drawbacks largely limit the nature of additives usable in silicone resins cured in this way.

2.2.1.2 Condensation Curing

Condensation curing occurs between hydroxy, alkoxy or acetoxy groups [22] in presence of tin or titanium catalysts, accompanied respectively with release of water, alcohol or acetic acid as by-products and formation of Si-O-Si or Si-O-C bonds. The condensation-curing silicones are formulated as one- or two-part products. Typical two-component systems are formulated from a first part (Part A) containing the silanol-terminated PDMS and a second one (Part B) composed of the cross-linker and catalyst (dialkyltin, tin (II or IV) dialkanoates or zinc

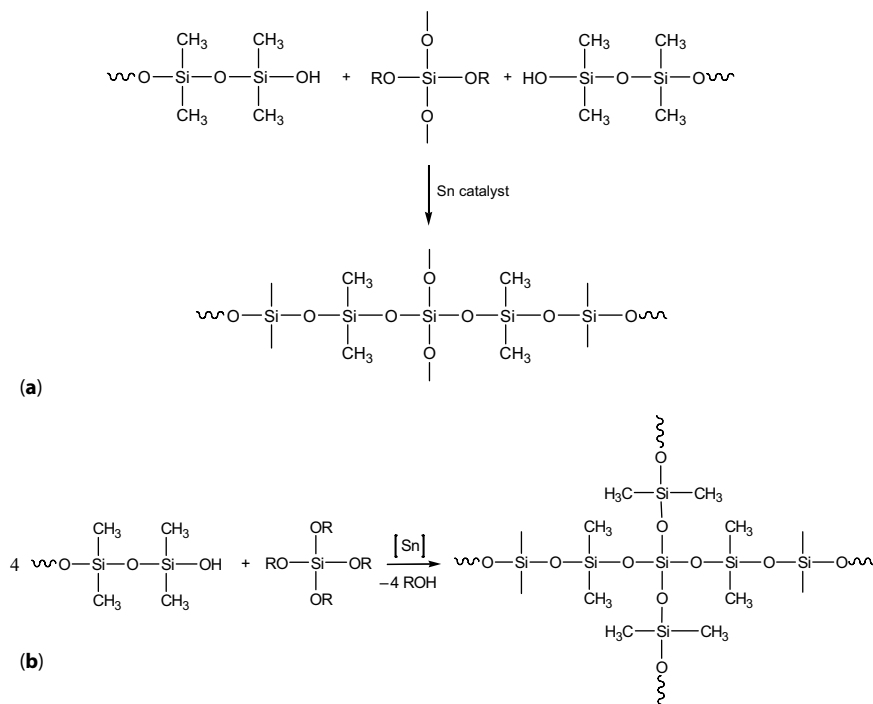


Figure 2.2 Condensation curing with multi-functional polysiloxane (a) and low molecular weight compounds (b), where R = Alkyl. Adapted from Ref. [23] with permission from Elsevier.

alkanoates). Thus, cross-linking starts after mixing the two parts (Figure 2.2 a,b). Reinforcing fillers and other additives may be added to Part A depending on the targeted application.

The curing process is fast and proceeds at low temperature while by-products are released. As a result, lightly cross-linked silicone films can be prepared, which are capable of dissipating normal and shear stresses at high temperatures (as in release coating applications), or are tough and flexible silicone elastomers which retain their elastic properties over a wide temperature range. The incorporation of reinforcing fillers such as fumed silica or calcium oxide improves the mechanical properties of the elastomers and affects the flow properties of the system. Introduction of a multifunctional cross-linker produces a three-dimensional network. Tri- and tetrafunctional low molecular weight compounds, such as trialkoxysilanes ($\text{R}'\text{Si}(\text{OR}')_3$), and tetraalkoxysilanes such as tetrapropoxysilane ($\text{Si}(\text{OPr})_4$) (Figure 2.2b) and multi-functional polysiloxane chains as poly(diethoxysiloxane) (Figure 2.2a) are usually used as cross-linking agents. These cross-linkers then condense with the silanol (SiOH)-terminated PDMS polymer producing a cross-linked network with release of the corresponding alcohol. The disadvantage of this kind of curing process is the formation of small by-product molecules which are released during condensation and can lead to some shrinkage of the film.

2.2.1.3 Hydrosilylation (Addition) Curing

Addition curing, known as hydrosilylation, is the third way for cross-linking of polysiloxanes. The reaction consists in formation of a new Si-C bond by addition of a hydrosilyl group ($\equiv\text{Si-H}$) to an unsaturated carbon-carbon bond in the presence of a transition metal-based catalyst (Figure 2.3). Usually the cross-linking occurs between silicone polymers with a vinyl or other alkenyl functionality and cross-linking functional oligomers as tetrakisdimethylsiloxysilane or tetravinyl tetramethylcyclotetrasiloxane. The position and concentration of both vinyl and hydrosilyl groups along the polysiloxane backbone govern the nature of the elastomeric network.

The reaction is catalyzed by complexes of platinum such as Speier ($\text{H}_2\text{Pt(IV)Cl}_6$) and Karstedt ($\text{Pt}_2(0)\{[(\text{CH}_2=\text{CH})\text{Me}_2\text{Si}_2\text{O}]_3\}$) catalysts. A three-step mechanism proposed by Chalk and Harrod [24] (Figure 2.4) consists of the oxidative addition of the Si-H on the Pt catalyst (oxidation state from II to IV), H transfer in the β -position of the carbon-carbon double bond, and reductive elimination of the product.

Elastomers featuring this type of curing system are supplied as two-part kits: one part (Part A) contains the vinyl-end capped PDMS, platinum catalyst, inhibitor, and the other part (Part B) contains the cross-linker. The cross-linking reaction starts after mixing of these two parts. This reaction is exothermic in nature, occurs even at room temperature and is reported to take place very rapidly. Some Pt-catalyzed samples have been observed to cure completely in less than 30 seconds. For slowing down the curing reaction, inhibitors (typically 3,5-dimethyl-1-hexyn-3-ol or acetylenic alcohols) are often added. The hydrosilylation reaction can also be slowed down by using rhodium-based catalysts, which are approximately five-to-ten times less reactive than Pt derivatives.

Compared to peroxide-cured silicone rubber, curing by hydrosilylation is less toxic due to the lower amount of cross-linker required. Compared to the condensation curing, hydrosilylation reaction does not produce any by-products, which usually eliminates the need for post-curing reactions. It gives well-cured elastomers with stoichiometric proportion of reagents making it one of the cleanest cross-linking methods. Some drawbacks of

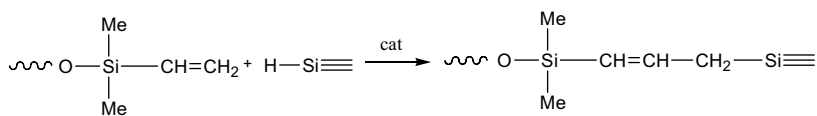


Figure 2.3 Hydrosilylation curing. Reproduced from Ref. [21] with permission from Elsevier.

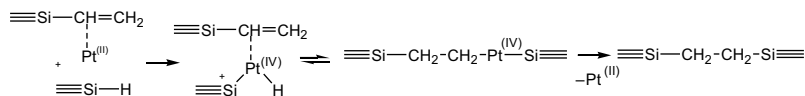


Figure 2.4 Reaction mechanism proposed for hydrosilylation. Adapted from Ref. [21] with permission from Elsevier.

the method are related to the use of catalysts. First, platinum catalysts are easily bonded to electron-donating substances like nitrogen (N-H are particularly detrimental), tin or sulfur-containing compounds to form stable complexes, these inhibiting the catalyst action. Secondly, due to their poor efficiency in basic environments the curing reaction may require some pH adjustment.

2.2.2 Surface Properties

The unique surface properties of cross-linked poly(dimethylsiloxane) (PDMS) are attributed to the backbone flexibility and mobility of silicone polymer chains. The flexibility of the chains can result in two potential conformations by exposing either methyl groups or the oxygen atoms at the surface (Figure 2.5). In air the apolar and hydrophobic methyl groups are pointing outwards and cover the surface of PDMS, which is the reason for its low surface energy (Figure 2.5a). In contact with water, because the chains are very flexible and mobile, they can potentially restructure to expose the polar oxygen groups at the PDMS/water interface, as shown in Figure 2.5b.

The restructuring of a PDMS surface in contact with water has been demonstrated by Chen *et al.* using Sum Frequency Generation (SFG) vibrational spectroscopy [25]. The results revealed that when PDMS chains come in contact with water, their methyl groups tilt more towards the silicone surface due to unfavorable interactions with water molecules. In 2005 Carlos *et al.* [26] and in 2009 Beigbeder *et al.* [27] reported decrease of contact angle of silicone coatings after immersion in water. They suggested that the increase of wettability after immersion in water was a consequence of the reorganization of the side chain and silicone backbone components. Due to the polar aqueous environment, the chains adapt their conformation in order to minimize energy. This type of molecular reorganization proved to be reversible.

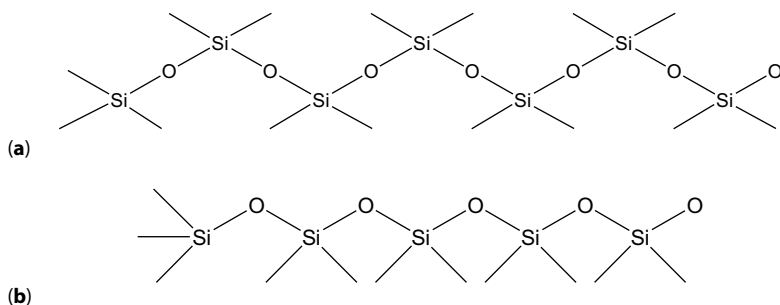


Figure 2.5 Schematic representations showing the two possible orientations of PDMS chains in air (a) and in water (b).

2.2.3 Adhesion Property

The main reasons for the low adhesion property of PDMS are its low surface free energy (γ_{sv} of 19.9 mJ/m²) [28], the lack of reactive surface groups leading to extremely low chemical reactivity, and the relatively high amount of low-molecular-weight (LMW) components having high mobility in the polymer bulk and a high tendency to migrate from bulk to the PDMS surface [17]. Silicone elastomers have also inherently low values of glass transition temperature (T_g) and elastic modulus. These properties make PDMS suitable for use in different advanced technologies as preparation of “fouling release” coatings [29–31] where adhesion is not desirable. However, in other applications as coatings, sealings, screen printings, and composites, requiring adhesion to a solid substrate its use evokes a high risk of adhesion failure [17]. This can be overcome with increasing the surface free energy of PDMS by introducing reactive functional groups into the polymer surface. Different techniques have been developed for silicone surface modification and they are discussed in the next section.

2.3 Methods for Cross-Linked PDMS Surface Modification

2.3.1 Physical Techniques

The physical techniques include flame treatment, corona treatment, cold plasma treatment, ultraviolet-ozone (UV/O₃) treatment, laser treatment, X-ray and γ -ray treatments, electron beam treatment, ion-beam treatment, etc. Among these, plasma, corona, UV/O₃ and laser treatments are most commonly used and will be discussed here.

2.3.1.1 Plasma Treatment

Conventional plasma treatment involves exposing of the substrate to a glow discharge between two electrodes or to a radio or microwave frequency generator at low pressure in different gases, e.g., argon, helium, oxygen or nitrogen. This results in introduction of polar functional groups on PDMS surface, which leads to the formation of hydrophilic surface. Attention should be paid as extended plasma treatment induces undesirable surface cracks, causing changes in the PDMS mechanical properties. The cracks also facilitate the migration of non-cured low molecular weight (LMW) PDMS chains to the surface. This migration is believed to play an important role in loss of surface hydrophilicity with time after plasma treatment. This phenomenon is known as “hydrophobic recovery” and is considered to be the main ongoing challenge with PDMS plasma treatment. Many studies have been performed aiming at surmounting this problem. Eddington *et al.* [32] have tried to remove the LMW species from the bulk phase through thermal aging. In this way the hydrophobic recovery of the oxidized surface is extended from minutes to days. An alternative method consisting in solvent extraction of oligomers from the bulk phase is introduced by Vickers *et al.* [33]. After storage in air for 7 days, the solvent extracted oxidized PDMS displayed a water contact angle (WCA) that increased from 30° to only 40°, while the WCA of PDMS that had not been solvent-extracted increased to the initial 110°. Hydrophobic recovery can be caused also by the reorientation of polar silanol groups from the surface towards the bulk

phase or the reorientation of nonpolar groups from the bulk to the surface. Several groups have successfully developed methods to avoid (or at least to slow down) PDMS reorganization at the surface. Tan *et al.* [34] reported an easy way to maintain the hydrophilicity of plasma treated samples for longer period. The PDMS samples were simply stored in water and under vacuum, thus prolonging the hydrophilicity for at least 7 days. This effect is explained by the high surface free energy of water which can prevent the reorganization of the silanol groups (SiOH) [35]. More recently Zhao *et al.* [36] have also shown that storing PDMS samples immediately after plasma treatment under water and Luria-Bertani broth (a common growth medium for bacteria) allowed for maintaining surface hydrophilicity for at least 7 days (with contact angles around 20–30° in water and 10–20° in LB broth), while the samples stored in air recovered their hydrophobicity in a week (contact angle above 100°). Oxygen plasma treatment of PDMS surfaces was found to improve adhesion to metal films, glass, acrylic tape, and cells [37–39]. The adhesion strength between plasma-treated PDMS surface and glass is shown in Figure 2.6. The remarkably improved adhesion was ascribed to the presence of surface silanol groups able to further react with the substrate surface thus creating permanent adhesion through covalent cross-linking [37].

Surface restructuring and functionality and therefore an adequate tuning of the PDMS surface physical chemistry are prerequisite to control adhesion property [38]. For this reason, non-oxygen plasma has been also applied to treat PDMS surface. Anand *et al.* used an atmospheric glow discharge with a fluorocarbon gas as precursor to modify the surface of PDMS [40]. After plasma treatment the WCA of PDMS decreased from 104° to an average of 80°. Vlachopoulou *et al.* [41] applied SF₆ plasma under conditions of anisotropic etching for surface nanostructuring of PDMS. The SF₆ plasma removes quickly the hydrophobic organic methyl groups, which reduces the contact angle of PDMS surface from 110° (untreated PDMS) to lower values depending on treatment time. Further treatment with O₂ plasma results in drastic increase of surface wettability for SF₆ plasma treatments longer than 2 min. The obtained super-hydrophilic surfaces were stable for at least one week. Another possibility is the surface modification by atmospheric pressure plasma (APP) as reported by Kim and Jeong [42]. Contact angle measurements of modified surface showed that hydrophilic stability of the product lasted for 20 days. The quantitative study performed on PDMS samples with different mixing ratios of base polymer to curing agent revealed that the PDMS sample with excess base polymer shows long-term hydrophilic stability with a low contact angle. Atmospheric-pressure plasma-enhanced chemical vapor deposition (AP-PECVD) has also been employed for ensuring long-lasting hydrophilicity of PDMS surface [43]. This long-lasting hydrophilicity is achieved by sequential plasma deposition of two kinds of layers on the bare PDMS surface – first highly cross-linked hydrocarbon layer is coated using CH₄ as the reactant, and then a hydrophilic upper layer is deposited using tetraethyl orthosilicate and oxygen (TEOS-O₂). The hydrocarbon layer between the bare PDMS and the SiO_x layer acts as a physical barrier that suppresses hydrophobic recovery. The results of static contact angle on the modified surfaces indicate high hydrophilicity of TEOS-O₂/CH₄/PDMS (with WCA almost equal to 0°) with no change for ca. 28 days. Water vapor-based plasma is another very attractive technique for increasing hydrophilicity and thus adhesion to various materials [44]. The method is found to result in

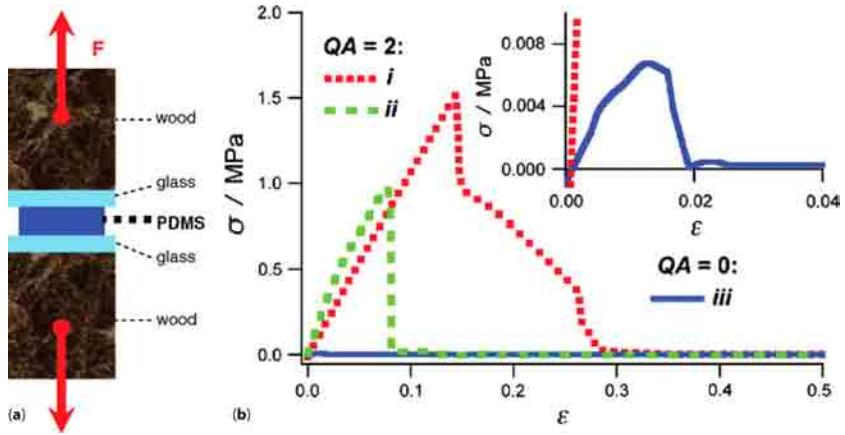


Figure 2.6 Tensile-strength measurements (TSMs) on PDMS–glass system. (a) Scheme of the wood/glass/PDMS/glass/wood junction used for the TSMs. (b) Tensile stress/strain, σ/ϵ , relation for quality of adhesion (QA) = 2 (curves *i* and *ii*), and QA = 0 (curve *iii*). For curve *i*, the permanent adhesion at both PDMS–glass interfaces was achieved by 30-s treatments with air plasma, radio-frequency power (P_{RF}) = 50 W and radio-frequency (RF) = 13.56 MHz. For curve *ii*, both PDMS substrates were treated with oxygen plasma under identical power, RF and time settings. For curve *iii*, one of the two PDMS substrates was treated under identical conditions as the samples for curve *i* and allowed to age for one day. Then at the other PDMS substrates, the materials were brought in contact without any plasma treatment to ensure QA = 0. The failure of *i*, at about 1.5 MPa, was a result of tearing the PDMS slab, while the failure of *ii* resulted from breaking one of the glass slides. No material deterioration was observed for *iii* after the disjointment at ~ 7 kPa. Adapted from Ref. [37] with permission from Elsevier.

highly hydroxylated surfaces and is effective in avoiding the creation of oxidized oligomers responsible for the hydrophobic recovery. Cell settling and spreading experiments revealed enhanced cell adhesion to modified PDMS surfaces. The as-obtained long-term (several months) stable hydrophilic surfaces with enhanced bio-integration enlarge the applications of the PDMS-based medical implants.

Despite all the benefits of these non-oxygen plasma treatments, the surface reconstruction by the mobile PDMS chains cannot be prevented, thus guiding the search for alternative surface modification methods.

2.3.1.2 Corona Treatment

As for plasma treatment, the reactions occurring on the PDMS surface under corona treatment are complex and the mechanisms behind are still not well understood [45]. It is basically considered that during the corona treatment, excited species such as ions, radicals and free electrons are accelerated into the surface of substrate, causing the rupture of long chains and producing free-radicals. The resulting free-radicals react rapidly with the products of the corona discharge and form new carbonyl groups with a higher surface

free energy. Oxidation of the surface increases the surface free energy allowing for better liquid wetting and thus promoting adhesion [18]. The results from corona treatment are very similar to those from plasma treated surfaces, i.e., creation of hydrophilic oxidized layer of silicon bonded to three or four oxygen atoms. The drawbacks of this type of surface modification have been demonstrated by AFM measurements [46]. It was shown that the initial wettability reverts to its original hydrophobic state within ca. 100 minutes. In addition, the adhesion force was found to increase immediately after the electrical exposure but eventually returned to the original value of the unexposed surface. The occurrence of such “oscillating” behaviour of the PDMS surface still shows the need for a method, which will allow obtaining of an intrinsically long-term stable surface.

2.3.1.3 UV/O₃ Treatment

The UV-ozone (UV/O₃) method involves a photo-sensitized oxidation process, in which a treated surface is exposed to short-wavelength (184.9 and 253.7 nm) UV radiation. As a result of UV-irradiation the excited molecules of the treated materials react with the atomic oxygen formed during O₃ formation and/or dissociation. They form volatile molecules (typically CO₂), which readily desorb from the surface [47]. The introduction of polar –OH groups to PDMS surface has been confirmed by contact angle measurements. Under the UV/O₃, silicone rubbers undergo drastic surface chemical changes that are similar to those induced by oxygen plasma. However, compared to oxygen plasma, UV/O₃ treatment is a milder type of physical modification (lack of high energy particles) and is much slower (by about one order of magnitude). This allows for better control over the surface modification, as different degrees of hydrophilicities can be obtained for different treatment times. Moreover, the method involves much deeper modification of the PDMS surface. The effect of the UV/O₃ treatment time on the atomic surface composition of PDMS has been reported by Oláh *et al.* [48]. The results from water contact angle and XPS measurements indicated the formation of hydrophilic silica-like (SiO_x) layer after 60 min UV/O₃ exposure. For shorter exposure times (<60 min) WCA measurements revealed an increase of contact angle hysteresis due to decreasing of receding contact angles, whereas the advancing angles remained unchanged. UV/O₃ treatment technique for fabrication of microfluidic chips has been developed by Berdichevsky *et al.* [49]. PDMS surfaces with long-term stable hydrophilicity were obtained. It was found that surfaces exposed to UV/O₃ for 120 min remained hydrophilic for more than three months, with contact angle of only 46° still recorded 130 days after treatment. For comparison those treated for 30 and 60 min recovered hydrophobicity in 3 days or the surfaces treated with radio-frequency oxygen plasma recovered hydrophobicity in 1–2 days. The difference between these results is explained with deeper penetration and higher degree of oxidation of thick-films caused by UV/O₃ treatment compared to oxygen plasma treatment. To maintain a stable surface wettability of PDMS-based microfluidic devices Ma *et al.* [50] use a very simple method, i.e., immersion of oxidized surfaces in water at low temperature. This proved efficient in hindering the migration of LMW species from PDMS bulk thus allowing better wettability control to be achieved.

As for plasma- and corona-treated surfaces, researchers have reported the creation of uniform silica-like layers with thickness around 10–30 nm (as measured by ellipsometry)

after UV/O₃ treatment. Similarly, hydrophobic recovery is strongly dependent on UV/O₃ exposure time, mainly due to the difference in the degree of transformation to silicon oxide-like species. However, the key issue related to wettability control over UV/O₃-treated PDMS surfaces is to control the diffusivity of LMW species for which low temperature and water immersion proved suitable.

2.3.1.4 Laser Treatment

Laser treatment is another technique used for PDMS surface modification. Lasers are photon sources characterized by energy and space coherence. Their main advantage is the narrow wavelength spread that can be tuned to the maximum absorption of the sample thus making laser treatment an energy efficient process. However, laser treatment has some drawbacks, including possible damage of both the surface and the bulk of polymer materials, caused by continuous irradiating with the laser beam. This problem can be overcome by pulsed lasers allowing optimization of the time intervals between pulses (shortened exposure times). When PDMS surface was treated with CO₂-pulsed laser [51], the samples showed variation in hydrophobicity that was strongly dependent on the number of laser pulses.

2.3.1.5 Physical Adsorption

Surface modification via physical adsorption (physisorption) is a very simple technique that can be a very promising approach for different applications. The method relies primarily on van der Waals interactions between the adsorbed molecules and the surface. The physisorbed molecules are known to desorb over time. Cunningham *et al.* [52], for example, investigated the cell adhesion efficiency and long-term stability of physisorbed fibronectin on PDMS substrates. They showed that initially the adsorbed amount (at a density of 310 ± 20 ng/cm²) desorbed almost 90% after 7 days in static culture, leaving only 10–20 ng/cm² proteins on the PDMS surface. Accordingly, cell adhesion tests showed poor attachment and spreading compared with tissue-cultured polystyrene. Similar results for protein physisorption were obtained by Pakstis *et al.* [53] in their study on screening different methods for PDMS surface modification. Another example is the use of a specific amino acid such as L-3,4-dihydroxyphenylalanine (L-Dopa) to enhance PDMS surface wetting and biocompatibility [54]. Coating process takes place through direct covering by L-Dopa solution of surface due to the interactions between the PDMS surface and the phenol group of L-Dopa, followed by subsequent immobilization of collagen on the hydroxyl-terminated PDMS surface. The improved wettability was confirmed by a decrease in the WCA from $112 \pm 3^\circ$ on native PDMS to $27 \pm 3^\circ$ for L-Dopa-collagen modified PDMS. Furthermore, this modified PDMS surface was shown to be suitable for protein immobilization and better cell adhesion, spreading and growth. Surfactant adsorption has also been investigated for hydrophilization of PDMS surfaces. The practice involves non-ionic poly(ethylene glycol)-based (Pluronic F127) [55] or ionic didodecyltrimethylammonium bromide (DDAB) compounds [56]. Despite the simplicity of this method, the performed studies revealed a) poor stability of the surfactant layer due to desorption, and b) significantly suppressed adhesion. The copolymer deposition consisting in simple dipping of PDMS samples in ethanol/water copolymer solutions is reported by Fukazawa and Ishihara [57]. The hydrophilicity of poly(2-methacryloyloxyethyl phosphorylcholine

(MPC)-co-2-ethylhexyl methacrylate (EHMA)-co-2-(N,N-dimethylamino)ethyl methacrylate) (PMED) and poly(MPC-co-EHMA) (PMEH) treated surfaces was confirmed by the recorded decrease of WCA from 90° to 20°.

2.3.2 Wet Chemical Techniques

The chemical methods commonly employed in surface modification of PDMS include etching, surface oxidation and etching, hydrolysis, functionalization, and surface grafting. These methods can be divided into two groups: the first one is modification by direct chemical reactions with a given solution (wet treatments) and the second one is modification by covalent bonding of various organic modifiers to the preliminarily introduced functional groups on the PDMS surface (grafting).

2.3.2.1 LbL Deposition

The layer-by-layer (LbL) assembly represents a simple and efficient technique first introduced by Decher *et al.* [58]. The method consists in the fabrication of polyelectrolyte multilayers (PEMs) on the substrate by sequential adsorption of polyanion and polycation from aqueous solutions. The driving forces for LbL film fabrication are electrostatic and other intermolecular interactions such as hydrogen bonding [59, 60], covalent bonding [61, 62], coordination bonding [63], charge-transfer (donor-acceptor) interactions [64], π - π interaction [65], cation-dipole interaction [66], etc. The important feature of LbL deposition is the achievement of a precise control on the layer thickness at the nanoscale level. The technique was successfully applied in improving adhesion property of PDMS substrates. Engineered PDMS microstructures and microchannel substrates were coated with multilayers of poly(styrene sulfonate) (PSS), poly(dimethyl diallylammonium chloride) (PDDA) and gelatin using electrostatic LbL self-assembly technique [67]. This surface treatment showed increased smooth muscle cells attachment to PDMS substrates and allowed for increasing the potential growth of cells. Ai *et al.* [68] have used alternating layers of cationic poly(ethyleneimine) (PEI) and anionic PSS to create bio-nanofilms on PDMS. Subsequently polypeptides and polysaccharides such as poly(D-lysine), gelatin, collagen, fibronectin, laminin, hyaluronic acid, and heparin were successfully adsorbed by LbL deposition. The obtained films as shown by contact angle measurement were hydrophilic and supported cell adhesion and growth compared to unmodified silicone elastomer. Park *et al.* [69] have produced various types of transferred PDMS patterns - positively embossed, negatively engraved, and edge-defined shapes using multilayer transfer printing (MTP) method. A weakly charged polyelectrolyte pair of linear poly(ethyleneimine) (LPEI) and poly(acrylic acid) (PAA) were LbL assembled on patterned PDMS stamps to produce multilayer films. The hydrophilicity of the polyelectrolytes increases the work of adhesion at the interface between the polymer and target substrate thus enabling transfer of a multilayer. A new LbL deposition method for preparation of silicone coatings to promote marrow cell attachment and spreading has been proposed by Mehta *et al.* [70] (Figure 2.7). PDDA, clay, type-IV collagen and fibronectin multilayers were deposited using automated microfluidic perfusion system developed by the authors [70]. The coatings revealed good cell spreading, proliferation and viability for the tested cells over

a 15-day period. However, the structures (especially those of PEMs) are dependent on many factors such as mixing ratio, polyelectrolyte ionic strength and concentration, solvent polarity, temperature and pH of the solution. Owing to these factors the use of LbL deposition has been limited.

2.3.2.2 Sol-Gel Method

Sol-gel process consists in the evolution of a colloidal suspension of particles (a 'sol') into a solid-like state - 'gel' via polymerization (polycondensation) of the hydrolyzed monomers of a metal alkoxide (for example, tetraethoxysilane or TEOS). Roman and Culbertson [71] modified PDMS using titanium isopropoxide, zirconium isopropoxide, and vanadium triisobutoxide as sol-gel precursors. This procedure resulted in the formation of surfaces with enhanced hydrophilicity. The WCAs of the so-obtained coatings were 90° for PDMS-ZrO₂, 61° for PDMS-TiO₂, and 19° for PDMS-VO₂. In addition, PDMS channels with inorganic coatings were modified with PEG, amino, perfluoro, or mercapto organic groups using silane chemistry. Similarly, TEOS was used as a precursor by Duo *et al.* [72] for preparation of PDMS/SiO₂ hybrid coatings. The atomic oxygen exposure tests revealed that these hybrid coatings have an excellent erosion resistance and can be used for Kapton® (DuPont) protection. The so-obtained modified surfaces showed good adhesion combined with cracking and spallation resistance.

2.3.2.3 Other Wet Chemical Treatments

Maji *et al.* [73] proposed a new and inexpensive approach for wet chemical modification of PDMS surface. Two-step process involving Piranha and KOH solution treatments has been exploited. The effects of surface modification were demonstrated by a reduced contact angle, i.e., $\sim 27^\circ$ for PDMS surface treated in Piranha solution with H₂O₂ and H₂SO₄ in the ratio of 2:3 followed by a dip in KOH solution for 15 min, and disappearance of methyl groups from the elastomer surface as revealed by FTIR-ATR study. The effectiveness of the method is also supported by improved adhesion and electrical continuity of deposited aluminum metal film over the modified PDMS surface. Hydrophobic recovery of the chemically treated PDMS surfaces was studied by measuring the contact angles at predetermined time intervals. The initial contact angle (74° or 27° depending on the surface composition) increased and saturated (at about 101.8° and 92.4°) after about 10 days of preservation in vacuum. A very simple, fast and low cost method for modifying the surface of PDMS has been reported by Park *et al.* [74]. Hydroxyl groups on the surface of Pt-cured PDMS membranes were generated by boiling in deionized water (Figure 2.8). The presence of SiOH groups was clearly revealed by the appearance of a broad band near 3400 cm^{-1} in the ATR-IR spectrum. Adhesion of human mesenchymal stem cells on the treated PDMS was enhanced compared to an untreated substrate.

2.3.3 Combination of Physical and Chemical Techniques

Among all the reported techniques the surface grafting is the most used one for tailoring the surface chemistry of PDMS. The method provides superior mechanical and chemical

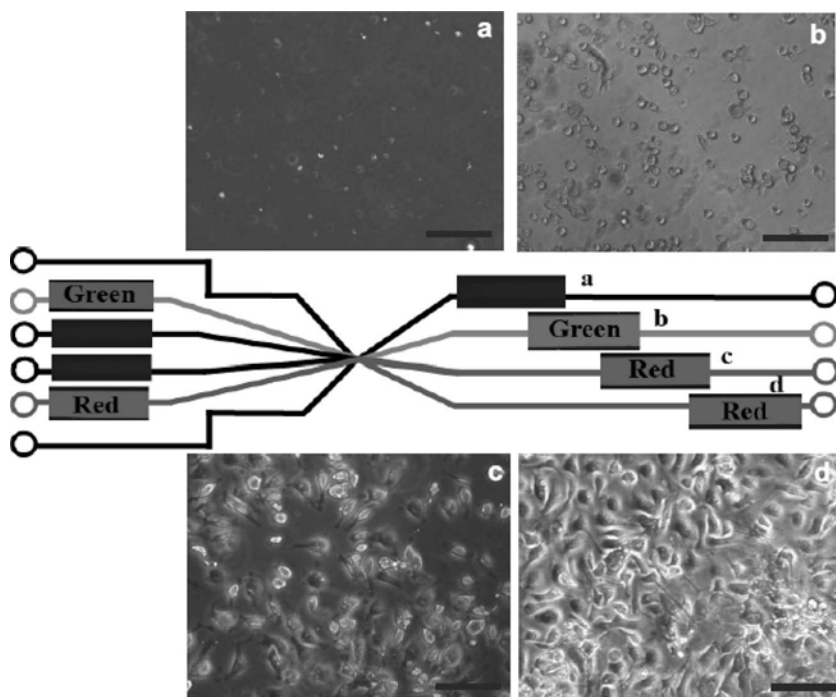


Figure 2.7 PDMS micro-bioreactor chip with multifunctional nanocomposite coatings. Four channels with compositions: (a) no coating, (b) (PDDA/Clay)_{3.5} (PDDA topped), (c) (PDDA/Clay)₄ coating (clay topped), and (d) (PDDA/Clay)₄ (Co/FN)₅. Indexes refer to the number of bilayers of PDDA and clay deposited. Co/FN refers to a polyelectrolyte multilayer built with one layer of positively charged collagen (Co) overlaid with one negatively charged fibronectin (FN). Adapted from Ref. [70] with permission from John Wiley & Sons.

robustness (when compared to physisorption, for example) and flexibility. It consists in grafting of low-molecular-weight molecules as sites where further polymerization can start (“grafting–from” technique) or reactive coupling of pre-formed chains (“grafting–to” technique) on the modified PDMS surface. The choice of the grafting technique depends on the substrate functional groups actually introduced prior to the reaction. For this purpose chemical treatments are applied followed by direct polymerization or physical treatments like plasma, corona, laser or γ -irradiation preceding “grafting–to” procedure with reactive monomers and their subsequent polymerization.

2.3.3.1 Covalent Surface Grafting

2.3.3.1.1 Plasma-Induced Grafting

The PDMS surface was modified by plasma induced graft polymerization of acrylic acid (AA), methacrylic acid (MAA), glycidylmethacrylate (GMA), 2-hydroxy ethyl methacrylate

(HEMA), vinyl alcohol (VA), etc., in order to improve its hydrophilicity and adhesion property. The oxygen and ammonia plasma treatments have been used for grafting of poly(ethylene-*alt*-maleic anhydride) (PEMA) and improving the adhesion property of silicone elastomer [17]. In the case of oxygen plasma-treated PDMS, “hydrophobic recovery” again occurred due to the surface segregation of its low-molecular-weight species. Amino-functional surface groups were generated after ammonia plasma treatment. This mechanically unstable top layer has been stabilized by grafting with PEMA directly or after using γ -aminopropyltriethoxysilane as a coupling agent. Pull-off tests have shown considerably improved adhesion between the PDMS and an epoxy resin after surface modification of PDMS film (Figure 2.9).

Völcker *et al.* [75] have succeeded to graft-*co*-polymerize AA, MAA and GMA onto the surface of PDMS samples by an argon plasma treatment prior to heat-induced solution polymerization. The synthetic procedure consists of exposing the plasma-treated samples to air in order to generate hydroperoxides. In a following step AA, MAA and GMA were

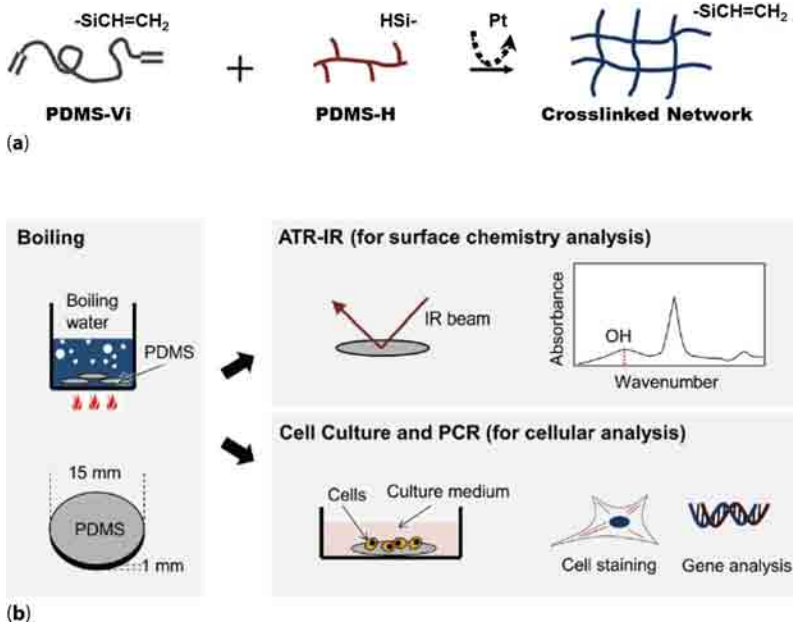


Figure 2.8 Theory and experiment. (a) Schematic of hydrosilylation cross-linking reaction used to cure SYLGARD[®] 184 PDMS elastomer. (b) Experimental procedure: PDMS substrates were cut into membranes (diameter: 15 mm, thickness: 1 mm). Deionized water was prepared and boiled within the prepared PDMS membranes for 30 min to 2 h. ATR-IR analysis was performed to confirm the surface chemistry modification. Human mesenchymal stem cells were cultured on PDMS membranes and analyzed by cell staining and polymerase chain reaction. PDMS-Vi stands for vinyl-functionalized PDMS, and PDMS-H for HSi-terminated PDMS. Adapted from Ref. [74] with permission from Elsevier.

graft-co-polymerized. In the case of AA copolymerization, argon plasma-treated samples were directly exposed to AA vapor in order to initiate graft-copolymerization. The cytocompatibility of as functionalized silicone was increased drastically, thus opening potential applications of these materials as ophthalmological implants. A plasma-induced graft copolymerization of acrylic acid has been used for permanent immobilization of collagen and gelatin on the silicone surface through covalent bonding between amino groups of proteins and carboxyl groups [76]. The same authors [77] have attached poly(acrylamide) (PAAm) onto corona pretreated PDMS surfaces. The grafted PAAm is further converted to poly(acrylic acid) by hydrolysis to introduce carboxyl groups and subsequently reacted with collagen to form covalent bonds. Plasma-induced graft copolymerization of HEMA on silica surface was demonstrated by Hsiue *et al.* [78], Bodas and Khan-Malek [79] and Almutairi *et al.* [80]. The resulted stable hydrophilic PDMS samples were very effective for attachment and growth of corneal epithelial cells. Polymerization of HEMA, poly(ethylene glycol) (PEG), and poly(vinylpyrrolidone) (PVP) was also performed by surface activation with oxygen plasma with several combinations of exposure time and RF. The hydrophilic silicone coatings with contact angle values of 30° or less and at least six-month stability have been prepared [81]. A final example of a recently reported air plasma grafting is the work by Li *et al.* [82]. They grafted poly(vinyl alcohol) (PVA) onto a nanopatterned PDMS, and the resulting surface was used for cell culture study. The experimental results show that the modified PDMS surface enhances cell growth and this was attributed to the lower contact angle (50–60°) after PVA coating.

2.3.3.1.2 Laser and UV Irradiation-Induced Grafting

The CO₂-pulsed laser grafting of HEMA and hydroxyethylmethacrylate phosphatidylcholine (HEMAPC) onto PDMS surface has been presented in the work of Khorasani and coworkers [83, 84]. The obtained surfaces were super-hydrophilic with water contact angles of about 35° and 10° for surfaced-grafted HEMA and HEMAPC, respectively. Results from *in vitro* testing showed that modified PDMS surfaces have excellent blood compatibility. The UV irradiation grafting of acrylic acid onto PDMS surface in an anhydrous benzophenone/acetone/acrylic acid solution has been also reported by Yang and coworkers [85, 86].

2.3.3.1.3 Hydrosilylation-Induced Grafting

Alauzun *et al.* have modified the PDMS surface with covalently linked hyaluronic acid (HA) in combination with PEG [87]. They prepared Si-H-rich PDMS surfaces using pre-curing and post-curing methods [88] on which allyl-*o*-tosylethyl-PEG was immobilized via hydrosilylation. Finally, HA was grafted onto the surface via amide linkage. HA-modified PDMS showed improved wettability and significant enhancement in 3T3 fibroblast and corneal epithelial cell proliferation, but reduced protein adsorption.

2.3.3.2 Modification by Amphiphilic Block Copolymers

Tuning of surface chemistry, wettability and topography of the silicone elastomers by incorporation of functionalized amphiphilic diblock copolymers in order to develop a new and

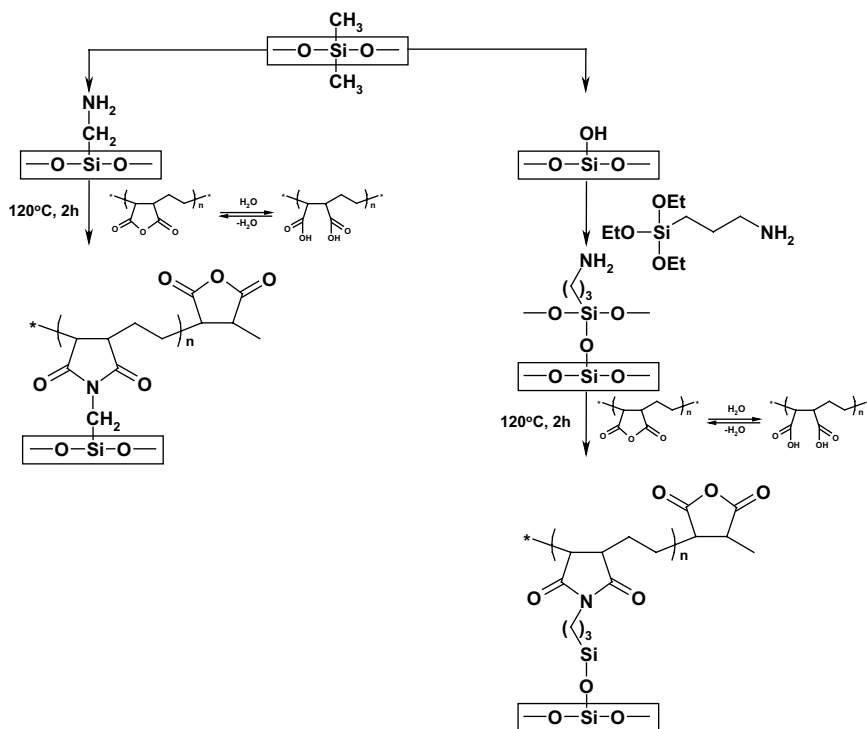


Figure 2.9 Scheme of the grafting procedure of poly(ethylene-*alt*-maleic anhydride) (PEMA) on plasma-treated PDMS surface. Adapted from Ref. [17] with permission from Elsevier.

very simple method for PDMS surface modification has been presented by Ngo *et al.* [89]. The method consists in incorporation of functionalized amphiphilic block copolymers, i.e., poly(dimethylsiloxane)-*b*-poly[2-(dimethylamino)ethyl methacrylate] diblock copolymers (PDMS-*b*-PDMAEMA), in silicone matrices, followed by PDMS cross-linking reaction and immersion of the obtained cured films in water. The immersion in water causes an increase of hydrophilicity due to the exposure of PDMAEMA block after surface reorganization. The surface reorganization was confirmed by atomic force microscopy with chemically-sensitive tips [90]. Adhesion force mapping with hydrophobic tips showed that immersed samples exhibited lower surface hydrophobicity due to the exposure of hydrophilic block copolymer chains at the PDMS surface. The adhesion experiments with mussels revealed that adhesion occurs preferably on block copolymer-filled coatings after immersion. Yao and Fang [91] have successfully prepared long-term stable hydrophilic PDMS surface by incorporating poly(ethylene oxide) (PEO)-*b*-PDMS with different concentrations in PDMS base and the curing agent. The contact angle for modified surfaces after curing decreased to $21.5\text{--}80.9^\circ$ depending on mixing ratio. After two-month storage in air the contact angle remained stable and then slightly increased in the next two months.

2.3.3.3 Other Combination of Physical and Chemical Techniques

Li *et al.* [92] attached the amino-terminated L-Arginyl-Glycyl-L-Aspartic acid (RGD peptide) onto PDMS surface through photochemical immobilization of functional N-hydroxysuccinimide (NHS) groups to facilitate adhesion of human skin fibroblasts. The results from cell culture study showed that RGD peptide-conjugated PDMS surface promoted human skin fibroblasts adhesion and proliferation for long-term (6 days) and enhanced collagen production.

2.4 Summary and Prospects

PDMS is a versatile material possessing many unique properties. It is used in many conventional (as sealants, adhesives, and cast materials) and advanced technologies (for cell culture and the fabrication of a unique range of medical devices, in the fabrication of microfluidic and laboratory-on-a-chip microfluidic devices). However, the strong hydrophobicity limits its usefulness. This review has covered various surface modification methods to increase the surface free energy of PDMS. It is shown that the use of physical treatments, like plasma, corona or laser discharge, leads to the generation of reactive surface groups resulting in an increased surface free energy and an improved adhesion to other materials. However, due to the high mobility of the (cross-linked) silicone chains these surface modifications are only temporary and the surface reverts to its native hydrophobic state in a short time scale. The loss of the improved adhesion property is connected to the disappearance of polar functional groups and the loss of surface reactivity, and wettability. Therefore, many efforts have been focused on grafting of different organic modifiers to stabilize the surface modification effect of silicone elastomers. Chemical grafting appears as a very promising approach to tailor the surface properties of PDMS, but the method generally requires multiple steps such as initiator formation, growth reaction, and distillation of some products prior to reaction. This could represent a serious limitation for large-scale production of PDMS elastomers. Finally, the relatively new attempts for PDMS surface modification by incorporation of amphiphilic block copolymers have been reported and have proved to be a promising approach. But still the design of long-term hydrophilic PDMS surfaces with well-tailored adhesion property remains a real technical challenge.

Acknowledgements

We gratefully acknowledge financial support by the ARC BIOMIME project (ARC AUWB-2008-08/12-UMH15), the Science Policy Office of the Belgian Federal Government (PAI 7/05) and the POLINNOVA project (EU FP7 “Capacities – Research Potential” program).

List of Abbreviations

AA	acrylic acid
AFM	atomic force microscopy
AP-PECVD	atmospheric-pressure plasma-enhanced chemical vapor deposition
APP	atmospheric pressure plasma
ATRP	atom transfer radical polymerization
DDAB	didodecyldimethylammonium bromide
GMA	glycidylmethacrylate
EHMA	2-ethylhexyl methacrylate
HA	hyaluronic acid
HEMA	2-hydroxy ethyl methacrylate
HEMAPC	hydroxyethylmethacrylate phosphatidylcholine
LbL	layer by layer
L-dopa	L-3,4-dihydroxyphenylalanine
LMW	low molecular weight
MAA	methacrylic acid
MPC	2-methacryloyloxyethyl phosphorylcholine
MTP	multilayer transfer printing
NHS	N-hydroxysuccinimide
PAA	poly(acrylic acid)
PAAm	poly(acrylamide)
PCBs	poly(chlorinated biphenyl)s
PDDA	poly(dimethyl diallylammonium chloride)
PDMAEMA	poly[2-(dimethylamino)ethyl methacrylate]
PDMS	poly(dimethylsiloxane)
PEG	poly(ethylene glycol)
PEI	poly(ethyleneimine)
PEMA	poly(ethylene- <i>alt</i> -maleic anhydride)
PEMs	polyelectrolyte multilayers
PEO	poly(ethylene oxide)

PMED	poly(2-methacryloyloxyethyl phosphorylcholine- <i>co</i> -2-ethylhexyl methacrylate- <i>co</i> -2-(N,N-dimethylamino)ethyl methacrylate)
PMEH	poly(2-methacryloyloxyethyl phosphorylcholine- <i>co</i> -2-ethylhexyl methacrylate)
P _{RF}	radio-frequency power
PSS	poly(styrene sulfonate)
PVP	poly(vinylpyrrolidone)
QA	quality of adhesion
RGD	L-Arginyl-Glycyl-L-Aspartic acid
RF	radio-frequency
SFG	sum frequency generation
T _g	glass transition temperature
TEOS	tetraethyl orthosilicate
TSMs	tensile-strength measurements
UV/O ₃	ultraviolet-ozone
VA	vinyl alcohol
WCA	water contact angle
XPS	X-ray photoelectron spectroscopy
γ _{sv}	surface free energy

References

1. J. Zhou, A.V. Ellis and N.H. Voelcker, Recent developments in PDMS surface modification for microfluidic devices, *Electrophoresis*, 31, 2–16 (2010).
2. J. Zhou, D. A. Khodakov, A.V. Ellis and N. H. Voelcker, Surface modification for PDMS-based microfluidic devices, *Electrophoresis*, 33, 89–104 (2012).
3. J.C. McDonald, D.C. Duffy, J.R. Anderson, D.T. Chiu, H. Wu, O.J. Schueller and G.M. Whitesides, Fabrication of microfluidic systems in poly(dimethylsiloxane), *Electrophoresis*, 21, 27–40 (2000).
4. Y. Hongbin, Z. Guangya, C.F. Siong, W. Shouhua and L. Feiwen, Novel polydimethylsiloxane (PDMS) based microchannel fabrication method for lab-on-a-chip application, *Sensors Actuators, B* 137, 754–761 (2009).
5. F. Abbasi, H. Mirzadeh and A.-A. Katbab, Modification of polysiloxane polymers for biomedical applications: A review, *Polym. Int.*, 50, 1279–1287 (2001).
6. M.C. Belanger and Y. Marois, Hemocompatibility, biocompatibility, inflammatory and in vivo studies of primary reference materials low-density polyethylene and polydimethylsiloxane: A review, *J. Biomed. Mater. Res. A*, 58, 467–477 (2001).

7. G.D. Friends, J.F. Kunzler and R.M. Ozark, Recent advances in the design of polymers for contact lenses, *Macromol. Symp.*, 98, 619–631 (1995).
8. J.F. Kunzler, Silicone hydrogels for contact lens application, *Trends. Polym. Sci.*, 4, 52–59 (1996).
9. V. Compan, A. Lopez-Aleman, E. Riande and M.F. Refojo. Biological oxygen apparent transmissibility of hydrogel contact lenses with and without organosilicon moieties, *Biomaterials*, 25, 359–365 (2003).
10. S.S. Lateef, S.B. Boateng, T. J. Hartman and L. Hanley, GRGDSP peptide bound silicone membranes withstand mechanical flexing *in vitro* and display enhanced fibroblast adhesion, *Biomaterials*, 23, 3159–3168 (2002).
11. C.A. Malpass, K.W. Millsap, H. Sidhu and L.B. Gower, Immobilization of an oxalate-degrading enzyme on silicone elastomer, *J. Biomed. Mater. Res.*, 63, 822–829 (2002).
12. W.R. Childs, M.J. Motala, K.J. Lee and R.G. Nuzzo, Masterless soft lithography: Patterning UV/ozone-induced adhesion on poly(dimethylsiloxane) surfaces, *Langmuir*, 21, 10096–10105 (2005).
13. R. Anderson, B. Arkles and G.L. Larson, *Silicon Compounds, Register and Review*, Petrarch Systems, Bristol, PA, USA (1987).
14. H. Meynen, M.V. Blucke, M. Gonzalez, B. Harkness, G. Gardner, J. Sudbury-Holtschlag, B. Vandavelde, C. Winters and E. Beyne, Ultra low stress and low temperature patternable silicone materials for applications within microelectronics, *Microelectronic Eng.*, 76, 212–218 (2004).
15. V.M. Graubner and D. Clemens, Neutron reflectometry and spectroscopic ellipsometry studies of cross-linked poly(dimethylsiloxane) after irradiation at 172 nm, *Langmuir*, 21, 8940–8946 (2005).
16. T. Meyer, H. Hedler, L. Larson and M. Kunselman: A new approach to wafer-level packaging employs spin-on and printable silicones, *Chip Scale Review*, 8, 65–71 (2004).
17. J. Roth, V. Albercht, M. Nitschke, C. Bellmann, F. Simon, S. Zchoche, S. Michel, C. Luhmann, K. Grundke and B. Voit, Surface functionalization of silicone rubber for permanent adhesion improvement, *Langmuir*, 24, 12603–12611 (2008).
18. K.L. Mittal, The role of the interface in adhesion phenomena, *Polym. Eng. Sci.*, 17, 467–473 (1977).
19. H. Makamba, J.H. Kim, K. Lim, N. Park and J.H. Hahn, Surface modification of poly(dimethylsiloxane) microchannels, *Electrophoresis*, 24, 3607–3619 (2003).
20. I. Wong and C.M. Ho, Surface molecular property modifications for poly(dimethylsiloxane) (PDMS) based microfluidic devices, *Microfluidics Nanofluidics*, 7, 291–306 (2009).
21. F. de Buyl, Silicones sealants and structural adhesives, *Int. J. Adhesion Adhesives*, 21, 411–422 (2001).
22. G. Heinrich and M. Kluppel, Recent advances in the theory of filler networking in elastomers, *Adv. Polym. Sci.*, 160, 1–44 (2002).
23. A. Colas and J. Curtis, B-Silicones, in: *Biomaterials Science. An Introduction to Materials in Medicine (Third Edition)*, Section 1.2 Classes of materials used in medicine, B.D. Ratner, A.S. Hoffman, F.J. Schoen and J.E. Lemons (Eds), pp. 82–91, Elsevier, Oxford (2013).
24. A.J. Chalk and J.F. Harrod, Homogeneous Catalysis. II. The mechanism of the hydrosilation of olefins catalyzed by group VIII metal complexes, *J. Am. Chem. Soc.*, 87, 16–21 (1965).
25. C. Chen J. Wang and Z. Chen, Surface restructuring behavior of various types of poly(dimethylsiloxane) in water detected by SFG, *Langmuir*, 20, 10186–10193 (2004).
26. A. Carlos, C.A. Barrios, Q. Xu, T. Cutright and B.Z. Newby, Incorporating zosteric acid into silicone coatings to achieve its slow release while reducing fresh water bacterial attachment, *Colloids Surfaces B*, 41, 83–93 (2005).

27. A. Beigbeder, M. Jeusette, R. Mincheva, M. Claes, P. Brocorens, R. Lazzaroni and Ph. Dubois, On the effect of carbon nanotubes on the wettability and surface morphology of hydrosilylation-curing silicone coatings, *J. Nanostruct. Polym. Nanocomposites*, 5, 37–43 (2009).
28. M.J. Owen, Siloxane surface activity, in: *Silicon Based Polymer Science: A Comprehensive Resource*, J.M. Zeigler and F.W.G. Fearon (Eds), pp. 705–739, American Chemical Society, Washington, D.C. (1990).
29. A. Beigbeder, P. Degee, S.L. Conlan, R.J. Mutton, A.S. Clare, M.E. Pettitt, M.E. Callow, J.A. Callow and P. Dubois, Preparation and characterisation of silicone-based coatings filled with carbon nanotubes and natural sepiolite and their application as marine fouling-release coatings, *Biofouling*, 24, 291–302 (2008).
30. A. Beigbeder, C. Labruyere, P. Viville, M.E. Pettitt, M.E. Callow, J.A. Callow, L. Bonnaud, R. Lazzaroni and P. Dubois. Surface and fouling-release properties of silicone/organomodified montmorillonite coatings, *J. Adhesion Sci. Technol.*, 25, 1689–1700 (2011).
31. E. Martinelli, M. Suffredini, G. Galli, A. Glisenti, M.E. Pettitt, M.E. Callow, J.A. Callow, D.J. Williams and G. Lyall, Amphiphilic block copolymer/poly(dimethylsiloxane) (PDMS) blends and nanocomposites for improved fouling-release, *Biofouling*, 27, 529–541 (2011).
32. D.T. Eddington, J.P. Puccinelli and D.J. Beebe, Thermal aging and reduced hydrophobic recovery of polydimethylsiloxane, *Sensors Actuators B*, 114, 170–172 (2006).
33. J.A. Vickers, M.M. Caulum and C.S. Henry, Generation of hydrophilic poly (dimethylsiloxane) for high-performance microchip electrophoresis, *Anal. Chem.*, 78, 7446–7452 (2006).
34. S.H. Tan, N.T. Nguyen, Y.C. Chua and T.G. Kang, Oxygen plasma treatment for reducing hydrophobicity of a sealed polydimethylsiloxane (PDMS) microchannel, *Biomicrofluidics*, 4, 032204 (2010).
35. L. Lavielle and J. Schultz, Surface properties of graft polyethylene in contact with water: I. Orientation phenomena, *J. Colloid Interface Sci.*, 106, 438–445 (1985).
36. L.H. Zhao, J. Lee and P.N. Sen, Long-term retention of hydrophilic behavior of plasma treated polydimethylsiloxane (PDMS) surfaces stored under water and Luria-Bertani broth, *Sensors Actuators A*, 181, 33–42 (2012).
37. K. Chau, B. Millare, A. Lin, S. Upadhyayula, V. Nuñez, H. Xu and V.I. Vullev, Dependence of the quality of adhesion between poly(dimethylsiloxane) and glass surfaces on the composition of the oxidizing plasma, *Microfluidics Nanofluidics*, 10, 907–917 (2011).
38. D. Fuard, T. Tzvetkova-Chevolleau, S. Decossas, P. Tracqui and P. Schiavone, Optimization of poly-di-methyl-siloxane (PDMS) substrates for studying cellular adhesion and motility, *Microelectronic Eng.*, 85, 1289–1293 (2008).
39. P. Bödö and J.E. Sundgren, Titanium deposition onto ion-bombarded and plasma-treated polydimethylsiloxane: Surface modification, interface and adhesion, *Thin Solid Films*, 136, 147–159 (1986).
40. V. Anand, S. Ghosh, M. Ghosh, G Mohan Rao, R. Railkar and R.R. Dighe, Surface modification of PDMS using atmospheric glow discharge polymerization of tetrafluoroethane for immobilization of biomolecules, *Appl. Surface Sci.*, 257, 8378–8384 (2011).
41. M.E. Vlachopoulou, P.S. Petrou, S.E. Kakabakos, A. Tserapi, K. Beltsios and E. Gogolides, Effect of surface nanostructuring of PDMS on wetting properties, hydrophobic recovery and protein adsorption, *Microelectronic Eng.*, 86, 1321–1324 (2009).
42. H.T. Kim and O.C. Jeong, PDMS surface modification using atmospheric pressure plasma, *Microelectronic Eng.*, 88, 2281–2285 (2011).

43. D. Lee and S. Yang, Surface modification of PDMS by atmospheric-pressure plasma-enhanced chemical vapor deposition and analysis of long-lasting surface hydrophilicity, *Sensors Actuators B*, 162, 425–434 (2012).
44. C. Jensen, L. Gurevich, A. Patriciu, J. Struijk, V. Zachar and C.P. Pennisi, Stable hydrophilic polydimethylsiloxane surfaces produced by plasma treatment for enhanced cell adhesion. In: IFMBE Proceedings, 15th Nordic-Baltic Conference on Biomedical Engineering and Medical Physics, pp 105–108 (2011).
45. K. Haubert, T. Drier and D. Beebe, PDMS bonding by means of a portable, low-cost corona system, *Lab Chip*, 6, 1548–1549 (2006).
46. M. Meincken, T.A. Berhane and P.E. Mallon, Tracking the hydrophobicity recovery of PDMS compounds using the adhesive force determined by AFM force distance measurements, *Polymer*, 46, 203–208 (2005).
47. K. Efimenko, W.E. Wallace and J. Genzer, Surface modification of Sylgard-184 poly(dimethylsiloxane) networks by ultraviolet and ultraviolet/ozone treatment, *J. Colloid Interface Sci.*, 254, 306–315 (2002).
48. A. Oláh, H. Hillborg and G.J. Vancso, Hydrophobic recovery of UV/ozone treated poly(dimethylsiloxane): Adhesion studies by contact mechanics and mechanism of surface modification, *Appl. Surface Sci.*, 239, 410–423 (2005).
49. Y. Berdichevsky, J. Khandurina, A. Guttman and Y.-H. Lo, UV/ozone modification of poly(dimethylsiloxane) microfluidic channels, *Sensors Actuators B*, 97, 402–408, (2004).
50. K. Ma, J. Rivera, G. J. Hirasaki and S.L. Biswal, Wettability control and patterning of PDMS using UV–ozone and water immersion, *J. Colloid Interface Sci.*, 363, 371–378 (2011).
51. M.T. Khorasani and H. Mirzadeh, BHK cells behaviour on laser treated polydimethylsiloxane surface, *Colloids Surfaces B*, 35, 67–71(2004).
52. J.J. Cunningham, J. Nikolovski, J.J. Linderman and D.J. Mooney, Quantification of fibronectin adsorption to silicone-rubber cell culture substrates, *BioTechniques*, 32, 876–887 (2002).
53. L.M. Pakstis, J.P. Dunkers, A. Zheng, T.V. Vorburger, T.P. Quinn and M.T. Cicerone, Evaluation of polydimethylsiloxane modification methods for cell response, *J. Biomed. Mater. Res. A*, 92, 604–614 (2010).
54. C.Y. Gao, Y.Y. Guo, J. He, M. Wu, Y. Liu, Z.L. Chen, W.S. Cai, Y.L. Yang, C. Wang and X.Z. Feng, L-3,4 dihydroxyphenylalanine-collagen modified PDMS surface for controlled cell culture, *J. Mater. Chem.*, 22, 10763–10770 (2012).
55. Z. Wu and K. Hjort, Surface modification of PDMS by gradient-induced migration of embedded Pluronic, *Lab Chip*, 9, 1500–1503 (2009).
56. B. Han, Y. Xu, L. Zhang, X. Yang and E. Wang, Surface modification of poly(dimethylsiloxane) microchips using a double-chained cationic surfactant for efficiently resolving fluorescent dye adsorption, *Talanta*, 79, 959–962 (2009).
57. K. Fukazawa and K. Ishihara, Simple surface treatment using amphiphilic phospholipid polymers to obtain wetting and lubricity on polydimethylsiloxane-based substrates, *Colloids Surfaces B*, 97, 70– 76 (2012).
58. G. Decher, J.D. Hong and J. Schmitt, Buildup of ultrathin multilayer films by a self-assembly process: III. Consecutively alternating adsorption of anionic and cationic polyelectrolytes on charged surfaces, *Thin Solid Films*, 210/211, 831–835 (1992).
59. W.B. Stockton and M.F. Rubner, Molecular-level processing of conjugated polymers. 4. Layer-by-Layer manipulation of polyaniline via hydrogen-bonding interactions, *Macromolecules*, 30, 2717–2725 (1997).

60. E. Kharlampieva, V. Kozlovskaya and S.A. Sukhishvili, Layer-by-layer hydrogen-bonded polymer films: From fundamentals to applications, *Adv. Mater.*, 21, 3053–3065 (2009).
61. G.K. Such, J.F. Quinn, A. Quinn, E. Tjipto and F. Caruso, Assembly of ultrathin polymer multi-layer films by click chemistry, *J. Am. Chem. Soc.*, 128, 9318–9319 (2006).
62. F. Wang, N. Ma, Q. Chen, W. Wang and L. Wang, Halogen bonding as a new driving force for layer-by-layer assembly, *Langmuir*, 23, 9540–9542 (2007).
63. H.M. Xiong, M.H. Cheng, Z. Zhou, X. Zhang and J.C. Shen, A new approach to the fabrication of a self-organizing film of heterostructured polymer/Cu₂S nanoparticles, *Adv. Mater.*, 10, 529–532 (1998).
64. Y. Shimazaki, M. Mitsuishi, S. Ito and M. Yamamoto, Preparation of the layer-by-layer deposited ultrathin film based on the charge-transfer interaction, *Langmuir*, 13, 1385–1387 (1997).
65. T. Tang, J. Qu, K. Müllen and S.E. Webber, Molecular layer-by-layer self-assembly of water-soluble perylene diimides through π - π and electrostatic interactions, *Langmuir*, 22, 26–28 (2006).
66. Y. Ogawa, Y. Arikawa, T. Kida and M. Akashi, Fabrication of novel layer-by-layer assembly films composed of poly(lactic acid) and polylysine through cation–dipole interactions, *Langmuir*, 24, 8606–8609 (2008).
67. M. Li, H. Ai, D.K. Mills, Y.M. Lvov, M.J. McShane and B.K. Gale, Using microfabrication and electrostatic layer-by-layer (LbL) self-assembly technologies to improve the growth and alignment of smooth muscle cells. in: Proc. 2nd Annual International IEEE-EMBS Special Topic Conference on Microtechnologies in Medicine and Biology 109–114 (2002).
68. H. Ai, Y.M. Lvov, D.K. Mills, H. Meng, X. Qiao, J.S. Alexander and S.A. Jones, Coating bio-nano-film on PDMS through layer-by-layer self-assembly. in: Proc. Annual International Conference of the IEEE Engineering in Medicine and Biology Society - EMBC 1, 608–609 (2002).
69. J.S. Park, S.M. Cho, G.Y. Han, S.J. Sim, J. Park and P.J. Yoo, Phase controllable transfer printing of patterned polyelectrolyte multilayers, *Langmuir*, 25, 2575–2581 (2009).
70. G. Mehta, M.J. Kiel, J.W. Lee, N. Kotov, J.J. Linderman and S. Takayama, Polyelectrolyte-clay-protein layer films on microfluidic PDMS bioreactor surfaces for primary murine bone marrow culture, *Adv. Funct. Mater.*, 17, 2701–2709 (2007).
71. G.T. Roman and C.T. Culbertson, Surface engineering of poly(dimethylsiloxane) microfluidic devices using transition metal sol–gel chemistry, *Langmuir*, 22, 4445–4451 (2006).
72. S. Duo, M. Li, M. Zhua and Y. Zhoua, Polydimethylsiloxane/silica hybrid coatings protecting Kapton from atomic oxygen attack, *Mater. Chem. Phys.*, 112, 1093–1098 (2008).
73. D. Maji, S.K. Lahiri and S. Das, Study of hydrophilicity and stability of chemically modified PDMS surface using piranha and KOH solution, *Surface Interface Anal.*, 44, 62–69 (2012).
74. J.Y. Park, D. Ahn, Y.Y. Choi, C.M. Hwang, S. Takayama, S.H. Lee and S.H. Lee, Surface chemistry modification of PDMS elastomers with boiling water improves cellular adhesion, *Sensors Actuators B*, 173, 765–771 (2012).
75. N. Völcker, D. Klee, H. Höcker and S. Langefeld, Functionalization of silicone rubber for the covalent immobilization of fibronectin, *J. Mater. Sci. Mater. Med.*, 12, 111–119 (2001).
76. T. Okada and Y. Ikada, *In vitro* and *in vivo* digestion of collagen covalently immobilized onto the silicone surface, *J. Biomed. Mater. Res.*, 26, 1569–1581 (1992).
77. T. Okada and Y. Ikada, Modification of silicone surface by graft polymerization of acrylamide with corona discharge, *Makromol. Chem.*, 192, 1705–1713 (1991).
78. G.H. Hsiue, S.D. Lee, C.C. Wang, M.H. Shiue and P.C. Chang, Plasma-induced graft copolymerization of HEMA onto silicone rubber and TPX film improving rabbit corneal epithelial cell attachment and growth, *Biomaterials*, 15, 163–171(1994).

79. D.S. Bodas and C. Khan-Malek, Fabrication of long-term hydrophilic surfaces of poly(dimethyl siloxane) using 2-hydroxy ethyl methacrylate, *Sensors Actuators B*, 120, 719–723 (2007).
80. Z. Almutairi, C.L. Ren and L. Simon, Evaluation of polydimethylsiloxane (PDMS) surface modification approaches for microfluidic applications, *Colloids Surfaces A*, 415, 406–412 (2012).
81. S. Hemmilä, J.V. Cauich-Rodriguez, J. Kreutzer and P. Kallio, Rapid, simple, and cost-effective treatments to achieve long-term hydrophilic PDMS surfaces, *Appl. Surface Sci.*, 258, 9864–9875 (2012).
82. J. Li, M. Wang and Y. Shen, Chemical modification on top of nanotopography to enhance surface properties of PDMS, *Surface Coat. Technol.*, 206, 2161–2167 (2012).
83. M.T. Khorasani, H. Mirzadeha and P.G. Sammes, Laser surface modification of polymers to improve biocompatibility: HEMA grafted PDMS, in vitro assay-III, *Radiat. Phys. Chem.*, 55, 685–689 (1999).
84. M. T. Khorasani and H. Mirzadeh, *In Vitro* blood compatibility of modified PDMS surfaces as superhydrophobic and superhydrophilic materials, *J. Appl. Polym. Sci.*, 91, 2042–2047 (2004).
85. H. Yang and Z. Hou, Homogeneous grafted poly(acrylic acid) brushes on ultra-flat polydimethylsiloxane (PDMS) films by UV irradiation, *Nano Biomed. Eng.*, 3, 42–46 (2011).
86. H. Yang, Z. Hou and J. Hu, Surface modification of ultra-flat polydimethylsiloxane by UV-grafted poly(acrylic acid) brushes, *J. Appl. Polym. Sci.*, 123, 2266–2271 (2012).
87. J.G. Alauzun, S. Young, R. D'Souza, L. Liu, M.A. Brook and H.D. Sheardown, Biocompatible, hyaluronic acid modified silicone elastomers, *Biomaterials*, 31 3471–3478 (2010).
88. H. Chen, M.A. Brook, H.D. Sheardown, Y. Chen and B. Klenkler, Generic bioaffinity silicone surfaces, *Bioconjugate Chem.*, 17, 21–28 (2006).
89. T.C. Ngo, R. Kalinova, D. Cossement, E. Hennebert, R. Mincheva, R. Snyders, P. Flammang, P. Dubois, R. Lazzaroni and P. Leclère, Modification of the adhesive properties of silicone based-coatings by block copolymers, *Langmuir*, DOI: 10.1021/la403995q.
90. A. Beaussart, T.C. Ngo, S. Derclaye, R. Kalinova, R. Mincheva, P. Dubois, P. Leclère and Y.F. Dufrêne, Chemical force microscopy of stimuli-responsive adhesive copolymers, *Nanoscale*, 6, 565–571 (2014).
91. M. Yao and J. Fang, Hydrophilic PEO-PDMS for microfluidic applications, *J. Micromech. Microeng.*, 22, 025012 (2012)
92. B. Li, J. Chen and J.H. Wang, RGD peptide-conjugated poly(dimethylsiloxane) promotes adhesion, proliferation, and collagen secretion of human fibroblasts, *J. Biomed. Mater. Res. A*, 79, 989–998 (2006).

Functionally Graded Adhesively Bonded Joints

M. Kemal Apalak*

Department of Mechanical Engineering, Erciyes University, Kayseri, Turkey

Abstract

Adhesively bonded joints exhibit a common problem, called edge effects, arising from peel and shear stress concentrations occurring around the free edges of the adherend-adhesive interfaces and affecting the overall joint strength considerably. Some joint geometry-specific measures were considered for adjusting the stiffness of joint members around these free edges in order to improve the joint strength. Functionally graded materials appear in nature with a role of reducing stress concentrations along bi-material interfaces. Biological interfaces, such as dentin-enamel junction or tendon to bone, utilize the concept of functionally graded materials. Today, this concept is considered to reduce stress concentrations appearing along the adherend-adhesive interfaces of the adhesive joints serving under static, dynamic and thermal loads. This review first discusses the mathematical models, solution methods related to the adhesive joint problem, the free edge effects, and measures to relieve these effects based on the current literature, and later evaluates how the concept of functionally graded materials can be implemented in adhesive joints, i.e. use of functionally graded adherends and adhesives.

Keywords: Adhesive joint, functionally graded material, functionally graded adhesive, bi-adhesive, mixed-joints

3.1 Introduction

Adhesive bonding technique is used successfully to join similar and dissimilar materials. The simplest geometry of an adherend is a bar, plate, shell, or tube. In order to join two adherends at least one needs to provide an adhesive layer between the two adherends and to apply a necessary gentle pressure by overlapping the adherends and a specific curing period.

*Corresponding author: apalakmk@erciyes.edu.tr

Despite the fact that the bonding surfaces need special cleaning and treatment before bonding process, the final joined configuration has some advantages, such as: uniform distribution of applied loads, no holes needed as for conventional fasteners, lower structural weight, and a better damage tolerance. Composite materials have found large applications in structural designs, aerospace, aeronautics and automotives, and can be joined successfully and safely using the adhesive bonding technique [1, 2].

Single-lap, double-lap, scarf, and stepped-lap joints are commonly used due to their simple geometries, whereas the strap, butt, butt strap, corner, T-shaped, L-shaped, double-doubler, and tubular lap joints are preferred due to type of applied external load, and orientations of bonded adherends. Some joint configurations are known as *balanced* joints since they do not cause any bending moment, such as double-lap, scarf, butt and stepped-lap joints, whereas others are *unbalanced* joints which cause large rotation and displacements due to the bending moment induced by the eccentricity of the load-axis, such as single-lap, T-shaped, L-shaped, and corner joints. The balanced joints also require simpler analysis methods than the unbalanced joints since the effect of the bending moment is mostly at negligible level [3–5].

In practice, the adhesive joints are expected to serve under static, dynamic, thermal and impulsive (impact) loads. To achieve an optimum design with high strength, light-weight and suitable geometry requires that the adhesion mechanisms and mechanical behaviour of the adhesive joints be understood. In order to predict failure loads of any adhesive joint one needs to know the stress and strain distributions through the adhesive layer as well as in the adherends under a specific type of external load. This requires a mathematical model to be established and solved for displacements, strains and stresses. A complete mathematical model should include some fundamental issues, such as: the mechanical behaviour of materials (adhesive and adherends), the effect of joint geometry on load transfer, the type of external load, the effect of duration of external load, fracture and failure models, etc. A simple mathematical model assumes linear elastic material properties for adhesive and adherends, and a single lap joint is considered for a tensile load and is analysed due to its simple geometry. This stress analysis is a shear-lag analysis, which considers only shear stresses and ignores the normal stresses induced by the bending moment as a result of the load eccentricity [6] or considers them [7].

As the external load is applied the overlap region rotates considerably, and this changes the orientation of the load transfer axis; consequently, there is a nonlinear joint behaviour, which is called *geometrical non-linearity* [8, 9]. Engineering materials, like metals and alloys as well as adhesives, exhibit ductility under applied load; therefore, they can withstand additional increases in external applied load after they begin to deform plastically. However, the stress-strain behaviour is non-linear in this plastic region until the failure load level. This is another type of non-linearity, called *material non-linearity*, that should be considered in the stress analysis [8, 10]. In case the material or/and geometrical non-linearity is/are considered the mathematical model yields non-linear differential equations subjected to linear or non-linear boundary conditions, whereas only linear assumption for geometrical and material behaviours yields linear differential equations. The solution of the non-linear differential equations requires implementation of iterative and corrective solution algorithms,

such as Newton-Raphson and arc-length methods. Another non-linearity arises during the re-contact of the adhesive layer and adherend surfaces, which are separated from each other (interfacial failure). Thus, the adhesive layer and the adherend surfaces are uniformly bonded and the adhesive layer does not contain any internal flaws before the external load is applied; whenever separations occur along the adhesive-adherend interfaces or local fractures occur at any location inside the adhesive layer the separated adhesive or adherend surfaces can contact each other and as a result the members of adhesive joint deform in the manner of large rotations and displacements. The stiffer one of the contacting deformed surfaces affects dominantly the deformation of other surfaces. This is a nonlinearity arising due to *the boundary conditions*, which also includes geometrical nonlinear effects. The surface-to-surface contact or general contact algorithms are generally used to consider these boundary conditions [11, 12].

The analytical methods, such as potential functions, Fourier series, Green functions, Laplace transforms, are used for the closed-form solutions. However, the analytical methods can be used on a limited basis only since the boundary conditions and the joint geometry make the problem more complex. Consequently, the closed-form solutions become possible only by making some assumptions, such as constant stresses across the adhesive thickness. However, the real nature of adhesive joint problem is non-linear and more complex, and all parameters affecting the mechanical response and failure mechanism of the adhesive joint should be taken into account in the mathematical model. This type of mathematical model generates nonlinear differential equations, which can be solved approximately by using the numerical methods, such as the finite element method, the finite difference method, the finite volume method, and the boundary element method. Today, the high performance computers allow to establish and solve numerically the mathematical models in simulating the stress and deformation states of any type of adhesive joint under any load type [13–15].

In general, adhesive joints exhibit interfacial failure, cohesive failure, thin-layer cohesive failure, fiber-tear, light-fiber-tear, stock-break failure, mixed modes (in case of composite adherends) [16]. The damage initiation and propagation through the adhesive layer and adherends require damage models in accordance with the material behaviours determined experimentally. Fracture mechanics offers simple linear elastic fracture models. The toughness values related to elastic energy can be determined in terms of normal and shear deformations at an existing crack tip appearing either along an adhesive-adherend interface or in an adhesive layer, and the crack propagation direction can be determined based on the local mixed mode energy release rate [4]. Alternatively, the stress singularity approach is useful to predict the fracture initiation in case an initial crack does not exist [17, 18]. The progressive damage models are new areas for study of adhesive joints, which allow to model the mechanical responses of the adhesive joints from the initiation of first local failure to the global failure of the adhesive joint [19]. The continuum approach models the damage over a finite region whereas the local approach, *cohesive zone model*, confines the damage to zero volume geometrical entities, such as lines and surfaces. The cohesive zone model can be implemented in case of the progressive damage and failure of an existing crack by specifying a traction-separation rule along the adhesive-adherend interfaces; thus, as the crack opening is increased the tractions reach a limiting level at which the crack initiates and then

these tractions decrease (softening stage), and then the crack propagates. The cohesive zone models differ only in terms of the traction-separation curves, i.e. linear or non-linear paths. The area covered by the traction-separation curve, namely toughness, and a characteristic displacement defined by the failure strain of the cohesive zone are necessary parameters for the cohesive law, which can be determined experimentally [20, 21].

The strength of a specific joint configuration depends on load type, stress distribution, joint geometry, and mechanical properties of joint members. The fundamental stress analysis of a simple lap joint indicates peak shear and normal stresses around the free edges of adhesive-adherend interfaces. The shear stresses are very low in a large area of the overlap region, increase uniformly towards the adhesive free edges, become maximum near the free edges and disappear at the adhesive free edges due to free surface conditions. However, the normal stresses are at peak level at the adhesive free edges and are uniformly low in the middle of overlap region. Consequently, the free edges of adhesive-adherend interfaces are critical regions in which the failure initiation is first expected [22]. The fibre-reinforced composite adherends exhibit high through-thickness stresses around their free edges, but the low through-thickness stiffness and strength of the composite adherends result in failures in the adherends rather than in the adhesive layer; and the adhesive joint fails prematurely [1, 2]. The failure mechanism is more complex for adhesively bonded metal-composite joints since the composite adherends have lower through-thickness stiffness and strength than metal adherends. The strength of adhesive joint is uncertain; therefore, designers tend to use large safety factors. The stress concentrations, especially peel stresses, at the free edges of the adhesive-adherend interfaces should be relieved with some design measures, such as modifying edge geometry of adherends or adhesive composition, size and geometry of adhesive spew fillet. This small modification of adherend edge geometry provides considerable reductions in stress levels. Shaping adherend edges presents two design parameters, such as tapering or scarfing angle and taper edge thickness. Increasing overlap area or length is another solution for reducing stress concentrations around the free edges. To bond adherends a pressure is applied to adherends, and excessive adhesive between adherends is squeezed out. These adhesive secretions around the free edges as well as lateral edges of the adhesive layer are gathered and formed in triangular or bubble shapes. These adhesive spew fillets provide a smooth load transfer between adhesive layer and adherends. Consequently, this smooth geometry transition provides comparatively lower stresses around the adhesive free edges, and the adhesive spew fillets are not removed [23–25].

In practice, the adhesive joints may experience thermal loads, such as a heat flux or prescribed temperature distribution. The heat is transferred from a fluid by convection or from a heat source by radiation to surfaces of the adhesive joint and through the adhesive joint by conduction and thus a uniform or non-uniform temperature distribution appears in the adhesive joint. A non-uniform temperature distribution or non-homogeneous mechanical or thermal material distributions are the origin of thermal stresses in the adhesive joints. Thermal strains on both sides of the adhesive-adherend interfaces are not identical but the total strains are identical. Consequently, internal normal and shear stresses occur, and peak adhesive stresses are observed at the adhesive free edges and along the adhesive-interfaces [26]. The residual thermal stresses may also remain in the adhesive joint after the curing

period of adhesive layer. The structural and thermal loads commonly cause stress concentrations around the adhesive free edges, and similar measures can be applied to relieve the peak stresses under both structural and thermal loads [27, 28].

3.2 Functionally Graded Materials

The peak stresses and strains around the adhesive free edges are the main drawbacks for any geometry of the adhesive joint under both structural and thermal loads. However, the geometrical measures to relieve these peak stresses cause losses in the stiffness and strength of the adhesive joint. The stresses and strains are strongly related to mechanical and thermal behaviour of continuum. The stress and strain levels are dependent on ductility, rigidity, thermal conductivity, and toughness of the material. The stress levels can also be controlled by tailoring the composition variation of adherends as well as adhesive with one or more other constituents. Especially this method is helpful for relieving thermal stresses due to thermal loads. Layered composite materials, which can be joined easily by adhesive bonding technique, have superior thermal and mechanical properties to single-composite material. However, critical stress concentrations, reason for material failure, occur along the bi-material interfaces due to the sharp discontinuities in the material properties. In case an engineering structure experiences a heat flux, the design requires a layer behaving like thermal barrier in front of the heat flux in order to prevent a fast heat transfer at a high gradient and its destructive effect through the remaining part of the material. In addition, a region with high toughness after this thermal barrier will provide a high strength for the structure against static and dynamic loads. Functionally graded materials (FGMs) were proposed to avoid the deficiencies of the layered composite materials. FGMs have been studied extensively since this concept was first introduced by the NKK Corporation in Japan in 1989 when the applications of FGMs to thermal-resistant structures of space shuttles were aimed [29].

The main aim of the functionally graded materials is to achieve performance similar to that of single-phase materials by unifying the best properties of the constituent phases, such as a ceramic phase with poor thermal conductivity and a metal with good toughness. FGMs have continuously varying material composition through one or more dimensions of the substances, such as bar, plate or shell, especially through the thickness. The material composition variation is expected to remove sharp discontinuity along the bi-material interface; consequently, sudden jumps in the thermal stresses induced by different thermal and mechanical properties of the material layers can be relieved. The variable through-thickness material properties, such as coefficient of thermal expansion and modulus, the thickness of the FGM layer between pure-ceramic and pure-metal layers affect the thermal and mechanical behaviours of the FGMs. During the production and service-life of functionally graded materials the environmental thermal conditions result in residual stresses to arise in the FGMs as in the adhesive joints and composite material problems [30, 31]. These thermal stresses can be minimized provided that the thermal and structural properties of both ceramic and metal constituents as well as their volume fraction variations be combined suitably.

The concept of FGMs is relatively new; however, a large number of research investigations have been carried out and this field continues to expand enormously. Many papers on different aspects of FGMs have been published in regular journals as well as in special issues of journals. The mechanical analysis of FGMs is rather difficult since the material microstructure has an arbitrary spatial variation. Two distinct approaches have been implemented so far. The first is the uncoupled micro-macrostructural approach limited to materials with very fine microstructures [32–35]. This approach aims to analyse FGMs at macroscopic level by reducing a given boundary-value problem to a system of differential equations with variable coefficients. The second one is the coupled approach, which takes into account explicitly the effects of microstructural variation and interaction between nonuniformly distributed inclusions [36–39]. This makes possible the analysis of heterogeneous materials with different microstructural scales. The philosophy behind the concept of the functionally graded materials is to smooth or to reduce thermal or structural stress concentrations. This explains easily the relations between functionally graded materials and adhesive bonding technique, and attempts for joining functionally graded adherends by adhesive bonding technique. Therefore, it would be useful to explain the problems arising in the functionally graded materials based on the available pioneering studies.

First, Noda [40] published an extensive review paper discussing the studies on the temperature and thermal stress fields arising in thermal barrier coatings based on the elastic or inelastic material behaviour. Shaw [41] investigated thermal residual stresses on both metal and ceramic faces of through-thickness functionally graded plates when a rapid change in volume fraction occurred near the metal face and showed that a linear compositional gradient resulted in minimum residual stresses for a uniform temperature distribution. Reddy [42] formulated theoretically the stress problem of through-thickness functionally graded plates with the finite element models based on the third-order shear deformation plate theory, which account for the thermomechanical coupling, time dependency, and the von Karman-type geometrical nonlinearity. He showed that the material distribution affected deflections and stresses in the functionally graded plates. Reddy and Cheng [43] studied 3D thermomechanical deformations of simply supported functionally graded rectangular plates for different volume fractions of the ceramic and metallic constituents, and determined that the assumption of a constant through-thickness deflection usually made by 2D plate theories was invalid for the case of the thermal load. Cho and Oden [44] observed different thermal stress characteristics for different material variations and different sizes of a functionally graded layer between ceramic and metal layers. Cho and Ha [45] compared averaging estimation methods with the finite element discretization approach for the thermomechanical properties and responses of dual-phase FGMs, and found that almost all of the averaging estimates produced considerably different stress distributions from those by the finite element discretized models. Cho and Ha [46] also optimized the volume fraction for minimizing thermal stresses in FGMs by using both penalty-function and golden-section methods. Goupee *et al.* [47, 48] proposed a methodology for the multi-objective optimization of material distribution in functionally graded materials with temperature-dependent material properties for steady thermomechanical processes. Bansal and Pindera [34] presented an overview of different approaches employed to

model the thermomechanical response of FGMs, and demonstrated that the higher-order theory is accurate and useful approach for the analysis of FGMs which accounts for micro- and macro-structural coupling. Apalak and Gunes [49] investigated thermal residual stress distributions in functionally graded composite plates having different composition rules with different dual constituents for various thermal fields. The thermal and mechanical properties of constituents had an important role in the stress magnitudes rather than on the profiles of the through-thickness variations of normal and shear stresses. The continuous temperature fields through the plate thickness also resulted in similar normal and shear stress variations.

Shukla *et al.* [50] presented a review of dynamic fracture studies in functionally graded materials and a discussion on the higher-order asymptotic analysis of the transient elastic field surrounding the tip of a dynamically growing crack in a functionally graded material. Birman and Byrd [51] presented a review of the principal developments in functionally graded materials with an emphasis on the work published between 2000–2007 in the diverse areas relevant to various aspects of the theory and applications of FGMs, which included homogenization of particulate FGM, heat transfer issues, stress, stability and dynamic analyses, testing, manufacturing and design, applications, and fracture. Liew *et al.* [52] published a review paper which focuses mainly on the developments of element-free or meshless methods and their applications in the analysis of laminated and functionally graded plates, and is organized as a brief introduction to the plate and shell theories with the first-order and higher-order shear deformation approaches, a review of meshless methods including static and dynamic analyses, free vibration, buckling, and non-linear analyses. Marzocca *et al.* [53] reviewed the state-of-the-art in linear and nonlinear aero-thermo-elasticity of FGM panels with emphasis on their own contributions to this topic. They presented first an overview of the pertinent literature discussing the linear and nonlinear behaviors of flat and curved panels when exposed to high temperature supersonic flow fields, and addressed the effect of material property dependency on temperature, divergence and flutter, and methodologies used to determine these aero-thermo-elastic instabilities. Jha *et al.* [54] presented a critical review of recent research on functionally graded plates, which covers the reported studies in the area of thermo-elastic and vibration analyses of functionally graded plates since 1998. This newest review includes all the important contributions and outlines the critical areas regarding future research needs for a successful implementation of FGMs.

3.3 Constitutive Relations

A graded interlayer (FGM) between the top ceramic-rich and bottom metal-rich surfaces of a bar, plate or shell can reduce and redistribute the stresses. In general, a functionally graded material is designed as a layer with continuous composition variation through a direction, especially through-the-thickness, of, for example, a plate so that a high-temperature resistance on one of the plate surfaces can be provided using the low thermal conductivity of the ceramic constituent. In practice, these structures, such as plates, shells, thick cylinders, can serve under not only thermal loads but also structural loads.

However, an actual functionally graded material consists of ceramic and metal particles with arbitrary shapes mixed up in random dispersion structures whose thermo-mechanical properties are function of the shape and orientation of ceramic and metal particles, the dispersion structure, as well as volume fraction (Figure 3.1). The simple estimation method is the linear rule of mixtures in which a generic material property P at any point Z in the graded region is determined by the linear combination of volume fractions V of ceramic (c) and metal (m) as:

$$P(y) = V_m(y)P_m(y) + V_c(y)P_c(y) \quad (3.1)$$

with

$$V_m + V_c = 1 \quad (3.2)$$

where y is considered the distance along the thickness of the functionally graded plate (Figure 3.2). The mechanical behaviour of FGMs is strongly dependent on the accurate estimation of their modulus of elasticity [45, 46, 55–59]. Here it is assumed that the functionally graded composite plates are composed of a graded layer between homogeneous isotropic ceramic and metal phases. The volume fractions of the metal and ceramic phases at any position y along the thickness of the plate follow the power law as

$$V_m(y) = \left(1 - \frac{y}{t}\right)^n \quad (3.3)$$

and

$$V_c(y) = 1 - V_m \quad (3.4)$$

for a metal-to-ceramic plate where n is compositional gradient exponent, y is distance from the metal-rich bottom face along the direction of the plate thickness, and t is the plate

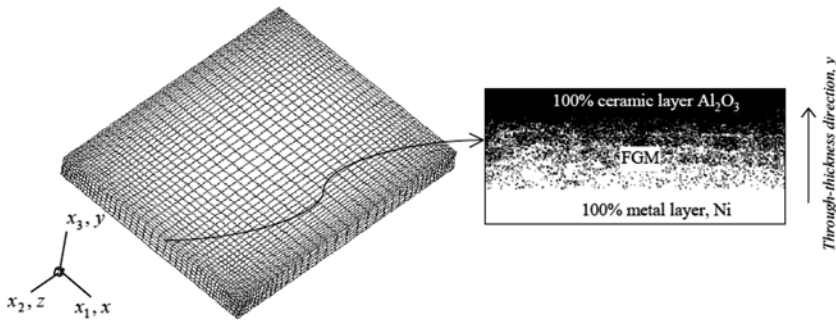


Figure 3.1 The through-thickness composition variation of a functionally graded adherend.

thickness. Tomota *et al.* [58] proposed a modified rule of mixtures for the modulus of elasticity as

$$E(y) = \left[\left(\frac{q + E_c}{q + E_m} \right) V_m E_m + (1 - V_m) E_c \right] \left[\left(\frac{q + E_c}{q + E_m} \right) V_m + (1 - V_m) \right]^{-1} \quad (3.5)$$

where E_m and E_c are moduli of metal and ceramic phases, respectively and the stress-strain transfer ratio is

$$q = \frac{\sigma_c - \sigma_m}{\varepsilon_c - \varepsilon_m} \quad (0 < q < +\infty) \quad (3.6)$$

The choice of value q affects the averaged modulus of elasticity based on the modified rule of mixtures. Thus, for a well dispersed metal- Al_2O_3 composite a value q of 500 GPa is recommended [45]. For the isotropic particulate composites, Wakashima-Tsukamoto [59] expressions require that the overall thermal expansion coefficient for dual-phase materials is related to the averaged bulk modulus using the Levin relation [60]

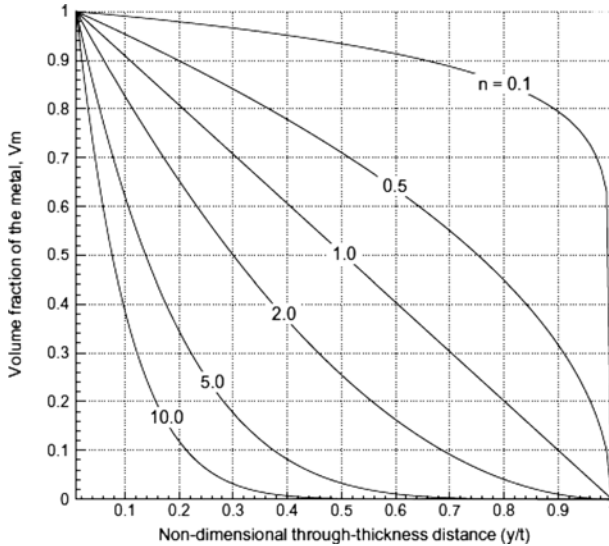


Figure 3.2 The through-thickness variation of metal constituent in the functionally graded region for different compositional gradient exponents, n .

$$\bar{\alpha}(y) = \alpha_m + \frac{\left(\frac{1}{\bar{K}} - \frac{1}{K_m}\right)(\alpha_c - \alpha_m)}{\frac{1}{K_c} - \frac{1}{K_m}} \quad (3.7)$$

and overall Poisson's ratio

$$\bar{\nu}(y) = \frac{3\bar{K} - 2\bar{\mu}}{2(3\bar{K} + \bar{\mu})} \quad (3.8)$$

where the overall bulk modulus \bar{K} is

$$\bar{K}(y) = K_m + \frac{aV_c K_m (K_c - K_m)}{V_m K_c + aV_c K_m} \quad (3.9)$$

and the overall shear modulus $\bar{\mu}$ is

$$\bar{\mu}(y) = \mu_m + \frac{bV_c \mu_m (\mu_c - \mu_m)}{V_m \mu_c + bV_c \mu_m} \quad (3.10)$$

and where a and b are

$$a = \frac{K_c (3K_m + 4\mu_m)}{K_m (3K_c + 4\mu_c)} \quad (3.11)$$

and

$$b = \frac{(1+e)\mu_c}{\mu_m + e\mu_c} \quad (3.12)$$

together with

$$e = \frac{9K_m + 8\mu_m}{6K_m + 12\mu_m} \quad (3.13)$$

The density, ρ , is defined based on the linear rule of mixtures as

$$\rho(y) = V_m \rho_m + V_c \rho_c \quad (3.14)$$

where ρ_m and ρ_c are densities of the metal and ceramic phases, respectively.

In addition, the variations of mechanical properties, such as modulus of elasticity, density and Poisson's ratio, through the thickness of a functionally graded bar, plate or shell are often assumed in exponential form as

$$E(y) = E_0 e^{\beta y} \quad (3.15)$$

$$\rho(y) = \rho_0 e^{\beta y} \quad (3.16)$$

$$\nu(y) = \nu_0 e^{\beta y} \quad (3.17)$$

where E_0 , ρ_0 and ν_0 are modulus of elasticity, density and Poisson's ratio defined along the center plane, and β is a constant describing the variation profiles of mechanical properties.

3.4 Joints with Functionally Graded Adherends

In adhesive joints the concept of functionally grading is used for smoothing/relieving stress distributions, thus, the adherends or the adhesive layer can be produced in the manner of a functionally graded material. First, Ganesh *et al.* [61] proposed that composite materials with continuously varying material properties can be produced by modifying the conventional braiding technology of fiber placement. The local variation of adherend modulus, especially along the overlap region of the adhesive joints, could be possible using an innovative braiding technology. Ganesh and Choo [62] implemented a new concept of adherend modulus grading in order to reduce the peak stress and non-uniform stress distribution in an adhesively bonded single lap joint. They fabricated composite materials with spatially and continuously varying material properties using a new fiber placement technique and reduced gradually the adherend longitudinal modulus from the loaded end to the unloaded end of the adherend. Their comparison of the traditional uniform modulus adherend to adherends with one or two assumed grading profiles showed that reductions in peak stress, especially about 20% in peak shear stress, and more uniform stress distribution in the overlap region were achieved. Boss *et al.* [63] examined the behaviour of single-lap adhesive joints with modulus and geometrically graded adherends. They controlled the modulus grading of the adherend by continuously varying the braid angle and the geometrical grading by varying the adherend thickness in the overlap region. They compared the performance of modulus grading and geometrical grading based on the stress distribution and transverse deformation along the mid-thickness of the adhesive layer. They observed that modulus grading and geometrical grading usually had similar effects whereas the material grading was more effective in reducing the shear stresses for thicker adherends, and showed that both geometrical grading and modulus grading can be combined to evolve an overall better performing adhesively bonded single-lap joints.

Apalak and Gunes [64] investigated three-dimensional elastic stress state of an adhesively bonded single lap joint with functionally graded adherends in tension. The adherends had a functionally graded layer through the adherend thickness between a pure ceramic layer and a pure metal layer. They implemented a layered three-dimensional finite element to the stress problem [65, 66]. Stress concentrations appeared along the free edges of the adhesive layer and through the corresponding adherend zones. The normal stresses and in-plane shear stresses were critical along the adhesive free edges. The normal stress

in the load direction varied uniformly from compression in the ceramic layer to tension in the metal layer through upper adherend thickness and from tension in the ceramic layer to compression in the metal layer through the lower adherend thickness. In the adhesive layer the peak stresses appeared at the free edges of both upper adherend-adhesive interface and the lower adherend-adhesive interface but at different edges. The peel stress varied uniformly through the adhesive thickness and attained peak level at the adhesive interfaces. They indicated that a suitable number of layers was needed through the thickness of layered finite element in order to model functionally graded region accurately, and increasing the ceramic phase in the material composition of the functionally gradient region did not affect the through-thickness profiles of von Mises and normal stresses in the adherends and adhesive, whereas their magnitudes in the ceramic-rich layer of both adherends and along the adherend-adhesive interfaces increased considerably. On the contrary, the layer number and compositional gradient exponent had an evident effect on the through-thickness profiles and magnitudes of the critical stress components in the adherends and adhesive layer of the functionally graded adhesively bonded joints.

Apalak and Gunes [67] also investigated three-dimensional elastic flexural behaviour of an adhesively bonded single lap joint with functionally graded adherends. Their study indicated stress concentrations along the the left free edge of the upper adherend-adhesive interface, the right free edge of the lower adherend-adhesive interface and through the corresponding adherend zones. The normal stress had a linear variation through the adherend thickness which reaches peak values in the ceramic and metal layers, whereas the normal stress in the adhesive layer reaches peak values at the left free edge of the upper adherend-adhesive interface and at the right free edge of the lower adherend-adhesive interface and then decreased uniformly across the adhesive layer towards the other adherend-adhesive interface. In addition, the ceramic-rich functionally gradient region did not affect the through-thickness profiles of both normal and shear stresses in both adherends and adhesive layer but affected the stress magnitudes considerably. The three-dimensional stress analyses of adhesively bonded single lap joints with functionally graded adherends subjected to structural loads, in tension and bending moment, show that the peak stress levels in both adherends and adhesive layer can be controlled by tailoring the through-thickness material composition of the adherends rather than through-thickness stress profiles [64, 67].

Apalak [68] carried out the three-dimensional stress analysis of an adhesively bonded tubular joint with functionally graded tubes in tension using the layered three-dimensional finite elements. In his study the stress concentrations appeared around the free edges of the adhesive layer, and the von Mises stress decreased uniformly through the adhesive thickness from the outer tube-adhesive interface towards the inner tube-adhesive interface. The different composition variations had only a minor effect on the stress profiles through the tube and adhesive thicknesses. However, as the ceramic phase was increased in the material composition of the tubes von Mises stress reached its peak levels. The peak adhesive stresses appeared at the edge of the outer tube-adhesive interface near the free edge of the inner tube and at the edge of the inner tube-adhesive interface near the free edge of the outer tube. Similarly, increasing the ceramic phase in the material composition resulted in higher von Mises stresses along the free edges of the adhesive-tube interfaces. The compositional

variation of the tubes affected only the stress levels rather than stress profiles. Apalak [69] also carried out the three-dimensional stress analysis of an adhesively bonded tubular joint with functionally graded tubes under an internal pressure. He observed that the peak stress concentrations occurred at the free edges of the adhesive-outer and inner tube interfaces, and the material composition variation affected only stress levels and not through-thickness profiles. In addition, the ceramic-rich composition through the tube thickness increased the peak stress levels. In case a suitable functionally graded composition is selected for the tubes of tubular joints both peak stress levels can be reduced reasonably and a uniform stress distribution can be achieved under structural loads, tension or an internal pressure in comparison with those in the tubular joints with uniform modulus and Poisson's ratio distributions [68, 69]. Thus, the concept of functionally graded adherends has superiority over geometrical grading for the tubular joints.

Apalak and Ekici [70] investigated the three-dimensional stress state of an adhesively bonded double containment cantilever joint in tension. The adherend had a functionally graded region, whose through-thickness variation of mechanical properties was defined based on a power law distribution, between ceramic (Al_2O_3) top layer and metal (Ni) bottom layer. In this study stress concentrations appeared inside adhesive fillets along the adhesive free edges, and the peak stresses occurred at the free edges of containment-adhesive interfaces. The compositional gradient considerably affected both through-thickness adherend stress profiles and levels. As the material composition was enriched with the ceramic phase the stress profiles became uniform. They also studied the effects of the geometrical parameters and the compositional gradient on the strain energy of the adhesive joint using the artificial neural networks, and determined the adherend thickness and the compositional gradient exponent as the most dominant design parameters affecting the strain energy. The adhesive thickness, the support length, and thickness were other parameters. They found that an optimum joint design required that the adherend thickness and the adhesive thickness be minimal, the support length and thickness be maximal, and the material composition consist of the constituent with as high modulus as possible. Apalak [71] also investigated the three-dimensional elastic flexural stress state of an adhesively bonded double containment cantilever joint. Similarly, she observed stress concentrations inside the adhesive fillets around the adhesive free edges and that von Mises stress increased uniformly from the adherend half-thickness to both the ceramic and metal layers and reached peak value in the ceramic layer, and increased from the adhesive-metal interface to the adhesive-support interface through the adhesive thickness at the adhesive free edge. A ceramic-rich material composition was found to result in similar smooth through-thickness stress profiles and to reduce large differences between the peak stresses in the ceramic and metal layers. By implementing the artificial neural networks the compositional gradient exponent, the support length and the adherend thickness were determined to affect considerably the elastic strain energy, whereas the adhesive thickness had only minor effect. As the support length was decreased the effect of the adherend thickness became apparent and the support thickness became more effective as the support length was kept constant.

Theotokoglou *et al.* [72] investigated the influence of an adhesive layer in a graded elastic wedge consisted of two subwedges radially bonded by simulating the adhesive layer either

by an interface or by an infinitesimal subwedge of very small wedge angle. They gave the graded character to the wedges either by a linearly varying or by an exponentially varying shear modulus, and analyzed the problem under plane strain and generalized plane stress conditions. Analytical solutions for the stress and displacements were deduced based on the separation of loading in each subwedge and on the continuity of displacements at the interface. Mustapha *et al.* [73] proposed a method for determining the elastic shear and peel stresses in an adhesive joint between a strengthening plate and a functionally graded beam, which was assumed to be isotropic with a constant Poisson's ratio and exponentially-varying elastic modulus through the beam thickness. They found that the inhomogeneities played an important role in the interfacial stress distributions. Their solutions were the basis for establishing simplified FGM theories or a benchmark to assess other approximate methodologies.

In practice, the adhesively bonded joints also serve under thermal loads as well as structural loads. The mismatches of thermal and mechanical properties of adhesive and adherends, non-uniform thermal fields, and non-uniform material distributions through the adherends and adhesive layer are the main reasons for the thermal residual stresses [3–5, 26]. Adhesives with high curing temperatures may cause severe thermal stresses in some low temperature applications. Functionally graded adherends can provide uniform low stress distributions in adherends and adhesive layer. First, Apalak and Gunes [74] investigated three-dimensional thermal residual stress distributions occurring in an adhesively-bonded functionally graded single lap joint subjected to uniform cooling for two boundary conditions: one fixed joint-edge, and two fixed joint edges. The adherends had a functionally graded region between ceramic and metal layers. The normal stress along the joint axis was dominant in the overlap region of the upper and lower adherends and adhesive layer, whereas the in-plane shear stress concentrated around the free edges of adhesive layer. von Mises stress decreased uniformly through the adhesive thickness from compressive in ceramic layer to tensile in metal layer. The two fixed joint edges resulted in much higher stress levels. The compositional variation had only minor effects on the through-thickness von Mises stress profiles but considerably affected the peak stress levels. The free edges of adhesive-adherend interfaces and the corresponding adherend regions were still the most critical regions for thermal loads as for structural load, and the critical peak stresses in adherends and adhesive layer could be reduced by tailoring through-thickness material compositions.

Das *et al.* [75] developed a boundary element method (BEM) capable of including functionally graded materials in order to capture the correct behaviour of underfill material in electronic packages. They coupled the BEM solution with the conventional FEM solution while satisfying the continuity of displacements and equilibrium of tractions along the interfaces in order to use the salient features of both FEM and BEM. Their FEM and BEM analyses covered the thermoelastic deformation involving dissimilar materials exhibiting functional gradation in material properties. They demonstrated the capability of analysis by considering an electronic package consisting of an assembly of dissimilar materials with one component having FGM properties. The gradation of elastic modulus increased the singularity arising from material mismatches, which was not a detrimental effect since the

yield stress of the rich region with silica (silicon dioxide) beads is much higher than that of epoxy. The reduction of the thermal mismatch through the coefficient of thermal expansion produced a weaker singularity.

Apalak *et al.* [76] carried out elastic thermal residual stress analysis on an adhesively bonded functionally graded tubular joint for a uniform temperature drop. In their study the tubes had a functionally graded region between ceramic and metal layers whereas the adhesive layer had a uniform material distribution. The hoop, axial and transverse shear stresses were dominant and concentrated around adhesive free edges, and peak stresses were observed along the left and right free edges of the inner tube-adhesive interface and the left free edge of the outer tube-adhesive interface. The directional material composition variation of both tubes had considerable effect on the stress profiles and levels through the tube thickness in the critical joint regions. However, the material compositional gradient of both tubes had only a minor effect on the stress profiles but not on the stress levels through the tube thickness. The layer number in the tubes also played an important role in the accurate estimation of peak stress values in the ceramic layer of the metal-rich composition and in the metal layer of ceramic-rich composition because of a sudden transition between the two phases in these layers, whereas its effect on through-thickness stress profiles was minor.

Apalak and Bagci [77] investigated the thermal residual stress and deformation states of adhesively bonded in-plane functionally graded clamped plates subjected to different edge heat fluxes by assuming that the material properties of the functionally graded plates varied with a power law along an *in-plane* direction and not through the plate thickness direction. They discretized the transient heat conduction and Navier equations describing the two-dimensional thermo-elastic problem using the finite-difference method, and the set of linear equations was solved using the pseudo singular value method. In this study the material properties of plates near the interfaces affected the adhesive stresses, the compositional gradient of the plates had an important effect on both in-plane temperature distributions, and heat transfer periods. Both plates experienced considerable compressive normal stresses and strains but the shear strains were more apparent. The compositional gradient and compositional direction played important role in the profiles and levels of both stresses and strains. The adhesive layer underwent considerable distortional deformation rather than volumetric deformation. The equivalent stress exhibited small changes through the thickness and along the overlap length. The peak stresses appeared at the free edges of the adhesive-plate interfaces, but the compositional gradient and direction affected the location of the peak stresses along the free edges of the interfaces. Only the adhesively bonded ceramic-metal-adhesive-metal-ceramic plate configuration could achieve the lowest in-plane deformations and stresses in both plates and adhesive layer.

Apalak and Demirbas [78] also investigated the effects of in-plane compositional gradient and composition variation direction on the thermal residual stress and deformations in adhesively bonded functionally graded clamped circular plates subjected to different in-plane heat fluxes. They assumed the material composition to vary with a power law along an *in-plane* direction and not through the plate thickness direction, and discretized the two-dimensional transient heat conduction and Navier equations in polar coordinates using finite-difference method. In this study the composition variation direction was

designed as Ceramic-Metal (CM)-CM, CM-Metal-Ceramic (MC), MC-CM, and MC-MC for the inner and outer plates. The compositional gradient and composition variation direction affected evidently temperature levels and heat transfer periods. The compressive radial and shear strains were more influential on the deformation states of the adhesive layer and of the plate regions near the plate-adhesive interfaces. The adhesive layer experienced considerable shear deformations. The equivalent strain and stresses exhibited sharp peaks, which were influenced by the compositional gradient and direction, on the plate regions near the plate-adhesive interfaces, and decreased towards the adhesive interfaces. The MC-MC and CM-CM joints were determined to result in lower temperature, stress and strain levels around the adhesive layer and along the adhesive interfaces for outer and inner edge heat fluxes, respectively.

In engineering structures, long-term service life of adhesive joints is very important under dynamic loadings as well as static loadings. In order to achieve most efficient designs of adhesively bonded structures, it is essential to understand and improve the dynamic characteristics of adhesive joints. Functionally graded materials can be used to control or improve the dynamic characteristics of adhesive joints. First, Gunes *et al.* [79] carried out three-dimensional free vibration and stress analyses of an adhesively bonded single lap joint with functionally graded adherends using the artificial neural networks combined with the finite element method. In this study the mechanical and physical properties of very thin adhesive layer, such as modulus, Poisson's ratio and density, had only a negligible effect on the first ten natural frequencies and mode shapes of the adhesive joint. However, the design parameters of the adhesive joint, such as the support length, the plate thickness and the compositional gradient exponent, played important role in the natural frequencies, mode shapes and modal strain energies of the adhesive joint, whereas the adhesive thickness had a minor effect. They indicated that the free vibration characteristics of the adhesive joint could be improved by tailoring the material composition of both adherends whilst the dimensions of the adhesive joint are kept constant. Gunes *et al.* [80] also studied the effects of the plate dimensions and the through-thickness compositional gradient and composition variation direction on the three-dimensional free vibration behaviour of adhesively bonded single lap joints with both wide and narrow functionally graded plates. They used the artificial neural networks combined with the finite element method as the analysis tools. The natural frequencies increased with increasing plate thickness or as the through-thickness material composition variation became ceramic-rich. The overlap length had a negligible effect, whereas the natural frequencies decreased suddenly with increasing plate width. For a plate width larger than 50 mm, the natural frequencies became very low and the effect of the other design parameters on the natural frequencies became minor. In case the upper and lower plates had similar or dissimilar material composition variations the mode shapes were affected considerably, and not the natural frequencies. Gunes *et al.* [81] investigated the three-dimensional free vibration behaviour of an adhesively bonded tubular single lap joint with functionally graded regions between ceramic and metal layers through tube thickness. They found the adhesive material properties, such as modulus, Poisson's ratio and density, to have only a minor effect on the free vibration characteristics (first ten mode shapes and natural frequencies) of the adhesive joint since the adhesive layer is very

thin in comparison with tube thickness. They also used the artificial neural networks and the genetic algorithms combined with the finite element method in order to determine the optimal design parameters of the adhesive joint, such as overlap length, inner radius of the inner tube, outer and inner tube thicknesses, and the through-thickness material composition variation, which satisfy both maximum natural frequency and minimum modal strain energy conditions for each mode of the tubular adhesive joint. The outer tube thickness, the inner tube inner radius, and the compositional gradient exponent were found to have considerable effect on the natural frequencies, mode shapes, and modal strain energies of the functionally graded tubular single lap joint, whereas the overlap length and the inner tube thickness had only a minor effect.

Bian *et al.* [82] presented an exact analysis based on the state space formulation to study functionally graded beams integrated with surface piezo-electric actuators and sensors. They considered the effect of adhesive layer by modelling the adhesive layer between the host beam and the piezoelectric layers by a spring layer. Perfect or imperfect bonding conditions were applied by different models of spring layer. The imperfect bonding between FGM beam and piezoelectric actuator and sensor layers led to a reduction in global stiffness of the integrated beam by the increase of deflection and the decrease of natural frequency.

Yan *et al.* [83] proposed an analytical model of a cracked functionally graded beam with attached Lead Zirconate Titanate (PZT) actuator/sensors for structural health monitoring. The model considered the dynamic behaviour of the piezoelectric patches and included a viscoelastic law to describe the bonding imperfection between piezoelectric patches and the functionally graded beam. They found that some parameters such as adhesive viscosity, the shear-lag parameter, and the gradient index of the beam material-composition have remarkable effects.

3.5 Functionally Graded Adhesives

In order to relieve high stress concentrations at the free edges of the overlap region and to have more uniform stress distributions, an adhesive layer with variable modulus has been proposed. This requires at least the use of two adhesives with different mechanical and thermal properties as the adhesive layer. This is a primitive approach for the functionally graded adhesive layer.

First, Hart-Smith [84] extended the elastic solution of Volkersen considering adhesive plasticity, adherend stiffness imbalance, and thermal mismatch between the adherends. He devoted a significant effort to the concept of using a high-modulus adhesive in the central region of the joint and low-modulus adhesive in the outer regions where the relative displacements between the adherends exceed the strain capabilities of the high-modulus adhesives. He found that this concept had no practical merit in comparison to a ductile adhesive alone while it did offer advantages over a brittle adhesive alone, and by softening the end zones of the joint an increase in strength was obtained. Srinivas [85] showed that the maximum peel and shear stresses in the bond-line could be reduced by using a combination of flexible and stiff adhesives for single-lap, flush and double-lap joints, and advised a flexible and ductile adhesive around the free edges of the overlap region, where the peak

stress occurs, and a rigid and brittle adhesive in the middle of overlap region, where low stresses exist uniformly. The National Materials Advisory Board of the National Research Council [86] proposed an adhesive joint with various adhesives, called graded seal concept, using one or more thin adhesive layers of suitably modified properties in order to reduce the stress concentrations. They expected this concept to be beneficial for bonded adherends with dissimilar coefficients of thermal expansion, and also aimed to reduce the peak adhesive shear stresses using a more ductile adhesive at the free edge of the less stiff adherend. Pires *et al.* [87] used two adhesives with different stiffnesses along the overlap region of an adhesive lap joint where a stiff adhesive was applied in the middle portion of the overlap and a less stiff adhesive was applied towards the edges prone to stress concentrations. Their experimental, linear and nonlinear analyses indicated a measurable increase in strength of the bi-adhesive bonded joints in comparison to those in which single adhesives were used over the full length of the bondline. Fitton and Broughton [88] described a practical method for joint optimisation using an adhesive layer with variable modulus. They achieved significant changes in the failure modes and improvement in the joint strength of lap joints in comparison to a single-modulus adhesive which is typically used to bond unidirectional carbon fibre-reinforced plastics. They achieved most significant improvements in the joint strength whereas failure occurred in un-optimised single adhesive joints at stresses considerably less than the shear strength of the adhesive, and were dominated by peel stresses. However, an improvement was not achieved for the adhesive joints which are subjected to a pure shear loading. Temiz [89] applied bi-adhesive concept to double-strap joints subjected to bending moments in order to reduce stress concentrations around the adhesive free edges with an expectation to increase the failure load levels of the adhesive joint. He used a stiff adhesive in the middle portion of the overlap and a flexible adhesive around the free edges of the overlap region, and his results showed that the adhesive joints with two different adhesives carried higher loads and had higher strength as compared to single-adhesively-bonded joints.

The concept of using multi-modulus adhesives can provide improvements in the overall joint strength. This concept can also be implemented to the thermal stress problems of the adhesive joints to withstand low and high temperatures. First, Hart-Smith [84] recognized the use of a mixed adhesive joint for low and high temperature applications. Thus, a high-temperature adhesive (HTA) in the middle of the overlap region keeps the strength by transferring the entire load, whereas a low temperature adhesive (LTA) withstands loads at the low temperatures by causing the high temperature adhesive to undergo moderate stress levels. da Silva and Adams [90] investigated theoretically Hart-Smith's proposition by assessing if a mixed adhesive joint could achieve an increased load bearing capacity over a single and a double lap joint with an HTA alone. They found that the mixed adhesive joint decreased the stresses in the HTA at low temperatures in comparison to a joint with an HTA alone; thus the higher the modulus of the LTA, the more was the decrease, and recommended that for low modulus LTAs, in order to decrease further the stresses in the HTA, the free ends of the overlap could be stiffened by reducing locally the bondline thickness. In case dissimilar adherends are bonded they pointed out two factors: the stiffness unbalance and the residual thermal stress unbalance, and the classic mixed adhesive joint design,

with an LTA at both ends of the overlap, could be modified so that the LTA is located only on the critical bondline edge. Their main predictions were that for identical adherends, the mixed modulus concept was of little benefit to the joint strength; however, for metal/composite joints, there was a real improvement, especially if the difference in coefficients of thermal expansion was large. da Silva and Adams [91] also investigated experimentally if a mixed adhesive joint was advantageous as predicted [90]. Based on their experiments for titanium/titanium and titanium/composite double lap joints, as a joint with dissimilar adherends, the combination of two adhesives gave a better performance (increased load capacity) over the temperature range than a high temperature adhesive alone. They also showed that mixed adhesive joints could be used at low temperatures after a period at high temperatures. da Silva and Lopes [92] examined the improvements in the strength of single lap joints using a brittle adhesive in the middle of the overlap and three different ductile adhesives of increasing ductility at the free ends of the overlap region. They pointed that this concept gave joint strength improvements compared to a brittle adhesive alone; and for a mixed adhesive joint to be stronger than the brittle adhesive and the ductile adhesive used individually, the load carried by the brittle adhesive was higher than that carried by the ductile adhesive.

Vallee *et al.* [93] studied the influence of stress reduction methods, such as adhesive rounding, chamfering and adhesive grading, on the strength of adhesively bonded joints with brittle adherends. They found that the peak adhesive stresses did not dictate the overall strength of the joints with brittle adherends made of fibre reinforced polymers and timber due to adherend failures. Their experimental work allowed a better insight into the relation between stress reduction and strength increase.

The concept of functionally graded adhesive implies, in fact, that one or more material properties, such as modulus, Poisson's ratio, or coefficients of thermal expansion and thermal conduction, are altered along one or more coordinate directions based on a distribution law: power or exponential. This concept is purely theoretical; consequently, today's production methods are not suitable for this new type of material. The bi-adhesive or mixed joint concepts are early stages of the concept of functionally graded adhesive but are convenient for production purposes. First, Kumar [15, 94] aimed to reduce the peak adhesive stresses around the free edges of bondline by employing a modulus graded adhesive layer in a tubular adhesive joint. The adhesive joint had similar or dissimilar adherends and a functionally modulus graded bondline, which was identified by smooth and continuous functions. The peel and shear stress peaks in the functionally modulus graded bondline were much smaller and stress distributions along the overlap region were more uniform than those of mono-modulus bondline adhesive joints. He indicated that the peel and shear strengths could be optimized by spatially controlling the adhesive modulus. Kumar and Pandey [95] carried out two- and three-dimensional nonlinear (geometric and material) finite element analyses of adhesively bonded single lap joints having modulus-graded bondline under monotonic loading conditions by modelling adhesives as an elasto-plastic multi-linear material and the substrates as both linear elastic and bi-linear elasto-plastic material. The static strength was higher for joints with bi-adhesive bondlines compared to those with single adhesives in bondline, and a higher joint strength was possible for an optimum bi-adhesive bondline

ratio. Their 3D analysis results revealed the existence of complex multi-axial stress/strain state at the free ends of the adhesive layer which cannot be observed in 2D plane strain analysis, and in-plane global stiffness of the joint was unaffected by modulus gradation of the adhesive layer. Kumar and Scanlan [96] investigated the stress state and strength improvement of a shaft-tube bonded joint with similar and dissimilar adherends and a functionally modulus graded bondline. The peel and shear peak stresses in the joint with a functionally modulus graded bondline were much lower and their distributions along the overlap region were more uniform than those of the joint having a conventional mono-modulus bondline. Kumar and Scanlan [97] presented an improved analytical model for the stress analysis of interface stiffness graded axisymmetric adhesive joints, composed of similar and dissimilar polar anisotropic and/or isotropic adherends and a functionally modulus graded bondline adhesive. The reductions in shear and normal stresses were predicted in comparison to the mono-modulus bondline model. Their model was applicable to examine the effects of loss of interface stiffness due to an existing defect and/or damage in the bondline.

Functionally graded adhesives have some potential drawbacks. Hart-smith [84] identified the first two: i) using the ductile adhesive alone may provide small gains, but this may be inadequate when the production difficulties are considered, ii) during manufacturing the stiff adhesive may tend to displace the ductile adhesive under the applied pressure; therefore, the bonded joint may be worse off than using the ductile adhesive alone. Aboudi *et al.* [98] investigated the response of the metal matrix composites designed in the manner of a functionally graded structure to the external load variations, and determined that a functionally graded structure may lose its usefulness in smoothing stress distributions in case of a sudden change in the direction and magnitude of the applied external load. Stapleton *et al.* [99, 100] aimed to increase the understanding of both bi-adhesive and non-stepwise functionally graded adhesives to make them a more viable, realistic, and advantageous choice for actual application in composite structures. They analysed the stress state of a butt-end joint with constant (single adhesive), discrete (bi-adhesive), linear and exponential modulus graded adhesives using a special adhesive finite element, and addressed the issue of adhesive flow during bonding by showing the sensitivity of the functionally graded adhesives to the gradation profiles, and later questioned if varying loading conditions for a specific gradation profile had detrimental effects on the stress state of adhesive joint. As long as the stress magnitude gradient in the adhesive remained unchanged under different loading conditions the adhesive joints may become a perfect application area for material grading. The grading was still optimum under different loading cases.

The concept of functionally graded materials with the adhesive bonding technique has also been applied successfully in bio-inspired dental multilayers. Unlike conventional crown structures in which ceramic crowns are bonded to the ground with an adhesive layer, real teeth do not have a distinct adhesive layer between the enamel and the dentin layers. Niu *et al.* [101] were inspired by the stress reduction associated with the functionally graded structures of the dentin-enamel junctions in natural teeth. They proposed a graded transition from enamel to dentin, a 10 to 100 μm thick regime, and used a micro-scale, bio-inspired functionally graded structure to bond the ceramic layer to a dentin-like ceramic-filled epoxy substrate. They found the bio-inspired functionally graded material to exhibit

higher critical failure loads. Du *et al.* [102] idealized the ceramic crown structures under occlusal contact as flat multilayered structures consisting of a crown-like ceramic top layer, an adhesive layer and a dentin-like substrate. Their bio-inspired design of adhesive layer is composed of functionally graded multilayers that mimic the dentin-enamel junction in natural teeth. Later, they examined the effects of FGM layer architecture on the contact-induced deformation of bio-inspired dental multilayers using the finite element method. They fabricated a layered nanocomposite structure by sequential rolling of micro-scale nanocomposite materials with local moduli that increase from the side near the soft dentin-like polymer composite foundation to the side near the top ceramic layer. They found that the loading rate dependency of the critical failure loads can be well predicted by a slow crack growth model, which integrates the actual mechanical properties obtained from nanoindentation experiments.

Nature offers many examples related to graded materials to reduce stress concentrations along the material interfaces. Tendon-to-bone joints are one of these examples, whose graded material properties allow more even stress distributions across the joint. Genin *et al.* [103] developed a model for the tendon-to-bone insertion similar to a functionally graded interface between tendon and bone formed by the human body. This model assumed a gradual and continuous change in: i) the orientation distribution of collagen fibers, and ii) the relative concentration of the organic and inorganic tissue constituents. Mineral volume fraction varied approximately linearly across the tendon-to-bone insertion. Their model can explain how tendon-to-bone attachment was achieved through a functionally graded material composition. Liu *et al.* [104] concentrated on the material mismatch at the attachment of tendon to bone, which is a tensile connection in nature, and studied especially functional grading of transitional tissue between tendon and bone. Liu *et al.* [105] also showed that stress concentrations, in the attachment of tendon to bone due to the greatest interfacial material mismatches in nature, could be reduced by a biomimetic grading of material properties, and suggested a new approach to functional grading for minimization of stress concentrations at interfaces.

3.6 Conclusions

Functionally graded materials appear in nature with a role of reducing stress concentrations along bi-material interfaces. Biological interfaces, such as dentin-enamel junction or tendon to bone, are best examples of the concept of functionally graded materials. In adhesive bonding process, the designers may apply the concept of functionally graded material to adherends and/or adhesive layer in order to reduce stress concentrations appearing along the adherend-adhesive interfaces. The adhesive joints serve under static, dynamic and thermal loads; therefore, as this concept was first discussed some drawbacks were asserted as: serious production difficulties, and detrimental effects on strength in case external load type was varied. Today, functionally graded materials can be produced and applied successfully to many engineering structures, especially to reduce thermal stress concentrations or to distribute these stresses uniformly. In case of adhesive joints with functionally graded adherends and single adhesive the present theoretical studies indicate that the stress

concentrations occurring at the free edges of the adhesive layer due to mechanical and thermal loads can be reduced and controlled by varying the material composition of adherends near the adherend-adhesive interfaces or through thickness of adherends. In case a functionally graded adhesive layer is included for adhesive joint with similar/dissimilar adherends the earlier method was to use bi-adhesives along the bondline: a ductile adhesive with low stiffness around the free edges experiencing peak stresses and a brittle adhesive with high stiffness in the middle region of bondline. As far as reducing the peak stress concentrations or achieving a uniform stress distribution is concerned the experimental and theoretical studies show that this method is successful only for adhesive joints with dissimilar adherends and only a small benefit is achieved for similar adherends. The penetration of adhesives with low and high stiffness due to the pressure applied to adherends during joining operation needs to be controlled, otherwise the results do not serve the purpose of using bi-adhesives. New theoretical analyses concentrate on the use of a continuous material grading, such as modulus or coefficient of thermal expansion, along one or two coordinate directions of the adhesive material, and improved strength for adhesive joints was achieved by controlling stress concentrations with an existing optimum material grading rule. However, the material grading distribution rules are not practical right now for production purposes. Consequently, the concept of functionally graded materials is still in the development stage, and needs much theoretical and experimental (if possible) studies which consider material non-linearity, viscoelasticity of adhesive layer, etc.

References

1. F.L. Matthews, P.P.F. Kilty, and E.W. Godwin, A review of the strength of joints in fiber-reinforced plastics: Adhesively bonded joints. *Composites* 13, 29–37 (1982).
2. M.D. Banea and L.F.M. da Silva, Adhesively bonded joints in composite materials: An overview. *Proc. Institution Mechanical Engineers, Part L: J. Mater. Design Appl.* 223, 1–18 (2009).
3. R.D. Adams and W.C. Wake, *Structural Adhesive Joints in Engineering*, Elsevier Applied Science, London (1984).
4. A.J. Kinloch, *Adhesion and Adhesives*, Chapman and Hall, London (1987).
5. L. Tong and G.P. Steven, *Analysis and Design of Structural Bonded Joints*, Kluwer Academic Publishers, Boston (1999).
6. O. Volkersen, Die Niekraftverteilung in Zugbeanspruchten mit Konstanten Laschenquerschnitten. *Luftfahrtforschung* 15, 41–68 (1938).
7. M. Goland and E. Reissner, The stresses in cemented lap joints. *Trans. ASME, J. Appl. Mech.* 11, A17–A27 (1944).
8. J.A. Harris and R.D. Adams, Strength prediction of bonded single lap joints by non-linear finite element methods. *Intl. J. Adhesion Adhesives* 4, 65–78 (1984).
9. U. Edlund and A. Klarbring, A geometrically nonlinear model of the adhesive joint problem and its numerical treatment. *Comput. Method. Appl. Mech. Eng.* 96, 329–350 (1992).
10. U. Edlund and A. Klarbring, Analysis of elastic and elastic-plastic adhesive joints using a mathematical programming approach. *Comput. Method. Appl. Mech. Eng.* 78, 19–47 (1990).
11. O. Allix and A. Corigliano, Geometrical and interfacial non-linearities in the analysis of delamination in composites. *Intl. J. Solids Struct.* 36, 2189–2216 (1999).

12. J. Mackerle, Finite element analysis of fastening and joining: A bibliography (1990–2002): A review. *Intl. J. Pressure Vessel Piping* 80, 253–271 (2003).
13. L.F.M. da Silva, P.J.C. das Neves, R.D. Adams, and J.K. Spelt, Analytical models of adhesively bonded joints-Part I: Literature survey. *Intl. J. Adhesion Adhesives* 29, 319–330 (2009).
14. L.F.M. da Silva, P.J.C. das Neves, R.D. Adams, A. Wang, and J.K. Spelt, Analytical models of adhesively bonded joints-Part II: Comparative study. *Intl. J. Adhesion Adhesives* 29, 331–341 (2009).
15. S. Kumar, Modeling of cylindrical joints with a functionally graded adhesive interlayer, in: *Advances in Modeling and Design of Adhesively Bonded Systems*, S. Kumar and K.L. Mittal (Eds.), pp 47–86, Wiley-Scrivener, Beverly MA, USA (2013).
16. ASTM D 5573–99. Standard practice for classifying failure modes in fiber-reinforced-plastic (FRP) joints. Annual Book of ASTM Standards, 15.03 (2002).
17. H.L. Groth, Stress singularities and fracture at interface corners in bonded joints. *Int. J. Adhesion Adhesives* 8, 107–113 (1988).
18. D.M. Gleich, M.J.L. VanTooren, and A. Beukers, Analysis and evaluation of bondline thickness effects on failure load in adhesively bonded structures. *J. Adhesion Sci. Technol.* 15, 1091–1101 (2001).
19. M.E.S.F. de Moura and J.A.G. Chousal, Simulation of bonded joints failure using progressive mixed-mode damage models, in: *Advances in Modeling and Design of Adhesively Bonded Systems*, S. Kumar and K.L. Mittal (Eds.), pp 147–170, Wiley-Scrivener, Beverly MA, USA (2013).
20. Z.J. Zhang and G.H. Paulino, Cohesive zone modeling of dynamic failure in homogeneous and functionally graded materials. *Intl. J. Plasticity* 21, 1195–1254 (2005).
21. C.Y. Hui, A. Ruina, R. Long, and A. Jagota, Cohesive zone models and fracture. *J. Adhesion* 87, 1–52 (2011).
22. R.D. Adams and J.A. Harris, The influence of local geometry on the strength of adhesive joints, *Intl. J. Adhesion Adhesives* 7, 69–80 (1987).
23. M.Y. Tsai and J. Morton, The effect of a spew fillet on adhesive stress distributions in laminated composite single-lap joints. *Composite Struct.* 32, 123–131 (1995).
24. A.R. Rispler, L. Tong, G.P. Steven, and M.R. Wisnom, Shape optimisation of adhesive fillets. *Intl. J. Adhesion Adhesives* 20, 221–231 (2000).
25. B. Kilic, E. Madenci, and D.R. Ambur, Influence of adhesive spew in bonded single-lap joints. *Eng. Fract. Mech.* 73, 1472–1490 (2006).
26. M.K. Apalak, Non-linear thermal stresses in adhesive joints, in: *Modeling of Adhesively Bonded Joints* L.F.M. da Silva and A. Oechsner (Eds.), pp 243–278, Springer-Verlag, Heidelberg (2008).
27. R. Kaye and M. Heller, Through-thickness shape optimisation of typical double lap-joints including effects of differential thermal contraction during curing. *Intl. J. Adhesion Adhesives* 25, 227–238 (2005).
28. K. Zhang, Z. Yang, and Y. Li, A method for predicting the curing residual stress for CFRP/Al adhesive single-lap joints. *Intl. J. Adhesion Adhesives* 46, 7–13 (2013).
29. M. Koizumi, FGM activities in Japan. *Composites Part B* 28, 1–4 (1997).
30. M. Takemura, A. Yoshitake, H. Hayakaurad, T. Hyakubu, and M. Tamura, Mechanical and thermal properties of FGM fabricated by thin lamination method. in: Proceedings of the 1st Int. Symposium on Functionally Graded Materials Forum, pp. 97–100 (1990).

31. A. Yoshitake, M. Tamura, I. Shito, and M. Niino, Fabrication of the functionally graded materials: The state of the art, in: Proceedings of ESA (European Space Agency) Symposium on Space Applications of Advanced Structural Materials, pp. 103–108 (1990).
32. M.J. Pindera, J. Aboudi, and S.M. Arnold, Limitations of the uncoupled, RVE-based micromechanical approach in the analysis of functionally graded composites, *Mech. Mater.* 20, 77–94 (1995).
33. Y. Bansal and M.J. Pindera, Efficient reformulation of the thermoelastic higher-order theory for FGMs, NASA CR 211909, NASA-Glenn Research Center, Cleveland, OH (2002).
34. Y. Bansal and M.J. Pindera, Efficient reformulation of the thermoelastic higher-order theory for functionally graded materials. *J. Thermal Stresses* 26, 1055–1092 (2003).
35. Y. Zhong and M.J. Pindera, Efficient reformulation of HOTFGM: Heat conduction with variable thermal conductivity, NASA CR 211910, NASA-Glenn Research Center, Cleveland, OH (2002).
36. J. Aboudi, M.J. Pindera, and S.M. Arnold, Thermoelastic response of large-diameter fiber metal matrix composites to thermal gradients, NASA TM 106344, NASA-Lewis Research Center, Cleveland, OH (1993).
37. J. Aboudi, M.J. Pindera, and S.M. Arnold, Higher-order theory for functionally graded materials, *Composites B* 30, 777–832 (1999).
38. M.J. Pindera and J. Aboudi, A coupled higher-order theory for cylindrical structural components with bi-directionally graded microstructures, NASA CR 210350, NASA-Glenn Research Center, Cleveland, OH (2000).
39. J. Aboudi, S.M. Arnold, and B.A. Bednarczyk, *Micromechanics of Composite Materials: A Generalized Multiscale Analysis Approach*, Butterworth-Heinemann, Oxford UK (2013).
40. N. Noda, Thermal stresses in functionally graded materials, *J. Thermal Stresses* 22, 477–512 (1999).
41. L.L. Shaw, Thermal residual stresses in plates and coatings composed of multi-layered and functionally graded materials. *Composites Part B* 29, 199–210 (1998).
42. J.N. Reddy, Analysis of functionally graded plates. *Int. J. Numer. Meth. Eng.* 47, 663–684 (2000).
43. J.N. Reddy and Z.Q. Cheng, Three-dimensional thermomechanical deformations of functionally graded rectangular plates. *Eur. J. Mech. A/Solids* 20, 841–855 (2001).
44. J.R. Cho and J.T. Oden, Functionally graded material: A parametric study on thermal-stress characteristics using the Clark-Nicolson-Galerkin scheme. *Comput. Method. Appl. Mech. Eng.* 188, 17–38 (2000).
45. J.R. Cho and D.Y. Ha, Averaging and finite element discretization approach in the numerical analysis of functionally graded materials. *Mater. Sci. Eng. A* 302, 187–196 (2001).
46. J.R. Cho and D.Y. Ha, Volume fraction optimization for minimizing thermal stress in Ni-Al₂O₃ functionally graded materials. *Mater. Sci. Eng. A* 334, 147–155 (2002).
47. A.J. Goupee, J.R. Cho, D.Y. Ha, and S.S. Vel, Two-dimensional optimization of material composition of functionally graded materials using meshless analyses and a genetic algorithm. *Comput. Method. Appl. Mech. Eng.* 195, 5926–5948 (2006).
48. A.J. Goupee, J.R. Cho, D.Y. Ha, and S.S. Vel, Multi-objective optimization of functionally graded materials with temperature-dependent material properties. *Mater. Design* 28, 1861–1879 (2007).
49. M.K. Apalak and R. Gunes, Thermal residual stress analysis of Ni-Al₂O₃, Ni-TiO₂ and Ti-SiC functionally graded composite plates subjected to various thermal fields. *J. Thermoplast. Composites* 18, 119–152 (2005)
50. A. Shukla, N. Jain, and R. Chona, A review of dynamic fracture studies in functionally graded materials. *Strain* 43, 76–95 (2007).

51. V. Birman and L.W. Byrd, Modeling and analysis of functionally graded materials and structures. *Appl. Mech. Rev.* 60, 195–216 (2007).
52. K.M. Liew, X. Zhao, and A.J.M. Ferreira, A review of meshless methods for laminated and functionally graded plates and shells. *Composite Struct.* 93, 2031–2041 (2011).
53. P. Marzocca, S.A. Fazelzadeh, and M. Hosseini, A review of nonlinear aero-thermo-elasticity of functionally graded panels. *J. Thermal Stresses* 34, 536–568 (2011).
54. D.K. Jha, T. Kant, and R.K. Singh, A critical review of recent research on functionally graded plates. *Composite Struct.* 96, 833–849 (2013).
55. T. Reiter, G.J. Dvorak, and V. Tvergaard, Micromechanical models for graded composite materials. *J. Phys. Solids* 45, 1281–1302 (1997).
56. T. Reiter and G.J. Dvorak, Micromechanical models for graded composite materials: II. Thermomechanical loading. *J. Phys. Solids* 46, 1655–1673 (1998).
57. M. Grujicic and Y. Zhang, Determination of effective elastic properties of functionally graded materials using Voronoi cell finite element method. *Mater. Sci. Eng. A* 251, 64–76 (1998).
58. Y. Tomota, K. Kuroki, T. Mori, and T. Tamura, Tensile deformation of two-ductile-phase alloys: Flow curves of α - γ Fe-Cr-Ni alloys. *Mater. Sci. Eng.* 24, 85–94 (1976).
59. K. Wakashima and H. Tsukamoto, Mean-field micromechanics model and its application to the analysis of thermomechanical behaviour of composite materials. *Mater. Sci. Eng. A* 146, 291–316 (1991).
60. V.M. Levin, On the coefficients of thermal expansion of heterogeneous materials. *Mech. Tverdops Tela* 2, 88–94 (1967).
61. V.K. Ganesh, S. Ramakrishna, and H.J. Leck, Fiber reinforced composite based functionally gradient materials. *Adv. Composites Lett.* 7, 111–115 (1998).
62. V.K. Ganesh and T.S. Choo, Modulus graded composite adherends for single-lap bonded joints. *J. Composite Mater.* 36, 1757–1767 (2002).
63. J.N. Boss, V.K. Ganesh, and C.T. Lim, Modulus grading versus geometrical grading of composite adherends in single-lap bonded joints. *Composite Struct.* 62, 113–121 (2003).
64. M.K. Apalak and R. Gunes, Investigation of elastic stresses in an adhesively bonded single lap joint with functionally graded adherends in tension. *Composite Struct.* 70, 444–467 (2005).
65. S. Ahmad, B.M. Irons, and O.C. Zienkiewicz, Analysis of thick and thin shell structures by curved finite elements. *Int. J. Numer. Method. Eng.* 2, 419–451 (1970).
66. S.M. Yunus and P.C. Khonke, An efficient through-thickness integration scheme in an unlimited layer doubly curved isoparametric composite shell element. *Int. J. Numer. Method. Eng.* 28, 2777–2793 (1989).
67. M.K. Apalak and R. Gunes, Elastic flexural behaviour of an adhesively bonded single lap joint with functionally graded adherends. *Mater. Design* 28, 1597–1617 (2007).
68. M.K. Apalak, Elastic stresses in an adhesively bonded functionally graded tubular single lap joint in tension. *J. Adhesion Sci. Technol.* 20, 1019–1046 (2006).
69. M.K. Apalak, Stress analysis of an adhesively bonded functionally graded tubular single lap joint subjected to an internal pressure. *Sci. Eng. Composite Mater.* 13, 183–211 (2006).
70. Z.G. Apalak and R. Ekici, Elastic stresses in an adhesively bonded functionally graded double containment cantilever joint in tension. *J. Reinf. Plast. Composites* 26, 1291–1318 (2007).
71. Z.G. Apalak, Elastic flexural stresses in an adhesively bonded functionally graded double containment cantilever joint. *J. Thermoplast. Composites* 23, 35–56 (2010).
72. E.E. Theotokoglou, I.H. Stampoulglou, and G.H. Paulino, An analytical approach for an adhesive layer in a graded elastic wedge, *Mech. Adv. Mater. Struct.* 17, 393–405 (2010).

73. M. Mustapha, B. Samir, T. Abdelouahed, E.A.A. Bedia, and M. Slimane, Interfacial stresses in plated beams with exponentially-varying properties. *J. Adhesion Sci. Technol.* 24, 1063–1081 (2010).
74. M.K. Apalak and R. Gunes, Thermal residual stresses in an adhesively bonded functionally graded single lap joint. *J. Adhesion Sci. Technol.* 20, 1295–1320 (2006).
75. M. Das, I. Guven, and E. Madenci, Coupled BEM and FEM analysis of functionally graded material layers. *J. Thermal Stresses* 29, 263–287 (2006).
76. M.K. Apalak, R. Gunes, and S. Eroglu, Thermal residual stresses in an adhesively bonded functionally graded tubular single lap joint. *Intl. J. Adhesion Adhesives* 27, 26–48 (2007).
77. M.K. Apalak and M.D. Bagci, Thermal residual stresses in adhesively bonded in-plane functionally graded plates subjected to an edge heat flux. *J. Adhesion Sci. Technol.* 25, 1861–1908 (2011).
78. M.K. Apalak and M.D. Demirbas, Thermal residual stresses in adhesively bonded in-plane functionally graded clamped circular hollow plates. *J. Adhesion Sci. Technol.* 27, 1590–1623 (2013).
79. R. Gunes, M.K. Apalak, and M. Yildirim, The free vibration analysis and optimal design of an adhesively bonded functionally graded single lap joint. *Int. J. Mech.Sci.* 49, 479–499 (2007).
80. R. Gunes, M.K. Apalak, M. Yildirim, and I. Ozkes, Free vibration analysis and adhesively bonded single lap joints with wide and narrow functionally graded plates. *Composite Struct.* 92, 1–17 (2010).
81. R. Gunes, M.K. Apalak, and M. Yildirim, Free vibration analysis of an adhesively bonded functionally graded tubular joint. *J. Adhesion* 87, 902–925 (2011).
82. Z.G. Bian, C.W. Lim, and W.Q. Chen, On functionally graded beams with integrated surface piezoelectric layers. *Composite Struct.* 72, 339–351 (2006).
83. W. Yan, J. Wang, W.Q. Chen, and W.C. Li, Electromechanical impedance response of a cracked functionally graded beam with imperfectly bonded piezoelectric wafers. *J. Intelligent Materials Systems Structures* 22, 1899–1912 (2011).
84. L.J. Hart-Smith, Adhesive-bonded double-lap joints. NASA CR 112235, NASA Langley Research Center, Hampton, Virginia (1973).
85. S. Srinivas, Analysis of bonded joints. NASA TN D-7855, NASA Langley Research Center, Hampton, Virginia (1975).
86. The National Materials Advisory Board of the National Research Council, in *Treatise on Adhesion and Adhesives: Structural Adhesives with Emphasis on Aerospace Applications*. Vol. 4, R.L. Patrick (Ed.), Marcel Dekker, New York (1976).
87. I. Pires, L. Quintino, J.F. Durodola, and A. Beevers, Performance of bi-adhesive bonded aluminium lap joints. *Intl. J. Adhesion Adhesives* 23, 215–223 (2003).
88. M.D. Fitton and J.G. Broughton, Variable modulus adhesives: An approach to optimised joint performance. *Intl. J. Adhesion Adhesives* 25, 329–336 (2005).
89. S. Temiz, Application of bi-adhesive in double-strap joints subjected to bending moment. *J. Adhesion Sci. Technol.* 20, 1547–1560 (2006).
90. L.F.M. da Silva and R.D. Adams, Adhesive joints at high and low temperatures using similar and dissimilar adherends and dual adhesives. *Intl. J. Adhesion Adhesives* 27, 216–226 (2007).
91. L.F.M. da Silva and R.D. Adams, Joint strength predictions for adhesive joints to be used over a wide temperature range. *Intl. J. Adhesion Adhesives* 27, 362–379 (2007).
92. L.F.M. da Silva and M.J.C.Q. Lopes, Joint strength optimization by the mixed-adhesive technique. *Intl. J. Adhesion Adhesives* 29, 509–514 (2009).
93. T. Vallée, T. Tannert, J. Murcia-Delso, and D.J. Quinn, Influence of stress-reduction methods on the strength of adhesively bonded joints composed of orthotropic brittle adherends. *Intl. J. Adhesion Adhesives* 30, 583–594 (2010).

94. S. Kumar, Analysis of tubular adhesive joints with a functionally modulus graded bondline subjected to axial loads, *Intl. J. Adhesion Adhesives* 29, 785–795 (2009).
95. S. Kumar and P.C. Pandey, Behaviour of bi-adhesive joints. *J. Adhesion Sci. Technol.* 24, 1251–1281 (2010).
96. S. Kumar and J.P. Scanlan, Stress analysis of shaft-tube bonded joints using a variational method. *J. Adhesion* 86, 369–394 (2010).
97. S. Kumar and J.P. Scanlan, On axisymmetric adhesive joints with graded interface stiffness, *Intl. J. Adhesion Adhesives* 41, 57–72 (2013).
98. J. Aboudi, M.J. Pindera, and S.M. Arnold, Elastic response of metal matrix composites with tailored microstructures to thermal gradients. *Int. J. Solids Struct.* 31, 1393–1428 (1994).
99. S.E. Stapleton, A.M. Waas, and S.M. Arnold, Functionally graded adhesives for composite joints. NASA TM-2011–217202, NASA Glenn Research Center, Cleveland, Ohio (2011).
100. S.E. Stapleton, A.M. Waas, and S.M. Arnold, Functionally graded adhesives for composite joints. *Intl. J. Adhesion Adhesives* 35, 36–49 (2012).
101. X. Niu, N. Rahbar, S. Farias, and W. Soboyejo, Bio-inspired design of dental multilayers: Experiments and model. *J. Mechanical Behavior Biomedical Materials* 2, 596–602 (2009).
102. J. Du, X. Niu, N. Rahbar, and W. Soboyejo, Bio-inspired dental multilayers: Effects of layer architecture on the contact-induced deformation. *Acta Biomaterialia* 9, 5273–5279 (2013).
103. G.M. Genin, A. Kent, V. Birman, B. Wopenka, J. D. Pasteris, P.J. Marquez, and S. Thomopoulos, Functional grading of mineral and collagen in the attachment of tendon to bone. *Biophys. J.* 97, 976–985 (2009).
104. Y. Liu, V. Birman, C. Chen, S. Thomopoulos, and G.M. Genin, Mechanisms of bimaterial attachment at the interface of tendon to bone. *J. Eng. Mater. Technol.* 133, 011006 (2011).
105. Y.X. Liu, S. Thomopoulos, V. Birman, J.S. Li, and G.M. Genin, Bi-material attachment through a compliant interfacial system at the tendon-to-bone insertion site. *Mech. Mater.* 44, 83–92 (2012).

Synthetic Adhesives for Wood Panels: Chemistry and Technology

A. Pizzi

*LERMAB, University of Lorraine, Epinal, France King Abdulaziz University,
Jeddah, Saudi Arabia*

Abstract

Synthetic polycondensation adhesives have dominated for the last 80 years, and still dominate, the field of wood panel bonding. They constitute about 50%–60% by volume of all adhesives produced in the world today. This review presents through their chemistry and technology the main categories of adhesives, namely urea-formaldehyde adhesives, melamine- and melamine-urea-formaldehyde adhesives, phenolic adhesives and isocyanate adhesives and their most recent industrial modifications.

Keywords: Wood panel adhesives, urea-formaldehyde, melamine-formaldehyde, melamine-urea-formaldehyde, phenol-formaldehyde, isocyanates

4.1 Introduction

A number of different adhesives are used for wood panels manufacture. Among these thermosetting adhesives based on the use of formaldehyde-based resins obtained by polycondensation have dominated the field for many decades, many of these being used mainly for their application to wood and wood fibre panel products of all types. The field is divided into formaldehyde-based adhesives, which even to-day constitute the majority of wood and wood fiber adhesives, and other products which have been adopted relatively recently in this field, namely isocyanates.

Formaldehyde-based thermosetting resins constitute more than 50% by volume (NB: not by value) of all the adhesives used today, in all fields included (not just wood). Thus, resins such as urea-formaldehyde (UF), phenol-formaldehyde (PF), melamine-formaldehyde (MF) and melamine-urea-formaldehyde (MUF), resorcinol-formaldehyde and other minor ones constitute today, with some notable exceptions, a low margin commodity products

*Corresponding author: antonio.pizzi@univ-lorraine.fr

produced in large quantities. The reason for such a wide use is mainly their relative ease of manufacture and the relatively low plant investment necessary to produce such resins. This apparent ease belies the high technology that is built in such resins; newcomers to this field can be easily deceived by the apparent simplicity of their chemistry and of their preparation. While their basic chemistry and technology is well understood, the development of applicable formulations acceptable to today's sophisticated markets is not an easy matter.

In the form in which they are delivered these adhesive resins are mainly liquid and consist mainly of linear or branched oligomeric and polymeric molecules in an aqueous solution or dispersion. During hardening and gelling they convert irreversibly into insoluble and non-melting three-dimensionally crosslinked networks. The hardening conditions used can be acidic (for aminoplastic resins such as those based on urea and melamine), or highly alkaline (phenolic resins).

The consumption of thermosetting formaldehyde-based wood adhesives, in North America and Europe in 1997 and 1999, respectively, based on resin solids, are as shown in Table 4.1.

Besides their main application as wood panel adhesives, other major fields of application for these adhesives are as foundry sand binders, and for the impregnation and bonding of paper with PF and MF resins to obtain laminates. There are other applications of these resins, other than as adhesives, such as their use to prepare rigid foams, for temperature-resistant binders for break lining, and many others.

From a purely technical point of view these resins have evolved during the last few decades to yield

- highly reactive adhesives with quick gelling and hardening behaviour and steep increase in bonding strength even at a low degree of chemical curing

Table 4.1 Estimated consumption of wood adhesives resin solids in North America and Western Europe.

Polymer type	North America*	Western Europe**	Total
	kTons	kTons	kTons
Urea-formaldehyde (UF)	960	2600	3560
Melamine-urea-formaldehyde (MUF)	–	350	350
Phenol-formaldehyde (PF)	567	260	827
Phenol-resorcinol-formaldehyde (PRF)	12	6	18

*1997

**1999

- highly reactive adhesive mixes by inclusion of additives such as accelerators, special hardeners, crosslinkers and others
- lower cost resins while maintaining the same performance, or even improving it.
- more environmentally acceptable adhesives

Thus, the minimization of the content of expensive melamine in exterior-grade MUF-resin, and the development of some fast-curing alkaline PF resols are conspicuous examples of these trends.

The impact of the resins on various environmental aspects, such as waste water and effluents, emission of noxious volatile chemicals (such as formaldehyde) during the production and from the finished boards, has been also an important concern in the last couple of decades and for the future which is of increasing importance for these resins. The emission of formaldehyde was a matter of concern in the past, a problem that has now been solved and solved well, as also possibly the effluent discharge of free phenols or other monomers.

It is necessary here to introduce the principal types of wood panels that are produced in this industry. The following types of wood panels are commercially produced: particleboard (*flakeboard* and *waferboard* are different products with slightly different chips dimensions. These terms are mostly used in North America and not in Europe), Medium Density Fibreboard (MDF), Oriented Strand Board (OSB), hardboard (high density fibreboard), plywood and Laminated Veneer Lumber (LVL).

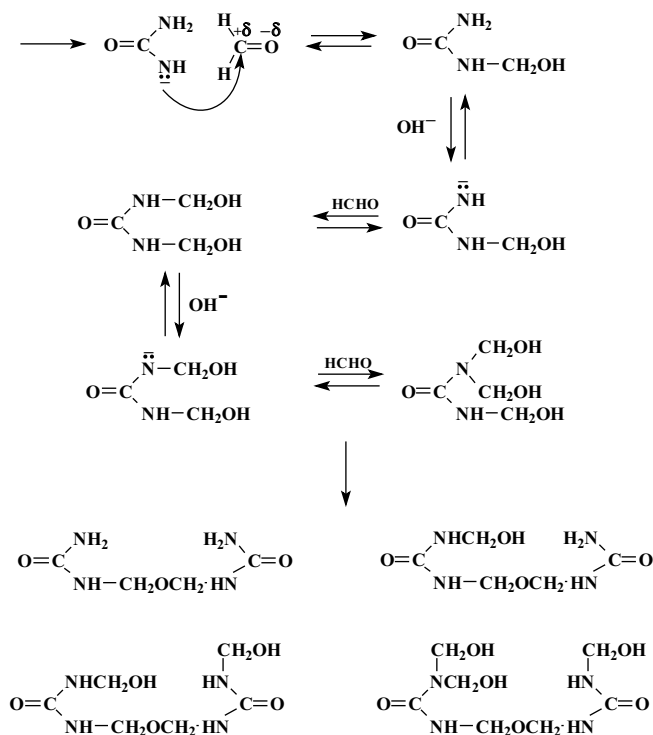
4.2 Urea-formaldehyde (UF) Adhesives

Urea-formaldehyde resins [1–11] are based on a multitude of reactions between urea and formaldehyde. Using different conditions of reaction and preparation innumerable condensed structures are possible. UF-resins are thermosetting resins and are constituted of a mix of linear or branched oligomers and polymers, always containing also some amount of monomers. Non-reacted urea is often desirable to achieve special effects, e.g. a better storage stability. Free formaldehyde, however, can have an ambivalent role. On the one hand it is necessary to induce the hardening reaction, while on the other hand it causes a certain amount of formaldehyde emission during hot pressing of the panel. At times, even in the hardened state some residual formaldehyde leads to some unpleasant subsequent emission from the finished boards. This concern has significantly changed UF-resins composition and preparation during the last 20 years. The problem of formaldehyde emission has now been solved for the last 10 years at least and stringent formaldehyde emission regulations are in place in most parts of the world.

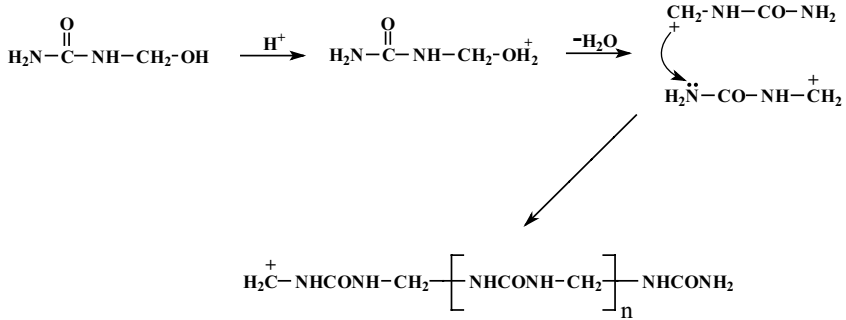
The reaction between urea and formaldehyde is complex. The combination of these two chemical compounds results in both linear and branched polymers, as well as three-dimensional networks in the cured resin. This is due to a functionality of 4 in urea (due to the presence of four replaceable hydrogen atoms) (in reality urea is only trifunctional as tetramethylol urea has never been isolated, except in the formation of substituted urons [1, 2, 11]) and a functionality of 2 in formaldehyde. The most important factors determining

the properties of the reaction products are (1) the relative molar proportion of urea and formaldehyde, (2) the reaction temperature, and (3) the pH value at which condensation takes place. These factors influence the rate of increase of the molecular weight of the resin. Therefore, the characteristics of the reaction products differ considerably when lower and higher condensation stages are compared, especially with respect to solubility, viscosity, water retention, and rate of curing of the adhesive. These all depend, to a large extent, on molecular weights.

The reaction between urea and formaldehyde is divided into two stages. The alkaline condensation to form mono-, di-, and trimethylolureas, (tetramethylolurea has never been isolated). The second stage is the acid condensation of the methylolureas, first to soluble and then to insoluble cross-linked resins. Under alkaline reaction conditions the reaction of urea and formaldehyde at room temperature leads to the formation of methylolureas. When condensed, they form methylene-ether links between the urea molecules. Under alkaline reaction conditions mono- and dimethylolureas are formed, as follows:



The methylolureas formed copolymerize by acid catalysis and produce polymers followed by highly-branched and cured networks, as shown below



The formation of monomethylolurea in weak acidic or alkaline aqueous solutions is characterized by an initial fast phase followed by a slow bimolecular reaction [12, 13]. The first reaction is reversible. The subsequent reaction of the methylolureas leads to methylene urea oligomers. The rate of reaction varies according to the pH with a minimum rate of reaction in the pH range 5 to 8 for a urea/formaldehyde molar ratio of 1: 1 and at a pH of 6.5 for a 1:2 molar ratio [8].

The rapid initial addition reaction of urea and formaldehyde is followed by a slower condensation, which results in the formation of polymers [14]. The rate of condensation of urea with monomethylolurea to form methylenebisurea (or UF "dimer") is also pH dependent. It decreases exponentially from a pH of 2 to 3 to neutral pH value. No condensation occurs at alkaline pH values.

The initial addition reaction of formaldehyde to urea is reversible and is subject to general acid and base catalysis. The forward methylation reaction is reported to have an activation energy of 13 kcal/mol while the reverse demethylation reaction has an activation energy of 19 kcal/mol [13]. Other sources report values of 17.5 and 17.1 kcal/mol for the same reactions respectively [7]. Thus, the inverse reaction of decomposition of the methylolureas will limit somewhat the proportion of methylolated urea obtained, the reaction going to completion only as methylolated ureas react to form dimers and higher oligomers when the pH is lowered in the condensation phase. If the reaction is stopped before the condensation phase a calculation of the degree of advancement of the reaction of methylation of urea under alkaline conditions [15] indicates that at equilibrium under the conditions used, 60% of the urea is present as methylol ureas. This compares well with a degree of conversion of 65%, at the equilibrium, of the more reactive melamine extrapolated from reported kinetic values [16] under the same reaction conditions. The reaction may eventually proceed to even higher degrees of conversion, even in alkaline environment, only as a consequence of the subsequent formation of methylene ether-linked oligomers.

The rates of incorporation into the urea molecule of one, two, and three methylol groups have been estimated to be in the ratio 9:3:1 respectively. The amount of N,N' -dimethylolurea from monomethylolurea is three times that of monomethylolurea from urea.

Methylenebisurea and higher oligomers undergo further condensation with formaldehyde [17] and monomethylolurea [18], behaving like urea. The capability of methylenebisurea to hydrolyze to urea and methylolurea in weak acid solutions (pH 3 to 5) indicates the reversibility of the amidomethylene link and its lability under weak acidic moist conditions. This explains the slow release of formaldehyde over a long period in particleboard and other wood products manufactured with UF resins.

After hardening, UF-resins consisting of insoluble, more or less three-dimensional, networks cannot be melted or thermoformed again. At their application stage UF-resins are still soluble or dispersed in water or spray dried powders, which, however, in most cases are redissolved and redispersed in water for application.

Notwithstanding that UF-resins consist mainly or only of urea and formaldehyde, a broad variety of possible reactions and structures in the resins can be obtained. At the molecular level the basic characteristics of UF-resins can be enumerated as follows:

- their high reactivity
- their waterborne behaviour, which renders the resins ideal for use in industry
- the reversibility of the aminomethylene link, which also explains the low resistance of the UF-resins against the influence of water and moisture, especially at higher temperatures, this being also one of the reasons for their subsequent formaldehyde emission.

The commercial preparation of UF resins is basically a two-step process, usually an alkaline methylation followed by an acidic condensation. The methylation step, which usually is performed at high molar ratio ($F/U = 1.8$ to 2.5), involves the addition of up to three (four in theory) molecules of the bifunctional formaldehyde to one molecule of urea to give the so-called methylolureas.

The UF-resin itself is formed in the acid condensation step, where the same high molar ratio as in the alkaline methylation step is used ($F/U = 1.8$ to 2.5): the methylolureas, urea and the residual free formaldehyde react to form linear and partly branched molecules with medium and even higher molar masses, forming polydispersed UF-resins composed of oligomers and polymers of different molar masses. Molar ratios lower than approx. 1.7 – 1.8 during this acid condensation step might cause resin precipitation.

The low molar ratio of the final UF-resin is adjusted by the addition of the so-called second urea, which might also be added in several steps [1–3, 9, 11, 19]. This last reaction step generally also includes the vacuum distillation of the resin solution to the usual 63%–66% solid content syrup and in this form the resin is delivered. Industrial preparation procedures are usually proprietary and are described in literature only in a few cases [1–3, 10, 11].

The types of bridges existing between the urea molecules of the resin depend on the conditions used, with methylene ether bridges ($-\text{CH}_2-\text{O}-\text{CH}_2-$) as well as the more stable methylene bridges ($-\text{CH}_2-$) being formed in different relative proportions according to the conditions used. Methylene ether bridges rearrange with relative ease to methylene bridges with emission of one molecule of formaldehyde. One ether bridge needs two formaldehyde molecules and also it is not as stable as a methylene bridge; hence, it is highly recommended to avoid and minimize when possible the proportion of such ether groups in UF-resins.

Formaldehyde emission from the finished bonded products is due to, on the one hand, the residual formaldehyde present as a gas in the wood and recesses of UF-bonded and MUF-bonded products as well as dissolved in the wood residual moisture content. On the other hand, the hydrolysis of weakly bonded formaldehyde from *N*-methylolgroups, acetals and hemiacetals, as well as in more severe cases of hydrolysis (e.g. at high relative humidity or higher temperatures) from methylene ether bridges, increases further the content of emittable formaldehyde. Contrary to phenolic and polyphenolic resins where an emission problem does not occur, in aminoplastic resins a permanent stream of supplementary, emittable formaldehyde is generated from these weakly bonded structures. This explains the constant, although nowadays low, release of formaldehyde from UF-bonded wood based panels even over long periods. However, it depends on the conditions whether this excess emittable formaldehyde leads to unpleasantly high emissions or not. The higher the hydrolysis rate, the higher is the proportion of formaldehyde which contributes to the subsequent formaldehyde emission from the wood panel. The so-called E1-emission class describes a product presenting formaldehyde emission which is low enough not to cause any danger, irritation or inflammation of the eyes, nose and mouth mucous membranes.

In the literature, various other types of resin binders preparation procedures are described, e.g. those yielding uron structures [11, 20, 21].

In the UF-resin itself the following chemical species are present:

- free formaldehyde, which is in steady state equilibrium with the remaining methylol groups and the post-added urea
- monomeric methylols, which have been formed mainly by the reaction of the post-added urea with the high content of free formaldehyde at the still high molar ratio in the acid condensation step
- oligomeric methylols, which have not reacted further in the acid condensation reaction or which have been formed by the above-mentioned post-added urea reaction
- molecules with higher molar masses, which are the main resin molecules.

The condensation reaction and the increase of the molar mass can also be monitored by gel permeation chromatography (GPC) [22]. With longer duration of the acid condensation step, oligomers of higher molar masses are progressively formed and the GPC peaks are shifted to lower elution volumes.

Forced by the necessity to limit the subsequent formaldehyde emission, the F/U molar ratio in UF resins has been progressively decreased to very low values. The main differences between UF-resins with high and with low content of formaldehyde are

- reactivities of the resin due to the different contents of free formaldehyde and
- different degrees of crosslinking in the cured network.

For example, a UF-resin for particleboard at the end of the 1970s would have had an F/U molar ratio of approx. 1.6–1.8. Today a UF resin for the same application has a molar ratio of between 1.02–1.08, and cases in which molar ratios as low as 0.95, or even slightly lower, are used are also known [9]. However, the requirements for the boards as given in the quality standards are still the same. Besides the degree of crosslinking of the cured resins, also the rate of hardening depends on the availability of free formaldehyde in the system.

Depending on the type of board and the manufacturing process applied, it is sometimes recommended to use a UF-resin with a low F/U molar ratio (e.g. F/U = 1.03), hence low content of free formaldehyde; while sometimes the use of a resin with a higher molar ratio (e.g. F/U = 1.10) and the addition of a formaldehyde catcher/depressant will give better results [8]. Which of these two, or other possible approaches, is a better one in practice can only be decided in each case by trial and error.

The higher the F/U molar ratio, the higher is the content of free formaldehyde in the resin. Assuming stable conditions in the resins, this means that post-added urea has enough time to react with the resin; the content of free formaldehyde is very similar even for different preparation procedures. As a rough estimate the content of free formaldehyde in a UF-resin is approx. 0.1% at F/U = 1.1 and 1% at F/U = 1.8 [22–24]. It also decreases with time, in storage, due to this free formaldehyde reacting further with urea.

There is a large variety of hybrid resins to which the same emission considerations as for UFs can be applied, these being melamine fortified UF-resins, MUFs, MUPFs, and PMFs. In UF-resins the methylene bridge is susceptible to hydrolysis and is, therefore, not stable at higher relative humidity, especially at elevated temperatures [25]. The influence of water also causes degradation of the UF-resin with greater devastating effect with the higher temperature of the water in which the boards are immersed. Hardened UF-resins can also be hydrolyzed under the influence of humidity or water, due to the weak bonding between the nitrogen of the urea and the carbon of the methylene bridge, especially at higher temperatures. During this reaction, formaldehyde can be liberated [26, 27]. The amount of this liberated formaldehyde can be taken under certain circumstances as a measure of the resistance of a resin against hydrolysis. The main parameters on which resin hydrolysis depends are the temperature, pH, and the degree of hardening of the resin [24]. Especially the acid which had induced the hardening of the resin can also induce its hydrolysis. Resin hydrolysis also leads to a loss of bonding strength. The degree of melamine fortification and especially the way in which melamine is incorporated in the resin can be very different. The

different resistance of formaldehyde polycondensation resins against hydrolysis is due to their differences in behaviour at molecular level. The chemical bond between the nitrogen of the urea or the melamine and the carbon of the methylolgroup can be easily cleaved in UF resins but not so easily in MF resins. In the latter case this is mainly due to the conjugated double bonds of the quasi-aromatic triazine ring of melamine. The methylene bridges connecting phenolic nuclei in phenolic resins are instead very stable against hydrolytic attack and hence are not subject to hydrolysis, making PF resins the only true exterior formaldehyde-based thermosetting resins. The melamine fortified products are much more expensive due to the manyfold price increase of melamine in recent years compared to urea. The content of melamine in these resins, therefore, is always as high as absolutely necessary but as low as possible.

Melamine can also be added to a UF resin in the form of melamine salts like acetates, formiates or oxalates [28–31], which decompose in the aqueous resin mix only at higher temperatures and enable considerable savings of melamine for the same degree of water resistance compared to traditionally prepared MUF resins. These salts can act additionally as hardeners.

Another approach to increase the resistance of UF-resins against hydrolysis is based on the fact that the acid hardening of the resin causes residue of acids or acidic substances in the bondline. Myers [32] pointed out that in the case of an acid hardening system the decrease in the durability of the adhesive bonds can be initiated by the hydrolysis of the wood cell wall polymers adjacent to the bondline as well as by an acid-catalyzed resin degradation in the case of UF-bonded products. A neutral bondline, therefore, should show a distinctly higher hydrolysis resistance. The amount of hardener (acids, acidic substances, latent hardeners) therefore always should be adjusted to the desired hardening conditions (press temperature, press time and other parameters) and never follow “the more the better”. Just the opposite is the case: too high an addition of hardener can cause brittleness of the cured resin and a very high acid residue level in the bondline.

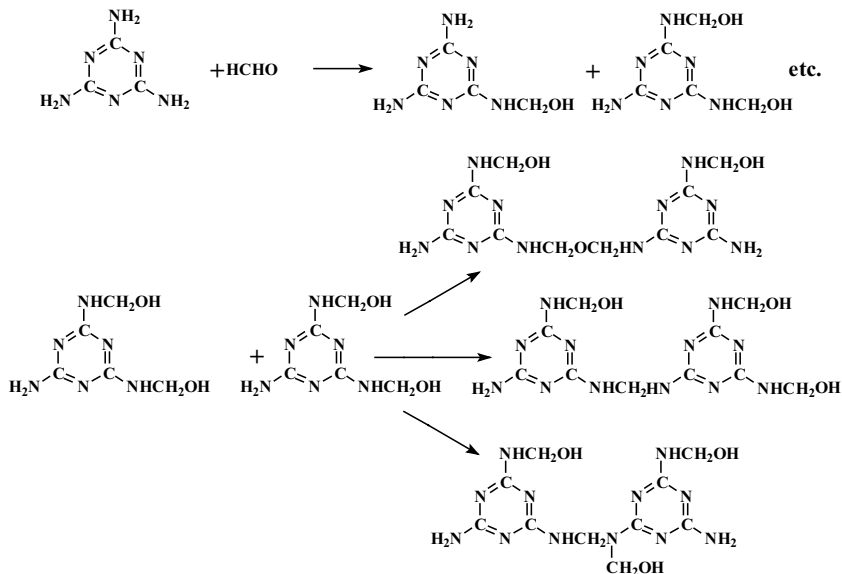
All UF, MF and MUF resins are used with addition of small amounts of hardeners. For UF resins these are salts such as ammonium sulphate and ammonium nitrate, used alone or in combination with small amounts of a carboxylic acid, mainly, but not only, formic acid. The acid generated by the decomposition of the salt at higher temperature during hot-curing, and by the simultaneous volatilization of ammonia, causes a marked and rapid decrease of pH inducing acid-hardening of the resin.

4.3 Melamine-formaldehyde (MF) and Melamine-urea-formaldehyde (MUF) Adhesives

UF resins are mainly used for interior products. Resins of higher hydrolysis resistance can be obtained by reacting melamine with formaldehyde to obtain MF resins. Today, due to the high cost of melamine, pure MF resins are not used anymore as adhesives; resin engineering has achieved the same results by using melamine-urea-formaldehyde (MUF) adhesives

with M:U weight ratios varying from 30:70 up to 50:50, and even as low as 20:80 in some less demanding applications,.

The condensation reaction of melamine with formaldehyde is similar to the reaction of formaldehyde with urea. It differs only in the much faster rate of reaction for melamine. As for urea, formaldehyde first attacks the amino groups of melamine, forming methylol compounds. The reaction proceeds according to the following scheme:

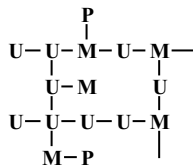


However, formaldehyde addition to melamine occurs more easily and completely than does addition to urea. The amino group in melamine accepts easily up to two molecules of formaldehyde. Thus a complete methylation of melamine is possible, which is not the case with urea [1]. Up to six molecules of formaldehyde are attached to a molecule of melamine. The methylation step leads to a series of methylol compounds with two to six methylol groups. Hydrophobic intermediates of the MF condensation appear early in the reaction. Another important difference is that MF condensation to give resins, and their curing, can occur not only under acid conditions, but also under neutral or even slightly alkaline conditions. The mechanism of the further reaction of methylol melamines to form hydrophobic intermediates is the same as for UF resins, with splitting off of water and formaldehyde. Methylene and ether bridges are formed and the molecular size of the resin increases rapidly. These intermediate condensation products constitute a large proportion of the commercial MF resins. The final curing process transforms the intermediates to the desired insoluble and infusible MF resins through the reaction of amino and methylol groups which are still available for reaction.

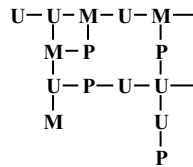
A simplified schematic formula of cured MF resins has been given by Koehler [33] and Frey [34]. They emphasize the presence of many ether bridges besides unreacted methylol groups and methylene bridges. This is because in curing MF resins at temperatures up to 100°C, no substantial amounts of formaldehyde are liberated. Only small quantities are liberated during curing up to 150°C. However, UF resins curing under the same conditions liberates a great deal of formaldehyde.

With regard to melamine-urea-formaldehyde, copolymers can be prepared which are generally used to reduce the cost of MF resins, but which also show some worsening of properties. Copolymerization was confirmed by means of model compounds and polycondensates [35]. MUF resins obtained by copolymerization during the resin preparation stage are superior in performance to MUF resins prepared by mixing pre-formed UF and MF resins, especially because processing of such mixtures is quite difficult [36]. The relative mass proportions of melamine to urea used in these MUF resins is generally in the range 50:50 to 30:70 [37].

Another type of resin also used today are the so-called PMUF (or MUPF depending on which author is writing) adhesives. These are fundamentally MUF resins in which a minor proportion of phenol (between 3% and 10%, P:M:U by weight of 10:30:60 just as an example) has hopefully coreacted with the MUF resin to further upgrade weather resistance of the bonded joint. Unfortunately, the alleged superior performance of such resins is often only wishful thinking as the phenol frequently does not react with the MUF resin, and consequently the PMUF resin will have a worse performance than an MUF resin. Analysis of the molecular structure of these resins in both their uncured and cured states appeared to show that often no co-condensates of phenol and melamine form and that these two separate resins coexist. This is due to the difference in reactivity of the phenolic and melamine methylol groups as a function of pH. This was confirmed by the demonstration that it depends exclusively on the resin manufacturing parameters, and materials reaction order used whether the phenol coreacts or not within many PMUF adhesives. This shows that often the phenol remains as a useless pendant group in the hardened aminoplastic (MUF) network without contributing at all to its performance [38, 39] or even stays unreacted as shown below;



**P pendant without
contribution to the
network
+ P unreacted**



P included in the network

The best reaction order necessary to obtain PMUF resins in which phenol contributes positively to the improved performance of the hardened network has also been defined [38]. PMUF resins are still used, and some good resins of this type do indeed exist. It is, however, unrealistic to expect that they will outperform equivalent MUF resins. It has been shown clearly that they perform at best as an MUF adhesive containing the same number of moles of melamine for the total moles of phenol plus melamine of the PMUF itself. The idea that the addition of small percentages of phenol to an MUF resin yields resins of better exterior durability is then incorrect, a myth even today perpetuated in the industry. They are also more expensive than equivalent MUF resins. Newer formulations of MUF resins always outperform the corresponding PMUF. PMUFs are not bad resins, they are simply resins in which one of the materials, phenol, is often wasted for no purpose.

Melamine can also be added in the form of melamine salts like acetates, formiates or oxalates to a UF resin or to an MUF resin to upgrade their melamine content and their exterior performance [28–31]. These salts decompose in the aqueous resin mix only at higher temperatures and enable considerable savings of melamine for the same degree of water resistance compared to traditionally prepared MUF resins. These salts can act additionally as hardeners.

The necessary melamine content in the resin depends on various parameters, e.g. the type of wood particle size, the pressing parameters (pressure profile, density distribution) and the percent resin load on wood; it can vary between a few percents up to more than 30%, based on liquid resin. Due to the considerable costs, the content of melamine must always be only as high as absolutely necessary but as low as possible. Other important parameters are the preparation procedure of the resin, which considerably influences the thickness swelling of the boards even at the same board resin content and the same content of melamine.

The production of melamine-fortified UF-resins and of MUF-resins can follow various paths:

- i. cocondensation of melamine, urea and formaldehyde in a multistep reaction [40–44]. A comprehensive study of various reaction types has been done by Mercer and Pizzi [37]. They especially compared the sequence of the additions of melamine and urea.
- ii. mixing of an MF-resin with a UF-resin according to the desired composition of the resin ([45, 46]
- iii. addition of melamine in various forms (pure melamine, MF/MUF-powder resin, melamine acetates or other salts) to a UF-resin during the application of the glue mix. In the case of the addition of pure melamine the UF-resin must have a rather high molar ratio, otherwise there is not enough formaldehyde available to react with the melamine in order to incorporate it into the resin [28, 29, 31, 47].
- iv. the addition of acetals such as ethylal and others [48–50] to upgrade the performance of aminoplastic resins has also been reported.

- v. The use of buffers to improve the performance of MUF resins to the level of PF resins and beyond has also been shown, with considerable advantages both in improved performance and considerable savings in the proportion of melamine used for the purpose [51–53]

The higher is the content of melamine, the higher is the stability of the hardened resin against the influence of humidity and water (hydrolysis resistance) [2]. This concept, however, is only valid for MUF resins prepared according to traditional ways. New resin engineering, especially with points (iii) and (v) above, has revolutionized the understanding of the field and in light of this the above concept has been proven incorrect. In short, traditional manufacturing approaches to MUF resins waste, for no purpose, considerable proportions of the melamine added [31, 54].

MUPF-resins (PMUF-resins) are mainly used for the production of so-called V100-boards according to standards DIN 68763 and EN 312–5 and EN 312–7. They contain only small amounts of phenol. Production procedures are described in patents and in the literature [55–59].

PMF-resins usually contain only little or no urea at all. The analysis of the molecular structure of these resins has shown that there is no cocondensation between the phenol and the melamine, but that there are two distinct networks [60–63]. The reason for this is the different reactivity of the phenol and the melamine methylols, depending on the existing pH.

During the curing process of a thermosetting adhesive resin a three-dimensional network is built up. This yields an insoluble resin which is not longer thermoformable. The hardening reaction is the continuation of the acid condensation step of the manufacturing process during resin production. The acid hardening conditions can be adjusted (i) by the addition of a so-called latent hardener or (ii) by the direct addition of acids (maleic acid, formic acid, phosphoric acid and others) or of acidic substances, which dissociate in water (e.g. aluminium sulphate). Common latent hardeners are ammonium sulphate and ammonium chloride. The latter one, however, has not been in use in the particleboard and MDF industry for several years because of the generation of hydrochloric acid during combustion of wood based panels causing corrosion problems, because of the suspected formation of dioxins and due to the need to decrease chlorides pollution of the environment which is now severely limited by government regulations. Ammonium sulfate reacts with the free formaldehyde in the resin to generate sulphuric acid, which decreases the pH; this low pH and hence the acidic conditions so generated enable the condensation reaction to start again, resulting finally in the gelling and hardening of the resin. The rate of the pH decrease depends on the amount of available free formaldehyde and of hardener and is greatly accelerated by heat [64, 65].

MUPF/PMUF-resin hardens primarily under acidic conditions as UFs and MUFs. Because MUF-resins harden in the acid pH range, whereas phenolic resins have a minimum of reactivity under these conditions, there is the real danger that the phenolic portion of the resin might not really be incorporated into the aminoplastic portion of the resin

during hardening. This does indeed occur if the sequence of reactions is not well chosen, negating often any advantage which could be derived by addition of phenol [59]. Proper reaction sequences do however yield acceptable copolymers and resins of acceptable performance [59].

During the hardening of PMF-resins no cocondensation occurs and in the hardened state two independent interpenetrating networks exist [66]. Only in model reactions between phenolmethylols and melamine indications for a cocondensation via methylene bridges between the phenolic nucleus and the amido group of the melamine has been found by $^1\text{H-NMR}$.

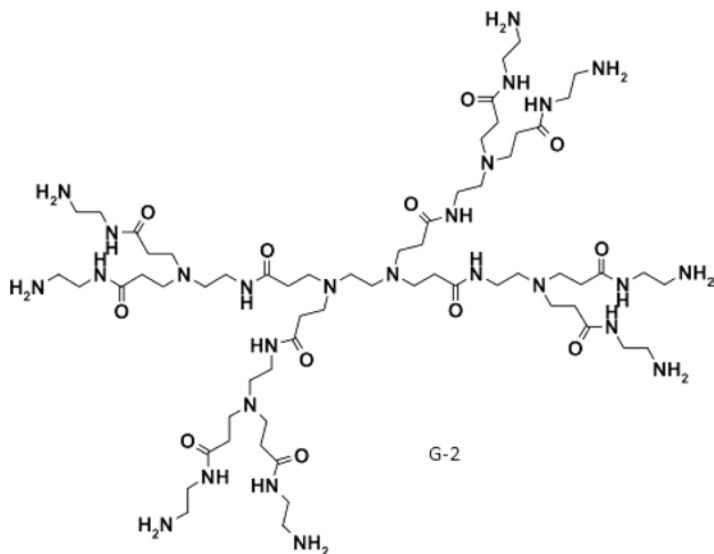
In order to increase the capacity of a production line especially by reducing the necessary press times, adhesive resins with a reactivity as high as possible should be used. This requires two parameters:

- a short gelation time
- a rapid bond strength increase, and this even at a low degree of chemical curing.

The reactivity of a resin at a certain molar ratio F/U or $\text{F}/(\text{NH}_2)_2$ is mainly determined by its preparation procedure.

Coreacted in situ, during hardening, UF-isocyanate resins and MUF-isocyanate resins, forming partly methylene partly urethane cross-linked networks, even in presence of water, have also been reported and are being used industrially [67, 68].

Recent work on the addition of very small amounts of hyperbranched acrylic polymers (dendrimers) of the G-2 type as shown below



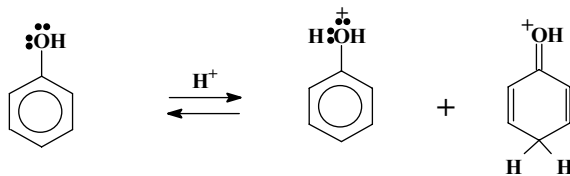
to MUF resins markedly upgrading their performance as exterior adhesives has also been reported and shows considerable promise. This is true also for UF resins [69].

4.4 Phenolic Resins

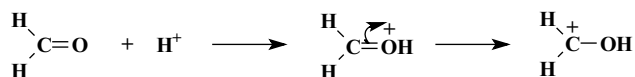
Phenolic resins, namely phenol-formaldehyde thermosetting adhesives, are the best panel adhesives for exterior grade application being both weather- and boil-proof. Their main disadvantages are the longer press times compared to UF- and MUF-resins, although this problem has now been solved; the dark colour of both the bondline and the board surface; as well as the higher moisture content of the boards on storage at high relative humidity of the surrounding air due to the hygroscopicity of the high alkali content used. In contrast to UF and melamine resins, PF adhesives cure well both under very acidic conditions as well as under very alkaline conditions. Where the acid does not react with the substrate the adhesive is acid cured (for example in sand binding for foundry cores). Where reaction of the acid with the substrate is deleterious, such as in wood binders where acid would attack and severely weaken the cellulose of the substrate, the PF adhesive is cured under strong alkaline conditions.

Phenol condenses initially with formaldehyde in the presence of either acid or alkali to form a methylolphenol or phenolic alcohol, and then dimethylolphenol. The initial attack may be at the 2-, 4-, or 6-position. The second stage of the reaction involves methylol groups with other available phenol or methylolphenol, leading first to the formation of linear polymers and then to the formation of hard-cured, highly branched structures [1].

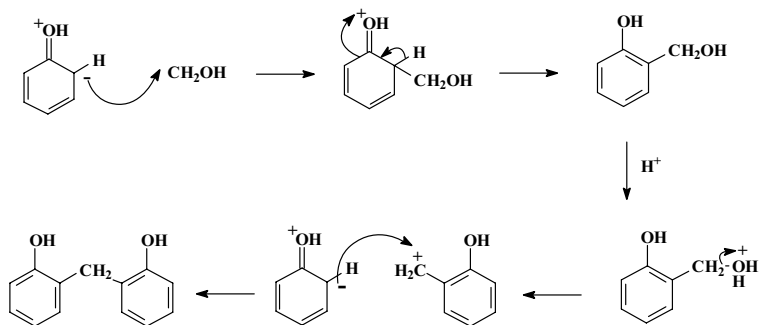
Novolak resins are obtained by acid catalysis with formaldehyde in lower molar proportion than phenol. A novolak resin has no reactive methylol groups in its molecule and therefore without hardening agents it is incapable of condensing with other novolak molecules on heating. To complete resinification, further formaldehyde is added to cross-link the novolak resin. Phenolic rings are considerably less active as nucleophilic centers at an acid pH, due to the protonation of their rings and hydroxyl groups, as shown below.



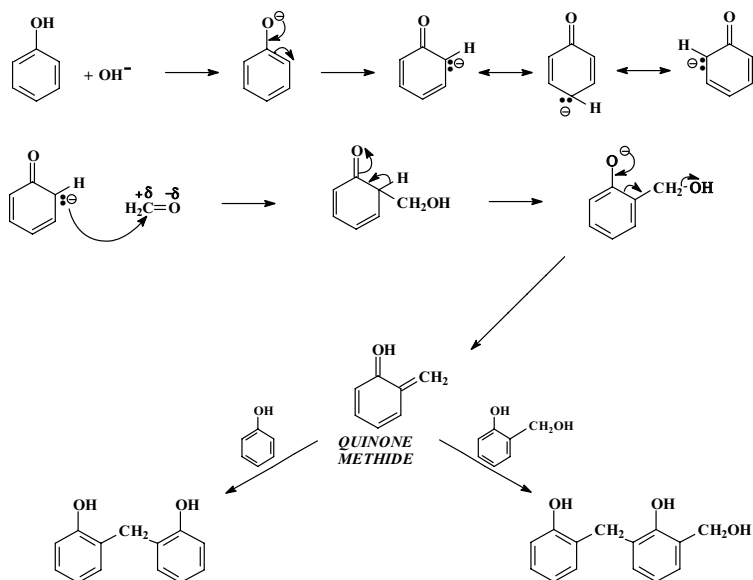
However, the aldehyde is activated by protonation, which compensates for this reduction in potential reactivity. The protonated aldehyde is a more effective electrophile as shown below.



The substitution reaction proceeds slowly and condensation follows as a result of further protonation and the creation of a benzylic carbonium ion that acts as a nucleophile, as shown below

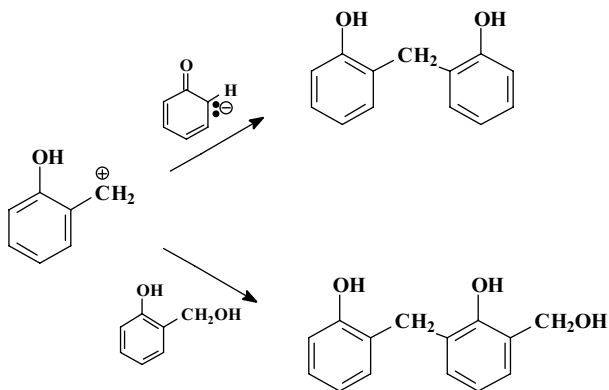


Resols are obtained as a result of alkaline catalysis and an excess of formaldehyde. A resol molecule contains reactive methylol groups. Heating causes the reactive resol molecules to condense to form large molecules, without the addition of a hardener. The function of phenols as nucleophiles is enhanced by ionization of the phenol, without affecting the activity of the aldehyde, as shown below



A carbonium ion mechanism is, however, more likely to occur for the condensation reaction although strong evidence for a quinone methide mechanism also exists [70–72]. Megson [70] also states that phenolic nuclei can be linked not only by simple methylene bridges but also by methylene ether bridges. The latter generally revert to methylol bridges if heated during curing with the elimination of formaldehyde.

The differences between acid-catalyzed and base-catalyzed processes are (1) in the rate of aldehyde attack on the phenol, (2) in the subsequent condensation of the phenolic alcohols, and, to some extent, (3) in the nature of the condensation reaction. With acid catalysis, phenolic alcohol formation is relatively slow. Therefore, this is the step that determines the rate of the overall reaction. The condensation of phenolic alcohols and phenols forming compounds of the dihydroxydiphenylmethane type is, instead, rapid. The latter are, therefore, predominant intermediates in novolak resins, as shown below



Novolaks are mixtures of isomeric polynuclear phenols of various chain lengths with an average of five to six phenolic nuclei per molecule. They contain no reactive methylol groups and consequently cross-link and harden to form infusible and insoluble resins only when mixed with compounds that can release formaldehyde and form methylene bridges (such as paraformaldehyde or hexamethylenetetramine).

In the condensation of phenols and formaldehyde using basic catalysts, the initial substitution reaction is faster than the subsequent condensation reaction. Consequently, phenolic alcohols are initially the predominant intermediate compounds. These phenolic alcohols, which contain reactive methylol groups, condense either: (i) with other methylol groups to form ether links, or more commonly, (ii) with reactive positions in the phenolic ring (ortho or para to the hydroxyl group) to form methylene bridges. In both cases water is eliminated.

Mildly condensed liquid resols, which are the more important of the two types of phenolic resins in the formulation of wood adhesives, have on average fewer than two phenolic nuclei in the molecule. The solid resols average three to four phenolic nuclei but with a wider distribution of molecular size. Small amounts of simple phenol, phenolic alcohols, formaldehyde, and water are also present in resols. Heating or acidification of these resins

causes cross-linking through uncondensed phenolic alcohol groups, and possibly also through reaction of formaldehyde liberated by the breakdown of the ether links.

As with novolaks, the methylolphenols formed condense with more phenols to form methylene-bridged polyphenols. The latter, however, quickly react in an alkaline system with more formaldehyde to produce methylol derivatives of the polyphenols. In addition to this mode of growth in molecular size, methylol groups may interact with one another, liberating water and forming dimethylene-ether links ($-\text{CH}_2-\text{O}-\text{CH}_2-$). This is particularly evident if the ratio of formaldehyde to phenol is high. The average molecular weight of the resins obtained by acid condensation of phenol and formaldehyde decreases from over 1000 to 200, with increase in the molar ratio of phenol to formaldehyde from 1.25:1 to 10:1.

Usually NaOH is used as catalyst, in an amount up to one mole per mole phenol (molar ratio NaOH/P), which corresponds to a portion of alkali in the liquid resin of approx. 10 weight%. The pH of a phenolic resin is in the range 10–13. The largest part of the alkali is free NaOH, and a smaller part is present as sodium phenolate. The alkaline medium is necessary to keep the resin water soluble via the phenate ion formation in order to achieve a degree of condensation as high as possible at a viscosity which still can be used in practice. Additionally, the alkali significantly drops the viscosity of the reaction mix. Hence the higher the alkali content, the higher is the possible degree of condensation of the resin, hence the higher is the hardening reactivity of the resin and, therefore, the shorter is the necessary curing time.

Higher alkali content has, however, also some important disadvantages. The equilibrium moisture content in a humid climate increases with the alkali content as well as some hygroscopic (longitudinal stability, thickness swelling, water absorption) and mechanical properties (creep behaviour) become worse. The alkali content also causes cleavage of the acetyl groups of the cellulose. This leads to an enhanced emission of acetic acid compared to UF-bonded boards. The higher is the alkali content, the higher is the emission of acetic acid from this source.

Besides NaOH, other basic catalysts can also be used, like $\text{Ba}(\text{OH})_2$, LiOH, Na_2CO_3 , ammonia or hexamine, some of these being commercially used and others are not. The type of catalyst significantly determines the properties of the resin [73–75]. Decreasing the proportion of alkali in PF-bonded products yields some advantages. Ammonia evaporates as a gas during the hot curing and therefore does not contribute to the alkaline behaviour and the hygroscopicity of the products. In wood panels applications, it is important to hold the pH fairly high as long as possible during hot pressing in order to guarantee a high reactivity and hence a short curing or pressing time [76, 77].

The penetration behaviour or the “grip” of the adhesive onto the substrate depends strongly on the molar mass of the resin: the higher the molar mass (more or less equivalent to the viscosity of the resin at the same solid content), the worse is its wetting capacity and the lower is its penetration into the wood surface [78, 79]. Lower molar mass chains are responsible for good surface wetting, however, too low a molar mass can cause overpenetration and hence starved bondlines. Contact angles of phenolic resins on wood increase strongly with increasing viscosity of the resins, and thus at higher molar masses [80]. The higher molar mass chains remain at the wood surface and form the bondline, but they will not anchor as well into the wood surface. Depending on the porosity of the wood surface, a certain part with higher molar masses must be present to avoid an overpenetration into

the wood, causing a starved bondline. This means a certain ratio between low and high molar masses is necessary [81–85]. Some authors found a decrease of the wood failure with increased molar mass averages of PF-resins [86].

The penetration behaviour of resins into the wood surface also is influenced by various parameters, such as wood species, amount of glue spread, press temperature and pressure, and hardening time. The temperature of the wood surface and of the bondline and hence the viscosity of the resin (which itself also depends on the already reached degree of hardening) influences the surface penetration behaviour of the adhesive [87].

4.4.1 Reactivity and Hardening Reactions of PF Adhesive Resins

PF adhesives for the core layer of panels usually have the highest average molar mass and hence show high reactivity and quick gelation. They contain a higher proportion of alkali than board surface resins in order to keep the resin soluble even at higher degrees of condensation. The higher the degree of condensation during the production process (the higher the viscosity), the shorter is the gel time [88]. The limit on the increase of the degree of condensation in the production process of the resin is dictated by (i) the viscosity of the resin (the resin must be able to be pumped, to have a certain storage stability as well as a proper distribution of the resin on the particles during blending) and (ii) the flow behaviour of the resin under heat, guaranteeing wetting of the unglued second wood surface and a sufficient penetration into the wood surface. Decreasing the solid content of the resin is limited if the moisture content of the glued particles is too high.

Alkaline PF-resins contain free reactive methylolgroups in sufficient number and can harden even without further addition of formaldehyde, a formaldehyde source, or catalysts. The hardening reaction is only initiated by heat. The methylol groups thus react to form methylene and methylene ether bridges. At higher temperatures ether bridges can rearrange to methylene bridges. The lowest possible temperature for a technically sufficient gelling rate is approx. 100°C. In some cases, potash in the form of a 50 weight% solution is added in the core layer resin mix in an amount of approx. 3–5 % potash based on resin solid content.

An in-depth investigation of the dependence of the gel time of an alkaline PF-resin on the pH [71] surprisingly found an unexpected lengthening of gel time in the very high pH value region (above 10). However, commercial PF resins for wood are prepared at high pHs (12 to 14), with a content of NaOH of 5 to 10 % by weight. The pH of the resin, however, may well change when the resin comes into contact with the acidic wood surface. Especially with rather acidic wood species, the pH of the resin could significantly drop [89] bringing back the resin to the pH for its highest reactivity.

It has also been shown that lignocellulosic substrates have a distinct influence on the hardening behaviour of PF-resins [90, 91], other formaldehyde-based adhesives and thermosetting wood adhesives (such as isocyanates): the activation energy of the hardening process is much lower than for the resin alone [91]. The reason is a catalytic activation of PF and other resins condensation by the surface of polymeric wood constituents, in particular carbohydrates like crystalline and amorphous cellulose and hemicellulose. Covalent bondings between the PF-resin and the wood, especially lignin, do not play any role under the conditions industrially prevalent today for wood adhesives application [91].

The acid-induced gelling reaction of PF resins can instead cause severe deterioration of wood and, therefore, has lost more or less completely its importance in the wood panels field. Procedures for the simultaneous neutralization of acid-hardened PF-bondlines during their curing have also been described [92]. This self-neutralisation of the bondline is obtained by adding to the PF glue-mix a strong acid coupled by complexes of morpholine and a weak acid. After hot curing, the complex re-formed is between the morpholine and the strong acid. This almost neutralizes the bondline and prevents acid deterioration of the wood substrate.

Acceleration of the hardening reaction is possible by using a resin with a degree of condensation as high as possible. A more effective PF accelerating system is the addition of esters such as propylene carbonate [71, 93–98] or even better of glycerol triacetate (triacetin) [15, 71, 99] or guanidine carbonate [99]. The higher is the addition of ester, the shorter is the gel time of the PF-resin [71]. Esters not only accelerate resin curing, but also increase the ultimate strength of the cured resin indicating that a more cross-linked hardened network has been obtained.

Potassium carbonate, sodium carbonate [93, 97, 98] or sodium- and potassium bicarbonates are just accelerators for PF resins curing, without contributing to an increase in the strength of the hardened network [93]. Also wood extractives, such as flavonoid tannins [1], other wood chemicals [97], and amines [93] have an accelerating effect on the hardening of PF-resins.

A further, very effective and relatively inexpensive method to accelerate the hardening of PF adhesives is by partly co-polymerizing them with urea during or after their preparation (see below).

Since alkaline phenolic resins harden only by heat, post-curing of wood panels during hot stacking is important. In contrast to UF-bonded boards, PF-bonded boards should be stacked as hot as possible to guarantee a maximum postcuring effect. However, too high a temperature during further stacking might start to cause some wood degradation.

Some special resins consist of a two-phase system with a highly condensed and no longer soluble PF-resin and an usual PF-resin [100]. Another two-phase resin is composed of a highly condensed PF-resin still in an aqueous solution and a PF-dispersion [101]. The purpose of such special resins is the gluing of wet wood, where the danger of overpenetration of the resin into the wood surface exists causing a starved bondline.

4.4.2 Modification of Phenolic Resins

4.4.2.1 Post-addition of Urea

Addition of urea to a phenolic resin at different levels of addition is current commercial practice and it causes several effects:

- decrease of the content of free formaldehyde
- decrease of the viscosity of the adhesive

- acceleration of the hardening reaction via the higher possible degree of condensation of the resin at the same viscosity
- reduction of the cost of the resin.

The urea usually is added to the finished PF-resin and causes a distinct decrease of the viscosity due to cleavage of hydrogen bonds [102] and also due to the dilution effect. There is obviously no co-condensation of this post-added urea with the phenolic resin. Some co-condensation has also been shown to occur during hot-pressing. Urea only reacts with the free formaldehyde of the resin forming methylols, which however do not react further due to the high pH [10]. Only at higher temperatures during hot pressing some phenol-urea co-condensation can occur [15, 99, 103].

The higher is the amount of post-added urea, the worse are the properties of the boards. A reason for this might be the dilution effect of urea on the PF-resin. Amelioration of the co-condensation process also could help in the optimization of the urea addition. In this respect one can explain the apparently surprising results of Oldörp and Marutzky [104] who found better board properties with increased urea post-addition, a clear indication that some co-condensation had indeed occurred.

4.4.2.2 Co-condensation Between Phenol and Urea

Real co-condensation between phenol and urea can be achieved in a number of different ways:

- Reaction of methylolphenols with urea [105–108].
- Reaction of UFC (urea-formaldehyde concentrate) with phenol under acidic conditions followed by an alkaline reaction [109, 110].
- Alkaline co-condensation to yield commercial resins and the products of reaction obtained thereof [15, 99] as well as the kinetics of the co-condensation of monomethylolphenols and urea [112, 113] have also been reported [2].

Model reactions proving urea-phenol-formaldehyde co-condensation are described both by Tomita and coworkers [105, 109, 113] and by Pizzi and coworkers [15, 99, 111]

4.4.2.3 Addition of Tannins, Lignins and Isocyanates

The purposes of the addition of tannins are:

- the acceleration of the hardening reaction [114, 115] but it has been unsuccessful with hydrolysable chestnut tannins [114] but successful when using polyflavonoid tannins [115].
- the replacement of phenol or part of the PF-resin [1, 116, 117].

The addition of lignins to phenolic resins can be (i) as an extender, e.g. in order to increase the cold tack or to reduce costs, or (ii) for a chemical modification of the resin,

whereby the lignin is chemically incorporated into the phenolic resin. The idea behind is based on the chemical similarity between the phenolic resin and lignin or between phenol and the phenylpropane unit of the lignin. The lignin can be added at the beginning, during the resin preparation procedure or at the end of the condensation reaction (with a following reaction step between the lignin and the phenolic resin). It is not fully clear whether the lignin really is incorporated into the phenolic resin or not. In practice lignin at the moment is used, if at all, only as a neutral filler in these adhesives, without offering any special advantage (sometimes even not in terms of costs).

The use of isocyanate as a fortifier for phenolic resins was not thought to be worthwhile; Deppe and Ernst [118] reported a precuring, hence a negative effect on reaction between the isocyanate and the phenolic resin, even if both components were applied separately to the wood particles of the panel. However, this was eventually found not to be the case. Thus, extensive industrial application to bond wood panel products of phenolic resins to which isocyanate has been added just in the glue-mix has shown to yield excellent results [119–121]. They yield copolymers linked by urethane bridges during curing of the wood panel in the hot press. The reactions involved and the reasons for their occurrence have also been clarified and presented [119]. Hse *et al.* [122] have described a similar system, however without pre-mixing the isocyanate and the phenolic resins but adding them separately to the wood particles. This also yielded some good results but not as good as the former system due to the decreased *in situ* mobility of the two resins and thus, the lower level of co-reaction of the two resins. These resins are now commercial in both the emulsified isocyanate/PF form, hence as single-component adhesives, and also incorporated directly in the glue mix, just before application by just mixing PF resin and non-emulsifiable isocyanate [119, 120, 123].

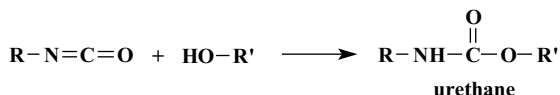
4.5 Isocyanate Wood Adhesives

Isocyanates have been used as adhesives in the wood panels industry since 1975, their first commercial introduction for this application was in Germany [1–3]. For several years these interesting materials struggled to find place in the market despite the fact they are excellent adhesives. Their initial struggle to be accepted in the wood panels industry was initially ascribed to a series of small but irritating side problems, such as binding of the panel board to the press during manufacture, the initial impossibility to use them for plywood or diluting them with water and their high costs. Notwithstanding that most of these problems have been solved, the main cause of this lack of acceptance was in reality the resistance of the wood industry to the introduction of bonding systems so different from the long-time accepted formaldehyde-based resins.

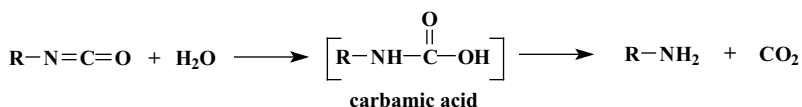
Isocyanates for wood bonding are excellent adhesives. To explain their behaviour different from traditional formaldehyde-based resins it was originally assumed that the very strong bonding they provided could only be obtained by forming a high proportion of covalent bonds between the resin and the wood substrate [124–126]. This assumption was very appealing, as wood teems with hydroxyl groups, one of the groups with which isocyanates readily react. The possibility or not of such an occurrence is briefly discussed later. The industrial polymers used for adhesives, i.e., polyisocyanates contain several repeat units and carry several reactive isocyanate groups on each molecule.

4.5.1 Chemistry of Isocyanate Wood Adhesives

The chemistry of polymeric isocyanates for wood adhesives is inextricably linked to the chemistry for preparation of polyurethanes. A number of reactions characteristics of an isocyanate group are of relevance to polyisocyanates application as wood adhesives. The first of these is the reaction between isocyanate and hydroxyl group to form a urethane bridge [125]:

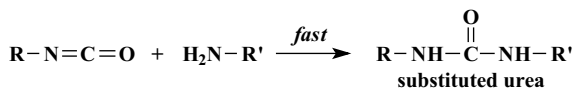


This extends to reaction with water, a hydroxyl-carrying molecule, with which the isocyanate reacts readily with the liberation of carbon dioxide and formation of urea groups. The first step in this reaction is the formation of unstable carbamic acid which then decomposes in a terminal amine end group and carbon dioxide [125]:

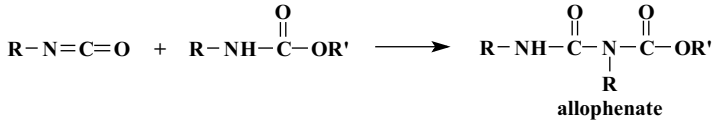


Although in itself it is unstable, carbamic acid has been found to be stable by ^{13}C NMR under certain conditions, namely in hardened networks formed by reaction of isocyanate with water where immobilization of the network renders difficult or unlikely any further reaction [127, 128]. Initially, the water reacts slowly with the isocyanate, allowing in the case of wood adhesives a certain time for handling before curing occurs rapidly at higher temperature. Notwithstanding this advantage, the reaction of water with isocyanate can be a source of problems, e.g. isocyanate containers need to be well closed to avoid hardening of the material due to atmospheric moisture content.

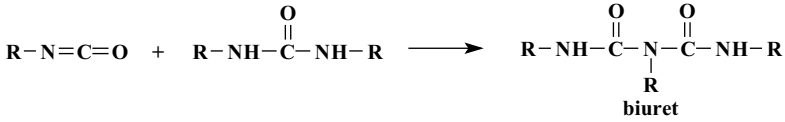
Primary and secondary amines also react readily with isocyanate groups. The amine generated by reaction of the isocyanate with water in the previous reaction reacts immediately with another isocyanate group to form a substituted urea [125].



The formation of substituted ureas is of particular interest in polyisocyanates used as wood adhesives as it is the starting point of reactions leading to molecules forming three-dimensional networks, namely allophanates and biurets (see below), which are considered responsible for the hardening of

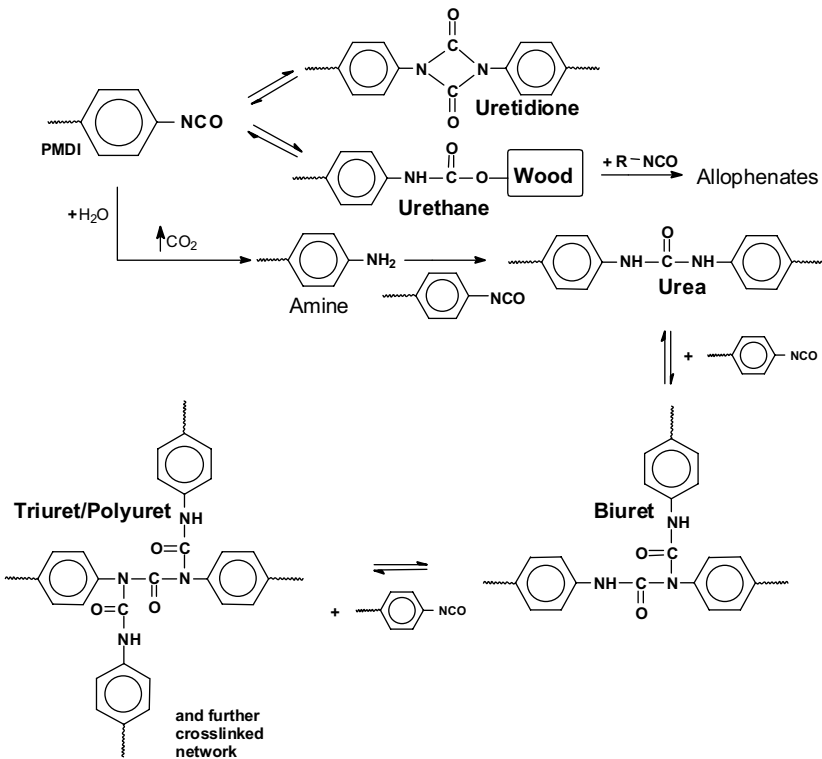


polyisocyanate adhesives in wood panel products. Thus, by reaction of an isocyanate group with a urethane bridge formed by previous reactions, allophenate and biuret bridges are formed [125]:



These two reactions account partly for the formation of three-dimensional covalently cross-linked networks [2].

The probable cure chemistry of the system is summarized by the following scheme of reactions [129]:

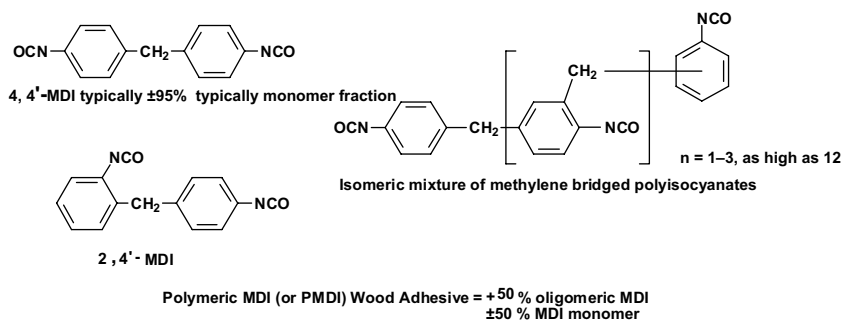


Thus, even one molecule of water, or reaction with a hydroxyl group, for instance of wood, is more than enough to start the chain reaction that produces gelling and hardening of the material [2].

Polyureas and biuret/polyuret linkages thus appear to be the main chemical linkages in the wood /isocyanate bondline, under industrial rate bonding conditions. The spurious claim still believed today that bonding wood with isocyanates is a “green” technology derives from the predominance of this reaction. Predominant, however, does not mean the only one. ^{13}C NMR spectrum of water/temperature hardened polymeric diphenylmethane diisocyanate (PMDI) still shows in the final network clear traces of unreacted isocyanate groups [127, 128], partly denying the “green” claim. This research work, for example, shows the spectra of such hardened pMDI cases. They show a peak or a shoulder at 125 ppm; this is the peak of the carbon of the $-\text{N}=\text{C}=\text{O}$ isocyanate group. This means that notwithstanding the high proportion of water and of UF reactive groups, unreacted isocyanate groups survive in no small proportion and remain in the hardened network. This is possibly due to early immobilization of the network during hardening. The argument that water vapour, or even water, during manufacture or afterwards, will eventually react with these still active, and toxic, isocyanate groups is an incorrect one. pMDI-generated networks are exterior/marine-grade, namely water repellent/resistant, and it is rather doubtful that either water vapour or water itself can get to all these unreacted $-\text{NCO}$ groups still present in the network to deactivate them. The use of hybrid PF/pMDI and UF/pMDI adhesives, described later in this review, greatly reduces this problem, but does not always eliminate it.

4.5.2 Technology of Isocyanate as Adhesives

The standard isocyanate adhesive used in the wood panels industry is 4,4' diphenylmethane diisocyanate (MDI), not in its monomer form but in its polymeric form. Polymeric MDI is generally referred to as simply pMDI, or PMDI or just MDI. It is an almost equal weight mixture of methylene bridged polyphenyl polyisocyanates and of MDI monomer. It is a dark, reddish-brown liquid containing no solvent. The monomer fraction is composed in great majority (> 90%–95%) of the 4,4' isomer and in minority of 2,4' isomer [125, 129] as shown below



The isocyanate (-NCO) groups content of industrial pMDI is in the 31%–32% range, viscosities of 175–250 cP, and surface tension of around 45 mN/m. In general, the number average and weight average molecular masses of industrial PMDI are, respectively, in the 250–280 g/mol and 470–550 g/mol [129]. As 4,4' diphenylmethane diisocyanate monomer is more reactive than its 2,2' equivalent isomer, PMDI is less reactive than pure 4,4' diphenylmethane diisocyanate monomer due to the presence in PMDI of ortho-substituted -NCO groups. Polyureas and biuret/polyuret linkages appear to be the main chemical linkages in the wood/isocyanate bondline, when PMDI is used under industrial rate hot pressing conditions. Under much slower bonding conditions urethane formation between the isocyanate adhesive and the wood constituents has been indeed shown to occur [130, 131]. However, it has also been shown that for all adhesives under fast bonding conditions prevalent in the wood panel industry the bondline is held together by strong secondary forces [91, 132, 133], hence without the need for any urethane formation between adhesive and wood [131, 134].

PMDI has been shown to penetrate down to the wood cell walls, with consequent wood cell walls plasticization [129, 135]. The hypothesis of PMDI forming an interpenetrating polymer network with wood has also been advanced [129, 136].

Advantages of bonding of wood products with PMDI are its tolerance to faster pressing, the water and weather resistance of the bondline obtained, and in particular lower amounts of adhesive needed than for more traditional adhesive systems [2, 124, 125]. Disadvantages are the tendency of PMDI-bonded particleboard to stick to the hot steel platens of the press, the need to provide a metering and pumping system devoid of water contamination, doubts as regards PMDI's level of toxicity and its higher cost than that of more traditional wood adhesives [2, 124, 125]. Most of these problems have already been solved, and solved well [2].

Polymeric polyisocyanate, PMDI, is very hygroscopic and must be stored in closed containers. Once cured, a PMDI bondline is very durable, these adhesives being classified as both exterior-grade as well as marine-grade. PMDI wood adhesives are not affected by the pH and buffering capacity of wood. In recent years, however, water dispersible, emulsified isocyanates have been used in industry, overcoming the problem to keep diisocyanates well away from water in the factory. The pot-life of these emulsified adhesives is sensitive to pH and temperature (Figures 4.1 and 4.2).

PMDI adhesives compete mainly with phenol-formaldehyde (PF) resins for the exterior panels market. Pure PMDI cannot be used for plywood. PMDI is used for plywood, but always in combination with other resins/compounds [67, 68, 119]. The great advantage of PMDI is that it can be used at much lower resin loads for the same bonding results. The other great advantage that PMDI had over PF resins was the much faster pressing/curing. PMDI does not have this advantage anymore, with the introduction of accelerated PF and PUF resins; on the contrary, today it can be slightly slower than this new generation of PF resins [71, 89, 104, 137]. PMDI adhesives have the further advantage of being one of the two thermosetting panel adhesives, the other being tannin adhesives [138], which can be used for bonding wood at higher moisture content during panel manufacture. Moisture content levels of the resinated wood particles from 12% to as high as 25% will still result in good laboratory panels and between 12% and 16% will result in good

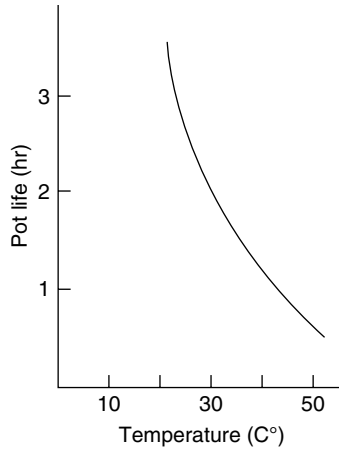


Figure 4.1 Dependence of PMDI pot-life on temperature in presence of water.

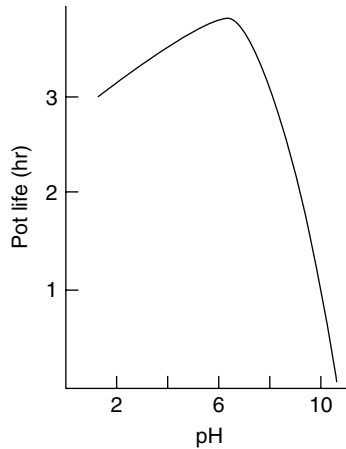


Figure 4.2 Dependence of PMDI pot-life on pH in presence of water.

industrial panels. This characteristic is applicable to both pure PMDI adhesives as well as to hybrid PF/PMDI and other similar hybrid adhesives [139].

Often in the panel industry hybrid panels are produced, i.e. panels using PMDI in the core of the board and a different adhesive on the panel surfaces. This practice derives from the early days of the use of isocyanates in the panel industry, when the problem of sticking to the press of PMDI-bonded wood was rather serious. Notwithstanding that this problem does not really exist anymore with the development of effective release agents, the fabrication of hybrid panels is still prevalent in the wood industry, sometimes for economic

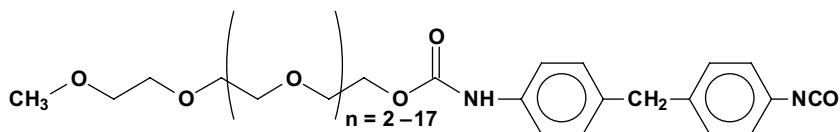
reasons. Thus, panels such as OSB bonded with PMDI in the core and PF or PMUF resins on the surfaces are still commonly used in industry.

Several variations in the type of isocyanates used in the wood panels industry exist. Each one of these was introduced in response to some particular need. The main ones are the use of emulsified/emulsifiable water-dispersed PMDI, hybrid PF/PMDI and UF/PMDI resins, PMDI/polyol adhesive systems, blocked pMDI, and sometimes combinations of these.

4.5.3 *Emulsified/emulsifiable Water-dispersed PMDI*

This is perhaps the most used modification of PMDI. Non-emulsifiable PMDI, being less expensive, still dominates the wood panel market, but emulsified/emulsifiable water-dispersed PMDI is also used in relatively high quantities. It was introduced to eliminate the need for separate lines and pumping due to the reactivity towards water of non-emulsifiable PMDI. It is a good product, and solves the problem it was introduced for, but has one drawback: the emulsifying agents used remain in the hardened bondline after curing, rendering it slightly more sensitive to water attack than in the case of non-emulsifiable PMDI. The problem is noticeable, but not to such an extent to be grave because emulsifiable pMDI performs well as an exterior adhesive. It just performs slightly worse than the non-emulsifiable type.

Emulsifiable PMDI is generally prepared by reaction of the pMDI with hydrophilic chains such as polyethylene oxide [129]. The general structure as shown below



can be seen from the ^{13}C NMR spectrum of one of these products with its relative assignments in Figure 4.3 [139].

The polyethylene oxide chains reacted with the PMDI act as a surfactant. The PMDI so reacted is used as a surfactant for mixing non-emulsified PMDI to render the resin water dispersible [140]. Depending on the emulsifier used and its proportion one obtains emulsified PMDIs that can have stability in water from 1 hour to several hours. These types of PMDI are used industrially but to a much lesser extent than the less expensive non-emulsifiable PMDI.

4.5.4 *PF/pMDI and UF/pMDI Hybrid Adhesives*

There has been growing interest in the last 15 years in the copolymerization of PMDI with traditional resins such as phenol-formaldehyde and urea-formaldehyde adhesives. These combinations yield adhesives with excellent performance. The reasons for this interest are: (a) to lower the cost of PMDI usage while still maintaining isocyanate-like performance; (2) to decrease by copolymerization the perceived toxicity of PMDI; (c) to allow the use of

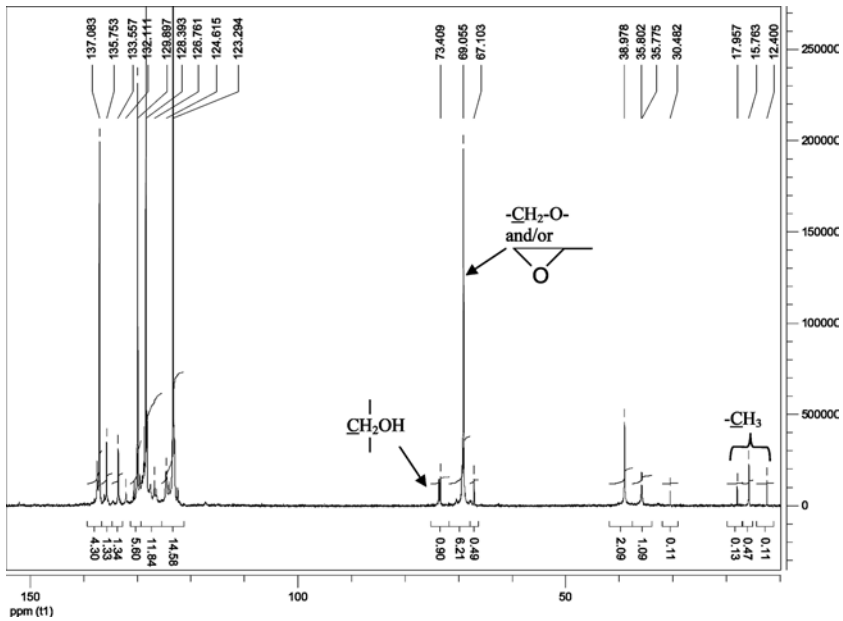


Figure 4.3 Liquid phase ^{13}C NMR spectrum of emulsifiable PMDI isocyanate [139].

PMDI in plywood manufacture where it cannot be used by itself alone; and (d) to upgrade the performance of cheaper adhesives. In this type of approach, PMDI becomes an upgrading additive for traditional adhesives and not a competitor. Both resin classes have something to gain by this combination.

Up to fairly recent times, knowledge of isocyanates and polyurethane chemistry had led to the assumption that in mixed resins such as PF/PMDI, UF/PMDI and others the isocyanate group could only react with the water carrier of the formaldehyde-based resins [142, 143]. However, it has been shown that the isocyanate group does react very rapidly, more rapidly than with water, with the hydroxymethyl groups ($\text{-CH}_2\text{OH}$) of formaldehyde-based resins such as PF resols, UF, MUF and similar resins [119, 141–143]. This is the only case known for formation of urethane bridges in water solution. This finding [142, 143], and the reactions on which it is based [119, 142], led to a series of new wood adhesives. The first which were applied industrially were PF/PMDI adhesives for plywood [67] and tannin-formaldehyde(TF)/PMDI adhesives for particleboard [141]. The PF/PMDI system is of particular interest as it allows the use of PMDI for plywood (alone it cannot be used for this application) and other panel types. It allowed bonding to marine-grade veneer species for which even the best PF resins could not give adequate results, and this at faster pressing, higher moisture content of wood veneers, and using simpler and cheaper PF resins. This mixed resin and its application are now well documented [67, 119].

Other resins carrying hydroxymethyl groups have also shown much improved performance when combined with small proportions of PMDI. Thus, use of the coreaction with

isocyanates to upgrade the performance of methylolated lignin adhesives [144, 145], UF resins [67, 68, 119, 127, 128], MUF resins [67, 119, 143], PUF resins [146] and PMUF resins [147] has been reported. Catalysts for polyurethanes preparation have been shown to be useful even for some of these mixed resins reactions, although these catalysts are not generally needed for wood panels bonding, other than perhaps in the case of lignin adhesives [121].

One of the positive characteristics of these mixed adhesives is that the lower proportion of formaldehyde resin in the combination yields lower formaldehyde emission without loss of bond strength (due to the presence of the isocyanate). Conversely, the presence of the formaldehyde-based resin decreases the percentage of unreacted toxic isocyanate groups immobilized in the hardened network. The decrease of the unreacted isocyanate groups in the case of the mixed resins is quite considerable, as has been proven by ^{13}C NMR analysis by comparing the UF/PMDI system with the system isocyanate/water only [127, 128, 139]. However, the presence, still, of some unreacted isocyanate groups (shoulder at 125 ppm) [127, 128, 139] in the hardened network, although a considerable improvement on the isocyanate/water alone case, again does not allow to designate isocyanate adhesives, even these hybrid ones, as “green” or environmentally friendly.

A particularly interesting and recent development of finely ground waste polyurethane powders is their use as additives to isocyanate adhesives in order to decrease the isocyanate adhesive resin load used on wood in panels bonding [148]. No active isocyanate groups are present in the waste polyurethane powder, which is generally obtained by grinding old polyurethane rigid foams [149]. Thus, the reaction between powder and isocyanates to incorporate the polyurethane powder in the final network occurs between the isocyanate group of the adhesive and the $-\text{NH}-$ residual groups of the urethane linkage in the powder. Substitution of up to 20% of the isocyanate adhesive is possible in this way without any loss of performance. Even more interestingly, the addition of polyurethane waste powder can be done with UF, MUF and PF resins [150]. For acid setting resins such as UFs and MUFs it is the hydroxymethyl groups of these resins which react with the $-\text{NH}-$ residual groups of the urethane linkage in the powder. For alkaline setting resins, such as PF resins for wood bonding, the additional cross-linking reaction is between the hydroxybenzyl groups of the PF resin and both the residual $-\text{NH}-$ groups and the still free aromatic ring sites of the polyurethane powder. In this way both the waste can be recovered and used as well, thus decreasing the cost of the adhesives.

4.5.5 Conditions for Application of Isocyanate Adhesives for Wood

Isocyanate adhesives are only used in the bonding of exterior grade wood panel products such as particleboard and oriented strandboard (OSB). By themselves they cannot be used for plywood because their rheology on heating causes total penetration in the wood veneer with migration away from the plywood-veneer interface. Thus, they harden within the wood veneer and not where they should, at the interface, and are thus incapable, when alone, to bond plywood. Nonetheless excellent plywood adhesives are obtained by coreaction directly in the panel hot press of isocyanates with traditional condensation adhesives such as PF, UF and MUF [67, 119].

In their application for particleboard they need as little as 5%–6% resin load on dry wood chips to give marine grade panels with excellent performance. Thus, the relatively low resin load required offsets the higher price disadvantage they have in relation to formaldehyde-based adhesives. Their conditions for application are generally short press times, around 5 seconds per mm panel thickness or shorter, for today's high press temperatures. Maximum pressure applied is 25 to 35 kg/cm² during the hot press cycle at temperatures between 190°C and 220°C.

Isocyanate adhesives, as well as isocyanate adhesives hybridized with other resins, have the exceptional characteristic of being much more tolerant than other adhesives to bonding at higher moisture content during panel manufacture. Moisture content levels of the resin-ated wood particles from 12% and as high as 25% will still result in good laboratory panels and between 12% and 17% will result in good industrial panels. Press cycle and the other characteristics of panel production with these adhesives are the same as for formaldehyde-based adhesives. The only thing that must be particularly kept in mind is that for isocyanate panels, when the isocyanate is used on the panel faces, it is necessary to add to the resin a specialized releasing agent, or alternatively a higher than usual level (around 1% or more on dry wood) of wax in the form of wax emulsion. This is necessary to avoid panel sticking to the press as the isocyanate is also a good metal adhesive. It must also be noted that recently isocyanates are starting to be also considered as higher value additives to upgrade traditional adhesives, simply by producing hybrid adhesives of excellent performance. Thus, one can find in the market prepacked PF/isocyanates, MUF/isocyanates and UF/isocyanates, as well as separate resins to compose hybrid adhesives as one wishes. Typical results for 12 mm thick particleboard bonded with different levels of PMDI are shown in Table 4.2.

It must be pointed out that in the new European directives PMDI is currently classified as harmful if inhaled, it is also irritating to eyes, skin and the respiratory system and may cause sensitization by inhalation or through skin contact [150]. Furthermore, PMDI apparently does not meet the criteria for classification as environment-friendly [150]. Some European

Table 4.2 Typical internal bond strength results for pMDI bonded wood particleboard (press temperature = 175°C) [129].

						Standard Requirements
PMDI % on dry wood	2	3	4	5	6	
Press time (s/mm)	15	15	10	10	10	
Density (kg/m ³)	680	680	680	680	680	
Dry internal bond (IB) strength (MPa)	0.15	0.53	0.63	0.75	0.81	≥ 0.35
2h boil IB strength, measured wet (MPa)	0.0	0.03	0.09	0.16	0.19	≥ 0.15

Union member states consider that chronic inhalation studies suggest the need to classify such a material as harmful on prolonged exposure through inhalation and with limited evidence of carcinogenic effect. Under what conditions its use is going to be permitted is still not clear at this stage.

4.6 Summary

Synthetic polycondensation adhesives have dominated for the last 80 years, and still dominate, the field of wood panel bonding. They are still likely to do so for quite some time. The increasing cost of oil has increased their costs and more stringent government regulations, particularly as regards their emission of formaldehyde in service, have both contributed to considerable innovation in this field as well as to more stringent controls in these adhesives application and manufacture. The considerable pressure exercised on these resins by the environmental awareness of public and governments has induced a positive innovation response in this field, rather than a decrease in their use and popularity. This has somewhat limited also the existing but growing competition from natural materials and adhesives. It is mainly innovation in resin engineering that has allowed these synthetic adhesives to hold their own quite successfully up to now. In short, it is difficult to substitute with anything else in the short and medium term the reputed, actual 10 million tons/year consumption of urea-formaldehyde wood adhesives and more than 3 million tons of phenolic wood adhesives. Thus, improvements in these resins and their continuous adaptation to ever more stringent requirements is likely to successfully continue for sometime to come.

References

1. A. Pizzi (Ed.), *Wood Adhesives, Chemistry and Technology*, Vol. 1, Marcel Dekker, New York (1983).
2. A. Pizzi, *Advanced Wood Adhesives Technology*. Marcel Dekker, New York (1994).
3. A. Pizzi and K.L. Mittal (Eds), *Handbook of Adhesive Technology*, 2nd edition, Marcel Dekker, New York (2003).
4. M. Dunky, Aminoplastic glue resins, in *Duroplastics* Vol. 10, W. Woebecken (Ed.), pp. 593–614, Carl Hanser, Munich (1988).
5. M. Dunky, Urea-formaldehyde glue resins, in *Polymeric Materials Encyclopedia* Vol. 11, J.C. Salamone (Ed.), CRC Press, Boca Raton, FL (1996).
6. K. Lederer, Aminoplaste, in *Polymere Werkstoffe* Vol. III, H. Batzer (Ed.), pp. 95–291, G. Thieme, Stuttgart (1984).
7. B. Meyer, *Urea-Formaldehyde Resins*. Addison-Wesley, London (1979).
8. H. Petersen, Amino-resins, in *Methods of Organic Chemistry* K.H. Büchel (Ed.), pp 1811–1890, G. Thieme, Stuttgart, (1987).
9. A. Pizzi, L. Lipschitz and J. Valenzuela, Theory and practice of the preparation of low formaldehyde emission UF adhesives for particleboard. *Holzforschung* 48, 254–261 (1994)
10. M.G. Kim, L.W. Amos and E.E. Barnes, Study of the reaction rates and structures of a phenol-formaldehyde resol resin by carbon-13 NMR and gel permeation chromatography, *Ind.Eng. Chem.Res.* 29, 2032–2037 (1990).

11. C. Soulard, C. Kamoun and A. Pizzi, Uron and uron-urea-formaldehyde resins. *J. Appl. Polym. Sci.* 72, 277–289 (1999).
12. L.E. Smythe, The reaction of urea and formaldehyde in presence of sulphuric acid, *J. Phys. Colloid Chem.* 51, 369 (1947).
13. G.A. Grove and C.C. Lynch, Curing of urea-formaldehyde adhesives under acid conditions, *J. Am. Chem. Soc.* 70, 3795 (1948); 71, 3731 (1949); 75, 574 (1953).
14. L. Bettelheim and J. Cedwall, The slow condensation to polymers of methylol ureas, *Svenska Kem. Tidskr.* 60, 208–214 (1948).
15. C. Zhao, A. Pizzi and S. Garnier, Fast advancement and hardening acceleration of low condensation alkaline PF resins by esters and copolymerized urea. *J. Appl. Polym. Sci.* 74, 359–378 (1999).
16. M. Gordon, A. Halliwell and T. Wilson, Kinetics of the addition stage in the melamine-formaldehyde reaction, *J. Appl. Polym. Sci.* 10, 1153 (1966).
17. J.I. de Jong and J. de Jonge, Kinetics of the reaction between mono-methylolurea and methylene diurea, *Recl. Trav. Chim. Pays-Bas* 72, 207 (1953).
18. J.I. de Jong and J. de Jonge, The reaction of methylene diurea with formaldehyde, *Recl. Trav. Chim. Pays-Bas* 72, 213 (1953).
19. A. Pizzi, UF resins adhesion to wood – A quantification method for adhesive formulators. *Holzforschung Holzverwertung* 43, 63–67 (1991).
20. K. Erhardt and H. Petersen, Aminoplastisches bindemittel fuer holzwerkstoffe, German Patent DE 2 207 921, assigned to BASF (1972).
21. D. Merkel and H. Petersen, Bindemittel fuer die holzverleimung, German Patent DE 2 550 739, assigned to BASF (1975).
22. M. Dunky, K. Lederer and E. Zimmer, Effect of molecular weight distribution of urea-formaldehyde resins on the technological properties of particle boards bonded with such resins, *Holzforschung Holzverwertung* 33, 61–71 (1981).
23. M. Dunky, Einfluss des Molverhaeltnisses auf die Eigenschaften der Leime und die erreichbaren Bindefestigkeiten bei Sperrholzverleimungen. Harnstoff-Formaldehyd-Leime, *Holzforschung Holzverwertung* 37, 75–82 (1985).
24. G.E. Myers, Resin hydrolysis and mechanisms of formaldehyde release from bonded wood products, in: Proceedings Wood Adhesives 2005: Status and Needs, Forest Products Society, Madison, WI, pp. 119–156 (1985).
25. H. Yamaguchi, M. Higuchi and I. Sakata, Hydrolytic dissolution behavior of a hardened urea-formaldehyde resin, *Mokuzai Gakkaishi* 26, 199–204 (1980).
26. G.E. Myers, Hydrolytic stability of cured urea-formaldehyde resins, *Wood Sci.* 15, 127–138 (1982).
27. G.E. Myers and J.A. Koutsky, Procedure for measuring formaldehyde liberation from formaldehyde-based resins, *Forest Prod. J.* 37, 56–60 (1987).
28. C. Cremonini and A. Pizzi, Improved waterproofing of UF plywood adhesives by melamine salts as glue-mix hardeners. *Holzforschung Holzverwertung* 49, 11–15 (1997).
29. C. Cremonini and A. Pizzi, Field weathering of plywood panels bonded with UF adhesives and low proportion of melamine salts. *Holz Roh Werkstoff* 57, 318 (1999).
30. C. Kamoun and A. Pizzi, Performance effectiveness of addition to UF of melamine salts vs. melamine alone in MUF adhesives for plywood. *Holz Roh Werkstoff* 56, 86 (1998).
31. M. Prestifilippo, A. Pizzi, H. Norback and P. Lavischi, Low addition of melamine salts for improved UF adhesives water resistance. *Holz Roh Werkstoff* 54, 393–398 (1996).

32. G.E. Myers, Use of acid scavengers to improve durability of acid-catalyzed adhesive wood bonds, *Forest Prod.J.* 33, 49–57 (1983).
33. R. Koehler, Über einige Versuche zur Härtung von Melaminformaldehyd-Kondensationsprodukten, *Kolloid Z.* 103, 138–144 (1943).
34. K. Frey, Kondensationsreaktionen von Anilin mit Formaldehyd und deren Bedeutung für die Herstellung plastischer Massen, *Helv. Chim. Acta* 18, 491–513 (1935).
35. D. Braun and H.J. Ritzert, Gemeinsame Kondensation von Harnstoff, Melamin und Formaldehyd. II. Modellreaktionen, *Angew. Makromol. Chem.* 156, 1–20 (1988).
36. D. Braun, M. de Lourdes Abrao and H.J. Ritzert, Gemeinsame kondensation von harnstoff, melamin und formaldehyd. I. Einfluß der reaktionsparameter, *Angew. Makromol. Chem.* 135, 193–210 (1985).
37. T.A. Mercer and A. Pizzi, Consideration on the principles of preparation of melamine-urea-formaldehyde adhesive resins for particleboard. *Holzforschung Holzverwertung.* 46(3), 51–54 (1994).
38. C. Cremonini, A. Pizzi and P. Tekely, Improvement of PMUF adhesives performance for fire-proof plywood. *Holz Roh Werkstoff.* 54(2), 85–88 (1996).
39. M. Higuchi, J.-K. Roh, S. Tajima, H. Irita, T. Honda and I. Sakata, Polymeric structures of melamine-based composite adhesives, in Proceedings of the Adhesives and Bonded Wood Symposium, Forest Products Society, Madison, pp. 429–449 (1994).
40. H. Czepel, Verfahren zur herstellung von formaldehyd-harnstoff-melamin kondensation-sprodukte, German Patent DE 2 455 420, assigned to Lentia (1974).
41. H. Etling and H. Diem, Process for the preparation of melamine-urea-formaldehyde condensates, German Patent DE 3 442 454, assigned to BASF (1984).
42. J.J. Houtjer, Manufacture of particle board and a novel suitable bonding agent, European Patent EP 62 389, assigned to Methanol Chemie Nederland (1982).
43. H.O. McCaskey, Resin coated substrate using a short-set, high-flow melamine-formaldehyde impregnating resin, US Patent 4,123,579, assigned to Westinghouse Electric Corp. (1978).
44. R.A. Breyer and S.G. Hollis, Low mole ratio melamine-urea-formaldehyde resin, US Patent 5,681,917, assigned to Georgia-Pacific Resins (1996).
45. F. Kauesbauer and W. Bolz, Process for the preparation of amino adhesive resins, German Patent DE 3 116 547, assigned to BASF (1981).
46. H. Diem and C. Dudeck, Method of preparing aminoplast resins, European Patent EP 52 212, assigned to BASF (1981).
47. M. Zanetti and A. Pizzi, Low addition of melamine salts for improved MUF adhesives water resistance. *J. Appl. Polym. Sci.* 88, 287–292 (2003).
48. A. Pizzi, M. Beaujean, C. Zhao, M. Properzi and Z. Huang, Acetals-induced strength increases and lower resin contents in MUF and other polycondensation adhesives *J. Appl. Polym. Sci.* 84, 2561–2571 (2002).
49. M. Zanetti, A. Pizzi, M. Beaujean, H. Pasch, K. Rode and P. Dalet, Acetals induced strength increase of MUF polycondensation adhesives, Part 2: Solubility and colloidal state disruption. *J. Appl. Polym. Sci.* 86, 1855–1862 (2002).
50. M. Zanetti and A. Pizzi, Variation of acetals on the performance of phenol-formaldehyde resin adhesives. *J. Appl. Polym. Sci.* 91, 2058–2060 (2004).
51. M. Zanetti, A. Pizzi and C. Kamoun, Upgrading of MUF particleboard adhesives and decrease of melamine content by buffer and additives. *Holz Roh Werkstoff* 61(1), 55–65 (2003).
52. C. Kamoun, A. Pizzi and M. Zanetti, Upgrading of MUF resins by buffering additives – Part 1: Hexamine sulphate effect and its limits. *J. Appl. Polym. Sci.* 90, 203–214 (2003).

53. M. Zanetti and A. Pizzi, Upgrading of MUF resins by buffering additives – Part 2: Hexamine sulphate mechanisms and alternate buffers. *J. Appl. Polym. Sci.* 90, 215–226 (2003).
54. A. Pizzi, 2001, High performance MUF resins of low melamine content by a number of novel techniques, in: Proceedings Wood Adhesives 2000, Forest Products Society, Madison, WI, pp 219–240 (2001).
55. J. Mayer and C. Schmidt-Hellerau, Wood adhesive, German Patent DE 2 020 481, assigned to BASF (1970).
56. H. Diem and H. Fritsch, Process for the preparation of cocondensates which form weatherproof adhesive bonds, German Patent DE 3 125 874, assigned to BASF (1981).
57. H. Diem and H. Fritsch, Process for the preparation of cocondensates which form a weather-proof adhesive bond, German Patent DE 3 145 328, assigned to BASF (1981).
58. M. Prestifilippo and A. Pizzi, Poor performance of PMUF adhesives prepared by final coreaction of a MUF with a PF resin. *Holz. Roh. Werkstoff.* 54, 272 (1996).
59. C. Cremonini, A. Pizzi and P. Tekely, Influence of PMUF resins preparation method on their molecular structure and performance as adhesives for plywood. *Holz. Roh. Werkstoff.* 54, 85–88 (1996).
60. D. Braun and W. Kraube, Gemeinsame Kondensation von Phenol, Melamin und Formaldehyd. I. Modellreaktionen, *Angew. Makromol. Chem.* 108, 141–159 (1982).
61. D. Braun and W. Kraube, Gemeinsame Kondensation von Phenol, Melamin und Formaldehyd, II. Chromatographische und spektroskopische Untersuchungen *Angew. Makromol. Chem.* 118, 165–182 (1983).
62. D. Braun, and H.J. Ritzert, Gemeinsame kondensation von phenol, melamin und formaldehyd. III. Vorkondensation, *Angew. Makromol. Chem.* 125, 9–26 (1984).
63. D. Braun, and H.J. Ritzert, Gemeinsame kondensation von phenol, melamin und formaldehyd. IV. Härtung, *Angew. Makromol. Chem.* 125, 27–36 (1984).
64. M. Higuchi and I. Sakata, Studies on the improvement of urea-formaldehyde resin adhesives (1). A possibility of water-resistance improvement, *Mokuzai. Gakkaishi* 25, 496–502 (1979).
65. M. Higuchi, H. Shimokawa and I. Sakata, Studies on the improvement of urea-formaldehyde resin adhesives (2). Effect of some urea derivatives and melamine as additives on water-resistance of a UF resin, *Mokuzai. Gakkaishi* 25, 630–635 (1979).
66. M. Higuchi, S. Tohmura and I. Sakata, Acceleration of the cure of phenolic resin adhesives V. Catalytic actions of carbonates and formamide, *Mokuzai. Gakkaishi* 40, 604–611 (1994).
67. A. Pizzi, J. Valenzuela and C. Westermeyer, Non-emulsifiables, water-based, diisocyanate adhesives for exterior plywood, Part 2: Industrial application. *Holzforschung* 47, 69–72 (1993)
68. C. Simon, B. George and A. Pizzi, UF/pMDI wood adhesives: Networks blend vs. copolymerization. *J. Appl. Polym. Sci.* 86, 3681–3688 (2002)
69. X. Zhou, H. Essawy, A. Pizzi, K. Li, K. Rode and G. Du, Upgrading of MUF wood adhesives for particleboard by highly-branched polymers. *J. Adhesion Sci. Technol* 27, 1058–1068 (2013).
70. N.J.L. Megson, *Phenolic Resin Chemistry*, Butterworth, London (1958)
71. A. Pizzi and A. Stephanou, On the chemistry, behaviour and cure acceleration of phenol-formaldehyde resins under very alkaline conditions. *J. Appl. Polym. Sci.* 49, 2157–2170 (1993).
72. K. Lenghaus, G.G. Qiao and D.H. Solomon, Model studies of the curing of resol phenol-formaldehyde resins Part 1. The behaviour of ortho quinone methide in a curing resin, *Polymer* 41, 1973–1978 (2000).
73. M. Duval, B. Bloch, and S. Kohn, Analysis of phenol-formaldehyde resols by gel permeation chromatography, *J. Appl. Polym. Sci.* 16, 1585–1602 (1972).

74. S. So and A. Rudin, Analysis of the formation and curing reactions of resole phenolics *J. Appl. Polym. Sci.* 41, 205–232 (1990).
75. E.R. Wagner and R.J. Greff, Analysis of resoles by gel permeation chromatography, *J. Polym. Sci. A1*, 9, 2193–2207 (1971).
76. K. Oldörp, Holzwerkstoffe: Neue entwicklungen, applikationen, in: Proceedings *Klebstoffe für Holzwerkstoffe und Faserformteile* J.Klein and R.Marutzky (Eds.), Braunschweig, Germany (1997).
77. K. Oldörp and H. Miertzsch, Untersuchungen zum Ersatz von Natriumhydroxid bei Phenolharzen durch Ammoniak, *Holz. Roh. Werkstoff* 55, 97–102 (1997).
78. St.E. Johnson and F.A. Kamke, Quantitative analysis of gross adhesive penetration in wood using fluorescence microscopy, *J. Adhesion* 40, 47–61 (1992).
79. St.E. Johnson and F.A. Kamke, Characteristics of phenol formaldehyde adhesive bonds in steam-injection pressed flakeboard, *Wood Fiber Sci.* 26, 259–269 (1994).
80. R.A.Haupt and T.Sellers. Jr., Characterizations of phenol-formaldehyde resol resins, *Forest Prod. J.* 44, 69–73 (1994).
81. S. Ellis, Natural adhesive-bonded particleboard, *Forest Prod. J.* 43, 66–68 (1993).
82. S. Ellis and P.R. Steiner, in: Proceedings Wood Adhesives 1990, Forest Products Society; Madison, Wisconsin, pp. 76–85 (1990).
83. S. Ellis and P.R. Steiner, The relationship between cure and flow parameters in powdered phenolic resins. *Wood Fiber Sci.* 23, 85–97 (1991).
84. W.L.-S. Nieh and T. Sellers, Jr., Performance of flakeboard bonded with three PF resins of different mole ratios and molecular weights, *Forest Prod.J.* 41(6), 49–53 (1991).
85. R.S. Stephens and N.P. Kutscha, Effect of resin molecular weight on bonding flakeboard, *Wood Fiber Sci.* 19, 353–361(1987).
86. L. Gollob, R.L. Krahrmer, J.D. Wellons and A.W. Christiansen, Relationship between chemical characteristics of phenol-formaldehyde resins and adhesive performance, *Forest Prod. J.* 35(3), 42–48(1985).
87. R.H. Young, Wood adhesives 1985: Status and needs, in: Proceedings, Wood Adhesives: Status and Needs, Forest Products Society, Madison, WI, pp. 267–276 (1985).
88. R.A. Haupt and T. Sellers, Jr., Characterizations of phenol-formaldehyde resol resins, *Ind. Eng. Chem. Res.* 33, 693–697 (1994).
89. A. Pizzi and A. Stephanou, Phenol-formaldehyde wood adhesives under very alkaline conditions, Part 1: Behaviour and proposed mechanism. *Holzforschung* 48, 35–40 (1994).
90. X. Lu and A. Pizzi, Curing conditions effects on the characteristics of thermosetting adhesives-bonded wood joints - Part 1: Substrate influence on TTT and CHT curing diagrams of wood adhesives. *Holz Roh Werkstoff* 56, 339–346 (1998).
91. A. Pizzi, B. Mtsweni and W. Parsons, Wood-induced catalytic activation of PF adhesives autopolymerization vs. PF/wood covalent bonding. *J. Appl. Polym. Sci.* 52, 1847–1856 (1994).
92. A. Pizzi, R. Vosloo, F.A. Cameron and E.Orovan, Self-neutralizing acid-set PF wood adhesives. *Holz. Roh. Werkstoff* 44, 229–234 (1986).
93. A. Pizzi, R. Garcia and S. Wang, On the networking mechanisms of additives accelerated PF polycondensates. *J. Appl. Polym. Sci.* 66, 255–266 (1997).
94. A. Pizzi and A. Stephanou, Phenol-formaldehyde wood adhesives under very alkaline conditions, Part 2: Acceleartion mechanism and applied results. *Holzforschung* 48, 150–156 (1994).
95. B. Riedl and B.-D. Park, in: Proceedings *Wood Adhesion Research*, Forest Products Society, Madison, WI, pp.115–121 (1998).

96. P.R. Steiner, G.E. Troughton and A.W. Andersen, Aqueous phenolic dispersions for bonding higher moisture content veneers, *Forest Prod. J.* 43, 29–34 (1993).
97. S. Tohmura, Acceleration of the cure of phenolic resin adhesives VII: Influence of extractives of merbau wood on bonding, *J. Wood Sci.* 44, 211–216 (1998).
98. S. Tohmura and M. Higuchi, Acceleration of the cure of phenolic resin adhesives VI. Cure-accelerating action of propylene carbonate, *Mokuzai Gakkaishi*. 41, 1109–1114 (1995).
99. C. Zhao, A. Pizzi, A. Kühn and S. Garnier, Fast advancement and hardening acceleration of low condensation alkaline PF resins by esters and copolymerized urea. Part 2: Esters during resin reaction and effect of guanidine salts. *J. Appl. Polym. Sci.* 77, 249–259 (2000).
100. P.R. Steiner, G.E. Troughton and A.W. Andersen, A new approach to phenol-formaldehyde adhesives for wood panels, in: *Proceedings Adhesives and Bonded Wood Products*, Seattle, WA, pp. 205–214 (1991).
101. M.R. Clarke, P.R. Steiner and A.W. Anderson, Phenol formaldehyde adhesive for bonding wood pieces of high moisture content and composite board and veneers bonded with such adhesive, US Patent 4,824,896, assigned to Georgia-Pacific (1988).
102. T. Gramstad and J. Sandstroem, Thioamides and nitriles as proton acceptors in hydrogen bond formation and a discussion of solvent shifts in electronic spectra, *Spectrochim. Acta* 25A, 31 (1969).
103. E. Scopelitis and A. Pizzi, Urea-resorcinol-formaldehyde adhesives of low resorcinol content. *J. Appl. Polym. Sci.* 48, 2135–2146 (1993).
104. K. Oldörp and R. Marutzky, Untersuchungen an Spanplatten mit harnstoffmodifizierten PF-Harzen, *Holz. Roh. Werkstoff* 56, 75–77 (1998).
105. B. Tomita and C.-Y. Hse, Cocondensation of urea with methylolphenols in acidic conditions, *J. Polym. Sci. Polym. Chem.* 30, 1615–1624 (1992).
106. B. Tomita and C.-Y. Hse, Syntheses and structural analyses of cocondensed resins from urea and methylolphenols, *Mokuzai Gakkaishi* 39, 1276–1284 (1993).
107. B. Tomita, M. Ohyama and C.-Y. Hse, Synthesis of phenol-urea-formaldehyde cocondensed resins from UF-concentrate and phenol, *Holzforschung* 48, 522–526 (1994).
108. B. Tomita, M. Ohyama, A. Itoh, K. Doi and C.-Y. Hse, Analysis of curing process and thermal properties of phenol-urea-formaldehyde cocondensed resins, *Mokuzai Gakkaishi*. 40, 170–175 (1994).
109. B. Tomita, Y. Yoshida, and C.-Y. Hse, Kinetics on cocondensation between phenol and urea through formaldehyde, in: *Proceedings, Adhesive Technology and Bonded Tropical Wood Products*, Taipei, Taiwan, pp. 71–83 (1993).
110. M. Ohyama, B. Tomita and C.-Y. Hse, Curing property and plywood adhesive performance of resol-type phenol-urea-formaldehyde cocondensed resins, *Holzforschung* 49, 87–91 (1995).
111. A. Pizzi, A. Stephanou, I. Antunes and G. de Beer, Alkaline PF resins linear extension by urea condensation with hydroxybenzyl alcohol groups. *J. Appl. Polym. Sci.* 50, 2201–2207 (1993).
112. Y. Yoshida, B. Tomita and C.-Y. Hse, Kinetics of cocondensation between phenol and urea through formaldehyde III. Concurrent reactions of monomethylolphenol and urea involving cocondensation and self-condensation, *Mokuzai Gakkaishi* 41, 652–658 (1995).
113. B. Tomita and C.-Y. Hse, Phenol-urea-formaldehyde (PUF) co-condensed wood adhesives, *Int. J. Adhesion. Adhesives* 18, 69–79 (1998).
114. E. Kulvijk, Chestnut wood tannin extract in plywood adhesives, *Adhesives Age*, 20, 33–34, (March 1977).
115. A. Trosa and A. Pizzi, Stability and performance of tannin-accelerated PF resins for plywood. *Holz. Roh. Werkstoff* 55, 306–308 (1997).

116. C.M. Chen, Effects of extraction on the quantity of formaldehyde requirement in reaction of extractives of bark and agricultural residues with formaldehyde, *Holzforschung* 36, 65–70 (1982).
117. B. Dix and R. Marutzky, Möglichkeiten der vermeilung von Holz mit kebstoffen auf der basis von natürlichen polyphenolen, *Adhäsion* 26(12), 4–10 (1982).
118. H.-J. Deppe and K. Ernst, Isocyanate als Spanplattenbindemittel, *Holz. Roh. Werkstoff* 29, 45–50 (1971).
119. A. Pizzi and T. Walton, Non-emulsifiable, water-based diisocyanate adhesives for exterior plywood, Part 1: Novel reaction mechanisms and their chemical evidence, *Holzforschung* 46, 541–547 (1992).
120. A. Pizzi, J. Valenzuela and C. Westermeyer, Non-emulsifiable, water-based, diisocyanate adhesives for exterior plywood, Part 2: Industrial application. *Holzforschung* 47, 69–72 (1993).
121. D.B. Batubenga, A. Pizzi, A. Stephanou, P. Cheeseman and R. Krause, Isocyanate/phenolic wood adhesives by catalytic acceleration of copolymerisation. *Holzforschung* 49, 84–86 (1995)
122. C.-Y. Hse, R.L. Geimer, W.E. Hsu and R.C. Tang, Effect of resin type on properties of steam-press-cured flakeboards, *Forest Prod. J.* 45(1), 57–62 (1995)
123. KW. Haider, M.A. Wittig, J.A. Dettore, J.A. Dodge and J.W. Rosthauser, On the trail to isocyanate/phenolic hybrid wood binders: Model compound studies., in: *Proceedings Wood Adhesives 2000*, Forest Products Society, Madison, WI, pp 376–378 (2000)
124. H.J. Deppe, Technische Fortschritte bei der Isocyanatverleimung von Holzspanplatten, *Holz. Roh. Werkstoff* 35, 295–297 (1977)
125. G.W. Ball and R.P. Redman, Isocyanates as adhesives for panels, in: *Proceedings FESYP International Particleboard Symp.*, Hamburg, pp 121–126 (1978)
126. K.C. Frisch, L.P. Rumao and A. Pizzi, Diisocyanate wood adhesives in *Wood Adhesives: Chemistry and Technology*, Vol. 1, A.Pizzi (Ed.), Marcel Dekker, New York (1983)
127. A. Despres, A. Pizzi and L. Delmotte, ¹³C NMR investigation of the reaction in water of UF resins with blocked emulsified isocyanates. *J. Appl. Polym. Sci.* 99, 589–596 (2006)
128. S. Wieland, A. Pizzi, W. Grigsby, S. Hill and F. Pichelin, The reaction in water of UF resins with isocyanates at short curing times: A ¹³C NMR investigation. *J. Appl. Polym. Sci.* 100, 1624–1632 (2006)
129. C.E. Frazier, Isocyanate wood adhesives, in: *Handbook of Adhesive Technology*, 2nd Edition, A. Pizzi and K.L. Mittal (Eds.), pp 681–694 Marcel Dekker, New York (2003)
130. F. Mora, F. Pla and A. Gandini, The interactions between wood components and formaldehyde-based resins. I. Monofunctional resin model compounds, *Angew. Makromol. Chem.* 173, 137–144 (1989)
131. G.C. Allan and A.N. Neogi, The mechanism of adhesion of phenol-formaldehyde resins to cellulosic and lignocellulosic substrates, *J. Adhesion* 3, 13–18 (1971).
132. H. Poblete and E. Roffael, Über chemische Veränderungen in Holzspänen bei der Herstellung von Harnstoff-Formaldehydharz-gebundenen Spanplatten, *Holz. Roh. Werkstoff* 43, 57–62 (1985).
133. G.E. Meyers, Adhesion of urea-formaldehyde resins to wood, in *Proceedings Wood Adhesives 1985: Status and and Needs*, Forest Products Research Society, Madison, Wisconsin, pp. 47–62 (1986).
134. A. Pizzi and N. Owens, Interface covalent bonding vs. wood-induced catalytic autocondensation of diisocyanate wood adhesives. *Holzforschung* 49, 269–272 (1995).

135. J.J. Marcinko, W.H. Newman, C. Phanopoulos and M.A. Sander, The nature of the MDI/wood bond, in: Proc. 2nd Washington State University International Symposium on Particleboard, Pullman, p. 175 (1995).
136. J. Ni and C.E. Frazier, On the occurrence of network interpenetration in the wood-isocyanate adhesive interphase, *Int. J. Adhesion Adhesives* 18, 81–87 (1998).
137. C. Zhao, A. Pizzi and S. Garnier, Fast advancement and hardening acceleration of low condensation alkaline PF resins by esters and copolymerized urea. *J. Appl. Polym. Sci.* 74, 359–378 (1999).
138. F. Pichelin, A. Pizzi and A. Frühwald, OSB adhesives rate of strength development on single strands couples. *Holz. Roh. Werkstoff* 58, 182–183 (2000).
139. A. Despres, Mise au point de nouvelles résines aminoplastes écologiques à base de diméthoxyéthanal et sans formaldéhyde pour application en tant que colles pour panneaux de particules, Ph.D. thesis, University of Nancy 1, France (2005).
140. F. Johnson, A.M. Wooler, O. Bengston and P. Mayrhofer, Emulsions of isocyanates and their manufacture, US Patent 3,996,154, assigned to ICI (1976).
141. A. Pizzi, E.P. von Leyser, J. Valenzuela and J.G. Clark, The chemistry and development of pine tannin adhesives for exterior particleboard. *Holzforschung* 47, 168–172 (1993).
142. A. Pizzi, A universal formulation for tannin adhesives for particleboard. *J. Macromol. Sci. Chem. Ed. A* 16, 1243–1248 (1981).
143. A. Pizzi, Pine tannin adhesives for particleboard. *Holz. Roh. Werkstoff.* 40, 293–300 (1982).
144. A. Pizzi and A. Stephanou, Rapid curing lignins-based exterior wood adhesives, Part 1: diisocyanates reaction mechanisms and application to panel products. *Holzforschung* 47, 439–445 (1993).
145. A. Pizzi and A. Stephanou, Rapid curing lignins-based exterior wood adhesives, Part 2: Acceleration mechanisms and application to panel products. *Holzforschung* 47, 501–506 (1993)
146. Z. Osman, A. Pizzi, W. Kantner and M.C. Triboulot, PUF panel adhesives mixed with additional urea and reinforced by isocyanates. *Holz. Roh. Werkstoff.* 63, 53–56 (2005).
147. H. Lei, A. Pizzi and G. Du, Coreacting PMUF/Isocyanate resins for wood panel adhesives. *Holz. Roh. Werkstoff.* 64, 117–120 (2006).
148. P. Berthevas, G. Santoro, R. Wevers, H. Gruenbauer and A. Pizzi, Recycled polyurethane foam powder can be used in conjunction with PMDI in particleboards to obtain the required properties while reducing costs, in: Proceedings 9th European Panel Products Symposium, Llandudno, Wales, UK, pp 40–47 (2005).
149. H.R. Mansouri and A. Pizzi, Recycled polyurethane micronized powders as active extenders of UF and PF wood panel adhesives. *Holz. Roh. Werkst.* 65, 293–299 (2007).
150. J. Dobbs and S. Baker, Regulatory trends and MDI resins, in: Proceedings 8th European Panel Products Symposium, Llandudno, Wales, UK, pp 2–52 to 2–56 (2004).

Adhesion Theories in Wood Adhesive Bonding

Douglas J. Gardner*, Melanie Blumentritt, Lu Wang and Nadir Yildirim

University of Maine, Advanced Structures and Composites Center, Orono, Maine, USA

Abstract

Investigating the theories or mechanisms responsible for wood adhesive bonding has been an important aspect of wood science and technology research over the past century. Understanding the nature of adhesion in wood and wood-based composites is of importance because of the fact that wood is adhesively bonded in over 80 percent of its applications. For wood bonding, studying adhesion theories requires an understanding of wood material characteristics, surface science, polymer characteristics, and the interactions between polymers and surfaces. The state-of-the-art categorizes adhesion theories or mechanisms into seven models or areas. These are: mechanical interlocking; electronic or electrostatic theory; adsorption (thermodynamic) or wetting theory; diffusion theory; chemical (covalent) bonding theory; acid-base theory; and theory of weak boundary layers. The goal of this paper is to provide a concise, critical, state-of-the-art review on adhesion theories in wood adhesive bonding with an emphasis on factors influencing bond creation in wood-based material applications. Over 200 papers were reviewed and information is presented with recommendations for future studies on wood adhesion.

Keywords: Adhesion, theories, covalent bonding, diffusion, mechanical interlocking, electrostatic, weak boundary layer, wetting, acid-base, wood

5.1 Introduction

It has been recognized over the past several decades that understanding the nature of adhesion in wood and wood-based composites is of great importance because of the fact that wood is adhesively bonded in over 80 percent of its applications [1]. There is a plethora of wood and wood-based composite products that rely on adhesives in their manufacturing

*Corresponding author: douglasg@maine.edu

processes [2]. Wood composite products include: glulam beams, oriented strand board, medium density fiberboard, particleboard, and paper just to mention a few [3]. Studying the theories or mechanisms responsible for wood adhesive bonding has been an important aspect of wood science and technology research over the past century. It is anticipated that improvements in the understanding of wood adhesion mechanisms have the potential to result in better adhesive systems and more efficient and effective processing methods for the wide array of wood and wood-based composite materials.

For wood bonding, studying adhesion theories requires an understanding of wood material characteristics, surface science, polymer characteristics, and the interactions between polymers and surfaces. At present no practical unifying theory describing all adhesive bonds exists, although a unified adhesion theory has been proposed [4]. The state-of-the-art categorizes adhesion theories or mechanisms into seven models or areas [5–7]. These are:

1. Mechanical interlocking theory
2. Electronic or electrostatic theory
3. Adsorption (thermodynamic) or wetting theory
4. Diffusion theory
5. Chemical (covalent) bonding theory
6. Acid-base theory
7. Theory of weak boundary layers

It should be noted that these theories are not self-excluding, and several may be occurring at the same time in a given adhesive bond depending on the particular circumstance. Recent applications of adhesion theories to describing the nature of wood adhesive bonding have focused effort on the durability of wood adhesive bonds [8–11].

5.1.1 Wood Material Properties Relevant to Adhesion

Wood can be classified into two broad groupings, i.e., softwoods and hardwoods [12]. Softwoods are from gymnosperms or those trees with needle-like leaves, generally evergreen, and bearing seeds in a woody cone. Hardwoods are from angiosperms or those trees with broad, deciduous leaves and bearing seeds in a fleshy fruit. Wood can be classified as an orthotropic, heterogeneous, cellular solid. The structure and properties of wood differ in three mutually-orthogonal planes: transverse (cross section), radial, and tangential. In the tree, wood can also be segregated into heartwood and sapwood. Sapwood, the periphery of the tree stem, is generally light in color, transports water, and stores food in the living tree. Heartwood, the central portion of the stem, is often darker in color, and contains extractives (fatty acids, waxes, etc.). The cellular structure of wood also varies between softwoods and hardwoods. Longitudinal tracheids account for over 90 percent of softwood volume, and the empty cell lumens suggest a honeycomb structure. Hardwoods contain fibers (analogous to softwood tracheids) that provide mechanical strength to the tree and large diameter vessel elements (“pores”) that mainly transport water and nutrients. The arrangement of cells and volumetric composition varies greatly among species. Softwood tracheids range

in size from 30 to 40 μm in diameter, and 3 to 4 mm in length. Hardwood vessel elements range from 20 to 300 μm in diameter and 0.5 to 1.5 mm in length while hardwood fibers range from 10 to 20 μm in diameter and 1 to 2 mm in length [3].

The chemical composition of wood also varies among species but the major structural organic polymers are similar in composition. Wood contains about 50 percent cellulose, 20 to 35 percent hemicellulose, and 16 to 33 percent lignin, on a dry weight basis [3]. Cellulose and hemicellulose are carbohydrate based polymers while lignin is a phenylpropane-based polymer. The non-structural components include extractives, typically 4 to 10 percent, and inorganic ash (0.2 to 0.5 percent in softwoods, 0.1 to 1.4 percent in hardwoods). Wood also contains water. Freshly cut trees may contain 30 to 200 percent or more water based on the oven dry weight of wood while "dry wood" contains 5 to 12 percent moisture content depending on the ambient interior environment, or up to 20 percent moisture content in exterior environments.

A simplified view of the cell wall structure suggests that cellulose microfibrils are embedded in a discontinuous lignin/hemicellulose matrix. Microfibril orientation varies in the wood cells as a function of the particular wall layer. Layers in the cell wall include the middle lamella between wood cells, the primary and three secondary wall layers: S1, S2, and S3. Several softwoods also exhibit a so-called "warty layer". The extractives in wood are low molecular weight organic chemicals specific to particular species and they contribute to wood odor, can provide decay resistance, concentrate at the wood surface during drying, and can negatively impact adhesion and finishing.

Wood adhesion is dictated by its anatomical, chemical, mechanical, and physical properties. The differences among wood species as a function of anatomy, chemistry, mechanical or physical properties reinforce its description as having a heterogeneous nature. Important characteristics of wood relevant to wood adhesion processes are wood's porosity, anisotropy, dimensional instability, and wood surface properties. Wood as a cellular material is porous and exhibits differing levels of porosity depending on species. Being an anisotropic material, wood exhibits different physical and mechanical properties depending on the orientation of the wood element. Because of its hygroscopic nature wood swells and shrinks as a function of moisture content, thus contributing to its dimensional instability.

Wood surface property issues include chemical heterogeneity, surface inactivation, weak boundary layers, and processing characteristics, i.e., machining, drying, and aging [13]. From a chemical perspective, it has long been recognized that extractives dominate wood surface properties [14, 15]. Because of the complex nature of wood structure and the myriad types of wood species, it is difficult to make sweeping generalizations about the surface properties of wood. It should be emphasized that although there are certain surface property behaviors that are similar among different wood species, it is usually prudent to learn about the specific species of wood type being adhesively bonded.

Approximately 50 years ago, a generalized representation of wood elements used in wood composites was promulgated that provided a practical length scale for wood composite elements [16]. The wood elements listed include logs, lumber, veneer, strands, chips, flakes, excelsior, particles, fiber bundles, fibers and wood flour. We have adapted this



Figure 5.1 Wood elements adapted from [16]. The question mark (?) denotes wood elements not yet defined.

representation and added microcrystalline cellulose and cellulose nanofibers, and a question mark is left in the table for elements not yet defined (Figure 5.1) [17, 18].

A practical look at the orders of scale for examining wood-adhesive interactions from the 1 meter scale down to the 1 nanometer scale are listed in Table 5.1. Evaluations of gross laminate adhesion failure surfaces in glulam beams are determined on the 1 m length scale whereas delamination measurements on glulam beam specimens subjected to accelerated aging regimes are made on the 10 cm length scale. Plywood lap shear specimen percent wood failure measurements are made on the centimeter length scale. Interactions between polymer droplets on individual cellulose fibers occur on the millimeter length scale, and microscopic evaluation of the wood-adhesive bondline is carried out on the 100 μm length scale. A bordered pit on a softwood tracheid is 10 μm in diameter, and the smallest resin droplets on medium density fiberboard furnish are on the order of 1 to 10 μm in diameter. Cellulose nanofibrils are on the scale of 100 nm in length and 10 to 20 nm in diameter.

The comparison of wood-adhesive interactions relative to length scale is shown in Table 5.2. Wood as a porous, cellular material has roughness on the micrometer scale but can also exhibit roughness on the millimeter scale depending on how a particular wood element to be bonded is produced. For example, production of rotary peeled veneer can produce roughness on a millimeter scale because of the creation of lathe checks. Fibers can exhibit roughness on the micro- or nanoscale depending on the method of preparation. Pores or free volume also occurs within the amorphous regions of the cell wall material on the molecular level.

Table 5.1 Orders of scale for wood-adhesive interactions.

Scale	Test specimen or material characteristic for determining wood-adhesive interactions
1 meter, 100 cm	Glulam beam laminates
10^{-1} meter, 10 cm	Glulam cycle delamination specimens
10^{-2} meter, 1 cm	Plywood lap shear test specimens
10^{-3} meter, 1 mm	Polymer microdroplet on wood or cellulose fiber
10^{-4} meter, 100 μm	Microscopic evaluation of wood-adhesive bondline
10^{-5} meter, 10 μm	Diameter of bordered pit
10^{-6} meter, 1 μm	Smallest resin droplets on medium density fiberboard furnish
10^{-7} meter, 100 nm	Scale of cellulose nanofibrils
10^{-8} – 10^{-9} meters, 1 to 10 nm	Scale of wood cell wall polymers

Table 5.2 Comparison of wood-adhesive interactions relative to length scale.*

Component	μm	nm
Adhesion forces	0.0002–0.0003	0.2–0.3
Cell wall pore diameter	0.0017–0.002	1.7–2.0
PF resin molecular length	0.0015–0.005	1.5–5.0
Diameter of particles that can pass through a pit	0.2	200
Tracheid lumen diameter	4–25	
Glueline thickness	50–250	

*Adapted from [203]

5.1.2 Objectives

The goal of this paper is to provide a concise, critical, state-of-the-art review on adhesion theories in wood adhesive bonding with an emphasis on factors influencing bond creation in wood-based material applications.

5.2 Mechanical Interlocking and Mechanics of Adhesive-Wood Interactions

Mechanical interlocking, which was proposed by McBain and Hopkins in the early 1900's [19] is one of the basic adhesion mechanisms that can be divided into two groups, specifically: locking by friction and locking by dovetailing (Figure 5.2) [20]. In mechanically interlocked systems, there are irregularities, pores or crevices where adhesives penetrate into and are adhered mechanically [21]. Mechanical interlocking strongly depends on the geometry

of the bonding sites and the mechanical properties of the materials involved [20]. Wood adhesive bonding is a good example where mechanical interlocking is observed because of wood's porous structure where it has open cells on the surface so that the adhesive can flow into the lumen of the cells and provide high strength [2].

In addition to geometry factors, surface roughness has a big effect on adhesion. Rougher surfaces provide better adhesion than smooth surfaces. Gent and Lin (1990) showed that a rough surface with a 60° peak angle has twice as much surface area as a flat surface [22]. Based on a model by Marra (1992), the linkage (chain link analogy) of a wood adhesive bond (Figure 5.3) can be divided into 9 links [16], where link 1 is the pure adhesive, link 2 and link 3 are the adhesive boundary layer which is no longer homogeneous because of the substrate influence while cured. Adhesion mechanisms may be mechanical interlocking, or chemical bonding which can be seen in links 4 and 5. Links 6, 7, 8 and 9 are the wood cells for this example, which are shown in Figure 5.3.

A study investigating the relationship between surface roughness and peel strength (N/m) showed that an increase in surface roughness produces an increase in the surface area (contact area), which produces higher peel strengths [23]. Wake (1982) proposed an equation defining the effects of mechanical interlocking and thermodynamic interfacial interactions for estimating adhesive joint strength G, as:

$$G = C \times M_k \times I_i \tag{5.1}$$

where: C is a constant, M_k is a mechanical keying component, and I_i is the interfacial interactions component [24].

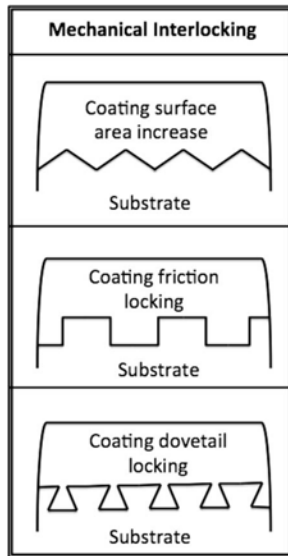


Figure 5.2 Schematic diagram of mechanical interlocking mechanisms.

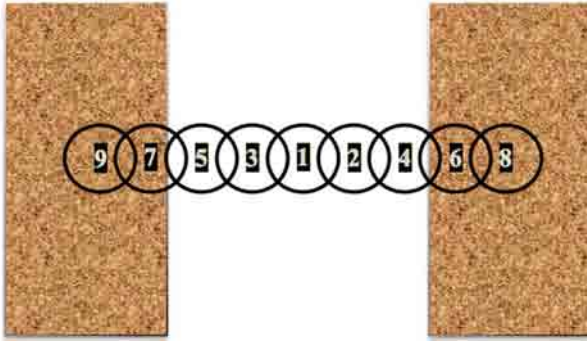


Figure 5.3 Chain link analogy for an adhesive bond in wood [16].

Table 5.3 Comparison of adhesion interactions relative to length scale.

Category of Adhesion Mechanism	Type of Interaction	Length Scale
Mechanical	Interlocking or entanglement	0.01–1000 μm
Diffusion	Interlocking or entanglement	10 nm–2 μm
Electrostatic	Charge	0.1–1.0 μm
Covalent bonding	Charge	0.1–0.2 nm
Acid-base interaction	Charge	0.1–0.4 nm
Lifshitz-van der Waals	Charge	0.5–1.0 nm

High-level adhesion can be attained by improving the surface properties and mechanical keying can be enhanced by increasing the surface area [24]. Cheng and Sun (2006) studied the adhesion between a soybean protein adhesive and wood, where they investigated the effects of wood surface roughness, adhesive viscosity, and the processing pressure on adhesion strength [25].

On the other hand, absorption has an important role in mechanical interlocking, because absorption affects the penetration of a liquid into pores or irregularities on the adherend surface. Therefore, higher absorption produces better adhesion in mechanical interlocking systems [26]. The length scale, which changes according to type of interaction, is another factor that affects adhesion. The detailed length scales for adhesion are listed in Table 5.3 [11].

Mechanical interlocking is an important factor for adhesion in wood and affects the mechanical stability of end grain adhesive joints. Follrich *et al.* (2007) examined grain angle effects on shear strength and showed that good mechanical interlocking is an important factor for the strength of adhesive joints [27]. In another study on the thermal and mechanical properties of polypropylene (PP)-wood powder (WP) composites, it was determined that better interfacial adhesion can be obtained with better mechanical interlocking [28]. Smith

et al. (2002) used scanning electron microscopy (SEM) to investigate mechanical interlocking of a thermoplastic adhesive and wood substrate. They showed that the extent of mechanical interlocking depends on the processing details of the adhesive joints and higher pressure and higher temperature with increased process time provides better interlocking than a short process cycle [29]. Kazayawoko *et al.* (1999) investigated the effects of adhesion on wood-polymer composites' mechanical performance and indicated that a decrease in the quality of mechanical interlocking because of pores or crevices produced lower shear strength [30]. A study on mechanical interlocking of adhesive in the cellular structure of wood showed that mechanical interlocking is the only effective bonding mechanism in preservative-treated wood because cell walls are physically blocked and chemically modified by metal complexes [31]. Backman and Lindberg (2004) investigated the interaction of *Pinus sylvestris* wood with poly (vinyl acetate) (PVAc) adhesive, poly(methyl methacrylate) (PMMA), and a hydrophilic acrylate, and, as a result, found that adhesion between wood and PVAc adhesive is mainly attributed to mechanical interlocking [32].

Mechanical interlocking is strongly dependent on the surface properties. While studying mechanical interlocking, the surface properties including the presence of crevices, pores, roughness and irregularities should be well understood. Optimizing the surface properties, for instance, increasing the roughness, of the surface will produce stronger or better mechanical interlocking.

5.2.1 Atomic Force Microscopy (AFM) & Nanoindentation

The atomic force microscope (AFM), an instrument that allows the measurement of surface characteristics using different interaction modes, is a useful tool to accurately measure the adhesion and pull-off forces between two surfaces. AFM allows researchers to investigate the adhesion properties of materials on the micro- and nano- levels so it is a valuable tool to aid in the understanding of the interactions in wood adhesive bonding systems where wood is comprised of micro- and nano- structures [33].

Over the last decade, there has been a significant increase in adhesion and pull-off force determinations, which depend on contact mechanics, specifically: Hertz, JKR (Johnson, Kendall and Roberts) and DMT (Derjaguin, Muller and Toporov). JKR and DMT incorporate the concepts developed by Hertz in 1896 [34]. The equations responsible for determination of the contact radius and pull-off forces according to Hertz, JKR and DMT are given in Table 5.4 [35]. The comparison of the theories discussed above is based on interactions between a flat plane and a sphere depicted in Figure 5.4 [35]. There is no attractive force in the Hertz model, only hard wall repulsion at contact. The JKR model includes short-range adhesion which is essentially a delta function with strength W_A , and thus only acts within the contact zone. The DMT curve shown represents a long-range surface force between the surface and a sphere. A volume integrated force, like the van der Waals force, can also lead to a DMT dependence, where the contact profile remains Hertzian and the attractive forces act like an additional external load. For an actual interaction force, the integral of the attractive well corresponds to the work of adhesion, W_A .

Table 5.4 Equations responsible for determination of the contact radius and pull-off forces according to Hertz, JKR and DMT.

Equation	Method	Source
$a = \left(\frac{PR}{K} \right)^{1/3}$	Hertz	[204]
$K = \frac{4}{3} \left(\frac{1 - \nu_1^2}{E_1} + \frac{1 - \nu_2^2}{E_2} \right)^{-1}$	Hertz	[204]
$a = \left(\frac{R}{K} * (P + 3\gamma\pi R) + \sqrt{(6\gamma\pi RP) + (3\gamma\pi R)^2} \right)^{1/3}$	JKR	[35]
$P_c = -\frac{3}{2} \gamma\pi R$	JKR	[34]
$a = \left(\frac{R}{K} * (P + 2\gamma\pi R) \right)^{1/3}$	DMT	[205]
$P_c = -2\gamma\pi R$	DMT	[205]

where;

P= Load

a= Contact radius

R= Sphere radius

E_1, E_2 = Young's moduli

K= Combined elastic modulus of tip

ν_1, ν_2 = Sphere and flat-plane Poisson ratios

γ = Dupré energy of adhesion

P_c = Pull-off force

Surface roughness characterization and adhesion force measurements have become an important topic with the increase in nanotechnology research and improvements in devices like AFM [36]. Hertz, JKR, and DMT theories have been modified and modeled by different researchers and applied to various materials [37]. A study on determining the adhesion between two rough surfaces showed that the modified model based on JKR theory may provide a useful approach for researchers studying adhesion [37].

Another technique that is used to measure the effect of adhesives and the adhesion between adhesives and wood is nanoindentation, which provides a more accurate way to make adhesion measurements. This technique allows researchers to apply the force to the surface vertically and protect the tip sliding on the surface and creating greater adhesion forces due to friction. Jakes *et al.* (2008) devised an experimental method to account for structural compliance in nanoindentation measurements, where they utilized the standard Oliver-Pharr [38] nanoindentation analysis where assumptions of the model include having a structurally rigid specimen with a homogeneous structure [39]. As a result of their

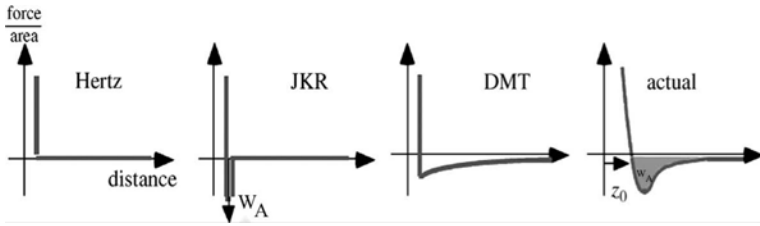


Figure 5.4 Interaction forces (per unit area) for the Hertz, JKR and DMT models, compared to an actual interaction. There is no attractive force in the Hertz model, only hard wall repulsion at contact. The JKR model includes short-range adhesion that is essentially a delta function with bond strength W_A , and thus only acts within the contact zone. The DMT curve shown represents a long-range surface force. A volume integrated force, like the van der Waals force, can also lead to a DMT dependence, where the contact profile remains Hertzian and the attractive force acts like an additional external load. For an actual interaction force, the integral of the attractive well corresponds to the work of adhesion, W_A [35].

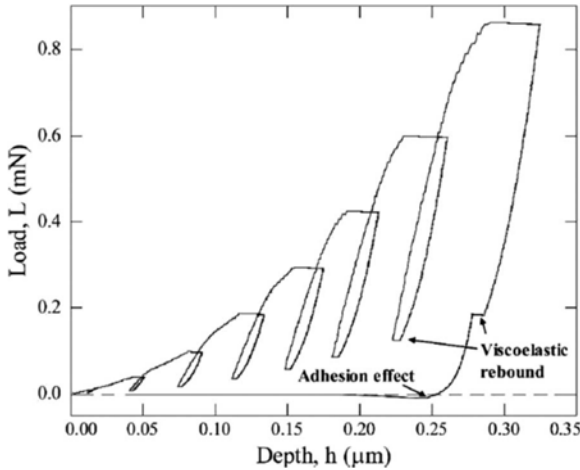


Figure 5.5 Typical load-depth (displacement) curve (drift subtracted) for multi-load indents performed in S2 layer of wood tracheid wall [39].

experimental study, they found a small amount of adhesion between the tip of the indenter and wood tracheid wall during the final unloading, which is shown in Figure 5.5 [39].

Konnerth and Gindl (2006) measured elastic modulus, hardness, and creep factor of wood cell walls in the interphase region of four different adhesive bonds specifically, melamine-urea-formaldehyde (MUF), phenol-resorcinol-formaldehyde (PRF), poly(vinyl acetate) (PVAc) and polyurethane (PU). They found that MUF and PRF bondlines produced improvement in elastic modulus and hardness and reduced the creep compared to reference cell walls (unaffected by adhesive) whereas PVAc and PUR bondlines decreased the elastic modulus and

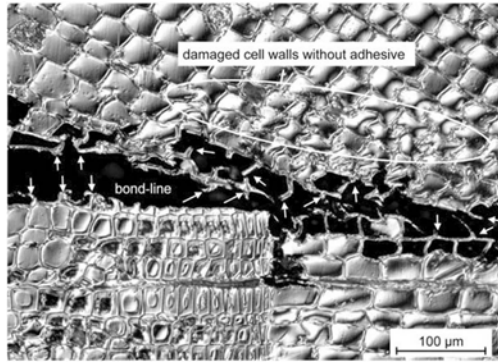


Figure 5.6 Optical micrograph of a wood-adhesive joint with a PVAc bondline (indicated by arrows) [40].

hardness and increased the creep. A sample optical micrograph, showing the tested (nanoin-dented) area of a wood joint with PVAc bondline, is provided in Figure 5.6 [40].

5.3 Electrostatic Adhesion

The electrostatic theory of adhesion was first proposed by Derjaguin in 1948 [41]. In the electrostatic theory, the adherend-adherend interface is viewed as analogous to the plates of an electrical condenser across which charge transfer occurs and adhesion strength is attributed to electrostatic forces (Figure 5.7) [6].

A list of the concepts and quantities important in electrostatic adhesion are shown in Table 5.5. Coulomb's Law describes the electrostatic interaction between electrically charged particles (Figure 5.8) as:

$$|F| = k_e \frac{|q_1 q_2|}{r^2} \quad (5.2)$$

where: F is force, k_e is Coulomb's constant, q_1 and q_2 are the charges and r is the distance between the charges. Capacitance C is defined as the ratio of charge Q on each conductor to the voltage V between them

$$C = \frac{Q}{V} \quad (5.3)$$

Derjaguin expressed the force $F(h)$ acting between two charges away from one another to the strength of an adhesion bond where:

$$F(h) = 2\pi R_{\text{eff}} W(h) \quad (5.4)$$

where: $W(h)$ is the interaction energy per unit area between the two planar walls and R_{eff} the effective radius.

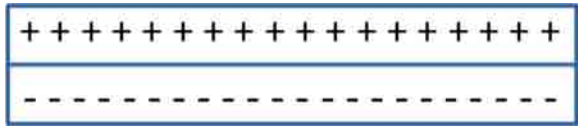


Figure 5.7 Schematic of the formation of an adhesion bond attributed to transfer of charge from an electropositive material to an electronegative material.

Table 5.5 Concepts and quantities important in electrostatic adhesion*.

Concept	Definition
Electric field	Generated by electrically charged particles
Coulomb's Law	Electrostatic interaction between electrically charged particles.
Capacitor	Consists of two conductors separated by a non-conductive region.
Charge density	Measure of electric charge per unit volume of space, in one, two or three dimensions.
Van der Waals force	Close-range force between two molecules attributed to their dipole moments
Hamaker constant	Augmentation factor for van der Waals force when many molecules are involved, as in the case of nanoparticles
DLVO Theory	Named after Derjaguin, Landau, Verwey and Overbeek. Theory explains the aggregation of particles in aqueous dispersions quantitatively and describes the force between charged surfaces interacting through a liquid medium. It combines the effects of the van der Waals attraction and the electrostatic repulsion due to the so-called double layer of counter ions.
Zeta potential	The potential difference between the dispersion medium and the stationary layer of liquid attached to the dispersed particle
Smoluchowsky approximation	Used to calculate the zeta potentials of dispersed spherical nanoparticles

*Adapted and augmented from [43]

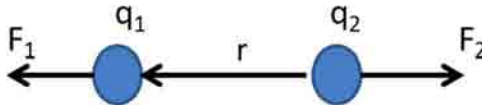


Figure 5.8 Interaction between electrically charged particles. F_1 and F_2 are the forces of interaction between two point charges (q_1 and q_2) and the distance (r) between them.

When dealing with electrostatic interactions in liquids, the Derjaguin, Landau, Verwey and Overbeek (DLVO) theory is used to describe interactions between charged surfaces where the total adhesion force F_A is equal to the sum of the van der Waals force F_{vdW} and the Electric Double Layer force F_{EDL}

$$F_A = F_{vdW} + F_{EDL} \quad (5.5)$$

The van der Waals force is a function of the system Hamaker constant, particle diameter, contact radius and particle-surface separation distance. The Electric Double Layer force is a function of liquid medium dielectric constant, zeta potential, reciprocal double layer thickness, particle diameter, and particle-surface separation distance.

The electrostatic theory is often used to describe adhesion behavior of powders to solid surfaces [41–43]. Practical applications of electrostatic adhesion in wood and wood-based materials include coating of furniture, sandpaper manufacture, xerography or photocopying paper, and ink jet and laser jet printing [44–46]. Typically, dry particles or powders (coatings, inks) are charged and deposited on an oppositely charged or grounded substrate. A novel application of inkjet printing is in the creation of bioactive papers for cellulose-based functional materials [47]. Waterborne coatings can also be applied to wood electrostatically [48]. Electrostatic coating of wood became viable and commercially applicable in the 1950s [49, 50]. However, the scientific literature has been somewhat limited on electrostatic adhesion applied to wood over the past 60 years. It should be noted that the patent literature on electrostatic powder coating over the same time period is significant [51].

Electrostatic adhesion that occurs in the liquid phase through colloidal interactions has received much greater emphasis in the scientific literature and practical applications are plentiful in paper manufacturing [52]. Electrostatic interactions have also been the subject of study regarding cellulose films [11]. Electrostatic self-assembly in liquids is an important area in nanoscience applications [43, 53] and has been applied to paper coatings with success [54]. Electrostatic self-assembly has also been applied to wood using layer-by-layer (LbL) nanoscale coatings (Figure 5.9) and the creation of conductive paper using nanoparticles [55–58].

5.4 Wettability, Surface Energy, Thermodynamic Adhesion

Thermodynamic adhesion or wetting refers to the atomic and molecular interactions between adhesives and adherends. Surface tension or surface energy represent these forces and are regarded as fundamental material properties to understand adhesion because they are associated with adhesive bond formation [5]. Bond formation arises from the highly localized intermolecular interaction forces between materials. Therefore, good wetting is beneficial to strong adhesive bonding. Mittal pointed out that the dominant surface chemical and energetic factor influencing joint strength is interfacial tension between the adhesive and the adherend (γ_{sl}): the joint strength increases as γ_{sl} decreases [59]. The atomic and molecular forces involved in wetting include: (a) acid-base interactions, (b) weak hydrogen bonding, or (c) van der Waals forces (dipole-dipole

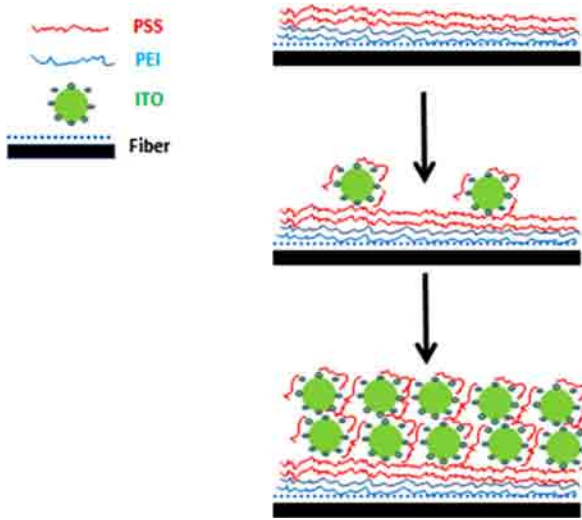


Figure 5.9 Schematic representation of LBL coating of wood fibers with polyethyleneimine (PEI), poly(sodium 4-styrenesulfonate) (PSS) and indium tin oxide (ITO) [57].

and dispersion forces) [5]. The condition necessary for spontaneous wetting is given below:

$$\gamma_{sg} \geq \gamma_{sl} + \gamma_{lg} \tag{5.6}$$

where: γ_{sg} , γ_{sl} and γ_{lg} are respectively the interfacial free energies for solid-gas, solid-liquid and liquid-gas interfaces. If γ_{sl} is insignificant, the criterion can be simplified to:

$$\gamma_{sg} \geq \gamma_{lg} \text{ or } \gamma_{substrate} \geq \gamma_{adhesive} \tag{5.7}$$

which means that the adhesive will wet the surface of the adherend when the surface free energy of the substrate is greater.

Usually the determination of surface free energies of solids can be made by measuring the contact angles of appropriate probe liquids on the solid surface. Different contact analysis techniques are applied in the measurements of various forms of substrates. One is the sessile drop method (Figure 5.10) which is also referred to as static contact angle technique. The angle can also be calculated by the following equation with obtained height (h) and radius (r) of the spherical drop.

$$\text{Contact angle } (\theta) = \sin^{-1} \frac{2rh}{r^2 + h^2} \tag{5.8}$$

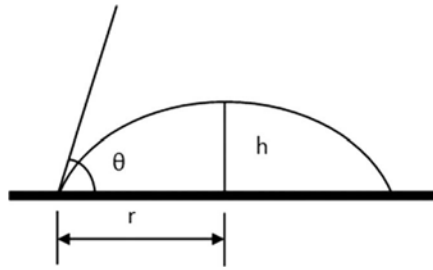


Figure 5.10 Schematic illustration of the sessile drop method.

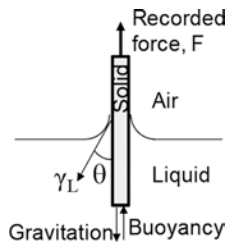


Figure 5.11 Schematic illustration of the Wilhelmy method.

Another method is the Wilhelmy Plate technique that is suitable for making contact angle measurements on thin plates and single fibers. According to Figure 5.11, the contact angle can be calculated using the Wilhelmy equation (Equation 5.9) [60].

$$F = \gamma_L P \cos \theta + mg - \rho_L Ahg \quad (5.9)$$

where:

F = advancing or receding force on the sample in liquid

γ_L = surface tension of the liquid

P = perimeter of the wetted cross section

m = mass of the specimen

g = acceleration due to gravity

ρ_L = liquid density

A = cross-sectional area of the specimen

h = depth of immersion.

For particles (also fibers), by recording the process of liquid going through a column attributed to capillary forces where particles of interest are packed inside, the contact angle

can be calculated from the Washburn equation (Equation 5.10) [61] that governs the wicking process:

$$h^2 = \frac{tR\lambda_L \cos \theta}{2\eta} \quad (5.10)$$

where:

h = height to which liquid has risen as a function of time t

R = effective interstitial pore radius between the packed particles

γ_L = surface tension of the liquid

η = viscosity of the liquid.

Recently a three-dimensional dynamic contact angle analysis method was developed that can determine the key parameters such as volume and contact angle during sessile droplet measurement [62]. A strong point of this method is that even when the orientation of the droplet's axis changes with time, the dynamic parameters of droplet on anisotropic surfaces can be determined. However, one limitation of this technique is that because the model is based on spherical and ellipsoidal droplets, the calculated volumes and contact angles for non-elliptical oblong droplets are not reliable.

The methods for determining surface free energy of solids based on contact angles are various, for example the Zisman approach [63], the Neumann (the equation of state) [64], the Chibowski approach [65], the harmonic mean approach [66], Owens and Wendt approach (the geometric mean) [67] and the acid-base approach [10], which are reported in a recent review by Etzler [65]. Most of the methods have already been applied to wood surface adhesion. Another way to compute surface free energy of fibers or particles is by inverse gas chromatography (IGC) which provides an alternative to the measurement of contact angles [68]. Regarding the wetting of wood materials, there are several influential factors: wood species, sapwood or heartwood, grain orientation, wood elements and chemical composition, surface roughness, absorption and capillary flow, sample aging, and machine test speed, different treatments, etc. [69–72].

5.4.1 Wood Anatomy Impact on Wetting

In general, hardwoods have lower contact angles than softwoods whose surfaces contain more hydrophobic substances, such as resins and unsaturated fatty acids, in addition to phenolic compounds in both species [73]. As reported, huge variability in surface free energy of wood exists along the stem [74]. The polar component of surface free energy is found to be high at the stem base and gradually decreases with height, but the dispersion component acts in an opposite manner. Because the polar component of surface free energy is markedly higher than the dispersion component, in general, the surface free energy decreases along the tree height. No significant difference in surface free energy is observed across the tree cross section. Wood is more easily wetted along the grain direction than across the grain direction [75, 76]. This results from the fact that the liquid drop placed on the surface

will spread easily along the wood cell lumen in the grain direction than across the lumen because of capillary effects during the adhesive wetting process [70].

Heartwood and sapwood have different influences on the wetting by adhesives. Heartwood normally contains extractives and hardened parenchyma cells. Additionally, closed pits in heartwood will greatly reduce the number of microscale pathways for adhesive penetration. Therefore, the heartwood is expected to be less wettable than sapwood in terms of instantaneous liquid spreading. However, the difference in equilibrium contact angles between heartwood and sapwood depends on the wood species and resin type [70]. On the microscale, earlywood consists of parenchyma and is distorted more by cutting tools, resulting in protruding cell fragments. Therefore, earlywood is often rougher than latewood [77]. So normally, wettability and surface free energy of earlywood are greater than latewood.

5.4.2 Extractives

The influence of extractives on the wettability of wood surface is significant because of both physical blocking of adhesive penetration and chemically affecting the curing process [78, 79]. Decreased wettability can also be attributed to the change in wood chemical composition [80] and acid-base property of the wood surface when it is covered by extractives [81]. Because the surface composition and surface free energy of the solid are altered, the measured contact angle is not representative of the state of the surface of interest. A detailed description of the effect of extractives on wood surface wettability can be found in the section on weak boundary layers.

5.4.3 Adhesive Wettability

The differences among contact angles are related to the nature of the adhesives. PF resins are more hydrophobic than UF resins because of the phenyl rings present in their structures. As a result, the contact angles of PF resins should be larger than that of UF resins. On the other hand, viscosity of UF and PF is also an important factor affecting wetting [82]. The contact angle increases with an increase in resin viscosity [83]. Wetting of soy protein adhesives modified by urea on wood surfaces was found to increase because the molecular attraction between the adhesive and the wood surface was greater than that between adhesive molecules after modification [83]. Incorporation of dendritic compounds which bear different end groups such as $-OH$, $-NH_2$, and NH_3^+ , Cl^- into urea-formaldehyde adhesive has been shown to be effective adhesion promoters for wood bonding. This promotion is partially attributed to the improved wetting caused by the large number of polar functional groups present at the interface [84].

5.4.4 Wood Modification

Within a short period of time, freshly-cut wood surfaces undergo a transformation that has been referred to as surface inactivation. The major reason for the change of wood surface

free energy is the migration of low molecular weight extractives to the wood surface and the oxidation of extractives thereafter. This will reduce the surface wettability and impair the bonding of wood elements. Several chemical, physical, and mechanical methods can be applied to activate the surface from hydrophobic to hydrophilic, which is further discussed in the weak boundary layer section. At the same time, a hydrophobic wood is usually favored since hydrophilicity is an intrinsic property of wood, which is detrimental to physical properties, mechanical properties, and utility and service life of wood-based products. To minimize the hydrophilic effect, acetylation and grafting of hydrophobic groups on wood are general methods. Besides the interaction with moisture, flammability and biodegradability are intrinsic properties of wood that hamper its application. These can be overcome or ameliorated by fire retardant and preservative treatments. For bonding wood to fiber-reinforced plastics (FRPs), hydroxymethyl resorcinol (HMR) is used as adhesion promoter to produce durable adhesive bonds in an exterior environment for a number of diverse resin adhesive systems [85]. All these modifications will affect the wettability and surface free energy of wood and a brief review is given below. A summary of these treatments on the wettability of wood is shown in Table 5.6.

5.4.4.1 Acetylation

Acetylation is basically an esterification process where the available hydroxyl groups of wood are reacted with acetic anhydride. A review on acetylation of wood was reported by Rowell [86]. Chemicals that have been studied include acids (carboxylic acids, phthaldehydic acids), aldehydes (formaldehyde, difunctional aldehydes, acetaldehyde, chloral), chlorides (acid chlorides, alkyl chlorides), esters (β -propiolactone), ketene, isocyanates, acrylonitrile, dimethyl sulfate and epoxides. It was reported that all of these chemicals can create a hydrophobic layer on the wood surface by reacting with hydroxyls, reducing the wetting of polar adhesives on wood [87].

5.4.4.2 Grafting

Grafting is referred to as the covalent bonding of various substances like polymers or monomers, as well as smaller organic or inorganic compounds onto functional groups on a surface. For wood surfaces, new functional groups are introduced by reacting with existing functional groups (mainly hydroxyl) in wood polymers. A grafting process can be achieved by plasma, wet chemical and even enzymatic methods. Wettability of treated wood surfaces is determined by the functional groups grafted onto the wood. Hydrophobic groups will reduce the wetting of wood [88–90]. Prolonging the reaction duration of grafting will add more polymers on the wood substrate, creating a less wettable surface.

5.4.4.3 Fire Retardants, Preservatives and Adhesion Promotion

Ayrilmis *et al.* (2009) studied the wettability of fire retardant treated laminated veneer lumber (LVL) with a borax-boric acid compound, monoammonium phosphate and diammonium phosphate [91]. They found that waterborne fire retardants such as boron compounds and phosphates can make more wettable wood surfaces attributed to the hygroscopic

characteristics of the reagents, which was confirmed by other researchers [92]. On the other hand, other research indicated that borax and boric acid used as preservative resulted in poor wettability of alder and beech veneer surfaces [93]. The authors pointed out that wettability is dependent on the type of impregnation chemical, and also the wood species and resin used for bonding wood. The effects of two wood preservatives (waterborne chromated copper arsenate (CCA) and organometallic copper naphthenate (CuN)) on the surface free energy of wood and E-glass/phenolic composite material were also investigated [94]. The CuN treatment increased the contact angle of water on southern yellow pine because of the oily non-polar nature of this kind of preservative. CCA treatment reduced the contact angle of water and increased the total surface free energy of wood by metallic salts with high surface energy.

Hydroxymethyl resorcinol (HMR) can produce durable adhesive bonds for application in exterior environments. The dynamic adhesive wettability of HMR treated wood with PF and PMDI was found to decrease because the dispersion component of surface free energy decreased in this treatment [85]. The principles and details of wood surface modifications can be found in a recent review by Petric [95].

5.4.5 *Test Methods*

Compared to homogeneous materials like plastics and metals, the wetting process of wood is more complex and is attributed to its intrinsic surface properties like heterogeneity, roughness, and liquid adsorption, which makes the thermodynamic equilibrium conditions assumed by Young's equation not applicable to wood surface [96]. Therefore, some modifications on contact angle measurements and calculations are applied by researchers to take into account these factors. The sessile drop contact angle technique also referred to as static contact angle measurement has appeared in most previous studies on determination of the thermodynamics of the liquid/solid interaction of wood where the instantaneous or equilibrium contact angles were usually used [97]. However, it has been reported that time is a significant factor affecting the measured surface parameters of the wood surface [75, 98, 99]. Thus, simply comparing initial or equilibrium contact angles is not as meaningful as investigating all other phenomena during the wetting process like spreading and penetration [70]. Models and parameters (decay ratio, spreading ratio and changing rates) can be used to illustrate the dynamic wetting process [99].

During the measurement of contact angles on wood surfaces by the Wilhelmy plate method, a hysteresis phenomenon is observed [71]. That is, the advancing contact angle on the wood surface during the immersion process is usually higher than the receding contact angle when the liquid is withdrawn from the wood surface. This phenomenon is attributed to two reasons: (1) wood surface is heterogeneous which represents the low-energy sites during advancing contact angle measurement, while the surface transforms to high-energy sites during receding angle measurement because it is already covered with the test liquid; (2) molecules or hydroxyl groups in the solid surface rearrange after contact with a polar liquid. For instance, hydroxyl groups on the wood surface try to avoid contact with inert air by hiding under the surface, but they reorient to form hydrogen bonds when the surface

Table 5.6 Change in wettability after different treatments on wood surfaces.

Treatment	Species	Contact angle	Surface free energy	Wetting	References
Acetylation	Scots pine (<i>Pinus sylvestris</i>)	↑	↓ (acid -base)	↓	[87]
Grafting	Pine (<i>Pinus sylvestris</i>)	↑	↓ (acid-base)	↓	[90]
Fire retardant	Beech (<i>Fagus orientalis lipsky</i>)	↓	-	↑	[91]
Preservative	Alder (<i>Alnus glutinosa subsp. barbata</i>)	↑ (Boric acid)	-	↓ (Boric acid)	[93]
	Beech (<i>Fagus orientalis</i>)	↑ Copper Naphthenate (CuN)	-	↓ (CuN)	[94]
	Southern yellow pine	↓ Chromated Copper Arsenate (CCA)	-	↑ (CCA)	
(Adhesion promoter Hydroxymethyl resorcinol) (HMR)	Southern pine (<i>Pinus</i> spp.) and Douglas-fir (<i>Pseudotsuga menziesii</i>)	↓	↑ (acid -base)	↓	[206]

↑ Increase, ↓ Decrease, acid-base: acid-base component of surface free energy

is in contact with water [71, 100]. End-sealing wood veneers or polymeric foams with poly (vinyl acetate) is recommended as a standard practice for Wilhelmy plate analysis because it can reduce capillary uptake of the probe liquid, reducing premature wetting of the wood surface. Another way to minimize the effect of capillarity is to increase the test speed to reduce the time for absorption.

It is not accurate to use column wicking measurements to determine the contact angle on swelling polymer substrates by the Washburn equation because the effective interstitial pore radius (R) in the wicking experiments changes after the particles swell. Two phenomena observed during the wicking process indicate that the equation needs further modification: (1) heat was released during the wicking process when the polar liquids contacted the swelling polymer particles, and (2) compared to using hexane (non-polar liquid), using methanol (polar liquid) resulted in a smaller average capillary radius (r) [101]. At the same time, Shi and Gardner (2000) reported one attempt to account for swelling and energy loss during the wicking tests [101].

5.5 Diffusion Theory of Adhesion

The diffusion theory is based on the concept that two materials are soluble in one another, i.e. compatible, and if they are brought into close contact, they dissolve in one another and form an interphase which is a solution of both materials in one another and therefore does not form a discontinuity of physical properties between the two materials (Figure 5.12) [6]. In the case of wood adhesive bonding, this theory is more applicable for an adhesive that diffuses/penetrates into the wood cell wall. Penetration is the ability of an adhesive to move into the voids on the surface of a substrate or into the substrate itself. The cellular nature of wood can cause significant penetration of an adhesive into the substrate. Adhesive penetration follows the path of least resistance into the porous structure, either by gross penetration or by cell wall penetration [102]. According to Frihart (2004) there are four scenarios of penetration: 1) occupation of free volume, 2) mechanical interlocking, 3) interpenetrating polymer networks, which form cross-links between the adhesive molecules within the free volume of the cell wall, and 4) chemical cross-links with cell wall polymers [103].

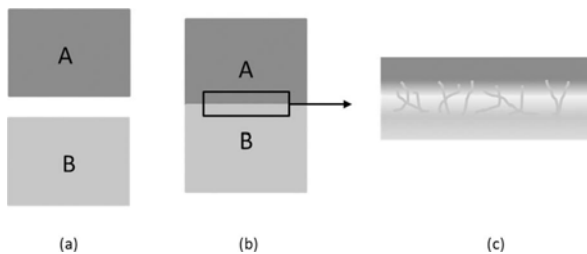


Figure 5.12 Schematic of diffusion theory of adhesion: (a) two compatible materials are brought into close contact (b) and an interphase (c) is formed where both materials mix and/or entangle with one another.

Adhesive bond performance between wood elements is presumed to be significantly influenced by the degree of penetration of the adhesive into the porous network of interconnected cells and is controlled by 1) adhesive variables (molecular weight (MW), distribution), 2) substrate variables (species, orthogonal plane, moisture content) and 3) processing variables (curing method i.e. time, pressure, and temperature). Swelling is defined as the uptake of liquid molecules by wood polymers in the wood cell wall and is driven by diffusion. The degree of swelling decreases with increasing size of the molecules in the liquid [104]. Mantanis *et al.* (1994) showed that even relatively large molecules, like pyridine (MW=79) and benzyl alcohol (MW= 108), are able to swell the wood cell wall significantly because of their high capacity to form hydrogen bonds [104]. Furuno *et al.* (2004) studied the penetration of PF resin at different MWs (290, 470, 820) into the wood cell wall and found that low MW resin penetrated more into the cell wall whereas the medium and high MW resins penetrated only slightly [105]. A lower MW resin is also more likely to contribute to dimensional stability and decay resistance [105]. Similar results were reported by Laborie and coworkers [106, 107] suggesting a nanoscale miscibility of low MW PF resin with wood polymers using solid-state NMR spectroscopy.

Research investigating bondline performance has focused on methods using microscopic examination and associated techniques with the goal of establishing a relationship between penetration and bond performance. Modzel *et al.* (2011) provide a good review on microscopic methods used and resin systems studied to examine adhesive penetration in wood [108]. Figure 5.13 gives an overview of the most commonly used methods and examples of attainable images to study resin penetration into wood.

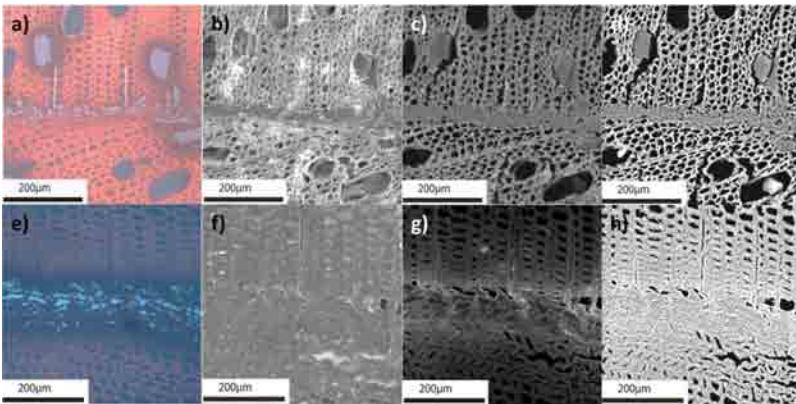


Figure 5.13 Photomicrographs of PF adhesive bondlines in hybrid poplar (a-d) and Douglas-fir (e-h) with rubidium replacing sodium in the PF formulation for better detection. Images show the same field of view for each species and were created using fluorescence microscopy (a+e), scanning electron microscopy (SEM) (b+f), SEM with back-scatter detector (BSE) (c+g), and SEM with wavelength-dispersive spectroscopy (WDS) (d+h). Images courtesy of Fred Kamke.

More recent work using micro- or synchrotron radiation X-ray computed tomography has shown its advantage over more conventional microscopic techniques in providing an accurate representation of the 3D microstructure of the wood and penetrating adhesive system [109–111]. Furthermore, it is possible to calculate the stress and strain in the adhesive bondline using a micromechanical model proposed by Kamke *et al.* [112]. Besides the adhesive type, especially the characteristics of the wood elements to be bonded play an important role in penetration and bond performance. Gruver and Brown (2006) investigated the penetration and bond performance of pMDI according to: 1) species, 2) anatomical bonding plane, and 3) moisture content by fluorescence microscopy and compression shear block test [113]. While a species and corresponding anatomical effect was observed, overall bond performance was mostly influenced by moisture content. The influence of species and corresponding anatomy is most apparent in hardwood species, where the penetration occurs mostly in the vessel network compared to softwoods where the penetration is more evenly distributed and interconnected [110]. Mendoza *et al.* (2012) developed a model to predict adhesive penetration into the interconnected vessel network of hardwoods taking into account adhesive hardening, capillary penetration, and processing techniques [114]. A different method to characterize resin penetration is described by Wang and Yan [115] who used mercury intrusion porosimetry to measure the pore volume with and without resin. Their work showed that processing parameters are an important factor, since pressure applied by hot-pressing promoted resin penetration into smaller pores.

While gross penetration into wood cells is relatively easy to study, the methods employed are often limited by their resolution and/ or contrast capabilities to investigate cell wall penetration on the nano- or even angstrom scale. To date, the most successful methods to investigate cell wall penetration use some form of tagging of the adhesive to make the tag detectable by the method employed. The penetration of UF/UMF resin into MDF fiber walls was shown by means of confocal scanning microscopy in combination with staining [116, 117]. Xing *et al.* (2005) observed that the penetration was directional through the outside of the fiber wall towards the lumen and not horizontal along cell wall layers, presumably through pores in the cell wall [116]. Gindl and coworkers (2002, 2003) used UV absorbance microscopy specifically for melamine in MUF and MF resin to study cell wall penetration. Their results confirm that resin diffusion into the wood microstructure occurs for these adhesive types [118, 119]. The UV absorbance microscopy method was further used to study the effect of resin diffusion on the stability of adhesively bonded joints of PUR and PRF resins on cell wall mechanical properties by nanoindentation [120]. PRF resin penetrated the cell wall microstructure while PUR resin did not. The elastic modulus determined by nanoindentation of resin infiltrated undamaged cells did not change significantly but hardness increased. The presence of PRF but not of PUR and epoxy resin in wood cell walls was also determined by scanning thermal microscopy [121].

Another more recently developed technique is the use of solid or solution state NMR spectroscopy to investigate polymer miscibility and therefore nano scale cell wall penetration of isotopic labeled PF and pMDI resins [107, 122–124]. NMR spectroscopy has also found application in investigating the adhesiveless bonding of wood by high speed rotation welding [125]. The mechanism for high speed rotation, as well as linear vibration welding,

relies on mechanical friction and corresponding temperature-induced softening and penetration of amorphous polymer material (mostly hemicelluloses and lignin) into the intercellular structure of the wood. The result is a high densification of the bonded interphase, yielding high quality wood-wood joints [125–127].

5.6 Covalent Bonding

A covalent bond is a bond where two atoms share an electron pair and is believed to improve the bond durability between wood and an adhesive. While covalent bonds occur in certain fields of adhesion their existence was for a long time not believed to occur between wood and adhesives [11, 128]. It is well established that the energy of activation of the condensation of wood adhesives (e.g. PF, UF, MF and MUF) is influenced by the presence of wood polymers compared to neat resin [129–132]. According to Pizzi *et al.* (1994) two effects are present when an adhesive cures on a wood surface, 1) catalytic self-activation of the resin self-condensation induced by carbohydrates and 2) formation of resin-substrate covalent bonds induced by lignin [130]. However, the contribution of the second one is very small and often negligible under the conditions pertaining to thermosetting adhesive applications [130, 131] and do not exist for MUF systems [133].

A limiting factor for the investigation of resin to wood substrate covalent bonding is the difference between conditions in the laboratory and industrial settings. Often used differential scanning calorimetry (DSC) and thermogravimetric analysis (TGA) techniques are subject to time and temperature limitations since heating rates are much slower (10–20°C/min) compared to a maximum heating and curing of only a few minutes in industrial composite board production processes. Even more extreme sampling requirements are necessary when infrared (IR) and ultraviolet (UV) spectrophotometries are used [130].

Most of the more recent research in wood-adhesive covalent bonding focuses on phenyl isocyanate-based adhesives, since they are most likely to form urethane (or carbamate) bonds with wood polymers and are shown to penetrate the wood cell wall and intimately associate with wood molecules [122–124, 132, 134]. Solid-state NMR spectroscopy can be used to study urethane formation using isotopic labeled isocyanate pMDI. However, this method cannot identify covalent bonds with certainty since urethane and polyurea signals display a significant overlap in the acquired spectra and are of low signal intensity [123, 124, 134]. A solution-state NMR spectroscopy technique was further developed to allow for a more accurate determination of isocyanate reactivity with wood. While this method was able to detect urethane formation between phenyl isocyanate and cell wall polymers no covalent bonds could be determined in experiments under typical conditions used for industrial oriented strand board (OSB) bonding using pMDI [135–137]. Bao *et al.* (2003) proposed a model for pMDI bonding and attribute the strength of this particular wood-adhesive bond to the deep penetration of adhesive molecules into the wood cell wall and middle lamella and the crosslinking between individual sections between and within cells [138]. All together it is very unlikely that covalent bonds form in any significant amount under conditions characteristic of thermosetting wood adhesive applications, even though

the formation of covalent resin-substrate bonds has been demonstrated to exist. If the advantages of covalent wood-adhesive bonds are desired for certain applications, future work in this field needs to focus on adjusting processing parameters to allow for the formation of covalent bonds and further development of detection methods.

5.7 Acid-base Theory

Based on the correlation of acid-base interactions by Drago *et al.* (1971) [139], Fowkes and Mostafa proposed a new method to interpret the interactions during polymer adsorption where the polar interaction is referred to as an acid-base interaction [140]. In this interaction, an acid (electron-acceptor) is bonded to a base (electron-donor) by sharing the electron pair offered by the latter, which forms a coordinate bond.

Thomas Young formulated (without using equations) the relation between the surface tension of a liquid and a solid, the interfacial tension between the solid and the liquid, and the contact angle θ for a drop of liquid deposited on a flat horizontal surface [141]. This formulation is usually expressed as Young's equation:

$$\gamma_{LG} \cos \theta = \gamma_{SG} - \gamma_{SL} \quad (11)$$

where: γ_{LG} and γ_{SG} are the surface free energies of the liquid and the solid, respectively, exposed to a gas (G), and γ_{SL} is the solid-liquid interfacial free energy.

Perhaps the most convenient way of interpreting the wettability of a low-energy surface, such as that of various polymers or ligno-cellulosic materials, is by the formulation of the work of adhesion, W_a , defined as the work required to separate unit area of the solid-liquid interface [142], i.e.

$$W_a = \gamma_s + \gamma_L - \gamma_{SL} \quad (5.12)$$

where: γ_s and γ_L are the surface free energies of the solid (S) and liquid (L) surfaces in vacuum, and γ_{SL} is the solid-liquid interfacial free energy.

The surface free energy per unit area (or surface tension) g_i of the substance i is defined as half the work of cohesion W_c , i.e.:

$$\gamma_i = \frac{1}{2} W_c \quad (5.13)$$

Assuming that $\gamma_L \approx \gamma_{LG}$ and $g_s \approx g_{SG}$, combination of equations (5.11) and (5.12) leads to the Young-Dupré equation:

$$W_a = \gamma_L (1 + \cos \theta) \quad (5.14)$$

Hence, if the contact angle, θ , of a well-defined probe liquid against a solid is measured, the work of adhesion can be determined.

The following descriptions briefly summarize the Lewis acid-base concept in wetting-related phenomena. According to Fowkes [143] and van Oss *et al.* [144], the total work of adhesion in interfacial interaction between solids and liquids can be expressed as the sum of the Lifshitz-van der Waals (LW) and the Lewis acid-base (AB) interactions, viz.

$$W_a = W_a^{LW} + W_a^{AB} \quad (5.15)$$

The separation of the work of adhesion into LW and AB components is also applicable to the surface free energies according to:

$$\gamma_i = \gamma_i^{LW} + \gamma_i^{AB} \quad (5.16)$$

A breakthrough in the understanding of wetting phenomena was the Good-Girifalco-Fowkes 'geometric mean' combination rule for the LW interactions between two compounds i and j, which can be expressed as [145, 146]:

$$W_a^{LW} = 2\sqrt{\gamma_i^{LW}\gamma_j^{LW}} \quad (5.17)$$

Hence, if the θ is determined for both a non-polar and a polar liquid, with known γ^{LW} parameters, on the same surface, then W_a^{LW} and W_a^{AB} can be determined using equations (5.14–5.17).

The acid-base theory plays a critical role in surface chemistry and adhesion and it has been exploited broadly on different materials [147, 148]. Several models of calculating the surface energy of solids were proposed where acid-base theory was applied, including Fowkes's method, Good's method, van Oss's method and Chang's method [65]. In terms of surface energy of wood determined by contact angle analysis, results from the Zisman approach deviate from other methods; the equation of state method is practical to an adhesion interaction only having a dispersion component because the polar part of the equations is not related to contact angle. For chemically heterogeneous materials like wood, the acid-base approach is a more valuable method because it can provide the most detailed information about the surface chemistry including the values of Lifshitz-van der Waals (dispersion) and Lewis acid-base (polar) components of surface free energy. Because the type of contact angle test liquid has an influence on the results of the acid-base approach, a minimum of three liquids is recommended for this method [10, 149].

Analysis of wood extractives reveals that they are the dominant factor influencing the acid-base properties [81]. Wood surfaces with extractives exhibit less acidic (electron-accepting) character and greater basic (electron-donating) character and the Lifshitz-van der Waals (dispersion) surface free energy component increases after the elimination of extractives from spruce wood particles [68].

5.8 Weak Boundary Layer

Bikerman first introduced the concept of a weak boundary layer (WBL) in adhesion science in 1961 [150]. In his model, three general classes of WBLs were specified, i.e., air

bubbles, impurities at the interface, and reactions between components and the medium. It was pointed out that the interface was the place where the failure of a bonded assembly will occur when a weak boundary layer was present. The WBL is important because people initially thought that an interface between an adhesive and a substrate would not fail, but actually it can fail if a WBL is present. Thus, to achieve satisfactory adhesive bonding performance, the weak boundary layer should be eliminated.

In regards to wood adhesion, Stehr and Johansson gave a detailed definition of the WBL (Figure 5.14) [151]. They classified wood weak boundary layers into two groups. The first group is referred to as a chemical weak boundary layer (CWBL) which is attributed to low-molecular-weight compounds on the wood surface. This contamination usually comes from extractives of wood, containing both hydrophobic and hydrophilic components. The second group is referred to as a mechanical weak boundary layer (MWBL) formed by damage to the wood surface. The MWBL derives from surfaces going through machining processes (planing, sanding, peeling, etc.), weathering (light delignification) and other forms of loose particles (dirt), as well as trapped air bubbles.

Christiansen (1990) focused on the influence of excessive drying (surface inactivation) on wood bonding. Physical responses to excessive drying include: 1) migration of extractives to the surface, lowering the wettability or covering the surface, 2) rearrangement of wood surface molecules, reducing wettability or sites for bonding, and 3) permanent closure of large micropores in cell walls [78]. Chemical responses to excessive drying include: 1) deteriorating wood surface strength, 2) degrading wood surface by oxidation and pyrolysis reactions, 3) chemical interference with resin cure or bonding, and 4) reducing the number of surface hydroxyl groups by etherification [79]. Besides, drying methods can have different impacts on wettability of wood [69]. For example, research found that polar components of oven and rotating-drum dried strands were greater than that of air and microwave dried strands [152].

5.8.1 *Extractives*

The mechanisms proposed for surface inactivation appear valid to some degree. The wood aging effect is generally attributed to the exudation of wood extractives to the exterior surfaces after machining processes, which decreases the wettability and surface free energy of wood surfaces [98, 153]. Overall, the chemical compositions of extractives have much lower oxygen to carbon (O/C) ratios compared with cellulose, causing a hydrophobic effect, which is detrimental to the wetting of polar adhesives [80, 154]. The hydrophobic components from bark extractives have more difficulty in being covered by the polar adhesive during gluing. Thus, bark extractives are adverse to the interaction of the particle/phenol-formaldehyde adhesive system [155].

Extractives often affect the curing process of adhesives because they contain both acidic and basic constituents. For PF resin, some previous studies on the effects of wood extractives on the curing reaction of resole (alkaline curing) resins showed that the acidity of the wood extractives inhibited the curing of the resole by changing them from weak basic to neutral, which resulted in the formation of a large quantity of dimethylene ether linkages [156, 157]. A definitive answer pertaining to the influence of wood extractives and

their chemical compositions on the hardening behavior of aminoplastic condensation resin adhesives (urea- and melamine-formaldehyde) is not clear: acceleration as well as retardation of the hardening process have been reported [158, 159]. Acceleration of the hardening process of aminoplastic resins usually results from a decrease in the adhesive pH after application onto a wood surface [160]. Resin curing retardation arises from the basic component in wood extractives. However, dissimilar to the former two cases, extractives of different wood species from cold water extraction had almost no effect on the curing process of UF resin and melamine-modified UF resin [158]. For wood-cement composites, hydration of cement was inhibited by low molecular weight carbohydrates and hemicelluloses [161].

Extractives also have a negative influence on the hydrogen bonding prevalent in wood pellet manufacturing [162, 163]. Detailed explanation was given that extractives block many binding sites on the particles, therefore, little hydrogen bonding or van der Waals forces occur between particles, forming a chemical weak boundary layer [164, 165]. A positive aspect of extractives during wood pellet production is that they have a beneficial effect on lowering the energy consumed during compression by acting as plasticizers and lubricants [162].

5.8.2 Heat Treatment

Heat-treated woods have outdoor applications attributed to their enhanced properties such as reduced hygroscopicity, improved dimensional stability, and improved resistance to degradation by microorganisms. Much research has focused on the change in wettability of heat-treated woods because excessive heat can cause problems during varnish or paint application. The wettability of wood decreases after high temperature treatment [166–172]. Contact angles on heat-treated wood surfaces increase because of a more hydrophobic character of the surface attributed to partial degradation of hemicelluloses and the plasticization of lignin, leading to a rearrangement of the wood polymer components [173–179] and exudation of extractives and VOC-like substances to the surface [80]. In contrast, an interesting result was that certain exterior waterborne coatings were found to exhibit much better wetting on oil-heat-modified Scots pines than on unmodified samples that should be more hydrophilic and readily wetted. It was believed that surface tensions of the tested waterborne coatings were low, attributed to the increased hydrophobicity by adding silicone

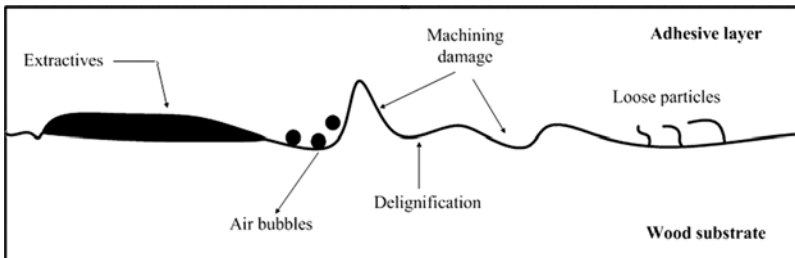


Figure 5.14 Revised scheme for weak boundary layer in wood adhesion [151].

and wax into the coating and the dispersion component of the surface free energy increased after heat treatment [180].

5.8.3 *Wood Impregnation and Densification*

After the first patented procedures appeared, wood densification methods have been available for at least a century [172]. Wood can be densified because it is constituted of cells whose lumens can be filled with other materials like polymers, wax, sulfur and molten metals. The surface energy of densified wood decreases slightly compared to hydro-thermally treated wood [181], which may be attributed to the hydro-thermal treatment induced during the densification process [182].

5.8.4 *Machining Processes*

It is difficult to generalize whether a rough wood surface has a positive or negative impact on adhesive bonding performance. On one hand, roughness is a disadvantage because it contains failure initiation sites and hinders adhesives and coatings to penetrate into the wood substrate [183, 184] and anchor to intact wood material [185]. On the other hand, roughness appears, to some extent, to improve the adhesive joint performance [186] because crushed fibers can mechanically interlock with adhesives [187] and offers a larger contact area on the surface of wood [82]. Moreover, a rougher surface can provide enhanced capillary forces and expose more porous structures in the wood [25]. Wood-adhesive bond performance deteriorates only when the damaged fibers become excessive and unattached.

Different machining methods applied in the process of making wood elements have various effects on the surface wettability. Overall, regardless of the tools used, an increase in surface roughness enhances wettability and adhesion. In contrast to sanding and face milling, helical planing produced higher surface roughness on birch wood, with better wetting properties [188]. Compared to peripheral knife planing, the sanding process on sugar maple wood caused cell wall fibrillation and only a few open vessels, while planed surfaces were smoother and consisted of more open cells. Thus, the surfaces of sanded wood were rougher than planed and more hydroxyl groups were displayed. As a result, the sanded wood surface has a higher surface energy and wettability [77]. Face-milled black spruce wood had more subsurface damage, fibrillation, and open lumens that favored coating penetration than oblique cutting and helical planing generated surfaces [189].

Wettability probe liquids most readily wet sanded surfaces, which have higher surface roughness and capillary forces compared with sawed, planed, and razor blade cut southern pine surfaces [183]. In addition, planing homogenizes surfaces, while sanding activates surfaces by mechanical cell modification [73]. However, since sanding redistributes non-wettable extractives on the wood surface, surface tension of sanded wood may decrease more rapidly with time than surface tension of microtome prepared or planed wood [98]. Planing parameters (rake angle and feed speed) have a significant effect on surface energy and the total surface energy is strongly influenced by the dispersion component of surface energy [190]. As pointed out by Cheng and Sun (2006), the final adhesive bonding property

of wood products depends on wettability which sometimes acts as a secondary effect, and also on processing factors such as curing time and pressure [25]. Therefore, comprehensive consideration is needed when dealing with bonding performance of an adhesive bonded wood product [25].

5.8.5 *Surface Degradation*

In the high temperature environment of wood element processing such as drying, it was speculated that a small amount of active hydroxyl groups were consumed in carboxylation reactions instead of reacting with phenolic adhesives [191]. Wood dried in a nitrogen environment is less inactivated than wood dried in air based on the values of bond strength and wood failure, which is a proof for oxidation occurring during drying. As temperature increased, the difference between the characteristic oxidation times of white spruce became smaller, indicated by the result from infrared spectroscopy measured in the atmosphere of nitrogen and air. The observation suggests that pyrolysis reactions are the predominant source of surface degradation.

Ugovšek *et al.* (2012) applied liquefied wood as an adhesive on the surface of beech (*Fagus sylvatica L.*) and used light microscopy, scanning electron microscopy, FT-IR microspectroscopy, and elemental carbon, nitrogen and sulfur (CNS) analysis techniques to investigate adhesive bonding [192]. The results showed that a layer of partially delignified cells, defined as a weak boundary layer, existed between the original wood cells on the adherend and carbonized cells. Because lignin is assumed to be a fortifying polymer of wood cells, the strength of the cell wall was dramatically weakened and bond shear strengths were relatively low.

Weathering is an important process affecting wood surface wetting. Wettability often increases after weathering since cracks propagate and a more hydrophilic surface is formed by transforming the crystalline area into an amorphous area [193, 194].

5.8.6 *Surface Activation*

Elimination of extractives usually results in wetting improvement, but it is also species dependent. For hot water extraction of red maple, this enhancement is attributed to the loss of lipophilic substances, higher pore volume created during the extraction process and increased acid-base characteristics from the hemicellulose cleavage which exposes high surface energy functional groups [195]. Douglas-fir was more wettable after extraction because the dispersion force attributed to low or nonpolar extractives was predominant before extraction, while after extraction, the polar force became relatively prevalent [196]. However, post-drying extraction by a variety of different organic solvents such as acetone, petroleum ether and benzene-ethanol did not increase the wettability of high-temperature-dried Douglas-fir veneer [197], which may be attributed to the wood surface reacting with fatty acids and forming ether bonds with the cellulose during the high temperature drying [198]. Boiling water extraction of oak chips before bonding increases internal bond (IB) strength and bending strength, which can also be achieved by sodium carbonate treatment [199].

Exposure of a wood surface to UV light is a simple and effective way to improve the wettability of the surface [200]. UV light can open the pits (spruce), change surface morphology and alter surface chemical composition to a certain extent. Because of the oxidative activation effect, wettability and carbonyl group concentration of bamboo surface increased with UV irradiation time [201].

5.9 Discussion and Future Research Prospects

Upon reviewing the literature for this paper, it became apparent that there were several wood adhesion theories that deserve greater attention because of the lack of a body of knowledge on the subject. The electrostatic theory of adhesion has received little scientific attention over the last half century relative to wood adhesion probably because it works well for coating applications and thus was readily accepted in the commercial marketplace. It is difficult for researchers to solicit and obtain financial backing for fundamental research on a topic that is well accepted in the commercial marketplace. However, there may be applications of electrostatic adhesion that could benefit the production of bonded wood materials especially in wood nanomaterial applications.

The contact mechanics between surfaces or particles and a surface remains an interesting topic for researchers. Many studies have been done on contact mechanics starting in late 1800's with Hertz and followed by DMT and JKR. Nowadays, with the newest state-of-the-art measurement equipment, new methods are used to measure the forces between surfaces. AFM is one of the most popular techniques to measure the adhesion forces between two surfaces, which uses force- deflection curves and calculates adhesion forces according to these nanomechanical interactions. A study investigating the adhesive bonding properties of wood- plastic composite (WPC) and continuous glass fiber reinforced (FPR) surfaces using AFM for measuring the surface roughness and adhesion forces is a good example [202]. On the other hand, nanoindentation is another novel technique which works with the same principle (force- deflection curves) as AFM but nanoindentation techniques give more accurate results because the setup is capable of applying the force to the surface with 90° while creating force- deflection curves. When the knowledge gained from previous studies is integrated with the newest measurement techniques, there will be less assumptions and more accurate studies on adhesion forces, and these measurements will be capable of addressing smaller length scales and adhesion forces.

The covalent or chemical bonding theory applied to wood adhesion is a challenging area because of the complex nature of both wood and the adhesives used to bond wood. This bonding mechanism has been addressed by a number of researchers, but many questions regarding this topic remain unanswered. Perhaps with newer imaging techniques and more sophisticated solid state chemistry analytical methods, the question of covalent bonding in wood adhesive applications can be addressed with greater certainty. The ability to create successful nonreversible covalent bonds between wood and an adhesive would ultimately lead to extremely durable wood adhesion for adverse environmental applications of wood products.

Ongoing research in studying wood adhesion theories using more easily accessible and tried and true techniques such as wettability and contact angle analysis, optical- and

electron microscopic techniques, thermal analysis, spectroscopic techniques as well as novel techniques like AFM and nanoindentation will continue. Following are some thoughts on future prospects for research on wood adhesion.

The effects of wood anatomical characteristics on wood wettability have already received considerable attention. Based on the articles cited in this review, certain aspects of wood wettability may need further investigation. For example, the different influences of tracheids in softwoods and vessel elements in hardwoods on wood wettability deserve more detailed study because they have different pore sizes that impact adhesive-wood interactions and subsequent penetration. Related articles discussed the wetting variations between along the grain direction and across the grain direction. However, even along the grain direction, there are still two distinguished faces (radial and tangential). Different amounts of cell wall microstructural inclusions (pits) exist on these faces, which will affect the penetration of adhesive into the wood cellular structure. Few articles have dealt with surface wettability of woods after modification by chemical reagents, where wettability becomes very important if the samples need further adhesive bonding or painting. In these cases, the wood modification processes may have significant effects on wood surface properties and wettability should be studied. For its heterogeneous nature, the contact angle measurements on the wood surface are quite complicated compared to homogeneous materials. Modifications have been adopted in the methods of contact angle measurements on wood which take the hygroscopic and heterogeneous characteristics of wood into account and certain improvements are observed. The modified and even original contact angle calculation equations contain simplifications and assumptions that are not necessarily accurate, which can lead to inaccurately calculated contact angles. Moreover, the prevalent surface free energy computations are based on the measured contact angles, thus an imprecise contact angle will result in surface free energy deviations that may lessen the significance of these methods. Therefore, more refined techniques are required to make contact angle measurements. From this perspective, IGC may be a better choice for surface free energy analyses because it is based on the affinities between column packing material and different probe gases, avoiding the inherent problems with contact angle measurements. Although IGC is relatively simple and accurate, its ability to obtain surface free energy is not perfect because the diluted gases are usually adsorbed on high energy sites during the testing of heterogeneous materials like wood whose mechanism should be explored in future research.

There are many constituents in wood extractives, which can influence the adhesion between wood and an adhesive. However, not all extractives have negative effects on adhesion. For example, cold water extraction had little or no effect on the curing process of UF and MUF resin. Though some research pointed out that lipophilic component of wood extractives interfered with adhesion, relationships are still unknown between the specific types of extractives and their influences on wood adhesion parameters, like formerly mentioned acid-base property, chemical compositions, number of hydrogen bonding sites, curing process of adhesives, etc. It will be beneficial to analyze the extractives' compositions and correlate them to adhesion.

One suggestion is that effort should be exerted on figuring out the influence of wood extractives and their chemical compositions on the hardening behavior of aminoplastic

condensation resin adhesives which is not entirely clear now. This is important to decide whether an extraction procedure is necessary for an aminoplastic resin system.

Regarding the effect of heat treatment on wood adhesion, the problem is that most previous papers dealing with this issue usually did not exclude the influence of extractives which also have the effect of reduced wetting of the wood surface as a result of heat treatment. Extractives may mask the mechanism of decreased wettability attributed only to heat treatment. The measured decreased surface free energy of densified wood has the same problem because this process is often associated with heat and moisture, and altered surface properties cannot be attributed solely to densification. Besides, the surface property of wood densified with materials like polymers and metals is not readily seen in past research, however, this is important because it is related to secondary processing like painting and overlaying laminates.

For the surface roughness caused by different machining methods, it is hard to generalize which method can produce the roughest surface because the roughness is not only dependent on the machining methods and processing parameters, but also on other factors such as wood species and anatomical characteristics. Therefore, if one wants to study the effects of different machining methods on wood surface properties, it is critical to make sure that other factors are the same. In addition, although roughness is beneficial to a product's mechanical properties as a result of mechanical interlocking with an adhesive, excessive wood cell wall damage can result in deteriorated bonding. Optimized surface roughness should be determined to maintain the roughness at a reasonable level. Combined with the roughness caused by different machining methods for certain species of woods, it should be possible to determine optimal machining process characteristics for each particular wood species.

The novel techniques of atomic force microscopy and nanoindentation can be used to determine adhesion forces and pull-off forces between wood and adhesives. The surface properties, pores, crevices, roughness of wood on the nanolevel should be investigated using these techniques. New adhesion models should be developed according to more accurately determined geometric properties of the wood surface. Future studies should be more focused on the effect of ambient conditions on adhesion forces at the nano level and determining the optimum conditions for adhesion. In addition to this, the adhesion between a single cellulose nanofiber and different adhesives should be studied in depth and the adhesion system based on a single cellulose nanofiber structure should be explained and compared to wood as a bonding substrate. As a result of these unique studies, the methods and conditions that will enhance the adhesion between cellulose nanofibers and adhesives can be determined and described in detail.

5.10 Summary

The study of wood adhesion theories has and will continue to be an important topic for researchers, and practitioners of wood adhesive bonding. The topics of wood wettability and the weak boundary layer have tended to dominate the study of wood adhesion over the past several decades. The diffusion theory of wood is beginning to receive greater attention

with the availability of improved analytical capabilities. Mechanical interlocking has long been accepted as a wood adhesion mechanism but is receiving new focus as researchers examine the nanometer length scale of wood-adhesive interactions. Both the electrostatic and covalent bonding theories deserve greater research attention from the wood research community. It is envisioned that much of the new knowledge being generated regarding wood adhesion theories will be incremental in nature unless researchers adopt non-conventional approaches and experimental methodologies to address this subject area. Are breakthroughs in understanding wood adhesion coming in the near term?

References

1. A. Pizzi, Guest editorial special issue on "Wood Adhesives". *J. Adhesion Sci. Technol.* 24, 1353–1355 (2010).
2. C.R. Frihart, Wood adhesion and adhesives, in *Handbook for Wood Chemistry and Wood Composites*, R.M. Rowell (Ed.), pp. 215–278, CRC Press, Boca Raton, FL. (2012).
3. Forest Products Laboratory, *Wood Handbook: Wood as an Engineering Material*, p. 508. General Technical Report FPL-GTR-190. U.S. Department of Agriculture, Forest Service, Forest Products Laboratory, Madison, WI. (2010).
4. F.H. Chung, Unified theory and guidelines on adhesion. *J. Appl. Polym. Sci.* 42, 1319–1331 (1991).
5. A. Baldan, Adhesion phenomena in bonded joints. *Int. J. Adhesion Adhesives* 38, 95–116 (2012).
6. A.V. Pocius, *Adhesion and Adhesives Technology—An Introduction*, 3rd edition, p. 370, Carl Hanser Verlag, München. (2012).
7. J. Schultz and M. Nardin, Theories and mechanisms of adhesion, in *Handbook of Adhesive Technology*, A. Pizzi and K.L. Mittal (Eds.), pp. 19–33, Marcel Dekker, New York. (1994).
8. J. Custódio, J. Broughton, and H. Cruz, A review of factors influencing the durability of structural bonded timber joints. *Int. J. Adhesion Adhesives* 29, 173–185 (2009).
9. C.R. Frihart, Adhesive groups and how they relate to the durability of bonded wood. *J. Adhesion Sci. Technol.* 23, 601–617 (2009).
10. D.J. Gardner, Application of the Lifshitz-van der Waals acid-base approach to determine wood surface tension components. *Wood Fiber Sci.* 28, 422–428 (1996).
11. D.J. Gardner, Adhesion mechanisms of durable wood adhesive bonds, in *Characterization of the Cellulosic Cell Wall*, D.D. Stokke and L.H. Groom (Eds.), pp. 254–265, John Wiley & Sons. (2005).
12. A.J. Panshin and C.de Zeeuw, *Textbook of Wood Technology*, 4th edition, p. 722, McGraw-Hill, New York. (1980).
13. D.D. Stokke and D.J. Gardner, Fundamental aspects of wood as a component of thermoplastic composites. *J. Vinyl Additive Technol.* 9, 96–104 (2003).
14. D.J. Gardner, M.P. Wolcott, L. Wilson, Y. Huang, and M. Carpenter, Our understanding of wood chemistry, in *Proc. 1995 Wood Adhesive Symposium*, pp. 29–36, Forest Products Society, Madison, WI. (1996).
15. V. Gray, The wettability of wood. *Forest Prod. J.* 12, 452–461 (1962).
16. A.A. Marra, *Technology of Wood Bonding: Principles and Practice*, p. 454, Van Nostrand Reinhold, New York. (1992).
17. D.J. Gardner, G.S. Oporto, R. Mills, and M.A.S.A. Samir, Adhesion and surface issues in cellulose and nanocellulose. *J. Adhesion Sci. Technol.* 22, 545–567 (2008).

18. C. Miao and W.Y. Hamad, Cellulose reinforced polymer composites and nanocomposites: A critical review. *Cellulose* 20, 2221–2262 (2013).
19. J.W. McBain and D.J. Hopkins, On adhesives and adhesive action. *J. Phys. Chem.* 29, 188–204 (1925).
20. H. Weiss, Adhesion of advanced overlay coatings: Mechanisms and quantitative assessment. *Surface Coatings Technol.* 71, 201–207 (1995).
21. S. Joo and D.F. Baldwin, Adhesion mechanisms of nanoparticle silver to substrate materials: Identification. *Nanotechnology* 21, 055204 (2010).
22. A.N. Gent and C.W. Lin, Model studies of the effect of surface roughness and mechanical interlocking on adhesion. *J. Adhesion* 32, 113–125 (1990).
23. B.S. Gupta, I. Reiniati, and M.G. Laborie, Surface properties and adhesion of wood fiber reinforced thermoplastic composites. *Colloids Surfaces* 302, 388–395 (2007).
24. W.C. Wake, *Adhesion and the Formulation of Adhesives*, p. 332, Applied Science Publishers, London. (1982).
25. E. Cheng and X. Sun, Effects of wood-surface roughness, adhesive viscosity and processing pressure on adhesion strength of protein adhesive. *J. Adhesion Sci. Technol.* 20, 997–1017 (2006).
26. W. Kim, I. Yun, L. Jung and H. Jung, Evaluation of mechanical interlock effect on adhesion strength of polymer-metal interfaces using micro-patterned topography. *Int. J. Adhesion Adhesives* 30, 408–417 (2010).
27. J. Follrich, A. Teischinger, W. Gindl and U. Müller, Effect of grain angle on shear strength of glued end grain to flat grain joints of defect-free softwood timber. *Wood Sci. Technol.* 41, 501–509 (2007).
28. M.G. Salemane and A.S. Luyt, Thermal and mechanical properties of polypropylene-wood powder composites. *J. Appl. Polym. Sci.* 100, 4173–4180 (2006).
29. M.J. Smith, H. Dai and K. Ramani, Wood-thermoplastic adhesive interface - Method of characterization and results. *Int. J. Adhesion Adhesives* 22, 197–204 (2002).
30. M. Kazayawoko, J.J. Balatinez and L.M. Matuana, Surface modification and adhesion mechanisms in woodfiber-polypropylene composites. *J. Mater. Sci.* 34, 6189–6199 (1999).
31. C.B. Vick and T.A. Kuster, Mechanical interlocking of adhesive bonds to CCA-treated Southern pine - A scanning electron microscopic study. *Wood Fiber Sci.* 24, 36–46 (1992).
32. A.C. Backman and K.A.H. Lindberg, Interaction between wood and polyvinyl acetate glue studied with dynamic mechanical analysis and scanning electron microscopy. *J. Appl. Polym. Sci.* 91, 3009–3015 (2004).
33. J. Drelich and K.L. Mittal (Eds.), *Atomic Force Microscopy in Adhesion Studies*, CRC Press, Boca Raton, FL. (2005).
34. K.L. Johnson, K. Kendall, and A.D. Roberts, Surface energy and the contact of elastic solids. *Proc. R. Soc. Lond. A.* 324, 301–313 (1971).
35. D.S. Grierson, E.E. Flater, and R.W. Carpick, Accounting for the JKR-DMT transition in adhesion and friction measurements with atomic force microscopy. *J. Adhesion Sci. Technol.* 19, 291–311 (2005).
36. C. Morrow, M. Lovell, and X. Ning, A JKR-DMT transition solution for adhesive rough surface contact. *J. Phys. D: Appl. Phys.* 36, 534–540 (2003).
37. C.S. Hodges, L. Looi, J.A.S. Cleaver, and M. Ghadiri, Use of the JKR model for calculating adhesion between rough surfaces. *Langmuir* 20, 9571–9576 (2004).

38. W.C. Oliver and G.M. Pharr, Improved technique for determining hardness and elastic modulus using load and displacement sensing indentation experiments. *J. Mater. Res.* 7, 1564–1583 (1992).
39. J.E. Jakes, C.R. Frihart, J.F. Beecher, R.J. Moon, and D.J. Stone, Experimental method to account for structural compliance in nanoindentation measurements. *J. Mater. Res.* 23, 1113–1127 (2008).
40. J. Konnerth and W. Gindl, Mechanical characterization of wood-adhesive interphase cell walls by nanoindentation. *Holzforschung* 60, 429–433 (2006).
41. B.V. Derjaguin, I.N. Aleinikova, and Y.P. Toporov, On the role of electrostatic forces in the adhesion of polymer particles to solid surfaces. *Powder Technol.* 2, 154–158 (1969).
42. A.G. Bailey, The science and technology of electrostatic powder spraying, transport and coating. *J. Electrostatics* 45, 85–120 (1998).
43. M.N. Horenstein, Electrostatics and nanoparticles: What's the same, what's different? *J. Electrostatics* 67, 384–393 (2009).
44. I.I. Inculet, Electrostatics in industry. *J. Electrostatics* 4, 175–192 (1978).
45. D. Rimai, K. Brown, M. Zaretsky, K. Lofftus, M. Aslam, W. Fowlkes, and D. Weiss, The role of adhesion in electrophotographic digital printing. *J. Adhesion Sci. Technol.* 24, 583–617 (2010).
46. L. Schein, W.S. Czarnecki, B. Christensen, T. Mu, and G. Galliford, Experimental verification of the proximity theory of toner adhesion. *J. Imaging Sci. Technol.* 48, 417–425 (2004).
47. S. Di Risio and N. Yan, Bioactive paper through inkjet printing. *J. Adhesion Sci. Technol.* 24, 661–684 (2010).
48. M.J. Dvorchak, Using high performance two-component waterborne polyurethane wood coatings. *J. Coating Technol.* 69, 47–52 (1997).
49. E.M. Ransburg, Electrostatic coating apparatus, US Patent 2684656 (1954).
50. W.A. Starkey, Electrostatic coating, US Patent 2723921 (1955).
51. T. Misev and R. Van der Linde, Powder coatings technology: New developments at the turn of the century. *Prog. Org. Coat.* 34, 160–168 (1997).
52. M.A. Hubbe, Bonding between cellulosic fibers in the absence and presence of dry-strength agents—A review. *BioResources* 1, 281–318 (2007).
53. K. Ariga, J.P. Hill, M.V. Lee, A. Vinu, R. Charvet, and S. Acharya, Challenges and breakthroughs in recent research on self-assembly. *Sci. Technol. Adv. Mater.* 9, 014109 (2008).
54. L. Wägberg, S. Forsberg, A. Johansson, and P. Juntti, Engineering of fibre surface properties by application of the polyelectrolyte multilayer concept. Part I: Modification of paper strength. *J. Pulp Paper Sci.* 28, 222–228 (2002).
55. M. Agarwal, Y. Lvov, and K. Varahramyan, Conductive wood microfibrils for smart paper through layer-by-layer nanocoating. *Nanotechnology* 17, 5319–5325 (2006).
56. Z. Lu, S. Eadula, Z. Zheng, K. Xu, G. Grozdits, and Y. Lvov, Layer-by-layer nanoparticle coatings on lignocellulose wood microfibrils. *Colloids Surfaces* 292, 56–62 (2007).
57. C. Peng, Y. Thio, and R. Gerhardt, Conductive paper fabricated by layer-by-layer assembly of polyelectrolytes and ITO nanoparticles. *Nanotechnology* 19, 505603 (2008).
58. S. Renneckar and Y. Zhou, Nanoscale coatings on wood: Polyelectrolyte adsorption and layer-by-layer assembled film formation. *ACS Appl. Mater. Interfaces* 1, 559–566 (2009).
59. K.L. Mittal, The role of the interface in adhesion phenomena. *Polym. Eng. Sci.* 17, 467–473 (1977).
60. L. Wilhelmy, Über die Abhängigkeit der Capillaritätskonstanten des Alkohols von Substanz und Gestalt des benetzten festen Körpers. *Annalen der Physik* 195, 177–217 (1863).

61. E.W. Washburn, The dynamics of capillary flow. *Phys. Rev.* 17, 273 (1921).
62. D. Baptista, L. Muszyński, D.J. Gardner, and E. Atzema, An experimental method for three-dimensional dynamic contact angle analysis. *J. Adhesion Sci. Technol.* 26, 2199–2215 (2012).
63. W.A. Zisman, Influence of constitution on adhesion. *Ind. Eng. Chem. Res.* 55, 18–38 (1963).
64. A. Neumann, R. Good, C. Hope and M. Sejpal, An equation-of-state approach to determine surface tensions of low-energy solids from contact angles. *J. Colloid Interface Sci.* 49, 291–304 (1974).
65. F.M. Etzler, Determination of the surface free energy of solids: A critical review. *Rev. Adhesion Adhesives* 1, 3–45 (2013).
66. S.H. Wu, Calculation of interfacial tension in polymer systems. *J. Polym. Sci. C: Polym. Symp.* 34, 19–30 (1971).
67. D.K. Owens and R. Wendt, Estimation of the surface free energy of polymers. *J. Appl. Polym. Sci.* 13, 1741–1747 (1969).
68. M.E. Wålinder and D.J. Gardner, Surface energy of extracted and non-extracted Norway spruce wood particles studied by inverse gas chromatography (IGC). *Wood Fiber Sci.* 32, 478–488 (2000).
69. T.F. Shupe, C.Y. Hse, and W.H. Wang, An investigation of selected factors that influence hardwood wettability. *Holzforschung* 55, 541–548 (2001).
70. S.Q. Shi and D.J. Gardner, Dynamic adhesive wettability of wood. *Wood Fiber Sci.* 33, 58–68 (2001).
71. D.J. Gardner, N.C. Generalla, D.W. Gunnells, and M.P. Wolcott, Dynamic wettability of wood. *Langmuir* 7, 2498–2502 (1991).
72. C. Piao, J.E. Winandy, and T.F. Shupe, From hydrophilicity to hydrophobicity: A critical review: Part I. Wettability and surface behavior. *Wood Fiber Sci.* 42, 490–510 (2010).
73. I. Santoni and B. Pizzo, Effect of surface conditions related to machining and air exposure on wettability of different mediterranean wood species. *Int. J. Adhesion Adhesives* 31, 743–753 (2011).
74. D. Rossi, S. Rossi, H. Morin, and A. Bettero, Within-tree variations in the surface free energy of wood assessed by contact angle analysis. *Wood Sci. Technol.* 46, 287–298 (2012).
75. S. Lee, T.F. Shupe, L.H. Groom, and C.Y. Hse, Wetting behaviors of phenol- and urea-formaldehyde resins as compatibilizers. *Wood Fiber Sci.* 39, 482–492 (2007).
76. Ü. Büyüksarı, T. Akbulut, C. Guler, and N. As, Wettability and surface roughness of natural- and plantation grown narrow leaved ash (*Fraxinus angustifolia vahl.*) wood. *BioResources* 6, 4721–4730 (2011).
77. L.F. de Moura and R.E. Hernández, Evaluation of varnish coating performance for two surfacing methods on sugar maple wood. *Wood Fiber Sci.* 37, 355–366 (2005).
78. A.W. Christiansen, How overdrying wood reduces its bonding to phenol-formaldehyde adhesives: A critical review of the literature. Part I. Physical responses. *Wood Fiber Sci.* 22, 441–459 (1990).
79. A.W. Christiansen, How overdrying wood reduces its bonding to phenol-formaldehyde adhesives: A critical review of the literature. Part II. Chemical reactions. *Wood Fiber Sci.* 23, 69–84 (1991).
80. M. Šernek, F.A. Kamke, and W.G. Glasser, Comparative analysis of inactivated wood surfaces. *Holzforschung* 58, 22–31 (2004).
81. M.E. Wålinder and D.J. Gardner, Acid–base characterization of wood and selected thermoplastics. *J. Adhesion Sci. Technol.* 16, 1625–1649 (2002).

82. I. Aydin, G. Colakoglu, and S. Hiziroglu, Surface characteristics of spruce veneers and shear strength of plywood as a function of log- temperature in peeling process. *Int. J. Solids Struct.* 43, 6140–6147 (2006).
83. H.-N. Xu, Q.-Y. Shen, X.-K. Ouyang, and L.-Y. Yang, Wetting of soy protein adhesives modified by urea on wood surfaces. *Eur. J. Wood Wood Prod.* 70, 11–16 (2012).
84. H.A. Essawy and H.A. Mohamed, Poly (amidoamine) dendritic structures, bearing different end groups as adhesion promoters for urea-formaldehyde wood adhesive system. *J. Appl. Polym. Sci.* 119, 760–767 (2011).
85. D.J. Gardner, C.E. Frazier, and A.W. Christiansen, Characteristics of the wood adhesion bonding mechanism using hydroxymethyl resorcinol, in *Proceedings of the Wood Adhesives 2005 Conference*, pp. 93–97, Forest Products Society, San Diego, CA. (2005)
86. R.M. Rowell, Acetylation. *Forest Prod. J.* 56, 4–12 (2006).
87. L.E. Bryne and M.E. Wälinder, Ageing of modified wood. Part 1: Wetting properties of acetylated, furfurylated, and thermally modified wood. *Holzforschung* 64, 295–304 (2010).
88. Y. Fu, G. Li, H. Yu, and Y. Liu, Hydrophobic modification of wood via surface-initiated ARGET ATRP of MMA. *Appl. Surface Sci.* 258, 2529–2533 (2012).
89. M.H. Drafz, S. Dahle, W. Maus-Friedrichs, J.C. Namyslo, and D.E. Kaufmann, Chemical improvement of surfaces. Part 2: Permanent hydrophobization of wood by covalently bonded fluoroorganyl substituents. *Holzforschung* 66, 727–733 (2012).
90. M.L. Mamiński, K. Mierzejewska, P. Borysiuk, P. Parzuchowski, and P. Boruszewski, Surface properties of octadecanol—grafted pine veneers. *Int. J. Adhesion Adhesives* 29, 781–784 (2009).
91. N. Ayrilmis, T. Dundar, Z. Candan, and T. Akbulut, Wettability of fire retardant treated laminated veneer lumber (LVL) manufactured from veneers dried at different temperatures. *BioResources* 4, 1536–1544 (2009).
92. R.H. Alamjuri, A. Zaidon, F. Abood, and U.K. Anwar, Adhesion and bonding characteristics of preservative-treated bamboo (*Gigantochloa scortechinii*) laminates. *J. Appl. Sci.* 10, 1435–1441 (2010).
93. I. Aydin and G. Colakoglu, Variation in surface roughness, wettability and some plywood properties after preservative treatment with boron compounds. *BUILD. Environ.* 42, 3837–3840 (2007).
94. C. Tascioglu, B. Goodell, R. Lopez-Anido, and D. Gardner, Surface energy characterization of preservative-treated wood and E-glass/phenolic composites. *Forest Prod. J.* 54, 262–268 (2004).
95. M. Petrič, Surface modification of wood. *Rev. Adhesion Adhesives* 1, 216–247 (2013).
96. M. de Meijer, S. Haemers, W. Cobben, and H. Militz, Surface energy determinations of wood: Comparison of methods and wood species. *Langmuir* 16, 9352–9359 (2000).
97. T. Nguyen and W.E. Johns, Polar and dispersion force contributions to the total surface free energy of wood. *Wood Sci. Technol.* 12, 63–74 (1978).
98. M. Gindl, A. Reiterer, G. Sinn, and S.E. Stanzl-Tschegg, Effects of surface ageing on wettability, surface chemistry, and adhesion of wood. *Holz Roh Werkst.* 62, 273–280 (2004).
99. J.Z. Lu and Q. Wu, Surface characterization of chemically modified wood: Dynamic wettability. *Wood Fiber Sci.* 38, 497–511 (2006).
100. M.E. Wälinder and G. Ström, Measurement of wood wettability by the Wilhelmy method. Part 2. Determination of apparent contact angles. *Holzforschung* 55, 33–41 (2001).
101. S.Q. Shi and D.J. Gardner, A new model to determine contact angles on swelling polymer particles by the column wicking method. *J. Adhesion Sci. Technol.* 14, 301–314 (2000).
102. F.A. Kamke and J.N. Lee, Adhesive penetration into wood—A review. *Wood Fiber Sci.* 39, 205–220 (2007).

103. C. R. Frihart, Adhesive Interactions with Wood, in *Fundamentals of Composite Processing. Proceedings of a Workshop*, Forest Products Laboratory, Madison, WI, Gen. Tech. Rep. FPL-GTR-149, p. 118 (2004).
104. G.I. Mantanis, R.A. Young, and R.M. Rowell, Swelling of wood. Part II. Swelling in organic liquids. *Holzforschung* 48, 480–490 (1994).
105. T. Furuno, Y. Imamura, and H. Kajita, The modification of wood by treatment with low molecular weight phenol-formaldehyde resin: A properties enhancement with neutralized phenolic-resin and resin penetration into wood cell walls. *Wood Sci. Technol.* 37, 349–361 (2004).
106. M.-P.G. Laborie, L. Salmén, and C.E. Frazier, A morphological study of the wood/phenol-formaldehyde adhesive interphase. *J. Adhesion Sci. Technol.* 20, 729–741 (2006).
107. M.-P.G. Laborie and C.E. Frazier, ¹³C CP/MAS NMR study of a wood/phenol-formaldehyde resin bondline. *J. Mater. Sci.* 41, 6001–6005 (2006).
108. G. Modzel, F. Kamke, and F. De Carlo, Comparative analysis of a wood: Adhesive bondline. *Wood Sci. Technol.* 45, 147–158 (2011).
109. J.L. Paris, F.A. Kamke, R. Mbachu, and S.K. Gibson, Phenol formaldehyde adhesives formulated for advanced x-ray imaging in wood-composite bondlines. *J. Mater. Sci.* 49, 1–12 (2013).
110. P. Hass, F. Wittel, M. Mendoza, H. Herrmann, and P. Niemz, Adhesive penetration in beech wood: Experiments. *Wood Sci. Technol.* 46, 243–256 (2012).
111. G. Standfest, S. Kranzer, A. Petutschnigg, and M. Dunky, Determination of the microstructure of an adhesive-bonded medium density fiberboard (MDF) using 3D sub-micrometer computer tomography. *J. Adhesion Sci. Technol.* 24, 1501–1514 (2010).
112. F.A. Kamke, J.A. Nairn, L. Muszynski, J.L. Paris, M. Schwarzkopf, and X. Xiao, Methodology for micromechanical analysis of wood adhesive bonds using X-ray computed tomography and numerical modeling. *Wood Fiber Sci.* 46, 1–14 (2014).
113. T.M. Gruver and N.R. Brown, Penetration and performance of isocyanate wood binders on selected wood species. *BioResources* 1, 233–247 (2006).
114. M. Mendoza, P. Hass, F. Wittel, P. Niemz, and H. Herrmann, Adhesive penetration of hardwood: A generic penetration model. *Wood Sci. Technol.* 46, 529–549 (2012).
115. W. Wang and N. Yan, Characterizing liquid resin penetration in wood using a mercury intrusion porosimeter. *Wood Fiber Sci.* 37, 505–513 (2005).
116. C. Xing, B. Riedl, A. Cloutier, and S.M. Shaler, Characterization of urea-formaldehyde resin penetration into medium density fiberboard fibers. *Wood Sci. Technol.* 39, 374–384 (2005).
117. P.-L. Cyr, B. Riedl, and X.-M. Wang, Investigation of urea-melamine-formaldehyde (UMF) resin penetration in medium-density fiberboard (MDF) by high resolution confocal laser scanning microscopy. *Holz Roh Werkst.* 66, 129–134 (2008).
118. W. Gindl, E. Dessipri, and R. Wimmer, Using UV-microscopy to study diffusion of melamine-urea-formaldehyde resin in cell walls of spruce wood. *Holzforschung* 56, 103–107 (2002).
119. W. Gindl, F. Zargar-Yaghubi, and R. Wimmer, Impregnation of softwood cell walls with melamine-formaldehyde resin. *Bioresource Technol.* 87, 325–330 (2003).
120. W. Gindl, T. Schöberl, and G. Jeronimidis, The interphase in phenol-formaldehyde and polymeric methylene di-phenyl-di-isocyanate glue lines in wood. *Int. J. Adhesion Adhesives* 24, 279–286 (2004).
121. J. Konnerth, D. Harper, S.-H. Lee, T.G. Rials, and W. Gindl, Adhesive penetration of wood cell walls investigated by scanning thermal microscopy (SThM). *Holzforschung* 62, 91–98 (2008).
122. S. Das, M.J. Malmberg, and C.E. Frazier, Cure chemistry of wood/polymeric isocyanate (PMDI) bonds: Effect of wood species. *Int. J. Adhesion Adhesives* 27, 250–257 (2007).

123. S.L. Wendler and C.E. Frazier, The effects of cure temperature and time on the isocyanate-wood adhesive bondline by ¹⁵N CP/MAS NMR. *Int. J. Adhesion Adhesives* 16, 179–186 (1996).
124. X. Zhou and C.E. Frazier, Double labeled isocyanate resins for the solid-state NMR detection of urethane linkages to wood. *Int. J. Adhesion Adhesives* 21, 259–264 (2001).
125. A. Pizzi, A. Despres, H.-R. Mansouri, J.-M. Leban, and S. Rigolet, Wood joints by through-dowel rotation welding: Microstructure, ¹³C-NMR and water resistance. *J. Adhesion Sci. Technol.* 20, 427–436 (2006).
126. B. Gfeller, M. Zanetti, M. Properzi, A. Pizzi, F. Pichelin, M. Lehmann, and L. Delmotte, Wood bonding by vibrational welding. *J. Adhesion Sci. Technol.* 17, 1573–1589 (2003).
127. A. Zoulalian and A. Pizzi, Wood-dowel rotation welding—A heat-transfer model. *J. Adhesion Sci. Technol.* 21, 97–108 (2007).
128. W.E. Johns, The chemical bonding of wood, in *Wood Adhesives, Chemistry and Technology*, Vol. 2, A. Pizzi (Ed.), pp. 75–96, Marcel Dekker, New York. (1989).
129. H. Mizumachi and H. Morita, Activation energy of the curing reaction of phenolic resin in the presence of woods. *Wood Sci. Technol.* 7, 256–260 (1975).
130. A. Pizzi, B. Mtsweni, and W. Parsons, Wood-induced catalytic activation of PF adhesives autopolymerization vs. PF/wood covalent bonding. *J. Appl. Polym. Sci.* 52, 1847–1856 (1994).
131. G. He and B. Riedl, Curing kinetics of phenol formaldehyde resin and wood-resin interactions in the presence of wood substrates. *Wood Sci. Technol.* 38, 69–81 (2004).
132. J.J. Marcinko, S. Devathala, P.L. Rinaldi, and S. Bao, Investigating the molecular and bulk dynamics of PMDI/wood and UF/wood composites. *Forest Prod. J.* 48, 81–84 (1998).
133. A. Pizzi and L.A. Panamgama, Diffusion hindrance vs. wood-induced catalytic activation of MUF adhesive polycondensation. *J. Appl. Polym. Sci.* 58, 109–115 (1995).
134. S. Bao, W.A. Daunch, Y. Sun, P.L. Rinaldi, J.J. Marcinko, and C. Phanopoulos, Solid state NMR studies of polymeric diphenylmethane diisocyanate (PMDI) derived species in wood. *J. Adhesion* 71, 377–394 (1999).
135. D.J. Yelle, J.E. Jakes, J. Ralph, and C.R. Frihart, Characterizing polymeric methylene diphenyl diisocyanate reactions with wood: 1. High-resolution solution-state NMR spectroscopy, in *Proceedings of the Wood Adhesives 2009 Conference*, Lake Tahoe, NV, pp. 338–342, Forest Products Society, Madison, WI. (2010).
136. D.J. Yelle, A Solution-State NMR Approach to Elucidating pMDI-Wood Bonding Mechanisms in Loblolly Pine, PhD thesis, University of Wisconsin, Madison, WI (2009).
137. D.J. Yelle, J. Ralph, and C.R. Frihart, Delineating pMDI model reactions with loblolly pine via solution-state NMR spectroscopy. Part 2. Non-catalyzed reactions with the wood cell wall. *Holzforschung* 65, 145 (2011).
138. S. Bao, W.A. Daunch, Y. Sun, P.L. Rinaldi, J.J. Marcinko, and P. Chris, Solid state two-dimensional nmr studies of polymeric diphenylmethane diisocyanate (pmdi) reaction in wood. *Forest Prod. J.* 53, 63 (2003).
139. R.S. Drago, G.C. Vogel, and T.E. Needham, Four-parameter equation for predicting enthalpies of adduct formation. *J. Am. Chem. Soc.* 93, 6014–6026 (1971).
140. F.M. Fowkes and M.A. Mostafa, Acid-base interactions in polymer adsorption. *Ind. Eng. Chem. Prod. R+D* 17, 3–7 (1978).
141. T. Young, An essay on the cohesion of fluids. *Philos. Trans. Roy. Soc.* 95, 65–87 (1805).
142. A. Dupré, *Théorie Mécanique de la Chaleur*, p. 585. Gustav Zeuner, Gauthier-Villars, Paris. (1869).

143. F.M. Fowkes, Acid-base interactions in polymer adhesion, in *Physicochemical Aspects of Polymer Surfaces*, Vol. 2, K.L. Mittal (Ed.), pp. 583–603, Plenum Press, New York. (1983).
144. C.J. van Oss, M.K. Chaudhury, and R.J. Good, Monopolar surfaces. *Adv. Colloid Interface Sci.* 28, 35–64 (1987).
145. R.J. Good and L.A. Girifalco, A theory for estimation of surface and interfacial energies, III. Estimation of surface energies of solids from contact angle data. *J. Phys. Chem.* 64, 561–565 (1960).
146. F.M. Fowkes, Additivity of intermolecular forces at interfaces. I. Determination of the contribution to surface and interfacial tension of dispersion forces in various liquids. *J. Phys. Chem.* 67, 2538–2541 (1963).
147. K.L. Mittal (Ed.), *Acid-Base Interactions: Relevance to Adhesion Science and Technology*, Vol. 2, CRC Press, Boca Raton, FL. (2000).
148. K.L. Mittal and H.R. Anderson, Jr. (Eds.), *Acid-Base Interactions: Relevance to Adhesion Science and Technology*, CRC Press, Boca Raton, FL. (1991).
149. M. Gindl, G. Sinn, W. Gindl, A. Reiterer, and S. Tschegg, A comparison of different methods to calculate the surface free energy of wood using contact angle measurements. *Colloids Surfaces* 181, 279–287 (2001).
150. J.J. Bikerman, *The Science of Adhesive Joints*, p. 258, Academic Press, New York. (1961).
151. M. Stehr and I. Johansson, Weak boundary layers on wood surfaces. *J. Adhesion Sci. Technol.* 14, 1211–1224 (2000).
152. S. Wang, Y. Zhang, and C. Xing, Effect of drying method on the surface wettability of wood strands. *Holz Roh Werkst.* 65, 437–442 (2007).
153. F. Englund, L.E. Bryne, M. Ernstsson, J. Lausmaa, and M. Wälinder, Spectroscopic studies of surface chemical composition and wettability of modified wood. *Wood Mater. Sci. Eng.* 4, 80–85 (2009).
154. P. Widsten, V.S. Gutowski, S. Li, T. Cerra, S. Molenaar, and M. Spicer, Factors influencing timber gluability with one-part polyurethanes – Studied with nine Australian timber species. *Holzforschung* 60, 423–428 (2006).
155. M. Claude, N. Yemele, A. Koubaa, P. Diouf, P. Blanchet, A. Cloutier, and T. Stevanovic, Effects of hot-water treatment of black spruce and trembling aspen bark raw material on the physical and mechanical properties of bark particleboard. *Wood Fiber Sci.* 40, 339–351 (2008).
156. E. Alamsyah, M. Yamada, and K. Taki, Bondability of tropical fast-growing tree species III: Curing behavior of resorcinol formaldehyde resin adhesive at room temperature and effects of extractives of *Acacia mangium* wood on bonding. *J. Wood. Sci.* 54, 208–213 (2008).
157. I. Abe and K. Ono, Effect of the acidity of some tropical wood extractives on the curing of the resol. *J. JWRS* 26, 686–692 (1980).
158. B. Stefke and M. Dunky, Catalytic influence of wood on the hardening behavior of formaldehyde-based resin adhesives used for wood-based panels. *J. Adhesion Sci. Technol.* 20, 761–785 (2006).
159. C.-Y. Hse and M.-L. Kuo, Influence of extractives on wood gluing and finishing—A review. *Forest Prod. J.* 38, 52–56 (1988).
160. G. Nemli, E.D. Gezer, S. Yildiz, A. Temiz, and A. Aydın, Evaluation of the mechanical, physical properties and decay resistance of particleboard made from particles impregnated with *Pinus brutia* bark extractives. *Bioresource Technol.* 97, 2059–2064 (2006).
161. M. Fan, M.K. Ndikontar, X. Zhou, and J.N. Ngamveng, Cement-bonded composites made from tropical woods: Compatibility of wood and cement. *Const. Build. Mater.* 36, 135–140 (2012).

162. N.P.K. Nielsen, D.J. Gardner, and C. Felby, Effect of extractives and storage on the pelletizing process of sawdust. *Fuel* 89, 94–98 (2010).
163. N.P.K. Nielsen, D.J. Gardner, T. Poulsen, and C. Felby, Importance of temperature, moisture content, and species for the conversion process of wood residues into fuel pellets. *Wood Fiber Sci.* 41, 414–425 (2009).
164. R. Samuelsson, S.H. Larsson, M. Thyrel, and T.A. Lestander, Moisture content and storage time influence the binding mechanisms in biofuel wood pellets. *Appl. Energy* 99, 109–115 (2012).
165. W. Stelte, J.K. Holm, A.R. Sanadi, S. Barsberg, J. Ahrenfeldt, and U.B. Henriksen, A study of bonding and failure mechanisms in fuel pellets from different biomass resources. *Biomass Bioenergy* 35, 910–918 (2011).
166. J. Follrich, U. Müller, and W. Gindl, Effects of thermal modification on the adhesion between spruce wood (*Picea abies karst.*) and a thermoplastic polymer. *Holz Roh Werkst.* 64, 373–376 (2006).
167. B. Esteves and H. Pereira, Wood modification by heat treatment: A review. *BioResources* 4, 370–404 (2008).
168. N. Ayrilmis and J.E. Winandy, Effects of post heat-treatment on surface characteristics and adhesive bonding performance of medium density fiberboard. *Mater. Manuf. Process.* 24, 594–599 (2009).
169. O. Unsal, Z. Candan, U. Buyuksari, S. Korkut, and M. Babiak, Effects of thermal modification on surface characteristics of OSB panels. *Wood Res.* 55, 51–58 (2010).
170. Z. Candan, U. Büyüksarı, S. Korkut, O. Unsal, and N. Çakıcıer, Wettability and surface roughness of thermally modified plywood panels. *Ind. Crop. Prod.* 36, 434–436 (2012).
171. Ü. Büyüksarı, Surface characteristics and hardness of MDF panels laminated with thermally compressed veneer. *Composites Part B* 44, 675–678 (2013).
172. U. Aleš, F.A. Kamke, M. Sernek, M. Pavlič, and A. Kutnar, The wettability and bonding performance of densified VTC beech (*Fagus sylvatica L.*) and Norway spruce (*Picea abies (L.) karst.*) bonded with phenol–formaldehyde adhesive and liquefied wood. *Eur. J. Wood Wood Prod.* 71, 371–379 (2013).
173. M. Pétrissans, P. Gérardin, I.E. Bakali, and M. Serraj, Wettability of heat-treated wood. *Holzforschung* 57, 301 (2003).
174. M. Hakkou, M. Pétrissans, A. Zoulalian, and P. Gérardin, Investigation of wood wettability changes during heat treatment on the basis of chemical analysis. *Polym. Degrad. Stabil.* 89, 1–5 (2005).
175. P. Gérardin, M. Petrič, M. Petrisans, J. Lambert, and J.J. Ehrhardt, Evolution of wood surface free energy after heat treatment. *Polym. Degrad. Stabil.* 92, 653–657 (2007).
176. D. Kocafee, S. Poncsak, G. Doré, and R. Younsi, Effect of heat treatment on the wettability of white ash and soft maple by water. *Holz Roh Werkst.* 66, 355–361 (2008).
177. A. Kutnar, F.A. Kamke, M. Petrič, and M. Sernek, The influence of viscoelastic thermal compression on the chemistry and surface energetics of wood. *Colloids Surfaces* 329, 82–86 (2008).
178. P. Boruszewski, P. Borysiuk, M. Mamiński, and M. Grzeskiewicz, Gluability of thermally modified beech (*fagus sylvatica l.*) and birch (*betula pubescens ehrh.*) wood. *Wood Mater. Sci. Eng.* 6, 185–189 (2011).
179. O. Unsal, Z. Candan, and S. Korkut, Wettability and roughness characteristics of modified wood boards using a hot-press. *Ind. Crop. Prod.* 34, 1455–1457 (2011).

180. M. Petrič, B. Knehtl, A. Krause, H. Militz, M. Pavlič, M. Pétrissans, A. Rapp, M. Tomažič, C. Welzbacher, and P. Gérardin, Wettability of waterborne coatings on chemically and thermally modified pine wood. *J. Coat. Technol. Res.* 4, 203–206 (2007).
181. J.D. Jennings, A. Zink-Sharp, C.E. Frazier, and F.A. Kamke, Properties of compression-densified wood, Part II: Surface energy. *J. Adhesion Sci. Technol.* 20, 335–344 (2006).
182. A. Kutnar, L. Rautkari, K. Laine, and M. Hughes, Thermodynamic characteristics of surface densified solid Scots pine wood. *Eur. J. Wood Wood Prod.* 70, 727–734 (2012).
183. M. Stehr, D.J. Gardner, and M.E. Wälinder, Dynamic wettability of different machined wood surfaces. *J. Adhesion* 76, 185–200 (2001).
184. V. Landry and P. Blanchet, Surface preparation of wood for application of waterborne coatings. *Forest Prod. J.* 62, 39–45 (2012).
185. A. Özçifçi and F. Yapici, Effects of machining method and grain orientation on the bonding strength of some wood species. *J. Mater. Process. Technol.* 202, 353–358 (2008).
186. J. Follich, O. Vay, S. Veigel, and U. Müller, Bond strength of end-grain joints and its dependence on surface roughness and adhesive spread. *J. Wood. Sci.* 56, 429–434 (2010).
187. S. Kuljich, J. Cool, and R.E. Hernández, Evaluation of two surfacing methods on black spruce wood in relation to gluing performance. *J. Wood. Sci.* 59, 185–194 (2013).
188. R.E. Hernández and J. Cool, Evaluation of three surfacing methods on paper birch wood in relation to water- and solvent-borne coating performance. *Wood Fiber Sci.* 40, 459–469 (2008).
189. J. Cool and R.E. Hernández, Performance of three alternative surfacing processes on black spruce wood and their effects on water-based coating adhesion. *Wood Fiber Sci.* 43, 365–378 (2011).
190. J. Cool and R.E. Hernández, Effects of peripheral planing on surface characteristics and adhesion of a waterborne acrylic coating to black spruce wood. *Forest Prod. J.* 62, 124–133 (2012).
191. S.-Z. Chow, Infrared spectral characteristics and surface inactivation of wood at high temperatures. *Wood Sci. Technol.* 5, 27–39 (1971).
192. A. Ugovšek, A. Sever Škapin, M. Humar, and M. Sernek, Microscopic analysis of the wood bond line using liquefied wood as adhesive. *J. Adhesion Sci. Technol.* 27, 1247–1258 (2012).
193. M. Kishino and T. Nakano, Artificial weathering of tropical woods. Part 1: Changes in wettability. *Holzforschung* 58, 552 (2004).
194. X. Huang, D. Kocaefe, Y. Kocaefe, Y. Boluk, and A. Pichette, Changes in wettability of heat-treated wood due to artificial weathering. *Wood Sci. Technol.* 46, 1215–1237 (2012).
195. J.J. Paredes, R. Mills, S.M. Shaler, D.J. Gardner, and A. van Heiningen, Surface characterization of red maple strands after hot water extraction. *Wood Fiber Sci.* 41, 38–50 (2009).
196. T. Nguyen and W. Johns, The effects of aging and extraction on the surface free energy of Douglas-fir and redwood. *Wood Sci. Technol.* 13, 29–40 (1979).
197. P. Northcott, The effect of dryer temperatures upon the gluing properties of Douglas-fir veneer. *Forest Prod. J.* 7, 10–16 (1957).
198. G. Sinclair, R. Evans, and H. Sallans, New methods for sizing fibrous products. *Pulp Paper Mag. Can.* 62, T23-T27 (1960).
199. E. Roffael and W. Rauch, Extraktstoffe in Eiche und ihr Einfluss auf die Verleimbarkeit mit alkalischen Phenol-formaldehydharzen. *Holz Roh Werkst.* 32, 182–187 (1974).
200. M. Gindl, G. Sinn, and S.E. Stanzl-Tschegg, The effects of ultraviolet light exposure on the wetting properties of wood. *J. Adhesion Sci. Technol.* 20, 817–828 (2006).

201. K.T. Lu and S.Y. Fan, Effects of ultraviolet irradiation treatment on the surface properties and adhesion of moso bamboo (*Phyllostachys pubescens*). *J. Appl. Polym. Sci.* 108, 2037–2044 (2008).
202. G.S. Oporto, D.J. Gardner, G. Bernhardt, and D.J. Neivandt, Forced air plasma treatment (FAPT) of hybrid wood plastic composite (WPC)-fiber reinforced plastic (FRP) surfaces. *Composite Interfaces* 16, 847–867 (2009).
203. T. Sellers, Jr., Adhesives in the wood industry, in *Handbook of Adhesive Technology*, A. Pizzi and K.L. Mittal (Eds.), pp. 599–614, Marcel Dekker, New York, NY. (1994).
204. K.L. Johnson, *Contact Mechanics*, p. 452, Cambridge University Press, Cambridge. (1987).
205. B.V. Derjaguin, V.M. Müller, and Y.P. Toporov, Effect of contact deformations on the adhesion of particles. *J. Colloid Interface Sci.* 53, 314–326 (1975).
206. D.J. Gardner, W.T. Tze, and S.Q. Shi, Adhesive wettability of hydroxymethyl resorcinol (HMR) treated wood, in *Proceedings of the Wood Adhesives 2000 Conference*, pp. 321–327, Forest Products Society, Madison, WI. (2000).

Adhesion and Surface Issues in Biocomposites and Bionanocomposites

Cintil Jose^{1,3}, Merin Sara Thomas^{2,4}, B. Deepa^{4,5}, Laly A. Pothan^{4,5}
and Sabu Thomas^{1,2,6,*}

¹*School of Chemical Sciences, Mahatma Gandhi University, Kottayam, Kerala, India*

²*International and Interuniversity Centre for Nanoscience and Nanotechnology, Mahatma Gandhi University, Kottayam, Kerala, India*

³*Department of Chemistry, Newman College, Thodupuzha, Kerala-685585, India*

⁴*Department of Chemistry, C.M.S. College, Kottayam, Kerala, India*

⁵*Department of Chemistry, Bishop Moore College, Mavelikara, India*

⁶*Faculty of Applied Science, Universiti of Teknologi MARA, Selangor, Malaysia*

Abstract

Biopolymers and biocomposites draw our attention in various applications due to their versatile properties. But the lack of good interfacial adhesion between the hydrophilic filler particles and hydrophobic polymer matrix make these composites less attractive for various applications. The use of adhesion promoters, additives or chemical modification of the filler surface can help to improve the interfacial adhesion between filler particles and polymer macromolecules and their dispersion in the matrix, and thus improve the overall mechanical performance of the composites. Interfacial adhesion between filler and matrix remains the key issue in terms of overall performance, since it influences the final properties of the composites. This review focuses on biopolymers, biomatrices, their modifications and processing techniques and characterization of interfacial modifications.

Keywords: Biopolymer, composites, interfacial adhesion, biocomposites, bionanocomposites

*Corresponding author: sabuchathukulam@yahoo.co.uk

6.1 Introduction

Materials derived from renewable biomaterials undoubtedly play a large role in the biocomposite research effort. Cellulose, chitin and starch are important biopolymers used in new materials development. The behavior of these material surfaces in different media and their interaction with different chemicals are of great importance in their current and future applications (like papermaking and development of composites and nanocomposites). The mechanical performance of composites, for instance, is dependent on the degree of dispersion of the fibres in the matrix polymer and the nature and intensity of fibre-polymer adhesion interactions. Biopolymers are increasingly used as matrix for biofibre reinforced composites. There is a growing trend to use biofibers as fillers in plastics composites. Their flexibility during processing, high specific stiffness, and low cost make them attractive to manufacturers. This century has witnessed ever-increasing utilization of plastics. More than 80% of such plastics are thermoplastics. Biofiber reinforced plastic composites are gaining more and more acceptance in structural applications. Natural fibres have several advantages like low density, low cost, good specific mechanical properties, reduced tool wear and biodegradability than traditional reinforcement materials such as glass fibres, carbon and talc. This review covers all important biopolymers, biomatrices and their modifications. It also discusses the processing techniques and various interface characterization techniques for assessing the properties of the composites.

6.2 Biopolymers

6.2.1 Cellulose

Cellulose is the most abundant biopolymer on the Earth. It is available in the form of renewable fibre in nature. Moreover, it can be produced from agricultural waste. This makes it more economically viable than any other source of fibres currently in use. Cellulose fibre offers an exceptional balance of excellent mechanical properties, low density, high crystallinity, safer handling and working conditions compared to synthetic fibres. The basic chemical structure of cellulose is given in Figure 6.1 and it is a homopolysaccharide consisting of β -D glucopyranose units linked together by β -1, 4-linkage.

The presence of hydroxyl groups enables the formation of hydrogen bonds which influences the crystalline structure as well as physical properties of cellulose. Nanosized cellulose fillers have been found to be very promising reinforcing elements for about 15 years [1]. There are two types of nanosized cellulose, cellulose whiskers and micro fibrillated cellulose. Depending on the source, the microfibrils of cellulose may be several micrometers in length.

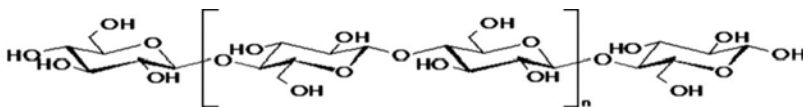


Figure 6.1 The basic chemical structure of cellulose [2].

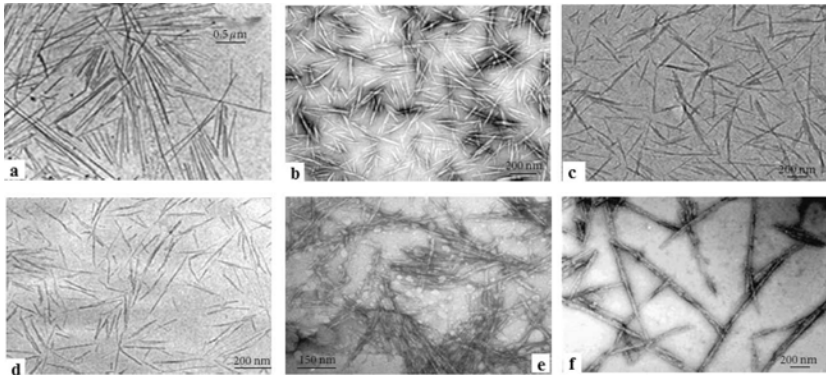


Figure 6.2 Transmission electron micrographs of dilute suspensions of hydrolyzed (a) tunicin [17], (b) ramie [13], (c) cotton [18], (d) sugar beet [15], (e) MCC [19], and (f) bacterial cellulose [20].

Each microfibril consists of crystalline domains intermixed with disordered amorphous regions [2]. On acid hydrolysis the amorphous phase can be removed and highly crystalline cellulose whiskers or nanocellulose can be obtained. Mechanical treatments can be employed to obtain nanofibrillated cellulose (NFC) [3–5]. As mentioned earlier, crystalline cellulose nanowhiskers can be obtained by simple acid hydrolysis. Cellulose whiskers are also known as cellulose nanocrystals, nanorods or nanowhiskers. These can be prepared from a variety of sources, eg. microcrystalline cellulose [6], bacterial cellulose [7], algal cellulose (valonia) [8], hemp [9], tunicin [10, 11], cotton [12], ramie [13], sisal [14], sugar beet [15], and wood [16]. Transmission electron microscopy (TEM) studies show that the colloidal suspensions after acidic treatment of cellulose can be dried to produce aggregates of needle-shaped particles [13, 15, 17–20] (Figure 6.2).

The shape, size and dimensions of nanocrystals depend on the nature of source as well as the hydrolysis conditions such as time, temperature, ultrasound treatment, and purity of materials. However, typical dimensions of whiskers range from 5 to 10 nm in diameter and from 100 to 500 nm in length. These are otherwise known as NFC. The degree of fibrillation and properties of the microfibrillated cellulose (MFC) are closely linked. For low degree of fibrillation the MFC separates out from water, as is the case with untreated fibres. However, with too much processing the MFC structure starts to break down, forming a film. This film can be used, for example, as a coating or packaging material for food products [21].

6.2.2 Chitin

Chitin is the second most abundant semicrystalline polysaccharide in nature after cellulose. It is a high molecular weight biopolymer found predominantly in exoskeleton shells of arthropods as well as in the internal flexible backbone of cephalopods. Chemically, a chitin molecule consists of N-acetyl-D-glucosamine units. Chitin is known to be non-toxic, odorless,

biocompatible with living tissues, and biodegradable [22]. Recently, the commercial value of chitin has increased because of the beneficial properties of its soluble derivatives, which are important in chemistry, biotechnology, agriculture, food processing, cosmetics, veterinary, medicine, dentistry, environment protection, and paper or textile production. Chitin also gives rise to two types of nanoparticles: nanowhiskers and nanofibres (Figure 6.3 and Figure 6.4). The incorporation of chitin whiskers (ChWs) as reinforcing nanofillers in polymer matrices has broadened the utilization of chitin in preparing a new class of biocomposite materials [23]. As in the case of cellulose whiskers, acid hydrolysis is the principal method adopted for the isolation of chitin nanocrystals [24]. Disordered regions of chitin are preferentially

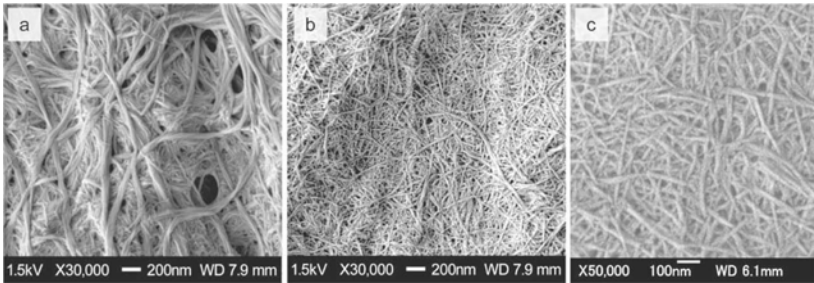


Figure 6.3 FE-SEM micrographs of chitin nanofibers from crab shell after one pass through the grinder (a) without acetic acid (pH 7) and (b,c) with acetic acid (pH 3). The length of the scale bar is (a) 200, (b) 200, and (c) 100 nm [41].

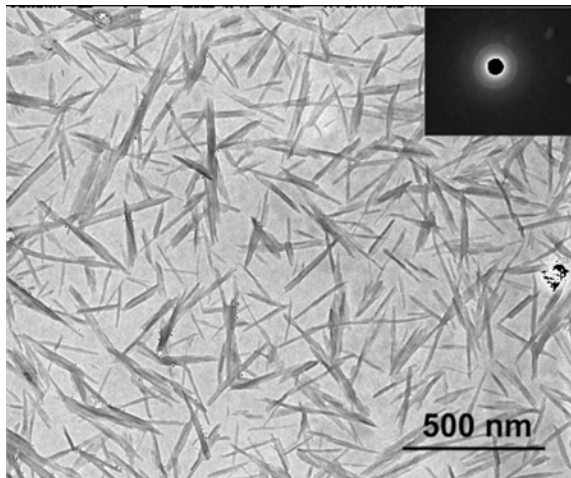


Figure 6.4 TEM image of a dilute suspension of chitin whiskers (inset: typical electron diffractogram recorded on chitin fragments) [29].

hydrolyzed and dissolved in the acid solution, whereas water-insoluble, highly crystalline residues that have a higher resistance to acid attack remain intact. Therefore, following an acid hydrolysis that removes disordered regions, chitin rodlike whiskers are produced [2, 11]. ChWs can be prepared by hydrolysis in HCl solutions. Revol and Marchessault [25] and Li *et al.* [26] reported an approach for preparation of suspension of chitin crystallites through acid hydrolysis in detail. In this approach, purified chitin was hydrolyzed by boiling in 3 N HCl for 90 min under stirring; after acid hydrolysis, the suspensions were diluted with deionized water, followed by centrifugation and decanting of the supernatant liquid; this process was repeated several times until the solution spontaneously transformed into a colloidal state. The obtained crystallites were rodlike particles with average size of 200 ± 20 nm in length and 8 ± 1 nm in width. Because of their nanoscale size, the crystals are named nanocrystals or whiskers. Based on this procedure, whiskers have been prepared from chitins of different origins such as squid pen chitin [27], riftia tubes [28], crab shells [29–32] and shrimp shells [33–37]. Mechanical treatment under acidic condition or neutral condition is important in the preparation of chitin nanofibers. Cationization of amino groups in the chitin by the addition of an acid facilitates the fibrillation of chitin into chitin nanofibers due to electrostatic repulsion [38]. Because of their linear (1,4)- β -N-acetyl glycosaminoglycan structure with two hydroxyl groups and an acetamide group, native chitins in crustacean shells are highly crystalline with strong hydrogen bonding, and are arranged as β -chitin microfibrils in an antiparallel fashion. These microfibrils consist of nanofibers about 2–5 nm in diameter and about 300 nm in length embedded in a protein matrix. Other methods used for the preparation of chitin nanofibers are: TEMPO (2,2,6,6-tetramethylpiperidine-1-oxyl) mediated oxidation, an ultrasonic technique [39], and an electrospinning method [40]. However, the nanofibers obtained by these methods are substantially different from the native chitin nanofibers in terms of width, aspect ratio, crystallinity, chemical structure, and/or homogeneity. Although Fan *et al.* [37] reported a procedure for preparing chitin nanofibers 3–4 nm in width from squid pen chitin by ultrasonication treatment under acidic conditions, crystallinity of the nanofibers from the squid pen is relatively low. In addition, the biomass quantity of the squid pen is considerably lower than those of crab and shrimp shells. Ifuku and coworkers [41, 42] have recently succeeded in isolating α -chitin nanofibers from crab and shrimp shells with a uniform width of 10–20 nm and a high aspect ratio by a simple process involving only grinding. Figure 6.3 shows the FE-SEM micrographs of chitin nanofibers from crab shell and Figure 6.4 shows TEM image of dilute suspension of chitin whiskers.

6.2.3 Starch

Starch is an abundant, inexpensive, naturally renewable, and biodegradable polysaccharide found in the roots, stalks, and seeds of staple crops such as rice, corn, wheat, tapioca, and potato [43–47]. Chemically starch is a mixture of two main components: amylose, a linear or slightly branched (1→4)- β -D-glucan; and amylopectin, a highly branched macromolecule consisting of (1→4)- β -D-glucan short chains linked through β -(1→6) linkages [48–50]. TEM images of starch nanocrystals in its longitudinal and planar view are shown in Figure 6.5. About 70% of the mass of a starch granule is amorphous and 30% is crystalline.

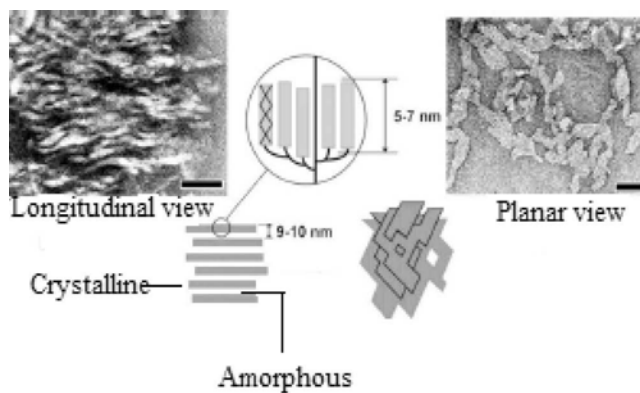


Figure 6.5 TEM observations of starch nanocrystals: longitudinal view and planar view [50].

The amorphous regions contain the main amount of amylose, and a considerable part of the amylopectin. The crystalline region consists primarily of the amylopectin [51]. Starch occurs naturally as discrete granules since the short branched amylopectin chains are able to form helical structures which crystallize. Starch granules exhibit hydrophilic property and strong inter-molecular association via hydrogen bonding formed by the hydroxyl groups on the granule surface [52]. Starch has been widely used in many industrial applications [53, 54] because of its attractive properties such as biodegradability and biocompatibility, as well as its universality, low-cost, versatility, and functional attributes. Starch nanoparticles can be divided into two types i) Nanocrystals and ii) Colloidal starch nanoparticles. The commonly used terms for starch nanocrystals are starch crystallites, microcrystalline starch, and hydrolyzed starch (Figure 6.5). Starch nanocrystals are obtained from mild acid hydrolysis of native starch granules using hydrochloric or sulfuric acid. The use of sulfuric acid leads to more stable aqueous suspensions due to resulting negatively charged surfaces. Starch nanoparticles are generally prepared by regeneration or mechanical treatment.

6.3 Chemical Modification of Cellulose, Chitin and Starch

Cellulose has three alcoholic hydroxyl groups in it, and chemical modifications can be exclusively performed on these hydroxyls. The primary hydroxyl group at C-6 and the two secondary ones at C-2 and C-3 can participate in all the classical reactions as the alcoholic hydroxyl group does, including esterification, etherification, and oxidation reactions. Chemical modifications can be conducted both in heterogeneous and homogeneous conditions. Among the various modification techniques, silylation, mercerization, peroxide treatment, benzylation, graft copolymerization, and bacterial cellulose treatment are the best methods for surface modification of cellulose fibres. Silane coupling agents usually improve the degree of cross-linking in the interface region and offer a perfect bonding. Silane coupling agents may reduce the number of cellulose hydroxyl groups at the fibre-matrix interface. In the presence

of moisture, hydrolysable alkoxy groups lead to the formation of silanols. The silanol then reacts with the hydroxyl group of the fibre, forming a stable covalent bond with the cell wall [55]. Mercerization is a common method used to produce high quality cellulose fibres [56]. Mercerization reduces fibre diameter, thereby increasing the aspect ratio and also leads to the development of a rough surface topography that results in better fibre-matrix interface adhesion and an increase in mechanical properties [57]. Moreover, mercerization increases the number of possible reactive sites and allows better fibre wetting. Several researchers have carried out work on alkali treatment and reported that mercerization leads to an increase in the amount of amorphous cellulose at the cost of crystalline [57, 58]. Figure 6.6 shows the probable mechanism of mercerization of cellulose fibres.

Many researchers make use of peroxide treatment of cellulose fibres because of its easy processability and improvement of mechanical properties. Organic peroxides tend to decompose easily to free radicals, which further react with the hydrogen atom of the matrix and cellulose fibres. In benzylation treatment, benzoyl chloride is most often used in fibre pretreatment and inclusion of benzoyl ($C_6H_5C=O$) group in the fibre is responsible for the decreased hydrophilic nature of the treated fibre [57]. In this treatment, a known amount of washed fibres are soaked in 18% NaOH solution for 30 minutes followed by filtration and washing with water. The treated fibres are then suspended in 10% NaOH solution and agitated with 50 ml benzoyl chloride. The reaction between the cellulosic $-OH$ group of sisal fibre and benzoyl chloride is shown in Figure 6.7 [57, 59].

Chitin nanowhiskers possess a reactive surface covered with hydroxyl groups, which provides the possibility of modification through chemical reaction. The purpose of chemical modification is to provide specific functions and to expand the applications of chitin nanowhiskers. Nair *et al.* [27] investigated the surface chemical modification of chitin nanowhiskers with different reagents. The surface of chitin nanowhiskers - prepared by acid hydrolysis of chitin from crab shells - was chemically modified using chemical reaction between hydroxyl groups and isocyanate groups (Figure 6.8). In TEMPO-mediated oxidation, the primary hydroxyl groups on the chitin nanowhisiker surfaces are selectively oxidized to carboxylate groups. (Figure 6.9).

Chemical modification of starch involves the polymer molecules of the starch granule in its native form. Modification is generally achieved through methods such as etherification, esterification and crosslinking, oxidation, cationization and grafting of starch. Starch modification using a combination of chemical and physical or chemical and enzymatical methods has grown rapidly. A combined method of modification using crosslinking and

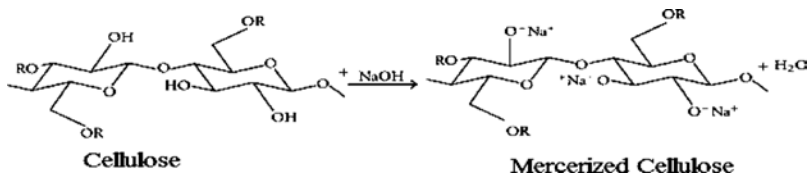


Figure 6.6 Mechanism of mercerization of cellulose fibres [56].

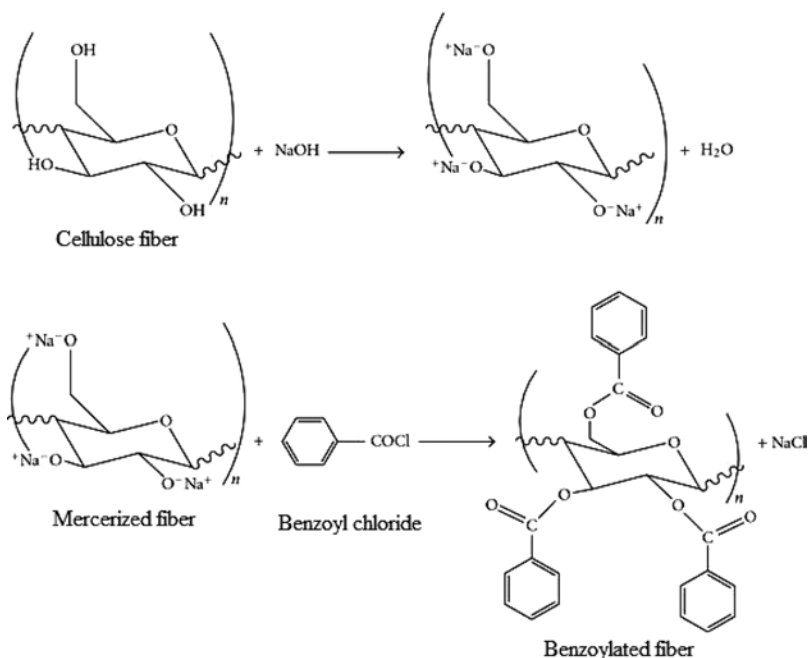


Figure 6.7 Mechanism of benzoylation of cellulose fibres [56].

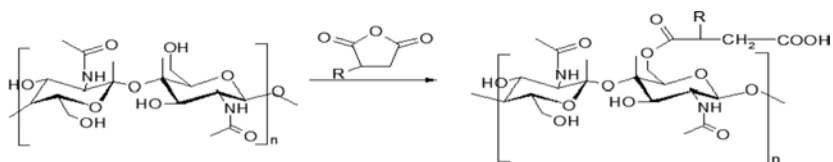


Figure 6.8 Chemical modification of chitin nanowhiskers with alkenyl succinic anhydride.

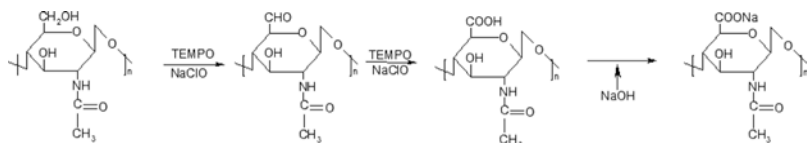


Figure 6.9 TEMPO oxidation of chitin nanowhiskers.

phosphorylation on rice starch provided modified rice starch with good freeze-thaw stability [60]. Starch modified through esterification with ferulic acid giving rise to starch ferulate showed lower viscosity and higher water holding capacity compared to native starch [61]. The high efficiency in producing succinylated cassava starch with microwave assistance was also observed [62]. This is a good method to decrease the use of chemicals to

enhance production. More enzymes are being identified for use in modification of starch. In another study by Hansen *et al.* [63] on gel texture formed in the modification of potato, high-amylose potato, maize and pea starch with amylopectinase, there was an improvement in gel texture compared to the parent starch. All modified starches showed broadened amylopectin chain length profiles [63]. Figure 6.10 shows a schematic representation of the reaction taking place.

Plasma surface modification [64, 65] is an effective and economical surface treatment technique to improve adhesion. There are different types of treatments and using oxygen plasma provides the possibility of carboxyl, carbonyl, ester, ether, epoxy, hydroxyl and carbonate moieties on a hydrocarbon surface. Pertile *et al.* [66] modified bacterial cellulose(BC)membranes with nitrogen plasma in order to enhance cell affinity. The surface properties of the untreated and plasma modified BC were analyzed through contact angle measurements, X-ray photoelectron spectroscopy (XPS) and scanning electron microscopy (SEM). The nitrogen plasma treatment did not increase the wettability of the material, but increased the porosity. In another study by Han *et al.* [67] cold plasma treatments created fluorine-rich layers on the surface of starch samples enhancing hydrophobic property. The treatment parameters affect the chemical mechanisms of modifications, which results in different levels of fluorine deposition and oxygen to carbon ratio [67].

6.4 Bio-based Matrices

6.4.1 Poly(lactic acid) (PLA)

Poly(lactic acid) (PLA) polymers have recently been introduced commercially for products where biodegradability is wanted. PLA is a versatile polymer made from renewable agricultural raw materials, which are fermented to lactic acid. The lactic acid then undergoes ring opening polymerisation to give PLA. The polymer is modified by certain means, which enhances the temperature stability of the polymer and reduces the residual monomer content. The resulting PLA can be processed similarly to polyolefins and other thermoplastics although the thermal stability could be better. Reinforcing with fibres is one possibility

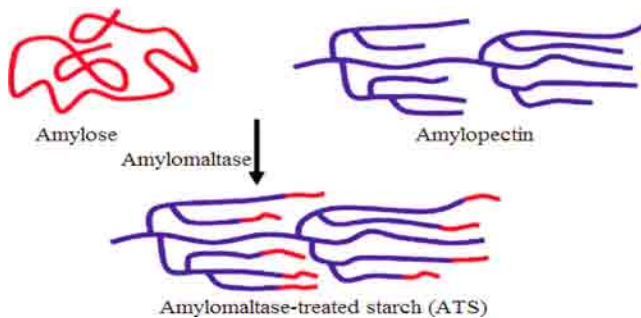


Figure 6.10 Schematic representation of the enzymatic conversion of potato-starch-derived amylose and amylopectin into ATS by amylopectinase [63].

to enhance thermal stability. Poly(lactide) polymers are brittle materials, and it is, therefore, necessary to use plasticizers to improve the elongation and impact properties. The poly(lactide) is fully biodegradable. The degradation occurs by hydrolysis to lactic acid, which is metabolised by micro-organisms to water and carbon dioxide. By composting together with other biomass the biodegradation occurs within two weeks, and the material fully disappears within 3–4 weeks [68].

Several reports are available in the literature regarding the usage of various fibres, flax, ramie, jute [69–71], as reinforcement in polymeric matrices. The interface which is termed the “heart” of the composite is the factor that controls the ultimate properties of the composite. Composites based on flax fibre have been reported by Duigou *et al.* [69]. They studied the interfacial bonding of flax fibre/poly(lactide) bio-composites. The interfacial characterization of flax fibre/poly(lactide) composites was performed on a micro-scale using the microbond method [69]. To understand the interfacial mechanisms of flax/poly(lactide) biocomposites, these were exposed to different thermal treatments (i.e., different cooling rates and annealing to release thermal stress). The treatments resulted in different microstructures and residual stress states within the material.

Yu *et al.* studied [70] the effect of fibre surface-treatments on the properties of PLA/ramie composites. Ramie was treated with alkali and silane (3-aminopropyltriethoxysilane and γ -glycidoxypropyltrimethoxysilane). The mechanical properties (tensile, flexural and impact strengths) of the composites showed significant improvements. The morphology of fracture surfaces evaluated by scanning electron microscopy (SEM) indicates that surface treatment can produce better adhesion between the fibre and the matrix.

Ji *et al.* reported [71] the electron beam effect on the tensile properties and topography of jute fibres and the interfacial strength of jute-PLA green composites. They concluded that electron beam irradiation played a contributing role in physically modifying the jute fibre surfaces and also in improving the interfacial adhesion between jute fibres and PLA in the green composite system.

Petinakis *et al.* [72] investigated the influence of interfacial adhesion on the mechanical properties of PLA micro-composites. According to them addition of up to 40% w/w of wood flour particles into PLA has only little influence on the tensile strength of the micro-composites, but is accompanied by a significant reduction in their elongation-at-break and also results in an increase of up to 95% in the tensile modulus. The lack of the effect of the wood flour particles on tensile strength indicated poor interfacial adhesion between the PLA matrix and the wood flour particles. The addition of a coupling agent, methylenediphenyl-diisocyanate (MDI) to the composition resulted in an increase in tensile strength and tensile modulus of the micro-composites, by 10 and 135%, respectively, indicating enhanced matrix–particle interfacial adhesion. The interfacial adhesion can also be improved by using a compatibilizing agent such as maleic anhydride [73].

6.4.2 Polyhydroxybutyrate (PHB)

Polyhydroxybutyrate (PHB) is a natural thermoplastic synthesized by bacterial microorganisms whose characteristics and potential applications have recently attracted the attention

of both academia and industry [74]. This material is a semicrystalline linear polyester with proven biocompatibility and biodegradability and, therefore, is harmless to the environment. The combination of these characteristics associated with its excellent barrier properties to gas and ultraviolet radiation (250–350 nm) makes it an outstanding candidate in the food packaging industry [75], where products are immediately disposed after consumption and are known to be responsible for the large amount of accumulated waste. The use of biodegradable packages can drastically diminish this solid waste.

Unfortunately, commercial use of PHB is still limited due to its poor mechanical properties as well as its high production cost compared with usual synthetic polymers. PHB presents high crystallinity after processing, as it undergoes secondary crystallization due to its low glass transition temperature (T_g), about 58°C. [76].

A new class of biodegradable “green” composites has been prepared by Luo and Netravali [77] using pineapple fibres and poly(3-hydroxybutyrate-co-3-hydroxyvalerate (PHBV) resin. Pineapple fibres have an average tensile strength of 445 MPa and Young’s modulus of 13.21 GPa. As is the case with all natural cellulosic fibres, pineapple fibres showed high variability in their mechanical properties. Pineapple fibre/PHBV resin interfacial shear strength measured using the microbond technique was found to be 8.23 MPa. This suggests that fibre surface may be treated to improve fibre/PHBV interfacial shear strength.

6.4.3 Cellulose

Cellulose from agricultural products has been identified as a source of biopolymer that can replace petroleum-based polymers. Green nanocomposites have been successfully produced from cellulose acetate (CA), triethyl citrate (TEC) plasticizer and organically modified clay via melt compounding [78]. The cellulosic plastic with 80 wt% pure cellulose acetate and 20 wt% triethyl citrate plasticizer has been used as the polymer matrix for nanocomposite fabrication. Mechanical properties of the nanocomposites were determined and correlated with observations from X-ray diffraction and transmission electron microscopy. Results showed that cellulosic plastic-based nanocomposites containing 5 and 10 wt% organoclay had better exfoliated and intercalated structure than those with 15 wt% organoclay. Tensile strength and modulus of cellulosic plastic reinforced with 10 wt% organoclay improved by 75 and 180% respectively. Thermal stability of the cellulosic plastic also increased.

Recently, a cellulose based nanocomposite material has been investigated as a flexible humidity and temperature sensor [79]. Cellulose was obtained from cotton pulp via acid hydrolysis using a solution of lithium chloride and N,N-dimethylacetamide. Nanoscale polypyrrole has been used as the second component of the nanocomposite. Cellulose-polypyrrole nanocomposite was fabricated by nanocoating polypyrrole layer onto cellulose membrane with varying polymerization time. The authors focused basically on the sensing ability and not on the structural integrity of the nanocomposite material. However, the analysis revealed that there was successful deposition of polypyrrole nanolayer onto the cellulose surface.

An active antimicrobial packaging material has been developed using methyl cellulose (MC) as the base material with montmorillonite (MMT) as reinforcement [80]. MC and

MMT were industrially prepared and mixed with carvacrol (CRV) to form nanocomposites and the resulting nanocomposites were characterized. TEM showed that there were both intercalated and exfoliated nanocomposite structures with exfoliated structures being more prevalent in nanocomposites with low concentration of MMT. Thermal stability of nanocomposite was found to increase with increase in concentration of MMT. The authors suggested that the slight thermal degradation shown by the nanocomposite was due to the structural degradation of MC at higher temperatures.

A new strategy was developed for cellulose diacetate (CDA) based biocomposites by melt processing [81]. It makes use of two different plasticizers: a primary “non-reactive-type” plasticizer, triacetin (TA), added prior to extrusion to enhance the “processing window” of the polymer, and a secondary “reactive-type”, glycerin polyglycidyl ether (GPE), added during the extrusion step to reduce the amount of potential volatiles or leachable products in the final product and to help in the reduction of viscosity and further improve the processability. It was observed that the adhesion of the polymer matrix to the fibres improved by the addition of GPE, possibly because of the formation of strong chemical bonds with the polymer matrix through the epoxy groups of GPE.

6.4.4 Chitosan

Chitosan (CH) offers a number of advantages over other materials for developing biomaterials due to its excellent properties, such as biocompatibility, biodegradability, bioadhesive nature, and antibacterial activity [82 - 84]. However, the poor processability and mechanical properties limit its applications [85]. The formation of organic–inorganic hybrids through incorporation of fillers is an effective approach for improving physical and mechanical properties of chitosan. For example, hydroxyapatite (HA) [86], cellulose nanocrystals [87], graphene oxide (GO) [88], polyhedral oligosilsesquioxanes (POSS) [89] etc can be used as the reinforcing phases.

Nikpour *et al.* [86] synthesized hydroxyapatite/chitosan composite membrane for biomedical application. Chitosan showed strong adsorption on HA. The HA nanoparticles well dispersed in the matrix and it was indicated that composite samples consist of homogeneous aggregates around 40–100 nm, in which many HA nanocrystals align along the chitosan molecules. This homogeneous distribution of inorganic nanoparticles reveals strong interfacial interaction between the nanoparticles and the polymer matrix.

deMesquita *et al.* [87] functionalized cellulose nanocrystal (CNC) surface with methyl ester end groups for creating reactive end groups on the nanocrystals which reacted with the amino groups of the chitosan biopolymer, leading to a bionanocomposite with covalent linkages between the CNCs and the chitosan. A remarkable increase in tensile strength and modulus with increasing concentration of the nanocrystals was observed. The strain-to-failure of the nanocomposites was similar to that of the pristine CH matrix when the concentration of CNCs was relatively low (up to approximately 10%). For higher concentrations of CNCs, a decrease in the strain-to-failure (from 12% for the pristine CH to 5% for the highest concentration used in this work) was observed. This behavior can be explained by the strong interfacial adhesion between the matrix and the cellulose nanofillers, which restricts the motion of the matrix.

Pan *et al.* [88] developed a simple and green approach for fabrication of graphene oxide (GO)/chitosan nanocomposite films. Mechanical properties of the nanocomposite were significantly enhanced without sacrificing the optical transparency. GO sheets are unidirectionally aligned in the chitosan matrix and parallel to the surface of nanocomposite film. With incorporation of 1 wt% GO, the fracture strength and tensile modulus of the nanocomposites were significantly enhanced i.e., by 93% and 51%, respectively. The simultaneous improvement of strength and toughness could be attributed to the homogeneous dispersion and alignment of GO sheets in the chitosan matrix.

Xu *et al.* [89] added hydrophilic and hydrophobic POSS with different charges into chitosan matrix to form composite membranes. Phase separation was observed in composite membranes containing hydrophobic POSS, whereas no phase separation was observed in the membranes containing hydrophilic POSS. Composite membranes containing hydrophilic POSS presented good mechanical properties due to good compatibility and strong interactions between POSS and the chitosan matrix. However, hydrophobic POSS with poor interfacial interaction with chitosan made the composite membranes more brittle.

6.4.5 Starch

Starch films have a strong and flexible structure and good transparency derived from the linear structure of amylose (one of the components of starch), and they are resistant to fats and oils [90]. In addition, they are odorless, tasteless, colorless, non-toxic and biologically absorbable. However, the use of starch based materials has been strongly limited because of their poor mechanical properties and high permeation compared to other non-natural polymers [91]. The incorporation of micro and nano-sized fillers into starch has been the topic of many studies in order to overcome these disadvantages [92].

Cassava starch based composites were prepared by Ramirez *et al.* [93] by incorporating fibres from Brazilian green coconuts with different amounts of coir fibres by thermal molding using glycerol as plasticizer for the starch. The matrix and composites were given thermal treatment. Both the untreated and treated matrices and their composites were characterized. The tensile properties of cassava starch improved with both the incorporation of fibres and thermal treatment. Fractographic studies through scanning electron microscopy were used to explain the observed strength properties. Water uptake, swelling and moisture absorption of thermoplastic starch (TPS) showed decrease with the incorporation of fibres, which is due to better interfacial bonding between the matrix and fibres as well as the hindrance to absorption caused by the fibres.

Castanoa *et al.* [94] reported the physical, chemical and mechanical properties of pehuen cellulosic husk and pehuen starch based composites. Thermo-mechanical properties of thermoplastic pehuen starch composites reinforced with pehuen husk showed the potential of this biofiber as an excellent reinforcement for composite materials. TPS composites showed a good interaction between the fibres and the plasticized starch matrix due to the natural affinity between husk and starch in the pehuen seed.

Starch/multi-walled carbon nanotube composites were prepared by Fama *et al.* [91]. These materials exhibited highly improved tensile and impact properties as a consequence

of wrapping the multi-walled carbon nanotubes (MWCNTs) with a starch–iodine complex composed of the same starch as the matrix. Thus, good dispersion of the filler in the matrix and excellent adhesion between the phases were achieved. SEM observations also indicated that carbon nanotubes were well dispersed in the starch matrix and good adhesion between matrix and filler was achieved. This is a consequence of the successful wrapping of the nanotubes with the complex composed of the same starch as the matrix. Thus, strong adhesion between matrix and filler was assured and also better dispersion of the MWCNTs was achieved by hindering van der Waals interactions among them and therefore CNTs agglomeration was avoided.

6.4.6 Natural Rubber

The second most consumed biopolymer after cellulose is natural rubber (NR) and it is the most widely studied elastomer. Different tropical trees produce different forms of poly(1,4-isoprene), which are exuded or extracted as an aqueous emulsion (latex) or as a sap-like dispersion, before coagulation. The *cis*-form of the polymer (Figure 6.11 (a)) tends to be amorphous and has a glass transition temperature of about -70°C , which makes it ideally suitable for application. The practical application of elastomers requires the addition of fillers to obtain an improvement in mechanical properties. It is impossible to use most elastomers without reinforcing with certain fillers, such as carbon black and highly structured silica. The *trans*-form (Figure 6.11 (b)), called gutta percha or balata, readily crystallizes forming rigid materials melting at about 70°C .

The primary effects of bio-fibre reinforcement on the mechanical properties of natural rubber composites include increased modulus, increased strength with good bonding at high fibre concentrations, decreased elongation at failure, greatly improved creep resistance over particulate-filled rubber, increased hardness, and a substantial improvement in cut, tear and puncture resistance. Biodegradation of vulcanized rubber material is possible, although it is difficult due to the interlinkages of the poly(*cis*-1,4-isoprene) chains, which however result in reduced water absorption and gas permeability of the material [95].

It is difficult for inorganic nanoparticles to be evenly dispersed in a polymer, such as rubber matrix, and attain the strong interface strength due to their surface characteristics (which generally cause strong filler–filler interaction and weak filler–rubber interaction). Therefore, it is very important and challenging to find an economic and effective technique to improve the dispersion of nano-particles in polymer matrix and strengthen

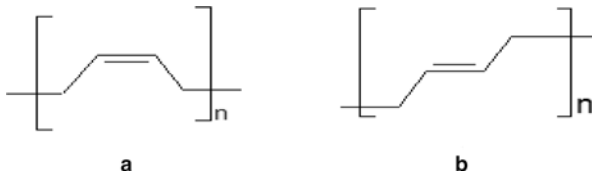


Figure 6.11 The two main structures of poly (1,4-isoprene) in natural rubber: (a) the *cis*-form and (b) the *trans*-form.

the interfacial interaction between inorganic nano-particles and polymer [96]. Peng *et al.* [97] prepared NR/MWCNT composites by a combination of latex compounding and self-assembly techniques. The morphological structures of the composites depended on the loading of acid treated MWCNTs, which were modified with poly(diallyl dimethyl ammonium chloride) (PDDA); MWCNTs were dispersed well in NR when the loading was less than 3 wt %, but aggregation was observed when more MWCNTs were added. These structural and morphological effects contributed directly to the thermal and mechanical properties of the composites. Significant improvements in tensile strength and modulus were observed when the MWCNT loading was between 1 and 2 wt %, whereas a further increase in the loading showed only limited reinforcement. The results indicate that the MWCNTs were homogeneously distributed throughout the NR matrix as single tubes and had good interfacial adhesion with the NR phase when the MWCNT loading was lower than 3 wt %.

Cellulosic nanoparticles (cellulose whiskers or microfibrillated cellulose) were used as reinforcing phase to prepare nanocomposite films using natural rubber latex as matrix using solvent casting technique. The swelling behavior of the polymeric matrix by toluene was found to strongly decrease even at only 1 wt.% of cellulose nanoparticles and was almost independent of the filler content and nature. Differences in properties between the two sets of nanocomposite films were analyzed from the differences between the two kinds of cellulosic nanoparticles, i.e., flexibility and possibility of entanglements, and presence of residual lignin, extractive substances and fatty acids at the surface of MFC. From the results Bendahou *et al.* [98] concluded that higher filler-matrix adhesion dominates the behavior of MFC-based composites. It results in lower water uptake and higher mechanical property in terms of stiffness.

Arvanitoyannis *et al.* [99] reported on biodegradable blends based on gelatinized starch and 1,4-transpolyisoprene (gutta percha) for food packaging or biomedical applications. Components are mixed to an adequate degree of dispersion by thermal pressing. A series of blends of gutta percha with gelatinized starch, with and without plasticizers or compatibilizers, were prepared in an attempt to preserve the excellent biocompatibility of gutta percha. A small amount of plasticizer was incorporated into the blends to improve mechanical properties. The gas and water permeability values of the blends were found to have intermediate values between the two components.

Mondragon *et al.* [100] used unmodified and modified natural rubber latex (uNRL and mNRL) to prepare thermoplastic starch (TPS)/natural rubber/montmorillonite type clay (TPS/NR/Na⁺-MMT) nanocomposites by twin-screw extrusion followed by injection molding. The dispersion of the nanoclay in the polymer blends was evaluated by XRD and TEM. The chemical modification of NR improved both the dispersion and interfacial adhesion of the rubber phase in the TPS matrix. This improvement combined with the NR crosslinking occurring during chemical modification resulted in very significant increase of tensile strength and elastic modulus as compared to TPS/uNR blends. Addition of 2 wt.% MMT led to exfoliated structures which further increased the tensile properties of the TPS/mNR blend, demonstrating the benefits of using both modified rubber molecules and nanoclay particles. Surprisingly, nanoclay particles were mainly dispersed in the NR domains.

6.5 Processing Techniques

Many methods have been employed for the production of nanocomposites in an attempt to achieve optimum dispersion of fibres in the matrix. The extrusion process is used by the plastics industry for the production of granules and also in the continuous production of semi-finished products or components. Single-screw as well as twin-screw extruders are used for this process. Single-screw extruders are used when the mixing effect does not have to be very high. Owing to the excellent mixing effect of the twin-screw extruder, natural fibre materials can be homogeneously distributed in and wetted by the thermoplastic melt [101]. One of the current limitations of compounding and extrusion is that only relatively short fibres (which impart limited reinforcement) can be used. If longer fibres are to be included, alternative methods may need to be employed [102].

Injection molding is the most common method of producing parts made of plastic. The process includes the injection or forcing of heated molten plastic into a mold which is in the form of the part to be made. Upon cooling and solidification, the part is ejected and the process continues. Extrusion followed by injection molding has been used [103]. Although the effect of the method on the properties of the resulting composite has not been reported, it is believed that this processing method leads to a better exfoliation of fibres in the matrix [103]. Majdzadeh -Ardakani and S-Ardakani [104] noted that when using the melt extrusion method, extrusion speed has a significant effect on the thermal properties, specific energy requirement, radial expansion ratio and compressibility of polymer foams. Another common method is film stacking which involves compressing a stack of polymer film and fibre for a period of time. Moulding method influences the tensile properties of the composites [105]. Melt compounding followed by compression moulding [100], injection moulding [106], solution casting after gelatinization [107], direct melting and solidification [108] and one-step in-situ intercalative solution polymerization [109] were some of the moulding techniques used. The one-step in-situ polymerization method involves the dispersion of nanofillers in monomer(s), followed by bulk or solution polymerization. The functional group modification of nanofillers helps to increase the interaction between the polymer and the nanofillers, which ultimately leads to a good dispersion in the polymer matrix.

In the processing of rubber composites, mixing is the most critical part. The primary purposes of mixing are incorporation, dispersion and distribution of the filler and other ingredients in elastomeric polymers. Usually, this is achieved by using batch mixing or continuous mixing of dry fillers and solid rubber or pellets, referred to as dry mixing. Mixing is done either in large enclosed mixing machines or in rubber mills. The Banbury mixer, a traditional compounder, which mixes components together that do not readily blend and require considerable energy to become homogeneous. Jong [110] compounded NR with a Brabender mixer equipped with a pair of Banbury blades. Visakh *et al.* [111] used two-roll mill mixing method for the preparation NR reinforced with cellulose nanofibres. Solvent casting is another widely used method which is based on dispersing the filler as well as matrix in an appropriate solvent, mixing it together followed by casting it into films by evaporating the solvent. Jiang *et al.* [112] fabricated a carbon nanotube (CNT) reinforced natural rubber composite by solvent casting method.

6.6 Interfacial Adhesion Issues

The utilization of polymer nanocomposites derived from renewable biomaterials has received much attention because of their low cost, low density, nonabrasiveness, combustibility, non-toxicity, and biodegradable characteristics. However, the lack of good interfacial adhesion between the hydrophilic filler particles and hydrophobic polymer matrix makes these composites less attractive for various applications. This is a very important issue, since the poor adhesion between the reinforcement and the matrix may lead to poor mechanical properties in comparison to the neat polymer. The use of adhesion promoters, additives or chemical modification of the filler surface can help to improve the interfacial adhesion between filler particles and polymer macromolecules as well as their dispersion in the matrix, thereby improving the overall mechanical performance of the composites.

6.6.1 *Challenges of Interfacial Adhesion of Natural Fibres in Polymer Matrix*

The major difficulties associated with the use of natural fibres as reinforcement in polymer matrix composites are related to their strong sensitivity to water, even moisture, relatively low thermal stability and fibre decomposition during compounding with the polymer matrix. These factors strongly influence the morphology and final properties of the composites.

One of the biggest problems encountered in the use of natural fibres lies in the difficulty in ensuring good dispersion of the fibres in the matrix material. Natural fibres are hydrophilic and polar in nature due to the high density of hydroxyl (-OH) groups on their surface, whereas common thermoplastic matrices are hydrophobic and non-polar. The weak bonding between the non-polar matrix and polar fibres is caused by the large difference in the respective surface energies of the two materials [113]. Bonding between the matrix and the fibre is dependent on the atomic arrangement and chemical properties of the fibre and on the molecular conformations and chemical constitution of the polymer matrix. Therefore, the interface is specific to each fibre/matrix system.

Interface plays an essential role in the physical and mechanical properties of composites. It has been established that the mechanical performance of the composites depends not only on the principal components but also on the nature and strength of the interface that is responsible for the load transfer from the matrix to the fibres. A strong interface allows effective stress transfer between the matrix and fibres and a weak interface causes insufficient stress transfer from the matrix to the fibres. When the interface is too strong then brittle scission of fibres occurs, whereas a too weak interface leads to pull-out of fibres [114]. Therefore, the optimization of interfacial properties is essential for effective stress transfer between the matrix and fibres. Physical and chemical modifications can be used to optimize the interface in natural fibre composites. A good interfacial adhesion can also be achieved by the use of coupling/compatibilizing agents, or the modification of the matrix [115–120]. The main aims of these modifications are to provide an efficient hydrophobic barrier and to minimize the interfacial energy between the fibres and the non-polar matrix, thus generating optimum

adhesion. A large number of adhesion theories have been proposed to understand how the modification of the matrix improves the fibre/matrix adhesion in natural fibre composites. These include adsorption, diffusion, mechanical interlocking, surface energy or wetting, electrostatic attraction, acid-base and weak boundary layer theory [121–125].

6.6.1.1 Challenges of Dispersion of Cellulose Nanofibres

Cellulose nanofibres have attracted widespread interest as a renewable reinforcing phase for polymers to increase their modulus, strength and heat distortion temperatures. Cellulosic nanofibers present a very high surface area and the most important parameter to be controlled for its ultimate application is the adhesion property. Key determinants of the performance properties of cellulose nanofibre reinforced composites include fibre-matrix adhesion, the mechanical properties of the fibre, moisture content, physical impact and fatigue, thermal stability, etc.

Cellulose nanofibres have a tendency to form hydrogen bonds with adjacent fibrils, which results in agglomeration or entanglement of the nanofibres and hence dispersion is an important challenge in non-polar solvents. In order to expand the horizon of bionanocomposites for high performance applications, it is necessary to reduce the entanglement of fibrils and improve their dispersion quality in the polymer by surface functionalization without deteriorating their reinforcing ability. The surfaces of cellulose nanoparticles have accessible –OH groups on which chemical functionalization can take place. Surface functionalization allows tailoring of particle surface chemistry to facilitate self-assembly, controlled dispersion in a wide range of matrix polymers, and control of both the particle-particle and particle-matrix bond strength. The main challenge in the chemical functionalization of different nanocelluloses is to conduct it in such a way that it only alters their surface while preserving their original morphology, avoiding any polymorphic conversion, and maintaining the integrity of their native crystalline structure [2].

Nanocelluloses are generally recognized to be effective in reinforcing polymers due to interaction between the nano-scale elements that form a network interconnected by hydrogen bonding. These hydrogen bonds present on the surface of nanofibers of cellulose are the key for a better manageability of these new materials to determine their future applications. These applications will be strongly dependent on the surface properties of nanocellulosic materials and their capability to be compatible with the matrix in which they are processed [126].

6.6.2 Strategies for Improving Interfacial Adhesion

Various strategies have been developed to improve the adhesion of the matrix to the fibre and the corresponding fibre/matrix interfacial strength in composites. These strategies include (i) physical treatments of fibres such as corona, plasma, laser, vacuum ultraviolet and γ -radiation, and (ii) chemical modification methods such as mercerization, acetylation, esterification, cationization, carboxylation, silylation, isocyanate treatment, and polymer grafting [127–133]. Polymer grafting improves wetting of the fibre by the matrix by hydrophobizing the fibre surface and thus promotes interfacial bonding by diffusion of the chain segments of the grafted molecules into the matrix. These methods have achieved various

levels of success in improving fibre strength and fibre/matrix adhesion in natural fibre composites. All chemical functionalizations have been mainly conducted (i) to tune the surface characteristics of nanocelluloses to promote their dispersion in nonpolar organic media and/or to improve their compatibility with hydrophobic matrices in nanocomposites; (ii) to introduce stable negative or positive charges on the surface of nanocellulose to obtain better electrostatic repulsion induced dispersion, especially when exploring their self-assembly properties [2].

Coupling agents and radical induced adhesion also enhance interfacial bonding through covalent bonds between the fibre and the matrix [122, 134]. The substance which promotes or establishes a stronger bond at the matrix/reinforcement interface is known as the coupling agent/compatibilizer. The role of the coupling agent/compatibilizer is to interact with both the fibre and matrix, in order to bridge the properties of the two different systems. In general, to enhance the compatibility between hydrophobic and hydrophilic components of a system, the compatibilizing agents have a functional group able to react with the hydroxyl groups of cellulose, and an alkyl chain which decreases the hydrophilicity of the fibre and, at the same time, makes its surface more compatible for good adhesion to the matrix.

Several strategies for surface modifications aiming at improving the compatibility between cellulose fibres and polymer matrices have been reported [135–136]. Coupling agents bearing two reactive groups can be used to chemically modify the surface of fibres and that of polymeric materials. Coupling agents usually improve the degree of cross-linking in the interface region resulting in a perfect bonding. Coupling agents such as maleated polymer [137], isocyanates [138] and alkoxy silanes [139–143] were used to improve the compatibility between the fibre and matrix. Within these different reagents, maleated polypropylene (MAPP) or polyethylene (MAPE) have reportedly shown significant enhancement in tensile and flexural strengths, ranging from 40% up to 80%, when they are blended with cellulose fibres before mixing with the matrix [142].

Similarly, silane coupling agents were also found to be effective in modifying the natural fibre-matrix interface. Coupling agents such as triethoxy (vinyl) silane, aminopropyl (trimethoxy) silane and aminopropylmethyl (diethoxy) silane were tested in fibre treatment in order to improve the interface properties. Silanes as a coupling agent have some major advantages, first these are commercially available; second these bear an alkoxy silane group that is capable of reacting with the OH-rich surface of natural fibres at one end while at the other end, a large number of organo functional groups are available which can be tailored to the matrix to be used [141].

Andresen *et al.* [143] have reported successful surface silylation of nanofibrillated cellulose with (chlorodimethyl) isopropylsilane. At moderate degree of substitution (between 0.6 and 1), hydrophobized silylated fibres maintained their morphological integrity and were able to stabilize water-in-oil emulsions [144]. Nishino *et al.* [145] reported that the interfacial adhesion strength of kenaf fibre can be effectively improved by the addition of silane coupling agents.

Surface-trimethyl silylation of cellulose nanocrystals extracted from bacterial cellulose and their resulting cellulose acetate butyrate [20] or polysiloxane [146] based nanocomposites were investigated. Cellulose nanocrystals functionalized by partial silylation through coupling with n-dodecyldimethylchlorosilane showed a very good dispersion in

poly(L-lactide) and acted as nucleating agents and hence accelerated the crystallization rate of poly(L-lactide) [147]. Similarly, the coupling of either cellulose nanocrystals or nanofibrillated cellulose with 3-aminopropyltriethoxysilane enhanced their compatibility with PLA, thus significantly improving mechanical performances of final nanocomposites [148].

Interaction of cellulose with surfactants or surface active agents has been another way to facilitate the adhesion of hydrophilic cellulose suspension to non-polar hydrophobic polymer matrix. A surfactant is a material that can greatly reduce the surface tension of water when used in very low concentrations. It has been found that the surface tension of polymeric material contributes significantly to adhesion forces. The concentration and dispersion of cellulose particles within polymer matrices will also change surface tension dynamics of nanocomposites relative to its interface. The value of interfacial tension generally lies between the surface tension values of the two immiscible phases. If the molecules of the two phases are similar, the interfacial tension will be zero.

Noncovalent surface modifications of nanocelluloses are typically made via adsorption of surfactants [149]. Surfactants consisting of mono- and di-esters of phosphoric acid having alkylphenols tails have been used to modify cellulose nanocrystals. The surfactant coated cellulose nanocrystals dispersed very well in nonpolar solvents [150]. Bondeson and Oksman [151] have reported the use of an anionic surfactant to enhance the dispersion of cellulose nanocrystals in PLA. Kim *et al.* [152] and Rojas *et al.* [153] reported the use of nonionic surfactants to disperse cellulose nanocrystals in polystyrene-based composites. Zhou *et al.* [154] reported a new and elegant way of noncovalent nanocellulose surface modification based on the adsorption of saccharide-based amphiphilic block copolymers. By mimicking the natural lignin-carbohydrate copolymers, they adsorbed xyloglucan oligosaccharide-poly(ethylene glycol)-polystyrene triblock copolymer onto the surface of cellulose nanocrystals. The resulting cellulose nanocrystals showed excellent dispersion ability in nonpolar solvents.

6.6.3 New Challenges and Future Trends in Fibre/Matrix Interfacial Adhesion

The potential of cellulose nanofibres as a reinforcement in nanocomposites has received much interest recently. These nanoscale cellulose fibre materials serve as promising candidates for the preparation of bionanocomposites. However, there are some challenges that can be identified for expanding their use in new composite materials. One of the challenges associated with the use of nanocellulose in composites preparation is that it is desirable to have a fine dispersion between the two main phases, i.e., cellulose nanofibres and matrices. In order to achieve improved dispersion of cellulose nanofibres in polymer nanocomposites, good filler-matrix interaction is essential because it dictates the overall performance of the composites. Better dispersion of cellulose nanofibres in polymer matrices improves the interfacial characteristics of the composite and thereby improves the strength and stiffness of the composite. Consequently, the direction of research has been focused on producing composites with maximized and reproducible properties by developing new processing routes. The ideal process has been found to be the one that produces a fine nanocellulose dispersion by avoiding large-scale nanofibre agglomeration, which increases the effective particle size and lowers the fibre-matrix interface area [155].

Next challenge is associated with the control of nanocellulose properties, i.e. to produce nanocrystalline cellulose with tightly controlled size and aspect ratio, minimized crystal defects and controlled surface chemistry. Development of such nanocellulose materials with controlled properties will help to produce repeatedly, optimised materials with minimum or zero defects – a challenge presently faced by manufactures in the production line. The other major challenge dealing with nanocellulose is cost. A factor in the cost of nanocellulose production is the low yield when starting from plant based raw materials, as opposed to bacterial sources. Additionally, the viscosity of a nanocellulose dispersion rapidly builds with concentration, forcing the use of only dilute nanocellulose content during processing and functionalization. In addition to increased capital costs for production, this can also lead to excessive waste [155].

Extensive research efforts for nanocellulose adhesion are necessary to obtain a better understanding of the adhesion interactions of nanocellulose beyond hydrogen bonding, including mechanical interlocking, interpenetrating networks, acid-base interactions, and covalent linkages on a fundamental level to improve interfacial properties with thermoplastics, thermosets and biopolymers.

6.7 Interface Characterization Techniques

In natural fibre reinforced polymer composites, the strength and type of interface play an important role in the overall performance of the composites. Therefore, the interface characterization is very important for assessing the properties of the composites. The techniques that allow investigation of different changes at the composite interface are important tools for establishing correlations between interface characteristics and composite properties. Various techniques have been extensively used to characterize the interface in polymer nanocomposites. The commonly used powerful techniques for morphological characterization are scanning electron microscopy (SEM), atomic force microscopy (AFM), transmission electron microscopy (TEM), wide-angle X-ray diffraction (WAXD) and small-angle X-ray scattering (SAXS). For thermal characterization and to study the cure behaviour of polymer nanocomposites, the commonly used techniques are differential scanning calorimetry (DSC), thermogravimetric analysis (TGA), thermomechanical analysis (TMA) and dynamic mechanical thermal analysis (DMTA). Spectroscopic techniques such as Fourier transform infrared spectroscopy (FTIR), Raman spectroscopy, Attenuated total reflectance infrared spectroscopy (ATR-IR) and nuclear magnetic resonance (NMR) spectroscopy provide complementary information about the chemical nature of materials, the investigation of the composition of surfaces, and the interactions developed at the interface of composite materials. In this section, we briefly describe the applications of these techniques in the field of cellulose-based nanocomposites.

6.7.1 Morphological Characterization

Techniques such as scanning electron microscopy (SEM), atomic force microscopy (AFM) and transmission electron microscopy (TEM) can be used to study the morphological changes on the surface and can predict the extent of mechanical bonding at the interface.

6.7.1.1 Scanning Electron Microscopy (SEM)

Scanning electron microscopy (SEM) is generally employed for morphological investigation and interface characterization in composites. It provides images of surface features associated with a sample.

Kim *et al.* [156] used atmospheric glow discharge (AGD) to modify the surface properties of wood powder as well as plant fibre to improve the compatibility between the fibre surface and polypropylene (PP) matrix. The AGD surface modification allows the reinforcing material to disperse evenly within the matrix with a strong interfacial bonding between the fibre and the polymer matrix (Figure 6.12 and Figure 6.13). The tensile strengths of the

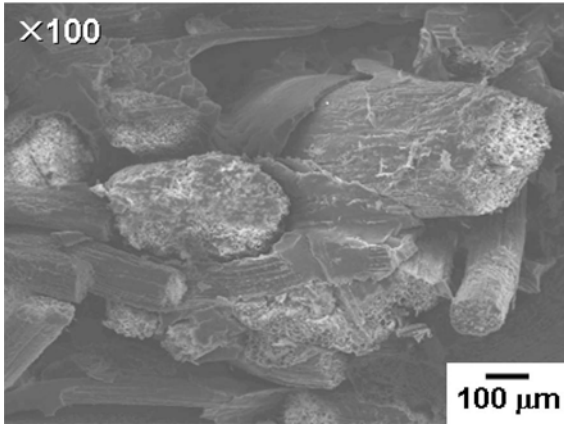


Figure 6.12 SEM micrograph of 50% jute fibre/PP composite [156].

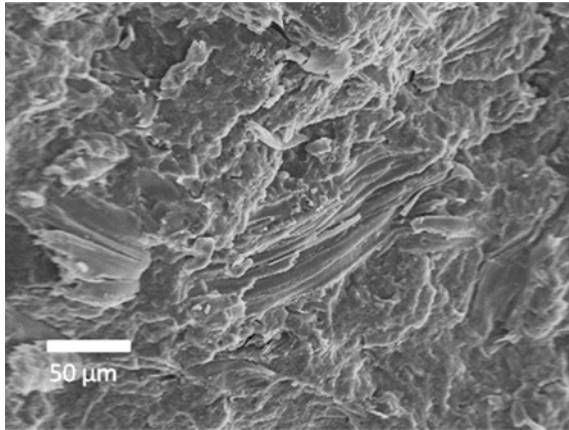


Figure 6.13 SEM micrograph of 50 wt% wood powder/PP composite [156].

wood powder/PP composites, coir/PP composites and jute/PP composites were examined. The tensile strength of AGD treated jute/PP composites increased by 50 and 114% and for coir/PP increased by 22 and 92% compared with NaOH treated and raw fibres, respectively.

Zhou *et al.* [157] investigated the effect of atmospheric pressure plasma jet (APPJ) treatments on ramie fibres and polypropylene (PP) composites reinforced with modified ramie fibres. APPJ treatment increased the roughness of the fibre surface in comparison to the untreated fibres which helps in the enhancement of the interfacial adhesion between the two phases and hence the mechanical properties (Figure 6.14).

Hernandez *et al.* [158] modified sugarcane bagasse fibres by various surface treatments like alkaline treatment, silane coupling agent, fibre coating with polystyrene (PS) and grafting of PS on the fibre (with and without crosslinker). SEM analysis revealed that after treatment PS aggregates distributed as dots which appeared along the fibre surface, resulting in more interlocking sites that contributed to the adhesion. The interfacial adhesion between the modified fibres and the polymer matrices was quantified using the single fibre pull-out test. The IFSS (interfacial shear strength) of all the chemically modified fibres increased significantly as compared to the untreated ones.

The influence of fibre surface treatment on the interfacial property of biocomposites based on PLA and ramie fibres was investigated by Chen *et al.* [159]. In order to improve the interfacial adhesion, ramie fibres were treated with permanganate acetone solution and silane acetone solution. SEM images (Figure 6.15) show that PLA biocomposites with treated ramie fibres exhibit better interfacial adhesion compared to the untreated fibres. Permanganate acetone solution removes the pectin, lignin and other components from the ramie fibre and the interaction between silane amino group and PLA matrix provides high interfacial adhesion between ramie fibre and PLA matrix.

The morphology and fracture surfaces of polyurethane (PU) nanocomposites have been examined by scanning electron microscopy (SEM) [160–162]. SEM images of PU nanocomposite films indicated a well dispersion of cellulose nanowhiskers in the matrix and good adhesion at the interface which has been attributed to strong hydrogen bonding.

Liu *et al.* [163] examined the morphological characteristics of flax fibre modified with poly(vinyl acetate) (PVAc) or PEG (poly(ethylene glycol)). Scanning electron micrographs of untreated, PVAc and PEG treated fibres are shown in Figure 6.16 (a-d). The SEM images

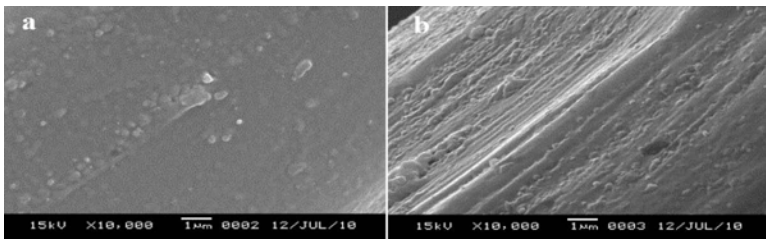


Figure 6.14 SEM micrographs of APPJ (a) plasma treated ramie fibres for 16 s with ethanol pretreatment (b) plasma treated ramie fibres for 24 s with ethanol pretreatment [157].

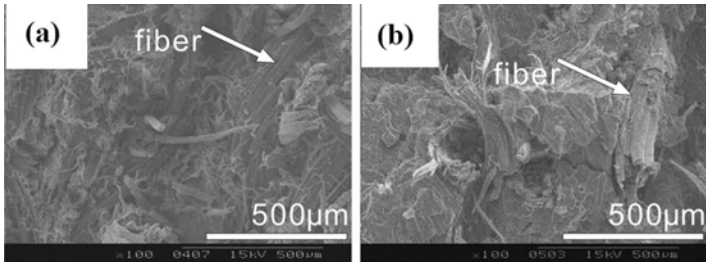


Figure 6.15 SEM micrographs of tensile fracture surfaces of (a) untreated ramie fibre/ PLA composite and (b) silane treated ramie fibre/ PLA composite [159].

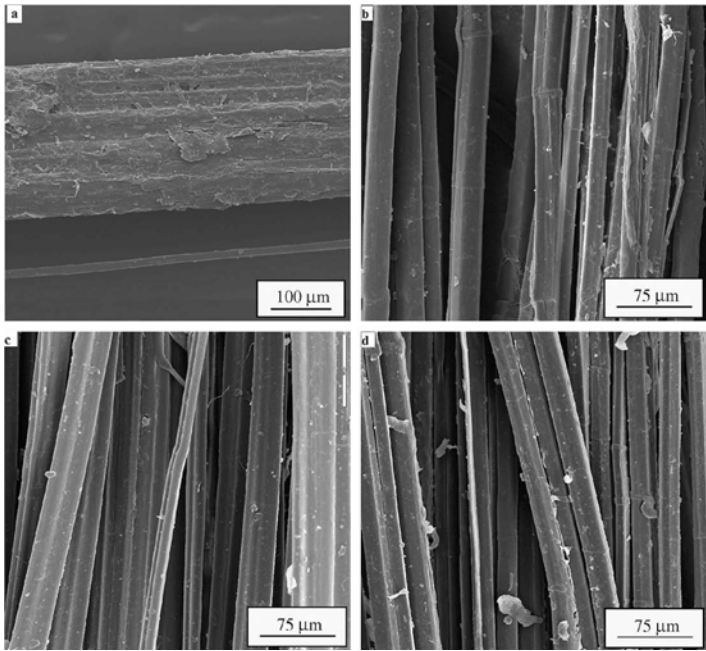


Figure 6.16 SEM micrographs of flax fibres that are untreated (a), pre-treated in a two stage (b), PEG (c) and PVAc (d) [163].

of the pre-treated fibres (Figure 6.16 (b)) are seen to be well separated and free from debris adhering to the fibre surface compared to the untreated fibre (Figure 6.16 (a)). After treatment with PEG and PVAc (Figure 6.16 (c) and Figure 6.16 (d) respectively), globular deposits were visible on the fibre surfaces which indicated the formation of a layer on the surface of the fibre. The authors suggested that a two-stage pre-treatment of flax fibre followed by modification with PEG and PVAc can improve the fibre/matrix interfacial adhesion.

Zhou *et al.* [164] used scanning electron microscopy (SEM) technique to understand the effect of nanocellulose isolation techniques on the surface morphological characteristics of nanocellulose reinforced poly (vinyl alcohol) (PVA) films. They introduced three techniques (acid hydrolysis (AH), 2,2,6,6-tetramethylpiperidine-1-oxyl radical (TEMPO)-mediated oxidation (TMO) and ultrasonication (US)) to isolate nanocellulose from microcrystalline cellulose, in order to reinforce poly(vinyl alcohol) films. The fractured surfaces after tensile tests on neat PVA and PVA nanocomposite films were examined using SEM (Figure 6.17). SEM images clearly showed the homogeneous distribution of the nanocellulose in both AH/PVA and TMO/PVA films, implying good adhesion between fillers and matrix. This should be attributed to the formation of a rigid hydrogen-bonded network of nanocellulose that is governed by percolation theory. However, some microfibril bundles are observed in fractured surfaces of US/PVA films, due to the lack of charge on the US-derived nanofibrils.

Vilela *et al.* [165] prepared novel low-density biocomposites based on cork and two biodegradable matrices, PLA and poly(caprolactone) by simple melting-mixing. The morphological characterization of the composites was done by SEM. The SEM results showed a good dispersion of cork and a strong interfacial adhesion between the cork particles and the polymeric matrices.

Shu *et al.* [166] presented a general methodology to enhance the interfacial adhesion in polymeric composites by creating nanoscale morphology on the surfaces of particles. The

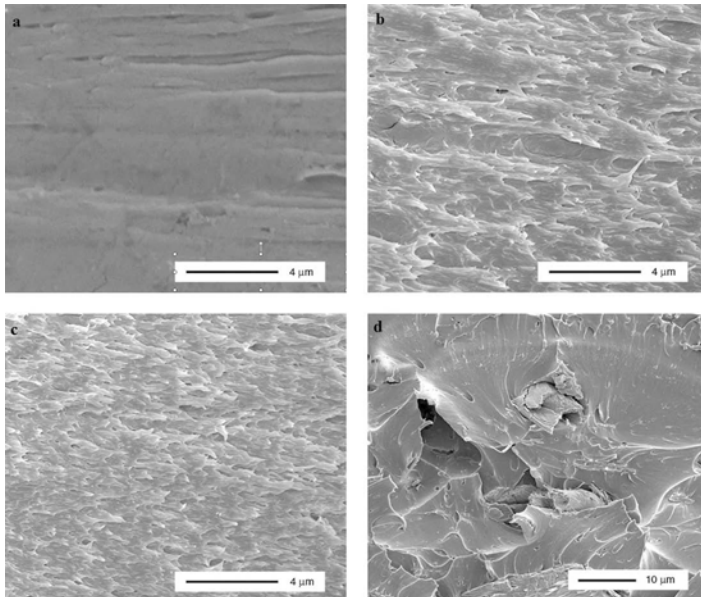


Figure 6.17 SEM images of fractured surfaces of (a) neat PVA, (b) AH/PVA, (c) TMO/PVA and (d) US/PVA films. (mag 20000x for (a), (b), (c), (mag 10000x for (d)) [164].

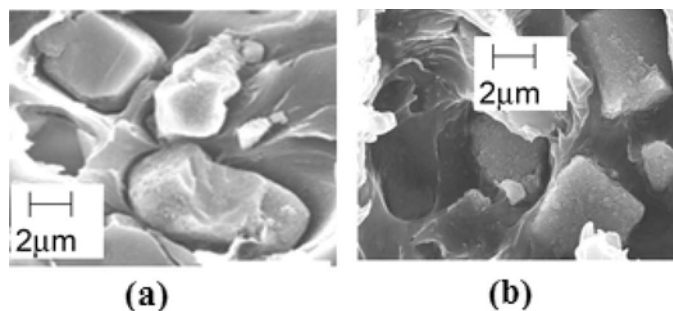


Figure 6.18 (a) Ultem[®] composite film containing unmodified silicate (zeolite 4A) particles, (b) Ultem[®] composite film containing modified silicate (zeolite 4A) particles [166].

surface morphology, which appears as inorganic whiskers, was achieved by treating silicate particles (zeolites 4A) with thionyl chloride, followed by reaction with methyl magnesium bromide (Grignard reagent). Poly (vinyl acetate) and Ultem[®] / PEI (polyetherimide) composites containing this type of modified particles exhibit defect-free interfaces. The authors examined the surface morphology of the particles as well as the interfacial morphology in the resultant composite films by scanning electron microscopy (SEM). SEM image of the film composed of Ultem[®] and unmodified 4A had apparent voids between the polymer and particles (Figure 6.18 (a)), indicating poor adhesion between these two phases. These undesirable voids were eliminated in the films embedded with the modified particles having the whisker surface morphology (Figure 6.18 (b)), implying enhanced interaction at the interface. The authors concluded from these results that the nanoscale whisker morphology stabilizes the polymer chains at the interface and promotes compatibility between the polymer and filler particles.

Perez *et al.* [167] investigated the influence of chemical surface modification of cellulose nanowhiskers (CNWs) on the morphological property of poly(lactide) based bionanocomposites by scanning electron microscopy (SEM). Poly(lactide) / CNW composites were grafted with n-octadecyl-isocyanate (ICN) by applying an in situ surface grafting method. SEM observation of the samples was made after cryofracture in liquid nitrogen. SEM image of neat poly(lactide) showed a flat and neat fracture surface. Upon dispersion of cellulose nanowhiskers (CNWs), fracture surfaces became rough. CNW and CNW composites were grafted with n-octadecyl-isocyanate (CNW-ICN) and with 2.5 wt% in poly(lactide) matrix showed a uniform distribution. For 15 wt% of nanofiller, aggregates of CNW and CNW-ICN were observed in the poly(lactide) matrix. However, the filler/matrix interaction was much better for CNW-ICN. It appeared to be better distributed in poly(lactide) compared to CNW and adhesion to the poly(lactide) matrix seemed to be improved.

6.7.1.2 Atomic Force Microscopy (AFM)

Atomic force microscopy (AFM) is another useful technique to characterize structures from nanometer to micrometer size scale. It has been applied to determine the structure of

nanocomposites and to provide three-dimensional morphology. AFM is considered to be a powerful tool for imaging the topography of the surfaces due to its high spatial and vertical resolution. The morphology of fractured and polished surfaces of polymer nanocomposites can be studied by AFM in tapping mode. In tapping mode, the AFM tip oscillates at a frequency close to its resonance and the tip is allowed to make contact with the sample for only a short duration in each oscillation cycle. During oscillation of the tip over the sample surface, the sample–tip interaction may alter the amplitude, resonance frequency, and phase angle of the oscillating cantilever. Detection of phase angle changes of the cantilever probe during scanning provides an image, called a phase image. Phase angle change is associated with energy dissipation during sample–tip interaction. Several parameters, such as topography of the sample, sample–tip interaction, deformation of sample–tip contact area, and experimental conditions, can cause energy dissipation. The phase image is very useful for compositional mapping of surfaces and interfaces of polymeric materials and generally provides better contrast than the topographic images.

Recently, Brown *et al.* [168] investigated the use of nanocrystalline cellulose (NCC) to reinforce the biocompatible fibrin matrix for artificial vascular graft application. NCC-fibrin nanocomposites were prepared which composed of homogeneously dispersed oxidized NCC (ONCC) in a fibrin matrix, with fibrin providing elasticity and ONCC providing strength. The maximum strength and elongation of the nanocomposites were determined by Atomic Force Microscopy (AFM) and compared with a native blood vessel. A representative AFM force curve is shown in Figure 6.19. They suggested that oxidized NCC and fibrin nanocomposites provided potential new biomaterials for small-diameter replacement blood vessels.

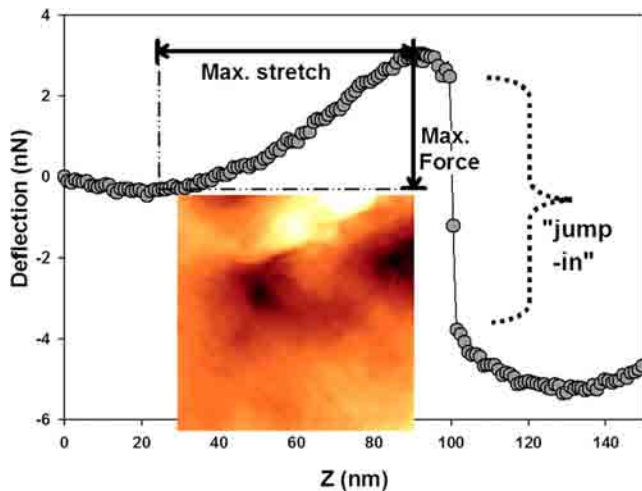


Figure 6.19 AFM force curve of ONCC-fibrin nanocomposite and illustration of maximum stretch and force measurement. Inset: AFM height image of an indented ONCC-fibrin nanocomposite surface by AFM tip [168].

6.7.2 Thermal Analysis

Thermal analysis of polymeric materials provides some basic information regarding thermal stability of materials. Thermal properties have a strong practical significance for the macroscopic performance of nanocomposites, in particular for the mechanical, barrier, and biodegradation. Additionally, in composites the main thermal transitions of a polymer matrix reflect the morphologies of both the matrix and the matrix/filler interface. Indeed, the relaxation behavior of a polymer matrix as well as the kinetics and thermodynamics of phase formation and transitions are all influenced by the level of miscibility between the polymer matrix and the reinforcement. Therefore, aside from the practical significance of thermal properties, their diagnostic capability for assessing filler/matrix miscibility, level of interactions, and microstructures at different length scales are particularly interesting.

In the case of nanosized reinforcements such as cellulose nanofibres (CNFs) and microfibrillated cellulose (MFC), a significant improvement in fibre/matrix interfacial interactions and compatibility between polymer matrix and filler was observed due to the formation of a percolating network and to an inherent entangled network morphology. CNFs are very efficient fillers to control the properties of polymer matrices. As for filled polymers, it is well established that the thermal properties of polymers, namely glass transition temperature (T_g), melting temperature (T_m), equilibrium viscoelastic properties, and thermal stability, are sensitive to the addition of fillers. This section highlights the impact of CNFs on the thermal properties of polymers.

The main thermal techniques applied for cellulose-based nanocomposites include differential scanning calorimetry (DSC), thermogravimetric analysis (TGA), thermomechanical analysis (TMA), and dynamic mechanical thermal analysis (DMTA). The application possibilities of these methods in the field of cellulose-based nanocomposites are so diverse that only a brief review can be given here.

6.7.2.1 Thermogravimetric Analysis (TGA)

TGA is used to characterize the decomposition and thermal stability of materials under a variety of conditions. Principally, in TGA analysis a change in thermal stability is examined in terms of percentage weight loss as a function of temperature while simultaneously differential thermal analysis (DTA) involves comparing the precise temperature difference between the sample and an inert reference material, while heating both. TGA measurements are often displayed as the first derivative of the TGA curve, the so-called derivative thermogravimetry (DTG) curve. Steps due to loss of mass in the TGA curve then appear as peaks in the DTG curves. The DTG curve corresponds to the rate of change of sample mass versus temperature. The influence of nanosized cellulose fibres on the thermal behavior of polymer composites has been studied by TGA. The thermal stability of nanocomposites is usually improved by incorporation of the cellulose nanofibers.

Liu *et al.* [169] have studied the thermal properties of clay nanopaper hybrid composites with montmorillonite (MTM) and nanofibrillated cellulose (NFC) using TGA and differential thermal analysis (DTA) techniques. TG-DTA results of NFC/clay nanopaper with different contents of MTM (50, 67, 80 and 89 wt %) are presented in Figure 6.20. TGA

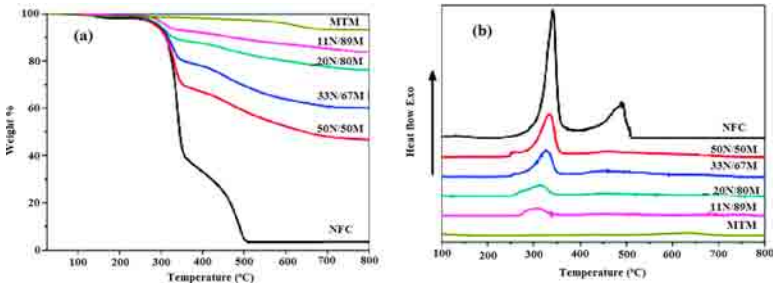


Figure 6.20 Data from TGA (a) and DTA (b) experiments in O_2 environment on NFC/clay nanopaper with different MTM contents (50, 67, 80, and 89 wt %).

curve of NFC shows two degradation stages, which can be divided into thermal cracking at 250–350°C and carbonization at 400–500°C. It has been observed that the decomposition rate for both stages increases with increasing NFC cellulose content. The TGA curves in Figure 6.20 demonstrate that the degradation of clay nanopaper is much slower compared to that of NFC cellulose nanopaper. Primarily because of its gas barrier properties, the clay nanopaper shows delayed thermal degradation of cellulose and self-extinguishing characteristics when it is subjected to open flames. From these results, the authors concluded that clay nanopaper has great potential for application in self-extinguishing composites and for further development into barrier layers in packaging applications.

Alemdar and Sain [170] investigated the thermal stability of nanocomposites obtained from wheat straw nanofibers with thermoplastic starch (TPS) polymer as the matrix and glycerol as the plasticizer. The TGA thermograms of the TPS and the nanocomposite filled with 5 wt % nanofibre showed that the starch starts to degrade at around 275°C. The degradation temperature for the nanofibres was around 296°C. The lower weight loss of the TPS and the nanocomposites is the result of evaporation of glycerol. TGA results also show that the degradation temperature of thermoplastic starch and the nanocomposites are close to each other.

Thermoplastic starch (TPS) nanocomposites reinforced with cellulose nanofibers (CNFs) extracted from wheat straw were prepared by Kaushik *et al.* [107] using the solution cast method. CNFs were dispersed in distilled water and sonicated for almost 3 hours. Maize starch was added with 30% glycerol and shear-mixed for 10 minutes using a Fluko FA25 homogenizer. Dispersed CNFs were added to the starch and glycerol mixture, and further shear-mixed for 20 minutes. Solution cast films of TPS-cellulose nanocomposites were made with 5%, 10%, and 15% nanofibers (as per dry weight of nanocomposites). The nanocomposites films were thermally analyzed by TGA and DSC. The results of TGA and DSC experiments indicated an interaction between the fibre and glycerol (plasticizer), causing the reduction in onset of degradation temperatures and a reduction in water sorption compared with the pure matrix.

Lee *et al.* [171] studied the thermal decomposition behaviour of nanocellulose reinforced PVA composite films by TGA. They observed that thermal stability of the composite films increased as the nanocellulose loading increased.

Similarly Zhou *et al.* [164] also investigated the thermal behaviour of nanocellulose reinforced PVA nanocomposites using TGA. They introduced three techniques including acid hydrolysis (AH), 2,2,6,6-tetramethylpiperidine-1-oxyl radical (TEMPO)-mediated oxidation (TMO) and ultrasonication (US) to isolate nanocellulose from microcrystalline cellulose (MCC), in order to reinforce PVA films. They observed that the thermal stability of the PVA nanocomposite films was much improved with addition of TMO-derived nanofibrils. The thermal stabilities of the neat PVA and PVA nanocomposite films examined by TGA are shown in Figure 6.21. All samples show a major weight loss in the range of 300–550 °C. For PVA nanocomposite films, a slight increase of the major degradation temperature was observed, in the sequence of TMO/PVA (287.8 °C) > AH/PVA (277.2 °C) > US/PVA (264.0 °C) > MCC/PVA (271.1 °C) > neat PVA (270.4 °C), further confirming the enhanced thermal stability due to a strong hydrogen bonding between the TMO-derived nanocellulose and the PVA matrix.

In another study, Li *et al.* [172] used TGA technique to understand the thermal degradation behaviour of nanocrystalline cellulose (NCC) reinforced PVA composites. Figures 22 (a) and (b) show TGA and DTG curves for the pure PVA and PVA/NCC nanocomposites respectively. According to the DTG (Figure 6.22 (b)) curves, the degradation of the pure PVA can be divided into three processes. These occur in the temperature ranges 77.5–210 °C, 210–350 °C and 380–500 °C. The second degradation process of the PVA/NCC begins at a slightly higher temperature than that of pure PVA, which indicates the increased thermal stability of PVA/NCC. The amount of char residue of PVA/NCC has been found to be slightly lower than that of pure PVA. TGA results indicate that the introduction of NCC in PVA/NCC lowers the maximum decomposition temperature of the first process by 5–15 °C, and that of the third process by 10–16 °C, while the maximum decomposition temperature of the second process changed only slightly,

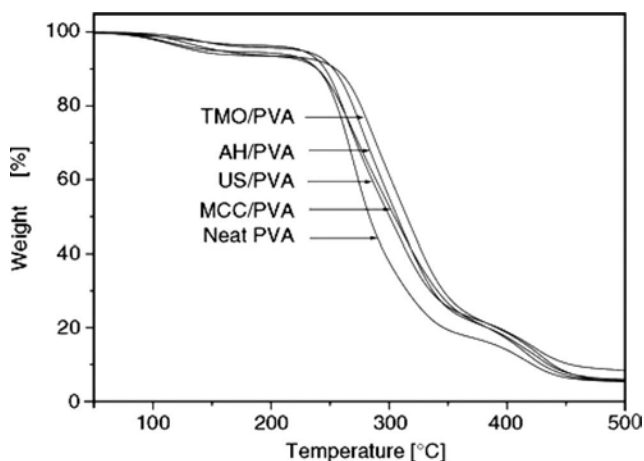


Figure 6.21 TGA curves of neat PVA and PVA nanocomposite films (6 wt% filler loading) [164].

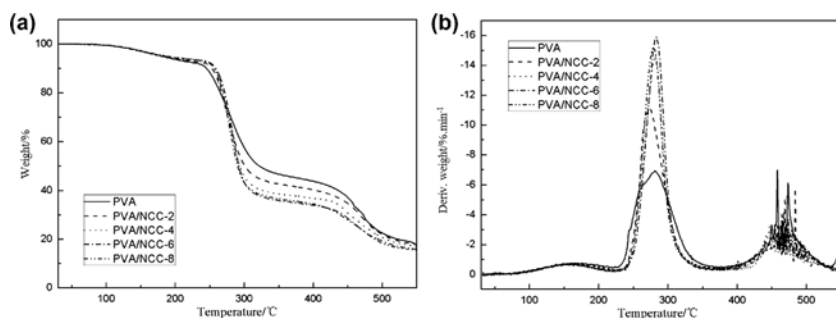


Figure 6.22 TGA (a) and DTG (b) curves for the PVA and PVA/NCC (PVA/NCC are composite films with NCC contents of 2–8 wt.%) [172].

6.7.2.2 Differential Scanning Calorimetry (DSC)

DSC can be used to investigate thermal events such as physical transitions (the glass transition, crystallization, melting, and vaporization of volatile compounds) and chemical reactions. Thermal properties such as heat capacity, glass transition temperature (T_g), melting temperature (T_m), and thermal stability can be determined using DSC.

Zhou *et al.* [164] carried out thermal characterization of neat PVA and PVA nanocomposite films using DSC measurements (Figure 6.23). The authors evaluated the glass rubber transition temperature (T_g), the melting temperature (T_m), heat of fusion (ΔH_m) and degree of crystallinity (X_c) from the DSC graphs. The glass transition temperature (T_g) of PVA nanocomposites ($T_g = 70.3^\circ\text{C}$) increased with the addition of AH-derived ($T_g = 75.1^\circ\text{C}$) and TMO-derived nanocellulose ($T_g = 76.9^\circ\text{C}$). The strong hydrogen bond formation between the PVA matrix and nanocellulose is expected to restrict the segmental mobility of polymer chains and thereby increase the T_g . The features of T_m , ΔH_m and X_c also enhanced as compared to neat PVA film.

Fujisawa *et al.* [173] determined the glass-transition temperatures (T_g) of the polystyrene matrix (PS) in the TEMPO-oxidized cellulose nanofibrils (TOCN)/PS nanocomposite films using DSC. The T_g of the neat PS was 102°C , and regardless of the TOCN content, the T_g value of the PS matrix remained almost constant around $98\text{--}100^\circ\text{C}$.

Suryanegara *et al.* [174] carried out DSC studies on PLA/MFC nanocomposites with nanofiber loading ranging from 3 wt% to 20 wt% using a two-step procedure based on solution-casting. For the amorphous PLA and the corresponding composites, T_g , cold crystallization temperature (T_{cc}) and T_m were determined in the first DSC heating scan, as well as a melt crystallization point (T_{mc}) upon cooling (Figure 6.24). The 10 wt% PLA/MFC composite showed a higher melt temperature (102.5°C) than the neat PLA (95.6°C) and much higher crystallinity after cooling (39.4%) compared with 17.3% for the neat PLA. The results reveal the faster and higher crystallization in the presence of MFC.

6.7.2.3 Dynamic Mechanical Thermal Analysis (DMTA)

Dynamic mechanical thermal analysis (DMTA) was used to measure the thermal transitions and temperature dependence of the materials' mechanical properties. In dynamic

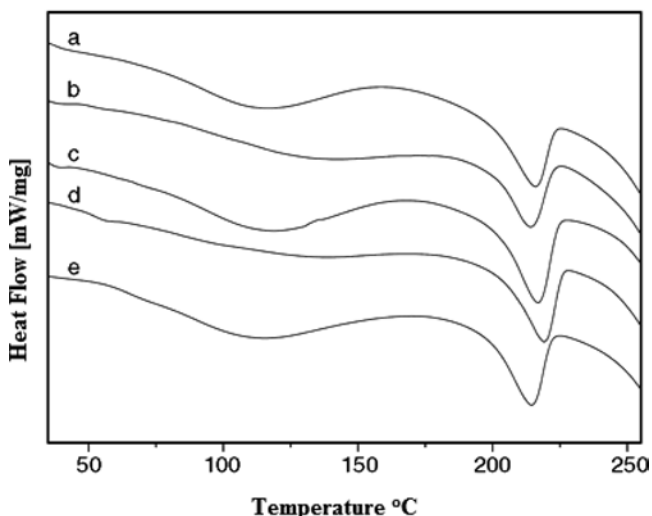


Figure 6.23 DSC curves of (a) neat PVA, (b) MCC/PVA, (c) AH/PVA, (d) TMO/PVA and (e) US/PVA films (6 wt% filler loading) [164].

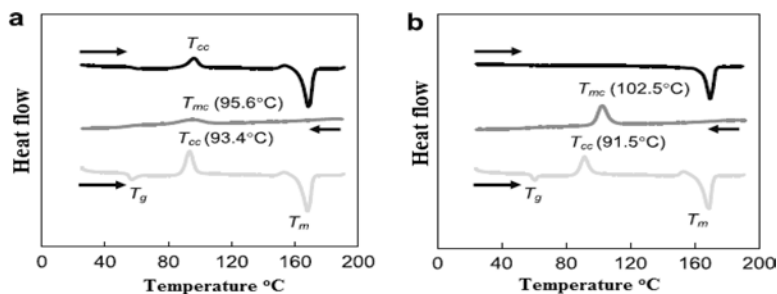


Figure 6.24 DSC thermograms of (a) neat PLA and (b) 10 wt% MFC/PLA nanocomposite [174].

mechanical thermal analysis (DMTA), mechanical modulus is determined as a function of temperature, frequency, and amplitude. The important properties of storage modulus, loss factor, T_g , and, especially, the influence of fillers and reinforcing effect on the modulus and T_g can be investigated by DMTA. Since the mechanical modulus depends on molecular condition, information can be gained about cross-linking and compatibility of polymer blends and additives. The T_g is often measured by DSC, but the DMTA technique is more sensitive and yields more precise data. It has been the most reported technique for evaluating the response of the mechanical properties of nanocellulose reinforced polymer composites.

Fujisawa *et al.* [173] investigated the storage modulus of TOCN/PS nanocomposite films by DMTA analysis (Figure 6.25). DMTA showed that the storage modulus of the TOCN/PS films increased significantly with TOCN content above the glass transition temperature

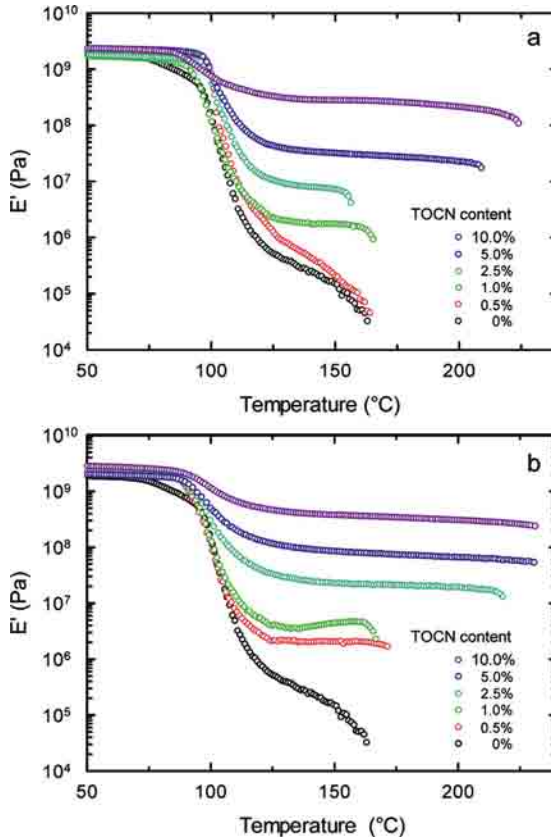


Figure 6.25 Storage moduli of (a) TOCN-93/PS and (b) TOCN-310/PS nanocomposite films. TOCNs were termed TOCN-93 and TOCN-310, corresponding to their aspect ratios. The average aspect ratios of the TOCNs were calculated to be 93 and 310, respectively, on the assumption that all TOCNs have the same and constant width of 3.5 nm [173].

of PS by the formation of an interfibrillar network structure of TOCNs in the PS matrix, based on percolation theory. The modulus of nanocomposite films maintained high values up to 230°C, whereas the neat PS fractured at 150°C. The dimensional stability of PS to temperature was enhanced significantly owing to the TOCN – matrix or TOCN – TOCN interactions. Compared to other fillers such as carbon nanotubes, TOCNs provide a superior reinforcement effect even at low addition levels.

Dynamic mechanical thermal analysis (DMTA) of nanocomposites from wheat straw nanofibers and TPS from modified potato starch has been reported. Results revealed that the T_g of the nanocomposites shifted to higher temperatures with respect to the pure TPS [170]. Lu *et al.* [175] observed no further improvement in mechanical properties when MFC was used above 10 wt%. In their study, MFC suspension was added at 1 wt%, 5 wt%, 10 wt%,

and 15 wt% loadings to the PVA matrix. A steady increase in film modulus and strength was observed until a plateau was reached at 10 wt% MFC. DMTA showed an increase of storage tensile modulus in the glassy state with increasing MFC content. The thermal stability of the PVA composite films was slightly increased with the addition of MFC.

Sehaqui *et al.* [176] studied the dynamic mechanical thermal properties of the wood fibre/NFC composites. Three materials were studied, namely the reference biocomposite (0% NFC), the 5% NFC composite, and the 100% NFC nanopaper. Results revealed that cellulose nanocomposites can be very stiff under conditions of low mobility and exhibit high modulus values at low temperatures. Modulus values are well preserved until temperatures as high as 200°C. The 5% NFC composite has higher storage modulus (E') than the 0% NFC composite and lower E' than the NFC nanopaper.

Cho and Park [177] investigated the thermomechanical properties of nanocellulose reinforced PVA nanocomposites by DMTA. The DMTA results showed a significant increase in the storage modulus (E') by about 74% at the 3 wt% nanocellulose loading level compared to that of the neat PVA film at 25°C. Figure 6.26 shows the $\tan \delta$ of the nanocomposites reinforced with various amounts of the nanocellulose as a function of temperature. As the nanocellulose content increased, the maximum $\tan \delta$ slightly increased at 1 wt% and then decreased up to 5 wt%. This result confirmed that a low tensile strength results in a decreased E' , which subsequently increases the $\tan \delta$.

The DMTA analysis of novel bionanocomposites using CNFs as reinforcement in PLA using acetone as the solvent has been reported [178]. Results showed that the storage modulus of the composites stayed constant above the glass transition temperature of the matrix polymer. In another study, Suryanegara *et al.* [174] applied the same method but exchanged the solvent acetone by dichloromethane and showed that the resulting nanocomposites had improved storage modulus when compared to neat PLA.

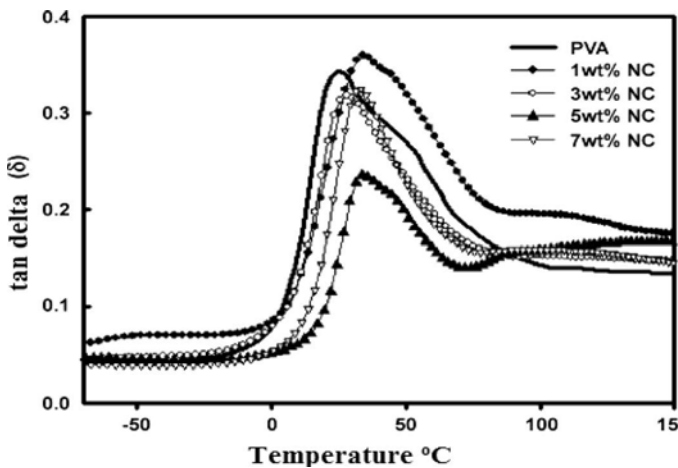


Figure 6.26 $\tan \delta$ as the function of temperature for nanocellulose-reinforced PVA nanocomposites [177].

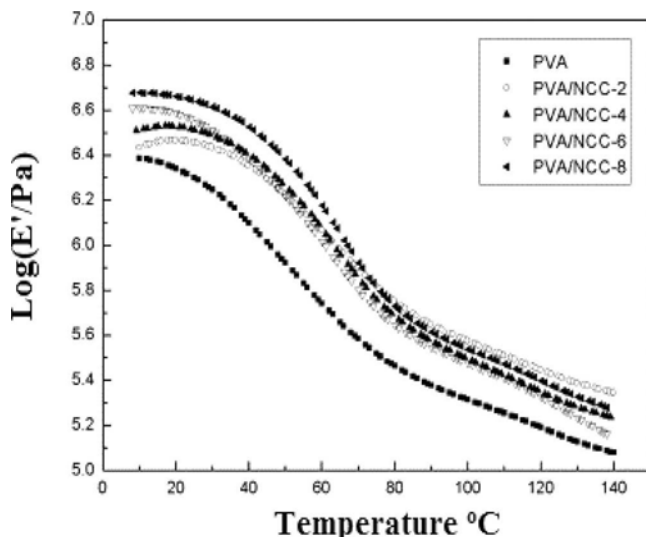


Figure 6.27 Temperature dependence of the storage modulus for PVA and PVA/NCC (PVA/NCC are composite films with NCC contents of 2–8 wt%) measured at 2.5 Hz [172].

Li *et al.* [172] investigated the reinforcing capability of nanocrystalline cellulose in PVA matrix via a solution casting method. They carried out DMTA analysis to investigate the reinforcement effect of the NCC in PVA matrix. Figure 6.27 shows the temperature dependence of the storage modulus (E') for PVA and PVA/NCC (2–8 wt% NCC content) composite films. The curve corresponding to the pure PVA showed the thermoplastic nature of the material. The α -relaxation transition temperature (T_{α}) corresponding to the glass transition of PVA was detected at about 44 °C. The T_{α} values of PVA/NCC with 0, 2, 4, 6 and 8 wt.% NCC were 59.2 °C, 64.5 °C, 59.1 °C, 67.8 °C and 65.3 °C, respectively. The DMTA data showed a marked increase in storage modulus from 1.7 GPa for pure PVA to 4.2 GPa for PVA/NCC-8 (PVA with 8 wt% NCC content) at 30°C, because of the high modulus of NCC. Results indicated that a strong reinforcement effect was achieved through the addition of NCC into the PVA matrix.

6.7.3 Spectroscopic Techniques

6.7.3.1 Fourier Transform Infrared (FTIR) and Raman Spectroscopies

Among the available spectroscopic techniques, the most commonly utilized is Fourier Transform Infrared Spectroscopy (FTIR). All materials absorb infrared radiation and the frequency intervals in which absorption bands appear are associated with the vibrational modes of specific functional groups. For a vibrational motion to be IR active, the dipole moment of the molecule must change, the higher the magnitude of this change, the higher the intensity of the band. Raman spectroscopy is also based on the vibrational motion of functional groups, detecting changes in polarizability of the molecule. The intensity of Raman vibration is proportional to the rate of change of polarizability. The polarizability of a

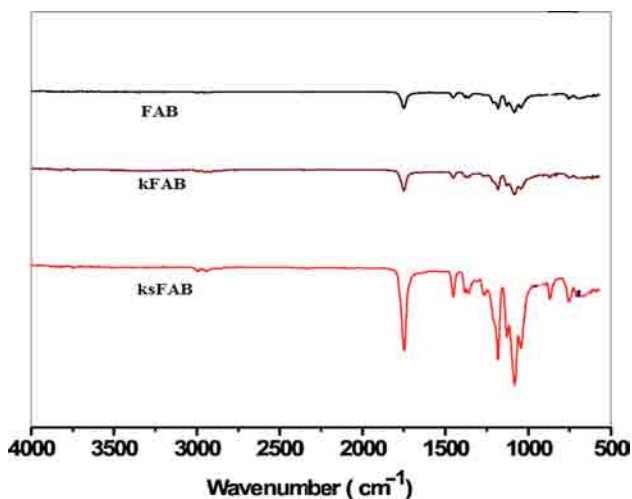


Figure 6.28 FTIR spectra of untreated ramie fibre (FAB), permanganate treated ramie fibre (kFAB) and silane treated ramie fibre (ksFAB) [159].

molecule decreases with increasing electron density, increasing bond strength and decreasing bond length. Both these techniques investigate the chemical composition of surfaces and also provide valuable information regarding possible interactions at the composite interface.

The effect of physical and chemical treatments on the interfacial property of bio-composites based on PLA and ramie fibres was analyzed by Fourier Transform Infrared Spectroscopy (FTIR) [159]. Figure 6.28 shows the infrared absorption spectra of untreated ramie fibre (FAB), permanganate treated fibre (kFAB) and silane treated fibre (ksFAB). The peaks at 1460cm^{-1} and 1378cm^{-1} are characteristic peaks of $-\text{CH}_2$, the strong absorption peak at 1749cm^{-1} is the C-O stretching vibration characteristic peak and the peaks at 1086cm^{-1} and 1178cm^{-1} are the C-O-C stretching vibration absorption peaks. There is no apparent change between the FAB and kFAB, this shows that the treatment by permanganate acetone solution does not change the chemical structure of ramie fibre. In the infrared spectrum of silane treated ramie fibres, the newly emerging characteristic peak at 860cm^{-1} is the characteristic peak of Si-cellulose, the characteristic peak at 950cm^{-1} is the Si-O-Si asymmetric stretching vibration characteristic peak. This shows that the silane coupling agent has reacted with ramie fibres through the hydrolysis effect.

Raman spectroscopy has been found to be a very powerful technique for the analysis of interfaces in cellulose fibre-based composite materials. It has been used to measure the anisotropy in cellulose nanowhisker composites [179]. Hot pressed samples of poly (vinyl acetate) resin with 15 wt% of tunicate cellulose nanowhiskers were compared with solution cast samples. It was shown that the former contained oriented domains of cellulose whiskers, whereas the latter only contained isotropic random networks. Both exhibited clearly different mechanical behaviours based on measurements of the local stress transfer using Raman spectroscopy. Therefore, this technique opens up the possibility of investigating orientation in cellulose nanocomposites, and also the local mechanics of these interesting materials.

In another study, Rusli *et al.* [180] monitored the mechanically induced molecular deformation of cellulose nanowhiskers embedded in subpercolation concentration in an epoxy resin matrix through Raman spectroscopy. Cellulose nanowhiskers isolated by sulfuric acid hydrolysis from tunicates and by sulfuric acid hydrolysis and hydrochloric acid hydrolysis from cotton were used in this study. Mechanically induced shift in the Raman peak initially located at 1095 cm^{-1} was used to express the level of deformation imparted to the nanowhiskers embedded in the resin. Much larger shifts of the diagnostic Raman band were observed for nanocomposites with tunicate nanowhiskers than for the corresponding samples comprising cotton nanowhiskers. In the case of nanocomposites comprising nanowhiskers produced by hydrochloric acid hydrolysis, no significant Raman band shift was observed. This suggested that Raman spectroscopic data are a useful diagnostic tool to elucidate the quality of mixing in cellulose nanocomposites.

6.7.3.2 Attenuated Total Reflectance Infrared Spectroscopy (ATR-IR)

ATR-IR technique has also been used to investigate the surface composition of composite materials. It is based on the multiple internal reflection of the beam incident on the sample. It is useful for studying the surface of materials (up to a depth of $0.5\text{--}5\text{ }\mu\text{m}$) that are placed in contact with the crystal.

Mohan *et al.* [181] prepared partially and fully regenerated cellulose model films from trimethylsilyl cellulose (TMSC) by a time-dependent regeneration approach. The surface composition of these thin films was investigated by ATR-IR technique. Figure 6.29 shows the ATR-IR spectra of the TMSC film and the regenerated cellulose films that were obtained with low volume of HCl (Method I) and a higher volume of HCl vapour (Method II) respectively. The spectra in Figure 6.29 show that the peaks due to Si-C rocking at $757, 848, \text{ and } 1252\text{ cm}^{-1}$ decrease concomitantly with the emergence of OH vibrations at $3000\text{--}3700\text{ cm}^{-1}$. From the ATR-IR spectra, it is evident that method

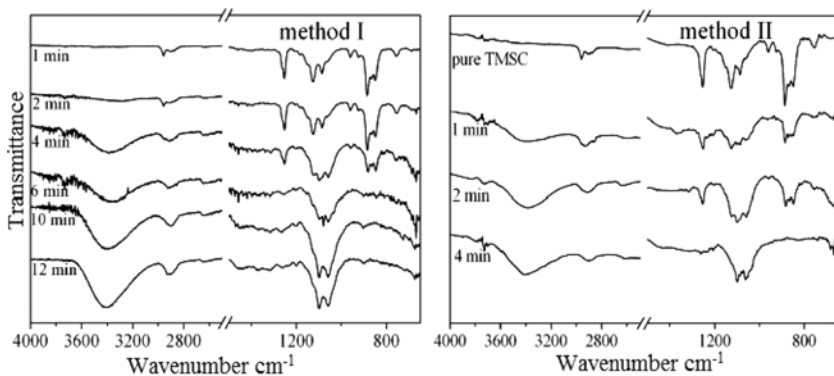


Figure 6.29 ATR-IR spectra of spin coated trimethylsilyl cellulose (TMSC) films after different regeneration times. Low volume of HCl (Method I) and a higher volume of HCl vapour (Method II) [181].

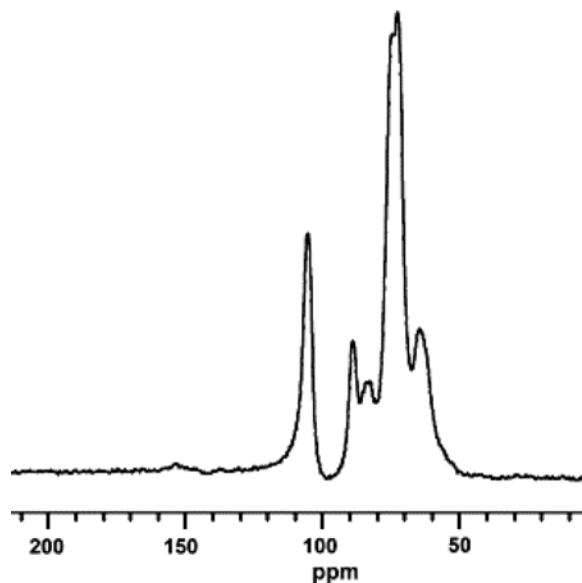


Figure 6.30 Cross polarization/magic angle spinning (Cp/MAS) ^{13}C NMR spectrum of freeze-dried bamboo cellulosic crystals (BCCs) [182].

II cleaved more TMS groups, introduced more -OH groups and improved wetting by water in shorter reaction times than method I. Nevertheless both methods allow controlled fabrication of partially and fully regenerated cellulose model films from TMSC and can be used to study the interaction ability of cellulose on these surfaces.

6.7.3.3 Nuclear Magnetic Resonance (NMR) Spectroscopy

Solid-state nuclear magnetic resonance (NMR) spectroscopy has been used to study the supramolecular structure of cellulose materials. The structure and morphology of bamboo cellulosic crystals (BCCs) were investigated by Liu *et al.* [182] using solid-state ^{13}C NMR. CP/MAS ^{13}C NMR spectrum of the freeze-dried BCCs is shown in Figure 6.30. The BCCs exhibited five main peaks at 105.6, 89.2 (83.9), 74.5 (72.9) ppm [assigned to the C1, C4, C5 (C3, C2)], as well as the C6 peak line at 64.6 ppm, which were all attributed to cellulose I. The C1 resonance region at 105.6 ppm, C4 at 89.2 ppm, as well as C6 at 64.6 ppm are all attributed to cellulose I β . The absence of cellulose I α (shoulder peak of C1 or C4) peak in the NMR indicates that higher plants contain no cellulose I α at all, only a distorted form of cellulose I β is located immediately below the surface of the crystalline units.

All the spectroscopic techniques mentioned above can be used as valuable tools for understanding the chemical composition and interactions at the composite interface.

6.8 Summary and Conclusions

Biopolymers and biocomposites have drawn attention in scientific community due to their versatile properties. Biopolymers can be used in several applications with substantially enhanced properties. Some drawbacks limit their use, such as aggregation, low concentration suspension, low compatibility with hydrophobic polymeric matrices. The lack of good interfacial adhesion between the hydrophilic filler particles and hydrophobic polymer matrix makes these composites less attractive for widespread applications. The use of adhesion promoters, additives or chemical modification of the filler surface can help to improve the interfacial adhesion between filler particles and polymer macromolecules and their dispersion in the matrices, thus improving the overall mechanical performance of the composites. Realization of functional modifications of nanowhiskers under mild reaction conditions would greatly improve their practical utility in the future. Interfacial adhesion between filler and matrix will remain the key issue in terms of overall performance, since it dictates the final properties of the composites. Many studies are examined, reviewed and highlighted in this review paper regarding the important biopolymers, biomatrices, their modifications, processing techniques, and characterization of interfacial modifications.

References

1. G. Siqueira, J. Bras, and A. Dufresne, Cellulosic bionanocomposites: A review of preparation, properties and applications. *Polymers* 2, 728–765 (2010).
2. Y. Habibi, L.A Lucia, and A.J. Rojas, Cellulose nanocrystals: Chemistry, self-assembly and applications. *Chem. Rev.* 110, 3479–3500 (2010).
3. E. Abraham, B. Deepa, L.A. Pothan, M. Jacob, S. Thomas, R. Anandjiwala, and S.S. Narine, Physico-mechanical properties of green nanocomposites based on cellulose nanofibre and natural rubber latex. *Cellulose* 20, 417–427 (2013).
4. D. Klemm, D. Schumann, F. Kramer, N. Hessler, D. Koth, and B. Sultanova, Nanocellulose materials – Different cellulose, different functionality. *Macromol. Symp.* 280, 60–71 (2009).
5. I. Siro and D. Placket, Microfibrillated cellulose and new nanocomposite materials: A review. *Cellulose* 17, 459–494 (2010).
6. D. Bondeson, A. Mathew, and K. Oksman, Optimization of the isolation of nanocrystals from microcrystalline cellulose by acid hydrolysis. *Cellulose* 13, 171–180 (2006).
7. A. Hirai, O. Inui, F. Horii, and M. Tsuji, Phase separation behavior in aqueous suspensions of bacterial cellulose nanocrystals prepared by sulfuric acid treatment. *Langmuir* 25, 497–502 (2009).
8. J. Sugiyama, H. Chanzi, and J.F. Revol, On the polarity of cellulose in the cell wall of valonia. *Planta* 193, 260–265 (1994).
9. X. Cao, Y. Chen, P.R. Chang, M. Stumborg, and M.A. Huneault, Green composites reinforced with hemp nanocrystals in plasticized starch. *J. Appl. Polym. Sci.* 109, 3804–3810 (2008).
10. C. Bonini, L. Heux, J.Y. Cavaille, P. Lindner, C. Dewhurst, and P. Terech, Rodlike cellulose whiskers coated with surfactant: A small-angle neutron scattering characterization. *Langmuir* 18, 3311–3314 (2002).

11. V. Favier, H. Chanzy, and J.Y. Cavaille, Polymer nanocomposites reinforced by cellulose whiskers. *Macromolecules* 28, 6365–6367 (1995).
12. W. Thielemans, C.R. Warbey, and D.A. Walsh, Permselective nanostructured membranes based on cellulose nanowhiskers. *Green Chemistry* 11, 531–537 (2009).
13. Y. Habibi, A.L. Goffin, N. Schiltz, E. Duquesne, P. Dubois, and A. Dufresne, Bionanocomposites based on poly(ϵ -caprolactone)-grafted cellulose nanocrystals by ring-opening polymerization. *J. Mater. Chem.* 18, 5002–5010 (2008).
14. N.L. Garcia de Rodriguez, W. Thielemans, and A. Dufresne, Sisal cellulose whiskers reinforced polyvinyl acetate nanocomposites. *Cellulose* 13, 261–270 (2006).
15. M.A.S. Azizi Samir, F. Alloin, M. Paillet, and A. Dufresne, Tangling effect in fibrillated cellulose reinforced nanocomposites. *Macromolecules* 37, 4313–4316 (2004).
16. S. Beck-Candanedo, M. Roman, and D. Gray, Effect of conditions on the properties behavior of wood cellulose nanocrystals suspensions. *Biomacromolecules* 6, 1048–1054 (2005).
17. S. Elazouzi-Hafraoui, Y. Nishiyama, J.L. Putaux, L. Heux, F. Dubreuil, and C. Rochas, The shape and size distribution of crystalline nanoparticles prepared by acid hydrolysis of native cellulose. *Biomacromolecules* 9, 57–65 (2007).
18. X.M. Dong, T. Kimura, J.F. Revol, and D.G. Gray, Effects of ionic strength on the isotropic-chiral nematic phase transition of suspensions of cellulose crystallites. *Langmuir* 12, 2076–2082 (1996).
19. I. Kvien, B.S. Tanem, and K. Oksman, Characterization of cellulose whiskers and their nanocomposites by atomic force and electron microscopy. *Biomacromolecules* 6, 3160–3165 (2005).
20. M. Grunert and W.T. Winter, Nanocomposites of cellulose acetate butyrate reinforced with cellulose nanocrystals. *J. Polymers Environment* 10, 27–30 (2002).
21. G. Chinga-Carrasco and K. Syverud, Computer-assisted quantification of the multi-scale structure of films made of nanofibrillated cellulose. *J. Nanoparticle Res.* 12, 841–852 (2010).
22. M.N. Ravi Kumar, A review of chitin and chitosan applications. *Reactive Functional Polymers* 46, 1–27 (2000).
23. A.J. Uddin, M. Fujie, S. Sembo, and Y. Gotoh, Outstanding reinforcing effect of highly oriented chitin whiskers in PVA nanocomposites. *Carbohydrate Polymers* 87, 799–805 (2012).
24. R.H. Marchessault, F.F. Morehead, and N.M. Walter, Liquid crystal systems from fibrillar polysaccharides. *Nature* 184, 632–633 (1959).
25. J.-F. Revol and R.H. Marchessault, In vitro chiral nematic ordering of chitin crystallites. *Int. J. Biological Macromolecules* 15, 329–335 (1993).
26. J. Li, J.F. Revol, and R.H. Marchessault, Rheological properties of aqueous suspensions of chitin crystallites. *J. Colloid Interface Sci.* 183, 365–373 (1996).
27. K. Gopalan Nair, A. Dufresne, A. Gandini, and M.N. Belgacem, Crab shell chitin whiskers reinforced natural rubber nanocomposites. 3. Effect of chemical modification of chitin whiskers. *Biomacromolecules* 4, 1835–1842 (2003).
28. A. Morin and A. Dufresne, Nanocomposites of chitin whiskers from riftia tubes and poly(ϵ -caprolactone). *Macromolecules* 35, 2190–2199 (2002).
29. K. Gopalan Nair and A. Dufresne, Crab shell chitin whisker reinforced natural rubber nanocomposites. 1. Processing and swelling behavior. *Biomacromolecules* 4, 657–665 (2003).

30. L.D. Feng, J.Y. Zhou, A. Dufresne, J. Zhang, M. Wie, and L. An, Structure and properties of new thermoforming bionanocomposites based on chitin whisker-graft polycaprolactone. *J. Appl. Polym. Sci.* 112, 2830–2837 (2009).
31. P.R. Chang, R. Jian, J. Yu, and X. Ma, Starch-based composites reinforced with novel chitin nanoparticles. *Carbohydrate Polymers* 80, 420–425 (2010).
32. P. Hariraksapitak and P. Supaphol, Preparation and properties of α -chitin-whisker-reinforced hyaluronan–gelatin nanocomposite scaffolds. *J. Appl. Polym. Sci.* 117, 3406–3418 (2010).
33. J. Sriupayo, P. Supaphol, J. Blackwell, and R. Rujiravanit, Preparation and characterization of α -chitin whisker-reinforced poly (vinyl alcohol) nanocomposite films with or without heat treatment. *Polymer* 46, 5637–5644 (2005).
34. J.D. Goodrich and W.T. Winter, α -Chitin nanocrystals prepared from shrimp shells and their specific surface area measurement. *Biomacromolecules* 8, 252–257 (2007).
35. A. Watthanaphanit, P. Supaphol, H. Tamura, S. Tokura, and R.J. Rujiravanit, Fabrication, structure, and properties of chitin whisker-reinforced alginate nanocomposite fibers. *J. Appl. Polym. Sci.* 110, 890–899 (2008).
36. J. Junkasem, R. Rujiravanit, B.P. Grady, and P. Supaphol, X-ray diffraction and dynamic mechanical analyses of α -chitin whisker-reinforced poly (vinyl alcohol) nanocomposite nanofibers. *Polym. Intl.* 59, 85–91 (2010).
37. Y. Fan, T. Saito, and A. Isogai, Preparation of chitin nanofibers from squidpen β -chitin by simple mechanical treatment under acid conditions. *Biomacromolecules* 9, 1919–1923 (2008).
38. A. Watthanaphanit, P. Supaphol, H. Tamura, S. Tokura, and R. Rujiravanit, Wet-spun alginate/chitosan whiskers nanocomposite fibers: Preparation, characterization and release characteristic of the whiskers. *Carbohydrate Polymers* 79, 738–746 (2010).
39. H. Zhao, X. Feng, and H. Gao, Ultrasonic technique for extracting nanofibers from nature materials. *Appl. Phys. Letters* 90, 073112 (2007).
40. B.M. Min, S.W. Lee, J.N. Lim, Y. You, T.S. Lee, P.H. Kang, and W.H. Park, Chitin and chitosan nanofibers: Electrospinning of chitin and deacetylation of chitin nanofibers. *Polymer* 45, 7137–7142 (2004).
41. S. Ifuku, M. Nogi, K. Abe, M. Yoshioka, M. Morimoto, H. Saimoto, and H. Yano, Preparation of chitin nanofibers with a uniform width as α -chitin from crab shells. *Biomacromolecules* 10, 1584–1588 (2009).
42. S. Ifuku, M. Nogi, M. Yoshioka, M. Morimoto, H. Yano, and H. Saimoto, Fibrillation of dried chitin into 10–20 nm nanofibers by a simple grinding method under acidic conditions. *Carbohydrate Polymers* 81, 134–139 (2010).
43. Y. Xu, W.Q. Ding, J. Liu, Y. Li, J.F. Kennedy, Q. Gu, and S.X. Shao, Preparation and characterization of organic-soluble acetylated starch nanocrystals. *Carbohydrate Polymers* 80, 1078–1084 (2010).
44. D.L. Corre, J. Bras, and A. Dufresne, Starch nanoparticles: A review. *Biomacromolecules* 11, 1139–1153 (2010).
45. S. Pérez and E. Bertoft, The molecular structures of starch components and their contribution to the architecture of starch granules: A comprehensive review. *Starch/Stärke* 62, 389–420 (2010).
46. A. Buléon, P. Colonna, V. Planchot, and S. Ball, Starch granules: Structure and biosynthesis. *Intl. J. Biological Macromolecules* 23, 85–112 (1998).
47. J. Preiss, Biochemistry and molecular biology of starch biosynthesis, in *Starch: Chemistry and Technology*, J. BeMiller and R.L. Whistler (Eds.), 3rd ed., pp. 83–147, Academic Press, New York. (2009).

48. N. Lin, J. Huang, P.R. Chang, D.P. Anderson, and J.H. Yu, Preparation, modification, and application of starch nanocrystals in nanomaterials: A review. *J. Nanomaterials* 2011, 20 (2011). Article ID 573687, 13 pages DOI 10.1155/2011/573687.
49. M. Paris, H. Bizot, J. Emery, J.Y. Buzaré, and A. Buléon, Crystallinity and structuring role of water in native and recrystallized starches by ¹³C CP-MAS NMR spectroscopy. 1: Spectral decomposition. *Carbohydrate Polymers* 39, 327–339 (1999).
50. H. Angellier, S.M. Boisseau, M.N. Belgacem, and A. Dufresne, Surface chemical modification of waxy maize starch nanocrystals. *Langmuir* 21, 2425–2433 (2005).
51. M.G. Sajilata, R.S. Singhal, and P.R. Kulkarni, Resistant starch – A review. *Comprehensive Rev. Food Sci. Food Safety* 5, 1–17 (2006).
52. D.R. Lu, C.M. Xiao, and S.J. Xu, Starch-based completely biodegradable polymer materials. *Express Polymer Letters* 3, 366–375 (2009).
53. S. Jobling, Improving starch for food and industrial applications. *Current Opinion Plant Biology* 7, 210–218 (2004).
54. D. Song, Y. Zhao, C. Dong, and Y. Deng, Surface modification of cellulose fibers by starch grafting with crosslinkers. *J. Appl. Polym. Sci.* 113, 3019–3026 (2009).
55. R. Agrawal, N.S. Saxena, K.B. Sharma, S. Thomas, and M. S. Sreekala, Activation energy and crystallization kinetics of untreated and treated oil palm fibre reinforced phenol formaldehyde composites. *Mater. Sci. Engg. A* 277, 77–82 (2000).
56. S. Kalia, A. Dufresne, B.M. Cherian, B.S. Kaith, L. Avérous, J. Njuguna, and E. Nassiopoulou, Cellulose-based bio- and nanocomposites: A review. *Int. J. Polym. Sci.* 24, 837–875 (2011).
57. K. Joseph, L.H.C. Mattoso, R.D. Toledo, S. Thomas, L.H. de Carvalho, L. Pothen, S. Kala, and B. James, Natural fiber reinforced thermoplastic composites. in *Natural Polymers and Agrofibers Composites*, E. Frollini, A.L. Leão, and L.H.C. Mattoso (Eds.), pp. 159–201, Embrapa Agricultural Instrumentation, São Carlos, Brazil. (2000).
58. M.S. Sreekala, M.G. Kumaran, S. Joseph, M. Jacob, and S. Thomas, Oil palm fibre reinforced phenol formaldehyde composites: Influence of fibre surface modifications on the mechanical performance. *Appl. Composite Mater.* 7, 295–329 (2000).
59. S. Kalia, V.K. Kaushik, and R.K. Sharma, Effect of benzylation and graft copolymerization on morphology, thermal stability, and crystallinity of sisal fibers. *J. Natural Fibers* 8, 27–38 (2011).
60. P. Deetae, S. Shobsngob, W. Varanyanond, P. Chinachoti, O. Naivikul, and S. Varavinit, Preparation, pasting properties and freeze-thaw stability of dual modified crosslink-phosphorylated rice starch. *Carbohydrate Polymers* 73, 351–358 (2008).
61. S. Ou, A. Li, and A. Yang, A study on synthesis of starch ferulate and its biological properties. *Food Chemistry* 74, 91–95 (2001).
62. A.N. Jyothi, K.N. Rajasekharan, S.N. Moorthy, and J. Sreekumar, Microwave assisted synthesis and characterization of succinate derivatives of cassava (*Manihot esculenta* Crantz) starch. *Starch/Stärke* 57, 556–563 (2005).
63. M.R. Hansen, A. Blennow, S. Pedersen, L. Nørgaard, and S.B. Engelsen, Gel texture and chain structure of amyloamylase-modified starches compared to gelatine. *Food Hydrocolloids* 22, 1551–1566 (2008).
64. M. Strobel, C.S. Lyons, and K.L. Mittal (Eds.), *Plasma Surface Modification of Polymers: Relevance to Adhesion*, CRC Press, Boca Raton, FL. (1994).
65. M. Thomas and K.L. Mittal (Eds.), *Atmospheric Pressure Plasma Treatment of Polymers: Relevance to Adhesion*, Wiley-Scrivener, Beverly, MA. (2013).

66. R.A. Pertile, F.K. Andrade, C. Alves, and M. Gama, Surface modification of bacterial cellulose by nitrogen-containing plasma for improved interaction with cell. *Carbohydrate Polymers* 82, 692–698 (2010).
67. Y. Han, S.O. Manolache, F. Denes, and R.M. Rowell, Cold plasma treatment on starch foam reinforced with wood fiber for its surface hydrophobicity. *Carbohydrate Polymers* 86, 1031–1037 (2011).
68. K. Meinander, M. Niemi, J.S. Hakola, and J.-F. Selin, Poly lactides—Degradable polymers for fibres and films. *Macromol. Symp.* 123, 147–154 (1997).
69. A.L. Duigou, P. Davies, and C. Baley, Interfacial bonding of flax fibre/poly(L-lactide) bio-composites. *Composites Sci. Technol.* 70, 231–239 (2010).
70. T. Yu, J. Ren, S. Li, H. Yuan, and Y. Li, Effect of fiber surface-treatments on the properties of polylactic acid/ramie composites. *Composites Part A* 41, 499–505 (2010).
71. S.G. Ji, D. Cho, W.H. Park, and B.C. Lee, Electron beam effect on the tensile properties and topology of jute fibers and the interfacial strength of jute-PLA green composites. *Macromol. Res.* 18, 919–922 (2010).
72. E. Petinakis, L. Yu, G. Edward, K. Dean, H. Liu, and A.D. Scully, Effect of matrix–particle interfacial adhesion on the mechanical properties of polylactic acid/wood-flour micro-composites. *J. Polymers Environment* 17, 83–94 (2009).
73. K. Hee-Soo, L. Byoung-Ho, L. Sena, K. Hyun-Joong, and R.D. John, Enhanced interfacial adhesion, mechanical, and thermal properties of natural flour-filled biodegradable polymer biocomposites. *J. Thermal Analysis Calorimetry* 104, 331–338 (2011).
74. C. Baltieri, L.H.I. Mei, and J. Bartoli, Study of the influence of plasticizers on the thermal and mechanical properties of poly(3-hydroxybutyrate) compounds. *Macromol. Symp.* 197, 33–44 (2003).
75. D.Z. Bucci, L.B.B. Tavares, and I. Sell, Biodegradation and physical evaluation of PHB packaging. *Polymer Testing* 26, 908–915 (2007).
76. A. El-Hadi, R. Schnabel, E. Straube, G. Muller, and S. Henning, Correlation between degree of crystallinity, morphology, glass temperature, mechanical properties and biodegradation of poly(3-hydroxyalkanoate) PHAs and their blends. *Polymer Testing* 21, 665–674 (2002).
77. S. Luo and A.N. Netravali, Interfacial and mechanical properties of environment-friendly “green” composites made from pineapple fibers and poly(hydroxybutyrate-co-valerate) resin. *J. Mater. Sci.* 34, 3709–3719 (1999).
78. A.K. Mohanty, P. Tummala, W. Liu, M. Misra, P.V. Mulukutla, and L.T. Drzal, Injection molded biocomposites from soy protein based bioplastic and short industrial hemp fiber. *J. Polymers Environment* 13, 279–285 (2005).
79. S.K. Mahadeva, S. Yun, and J. Kim, Flexible humidity and temperature sensor based on cellulose-poly pyrrole nanocomposite. *Sensors Actuators A* 165, 194–199 (2011).
80. S. Tunc and O. Duman, Preparation of active antimicrobial methyl cellulose/carvacrol/montmorillonite nanocomposite films and investigation of carvacrol release. *LWT-Food Sci. Technol.* 44, 465–472 (2011).
81. V.T. Phuong and A. Lazzeri, “Green” biocomposites based on cellulose diacetate and regenerated cellulose microfibers: Effect of plasticizer content on morphology and mechanical properties. *Composites: Part A* 43, 2256–2268 (2012).
82. M. Ionita and H. Iovu, Mechanical properties, urea diffusion, and cell cultural response of poly(vinyl alcohol)–chitosan bioartificial membranes via molecular modelling and experimental investigation. *Composites Part B* 43, 2464–2470 (2012).

83. F. Goktepe, S.U. Celik, and A. Bozkurt, Preparation and the proton conductivity of chitosan/poly(vinyl phosphonic acid) complex polymer electrolytes. *J. Non-Crystalline Solids* 354, 3637–3642 (2008).
84. M. Fang, J. Long, W. Zhao, L. Wang, and G. Chen, pH-Responsive chitosan-mediated graphene dispersions. *Langmuir* 26, 16771–16774 (2010).
85. A. Borzacchiello, L. Ambrosio, P.A. Netti, L. Nicolais, C. Peniche, A. Gallardo, and J.S. Roman, Chitosan-based hydrogels: Synthesis and characterization. *J. Mater. Sci.: Mater. in Medicine* 12, 861–864 (2001).
86. M.R. Nikpour, S.M. Rabiee, and M. Jahanshahi, Synthesis and characterization of hydroxyapatite/chitosan nanocomposite materials for medical engineering applications. *Composites: Part B* 43, 1881–1886 (2012).
87. J.P. de Mesquita, C.L. Donnici, I.F. Teixeira, and F.V. Pereira, Bio-based nanocomposites obtained through covalent linkage between chitosan and cellulose nanocrystals. *Carbohydrate Polymers* 90, 210–217 (2012).
88. Y. Pan, T. Wu, H. Bao, and L. Li, Green fabrication of chitosan films reinforced with parallel aligned graphene oxide. *Carbohydrate Polymers* 83, 1908–1915 (2011).
89. D. Xu, L.S. Loo, and K. Wang, Characterization and diffusion behavior of chitosan–POSS composite membranes. *J. Appl. Polym. Sci.* 122, 427–435 (2011).
90. R.N. Tharanathan, Biodegradable films and composite coatings: Past, present and future. *Trends Food Sci. Technol.* 14, 71–78 (2003).
91. L.M. Fama, V. Pettarin, S.N. Goyanes, and C.R. Bernal, Starch/multi-walled carbon nanotubes composites with improved mechanical properties. *Carbohydrate Polymers* 83, 1226–1231 (2011).
92. N.L. García, L. Ribba, A. Dufresne, M. Aranguren, and S. Goyanes, Physicomechanical properties of biodegradable starch nanocomposites. *Macromol. Mater. Eng.* 294, 169–177 (2009).
93. M.G.L. Ramírez, K.G. Satyanarayana, S. Iwakiri, G.B. de Muniz, V. Tanobe, and T.S.F. Sahagun, Study of the properties of biocomposites. Part I. Cassava starch-green coir fibers from Brazil. *Carbohydrate Polymers* 86, 1712–1722 (2011).
94. J. Castano, S.R. Llamazares, C. Carrasco, and R. Bouza, Physical, chemical and mechanical properties of pehuen cellulosic husk and its pehuen-starch based composites. *Carbohydrate Polymers* 90, 1550–1556 (2012).
95. K.J. Seal and L.H.G. Morton, Chemical materials. *Biotechnology* 8, 583–590 (1996).
96. L.X. Kong, Y. Chen, Z. Peng, and P. Li, Latex-based nanocomposites, in *Progress in Polymer Nanocomposite Research*, S. Thomas and G.E. Zaikov (Eds.), pp. 83–104, Nova Science Publishers, Hauppauge, NY (2008).
97. Z. Peng, C. Feng, Y. Luo, Y. Li, Z. Yi, and L.X. Kong, Natural rubber/multiwalled carbon nanotube composites developed with a combined self-assembly and latex compounding technique. *J. Appl. Polym. Sci.* 125, 3920–3928 (2012).
98. A. Bendahou, H. Kaddami, and A. Dufresne, Investigation on the effect of cellulosic nanoparticles' morphology on the properties of natural rubber based nanocomposites. *European Polym. J.* 46, 609–620 (2010).
99. I. Arvanitoyannis, I. Kolokuris, J.M.V. Blanshard, and C. Robinson, Study of the effect of annealing, draw ratio, and moisture upon the crystallinity of native and commercial gutta percha (transpolyisoprene) with DSC, DMTA, and X-rays: Determination of the activation energies at Tg. *J. Appl. Polym. Sci.* 48, 987–998 (1993).

100. M. Mondragon, E.M. Hernandez, J.L. Rivera-Armenta, and F.J. Rodriguez, Injection molded thermoplastic starch/natural rubber/clay nanocomposites: Morphology and mechanical properties. *Carbohydrate Polymers* 77, 80–86 (2009).
101. O. Faruk, A.K. Bledzki, H-P Fink, and M. Sain, Biocomposites reinforced with natural fibers: 2000–2010. *Prog. Polym.Sci.* 37, 1552–1596 (2012).
102. P.A. Fowler, J.M. Hughes, and R.M. Elias, Biocomposites: Technology, environmental credentials and market forces. *J. Sci. Food Agriculture* 86, 1781–1789 (2006).
103. S.O. Adeosun, G.I. Lawal, S.A. Balogun, and E.I. Akpan, Review of green polymer nanocomposites. *J. Minerals Mater. Charact. Eng.* 11, 483–514 (2012).
104. K. Majdzadeh-Ardakani and S.S. Ardakani, Experimental investigation of mechanical properties of starch/natural rubber/clay nanocomposites. *Digest J. Nanomaterials Biostructures* 5, 307–316 (2010).
105. E. Bodros, I. Pillin, N. Montrelay, and C. Baley, Could biopolymers reinforced by randomly scattered flax fiber be used in structural applications? *Composites Sci. Technol.* 67, 462–470 (2007).
106. S.M. Zabihzadeh, Water uptake and flexural properties of natural filler/HDPE composites. *Bioresources* 5, 316–323 (2010).
107. A. Kaushik, M. Singh, and G. Verma, Green nanocomposites based on thermoplastic starch and steam exploded cellulose nanofibrils from wheat straw. *Carbohydrate Polymers* 82, 337–345 (2010).
108. E. Teixeira, D. Pasquini, A.S. Antonio, C.E. Corradini, M.N. Belgacem, and A. Dufresne, Cassava bagasse cellulose nanofibrils reinforced thermoplastic cassava starch. *Carbohydrate Polymers* 78, 422–431 (2009).
109. M. Huskic and M.Z. Igon, PMMA/MMT nanocomposites prepared by one-step in situ intercalative solution polymerization. *European Polym. J.* 43, 4891–4897 (2007).
110. L. Jong, Natural rubber protein as interfacial enhancement for bio-based nano-fillers. *J. Appl. Polym. Sci.* 130, 2188–2197 (2013).
111. P.M. Visakh, S. Thomas, K. Oksman, and A.P. Mathew, Crosslinked natural rubber nanocomposites reinforced with cellulose whiskers isolated from bamboo waste: Processing and mechanical/thermal properties. *Composites Part A* 43, 735–741 (2012).
112. H.X. Jiang, Q.Q. Ni, and T. Natsuki, Effect of carbon nanotubes on the properties of natural rubber composites. *Key Eng. Mater.* 464, 660–662 (2011).
113. M.N. Belgacem, P. Bataille, and S. Sapiaha, Effect of corona modification on the mechanical properties of polypropylene/cellulose composites. *J. Appl. Polym. Sci.* 53, 379–385 (1994).
114. K.M. Almgren, E.K. Gamstedt, P. Nygård, F. Malmberg, J. Lindblad, and M. Lindström, Role of fibre–fibre and fibre–matrix adhesion in stress transfer in composites made from resin-impregnated paper sheets. *Intl. J. Adhesion Adhesives* 29, 551–557 (2009).
115. S. Kalia, K. Thakur, A. Celli, M.A. Kiechel, and C.L. Schauer, Surface modification of plant fibers using environment friendly methods for their application in polymer composites, textile industry and antimicrobial activities: A review. *J. Environ. Chem. Eng.* 1, 97–112 (2013).
116. M.Z. Rong, M.Q. Zhang, Y. Liu, G.C. Yang, and H.M. Zeng, The effect of fiber treatment on the mechanical properties of unidirectional sisal-reinforced epoxy composites. *Composites Sci. Technol.* 61, 1437–1447 (2001).
117. K.L. Mittal (Ed.), *Silanes and Other Coupling Agents*, Vol. 5, CRC Press, Boca Raton, FL. (2009).
118. J. George, M.S. Sreekala, and S. Thomas, A review on interface modification and characterization of natural fiber reinforced plastic composites. *Polym. Eng. Sci.* 41, 1471–1485 (2001).

119. J. Wu, D. Yu, D. Chan, and Y.W. Mai, Effect of fiber pretreatment condition on the interfacial strength and mechanical properties of wood fiber/PP composites. *J. Appl. Polym. Sci.* 76, 1000–1010 (2000).
120. G. Mehta, L.T. Drzal, A.K. Mohanty, and M. Misra, Effect of fiber surface treatment on the properties of biocomposites from nonwoven industrial hemp fiber mats and unsaturated polyester resin. *J. Appl. Polym. Sci.* 99, 1055–1068 (2006).
121. S. Kalia, B.S. Kaith, and I. Kaur, Pretreatments of natural fibers and their application as reinforcing material in polymer composites—A review. *Polym. Eng. Sci.* 49, 1253–1272 (2009).
122. M. Abdelmouleh, S. Boufi, M.N. Belgacem, and A. Dufresne, Short natural-fibre reinforced polyethylene and natural rubber composites: Effect of silane coupling agents and fibres loading. *Composites Sci. Technol.* 67, 1627–1639 (2007).
123. Y. Xie, C.A. Hill, Z. Xiao, H. Militz, and C. Mai, Silane coupling agents used for natural fiber/polymer composites: A review. *Composites Part A* 41, 806–819 (2010).
124. K.L. Mittal (Ed.), *Acid-Base Interactions: Relevance to Adhesion Science and Technology*, Vol. 2, CRC Press, Boca Raton, FL. (2000).
125. K.L. Mittal, The role of the interface in adhesion phenomena. *Polym. Eng. Sci.* 17, 467–473 (1977).
126. D.J. Gardner, G.S. Oporto, R. Mills, and M.A.S.A. Samir, Adhesion and surface issues in cellulose and nanocellulose. *J. Adhesion Sci. Technol.* 22, 545–567 (2008).
127. C. Gouss, H. Chanzy, G. Excoffi, L. Soubeyrand, and E. Fleury, Stable suspensions of partially silylated cellulose whiskers dispersed in organic solvents. *Polymer* 43, 2645–2651 (2002).
128. Y. Habibi, H. Chanzy, and M. Vignon, TEMPO-mediated surface oxidation of cellulose whiskers. *Cellulose* 13, 679–687 (2006).
129. M. Hasani, E.D. Cranston, G. Westman, and D.G. Gray, Cationic surface functionalisation of cellulose nanocrystals. *Soft Matter* 4, 2238–2244 (2008).
130. G. Morandi, L. Heath, and W. Thielemans, Cellulose nanocrystals grafted with polystyrene chains through surface-initiated atom transfer radical polymerization (SI-ATRP). *Langmuir* 25, 8280–8286 (2009).
131. B. Braun and J.R. Dorgan, Single-step method for the isolation and surface functionalisation of cellulosic nanowhiskers. *Biomacromolecules* 10, 334–341 (2009).
132. B.L. Peng, N. Dhar, H.L. Liu, and K.C. Tam, Chemistry and applications of nanocrystalline cellulose and its derivatives: A nanotechnology perspective. *Canadian J. Chem. Eng.* 89, 1191–1206 (2011).
133. J. George, R. Janardhan, J. Anand, S. Bhagawan, and S. Thomas, Melt rheological behaviour of short pineapple fiber reinforced low density polyethylene composites. *Polymer* 37, 5421–5431 (1996).
134. M. Brahmakumar, C. Pavithran, and R.M. Pillai, Coconut fibre reinforced polyethylene composites: Effect of natural waxy surface layer of the fibre on fibre/matrix interfacial bonding and strength of composites. *Composites Sci. Technol.* 65, 563–569 (2005).
135. P.J. Herrera and A. Valadez, A study of the mechanical properties of short natural-fiber reinforced composites. *Composites Part B* 36, 597–608 (2005).
136. I.V. Weyenberg, J. Ivens, A.D. Coster, B. Kino, E. Baetens, and I. Verpoest, Influence of processing and chemical treatment of flax fibres on their composites. *Composites Sci. Technol.* 63, 1241–1246 (2003).

137. S. Panthapulakkal, M. Sain, and S. Law, Effect of coupling agents on rice-husk-filled HDPE extruded profiles. *Polymer Intl.* 54, 412–425 (2005).
138. W. Qiu, F. Zhang, T. Endo, and T. Hirotsu, Isocyanate as a compatibilizing agent on the properties of highly crystalline cellulose/polypropylene composites. *J. Mater. Sci.* 40, 3607–3614 (2005).
139. X. Colom, F. Carrasco, P. Pages, and J. Canavate, Effects of different treatments on the interface of HDPE/lignocellulosic fiber composites. *Composites Sci. Technol.* 63, 161–169 (2003).
140. M.N. Belgacem and A. Gandini, The surface modification of cellulose fibres for use as reinforcing elements in composite materials. *Composite Interfaces* 12, 41–75 (2005).
141. I.S. Aji, S.M. Sapuan, E.S. Zainudin, and K. Abdan, Kenaf fibres as reinforcement for polymeric composites: A review. *Int. J. Mechanical Mater. Eng.* 4, 239–248 (2009).
142. T.J. Keener, R.K. Stuart, and T.K. Brown, Maleated coupling agents for natural fibre composites. *Composites Part A* 35, 357–362 (2004).
143. M. Andresen, L.S. Johansson, B.S. Tanem, and P. Stenius, Properties and characterisation of hydrophobised microfibrillated cellulose. *Cellulose* 13, 665–677 (2006).
144. M. Andresen and P. Stenius, Water-in-oil emulsions stabilized by hydrophobized microfibrillated cellulose. *J. Dispersion Sci. Technol.* 28, 837–844 (2007).
145. T. Nishino, K. Hirao, and M. Kotera, X-ray diffraction studies on stress transfer of kenaf reinforced poly(L-lactic acid) composite. *Composites Part A* 37, 2269–2273 (2006).
146. M. Grunert and W.T. Winter, Progress in the development of cellulose reinforced nanocomposites. *Polym. Mater. Sci. Eng.* 82, 232–233 (2000).
147. A. Pei, Q. Zhou, and L.A. Berglund, Functionalized cellulose nanocrystals as biobased nucleation agents in poly(L-lactide) (PLLA)—Crystallization and mechanical property effects. *Composites Sci. Technol.* 70, 815–821 (2010).
148. A.N. Frone, S. Berlioz, J.F. Chailan, D.M. Panaitescu, and D. Donescu, Cellulose fiber-reinforced polylactic acid. *Polymer Composites* 32, 976–985 (2011).
149. L. Heux and C. Bonini, Microfibrillated and/or microcrystalline dispersion, in particular of cellulose, in an organic solvent. U.S. Patent No. 6,967,027 (2005).
150. L. Heux, G. Chauve, and C. Bonini, Nonfloculating and chiral-nematic self-ordering of cellulose microcrystals suspensions in nonpolar solvents. *Langmuir* 16, 8210–8212 (2000).
151. D. Bondeson and K. Oksman, Dispersion and characteristics of surfactant modified cellulose whiskers nanocomposites. *Composite Interfaces* 14, 617–630 (2007).
152. J. Kim, G. Montero, Y. Habibi, J.P. Hinstroza, J. Genzer, D.S. Argyropoulos, and O.J. Rojas, Dispersion of cellulose crystallites by nonionic surfactants in a hydrophobic polymer matrix. *Polym. Eng. Sci.* 49, 2054–2061 (2009).
153. O.J. Rojas, G.A. Montero, and Y. Habibi, Electrospun nanocomposites from polystyrene loaded with cellulose nanowhiskers. *J. Appl. Polym. Sci.* 113, 927–935 (2009).
154. Q. Zhou, H. Brumer, and T.T. Teeri, Self-organization of cellulose nanocrystals adsorbed with xyloglucan oligosaccharide-poly(ethylene glycol)-polystyrene triblock copolymer. *Macromolecules* 42, 5430–5432 (2009).
155. J.M. Robert, M. Ashlie, J. Nairn, J. Simonsen, and J. Youngblood, Cellulose nanomaterials review: Structure, properties and nanocomposites. *Chem. Soc. Rev.* 40, 3941–3994 (2011).
156. B.S. Kim, M.H. Nguyen, B.S. Hwang, and S. Lee Effect of plasma treatment on the mechanical properties of natural fiber/PP composites, in *High Performance Structures and Materials IV*, W.P. De Wilde and C.A. Brebbia (Eds.), pp. 159–166, WIT Press, Algarve, Portugal. (2008).

157. Z. Zhou, X. Liu, B. Hu, J. Wang, D. Xin, Z. Wang, and Y. Qiu, Hydrophobic surface modification of ramie fibers with ethanol pretreatment and atmospheric pressure plasma treatment. *Surf. Coat. Technol.* 205, 4205–4210 (2011).
158. E.G. Hernández, A.L. Claverie, A. Zizumbo, A. Castillo, and P.H. Franco, Improvement of the interfacial compatibility between sugar cane bagasse fibers and polystyrene for composites. *Polymer Composites* 25, 134–145 (2004).
159. D. Chen, L. Jing, and J. Ren, Influence of fiber surface-treatment on interfacial property of poly(L-lactic acid)/ramie fabric biocomposites under UV-irradiation hydrothermal aging. *Mater. Chem. Phys.* 126, 524–531 (2011).
160. N.E. Marcovich, M.L. Auad, N.E. Bellesi, S.R. Nutt, and M.I. Aranguren, Cellulose micro/nanocrystals reinforced polyurethane. *J. Mater. Res.* 21, 870–881(2011).
161. X.D. Cao, H. Dong, and C.M. Li, New nanocomposite materials reinforced with flax cellulose nanocrystals in waterborne polyurethane. *Biomacromolecules* 8, 899–904 (2006).
162. M.L. Auad, V.S. Contos, S. Nutt, M.I. Aranguren, and N.E. Marcovich, Characterization of nanocellulose-reinforced shape memory polyurethanes. *Polymer Intl.* 57, 651–659 (2008).
163. Q. Liu, T. Stuart, M. Hughes, H.S.S. Sharma, and G. Lyons, Structural biocomposites from flax – Part II: The use of PEG and PVA as interfacial compatibilising agents. *Composites: Part A* 38, 1403–1413 (2007).
164. Y.M. Zhou, S.Y. Fu, L.M. Zheng, and H.Y. Zhan, Effect of nanocellulose isolation techniques on the formation of reinforced poly(vinyl alcohol) nanocomposite films. *Express Polymer Letters* 6, 794–804 (2012).
165. C. Vilela, A.F. Sousa, C.S.R. Freire, A.J.D. Silvestre, and C.P. Neto. Novel sustainable composites prepared from cork residues and biopolymers. *Biomass Bioenergy* 55, 148–155 (2013).
166. S. Shu, S. Husain, and W.J. Koros, A general strategy for adhesion enhancement in polymeric composites by formation of nanostructured particle surfaces. *J. Phys. Chem. C* 111, 652–657 (2007).
167. E. Perez, J. Bras, V. Ducruet, A. Guinault, A. Dufresne, and S. Domenek, Influence of chemical surface modification of cellulose nanowhiskers on thermal, mechanical, and barrier properties of poly(lactide) based bionanocomposites. *European Polymer J.* 49, 3144–3154 (2013).
168. E. Brown, D. Hu, N. Lail, and X. Zhang, Potential of nanocrystalline cellulose-fibrin nanocomposites for artificial vascular graft applications. *Biomacromolecules* 14, 1063–1071 (2013).
169. A. Liu, A. Walther, O. Ikkala, L. Belova, and L.A. Berglund, Clay nanopaper with tough cellulose nanofiber matrix for fire retardancy and gas barrier functions. *Biomacromolecules* 12, 633–641 (2011).
170. A. Alemdar and M. Sain, Biocomposites from wheat straw nanofibers: Morphology, thermal and mechanical properties. *Composites Sci. Technol.* 68, 557–565 (2008).
171. S.Y. Lee, D.J. Mohan, I.A. Kang, G.H. Doh, S. Lee, and S.O. Han, Nanocellulose reinforced PVA composite films: Effects of acid treatment and filler loading. *Fibers Polymers* 10, 77–82 (2009).
172. W. Li, J. Yue, and S. Liu, Preparation of nanocrystalline cellulose via ultrasound and its reinforcement capability for poly(vinyl alcohol) composites. *Ultrasonics Sonochemistry* 19, 479–485 (2012).
173. S. Fujisawa, T. Ikeuchi, M. Takeuchi, T. Saito, and A. Isogai, Superior reinforcement effect of TEMPO-oxidized cellulose nanofibrils in polystyrene matrix: Optical, thermal, and mechanical studies. *Biomacromolecules* 13, 2188–2194 (2012).

174. L. Suryanegara, A.N. Nakagaito, and H. Yano, The effect of crystallization of PLA on the thermal and mechanical properties of microfibrillated cellulose reinforced PLA composites. *Composites Sci. Technol.* 69, 1187–1192 (2009).
175. J. Lu, T. Wang, and L.T. Drzal, Preparation and properties of microfibrillated cellulose polyvinyl alcohol composite materials. *Composites Part A* 39, 738–746 (2008).
176. H. Sehaqui, M. Allais, Q. Zhou, and L.A. Berglund, Wood cellulose biocomposites with fibrous structures at micro- and nanoscale. *Composites Sci. Technol.* 71, 382–387 (2011).
177. M.J. Cho and B.D. Park, Tensile and thermal properties of nanocellulose reinforced poly (vinyl alcohol) nanocomposites. *J. Ind. Eng. Chem.* 17, 36–40 (2011).
178. A. Iwatake, M. Nogi, and H. Yano, Cellulose nanofiber-reinforced polylactic acid. *Composites Sci. Technol.* 68, 2103–2106 (2008).
179. R. Rusli, K. Shanmuganathan, S.J. Rowan, C. Weder, and S.J. Eichhorn, Stress-transfer in anisotropic and environmentally adaptive cellulose whisker nanocomposites. *Biomacromolecules* 11, 762–768 (2010).
180. R. Rusli, K. Shanmuganathan, S.J. Rowan, C. Weder, and S.J. Eichhorn, Stress transfer in cellulose nanowhisiker composites – Influence of whisker aspect ratio and surface charge. *Biomacromolecules* 12, 1363–1369 (2011).
181. T. Mohan, R. Kargl, A. Doliška, H. Ehmann, V. Ribitsch, and K. Stana-Kleinschek, Enzymatic digestion of partially and fully regenerated cellulose model films from trimethylsilyl cellulose. *Carbohydrate Polymers* 93, 191–198 (2013).
182. D. Liu, T. Zhong, P.R. Chang, K. Li, and Q. Wu. Starch composites reinforced by bamboo cellulosic crystals. *Bioresource Technol.* 101, 2529–2536 (2010).

Adhesion Phenomena in Pharmaceutical Products and Applications of AFM

Emily Callard Preedy¹, Stefano Perni^{1,3} and Polina Prokopovich^{1,2,3,*}

¹*Cardiff School of Pharmacy and Pharmaceutical Science, Cardiff University, Redwood Building, Cardiff, UK*

²*Cardiff School of Engineering, Cardiff University, Queen's Buildings, Cardiff, UK*

³*Department of Biological Engineering, Massachusetts Institute of Technology, 77, Cambridge, MA, USA*

Abstract

This review aims at pinpointing the issues commonly associated with the production of pharmaceutical formulations and biomedical devices regarding adhesion and cohesion interactions through utilisation of atomic force microscopy (AFM) techniques. Adhesion and cohesion phenomena have been of interest for many years as they are encountered on a daily basis from activities such as walking to geckos climbing a tree. Many models for adhesion interactions have been developed since the early 1970s: Derjaguin, Landau, Verwey, and Overbeek (DLVO) assumed a physical approach to understanding adhesion; whilst, Johnson, Kendall, and Roberts (JKR) as well as Derjaguin, Muller and Toporov (DMT) both assumed a mechanical approach for understanding the adhesion phenomena. However, these theories were not without limitations, therefore models have been developed including the extended DLVO (xDLVO), as well as mathematical models based on data collected using AFM.

This review highlights the issues in the development of pharmaceutical formulations and where adhesion impacts the development of medical preparations. As many pharmaceutical products possess aspects of colloidal systems, so they are often affected by adhesion and cohesion interactions causing problems such as aggregation, sedimentation and flocculation. These phenomena can influence the overall adhesion and alter the outcome of formulations causing undesirable effects to medications; these issues are governed by the physicochemical

*Corresponding author: prokopovichp@cf.ac.uk

properties of materials. Such characteristics include surface topography and morphology and are influenced by humidity, and all these parameters can be analysed using the AFM. Therefore, such methodology has shown advantages over traditional techniques employed in the pharmaceutical industry including centrifugation, near-infrared spectroscopy and inverse gas chromatography in the understanding of adhesion at the nanoscale.

Keywords: Adhesion, cohesion, pharmaceutical industry, atomic force microscopy, pMDIs, DPIs, inhalers

7.1 Introduction

Adhesion is a complex phenomenon which spans many aspects of daily life, from the simplest task of a toddler gluing a pretty collage, to a cell adhering to a surface to form a new tissue [1]. Many aspects of day to day living may, therefore, be affected by the extent of attraction at these contact points. For instance, these interactions apply to many industrial as well as natural processes, such as cell to cell interactions, cells to materials interactions, drug delivery systems as well as drug formulations [1–3] and in medical prosthesis [4] in which adhesion can have impact on the wear and tear of the contacting materials through forces such as friction [4, 5]. Natural occurrences of adhesion appear throughout the animal world. An interesting example is the adhesion property of geckos toes [6]. There are millions of setae on the toes of geckos which utilize van der Waals (vdW) forces; studies have shown that the toes are highly hydrophobic and adhere well to hydrophobic, hydrophilic and polarisable surfaces [7]. Another adhesion encounter in nature includes adhesive pads on the toes of tree frogs [8], whereby friction forces generate large adhesion forces.

A simple analogy to describe adhesion could be when two bodies join resulting in a shared surface zone defined as a contact zone [9]. Yet, adhesion is often classified according to the different types of interacting forces such as electrostatic interactions, acid-base interactions, hydrophobic interactions and van der Waals (vdW) forces [10–13]. For example, fluid flow initially increases attachment by transporting materials to a surface, yet this also alters the hydrodynamic detachment forces especially in an aqueous environment [13]. Moreover, the differences between adhesion and cohesion have been highlighted [14]: adhesion is the propensity of particles to adhere to other surfaces, whereas cohesion is the propensity of like particles sticking together, i.e., the internal strength [15].

However, there are some theories of adhesion that attempt to describe/predict the contact zone which include a physical approach by Derjaguin, Landau, Verwey and Overbeek (DLVO) [16] with an additional extension (xDLVO); and Johnson, Kendall, and Roberts (JKR) [17] theory, as well as the Derjaguin, Muller and Toporov (DMT) theory which are based on a mechanical approach to understanding adhesion [18].

The former physical model of adhesion considers what happens at the point of contact, forming the basis of modern colloid and interface science [19]. DLVO theory has often been applied to explain the physical interactions in colloidal systems, such as emulsions, aerosols and foams. Generally, the total interaction potential (V_{TOT}) depends on the separation distance (d) and it is assumed to be the sum of the attractive (V_A) van der Waals (vdW)

and repulsive (V_R) electrostatic interactions [19]. DLVO theory calculates the electrostatic double layer (EDL) energy usually between two macro-bodies and is limited to investigating two parallel infinitely flat surfaces [20, 21], obviously this approximation has limitations such as in pharmaceutical powders and microbial adhesion. An alternative version is a smooth surface contacting a rougher surface which has been considered at the macro-scale, which includes the use of the extended DLVO (xDLVO) [11] theory. Similarly to the DLVO model, the xDLVO theory considers the energy associated with two surfaces immersed in an aqueous environment, the main difference between DLVO and xDLVO is that the latter includes also Lewis acid-base polar interactions (AB) and the Brownian motion (BR) to the Lifshitz-van der Waals (LW) and the electrostatic double layer (EDL) interactions [11, 22]. Yet, xDLVO predictions differ from experimental adhesion measurements especially when micro-organisms are concerned, which may be due to their complex surface which is far from the ideal colloidal particle [23, 24].

The JKR theory only applies to mechanical interactions that occur inside the contact zone, particularly to the deformation which influences the extent of adhesion and was developed in 1971 [17, 25]. JKR theory balances the stored elastic energy and the loss in surface energy through the deformation of interacting surfaces, i.e., it predicts the critical pull-off force over a contact area larger than the Hertzian contact [26], and considers the short-range surface forces that act in the contact zone. Whereas DMT theory considers the tensile stress which exists in an annular zone around the contact area with no deformation, i.e., the non-contact regions that lie outside the contact zone. Furthermore, both mechanical models, JKR and DMT, are often only applied to thermodynamically equilibrated conditions [27] otherwise other influencing factors must be considered that are not included in these theories of attachment such as temperature, relative humidity, as well as the morphology of the surfaces, and the viscoelastic deformation, and surface roughness.. These theories, however, are further complicated when real materials and interactions are concerned. For example, both physical, DLVO and xDLVO, as well as the mechanical JKR and DMT theories consider only ideal colloidal particles that have smooth surfaces contacting a flat surface.

The interest in adhesion from animal studies has opened avenues to study the micro- and nano- adhesion inherent in microelectromechanical systems (MEMS) [28, 29]; these systems are susceptible to stiction which is an unintentional adhesion of the structural elements when forces of elasticity cannot overcome the attractive effects due to interfacial forces from capillary, vdW and electrostatic interactions [30]. Adhesion is often detrimental in biomedical applications, for example, when considering total hip and knee prostheses, whereby constant movement of these joints can lead to fractures and wear impacting the longevity of the device. Another problem occurs in medical devices such as inhalers where there is an issue with the powders in dry powder inhalers (DPIs) to agglomerate and, consequently, the desired dose and size of the inhaled particles are affected, with the dose reduced and the size of the particle increased [31]. On the other hand, adhesion is essential in some aspects of drug delivery systems for rapid absorption of the active compound [32], as well in understanding the role of the extracellular polymeric substances (EPS) involved in bacterial attachment [33].

In this article we will describe the problem of adhesion in the pharmaceutical context through AFM techniques.

7.2 Adhesion in Pharmaceuticals

Adhesion has been of great interest to the pharmaceutical industry as the adhesion phenomena can affect many areas such as colloidal dispersion, aggregation, and lubrication processes [34–36]. It is vital to take into account adhesion and interaction forces when considering pharmaceutical materials, as caking of colloidal particles to the walls of machines often results in a reduction of production capacity [34]. Figure 7.1 demonstrates the common problems which occur when a colloidal system becomes unstable from a stable form.

In general, tablets are the most popular product in the pharmaceutical industry [14, 37]; however, there are often concerns during the development of tablets such as formulation materials sticking to tooling surfaces causing a build-up of product on punch surfaces leading to potential defects and alterations to the end product [15, 38]. Therefore, it is essential for correct production to select suitable excipients as well as manufacturing processes to minimise sticking from occurring, as this issue is normally recognised late in the development of tablets. Any changes in the structure and formulation may, therefore, cause an adverse effect on the overall application of a particular drug, for instance, in the gas phase, humidity can deteriorate many pharmaceutical particles if relative humidity (RH) is over 75% [34, 39, 40] causing capillary force contributions by forming a liquid meniscus between particles that are in contact. Thus, identification and control of adhesion is essential for industrial processes as well as for the delivery of medications [32]. For example, in inhalers, if the powder aggregates before the dose is expelled, then the active

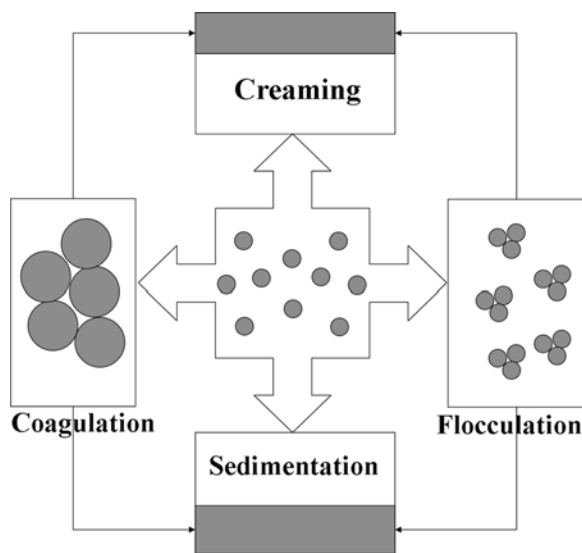


Figure 7.1 An illustration depicting the effect of destabilisation of a colloidal system.

pharmaceutical ingredient (API) may not reach its target, as agglomerated powder can collect in the upper airways causing hoarseness and oropharyngeal candidiasis [31, 41, 42].

Granulation is a common process that needs particular control on adhesion [43] as agglomeration of powders is achieved by controlled crushing using high stress to form compacted powders [44]. It is also known as particle bonding and is of relevance in both dry and wet compaction processes [44, 45]. There are two main mechanisms associated with particle bonding especially in pharmaceutical powders and tablet formation [45]. For example, if liquid is present in a powder formulation, then a thin layer of immobile particles may form on a powder particle which increases the area for contact to take place between powder particles. This increases the bond strength as the van der Waals (vdW) forces are proportional to the particle diameter and inversely proportional to the distance of separation [45]. Secondly, the interfacial forces of the mobile film must be taken into consideration. For example, during industrial processes of wet granulation, the added liquid is distributed as films around the particles, this holds the particles together by surface tension forces [45, 46].

Another major concern that has been highlighted in the developmental stages of tablet formulations is the sticking of the tablet materials to the tooling surfaces [14, 15]. Sticking can affect the surface chemistry and topography of the compacted tablet; this can cause destabilisation of the original formulation resulting in disintegration and drug dissolution. This can lead to changes in the surface structure and chemistry of the formulation, thus causing variations in the formulations from batch to batch [14].

A common example of batch to batch alterations has been a concern in aerosol based medications [47], such as those used in dry powder inhalers (DPIs) and pressurised metered dose inhalers (pMDIs) to treat asthma [47]. Especially in these cases, there is significant concern to control interactions between drug-drug, drug-carrier, and drug-device in order to effectively and efficiently deliver fine drug particles into the human body.

7.2.1 Adhesion Interactions

In the literature [48–50], it has been highlighted that there are three main concepts whereby adhesion can influence the outcome of pharmaceutical applications, i.e. drug-drug, drug-carrier, and drug-device (canister) interactions. The switch from chlorofluorocarbon propellants (CFCs) to hydrofluoroalkanes (HFAs) according to the Montreal Protocol [51, 52] has led to an increase in the study of drug-drug, drug-carrier, and drug-device interactions [1, 51, 53]. Results have revealed that modifications to the drug substance, co-solvents, design of the device, and excipients are needed to improve the performance of formulations using HFAs [54]. For example, excipients did not provide adequate stability to the systems causing flocculation (Figure 7.1) leading to sedimentation of particles (drug-drug/drug-carrier) [51]; therefore, one notable change was the use of oleic acid previously used in CFC products as a stabiliser but it can only be used in new HFA products when ethanol is present in the formulations [51].

7.2.1.1 Drug-Drug/Carrier Interactions

Inhalers are common examples where there are many problems associated with drug-drug, drug-carrier and drug-canister/packaging. The two main devices used are pressurised metered dose inhalers (pMDIs) and dry powder inhalers (DPIs): pMDIs contain the active

ingredient suspended in a propellant gas as solid micronized particles; DPIs contain particles in a blister for respiration. Both devices often have excipients or carriers which act as stabilisers to minimise the effects of adhesion in the formulations [55]. Thus, the micronisation process used in the pharmaceutical industry is a well-established procedure for the production of micron-sized particles for both orally and inhaled medications [48], however it is reported to contribute to some metal contamination. Micronisation often results in particulates with high surface area, which has the risk of forming unstable cohesive systems that often agglomerate and adhere to surfaces [55], thus making it difficult to control the dosage.

Aggregation is not a desirable attribute, especially in inhaled medications [51, 56] as this affects the size and morphology of the formulation through flocculation or coagulation of particles, contributing to the lack of stability [54]. Such interactions are dominant in the manufacturing of pharmaceutical powders which can influence the adhesion of these powders to each other or to devices used in industry and have been reported to interact with the packaging of oral medications [50, 57, 58]. For example, electrostatic charges can be used as a beneficial aspect when mixing powders of controlled size distributions, such as those in dry powder inhalers (DPIs), to ensure homogeneous mixtures to increase the quality of the product [50, 57] as this introduces a repulsive force which can overcome the attraction causing agglomerates to form. It is often generated when two different materials contact and are then separated through sliding; unfortunately, this particle electrification can result in dust explosions [50]. Yet electrification is exploited in powder flow measurements, separation processes as well as in electrophotography in photocopiers and laser printers [50]. However, in the pharmaceutical industry it has become a priority to control this process as it can affect the particle dose by governing the deposition rate in the human lung, and by influencing the aerosol dispersion behaviour in the air stream [50, 57]. Another effective way to combat this issue is by steric effects through the addition of a polymer to stabilise the formulation [51].

Normally carrier particles are required in DPI systems and excipients are required in pMDIs and tablet formulations [39]. These act as bulking agents, while stabilisers aid in the metering and fluidisation within DPIs. When stress is introduced to the system, these carriers aid in the de-agglomeration and deposition of the drug. The adhesion interactions between carrier and drug are the result of manufacturing processes as well as of the physicochemical characteristics of the drug and carrier used [39, 59]. Although carrier particles have been successfully used [39], influencing factors that may play a relevant role during storage still lead to a number of fundamental effects on the particles properties. These factors are responsible for the inter- and intra-batch variations observed in pharmaceutical formulations [39]. It is important, therefore, to control the ambient conditions to ensure the integrity of these systems as particle adhesion is often dominated by non-surface-specific capillary forces arising from a thin layer of water molecules adsorbed on the surface forming a concave meniscus between drug and carrier. This has been described as Laplace vapour pressure which acts across the meniscus at the air-liquid interface [35, 39, 60].

7.2.1.2 Drug-Device/Packaging Interactions

Drug-packaging or device interactions are another potential issue in pharmaceutical industrial processes, which can be a result of the micronisation methods used [55]. This problem

involves the agglomeration of particles forming larger particles which govern the particle-particle and particle-canister adhesion especially in DPI systems. Such adhesion also controls the powder flow often influenced by van der Waals forces and electrostatic interactions resulting from charged particles [50, 55]. Other issues associated with drug and packaging interactions in pharmaceutical industry include leaching and sorption. Leaching is the migration of chemical components from the packaging to the drug, whilst sorption is the opposite with the drug adhering to the packaging material [58]. Therefore, either process has a significant effect on product safety by either altering the toxicity levels due to leaching or causing alterations in the efficacy and stability through sorption [58]. Compaction processes have been shown to alter the interactions in formulations by modification of the particles surface [61].

A further problem with drug-device interactions is the attraction of the formulation to the seals and valves of the device [54, 62]. As HFA is inert it does not interact with elastomeric seals. However, it lacks lubrication for a smooth actuation [62], hence a suitable lubricant must be used to minimise the adhesion of the formulation to seals and to prevent leakage of highly volatile formulations from pressurised canisters [62]. Also, variations in the valve designs can cause alterations in the drug dose as valves in contact with the suspension may become coated and enriched with the suspended drug; furthermore, any small orifices or long nozzles within the device can result in de-aggregation [54].

7.2.2 Factors Influencing Adhesion

There are many factors that influence the extent of adhesion and cohesion interactions which directly affect the outcome of pharmaceutical formulations. The most recognised parameters that directly govern adhesion include: roughness, morphology and topography; humidity and moisture; surface energy and tension (when liquids are concerned) [23, 25, 47, 50, 56, 63, 64].

Electrostatic charging of pharmaceutical powders is also a prevalent issue due to collisions and sliding contact of particles with other particles as well as with the walls of devices, this is known as triboelectrification [57]. This frictional contact or sliding often occurs with charged pharmaceutical particles which can then dominate the overall adhesion and deposition processes and thus has become of great importance in DPI devices. Not only does electrostatic charging cause adhesion to walls and other particles but also causes problems during manufacturing by affecting the powder flow and disrupting the dose uniformity [57]. On the other hand, this phenomenon has been used for controlling the mixing of powders [57].

Also micronisation impacts the crystalline structure of materials [48, 56], as the forces generated induce lattice defects as well as weakening of the intermolecular bonds in the crystalline material altering the overall physical and chemical stability [48]. This process of crystallisation can also influence the size and shape of the particle. It has been noted that the principal factor governing crystallisation is supersaturation which is the ratio of actual concentration to the solubility at a specific temperature [56]. Additionally, any alterations in the physicochemical characteristics of a particle affect the way in which it will interact with other particles [48]. The crystallisation of lactose causes drug particles to adhere causing

sedimentation due to the morphological change of the surface of the lactose carrier from smooth to a rougher texture due to crystallisation [56].

Surface roughness often correlates with the surface topography of a material or substrate, thus has a definite effect on the adhesion as the roughness governs the contact area [61]. Often the roughness of a surface is described in terms of asperities [4, 65] which are the peaks and troughs of a surface (Figure 7.2). Therefore, contact occurs when these peaks contact another surface. Recently, it has been noted that more often than not, surfaces exhibit multi-asperities [4], whereby the peaks and troughs at the micro-scale are covered by nano-scale asperities (Figure 7.2) which also affect adhesion process, as real surfaces possess roughness is several length scales, and ultimately nano-scale roughness determines the strength of adhesion [66]. For example, when two bodies contact, only the peaks will touch the opposite surface; therefore, the total amount of contact will be small giving a low adhesion, resulting in a non-permanent contact [66].

On the other hand, permanent adhesion tends to occur when whole surfaces, including the troughs, are in contact; this type of adhesion is useful for wound dressings and medical glues [67, 68]. Nevertheless, adhesion governed by asperities is important in tablet and powder formulations in pharmaceutical applications, as the rougher the surface the lower the adhesion. Morphology of interacting particles or materials is also important and is related to the topography and roughness of the surfaces. When particles are in contact, the adhesion interactions are dominated by the vdW interactions, and the extent of this attraction is governed by the surface roughness and asperities [64]. The mechanical properties of the materials surfaces are also an important factor to consider in adhesion [69]; for example, in biomimetic devices mushroom shaped fibrils have exceptionally high adhesion strength which exceeds that of

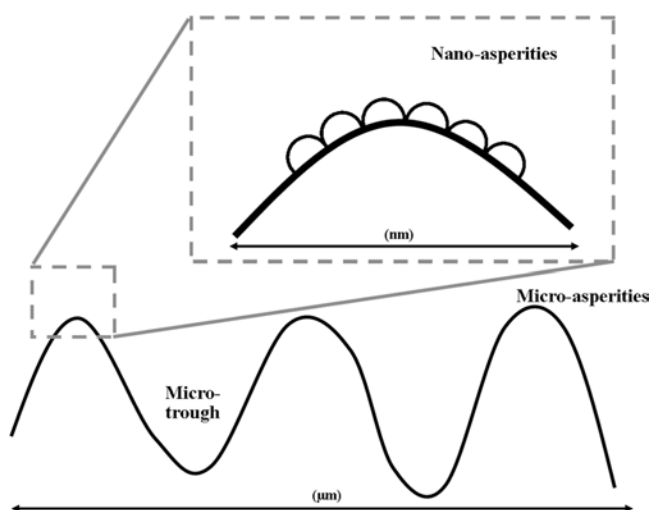


Figure 7.2 Three micro-asperities are shown as large peaks with a trough in-between, with nano-scale asperities shown in the dotted grey square and are present on all asperities.

natural fibrils found in gecko toes [69, 70]. Also, it is important to note that the shape of these asperities can have an influential role in adhesion [64, 65]; average asperity height, curvature radius of asperity tip and distribution of these parameters control the contact zone. Many models have been developed to consider asperities [4, 64, 71–73] which have been derived from JKR and DMT contact theories of single asperities, and recently the Prokopovich and Perni model [4, 25, 65] has taken into consideration the variability of the height and curvature of radius of each asperity [4]. This model assumes a rough surface contacting a flat surface as represented by Figure 7.3, so the total contact force can be assumed to be the sum of the individual asperities each with individual height and curvature radius.

The size of the particle is also an important aspect to consider when investigating adhesion behaviour [74]. Centrifugal technique has been employed to analyse the effects of the particle size [75–77] as the behaviour and mechanical properties of particles are dependent on the particle size and distribution. In the pharmaceutical industry especially, particle adhesion as a function of size has been quantified as tensile strength of a powder mass [74]. Adhesion of small particles to rough surfaces is governed by the geometrical effect on the surface-particle system. Adhering particles to a surface that are smaller or similarly sized to the asperities tend to be weakly dependent on the particle size and the interaction is limited to contact of a single asperity (Figure 7.4) demonstrating linear dependence of the pull-off force, and therefore adhesion is based on this contact alone [66, 78]. On the other hand, particles larger than the surface features will have several contact points so the asperity geometry and the size of the particle will have a greater influence over the extent of adhesion [66].

Humidity can be detrimental for pharmaceutical powders [47] especially in inhaler devices as this can cause agglomeration, altering the size and shape of the particles and consequently the drug deposition kinetics. Humidity tends to govern the particle-particle interactions that are influenced by capillary forces [79–81] which in dry powder inhalers (DPIs) become dominant [49] with possible detrimental effects. Capillary forces have a significant effect on the flow and adhesion behaviour of fine powders [80] through capillary

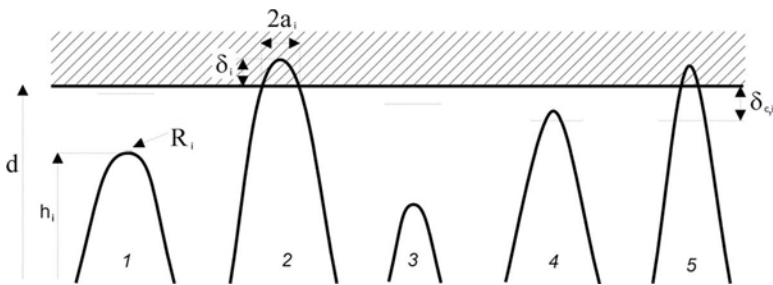


Figure 7.3 Multiasperity model of a rough and flat surface in contact, only asperities 2 and 5 are in contact as their height (h_i) is greater than distance (d), also asperity 4 is in contact as $d-h_i < \text{critical deformation } (\delta_{c,i})$. Reprinted from Journal of Colloid and Interface Science, volume 168, issue 1-2, Prokopovich, P and Starov, V, Adhesion models: From single to multiple asperity contacts, pages 210-222. Copyright 2011, with permission from Elsevier.

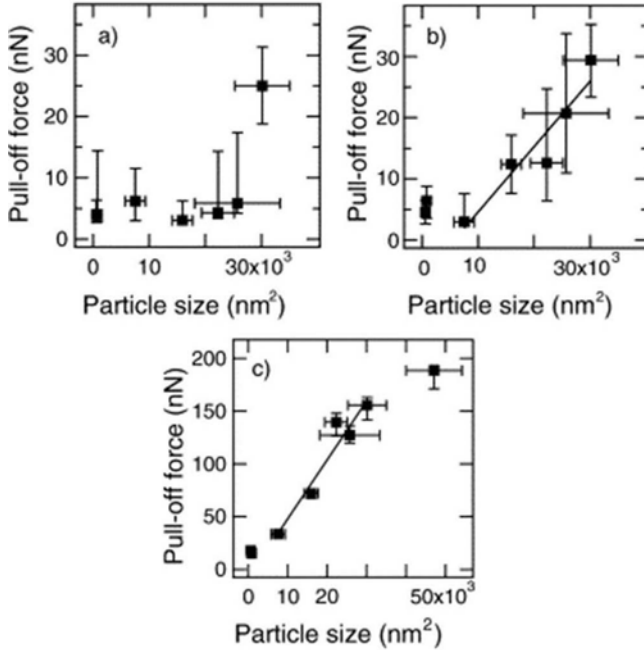


Figure 7.4 Pull-off forces measured from rough surfaces as a function of particle size expressed as area of maximum contact, with varying TiO₂ thin film coatings with a thickness of (a) 500, (b) 130 and (c) 10 nm [66]. The solid lines are to show the fit only. Journal of Colloid and Interface Science, volume 304, issue 2, Katainen, J, Paajanen, M, Ahtola, E, Pore, V, and Lahtinen, J, Adhesion as an interplay between particle size and surface roughness, pages 524–529. Copyright 2006 with permission from Elsevier.

condensation, especially between two hydrophilic surfaces in contact [79]. Capillary condensation is often described by the Kelvin equation [79, 82]), with Figure 7.5 representing a particle and flat surface attraction, and Figure 7.6 illustrates a particle-particle capillary force [79, 80]. Capillary condensation is described by the Kelvin equation [79]:

$$-\frac{\ln(P/P_0)}{\lambda_K} = \frac{1}{r} - \frac{1}{l} \tag{7.1}$$

Where:

$$\lambda_K = \frac{\gamma V_m}{K_B T} \tag{7.2}$$

Where r is the meridional radius of curvature of the meniscus and l is the azimuthal curvature parallel to the surface. P denotes the vapour pressure, and P_0 is the saturation vapour

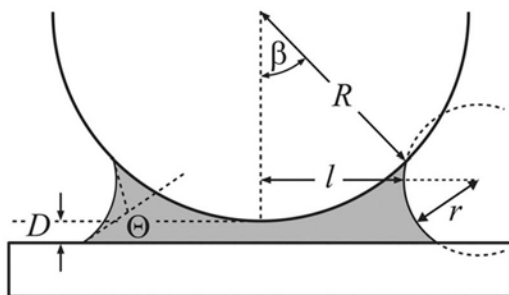


Figure 7.5 Spherical particle interacting with a flat surface via a liquid meniscus. Reprinted with permission from H.J. Butt, 2008 [79]. Copyright (2008) American Chemical Society

pressure. V_m represents the molecular volume of the molecules in the liquid phase, k_B the Boltzmann's constant, g the surface energy of the liquid and T is the temperature. The Kelvin length is shown as the constant λ_K which characterises the length scale for capillary condensation. Figure 7.5 represents the capillary interaction between a particle and flat surface, Figure 7.6 demonstrates that the capillary interaction between two particles can be predicted in a similar manner as a particle and flat surface with a capillary bridge formation [79, 83].

Recently, a model has been devised to predict adhesion forces between rough particles and surfaces by including vdW interactions and capillary forces [73]. This model considers a multiscale roughness feature as well as capillary forces as DPI systems are not limited to the nanoscale, and employs the fractal theory and Gaussian roughness distribution to account for the surface roughness. It also considers two important components for capillary forces, the capillary pressure and the surface tension force which tends to have a smaller influence as compared to the capillary pressure [73]. Figure 7.7 demonstrates the influence of surface roughness and vdW forces and capillary forces based on the You and Wan 2013 model and a graph representing the relative humidity effects on the forces of interactions that govern the overall adhesion of particles [73].

An understanding of all surface properties is important, as well as the surface tension [84] which is caused by the contraction of the exposed surface of a liquid to the smallest possible area [46]. The surface energy and tension of a system can, therefore, influence the overall adhesion [84]. As adhesion initially occurs through contact of two surfaces, surface interactions play a role and can explain the variability often found from batch to batch in pharmaceutical formulations [84]. Usually, the surface tension of the liquid must be lower than or equal to the surface tension of the substrate, i.e. liquid must have stronger attraction to the substrate than to itself for ease of adhesion [46]; the reverse is also true in order for interacting bodies to detach.

7.2.2.1 Monitoring and Controlling Influential Factors

Certain techniques have been employed within the pharmaceutical industry to investigate and control adhesion. It is important in industry to consider the cost of the process and

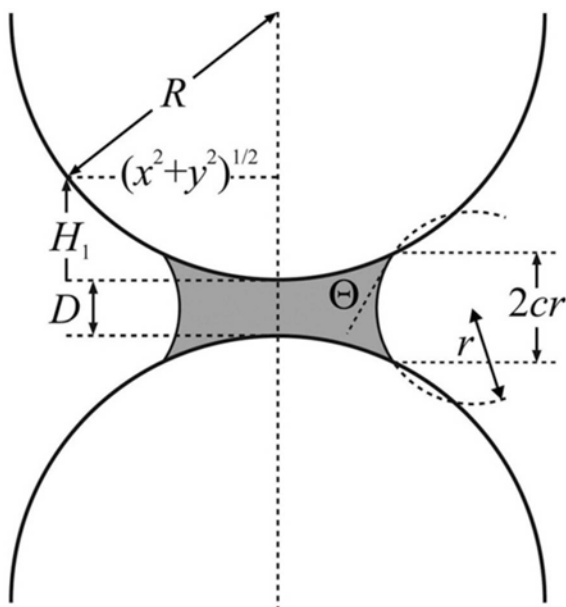


Figure 7.6 Schematic of two equal spheres interacting with each other via a liquid meniscus. c represents the mean of the cosines of the contact angles of the liquid on the two surfaces of the spheres. Reprinted with permission from H.J. Butt, 2008 [79]. Copyright (2008) American Chemical Society

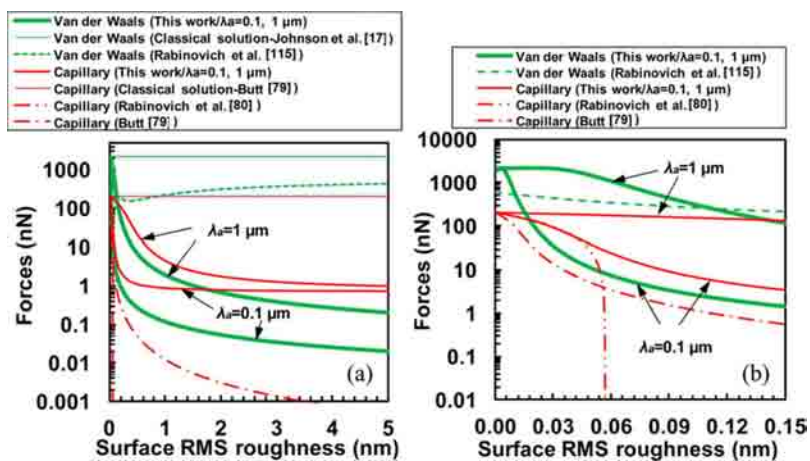


Figure 7.7 Surface roughness influence on van der Waals interactions and capillary forces using prediction models (You and Wan 2013 [73] and others), for (a) RMS roughness range of 0-5nm and (b) RMS roughness range of 0-0.15nm [73]. Reprinted with permission from [73]. Copyright (2013) American Chemical Society.

therefore it is essential to have quality assured products balanced with an acceptable level of testing taking into consideration the overall cost [85, 86].

Centrifugation is a common technique used in the pharmaceutical industry [77], where the concentration gradients of sedimenting particles are measured during application of centrifugal forces [77]. This technique separates particles from solutions according to their size, shape, density, and viscosity of the medium and rotor speed; and it has been used as an analytical investigative tool to separate natural and synthetic macromolecules and colloids in solution, dispersions and suspensions [75, 76]. The basic theory of centrifugation is that any object moving in a circle at a steady angular velocity is subject to an outwardly directed force, F also known as the relative centrifugal force (RCF), the magnitude of this force will depend on the angular velocity in radians, ω , and the distance from the rotation axis, r , as:

$$F = r\omega^2 \quad (7.3)$$

Sedimentation takes place due to a number of characteristic properties such as the size, shape and density of the molecules or particles, as well as the solvent properties [75–77]. These physicochemical characteristics will also influence the interactions between particles [75]. During the centrifugation process, two forces counteract the buoyancy force which are the displacement force and the frictional force. Analytical ultracentrifugation (AUC) techniques [75, 76] can also quantitate the concentration distribution of particles during sedimentation, providing hydrodynamic and thermodynamic information on the size, shape, molar mass, association energy, stoichiometry and thermodynamic non-ideality of the particles in solution [76]. AUC is becoming increasingly important in the study of biomaterials and biomedical devices [75]. It is often used in a non-conventional manner by employing layer by layer procedure to study hydrogel formation at the interface [75].

Inverse gas chromatography (IGC) has been utilised to monitor molecular mobility, crystallisation, relaxation; all of these can impact adhesion [84]. This technique has been employed [87] to study the characteristics of DPI formulation powders to monitor batch to batch variability. Many novel techniques including non-contact procedures to monitor the quality of formulation have emerged, such as acoustic, near-infrared (NIR), and focused beam reflectance measurements (FBRM), which aim to assess the desirable aspects of powders and tablets throughout their production [45, 88–90]. The acoustic process aims to obtain granulation signatures using an acoustic transducer which monitors changes in particle size, flow and compression properties [45]. The advantages of this technique are it is non-invasive, relatively inexpensive and sensitive. NIR is often used in pharmaceutical monitoring as a moisture sensor but is limited to only measuring liquid on the surface of a powder [45, 86, 91]. FBRM is used to determine the particle size of powders during formulations [45, 90]. It is based on a laser beam which follows a circular path intersecting the edges of particles, it passes through a sapphire window and the backscatter signal is collected. FBRM measures the dynamic changes in the particle size, morphology, concentration and rheology when liquids are concerned [45]. Further preparation techniques have been used for particles less than $2.5\mu\text{m}$ as used in DPI devices. FBRM uses a micromanipulator and video microscope to measure the adhesion force distribution between spherical

polycrystalline drug particle and lactose as a DPI carrier and to stainless steel as the wall of the inhaler device [47]

Another useful technique that has been used recently is a wireless transmission of ultrasonic waveforms to monitor tablet properties and deviations from the required specification during the formulation stage in pharmaceutical industrial processes [85]. This technique is of interest to industry as it has the capability of rapid and extensive inspection of a product with minimal time or interruption, and this is achieved through a non-contact procedure. The wireless technology is capable of monitoring such properties as geometry and mechanical properties which are important for the therapeutic effect of the drug formulations [85], as well as tablet thickness, mass density, integrity of the tablet, and even the layer by layer bonding quality as the powders are compacted.

Isothermal calorimetry (ITC) has also been utilised by the pharmaceutical industry to characterise physicochemical changes in the active pharmaceutical ingredients (APIs) [92]. This method is robust to handle the volatility of hydrofluoroalkanes as propellants unlike previously used techniques such as zeta potential and in situ laser diffraction [92]. ITC is a quantitative physical technique employed to determine reaction thermodynamics and kinetics, and can be used with a large variety of samples from liquids to solids and heterogeneous mixtures during the various stages of drug manufacturing including pre-formulation, determination of solubility as well as crystallinity and interactions between drug and carrier [92].

Near-infrared (NIR) spectroscopy is commonly used in the industrial setting for the qualitative analysis of large numbers of pharmaceutical products [86]. NIR spectroscopy is beneficial as a non-destructive analytical tool enabling simultaneous measurements of physicochemical properties such as chemical composition, the active pharmaceutical ingredient (API), as well as tablet hardness and dissolution profile [86, 91]. Usually, API is analysed using high performance liquid chromatography (HPLC) but this is a destructive technique and can be time consuming [86], and NIR spectroscopy can provide the same information as gained with HPLC but in less time and less labour-intensive manner. However, multivariate calibrations are required when simultaneously analysing both chemical and physical aspects of pharmaceutical products just to ensure adequate accuracy, precision and robustness of the technique [86]. Yet HPLC is still required to quantify the API ingredients as a complimentary technique to NIR spectroscopy [91].

7.3 Atomic Force Microscopy

Atomic force microscopy (AFM) has been employed by the pharmaceutical industry as it provides a simple and sensitive technique for measuring a wide variety of surface characteristics of complex pharmaceutical systems. For example, interaction forces are measured as a function of sample displacement by recording the cantilever deflection. Unlike other techniques, AFM can focus on individual particles to further understand adhesion issues associated with pharmaceutical systems which can then be used to improve bulk formulations [3, 93].

Throughout its history, atomic force microscopy (AFM) has been utilized to provide high resolution topographical images of a wide variety of samples, from conducting to

non-conducting materials [94]. It was initially developed to overcome the limitations associated with other microscopy techniques, especially with scanning electron microscopy (SEM) [95]. SEM requires a conducting coating, often resulting in artefacts particularly in biological samples.

AFM is a very versatile technique allowing for in situ imaging of a range of samples in their physiological conditions [96]. It has been employed to characterise the cohesive nature of pharmaceutical powders for inhalation therapy, to quantitatively study the elasticity of cells, and to measure molecular interactions forces [97]. It can also be used to image the topography of materials in their native environments, giving significant information about surface features with unprecedented clarity [98]. One aspect which enables AFM to effectively produce accurate representation of the topography is its ability for three-dimensional mapping of the surface [96, 98]. AFM creates images by scanning a micro-scale cantilever with a sharp tip across the surface in a non-destructive manner and can be performed on bulk samples to reveal nano-scale topographical information about soft matter, without the need for complex sample preparation [99].

The tip is the heart of the instrument [98], giving rise to the image through force interactions; and it is mounted on the end of the cantilever. Important characteristics of the tip are the sharpness of the apex, the radius of curvature, and the ratio of the tip curvature to tip height [98]. AFM images are formed by the interaction forces that are recorded between the tip and the sample, and a feedback loop is essential for the accuracy of the images produced. Principally, the AFM utilizes the tip to scan across a surface in a horizontal pattern and back, controlled by the AFM electronics [98], [100].

Normally, the AFM cantilever has three modes of operation: contact, non-contact, and tapping mode [101]. The non-contact mode is utilized by moving the cantilever away from the sample surface and oscillating the cantilever at/near its natural resonance frequency. Contact mode monitors the interaction forces while the cantilever tip is in contact with the sample. Tapping mode combines characteristics of both contact and non-contact modes by gathering sample data and oscillating the cantilever tip at/near its natural resonance frequency while allowing the cantilever tip to impact the target sample for a minimal duration of time [101].

7.3.1 AFM and Pharmaceutical Formulations

From a pharmaceutical aspect, AFM has been used to study important factors that may affect the formulation of the end product and all these influence adhesion interactions [53]. A common example that has been extensively studied using the AFM is salbutamol sulphate found in DPIs [53]. This powder was of interest due to its cohesion and de-agglomeration aspects which can be detrimental to the efficacy of the delivered dose as a result of alterations in the size of particles in the dose. Consequently, Young et al. [53] studied the forces between a drug functionalised cantilever and the drug powder to determine drug-drug interaction. As humidity also can affect the homogeneity of pharmaceutical powders, so this aspect was taken into account by using a custom-built perfusion apparatus; this resulted in a domination of capillary interactions with increasing humidity [47, 49, 53].

These studies have successfully demonstrated the strength of AFM as an investigative tool for the quantification of separation energies between micronized particles [2].

Interestingly, the development of the colloidal probe, i.e. an AFM tip with an attached particle, has led to investigations using single particles to understand the fundamental forces which influence pharmaceutical formulations, including understanding of vdW, electrostatic, and capillary forces; and can be applied to understand particle-particle, particle-carrier, and particle-canister/packaging interactions [93]. This technique can be employed to study the forces of interactions, as the morphology of contact area and asperities and surface roughness are directly related [102].

To assess the surface roughness of materials, AFM scans samples using the topography function whereby surface features and asperities can be represented as three-dimensional (3D) images. Data can also be extracted to explore the roughness of samples using the average roughness (Ra) measurements. This technique has been utilised to understand the extent of roughness and the inter-particle interactions between lactose carrier and the drug particles in DPI formulations [103]. Interactions between surfaces of different work functions result in contact potential between the surfaces in question; Coulombic interactions are usually between oppositely charged particles or a charged particle and a neutral surface; whereas capillary forces tend to be influenced by humidity because of the influence of RH on the liquid bridge formation between particles [103]. The AFM has also qualitatively identified intermolecular interactions such as vdW forces and hydrogen bonding [103, 104].

Pharmaceutical powders are susceptible to humidity, and the AFM can monitor changes in adhesion with humidity [105, 106]. From the literature [36, 39, 105, 107] humidity influences the physical and chemical stabilities of the product, control of drug release as well as the properties of the solid dosage form and excipient. Moisture can also govern the dispersion and de-agglomeration behaviour especially in DPIs [36] which influences the performance of the respiratory drug delivery by affecting the aerodynamic properties which are often dependent on the carrier particles [3, 49]. Interestingly, it has been noted through the use of AFM that storage humidity which influences the aerosolisation efficiency is drug dependent [108].

The surface energy, to understand its role in adhesion, has been assessed by AFM [93, 109]. Pierce et al. [110] used AFM to assess the surface energy and work of adhesion of flat surfaces, which could then be adopted for pharmaceutical applications [111, 112]. This investigation emphasised the need for free-flowing particles of controlled size and morphology to ensure homogeneous powders for pharmaceutical formulations, Hooton et al. [111] applied this concept to study interactions between pharmaceutical particles by determining the contact area [93, 111]. More recently, it has been highlighted that the contacting asperities must be considered rather than the overall contact area [65, 112].

7.3.2 Advantages of AFM

It has also been demonstrated [49] that there are three main inter-particle forces within DPI systems: vdW dispersion interactions, electrostatic forces, and capillary interactions. These forces and their contributions to a system are dependent on the material properties and

the environmental conditions (temperature, relative humidity (RH) [47, 49]. The measurements of these fundamental interactions has previously been limited to bulk techniques [47], however, now the AFM has been found to be capable of measuring such forces between individual particles and substrates at specific environmental conditions.

It is important to point out that atmospheric humidity and surface roughness play a role in the adhesion forces; for example, Tsukada et al. [47] noted that with increasing surface roughness of the lactose plate, to mimic lactose carriers by coating a surface, i.e., a plate with lactose, the distributions of adhesion forces between a drug particle and the plate were widely spread and their mean values decreased. Furthermore, adhesion force increased with atmospheric humidity [47]. Humidity also affects the water layer thickness adsorbed on the surface of pharmaceutical particles and it was also determined by AFM. The forces between particles having hydrophilic surfaces were affected more by atmospheric humidity than those with hydrophobic surfaces. In general, adhesion force of more hydrophilic material increased remarkably with increasing humidity and this was precisely evaluated by adhesion force measurement between silica particles with a silica colloid probe. The increase in adhesion force at higher humidity conditions can be caused by the capillary force and surface tension of water due to the formation of a condensed water bridge between the particle and the plate. In addition, the powder once exposed at high humidity did not show the same adhesion force after returning to lower humidity conditions, i.e., the change in adhesion force was irreversible. To conclude, a small curvature particle, rough surface plate with low Hamaker constant material and low humidity in the atmosphere have the tendency to decrease the adhesion force [47].

In order to directly measure the force using the AFM, the tip approaches vertically towards and away from the sample in the z direction, and the relative deflection of the cantilever produces a force-distance curve. The attachment of a drug particle to the apex of a tipless cantilever may be a route for the measurement of drug–drug interactions (Figure 7.8) [49, 53].

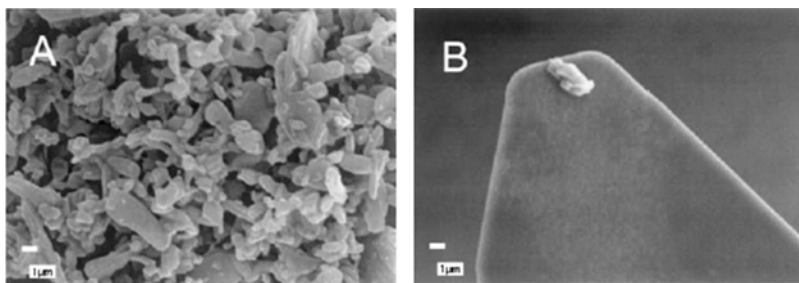


Figure 7.8 Image A represents an SEM image of salbutamol sulphate powder (5000x) and image B demonstrates a salbutamol drug probe attached to AFM cantilever (5000x). *Journal of Pharmaceutical Sciences*, volume 92, issue 4, Young. P. M, Price. R, Tobyn. M. J, Buttrum. M, and Dey, F, Investigation into the Effect of Humidity on Drug-Drug Interactions Using the Atomic Force Microscope, pages 815-822. Copyright 2003, with permission from John Wiley and Sons.

Thus, the degree of cohesiveness between salbutamol sulphate particles will directly influence the aerosolization performance of the drug when administered to a patient via a dry powder inhaler (DPI). Recent *in vitro* aerosolization studies have reported humidity to cause a significant decrease in aerosolization efficiency of micronized salbutamol sulphate from a model DPI [47, 49]. This decrease in aerosolization performance is possibly related to an increase of particle cohesion due to capillary interactions. Such increases in the cohesion and adhesion between micronized pharmaceutical materials at elevated humidities were also demonstrated using the centrifugal technique [49].

Another useful investigation supporting the benefits of using AFM in pharmaceutical investigations is the study of the influence of cohesion-adhesion balance on DPI formulations [113, 114] for drug delivery through the respiratory tract. It is important when formulating powders for use in aerosols to consider their size [113], typically DPI formulations are binary blends of coarse carriers and micronized drugs. The homogeneity, de-aggregation, and dispersion properties tend to be governed by the resulting cohesion due to drug-drug interaction, and adhesion due to drug-excipient interactions [113]. Problems in DPI systems occur when there is excessive adhesion as this may prevent elutriation or separation of particles from the carrier, resulting in upper airway deposition leading to hoarseness as the particles are too large [113]. Likewise, excessive cohesion could enhance the segregation and agglomeration, which directly affects the dispersion characteristics of the formulation. Not only are the drug-drug and drug-excipient adhesion and cohesion interactions important factors when considering the dispersion aspects of the formulation, but the actual inhaler device can directly affect the fluidisation and aerosol characteristics too. Therefore, the aerodynamic forces that are generated within the device have an influential role in the aerosolisation of the powders [113].

Also Begat et al.[113] have used a predictive cohesion-adhesion balance (CAB) which provides a graph of binary and complex formulations which is used to as a rapid pre-formulation tool to determine the relative strength of various interactions forces and to predict the DPI behaviour. AFM was used for this investigation to evaluate interaction forces using a colloid probe technique, to study the specific role of the cohesion and adhesion force balance in the de-agglomeration efficiency and deposition characteristics of the drug. The results revealed a relationship between particle cohesive strength and the de-agglomeration efficiency of drug only formulations. It was also noted that addition of fine particles such as lactose carrier influenced the drug deposition patterns, and was thought to be dependent on the relative cohesion and adhesion force balance in the formulation.

7.4 Prospects

It is evident that the AFM can offer realistic results regarding individual components in formulations. That said, an advantage to the pharmaceutical industry could be to combine this analytical tool with techniques already in use, such as IGC [84], ITC [92], and even NIR [86] to understand formulations at their nano-level, in order to improve and develop aspects of these pharmaceutical products at the macro-level. AFM has and will provide new insights into its extended applications due to its capability for spatial mapping of adhesion

under a range of environments, allowing for specific identification of high adhesion areas and relate these to local morphology and composition [93].

7.5 Summary

Atomic force microscopy since its invention in the early 1980s has proved to be a useful technique to quantify the morphology of surfaces by producing detailed two-dimensional and three-dimensional images. Not only can AFM produce real images of a wide range of materials from hard metals to delicate biological samples in optimum environmental conditions, but can also analyse interfacial interactions associated with these materials by employing colloidal probe techniques. Over the years many models of adhesion have been proposed considering the physical and mechanical aspects of adhesion, including DLVO, XDLVO, JKR and DMT. Yet it has been observed that these traditional theories are limited to ideal colloidal materials approaching atomically flat surfaces; therefore, new models have been introduced recently which include a more rounded approach to understanding adhesion. These new models have been built on the original theories by adding protocols to include certain characteristics known to govern the extent of adhesion, including the physicochemical properties of materials including size, shape, surface topography and morphology. Others have considered the interactions that often occur such as van der Waals forces of attraction, electrostatic repulsive interactions, as well as capillary forces, all of which can have a detrimental impact on the formulation of pharmaceutical and biomedical products. A greater understanding of the adhesion phenomena by employing better techniques to investigate adhesion, should be beneficial for industry, and AFM is the technique for this purpose in combination with some traditional procedures already in place in the pharmaceutical industry. Improvements in formulations would help produce cost-effective, less time consuming quality assured products which is advantageous for the industry as well as beneficial to patients care and well-being.

Acknowledgments

The authors would like to acknowledge financial support from Arthritis Research UK (ARUK:18461) and Cardiff University School of Pharmacy and Pharmaceutical Science.

References

1. P.G.A. Rogueda, R. Price, T. Smith, P.M. Young, and D. Traini, Particle synergy and aerosol performance in non-aqueous liquid of two combinations metered dose inhalation formulations: An AFM and Raman investigation. *J. Colloid Interface Sci.* 361, 649–655 (2011).
2. P.M. Young, H. Adi, T. Patel, K. Law, P. Rogueda, and D. Traini, The influence of micronised particulates on the aerosolisation properties of pressurised metered dose inhalers. *J. Aerosol Sci.* 40, 324–337 (2009).
3. D. Traini, P.M. Young, P. Rogueda, and R. Price, The use of AFM and surface energy measurements to investigate drug-canister material interactions in a model pressurized metered dose inhaler formulation. *Aerosol Sci. Technol.* 40, 227–236 (2006).

4. P. Prokopovich and V. Starov, Adhesion models: From single to multiple asperity contacts. *Adv. Colloid Interface Sci.* 168, 210–222 (2011).
5. P. Prokopovich, S. Perni, J. Fisher, and R.M. Hall, Spatial variation of wear on Charité lumbar discs. *Acta Biomaterialia* 7, 3914–3926 (2011).
6. K. Autumn, M. Sitti, Y.A. Liang, A.M. Peattie, W.R. Hansen, S. Sponberg, T.W. Kenny, R. Fearing, J.N. Israelachvili, and R.J. Full, Evidence for van der Waals adhesion in gecko setae. *Proc. Nat. Acad. Sci.(USA)* 99, 12252–12256 (2002).
7. K. Autumn, Y.A. Liang, S.T. Hsieh, W. Zesch, W.P. Chan, T.W. Kenny, R. Fearing, and R.J. Full, Adhesive force of a single gecko foot-hair. *Nature* 405, 681–685 (2000).
8. T. Endlein, A. Ji, D. Samuel, N. Yao, Z. Wang, W.J.P. Barnes, W. Federle, M. Kappl, and Z. Dai, Sticking like sticky tape: Tree frogs use friction forces to enhance attachment on overhanging surfaces. *J. R. Soc. Interface* 10, 20120838 (2013).
9. O. Dos Santos Ferreira, E. Gelinck, D. De Graaf, and H. Fischer, Adhesion experiments using an AFM--Parameters of influence. *Appl. Surf. Sci.* 257, 48–55 (2010).
10. A.D. Zimon, *Adhesion of Dust and Powder*, second edition, pp. 1–30, Springer, New York (1982).
11. E.M.V. Hoek and G.K. Agarwal, Extended DLVO interactions between spherical particles and rough surfaces. *J. Colloid Interface Sci.* 298, 50–58 (2006).
12. A. Baldan, Adhesion phenomena in bonded joints. *Int. J. Adhesion Adhesives.* 38, 95–116 (2012).
13. N.P. Boks, W. Norde, H.C. Van der Mei, and H.J. Busscher, Forces involved in bacterial adhesion to hydrophilic and hydrophobic surfaces. *Microbiology* 154, 3122–3133 (2008).
14. T.S. McDermott, J. Farrenkopf, A. Hlinak, J.P. Neilly, and D. Sauer, A material sparing method for quantitatively measuring tablet sticking. *Powder Technol.* 212, 240–252 (2011).
15. F. Waimer, M. Krumme, U. Danz, P. Tenter, and C. Wchmidt, A novel method for the detection of sticking of tablets. *Pharm. Dev. Technol.* 4, 359–367 (1999).
16. B.V. Derjaguin, V.M. Muller, and Y.P. Toporov, Effect of contact deformation on the adhesion of particles. *J. Colloid Interface Sci.* 53, 314–326 (1975).
17. K.L. Johnson, K. Kendall, and A.D. Roberts, Surface energy and the contact of elastic solids. *Proc. Royal Soc. (London) A* 324, 301–313 (1971).
18. L. Espinasse, L. Keer, F. Borodich, H. Yu, and Q. Jane Wang, A note on JKR and DMT theories of contact on a transversely isotropic half-space. *Mech. Mater.* 42, 477–480 (2010).
19. N.V. Churaev, The DLVO theory in Russian colloid science. *Adv. Colloid Interface Sci.* 83, 19–32 (1999).
20. K. Li and Y. Chen, Evaluation of DLVO interaction between a sphere and a cylinder. *Colloids Surfaces A* 415, 218–229 (2012).
21. S.J. Chidlow, W.W.F. Chong, and M. Teodorescu, On the two-dimensional solution of both adhesive and non-adhesive contact problems involving functionally graded materials. *Eur. J. Mech. A* 39, 86–103 (2013).
22. J. Azeredo, J. Visser, and R. Oliveira, Exopolymers in bacterial adhesion: Interpretation in terms of DLVO and XDLVO theories. *Colloids Surfaces B* 14, 141–148 (1999).
23. V.T. Nguyen, T.W.R. Chia, M.S. Turner, N. Fegan, and G.A. Dykes, Quantification of acid–base interactions based on contact angle measurement allows XDLVO predictions to attachment of *Campylobacter jejuni* but not *Salmonella*. *J. Microbiol. Methods* 86, 89–96 (2011).
24. C.V. Chrysikopoulos and V.I. Syngouna, Attachment of bacteriophages MS2 and Φ X174 onto kaolinite and montmorillonite: Extended-DLVO interactions. *Colloids Surfaces B* 92, 74–83 (2012).

25. P. Prokopovich and S. Perni, Comparison of JKR- and DMT-based multi-asperity adhesion model: Theory and experiment. *Colloids Surfaces. A* 383, 95–101 (2011).
26. G. Liu, S. Li, and Q. Yao, A JKR-based dynamic model for the impact of micro-particle with a flat surface. *Powder Technol.* 207, 215–223 (2011).
27. M. Rundlöf, M. Karlsson, L. Wågberg, E. Poptoshev, M. Rutland, and P. Claesson, Application of the JKR method to the measurement of adhesion to Langmuir–Blodgett cellulose surfaces. *J. Colloid Interface Sci.* 230, 441–447 (2000).
28. G. Carbone and F. Bottiglione, Asperity contact theories: Do they predict linearity between contact area and load? *J. Mech. Phys. Solids* 56, 2555–2572 (2008).
29. S.H. Kim, M.T. Dugger, and K.L. Mittal, (Eds.) *Adhesion Aspects in MEMS and NEMS*, CRC Press, Boca Raton, FL (2011).
30. J.A. Williams and H.R. Le, Tribology and MEMS. *J. Phys. D: Appl. Phys.* 39, R201 (2006).
31. H.W. Frijlink and A.H.D. Boer, Dry Powder Inhalers for pulmonary drug delivery. *Expert Opin. Drug Deliv.* 1, 67–86 (2004).
32. E. Meng-Lund, C. Muff-Westergaard, C. Sander, P. Madelung, and J. Jacobsen, A mechanistic based approach for enhancing buccal mucoadhesion of chitosan. *Int. J. Pharm.* 461, 280–285 (2014).
33. B. Tansel and D.Z. Tansel, Adhesion strength and spreading characteristics of EPS on membrane surfaces during lateral and central growth. *Colloids Surfaces B* 111, 594–599 (2013).
34. M. Fuji, K. Machida, T. Takei, T. Watanabe, and M. Chikazawa, Effect of surface geometric structure on the adhesion force between silica particles. *J. Phys. Chem. B* 102, 8782–8787 (1998).
35. J. Israelachvili and H. Wennerstrom, Role of hydration and water structure in biological and colloidal interactions. *Nature* 379, 219–225 (1996).
36. K. Zhu, R.B.H. Tan, W. Kiong Ng, S. Shen, Q. Zhou, and P.W.S. Heng, Analysis of the influence of relative humidity on the moisture sorption of particles and the aerosolization process in a dry powder inhaler. *J. Aerosol Sci.* 39, 510–524 (2008).
37. D. Weber, Y. Pu, and C.L. Cooney, Quantification of lubricant activity of magnesium stearate by atomic force microscopy. *Drug Dev. Ind. Pharm.* 34, 1097–1099 (2008).
38. J.J. Wang, M.A. Guillot, S.D. Bateman, and K.R. Morris, Modeling of adhesion in tablet compression. II. Compaction studies using a compaction simulator and an instrumented tablet press. *J. Pharm. Sci.* 93, 407–417 (2004).
39. R. Price, P.M. Young, S. Edge, and J.N. Staniforth, The influence of relative humidity on particulate interactions in carrier-based dry powder inhaler formulations. *Int. J. Pharm.* 246, 47–59 (2002).
40. X. Xiao and L. Qian, Investigation of humidity-dependent capillary force. *Langmuir* 16, 8153–8158 (2000).
41. H.W. Frijlink and A.H. De Boer, Trends in the technology-driven development of new inhalation devices. *Drug Discov. Today: Technol.* 2, 47–57 (2005).
42. Patient.co.uk, Oral Thrush. <http://www.patient.co.uk/health/oral-thrush> accessed on 27/04/2014
43. C. Vervaet and J.P. Remon, Continuous granulation in the pharmaceutical industry. *Chem. Eng. Sci.* 60, 3949–3957 (2005).
44. P. Kleinebudde, Roll compaction/dry granulation: Pharmaceutical applications. *European J. Pharm. Biopharm.* 58, 317–326 (2004).
45. R.P. Patel and A.M. Suthar, Ensuring better control of granulation. *Eur. J. Pharm. Sci.* 21, 533–543 (2008).

46. J. Krawczyk, K. Szymczyk, A. Zdziennicka, and B. Jańczuk, Wettability of polymers by aqueous solution of binary surfactants mixture with regard to adhesion in polymer–solution system II. Critical surface tension of polymers wetting and work of adhesion. *Int. J. Adhesion Adhesives* 45, 106–111 (2013).
47. M. Tsukada, R. Irie, Y. Yonemochi, R. Noda, H. Kamiya, W. Watanabe, and E.I. Kauppinen, Adhesion force measurement of a DPI size pharmaceutical particle by colloid probe atomic force microscopy. *Powder Technol.* 141, 262–269 (2004).
48. M.H. Shariare, M. De Matas, P. York, and Q. Shao, The impact of material attributes and process parameters on the micronisation of lactose monohydrate. *Int. J. Pharm* 408, 58–66 (2011).
49. P.M. Young, R. Price, M.J. Tobyn, M. Buttrum, and F. Dey, Investigation into the effect of humidity on drug–drug interactions using the atomic force microscope. *J. Pharm. Sci.* 92, 815–822 (2003).
50. K. Zhu, R.B.H. Tan, F. Chen, K.H. Ong, and P.W.S. Heng, Influence of particle wall adhesion on particle electrification in mixers. *Int. J. Pharm.* 328, 22–34 (2007).
51. R. Ashayer, P.F. Luckham, S. Manimaaran, and P. Rogueda, Investigation of the molecular interactions in a pMDI formulation by atomic force microscopy. *Eur. J. Pharm. Sci.* 21, 533–543 (2004).
52. K.J. McDonald and G.P. Martin, Transition to CFC-free metered dose inhalers — into the new millennium. *Int. J. Pharm.* 201, 89–107 (2000).
53. P.M. Young, R. Price, D. Lewis, S. Edge, and D. Traini, Under pressure: Predicting pressurized metered dose inhaler interactions using the atomic force microscope. *J. Colloid Interface Sci.* 262, 298–302 (2003).
54. C. Vervaet and P.R. Byron, Drug–surfactant–propellant interactions in HFA-formulations. *Int. J. Pharm.* 186, 13–30 (1999).
55. J.K. Eve, N. Patel, S.Y. Luk, S.J. Ebbens, and C.J. Roberts, A study of single drug particle adhesion interactions using atomic force microscopy. *Int. J. Pharm.* 238, 17–27 (2002).
56. X.M. Zeng, G.P. Martin, C. Marriott, and J. Pritchard, The influence of crystallization conditions on the morphology of lactose intended for use as a carrier for dry powder aerosols. *J. Pharmacol. Pharmacother.* 52, 633–643 (2000).
57. H. Watanabe, M. Ghadiri, T. Matsuyama, Y.L. Ding, K.G. Pitt, H. Maruyama, S. Matsusaka, and H. Masuda, Triboelectrification of pharmaceutical powders by particle impact. *Int. J. Pharm.* 334, 149–155 (2007).
58. P. Feenstra, M. Brunsteiner, and J. Khinast, Prediction of drug–packaging interactions via molecular dynamics (MD) simulations. *Int. J. Pharm.* 431, 26–32 (2012).
59. V. Bérard, E. Lesniewska, C. Andrès, D. Pertuy, C. Laroche, and Y. Pourcelot, Affinity scale between a carrier and a drug in DPI studied by atomic force microscopy. *Int. J. Pharm.* 247, 127–137 (2002).
60. J.N. Israelachvili, *Intermolecular and Surface Forces*. third edition, pp. 415–467, Elsevier, London (2011).
61. V. Mazel, V. Busignies, H. Diarra, I. Reiche, and P. Tchoreloff, The surface layer of pharmaceutical compacts: The role of the punch surface and its impact on the mechanical properties of the compacts. *Int. J. Pharm.* 442, 42–48 (2013).
62. D.W. Grimbale, S. Theodossiadis, H. Rahnejat, and M. Wilby, Thin film tribology of pharmaceutical elastomeric seals. *Appl. Math. Model.* 37, 406–419 (2013).

63. G. Hwang, I.-S. Ahn, B.J. Mhin, and J.-Y. Kim, Adhesion of nano-sized particles to the surface of bacteria: Mechanistic study with the extended DLVO theory. *Colloids Surfaces. B* 97, 138–144 (2012).
64. S. Eichenlaub, A. Gelb, and S. Beaudoin, Roughness models for particle adhesion. *J. Colloid Interface Sci.* 280, 289–298 (2004).
65. P. Prokopovich and S. Perni, Multiasperity contact adhesion model for universal asperity height and radius of curvature distributions. *Langmuir* 26, 17028–17036 (2010).
66. J. Katainen, M. Paaanen, E. Ahtola, V. Pore, and J. Lahtinen, Adhesion as an interplay between particle size and surface roughness. *J. Colloid Interface Sci.* 304, 524–529 (2006).
67. A. Barnett, R.L. Berkowitz, R. Mills, and L.M. Vistnes, Comparison of synthetic adhesive moisture vapor permeable and fine mesh gauze dressings for split-thickness skin graft donor sites. *Am. J. Surg.* 145, 379–381 (1983).
68. M.G. Jeschke, C. Rose, P. Angele, B. Füchtmeier, M.N. Nerlich, and U. Bolder, Development of new reconstructive techniques: Use of integra in combination with fibrin glue and negative-pressure therapy for reconstruction of acute and chronic wounds. *Plast. Reconstr. Surg.* 113, 525–530 (2004).
69. A.V. Spuskanyuk, R.M. Mcmeeking, V.S. Deshpande, and E. Arzt, The effect of shape on the adhesion of fibrillar surfaces. *Acta Biomaterialia* 4, 1669–1676 (2008).
70. H. Gao, X. Wang, H. Yao, S. Gorb, and E. Arzt, Mechanics of hierarchical adhesion structures of geckos. *Mech. Mater.* 37, 275–285 (2005).
71. Y.I. Rabinovich, J.J. Adler, A. Ata, R.K. Singh, and B.M. Moudgil, Adhesion between nanoscale rough surfaces: I. Role of asperity geometry. *J. Colloid Interface Sci.* 232, 10–16 (2000).
72. K. Cooper, A. Gupta, and S. Beaudoin, Simulation of the adhesion of particles to surfaces. *J. Colloid Interface Sci.* 234, 284–292 (2001).
73. S. You and M.P. Wan, Mathematical models for the van der Waals force and capillary force between a rough particle and surface. *Langmuir* 29, 9104–9117 (2013).
74. K.K. Lam and J.M. Newton, Influence of particle size on the adhesion behaviour of powders, after application of an initial press-on force. *Powder Technol.* 73, 117–125 (1992).
75. C. Wandrey, U. Hasegawa, A.J. van der Vlies, C. O’Neil, N. Angelova, and J.A. Hubbell, Analytical ultracentrifugation to support the development of biomaterials and biomedical devices. *Methods* 54, 92–100 (2011).
76. T. Laue, Analytical ultracentrifugation: A powerful ‘new’ technology in drug discovery. *Drug Discov. Today: Technol.* 1, 309–315 (2004).
77. J. Liu, and S.J. Shire, Analytical ultracentrifugation in the pharmaceutical industry. *J. Pharm. Sci.* 88, 1237–1241 (1999).
78. M. Paaanen, J. Katainen, J. Raula, E.I. Kauppinen, and J. Lahtinen, Direct evidence on reduced adhesion of Salbutamol sulphate particles due to L-leucine coating. *Powder Technol.* 192, 6–11 (2009).
79. H.J. Butt, Capillary forces: Influence of roughness and heterogeneity. *Langmuir* 24, 4715–4721 (2008).
80. Y.I. Rabinovich, J.J. Adler, M.S. Esayanur, A. Ata, R.K. Singh, and B.M. Moudgil, Capillary forces between surfaces with nanoscale roughness. *Adv. Colloid Interface Sci.* 96, 213–230 (2002).
81. F.M. Etzler, Particle adhesion in the pharmaceutical sciences, in: *Recent Advances in Adhesion Science and Technology* (in honor of Dr. Kash Mittal), W. Gutowski and H. Dodiuk (Eds.) pp. 41–66, CRC Press, Boca Raton, FL (2014).
82. H.J. Butt and M. Kappl, Normal capillary forces. *Adv. Colloid Interface Sci.* 146, 48–60 (2009).

83. K.L. Mittal, The role of the interface in adhesion phenomena. *Polym. Eng. Sci.* 17, 467–473 (1977).
84. G. Buckton and H. Gill, The importance of surface energetics of powders for drug delivery and the establishment of inverse gas chromatography. *Adv. Drug Deliver. Rev.* 59, 1474–1479 (2007).
85. J.D. Stephens, M.V. Lakshmaiah, B.R. Kowalczyk, B.C. Hancock, and C. Cetinkaya, Wireless transmission of ultrasonic waveforms for monitoring drug tablet properties and defects. *Int. J. Pharm.* 442, 35–41 (2013).
86. M. Blanco, M. Alcala, J.M. Gonzalez, and E. Torras, A process analytical technology approach based on near infrared spectroscopy: Tablet hardness, content uniformity, and dissolution test measurements of intact tablets. *J. Pharm. Sci.* 95, 2137–2144 (2006).
87. M.D. Jones, P. Young, and D. Traini, The use of inverse gas chromatography for the study of lactose and pharmaceutical materials used in dry powder inhalers. *Adv. Drug Deliver. Rev.* 64, 285–293 (2012).
88. S. Montecinos and S.N. Simison, Study of the corrosion products formed on a multiphase CuAlBe alloy in a sodium chloride solution by micro-Raman and in situ AFM measurements. *Appl. Surf. Sci.* 257, 7732–7738 (2011).
89. M. Muniz-Miranda and M. Innocenti, AFM and micro-Raman investigation on filters coated with silver colloidal nanoparticles. *Appl. Surf. Sci.* 226, 125–130 (2004).
90. V. Kumar, M.K. Taylor, A. Mehrotra, and W.C. Stagner, Real-time particle size analysis using focused beam reflectance measurement as a process analytical technology tool for a continuous granulation-drying-milling process. *AAPS Pharma.Sci.Technol.* 14, 523–530 (2013).
91. M. Blanco, M. Bautista, and M. Alcala, API determination by NIR spectroscopy across pharmaceutical production process. *AAPS Pharma.Sci.Technol.* 9, 1130–1133 (2008).
92. J. Ooi, S. Gaisford, B.J. Boyd, P.M. Young, and D. Traini, Isothermal calorimetry: A predictive tool to model drug-propellant interactions in pressurized metered dose systems. *Int.J.Pharm.* 461, 301–309 (2014).
93. C.J. Roberts, What can we learn from atomic force microscopy adhesion measurements with single drug particles? *Eur. J. Pharm. Sci.* 24, 153–157 (2005).
94. J. Ralston, I. Larson, M.W. Rutland, A.A. Feiler, and M. Kleun, Atomic force microscopy and direct surface force measurements. *Pure Appl. Chem.* 77, 2149–2170 (2005).
95. J.A. Last, P. Russell, P.F. Nealey, and C.J. Murphy, The applications of atomic force microscopy to vision science. *Invest. Ophth. Vis. Sci.* 51, 6083–6094 (2010).
96. J.L. Alonso and W.H. Goldmann, Feeling the forces: Atomic force microscopy in cell biology. *Life Sci.* 72, 2553–2560 (2003).
97. H.X. You, J.M. Lau, S. Zhang, and L. Yu, Atomic force microscopy imaging of living cells: A preliminary study of the disruptive effect of the cantilever tip on cell morphology. *Ultramicroscopy* 82, 297–305 (2000).
98. P.C. Braga and D. Ricci, Imaging methods in atomic force microscopy, in *Atomic Force Microscopy: Biomedical Methods and Applications, Methods in Molecular Biology*, P.C. Braga and D. Ricci, (Eds.), pp. 13–23, Humana Press, Totowa, New Jersey (2004).
99. J.M.R. Tilley, A.J. Carr, and J.T. Czernuszka, Atomic force microscopy of bulk tendon samples: Effect of location and fixation on tissue ultrastructure. *Micron* 42, 531–535 (2011).
100. D. Fotiadis, S. Scheuring, S.A. Müller, A. Engel, and D.J. Müller, Imaging and manipulation of biological structures with the AFM. *Micron* 33, 385–397 (2002).
101. N. Jalili and K. Laxminarayana, A review of atomic force microscopy imaging systems: Application to molecular metrology and biological sciences. *Mechatronics* 14, 907–945 (2004).

102. U. Sindel and I. Zimmermann, Measurement of interaction forces between individual powder particles using an atomic force microscope. *Powder Technol.* 117, 247–254 (2001).
103. N. Islam, P. Stewart, I. Larson, and P. Hartley, Surface roughness contribution to the adhesion force distribution of salmeterol xinafoate on lactose carriers by atomic force microscopy. *J. Pharm. Sci.* 94, 1500–1511 (2005).
104. J. Drelich and K.L. Mittal (Eds.), *Atomic Force Microscopy in Adhesion Studies*. CRC Press, Boca Raton, FL (2005).
105. V. Bérard, E. Lesniewska, C. Andrès, D. Pertuy, C. Laroche, and Y. Pourcelot, Dry powder inhaler: Influence of humidity on topology and adhesion studied by AFM. *Int. J. Pharm.* 232, 213–224 (2002).
106. E.R. Beach and J. Drelich, Atomic force microscope pull-off force measurements for insulin in contact with acrylonitrile-butadiene-styrene and polypropylene surfaces at various humidities. *J. Adhesion. Sci. Technol.* 25, 435–449 (2011).
107. A. Elajnaf, P. Carter, and G. Rowley, Electrostatic characterisation of inhaled powders: Effect of contact surface and relative humidity. *Eur. J. Pharm. Sci.* 29, 375–384 (2006).
108. R.N. Jashnani and P.R. Byron, Dry powder aerosol generation in different environments: performance comparisons of albuterol, albuterol sulfate, albuterol adipate and albuterol stearate. *Int. J. Pharm.* 130, 13–24 (1996).
109. E.M. Etzler and J. Drelich, Atomic force microscopy for characterization of surfaces, particles and their interactions, in: *Developments in Surface Contamination and Cleaning*, Vol. 4, R. Kohli and K.L. Mittal (Eds.), pp. 307–331, Elsevier, Oxford, UK (2012).
110. M. Pierce, J. Stuart, A. Pungor, P. Dryden, and V. Hlady, Adhesion force measurements using an atomic force microscope upgraded with a linear position sensitive detector. *Langmuir* 10, 3217–3221 (1994).
111. J. Hooton, C. German, S. Allen, M. Davies, C. Roberts, S.B. Tendler, and P. Williams, Characterization of particle-Interactions by atomic force microscopy: Effect of contact area. *Pharmaceut. Res.* 20, 508–514 (2003).
112. J.C. Hooton, C.S. German, M.C. Davies, and C.J. Roberts, A comparison of morphology and surface energy characteristics of sulfathiazole polymorphs based upon single particle studies. *Eur. J. Pharm. Sci.* 28, 315–324 (2006).
113. P. Begat, D.A. Morton, J.N. Staniforth, and R. Price, The cohesive-adhesive balances in dry powder inhaler formulations II: Influence on fine particle delivery characteristics. *Pharma Res.* 21, 1826–1833 (2004).
114. F.L. Leite and P.S.P. Herrmann, Application of atomic force spectroscopy (AFS) to studies of adhesion phenomena: A review, in: *Atomic Force Microscopy in Adhesion Studies* J. Drelich and K.L. Mittal (Eds.) pp. 3–43, CRC Press, Boca Raton, FL (2005).
115. Y.I. Rabinovich, J.J. Adler, A. Ata, R.K. Singh, and B.M. Moudgil, Adhesion between nanoscale rough surfaces: II. Measurement and comparison with theory. *J. Colloid Interface Sci.* 232, 17–24 (2000).

Cyanoacrylate Adhesives in Surgical Applications

Edward M. Petrie

Industry Consultant, EMP Solutions, Cary, NC, USA

Abstract

Medical adhesives are considered to be a strong alternative to sutures in future clinical applications. Cyanoacrylates were first used for clinical applications in the early 1960s and have received prominent attention as a medical polymer. However, even today, few surgeons use cyanoacrylate adhesives except in unusual circumstances or in emergency cases. Improvements in biocompatibility, adhesion, and application characteristics will need to be addressed before these materials gain greater acceptance. This review provides a description of the chemistry, main categories, formulation modifications, and clinical applications of medical-grade cyanoacrylate adhesives that have been developed over the last 50 years. The review also recognizes the value of cyanoacrylate adhesives in surgery today, their future potential if unmet needs can be satisfied, and the most likely pathways for improvement.

Keywords: Cyanoacrylate, tissue, surgery, toxicity, medical, biocompatibility, sutures, adhesives, sealants, hemostats

8.1 Introduction

The subject of medical adhesives has a long history, is very wide-ranging, and encompasses a variety of materials that can be applied to a number of clinical procedures including surgery. As a result of advances in healthcare, such as non-invasive surgery and laparoscopic surgery, there are many clinical trials underway to evaluate the efficacy of surgical adhesives. However, the application of surgical adhesives in the operating room is still controversial and must be matched to specific tissue types as well as to a large and increasing number of procedures.

*Corresponding author: empetrie@hotmail.com

A universal adhesive does not exist, and there is very limited choice for applications inside the human body.

The medical community is, therefore, in search of adhesives which swiftly bond tissues, replace mechanical fasteners such as staples and sutures and which are biocompatible, biodegradable, and do not interfere with the healing process. Continued research and development is necessary to find new or improved adhesive systems. However, the following fundamental functions of surgical adhesives have not changed over time:

- Fixation of the structures and surfaces which are to be bonded
- Filling of cavities and gaps
- Reduce or eliminate bleeding
- Regulation of moisture content
- Protection of the wound from outside environment (water, stress, bacteria, etc.)
- Support the healing process.

Over the entire range of surgical adhesives, cyanoacrylates have unique properties that set them apart from others and have been exploited for topical tissue repair and closure. For example, cyanoacrylate adhesives are replacing sutures in external applications, and they are the most widely used adhesives for bonding traumatized tissues[1]. Cyanoacrylates are also being suggested and clinically tested in many internal surgical procedures.

Cyanoacrylate adhesives were originally developed in the late 1940s, and their potential as a medical adhesive became evident during the Vietnam War as a hemostat for soldiers wounded in field combat. These compounds entered the clinical market in the 1980s as dental products, liquid bandages, and wound closure adhesives. Today, several products are approved by the FDA and other regulatory agencies.

The use of cyanoacrylate adhesives in surgery is significant because of their unique combination of chemical and physical properties. They are single-component, catalyst-free adhesives capable of bonding at room temperature within just a few seconds. Cyanoacrylates require no external initiation, relying only on the small amounts of adsorbed water and chemicals on the tissue surface for cure. Unlike sutures, which leave small openings in the wound, cyanoacrylates form a continuous seal which efficiently distributes the load and leads to decreased scarring. These adhesives can also act as a liquid bandage to protect the wound and even act as a reservoir for antibacterial medication.

8.1.1 Basic Requirements of Surgical Adhesives

One can understand how far cyanoacrylates have come and also how far they still need to go by considering the general requirements imposed on a surgical adhesive. Five criteria are important in the use of surgical adhesives: safety, effectiveness, usability, cost, and regulatory approval[2]. Cost is an important consideration because some adhesives are relatively expensive compared to traditional surgical techniques. Only products that satisfy all of these criteria will be recognized and widely accepted by the surgical community.

General requirements for surgical adhesives are listed in Table 8.1, but most requirements will depend on the surgical procedure. Surgical adhesives must be nontoxic, safe, and free from risk of infectious transmission. Ideally, they should be bioabsorbable and not persist for a long time as a substance that is foreign to the body. Surgical adhesives should not hinder the healing processes. Appropriate working life, gel time, and mechanical properties will be required for specific procedures. They should bond rapidly to the surrounding tissues in the presence of water or other bodily fluids and provide high adhesive strength. However, the working life and gel time should be long enough for the surgeon to apply

Table 8.1 General Requirements of Surgical Adhesives

Chemical:

- Curable from the liquid state (wetable and spreadable) through polymerization, chemical crosslinking, or solvent evaporation
- Rapidly curable under wet physiological conditions (e.g., blood) at body temperature
- The adhesive should provide sufficient tack for early fixation and opportunity for rearrangement
- Any exothermic or chemical process involved in the curing of the adhesive should not damage the surrounding tissue

Physical:

- Once cured, the adhesive should mimic the mechanical performance of undamaged tissue
- Should not shrink excessively after application
- High bonding strength to tissues
- Tough but pliable

Clinical:

- Should be simple to handle and be easy to store (long shelf-life)
- Viscosity, bond strength, working life, and strength development time should be suitable for the procedure
- Should be sterile

Biological:

- Should not influence the healing process and the regrowth of new tissue where possible
- Adhesive product or degradation products should not affect the tissue (dermatitis, heat and chemical sensitization, etc.) or histotoxicity
- Adhesive or degradation products should not be transferable through the body
- Nontoxic components and degradation products that are bioabsorbable or are metabolized in a reasonable time

Regulatory:

- Should meet appropriate standards and regulations relevant for the procedure (e.g., United States Pharmacopoeia (USP) Class VI Standard and International Standards Organization (ISO) ISO-10993).

the dressing without being rushed. Other properties such as hardness, flexibility, exotherm temperature, etc. are important considerations as they can cause discomfort to the patient.

As with other surgical techniques, the use of surgical adhesives and sealants requires special training in order to attain full value and minimize complications. As with most adhesives and sealants, mixing and application procedures can be critical factors for success. Working time is an important factor that can cause complications and limit the type of procedures that can be performed. Due to toxicological concerns, not all substances are approved by the FDA or other regulatory agencies and some adhesives are limited as yet to only external procedures.

8.1.2 Surgical Substrates

For surgical adhesives, one substrate will always be a bodily tissue (skin, bone, muscle, etc.). These tissues can be external or internal. External substrates are exposed to air, sweat, and other elements, while internal substrates are constantly submerged in bodily fluids. As a result, surgical adhesives must generally bond to wet substrates and provide lasting strength in wet environments. This is indeed a challenge for many adhesive systems.

However, the substrates have many functional groups on their surface which can be used to develop adhesion. Table 8.2 describes tissue surfaces with regard to their functional groups and requirements. Blume and Schwotzer[3] provide an excellent review of the properties of tissue substrates as related to the development of adhesion.

Researchers have also shown that tissue adhesion can strongly be improved by adding functional groups to yield engineered hybrid adhesive materials[4]. These adhesive materials have a blend of different functional groups with specific hydrophobic / hydrophilic ratios.

Table 8.2 Specifics of Tissue Substrates[3]

Tissue Type	Functional Groups on Surface	Specific Requirements for Applied Adhesive
Skin	Waxy lipids: -OH, -NH ₂ Fatty acids: -COOH Proteins: -OH, -COOH, -NH ₂ , -CONH ₂ , -S-S Triglycerides: -COOR	Resistant to water (sweat) and hydrophobic compounds (>C ₂₄)
Teeth	Proteins: -OH, -COOH, -NH ₂ , -CONH ₂ , -S-S Carbonated hydroxyapatite: -OH, PO ₄	Resistant to water (saliva)
Bones	Glycoproteins: -OH, -CHO, -S-S Proteins: -OH, -COOH, -NH ₂ , -CONH ₂ , -S-S Calcium hydroxyapatite: -OH, PO ₄ , Ca ²⁺ Phospholipids: -OH, -COOH, -NH ₂ , PO ₄	Wet bonding process, injectable, resorbable
Blood vessels	Phospholipids: -OH, -COOH, -NH ₂ , PO ₄ Proteins: -OH, -COOH, -NH ₂ , -CONH ₂ , -S-S	Wet bonding process, injectable, resorbable

8.1.3 Scope and Objectives of this Review

From the above requirements it is apparent that there is no single surgical adhesive that is currently acceptable in the majority of procedures. Arguably, cyanoacrylates have generated the most interest and have the greatest potential. Cyanoacrylate adhesives have several benefits and limitations in surgical applications (Table 8.3), and today their surgical applications are limited mainly to external or temporary use. However, their formulation opportunities promise new developments that will compete strongly not only for wound closures but for other surgical procedures as well.

As a result of this anticipated success, cyanoacrylate surgical adhesives are the focus of this review article. Improvements in safety, biodegradation rate, tissue adhesion, and application characteristics will need to be addressed before these materials gain greater acceptance. This review provides a description of the chemistry, categories, formulation modifications, and clinical applications of medical-grade cyanoacrylate adhesives that have been developed over the last 50 years. The value of cyanoacrylates in today's surgery, their unmet needs, and likely pathways for improvement are identified.

8.2 Types of Surgical Adhesives

8.2.1 Full Scope of Surgical Adhesives

The full scope of medical adhesives (Figure 8.1) includes those used for surgery (tissue adhesives), pressure-sensitive adhesives used for bandages, tapes, labels, etc. and assembly adhesives used to assemble various medical products. This review focuses on cyanoacrylate

Table 8.3 Benefits and Limitations of Cyanoacrylate Adhesives in Surgical Procedures

Benefits	Limitations
<ul style="list-style-type: none"> • Simple cure mechanism • Rapid strength development • No measuring or mixing required • High tensile-shear strength (approximately an order of magnitude greater than other surgical adhesives) • Excellent adhesion to a wide variety of substrates including human tissues and graft materials • High strength possible on polyolefins and fluorocarbons using primers • Available in FDA approved, USP Class VI, and ISO 10993 compliant formulations 	<ul style="list-style-type: none"> • Significant reactivity results in short shelf-life • Due to reactivity, precautions are needed for application and delivery • Limited gap cure • Soluble in polar solvents • Relatively high material cost • Toxic byproducts (e.g., formaldehyde) can form on degradation causing inflammation (additive scavengers can reduce this risk) • Heat produced from the curing reaction can cause inflammation • N-butyl-cyanoacrylate is relatively rigid (octyl-cyanoacrylate has significantly higher flexibility)

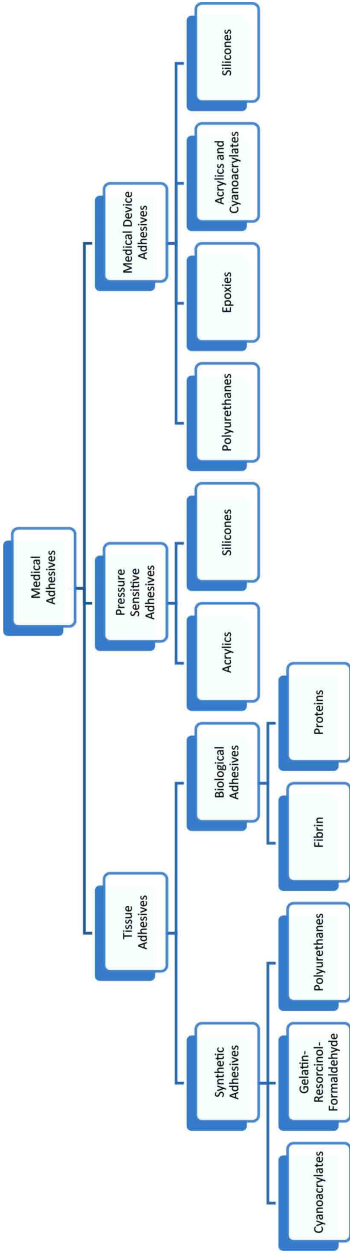


Figure 8.1 The full scope of medical adhesives[5].

adhesives for surgical applications, and this section deals with other surgical adhesives that may be considered for similar functions. These adhesives can be considered competitors of cyanoacrylate adhesives in certain procedures.

Surgical adhesives are used during a surgery or after a traumatic injury to bond together external or internal bodily tissues. Surgical adhesives can be used as alternatives to or in conjunction with more conventional methods of closure such as sutures or staples.

Confusion sometimes exists regarding the differences between a surgical “adhesive”, “sealant”, and “hemostat”. They do similar tasks such as sealing post-operative internal air or fluid leaks or closing a topical wound, but each has specific advantages and disadvantages.

Surgical sealants are absorbable materials used primarily to control internal bleeding and to seal tissue. Sealants prevent the leakage of body elements, thereby reducing risk of complications and enhancing the ability to manipulate fragile tissues. Sealants are generally intended for light bleeding, and they generally degrade rapidly (in a few days to a few weeks). They are often applied over incisions as hemostatic agents. Often they have low or no adhesive strength. The most common type of surgical sealant is fibrin.

Certain sealants have only one function, to help blood clotting, and these are known as “hemostats”.

Intraoperative and postoperative blood losses have always been a primary concern in modern surgery. Sealants as well as adhesives have also been used to stem the flow of blood. In addition, several modern techniques exploit different types of energy to induce blood clotting: monopolar energy (Tissuelink, Salient Surgical Technologies, Dover, NH, USA) or bipolar energy (Ligasure, Covidien, Boulder, CO, USA), and electrocoagulators based on radiofrequency and ultrasound (Ultracision, Johnson & Johnson, New Brunswick, NJ, USA).

Surgical adhesives are stronger than sealants, and they are typically non-absorbable. They provide tissue fixation and attachment to allow easy and rapid operative procedures. Adhesives may have a hemostatic effect if used to reduce the potential for blood loss even though they do not directly cause blood to clot. Surgical adhesives are generally considered to be alternatives to more conventional methods of tissue fastening such as sutures or staples. Adhesives are used in procedures requiring higher bonding strength, sealing of heavy bleeding, and long-term durability. Adhesives are used primarily for bonding tissue-to-tissue and tissue-to-grafts of various types. The most common surgical adhesives are based on cyanoacrylate.

In all cases, these materials go from a liquid phase (during application) to a solid phase (during service) based on some mechanism. These mechanisms include chemical cross-linking by mixing several reactive components together, solvent evaporation or absorption, heat activation, light (laser) activation, and a variety of other energetic methods (ultrasonic, magnetic, etc.).

The combination of formulation and activation mechanism will control how fast the adhesive / sealant sets and this will generally be dictated by the application. For example, cyanoacrylate adhesives are very rapid setting polymers that have been effective embolic agents for brain vascular malformation. However, its application to other procedures, such as aneurysm repair, has been limited seemingly because of the technical difficulties of using the adhesive, such as too rapid a polymerization, precise positioning of the delivery

catheter, accidental bonding to the catheter, premature gellation in the delivery tube, and so forth. Considerable skill is required for cyanoacrylate embolization.

The functions of surgical adhesives and sealants often do not have strict boundaries. Although the adhesive strength of sealants is often considered to be too low to bond wet tissue on their own, they are still considered viable adjuncts for many closure applications such as microvascular surgery and fixation of vascular grafts. Also, cyanoacrylate adhesives are often used to seal and provide embolization even though they are not as elastic as a “sealant”[6]. Surgical sealants and adhesives are often considered together when the surgeon goes through a selection process. In many articles and reports, surgical sealants and adhesives are often colloquially referred to as “glues”.

8.2.2 The Surgeon’s Toolbox

Currently there are several types of surgical or tissue adhesives, which are traditionally classified as either natural (biological) or synthetic. Recently another class of surgical adhesives has been suggested – “biomimetic” adhesives. These are adhesives that attempt to mimic the function of an animal such as a gecko or mussel. In recent years a gecko-mimicking adhesive has been developed for wet tissue adhesion[7]. Biomimetic surgical adhesives are as yet not commercially available.

There are many tissue glues that are currently used in clinical and experimental procedures. Each of these has an optimal clinical application depending on physical and chemical characteristics (bond strength, fluid or solid consistency, activation mechanism, etc.). The strength of these products to tissue varies considerably from product to product, with cyanoacrylate adhesive having the strongest bond strength.

Of these tissue adhesives, five main types appear to be preferred by surgeons:

- Fibrin sealants
- Cyanoacrylates
- Collagen-based compounds (made from bovine collagen and thrombin or human plasma)
- Poly(ethylene glycol) polymers
- Glutaraldehyde products (made from bovine albumin).

Several examples of the manufacturers and their products are provided in Table 8.4. The composition, function, and value of these materials are summarized in the following sections.

8.2.2.1 Fibrin Sealants

Fibrin sealants are a type of surgical adhesive derived from human or animal (bovine) blood products. Fibrin sealants are absorbable, relatively easy to use, and can be kept at room temperature or in a refrigerator prior to use. They are generally used by surgeons for hemostasis and sealing during cardiac surgery, liver surgery, and splenic trauma. Fibrin sealants are commonly used because they are relatively safe, and they have a long history and a wide range of applications.

Table 8.4 Examples of Commercially Available Surgical Adhesives and Sealants by Type

Type of Surgical Adhesive / Sealant	Trade Name / Supplier
Fibrin	TachoComb / CSL Behring, Tokyo, Japan
	Haemseal APR / Haemacure Corp., Sarasota, FL, USA
	Tissel VH / Baxter Healthcare Corp, West Lake Village, CA, USA
Cyanoacrylate	Aventis / Berring GmbH, Marburg, Germany
	Dermabond / Ethicon, Somerville, NJ, USA
	Trufill / Cordis Neurovascular, Inc., Miami Lakes, FL, USA
	Histoacryl / B. Braun, Tuttlingen, Germany
Collagen	Glubran 2 / GEM s.r.l., Viareggio, Italy
	FloSeal/ Sulzer Spine-tech, Anaheim, CA, USA
	Proceed/Fusion Medical Technologies, Mountain View, CA, USA
Poly(ethylene glycol)	CoStasis / Cohesion Technologies, Palo Alto, CA, USA
	AdvaSeal / Ethicon Inc., Somerville, NJ, USA
	CoSeal / Cohesion Technologies Inc., Palo Alto, CA, USA
Glutaraldehyde products	FocalSeal-L / Genzyme Biosurgery Inc., Cambridge, MA, USA
	BioGlue / CryoLife, Inc., Kennesaw, GA, USA
	Cardial / Technopole, Sainte-Etienne, France

It is claimed that the fibrin glues have a powerful hemostatic effect and promote healing by inducing blood clotting. Fibrin sealants essentially mimic the final stages of the coagulation cascade in the human body. They comprise two components: fibrin and thrombin. In the presence of calcium ions, thrombin cleaves the fibrinogen chains to form fibrin monomers, which can then polymerize to produce a physiological fibrin clot. This fibrin clot degenerates by physiologic fibrinolysis in two weeks. The sealant is completely reabsorbed by the body and does not induce an adverse inflammatory tissue reaction.

Formulations of fibrin glues contain two separate components that are reconstituted as two separate systems with sterile water immediately before use and then mixed immediately prior to application. Fibrin sealants tend to polymerize rapidly. Hence, the individual components are generally applied through a double plunger syringe or a double lumen injection needle catheter.

The tensile strength of the fibrin clot is mainly a function of the fibrinogen concentration of the glue. The speed of cure is determined by the thrombin concentration. Fibrin glues usually lack sufficient adhesive strength without the support of suture, staples, or other fixation devices. The adhesive strength is weak (~13 kPa) compared to cyanoacrylate (~68 kPa). TachoComb (CSL Behring, Tokyo, Japan) was determined in one investigation[8] to have a stronger adhesive and sealing potential than other fibrin based adhesives.

Fibrin glue has been used since the 1970s for hemostasis in cardiac surgery[9] and for sealing of vascular grafts and treatment of aortic dissections in vascular surgery[10], as well as many other surgical procedures. Optimal application requires a dry operative field, which can be difficult to achieve, and thus fibrin sealants are most used while the suture line is dry to prevent possible hemorrhage. Fibrin sealants have been applied by endoscopic procedures for the treatment of peptic ulcers and for the prevention of anastomotic leaks during gastric bypass surgery. While fibrin glues have been used in Europe for endoscopic hemostasis in bleeding ulcers and varices, in the US product labeling does not endorse intravascular injection. The University of Virginia Tissue Adhesive Center is a multidisciplinary center that provides educational programs and clinical consultation of sealant use. Their focus appears primarily to be on fibrin based sealants.

The main advantage of using fibrin based adhesives is their lack of toxicity, complete biocompatibility, and a natural degradation process so that healing is not affected. Drawbacks of fibrin products include the method of preparation, relatively low bonding strength, and somewhat variable response time.

8.2.2.2 Cyanoacrylates

The cyanoacrylate tissue adhesives are liquid monomers that polymerize quickly on contact with tissue surfaces in an exothermic reaction creating a strong yet somewhat flexible film that bonds the wound edges. The two primary types of cyanoacrylates used as tissue adhesives are:

- N-butyl-2-cyanoacrylate (Histoacryl, B. Bruan, Tuttlingen, Germany; Glubran 2, GEM S.r.l., Viareggio, Italy; Trufill, Cordis Neurovascular, Inc., Bridgewater, NJ, USA, and others)
- 2-Octyl-cyanoacrylate (Dermabond, Ethicon, Raleigh, NC, USA, and others)

Dermabond and Trufill are approved by the FDA for superficial wound closure, and are used by emergency room physicians, dermatologists, and plastic surgeons for external tissue adhesives. The 2-octyl-cyanoacrylate (OCA) is about three times stronger and more flexible than N-butyl-2-cyanoacrylate[11]. OCA is comparable to 5-0 sutures yet should not be used alone in tissue joints where there may be high post-operative stress.

Unlike fibrin sealants, cyanoacrylates are not bioabsorbable and the body cannot break them down. The degradation products are cyanoacetate and formaldehyde. These products can accumulate in tissues and produce significant histotoxicity characterized by both acute and chronic inflammation. Fibrin glues are generally less toxic than cyanoacrylates; however, they are less strong, less available, and more expensive.

Using cyanoacrylates can avoid sutures -- a great advantage when operating on young children. Cyanoacrylates are waterproof, flexible and require no dressing on the wound. Cyanoacrylate adhesives have many different uses and considerable research is underway on the application of certain cyanoacrylate products in a drug delivery system. The various types of cyanoacrylate surgical adhesives, their formulations, and history of development and clinical use are more fully described in other sections of this review.

8.2.2.3 Collagen-Based Adhesives

Collagen-based adhesives are relatively new, but they show significant potential. Collagen-based compounds are surgical adhesives made from bovine collagen, bovine thrombin, and human plasma. Collagen based compounds assist with coagulation by delivering fibrinogen to the wound area, which helps to control bleeding. Collagen-based adhesives are bioabsorbable and suitable for cardiovascular surgery, though further study is needed to assess long-term risks.

Two of these products are approved for use in the US: FloSeal (Sulzer Spine-tech, Anaheim, CA, USA) and Proceed (Fusion Medical Technologies, Mountain View, CA, USA). FloSeal is marketed for vascular surgery hemostasis, and Proceed is intended for prevention and treatment of cerebrospinal fluid leakage.

CoStasis (Cohesion Technologies, Inc, Palo Alto, CA, USA) is another collagen product that adds autologous human plasma to the bovine collagen and thrombin. The literature suggests that CoStasis provides significant improvement in the control of surgical bleeding in general, as well as in hepatic, cardiovascular, and orthopedic procedures. CoStasis has been successfully used for endoscopic control of severe upper gastrointestinal bleeding from metastatic cancer[12].

8.2.2.4 Poly(ethylene glycol) Polymers

Poly(ethylene glycol) (PEG) polymers are biodegradable agents that can be used to act both as a fluid barrier and as a hemostatic agent. PEG sealant can be applied as a two-component system that crosslinks during bonding. PEG gels can also be crosslinked with visible light in order to provide a seal.

They form an adhesive bond rapidly and are biodegradable in about 1-6 weeks. PEG surgical glues may be more expensive than other products.

PEG sealants have been shown to be useful in preventing dural leaks after neurosurgical procedures. Dural leaks are potentially dangerous because of the possibility of meningitis, and the leaks can lead to severe headache. PEG sealants have also been used in the control of pulmonary air leaks. However, the product swells within the body and must be used sparingly in tight spaces such as intracranial cavities.

One example of this is FocalSeal (Genzyme Biosurgery Inc., Cambridge, MA, USA), which is based on a primer and a sealant. The primer is first brushed on and absorbed by the tissue where it crosslinks. The sealant is applied in the form of an aqueous solution. The sealant is then cured into a gel by photopolymerization with visible blue-green light (450-550 nm). FocalSeal is FDA approved. Another example of this type of adhesive is AdvaSeal, Ethicon, Somerville, NJ, USA. It is a one-component bioabsorbable poly(ethylene glycol) based synthetic compound that undergoes photopolymerization to form a flexible and strongly adhered hydrogel.

PEG polymers have the potential to be very useful. However, at this point the application process is complicated and adds a significant amount of time to the procedure. The photoactivation makes application of the compound difficult and nearly impossible in hemorrhage situations. This obstacle is claimed to be overcome by yet another PEG product

currently being evaluated in the US (CoSeal, Cohesion Technologies, Inc., Palo Alto, CA, USA).

Hydrogels are synthetic PEG polymers commonly used in lung and thoracic surgery due to their ability to seal air leaks. Hydrogels are bio-absorbable and stronger than fibrin sealants. They are also photoactivated, meaning that the sealant sets with exposure to light, which can be a drawback in situations where a patient is hemorrhaging.

8.2.2.5 Albumin and Glutaraldehyde Products

This group of adhesives is based on the combination of albumin and organic compounds to provide adhesion. They are sometimes referred to in the literature as gelatin-resorcinol-formalin (GRF) glues, and contain formaldehyde and glutaraldehyde as an activator. Currently, there is one GRF compound approved in the US (BioGlue, CryoLife Inc., Kennesaw, GA, USA). In BioGlue, the formaldehyde component is left out because of its toxic potential. To date, none of the other GRF glues have been approved by the US FDA because long term outcomes are not yet known.

The glue is composed of purified bovine serum albumin and glutaraldehyde. It utilizes the crosslinking reaction between glutaraldehyde and amine groups for its adhesive effect. The amine groups are supplied by the amino acid lysine, which is abundantly present in bovine serum albumin as well as in extracellular matrices and cell surface proteins. The reaction is rapid (2-3 min) and the resulting scaffold is relatively strong. GRF BioGlue is delivered via a proprietary device that requires minimal set-up time.

BioGlue has been used worldwide in many different surgical locations and procedures including: cardiac (aortic valve replacement, coronary artery bypass grafting, aortic dissection repair, and aneurysm repair of the abdominal aorta), vascular, pulmonary, gastrointestinal tract, and general surgery procedures[13, 14].

Currently BioGlue is limited in the US to the repair of aortic dissection (i.e., filling in of the false lumen)[15]. BioGlue fills in the dissection, thus closing the cavity and providing a stronger arterial wall for repair. BioGlue's properties allow it to be used in sealing, reinforcement, and in rebuilding of tissues. It has a half-life of approximately 30 days.

Potential complications include vascular strictures at the site of application or embolization of adhesive substance from the local site to a distant site. Like cyanoacrylate adhesives, GRF adhesives are considered cytotoxic and are poorly reabsorbed.

8.2.2.6 Others

Other organic compounds are currently being considered for surgical adhesive applications. For example, polyurethanes[16, 17] and proteins[18] from marine organisms (e.g., mussels) are actively being studied but are not yet widely available on a commercial basis.

Researchers[19] have developed a biological glue from gelatin and poly(L-glutamic acid), PLGA. This is a hydrogel that can be used for soft tissues. Water soluble carbodimides can be used to crosslink the aqueous mixture of gelatin and PLGA. The mixed solution sets to a hydrogel as rapidly as fibrin glue. Gel time can be controlled by the PLGA and carbodimide concentrations, and tensile strength is controlled by the PLGA concentration. The cured

hydrogel exhibited firm adhesion to mouse skin and other soft tissues with a higher bonding strength than fibrin glue. The adhesive is gradually absorbed with time in vivo.

8.2.3 *Comparison of Adhesive Types*

An adhesive used for tissue bonding must possess a number of attributes, and many of the basic requirements have been identified in the previous section of this review. The advantages and disadvantages of the main surgical adhesives and examples of commercial products are listed in Table 8.5.

Above all else the adhesive must hold the tissue together with adequate bond strength for sufficient time. Once cured it must also have physical properties (elongation, conformability, etc.) that are suitable for the application. The tissue should regrow to heal the defect naturally, in which case the adhesive must also degrade at a rate which is consistent with its replacement. It must be chemically acceptable to the body, and any degradation products must be able to be removed by natural processes. Although there is no specific set of criteria for the surgeon to use in selecting a surgical adhesive, Table 8.6 provides a list of certain essential properties that are important.

Bond strength and physical properties such as elongation provide a method of comparing adhesives. Bond strength will depend on the substrate. Most adhesives bond well to graft materials due to penetration and mechanical bonding. The bond strength to the bodily tissues is expected to be the “weak-link” in the joint.

Chivers and Wolowacz[21] conclude from their investigation that the bond strength will depend strongly on the nature of the adhesive and the condition of the tissue, with adhesive bond strengths showing the following orders of magnitude:

- Cyanoacrylate: 1 MPa
- GRF: 0.1 MPa
- Fibrin: 0.01 MPa

The bond strengths measured in their study depended somewhat on the type of tissue being bonded (Table 8.7). However, the order of bond strength remained constant (cyanoacrylate>GRF>fibrin).

The rigidity of the adhesives follows the same ranking. Cyanoacrylates are relatively brittle and show an interfacial failure mode. Fibrin adhesive / sealants are relatively soft and provide cohesive failures. As a result, fibrin is more often used as a sealant than an adhesive and is usually applied only to softer tissue.

8.3 *History of Cyanoacrylate Surgical Adhesives*

8.3.1 *Development of Cyanoacrylates as Industrial Adhesives*

Cyanoacrylate resins were developed during the 1940s. The earliest patents on the preparation of cyanoacrylates were issued in 1949 and assigned to B.F. Goodrich Company[22, 23]. The adhesive properties were later realized accidentally. Between the years 1955 and 1957, a

Table 8.5 Advantages and Disadvantages of Selected Surgical Adhesives

Type of Surgical Adhesive / Sealant	Trade Name (Manufacturer)	Advantages	Disadvantages
Fibrin	<ul style="list-style-type: none"> • Tisseel (Baxter) • Beriplast P (Behring) • Tssuccol (Baxter) • Green Plast (Orleant) • Cryoseal (ThermoGenesis) 	<ul style="list-style-type: none"> • Ideal to secure hemostasis • Cures on mixing 	<ul style="list-style-type: none"> • Manufactured from bovine or human blood (must be treated / tested to prevent transmission of infection or viruses) • Requires >2min to set
Cyanoacrylate	<ul style="list-style-type: none"> • Dermabond (Ethicon) • Liquibrand (Med Logic) • Histoacryl (B. Braun) • Glubran 2 (GEM s.r.l.) • Floreseal (Adhesion Biomedical) • Indermil (Henkel) 	<ul style="list-style-type: none"> • Polymerizes rapidly (30-60 s) in presence of moisture, blood, etc. • Good cosmetic outcome (no sutures) • No risk of transmission of infection • Waterproof 	<ul style="list-style-type: none"> • Low elasticity • Sometimes cure is too fast depending on procedure • Dermatitis with certain individuals • More data needed to understand toxicity • Not bioabsorbable • Currently restricted to external and temporary applications

Table 8.5 cont.

Collagen compounds	<ul style="list-style-type: none"> FloSeal, (Sulzer Spine-tech) Proceed (Fusion Medical Technologies) CoStasis (Cohesion Technologies) 	<ul style="list-style-type: none"> Similar to fibrin but absorbs into body faster Swells in the presence of blood and provides a mechanically stable matrix for a clot to form 	<ul style="list-style-type: none"> Manufactured from bovine or human blood (must be treated / tested to prevent transmission of infection or viruses) Low adhesion (stays in place only mechanically) Requires >2min to set
Poly(ethylene glycol) polymers	<ul style="list-style-type: none"> CoSeal (Cohesion Technologies) FocalSeal-L (Genzyme Biosurgery Inc.) AdvaSeal (Ethicon) 	<ul style="list-style-type: none"> Hydrogels prevent air or liquid leakage Good adhesion Biocompatible Reabsorption in about 30 days Cures in <60 s (photopolymerized) Sprayable formulations 	<ul style="list-style-type: none"> Short shelf-life Hydrogels unsuitable as an adhesive
Glutaraldehyde products	<ul style="list-style-type: none"> Bioglue (CryoLife) Cardial (Technopole) 	<ul style="list-style-type: none"> Cures by mixing Sets in 30-60 s Flexible seal 	<ul style="list-style-type: none"> Long absorption time (2 years) Bacterial growth Not suitable for external or topical use

Table 8.6 Suggested Criteria for Comparing Sutureless Adhesives (Required value will depend on nature of surgical procedure)[20]

Curing	<ul style="list-style-type: none"> • Time to set, seconds • Time to reach 100% bond strength, seconds
Physical	<ul style="list-style-type: none"> • Tensile strength, MPa • Modulus, MPa • Cyclic fatigue, Hz/cycles • Tear / peel strength, MPa
Biodegradability	<ul style="list-style-type: none"> • Time to degrade, hours-days • Time to absorb into the body, hours-days

Table 8.7 Measured Bond Strength Between Different Tissue Types for Butt Joints[21]

Adhesive	Bond Strength, MPa		
	Cartilage	Bone	Skin
n-Butyl-2-cyanoacrylate	1.0 (4) [1.4]	1.4 (2) [1.6]	1.2 (5) [1.8]
Gelatin-resorcinol-formalin (GRF)	0.15 (5) [0.23]	0.2 (1) [0.20]	0.07 (5) [0.12]
Fibrin	0.0049 (4) [0.0070]	0.011 (5) [0.019]	0.019 (6) [0.028]

Note: The mean is quoted first, followed by the number of specimens in parentheses and then the highest value measured is in square brackets.

number of patents were issued to Eastman Kodak including the use of cyanoacrylates as adhesives[24]. These materials only had limited use at first mainly because of their cost. However, the small amounts of adhesive required to achieve high bond strength lessened this as an issue, and cyanoacrylates commercially were introduced to the industry in 1958 and then to the general public as do-it-yourself type adhesives in 1973.

The first commercial cyanoacrylate adhesive was Eastman 910. Later similar compositions were introduced into the market under brand names such as Crazy Glue, Super Glue, Permabond, etc. These adhesives grew rapidly in the consumer market as well as many industrial markets because of their ability to bond a wide variety of substrates in a few seconds. Table 8.8 summarizes the general benefits and limitations of cyanoacrylate adhesive systems.

Early generations of cyanoacrylate adhesives had significant performance limitations. Since they were essentially thermoplastic in nature, cyanoacrylate adhesives exhibited poor thermal and chemical resistance. Since they were hard and brittle when cured, they exhibited poor impact and peel properties. These drawbacks limited their industrial applications to high volume assembly operations with minimal performance requirements.

Table 8.8 General Benefits and Limitations of Industrial-Grade Cyanoacrylate Adhesives

Benefits	Limitations
<ul style="list-style-type: none"> • Excellent adhesion to a wide variety of substrates • Simple cure mechanism • Rapid strength development • High strength possible on polyolefins and fluorocarbons using primers • Available in USP Class VI compliant formulations • High shear strength • No measuring or mixing required 	<ul style="list-style-type: none"> • Blooming/frosting • Difficult to cure fillet or exposed liquid adhesive without activator • Limited gap cure • Stress cracking could occur to some plastics • Soluble in polar solvents • Thermal and chemical stability not as good as with certain other structural adhesives • Unmodified formulations have low peel and impact strengths • Relatively high materials cost • Pungent odor associated with early formulations

Over the years the various properties of these adhesives were improved for specific end-uses. New cyanoacrylate resin monomers (Table 8.9) have also been introduced to provide faster cures, higher strength with some plastics, and greater thermal and impact resistance. These newer products continue to offer the ease of use of a cyanoacrylate but now with the added performance properties of a truly structural adhesive.

Improved heat resistance is addressed by the addition of crosslinking agents, heat resistant modifying monomers, or both. The use of phthalic anhydride has been reported to improve both the moisture resistance and heat resistance of the cyanoacrylates[26]. Rubber toughened cyanoacrylates generally also show the best performance in water and humid environments. Crosslinking monomers such as biscyanoacrylates or alkenyl cyanoacrylates can be used to generate some amount of crosslinking in the adhesive[27].

Whereas unmodified cyanoacrylates normally have a maximum operating temperature of about 82°C, new thermally resistant formulations offer continuous service at temperatures as high as 120°C. Several formulations are commercially available that claim short term service temperatures up to 150°C. These high temperature formulations are very useful in electrical / electronic applications such as wire tacking and component bonding to printed circuit boards.

Typically unmodified cyanoacrylate adhesives have a high lap shear strength, on the order of 14-21 MPa, on most substrates. Lap shear strength can be further improved by 10-30% and peel and impact resistance can be greatly improved by incorporation of tougheners or plasticizers to the unmodified cyanoacrylate adhesive formulation[25, 27]. Products have been developed which have 5-10 times higher peel strength than conventional compositions.

Plasticizers such as aliphatic esters, aromatic phosphates, and phthalates can also be added to the cyanoacrylate formulations for flexibilizing the bondline. Plasticizers help

Table 8.9 Relationship of Cyanoacrylate Monomer to Basic Adhesive Properties[25]

Property	Methyl-	Ethyl-	beta-Methoxy	n-Butyl	n-Hexyl
Tensile-shear strength on grit blasted mild steel, N / mm ²	22	20	18	15	8
Typical setting time/s					
- Steel	50	20	50	60	120
- Rubber	5	5	10	20	30
- PVC*	10	5	15	30	60
Moisture resistance	Good	Good	Good	Good	Fair – good
Solvent resistance	Very good	Good	Good	Fair	Fair
Maximum operating temperature, °C	90	90	90	90	80
Odor	Pungent	Pungent	Negligible	Pungent	Negligible
Blooming	Significant	Significant	Very slight	Slight	Very slight

*poly(vinyl chloride)

Table 8.10 A Typical Cyanoacrylate Adhesive Formulation[28]

Component	Amount (pph)	Function
Ethyl cyanoacrylate	91	Resin former
Poly (methyl methacrylate)	4	Thickener, flow control agent
Dimethyl sebacate	5	Flexibilizer
p-Methoxyphenol	0.1	Free radical inhibitor
Sulfur dioxide	0.005	Anionic polymerization inhibitor

improve the peel strength and shock resistance of the cured cyanoacrylate adhesive. Table 8.10 illustrates a typical early cyanoacrylate adhesive formulation.

Significantly improved impact strength has been accomplished using various elastomeric tougheners[29]. Modern cyanoacrylate adhesives include toughening agents such as acrylonitrile-butadiene-styrene, ethylene-methyl acrylate copolymers, styrene butadiene rubber grafted with styrene and methyl methacrylate as well as other copolymers and grafted polymers. The toughening agent is usually added at a concentration of 15-20 percent by weight of the cyanoacrylate monomer. The toughening mechanism is primarily one of phase separation.

Unmodified cyanoacrylate adhesives do not polymerize readily on acidic surfaces such as wood or dichromated metals. The incorporation of poly-n-vinyl pyridine or polyethyleneimine or even simple amines presumably serves the dual purpose of thickening the liquid (for better bonding to the porous wood surface) and increasing the pH to speed cure. Surface insensitive and fast reacting cyanoacrylates have been developed by adding agents such as silacrown compounds, crown ethers, and calixarenes to ethyl cyanoacrylates.

Cyanoacrylates are now available in gel form in addition to the conventional low viscosity liquids. These systems provide the ability to bond to substrates such as wood, leather, and fabrics, which have been notoriously difficult substrates for bonding with cyanoacrylate adhesives. Fumed silica and high molecular weight acrylates are generally employed in these formulations.

Recently light curing cyanoacrylate adhesives have been developed that offer the rapid light cure properties of a thermosetting acrylic adhesive coupled with the ease and speed of a secondary cyanoacrylate cure[30]. Light curing cyanoacrylates are ethyl based products that have photoinitiators added to the formulation, allowing them to set rapidly on exposure to low intensity light, and to cure in shadowed areas.

A major benefit of light curing cyanoacrylate adhesives is that liquid adhesive can be cured to a tack-free surface in less than three seconds through exposure to a low intensity light. This prevents blooming (frothing of substrate surfaces) and stress cracking of plastics, and greater gap thicknesses can be cured. Light curing cyanoacrylate adhesives can be cured to depths in excess of 0.64 cm within 15 s. Since light cured cyanoacrylate adhesives are thermosetting, they provide improved creep resistance at elevated temperatures.

8.3.2 Development of Cyanoacrylate Tissue Adhesives

The high bonding strength and ability to bond in wet environments attracted the medical community to cyanoacrylate adhesives in the 1960s. The surgical use of cyanoacrylate was first proposed by Coover in 1959[31]. A series of reviews on medical applications of cyanoacrylate applications have since been published[1, 11, 32]. The various cyanoacrylate adhesive derivatives are effective and recommended mainly for superficial skin closure. The clinical applications of cyanoacrylate surgical adhesives are described in a later section of this review.

Unfortunately, the short chain early butyl-cyanoacrylates (e.g., Eastman 910) proved to be extremely toxic to tissue, preventing their widespread use at the time. The mechanical (poor tensile strength and brittle nature) also limited their use to small lacerations and incisions where post-operative stress was small. While the FDA prohibited their early surgical use, research was being done to develop fast setting and strong n-butyl-cyanoacrylates that were less toxic (e.g. Histoacryl (Braun), Indermil (Henkel), or LiquiBand (Advanced Medical Solutions)). Then Ethicon developed Dermabond, a slower setting octyl-cyanoacrylate adhesive with more flexibility. It was approved for external clinical use by the FDA in 1998.

Concerns with toxicity as well as mechanical properties (primarily flexibility) have led to a series of improvements. Quite a few cyanoacrylate surgical products are commercially available. They differ primarily in monomer type, formulation, and the design of their application system.

Today's commercially available cyanoacrylate surgical adhesives are listed in Table 8.11. Of these Dermabond, Indermil, and Turfill are FDA approved for topical wound closure applications. Turfill is FDA approved for neurological embolization. The FDA, as yet, approves no cyanoacrylate adhesive for internal use. However, internal use is not prohibited in other countries or in clinical trials in the US. Many clinical studies have been made and are underway. The major clinical studies will be described in a later section of this review.

Some commercial cyanoacrylate adhesives have been developed only for veterinarian use. The main n-butyl-2-cyanoacrylate manufacturers are Vetbond (3M), VetGlu (GluStitch), LiquiVet (Oasis Medical) and the main 2-octyl-cyanoacrylate manufacturer in this category is Nexaband (Abbott).

8.3.2.1 n-Butyl-2-Cyanoacrylate

n-Butyl-2-cyanoacrylate surgical adhesives have been in use the longest. It has been widely used in endoscopic therapy for more than 10 years. After polymerizing, the adhesive becomes relatively brittle and is subject to fracturing when used in skin creases or long incisions. Although this limits the application somewhat to low tension joints, n-butyl-2-cyanoacrylate has been used with good cosmetic outcomes for various plastic surgery procedures[33]. Several studies have shown that the strength of tissue joints made with n-butyl-2-cyanoacrylate are equal to suture joints after 5-7 days; however, the initial breaking strength is much less than for a wound sutured with 5-0 monofilament[34].

The following summarizes the properties and applications of some of the more common n-butyl-2-cyanoacrylate surgical adhesives.

Histoacryl Blue

Histoacryl Blue tissue adhesive has been widely used in hospital accident and emergency departments for the treatment of pediatric patients and traumatic skin incisions in adults. It has been compared with silk sutures as a means for closing incisions and was found to be less inflammatory but the healing process was slower than sutures[35].

Histoacryl Blue has been the most widely used cyanoacrylate for internal operative procedures. For endovascular treatment, it has been mixed with Lipiodol for visualization and retardation of the polymerization reaction. Histoacryl Blue contains a blue dye; Histoacryl contains no dye. The manufacturer claims higher tensile strength than 2-octyl-cyanoacrylate (Figure 8.2), but the bond strength to tissue is debated by others.

Glubran 2

Glubran 2 is a modified n-butyl-2-cyanoacrylate with high adhesive and hemostatic properties. It is certified (European Directive on Medical Devices 93/42/EU) for internal or external use outside of the U.S. and has been used for endoscopic surgery. Kull, *et al.*, evaluated the properties of Glubran 2 on biological substrates and found it to be far superior to fibrin adhesives[37].

Table 8.11 Commercially Available Cyanoacrylate Surgical Adhesives

Chemical Type	Trade Name	Manufacturer	Characteristics
n-Butyl-2-cyanoacrylate	Histoacryl and Histoacryl Blue	B. Bruan, Tuttlingen, Germany	<ul style="list-style-type: none"> • Manufacturer claims higher tensile strength than OCA*
	Trufill	Cordis Neurovascular, Inc., Miami Lakes, FL, USA	<ul style="list-style-type: none"> • FDA approved for wound closure • FDA approved for neurological embolization
	Indermil	Henkel Loctite, Rocky Hill, CT, USA	<ul style="list-style-type: none"> • Commercialized by Covidien in the USA • FDA approved for wound closure
	Glubran 2	GEM s.r.l., Viareggio, Italy	<ul style="list-style-type: none"> • No research data available • Contains a monomer in addition to cyanoacrylate
	GluStitch, Twist CE	GluStitch, Inc., Delta, BC, Canada	<ul style="list-style-type: none"> • Primary first aid and sports bandage • No research data available
	PeriAcryl 90	GluStitch, Inc., Delta, BC, Canada	<ul style="list-style-type: none"> • Oral tissue adhesive
	Xion	Reevax Pharma, Hyderabad, India	<ul style="list-style-type: none"> • Long shelf-life tissue adhesive

Table 8.11 cont.

2-Octyl-cyanoacrylate	Dermabond	Ethicon, Somerville, NJ, USA	<ul style="list-style-type: none"> FDA approved for wound closure A higher viscosity form is now available Slower to polymerize than NBCA* (60 s vs. 30 s)
	SurgiSeal	Adhezion Biomedical, Wyomissing, PA, USA	<ul style="list-style-type: none"> Similar to Dermabond but with slightly faster cure and not FDA approved Claimed to be slightly stronger than Dermabond
	Octylseal	Medline, Research Triangle Park, NC, USA	<ul style="list-style-type: none"> High viscosity tissue adhesive
	Derma+flex QS	Chemence, Northamptonshire, UK	<ul style="list-style-type: none"> High viscosity, highly flexible tissue adhesive
	FloraSeal	Adhezion Biomedical, Wyomissing, PA, USA	<ul style="list-style-type: none"> Microbial protection High moisture permeability
Monomer blend	Liquiband Surgical S	Advanced Medical Solutions, Howell, MI, USA	<ul style="list-style-type: none"> Considered to be an "octyl-blend" (likely OCA blended with NBCA) Claimed to combine the fast set of NBCA with the flexibility of octyl-cyanoacrylates
2-Hexyl cyano-acrylate	Neuracryl	Provasis Therapeutics, Inc., San Diego, CA, USA	<ul style="list-style-type: none"> Much lower adhesion than other cyanoacrylates Suggested for non-bonding applications such as embolization (will not stick to catheter)
2-Ethyl cyano-acrylate	EpiGlue	Meyer-Haake, Ober- Mortlin, Germany	<ul style="list-style-type: none"> No research data available

*OCA: 2-octyl-cyanoacrylate

NBCA: n-butyl-2-cyanoacrylate

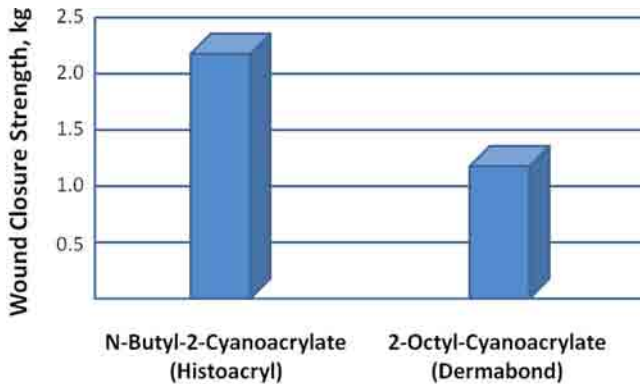


Figure 8.2 Comparative wound closure strength of Histoacryl and Dermabond in accordance with ASTM F 2458-05 (adhesive is applied across the seam of a butt joint made with freshly harvested porcine skin)[36].

Trufill

Trufill is a relatively new type on n-butyl-cyanoacrylate. It has received FDA approval for use in neurological embolization procedures as well as for topical tissue closure. Although much slower reacting than Histoacryl, Trufill also may require the addition of an inhibitor (e.g., Lipiodol) to slow the polymerization rate to allow for practical microcatheter application[38].

Trufill is a three-component system containing n-butyl-cyanoacrylate, ethiodized oil, and tantalum powder. It is used under fluoroscopic guidance to obstruct or reduce the blood flow to cerebral arteriovenous malformation via catheter delivery. The ethiodized oil is a radiopaque polymerizing retardant and will decrease the rate of polymerization of the cyanoacrylate. The tantalum powder is used to provide additional visualization.

8.3.2.2 2-Octyl-Cyanoacrylate

2-Octyl-cyanoacrylate overcomes some of the deficiencies of the shorter-chain butyl derivatives. Dermabond, the first 2-octyl-cyanoacrylate surgical adhesive, was approved by the FDA for closure of superficial skin lacerations in 1998, and in 2002 it was approved by the FDA as a barrier protection against common microbes.

The longer chain 2-octyl-cyanoacrylate adhesives are more flexible than the n-butyl-2-cyanoacrylate derivatives. Additionally, plasticizers are added to produce a more pliable and tissue-compatible product that flexes with the tissue and remains adhered for longer periods. Because of this flexibility it is preferred over n-butyl-2-cyanoacrylate for long incisions.

The longer chain length of the 2-octyl-cyanoacrylate monomer will also provide extended cure times. The monomer is slower to polymerize than its butyl counterpart, taking up to one minute to polymerize on skin tissue compared to 30 seconds for the butyl derivative.

The bond strength of 2-octyl-cyanoacrylate is claimed to be about 3 times that of n-butyl-2-cyanoacrylate and is closer to that of 5-0 monofilament suture. This stronger, more flexible bond may allow its use in clinical applications not possible with n-butyl-2-cyanoacrylate. However, the relative bond strength of n-butyl-2-cyanoacrylate and 2-octyl-cyanoacrylate adhesives is heavily debated.

A review of octyl-cyanoacrylate surgical adhesives has been made for animal and human studies in a variety of surgical indications and specialties[11]. The 2-octyl-cyanoacrylate derivatives are effective and recommended mainly for superficial skin closure. Use of the material below the level of the skin can result in acute and chronic inflammation and tissue necrosis[39].

However, cyanoacrylates have been used for embolization[38, 40] and repair of endoleaks after conventional aortic abdominal aneurism surgery[41, 42]. Injection therapy with cyanoacrylates is now considered the first line of endoscopic intervention of bleeding gastric varices as well as secondary prevention of gastric variceal bleeds outside of the US[43].

The following summarizes the properties and applications of some of the more common 2-octyl-cyanoacrylate surgical adhesives.

Dermabond

Dermabond is a 2-octyl-cyanoacrylate adhesive. Its larger molecular weight is claimed to provide flexibility and toughness. The manufacturer claims that Dermabond has tensile shear strength 3X that of Histoacryl and an order of magnitude greater than other surgical adhesives or sealants (i.e., fibrin, GRE, BioGlue). Dermabond is FDA approved only as a topical skin adhesive. However, it has been used clinically for embolization. Dermabond can be successfully applied on surgical incisions from 0.1 cm to more than 50 cm long. With an average tensile strength of 68 kPa it is indicated for cornea, skin wounds, or endoscopic therapy[44].

Dermabond is a relatively slow cyanoacrylate adhesive having a slower polymerization rate than n-2-butyl-cyanoacrylate type adhesives (60+ s vs. < 30 s). In fact, it is considered far too slow on its own for certain topical skin applications. As a result, an accelerator is added to the tip of the Dermabond applicator so that the flexible properties of the monomer can be utilized. The monomer becomes activated as it moves through the pores of the tip to give a desired setting time and provide a topical wound closure. Even in this mode of application, the Dermabond product is considered to be slower setting than n-2-butyl-cyanoacrylate derivatives.

SurgiSeal

SurgiSeal is a newer 2-octyl-cyanoacrylate from Adhezion Biomedical. It does not have FDA approval as yet, but it appears to be similar to Dermabond in properties. However, the moisture permeability rate for SurgiSeal is much higher which should provide better healing properties. SurgiSeal is claimed to have a slightly faster polymerization rate than Dermabond, and the accelerator is included in the formulation rather than incorporated in the applicator. Adhezion Biomedical claims that SurgiSeal has higher T-peel strength than Dermabond (Table 8.12).

Table 8.12 Comparative Test Results of SurgiSeal and Dermabond[45]

Property	SurgiSeal	Dermabond	ASTM Test Method
Tensile strength, MPa	0.979	0.075	F2255-05
Lap shear strength, MPa	0.101	0.108	F2258-08
T-peel strength, kg/cm	707	484	F2256-05
Wound closure strength, kg	1.22	1.09	F2458-05

8.3.2.3 Newer Cyanoacrylate Surgical Adhesives

More recently in the UK there has been the development of blended butyl- and octyl-cyanoacrylates (LiquiBand, Advanced Medical Solutions, Plymouth, Devon, UK) providing both a fast setting adhesive and a good degree of flexibility[46].

Recent research has also demonstrated that the new family of cyanoacrylate hemostatic agents (OMNEX, Ethicon, Somerville, NJ, USA), which had previously proven their safety and efficacy in topical use, are now safe and effective absorbable surgical sealants for internal use. OMNEX is a cyanoacrylate-based synthetic surgical sealant. To date, the use of OMNEX has only been described in a limited number of vascular surgery procedures.

8.4 Formulation Development

Cyanoacrylates can be synthesized by reacting formaldehyde with alkyl cyanoacetate to obtain a prepolymer that, by heating, is depolymerized into a liquid monomer. The resulting monomer can be modified by altering the alkoxy-carbonyl (-COOR) group to obtain compounds with different chain lengths. The properties of various monomeric derivatives are discussed in the first part of this section.

Additives can be incorporated at the end of the manufacturing process, although certain additives are required early in the manufacturing process to prevent premature polymerization. The additives that are incorporated during the final step are used to modify the application properties (viscosity, set time, etc.) and performance properties (bond strength, flexibility, etc.). Such additives normally used in medical grade cyanoacrylate adhesive formulations are discussed in the second part of this section.

The final adhesive product must be carefully packaged to provide a practical shelf-life since it is such a reactive resin. The cyanoacrylate can be packaged in tubes using conventional, humidity-free, techniques. Because most metal tubes would react with the cyanoacrylate, packaging tubes are usually made of plastic such as polyethylene although coated aluminum tubes are possible. Once the cyanoacrylate is exposed to moisture or an alkaline material, the monomers will repolymerize and harden.

Formulation of cyanoacrylate adhesives is typically difficult because of the sensitivity of cyanoacrylates to contaminants and the extreme reactivity of the cyanoacrylate curing mechanism. The difficulty in manufacturing is one reason for the high price of

cyanoacrylate resins. Medical grade cyanoacrylate is even more expensive to manufacture and purchase than commercially available industrial cyanoacrylates.

8.4.1 Monomeric Derivatives

There are several known methods of synthesizing cyanoacrylate monomers. The most important industrial method uses the following sequence:

1. Base-catalyzed Knoevenagel reaction of formaldehyde with a cyanoacetate ester to produce the 2-cyanoacrylate ester, which spontaneously polymerizes.
2. Thermal depolymerization (cracking) under acidic conditions and in the presence of an inhibitor (e.g., sulfur dioxide, phosphorous pentoxide, or nitric oxide) to generate the monomer.
3. Purification of the monomer by one or more distillations.
4. Addition of stabilizers, thickeners, and other additives to produce a commercial adhesive product.

The details of the reaction processes, pertinent manufacturing equipment, and quality control methods can be found in several publications[47, 48].

Cyanoacrylate adhesive monomers are alkyl-2-cyanoacrylates with a basic structure which is shown in Figure 8.3. Different monomers can be manufactured by altering the -R group. Development efforts have focused on modifying the chemical structure of the cyanoacrylate monomer itself.

Ethyl and methyl are the most commonly used alkyl groups in industrial or do-it-yourself cyanoacrylate adhesive markets. N-butyl-2-cyanoacrylate and 2-octyl-cyanoacrylate encompass the expanding range of potential surgical adhesives. The uses and properties of several cyanoacrylate monomers are shown in Table 8.13.

The longer the hydrocarbon group at the -R position, the slower the rate of polymerization, the less heat released during polymerization, and the lower the histotoxicity. The shorter-chain derivatives tend to have a higher degree of tissue toxicity than do the longer-chain derivatives. The inflammatory or carcinogenic potential of cyanoacrylates, as well as their degradation rates, are inversely proportional to the length of their alkyl (-COOR) side chains. Thus, the longer the side chains the slower the breakdown and formation of toxic degradation products (formaldehyde and cyanoacetate). In large quantities, these

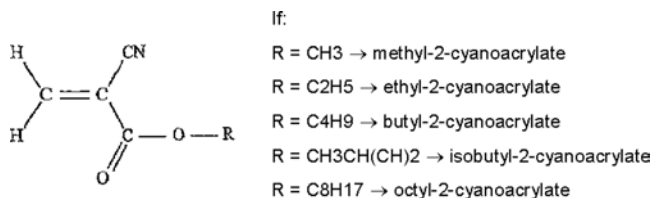
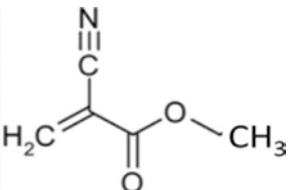
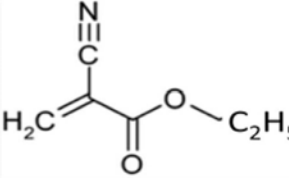
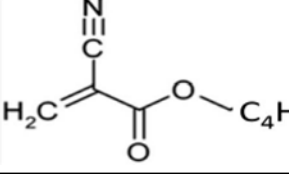
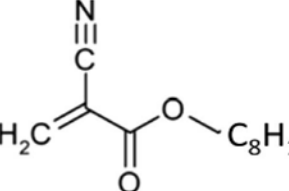


Figure 8.3 Monomeric cyanoacrylate. The R represents an alkyl group.

Table 8.13 Commercially Available Alkyl-2-Cyanoacrylate Monomers

Alkyl	Chemical Structure	Uses and Properties
Methyl		Industrial adhesive; strongest bonds to metals; good solvent and heat resistance
Ethyl		General purpose industrial adhesive; forms strong bonds to metals, plastics, and rubbers
Butyl		Surgical adhesive, adhesive also for plastics and rubber; improved flexibility; less irritating vapor than the lower cyanoacrylates
Octyl		Surgical adhesive; low toxicity; very good flexibility; moderate bond strength; slower setting than the lower cyanoacrylates

breakdown products can be histotoxic. Formaldehyde and cyanoacetate have the potential to cause inflammatory reactions and impair wound healing. Therefore, 2-octyl-cyanoacrylate (Dermabond) and n-butyl-2-cyanoacrylate (Turfill and Indermil) with longer side chains have had safety profiles satisfactory for human topical application and regulatory approval by the FDA.

The alkyl side chain has an important impact on the application properties and eventual performance of the cyanoacrylate adhesive. In general, reactivity can be increased by incorporating shorter alkyl side chains or by increasing branching off the side chain. A highly reactive compound will set fast and will be cohesively strong. However, short chain monomers tend to form brittle bonds which do not distribute stress well and can fracture easily. Also, short chain monomers, when exposed to moist or alkaline tissues, will result in very rapid polymerization and can cause significant heat (exotherm) during polymerization. Such heat can cause pain and inflammation.

Longer chain monomers (particularly four carbon chains or longer) have been found to be optimal for clinical uses. The polymer degrades by hydrolysis, and the longer the alkyl chain, the more hydrophobic the polymer becomes. The alkyl chain of the octyl polymer is so long and hydrophobic that it can take years to degrade[49, 50]. The degradation products from the longer chain compounds are barely detectable in extraction studies. Thus, it is not surprising that the longer chain cyanoacrylate monomers have passed FDA standards for a medical device adhesive.

The low reactivity of these compounds also is accompanied by a slow polymerization process, resulting in longer setting times, which is of benefit in surgical processes such as endovascular embolization. In fact, in some clinical settings (topical wound closure), longer chain compounds such as octyl-cyanoacrylate need an accelerator to polymerize in a clinically useful time period. This is particularly true if the formulation has had stabilizers added to improve stability during sterilization and to improve shelf-life.

The length and structure of the alkyl side chain also impart other important physical properties to the cured product, such as flexibility. In general, the longer or more complex the side chain, the more flexible the monomer. Such flexibility adds to the toughness of the adhesive and is considered to be of importance in dynamic situations such as topical wound closure (flexing of the skin) or for blood pulsation through an attached graft section.

8.4.2 *Optimal Formulation Development*

Commercial cyanoacrylate adhesives such as Dermabond or Histoacryl are fully formulated products. They contain a certain base monomer as well as additives to provide for the specific properties required for topical tissue adhesives. In the formulation process consideration must be given to the base cyanoacrylate monomer, inhibitors, accelerators, and other additives. As a result, there exist many cyanoacrylate formulation possibilities.

The methods to synthesize cyanoacrylates are elaborate and expensive. Although distributors and even surgeons can add modifiers to commercial cyanoacrylate adhesives to optimize properties for a specific application, this practice is best left to those experienced and having the proper processing equipment (i.e., the monomer manufacturer).

Once the liquid cyanoacrylate monomer is produced it is then stabilized with a free radical inhibitor, such as hydroquinone. This serves as a free radical trap, preventing repolymerization. Finally, various cyanoacrylate adhesive formulations can be manufactured by adding components to vary viscosity, spreadability, set time, bond strength, degradation rate, and other physical, chemical, and mechanical properties.

Cyanoacrylate adhesives are rarely sold as pure monomers. A simplified formulation for a cyanoacrylate tissue adhesive is shown in Table 8.14. In fact, most surgical adhesive formulations are even more complex, being customized for specific procedures. In addition to the base alkyl-2-cyanoacrylate monomer, they may contain initiators, adhesion promoters, thickeners, fillers, inhibitors, plasticizers, and dyes to modify both the application properties and final performance properties. In addition to the additives that the commercial cyanoacrylate adhesive manufacturers incorporate, the surgeon or end-user may deem it necessary to add modifiers to provide for a practical working time, radiopacity, etc.

Table 8.14 Simplified Formulation of a Cyanoacrylate Adhesive[51]

Component	Amount	Function
Alkyl cyanoacrylate	75-82 wt %	Base monomer
Acyl trialkyl citrate	18-25 wt %	Plasticizer
Sulfur dioxide	50-500 ppm	Anionic polymerization inhibitor

Components can be added to the cyanoacrylate adhesive formulation to modify the application or performance properties. However, this approach should be considered only with caution because:

1. Additives and modifiers are likely to affect FDA or other regulatory approval since most additives have lower molecular weight than the cured cyanoacrylate.
2. Unlike other adhesive types, the formulation of cyanoacrylate adhesives is difficult because of the sensitivity of cyanoacrylate reaction rate to additives or contaminants.

Thus, most development work regarding new formulations has been focused on changes in the chemical structure of the cyanoacrylate monomer itself. Several exceptions are noted below.

8.4.2.1 Inhibitors

Inhibitors or stabilizers are added by the adhesive manufacturers to prevent polymerization during storage. The specific type and concentration of inhibitor are chosen to provide stability during storage yet fast cure on application to a substrate. The two main types of inhibitors are radical polymerization inhibitors and anionic polymerization inhibitors.

Protection from anionic polymerization is provided by chemical compounds that are electron acceptors (i.e., protonic and Lewis acids). Some commonly used inhibitors are volatile acid gases and nonvolatile acids such as phosphoric acid, partial esters of phosphoric acid, sulfonic acids, and sulfur dioxide. These are used in various concentrations, depending upon the type of stabilizer (Table 8.15). Sulfur dioxide gas was the earliest used inhibitor. It is functional both during the manufacturing process as well as during packaging and storage. More recently, solid inhibitors have been preferred.

The earliest patents in this area recommend the use of SO_2 . The SO_2 was used in concentrations of 10 ppm to several hundred ppm. The gaseous inhibitors, however, presented several problems. Being gases, they are difficult to handle, and the determination of exact concentration of the gas in the adhesive is difficult. When SO_2 or other acidic gases are used as a stabilizer, they have been noticed to separate from the liquid adhesive causing reduced shelf-life[52, 53]. In prolonged storage, the inhibitors may evaporate and change the cure rate and stability of the adhesive, particularly when polyethylene containers are used. These problems have been generally overcome by using nonvolatile acid inhibitors,

Table 8.15 Anionic Polymerization Inhibitors

Inhibitor	Concentration
SO ₂	10-500 ppm
SO ₃	10-100 ppm
ArSO ₃ H	10-30 ppm
Sulfones	0.1-0.2%
Sulfamides	10-500 ppm
Cation exchange resins	5%
Boric acid chelates	10-600 ppm

such as aromatic sulfonic acids, or to complex the SO₂ with chelates, or to provide the adhesive in a gas barrier (e.g. aluminum foil) package.

Cyanoacrylate manufacturers also add inhibitors for free radical polymerization, usually phenolic types, such as hydroquinone or t-butyl catechol. Typical levels are 50-1000 ppm. These inhibitors protect the adhesive from polymerization induced by heat or light and other radical sources during storage. If used in reasonable quantities, they do not affect the cure speed of the adhesive. Radical inhibitors not only protect the formulated adhesive during storage, but they also may be needed during distillation of the monomer to prevent polymerization. Free radical inhibitors are generally also used to protect medical-grade cyanoacrylate adhesives during package sterilization.

A free radical stabilizer system consisting of hydroquinone and butylated hydroxyanisole is described in a US patent application[54]. The stabilized adhesive composition comprises cyanoacrylate monomers along with a first free radical stabilizer consisting of hydroquinone in an amount of 5 to 70 ppm and a second free radical stabilizer consisting of butylated hydroxyanisole in an amount of 500 to 10,000 ppm. This type of inhibitor system can be used in both industrial and medical cyanoacrylate adhesives.

8.4.2.2 Stabilizers Added Depending on the Surgical Procedure

Two problems with commercial surgical cyanoacrylate adhesives are that (1) their polymerization rate is too rapid for the specific procedure being undertaken and (2) their lack of radiopacity to detect the adhesive's presence or location during the procedure. These problems can make precise, safe application difficult to achieve.

Speed of setting can be modified by the proper choice and concentration of inhibitors or accelerators. One must be aware that cyanoacrylates have the potential for distal embolization of untargeted sites if the injection rate is too rapid or the adhesive polymerization time is so long that unpolymerized adhesive enters the blood stream[40]. Ideally, the surgeon wants an adhesive that will set "on-demand" or at least provide sufficient working time to be able to reach the surgical site through a microcatheter and wet the substrates before setting. But once at the correct location, the adhesive should set as quickly as possible.

Modifications to address these problems include the addition of powdered metals, typically tantalum or tungsten, and iodized oils. Tantalum has been noted to result in a slow initiation of polymerization. For embolic applications it should be added to the adhesive shortly before its use. Iodized oils not only act as a contrast medium to opacify the adhesive, but also reduce the polymerization time. However, the effect was found to be less pronounced when mixing n-2-butyl-cyanoacrylate with iophendylate (Pantopaque, Lafayette Pharmacol, Lafayette, IN, USA). Another side effect of the oils is to promote a less uniform, more flocculent polymer. The addition of glacial acetic acid has also been described as a method of delaying polymerization.

Most endoscopists mix cyanoacrylates with the lipid soluble Lipiodol to retard polymerization and enhance imaging. A mixture that is too concentrated risks premature polymerization, a mixture that is too dilute increases the risk of embolization. Lipiodol is also used to coat the interior of the injection needle catheter, the interior of the endoscope channel, and the tip of the endoscope to avoid damage to the endoscope.

In vitro measurements have shown that the polymerization of cyanoacrylates can be delayed markedly and controlled by adding an oily radiopaque material such as Lipiodol ultrafluid[55]. For example, a volumetric ratio of 1:4 of Histoacryl: Lipiodol provided good flow properties with polymerization time of approximately 12 seconds and excellent contrast definition (Table 8.16). Pollak and White use a mixture of monomeric cyanoacrylate adhesive with Ethiodol (Savage Laboratories, Melville, NY, USA) in ratios varying from 1:1 to 1:4[56].

Overstabilization is a temptation to ensure long shelf and working lives for cyanoacrylate adhesives. This practice, however, should be avoided because it leads to sluggish cure rates and inferior bond strengths. Overstabilization with strong acids should also be avoided in order to minimize hydrolysis.

Researchers have explored the possibility of non-adhesive cyanoacrylates to reduce the potential for adhesion between the tip of a microcatheter and an artery. An isostearyl-2-cyanoacrylate (ISCA) was developed to polymerize on contact with blood and does not demonstrate strong adhesion to the catheter. The ISCA required mixing with n-2-butyl-cyanoacrylate

Table 8.16 Polymerization Time of Various Volumetric Mixtures of Histoacryl and Lipiodol or Pantopaque[55]

Volume Mixing Ratio	Polymerization time, s	
	Histoacryl / Lipiodol	Histoacryl / Pantopaque
1:1	3.2	3.6
1:2	4.7	4.9
1:3	7.5	6.3
1:4	11.8	10.2

to give reasonable tissue adhesion, but much lower than with the adhesive alone[57]. Other possible non-adhesive cyanoacrylate products have been proposed, such as derivatives with long alkyl chains or 2-hexyl cyanoacrylate (Neuracryl M, Prohold Technologies Inc., San Diego, CA, USA)[58].

8.4.2.3 Accelerators

Accelerators are substances that increase the rate of polymerization but are not initiators in their own right. Accelerators can be compounded into the adhesive and do not significantly detract from storage stability. Among the earliest accelerators was common chalk, a natural carbonate. Certain chelating agents, such as crown ethers (10-1000 ppm) and polymers of ethylene oxide (0.5-10%) decrease the setting time without markedly reducing stability[59]. Presumably, they function by producing anions. The incorporation of poly-n-vinyl pyridine or polyethyleneimine or even simple amines serves the dual purpose of thickening the liquid and increasing the pH to speed cure.

Cooke and Allen provide an interesting test methodology for determining the effect of weak bases (e.g., N,N-dimethyl-p-toluidine and piperidine) on the polymerization time of various commercial adhesives[60]. Such a methodology may be used to measure the effect of inhibitors or accelerators. The authors also show that the acid value of the adhesive has a significant effect on the polymerization time.

Accelerators such as long chain amines, quaternary ammonium salts, and phosphine can be supplied in a solvent carrier and applied as a substrate primer or the accelerator can be added to the applicator tip. This prevents premature cure of the bulk adhesive by the accelerator before the parts can be mated. Also, liquid adhesive not cured by reacting between the substrates (e.g., excess adhesive at a filet) can generally be cured within seconds with activators. In these cases the activator can be sprayed or brushed directly onto the liquid cyanoacrylate.

Primer / accelerators are generally used on acidic surfaces or on surfaces where there is no adsorbed water or hydroxide ions (e.g., many plastic or elastomeric substrates). Most manufacturers supply suitable accelerators for their adhesives and can recommend specific combinations for most bonding applications. The use of accelerators / primers in surgical adhesives has not been reported in the technical literature but may be advantageous as a primer on synthetic grafts.

Several companies have discovered new primers that effectively interact with the cyanoacrylates. Triphenylphosphine or cobalt acetylacetonate primers used with cyanoacrylate adhesives produce adhesive bonds with polypropylene and low density polyethylene that are sufficiently strong to exceed the bulk shear strength of the substrate. They are also sufficiently durable as to withstand immersion in boiling water for long periods of time. Dimethyl-p-toluidine (DMPT) is an effective and common activator for cyanoacrylate adhesives. Since it is classified as a toxic substance, this activator is used only in industrial applications. Diethanol-p-toluidine (DEPT) is preferred in many applications based mainly on its relatively low toxicity and color retention.

Several patents describe methods of inducing cure of cyanoacrylate by passing the adhesive through a porous applicator tip containing substances that initiate the

polymerization[61]. These substances co-elute and dissolve into the adhesive as it is forced through the porous tip.

8.4.2.4 Thickeners

Thickeners are added to control the rheology of the adhesive and to prevent the adhesive from being absorbed into the substrate or from running off the surface. The higher viscosity grades are also necessary when large gaps exist between two substrates. The viscosities of commercial cyanoacrylates range from 0.002 Pa·s for unmodified monomers to 30 Pa·s for monomers thickened with organic polymers.

Thickeners are typically high molecular weight acrylates soluble in the cyanoacrylate monomer. Suitable thickeners include poly(alkyl acrylates), poly(alkyl methacrylates), poly(vinyl acetate), and poly(alkyl-2-cyanoacrylates). The addition of elastomeric material or a polymer such as poly(methyl methacrylate) has been found to increase impact strength and elongation-to-break values.

Because of their low viscosity, cyanoacrylates are easy to deliver through microcatheters; however, the high flow characteristics may be a detriment in certain applications. Thixotropic cyanoacrylates have been formulated with hydrophobic silica along with an organic thickener. The rheological properties of these adhesives provide a low viscosity under high strain rates such as when pumped through a microcatheter and high viscosity under low strain rates such as after application between substrates.

Manufacturers have increased viscosity of the adhesive by dissolving polymer back into the monomer. By incorporating flexible viscosifying agents and adding nontoxic plasticizer, one can possibly use shorter chain cyanoacrylate monomer in formulation and overcome their brittleness[62].

8.4.2.5 Plasticizers

Early in the development of cyanoacrylate adhesives, brittleness was recognized as a deficiency and many efforts have been made to solve this problem. Two generic approaches have been taken: (1) to use plasticizers or flexibilizers as additives or (2) to internally plasticize the molecule by adding longer side chain groups and/or increasing molecular weight.

Plasticizers are occasionally added to increase the flexibility of the cured adhesive and to improve impact resistance. Those most commonly used are C_1 through C_{10} esters of dicarboxylic acids, such as phthalic acid and sebacic acid. High concentrations of plasticizer reduce both the cure rate and bond strength. Limiting the plasticizer concentration to less than 5% will not generally retard the cure speed, from 5-20% will retard the cure rate, and over 20% plasticizer concentration seriously slows the cure rate of the adhesive[63].

High levels of lactones (e.g., propiolactone, butyrolactone, and heptodilactone) however, have been found to plasticize the cyanoacrylates without retarding the cure rate. In fact, some of the lactones apparently increase the cure speed after long-term storage of the adhesive. This is an indication that the lactones copolymerize with the cyanoacrylate in some fashion.

Plasticization may also result from internal modification of the cyanoacrylate molecular structure. This is the case for octyl-2-cyanoacrylate. The longer chain segments and the

higher molecular weight provide flexibility in the cured molecule, which translates into greater flexibility and impact strength. Such internal plasticization does not result in a significant decrease in adhesive strength and, in fact, may result in improvements depending on the specific substrate and joint geometry.

8.5 Properties

The properties of cyanoacrylate adhesives that set them apart from nearly all other adhesives are that they are single component and capable of bonding at room temperature within just a few seconds.

The “cure-on-demand” characteristic of cyanoacrylate adhesives has interested surgeons for decades. However, other properties are also vital, and often they will determine the extent of application and define the risks and benefits. The utility of various cyanoacrylate adhesives in surgery is directly related to their application and performance properties. This section reviews and compares important performance properties of commercial cyanoacrylate surgical adhesives.

8.5.1 Curing Mechanism

The reaction chemistry of cyanoacrylate adhesives is an important factor to the use and success of cyanoacrylates in surgical applications. On application to living tissues, the cyanoacrylate monomer undergoes an exothermic hydroxylation reaction that results in polymerization of the adhesive.

When the adhesive contacts a slightly alkaline surface, trace amounts of adsorbed water or hydroxide ions (OH⁻) that are present on the substrate’s surface neutralize the acidic stabilizer in the adhesive, resulting in rapid polymerization as shown in Figure 8.4. Thus, human tissue can be bonded very quickly with cyanoacrylate adhesive, not only due to the water content, but also to the amino acids present, which are quite basic to the adhesive. This has encouraged the use of cyanoacrylates in many surgical and dental applications.

Initiation:



Propagation:

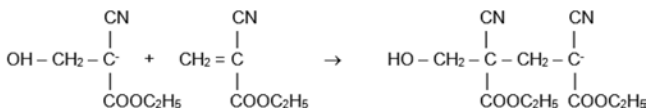


Figure 8.4 Chemical reaction of cyanoacrylate adhesives[59].

Cyanoacrylates typically reach significant bond strength within one minute at room temperature and achieve full strength in a few hours. In general, ambient humidity in the air or moisture on the bonding surface is sufficient to initiate curing within a few seconds. Therefore, substrates must be joined quickly. The setting time is dependent on the grade of adhesive, the ambient temperature and relative humidity, and the nature of the substrate surface (pH and amount of adsorbed water). Most cyanoacrylate development has been either to increase reaction rate (especially to less reactive surfaces such as low surface energy polymers) or to improve shelf-life without sacrificing set time.

8.5.1.1 Comparative Shelf-Life

It is generally assumed that the shelf-life of cyanoacrylate adhesives is in the range of 6-12 months at room temperature and almost indefinite when stored under refrigeration[47]. Medical cyanoacrylate tissue adhesives generally claim a longer shelf-life than industrial cyanoacrylates.

A comprehensive stability study was performed over a three-year period and results indicated that many cyanoacrylate adhesives were stable for two years after which their stability and performance degraded[64]. The cyanoacrylate adhesives studied were stored in a cool, dark, and dry location in order to prevent premature polymerization by heat, sunlight, or moisture.

Generally, octyl-cyanoacrylate adhesives have better stability and a longer shelf-life than n-butyl-2-cyanoacrylate adhesives as they are inherently less reactive. Refrigeration is usually recommended for n-butyl-2-cyanoacrylate adhesives, while octyl-cyanoacrylate does not require refrigeration. The shelf-lives that are claimed for commercial cyanoacrylate adhesives used in surgical applications are indicated in Table 8.17.

As a rule, if the viscosity of a stored adhesive has not increased and the rate of cure has not diminished during storage, the adhesive will perform as specified. Henkel uses an accelerated aging test for cyanoacrylate adhesive products consisting of 50°C aging and testing after 0, 2, 4, 6, and 8 weeks of aging. Two weeks of aging is roughly equivalent to six months of aging at room temperature[65]. Based on ASTM F1980-2 (Standard Guide for Accelerated Aging of Sterile Barrier Systems for Medical Devices), 12 days accelerated aging at 80°C or 6 months at 40°C is equal to 2 years shelf-life at room temperature.

According to Adhezion Biomedical, the shelf-life of SurgiSeal adhesive (an octyl-cyanoacrylate) was determined by real time shelf-life stability of 2 years and by the accelerated aging test at 80°C for 12 days, as well as the accelerated aging test at 40°C for 6 months. The stability of SurgiSeal was assessed based on five chemical characteristics: purity (2-OCA percentage), setting time, viscosity, color and sterility.

8.5.1.2 Container Materials for Packaging

The fast setting property of cyanoacrylates which makes them useful as a surgical adhesive raises serious problems in regard to packaging for a suitable shelf-life. A suitable container for cyanoacrylate monomer must have a high degree of gas and water vapor impermeability. This is to prevent water vapor in the air from permeating the

Table 8.17 Shelf-Life of Commercial Cyanoacrylate Surgical Adhesives

Cyanoacrylate Type	Trade Name	Company	Shelf-life
2-Octyl-cyanoacrylate	Dermabond	Ethicon, Somerville, NJ, USA	2 years at <30°C
	SurgiSeal	Adhezion Biomedical, Wyomissing, PA, USA	2 years at <30°C
n-Butyl-2-cyanoacrylate	Histoacryl	B. Braun, Tuttlingen, Germany	2 years at <-5°C
	Indermil	Henkel Loctite, Rocky Hill, CT, USA	2 years refrigerated or four months ambient
	Glubran 2	GEM s.r.l., Viareggio, Italy	2 years at 0°C to -4°C
	Liquiband*	Advanced Medical Solutions, Howell, MI, USA	18 months at 5°C to 25°C

* Liquiband is a blend of 2-octyl-cyanoacrylate and n-butyl-2-cyanoacrylate

container and, thereby, causing the monomer to polymerize before it can be used. It is also important that the container be impermeable to vapors other than water which could similarly polymerize the monomer should they gain entry into the container.

An example of the latter problem occurs when one wants to sterilize the outer surface of an adhesive container by conventional ethylene oxide technology. Ethylene oxide may be a preferred method of sterilization of cyanoacrylate adhesives since it avoids the high temperature encountered in autoclaving. However, during the ethylene oxide sterilization cycle, the container is ordinarily subjected to a mixture of pressurized ethylene oxide, carbon dioxide, and water for extended periods of time. Should appreciable amounts of water or ethylene oxide penetrate the container, the product will polymerize.

It is also important that the container have a high degree of impermeability toward cyanoacrylate monomer, both liquid and vapor. Should vapor or liquid escape from the container it will polymerize on contact with the ambient moist environment surrounding the container to produce an effect called "blooming". It is also important that the container material be hermetically sealable so as to prevent leaks either into or out of the package at the seal points.

As a result, packaging containers are generally made of polyethylene or polytetrafluoroethylene products since these surfaces are relatively non-reactive with cyanoacrylate and they provide a moderate barrier to ambient moisture. Since polyethylene and polytetrafluoroethylene are somewhat permeable to moisture, the container is often shipped and stored in a barrier package, such as metal foil. US Patent 3,524,537 provides a good description of early problems noticed with cyanoacrylate monomer packaging materials[66]. These are summarized in Table 8.18.

High density polyethylene (HDPE) is the primary packaging material for industrial grade cyanoacrylates because it provides adequate containment and shelf-life for many

Table 8.18 Problems Noticed with Early Cyanoacrylate Packaging Materials

Container Material	Problems Noticed
Low and high density polyethylene	Noticeable and rapid diffusion of monomer vapor out of the container as evidenced by the appearance of a substantial amount of white polymer film (blooming) on the surface of the container in only a few hours.
Saran (vinyl chloride – vinylidene chloride copolymer)	Generally known to have good vapor barrier properties, but permitted cyanoacrylate monomer to escape and polymerize on the external surfaces of the packaging after three weeks of storage at 37°C. In addition the Saran film was badly and permanently distorted.
Cellulose acetate and a laminate of cellulose acetate, Saran, and polyethylene	Similarly permitted cyanoacrylate monomer to escape as evidenced by polymer film on the surface of the container within 16 hr at 37°C.
Mylar – polyethylene laminate	Caused the contents of the container to polymerize within about two months after preparation of the package, thereby indicating entry of polymerization initiators into the contents of the container.
Haloethylene polymer (polytetrafluoroethylene)	Provided storage-stable containers; however, they were not transparent and are known to be quite difficult to fabricate into sheets or tubing suitable for containers (heat sealing is difficult).

compositions including butyl-cyanoacrylate monomers. These lower chain length cyanoacrylate adhesive monomers can be stably contained in HDPE containers for over one year without significant degradation of the monomer composition in the container, and for over 17 months without the container becoming noticeably degraded[67].

However, even with the stability provided by HDPE containers, cyanoacrylate suppliers have continued to develop innovative packaging designs that promised to even further improve the stability and shelf-life of the adhesive. This has generally been in response to the need to have a very fast reacting adhesive with surface insensitivity (good strength development on both basic and acidic substrates) and the desire to have greater purity (lack of inhibitors) in medical grade cyanoacrylates. Some of these developments are described below:

- Schaefer and Eckstein[68] disclose a multilayer packaging tube. The tube has a layer of HDPE positioned on the side of the tube that comes into contact with the cyanoacrylate. A primer layer of polyethyleneimine is located on the outside of the high density polyethylene layer to act to block migration to the outside surface of any cyanoacrylate product that passes through the polyethylene.

- Colvin[69] discloses the use of halogenated hydrocarbon polymers such as Teflon and poly(vinyl fluoride) for packaging.
- Winter[66] discloses a hermetically sealed package comprising a polymonochlorotrifluoroethylene container for a sterilized cyanoacrylate adhesive.
- D'Alessio[70] discloses a post-fluorinated process for treating a packaging material to contain a cyanoacrylate monomer.
- Monteneri and Termley[71] describe a squeezable multilayer container made of external and internal layers of polyolefin and a barrier layer formed of a barrier material blended with an adhesive.
- Azevedo and Zimmerman[72] describe a polypropylene package for cyanoacrylate with a nitrile polymer barrier layer as the inner layer of the package. The nitrile polymer material is sold under the Barex brand by BP Petrochemicals. The combination of materials is claimed to offer a shelf-life for cyanoacrylate adhesive products of two years or longer.

8.5.2 Bond Strength

Common tests used to determine the adhesive strength of cyanoacrylate surgical adhesives have been described by ASTM.

- ASTM F 2255, Standard Test Method for Strength Properties of Tissue Adhesives in Lap- Shear by Tension Loading.
- ASTM F 2256, Standard Test Method for Strength Properties of Tissue Adhesives in T-Peel by Tension Loading.
- ASTM F 2258, Standard Test Method for Strength Properties of Tissue Adhesives in Tension.
- ASTM F 2458, Standard Test Method for Wound Closure Strength.

Further reading regarding the chemistry, method of preparation, and application of cyanoacrylates is covered in several excellent reviews[73-76].

Chivers and Wolowacz[21] provide a thorough review of the strength of adhesive bonded tissue joints. Bonds described were formed *in vitro* and tested with a standard tensile test procedure. Bond strengths were strongly dependent on the adhesive type, with cyanoacrylate adhesives outperforming the others by at least an order of magnitude (as was previously shown in Table 8.7). Bond strengths of cyanoacrylate adhesives are dependent on its specific formulation, the nature of the substrate(s), and the application / curing method utilized.

Although n-butyl-2-cyanoacrylate is effective in closing superficial lacerations under low tension, it has several limitations. Studies have shown wound breaking strength in wounds repaired with n-butyl-2-cyanoacrylate to be equal to that in wounds repaired with sutures at 5-7 days; however, on day 1 the breaking strength with the tissue adhesive is only approximately 10-15% of that in a wound sutured with 5-0 monofilament. After polymerizing, the adhesive becomes brittle and is subject to fracturing when used in skin

creases or long incisions. This restricts the use of adhesive to areas of relatively low tension, thus limiting their use.

The 2-octyl-cyanoacrylate adhesive (Dermabond) has greatly improved flexibility due to its internal plasticization and several researchers have reported bond strength to tissue to be greater than n-butyl-2-cyanoacrylate[77, 78]. However, there is debate regarding this due to differences in test procedures, substrates, etc. It may be possible that n-butyl-2-cyanoacrylate has a greater tensile strength while 2-octyl-cyanoacrylate has greater shear strength. Generally more rigid adhesives perform better in tension while more flexible systems perform better in shear.

Several studies have been made with regard to a comparison of the bond strengths of surgical cyanoacrylate adhesives with the strength of conventional sutures. Early studies indicated that the initial strength of n-butyl-2-cyanoacrylate or 2-octyl-cyanoacrylate was not as strong as sutures and the breaking strength only equalized after several days[79, 80]. However, more recent publications indicate that Dermabond and Histoacryl are both significantly stronger than Steri-Strips (3M, St. Paul, MN, USA) but inferior to staples[81, 82].

8.5.3 Toxicity

When used as a tissue adhesive, cyanoacrylates have been reported to cause inflammation and tissue necrosis *in vivo*. An excellent recent review of the toxicity of cyanoacrylate adhesive in surgical applications has been published by Leggat *et al.*[83].

Inflammation, tissue necrosis, granulation formation, and wound breakdown can occur when cyanoacrylates are implanted subcutaneously. The process causing the histologic toxicity is thought to be related to the byproducts of degradation: cyanoacetate and formaldehyde[84]. The liberation of formaldehyde inside the body represents a significant issue regarding the acceptance of cyanoacrylates as internal tissue bonding adhesives. However, this is not believed to be a major issue in topical applications.

An alternative degradation mechanism has been proposed where the cyanoacrylate breaks down by the hydrolysis of the ester group. This seems to be verified by the fact that the measured amount of formaldehyde produced is only 5% of the amount of the theoretical quantity that would have been produced if the polymer had been entirely degraded by the cyanoacetate / formaldehyde pathway.

It is possible that the formaldehyde levels released from cyanoacrylates *in vivo* are low enough to be processed by tissue metabolic systems and/or cleared by the normal flow of physiological fluids over the site[85]. Research has shown that longer-chain cyanoacrylate derivatives degrade at a slower rate, thereby permitting the degradation products to be more safely metabolized with the generation of a less intense inflammatory response[86].

The local concentration of these breakdown products is proportional to the rate of degradation of the parent compound. Therefore, slower degradation rates result in less toxicity to the tissues. The slower degradation rate results in more effective clearance and invokes a less intense inflammatory response. The longer-chain compounds degrade much more slowly than the shorter chain compounds (Figure 8.5). The biodegradation rate of other surgical adhesives (e.g., fibrin, GRF) is much faster than any cyanoacrylate.

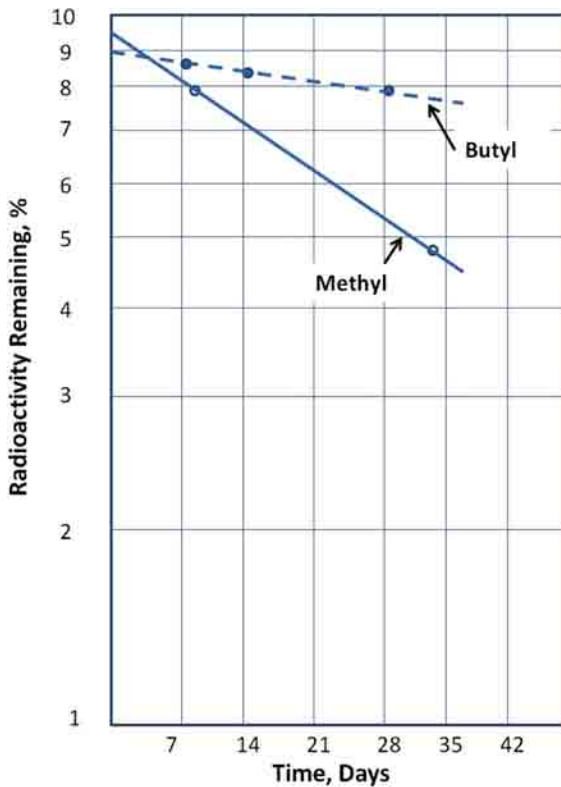


Figure 8.5 In vivo degradation rates measured as remaining radioactivity of tagged alkyl cyanoacrylate adhesives after days of body implantation[87]. (In vivo degradation of radioactivity is considered to be analogous to biological degradation.)

8.5.4 Biocompatibility

Adhesives used in medical devices are tested for their effect on cells (cytotoxicity), blood constituents (hemolysis), adjacent tissues, and for overall systemic effect. Several standards exist for biocompatibility testing. Adhesive suppliers, however, generally test according to the following guidelines that have been established for toxicological properties and biocompatibility:

- United States Pharmacopoeia (USP) – Class VI Standard
- International Standards Organization (ISO) – ISO-10993.

These guidelines were originally developed for testing the suitability of plastics used in medical devices that may come into contact with bodily fluids, but they have been extended

to adhesives as well. The two standards specify slightly different tests and follow different methodologies.

According to the injection and implantation testing requirements specified under the USP biological reactivity tests, *in vivo* polymers are classified on a scale of I to VI. To test a polymer, extracts of the material are generated in various media. The extracts are then injected systemically and intracutaneously into rabbits or mice to evaluate their biocompatibility. Class I, II, III, and V polymers do not require implantation testing; Class IV and VI polymers do require such testing. The USP Class VI test method consists of acute systemic (over the tissue), intracutaneous (under the skin), and muscle implantation (in the muscle) tests.

The Class VI rating merely states that the products exhibit a low level of toxicity under the test conditions. Merely passing the USP Class VI standard does not guarantee that an adhesive will meet FDA requirements in a particular application; however, passing the test is a strong indication of the nontoxicity of an adhesive.

The ISO-10993 standard is generally recognized as the standard of choice for companies operating globally and is widely recognized by North American, European, and Asian countries. It is also more extensive than the USP Class VI standard. The ISO-10993 biocompatibility testing includes:

- Intracutaneous injection tests to evaluate the irritation potential of the material,
- Acute systemic injection tests to evaluate the material for potential toxic effects as a result of single dose systemic injections,
- Cytotoxicity tests to determine the biological reactivity of cell cultures to the material, and
- Hemocompatibility tests to evaluate the hemolytic potential of the material with rabbit blood. (*In vitro* hemocompatibility tests ensure that the test material extract does not adversely affect the cellular components of the blood.)

ISO Standard 10993 consists of 16 parts. Each part describes specific tests that include a variety of toxicity tests. Table 8.19 indicates the biological effects that are tested in ISO 10933 for various combinations of procedures, tissues, and contact duration.

8.6 Clinical History

Cyanoacrylates have been used in many surgical disciplines[88]. Skin closure is a major application area for cyanoacrylate adhesives and this has received extensive attention. There are also literature reports documenting the use of cyanoacrylates to bond bone and cartilage, nerve tissue, vascular tissue, and intestines. Table 8.20 lists just some examples of the surgical and medical applications for cyanoacrylate adhesives. Other specific procedures include repair of blood vessels[89], placement of dural substitutes[90], animal limb reimplantation[91], kidney[92] and bronchial[93] closure, and repair of bone fractures[88, 94].

Table 8.19 Biocompatibility Tests for Medical Adhesives and Medical Devices According to ISO 10993 [3]

Adhesive Category		<i>Biological Consideration</i>											
Nature of body contact	Contact duration: A: <24 hr B: 1-30 days C: >30 days	Cytotoxicity	Sensitization	Irritation	Acute toxicity	Subchronic toxicity	Genotoxicity	Implantation	Hemocompatibility	Chronic toxicity	Carcinogenicity	Reproductive toxicity	Biodegradation
		Adhesive applied to the surface	A	X	X	X							
	B	X	X	X									
	C	X	X	X									
	A	X	X	X									
	B	X	X	X	O	O		O					
	C	X	X	X	O	X	X	O		O			
	A	X	X	X	O								
	B	X	X	X	O	O							
	C	X	X	X	O	O							
	A	X	X	X	O								
	B	X	X	X	O	O		O					
	C	X	X	X	O	X	X	O		O			O

Table 8.19 cont.

Adhesive Category		Biological Consideration													
Nature of body contact		Contact duration: A: <24 hr B: 1-30 days C: >30 days	Cytotoxicity	Sensitization	Irritation	Acute toxicity	Subchronic toxicity	Genotoxicity	Implantation	Hemocompatibility	Chronic toxicity	Carcinogenicity	Reproductive toxicity	Biodegradation	
External adhesive contact- ing internal tissues	Blood path direct	A	X	X	X	X				X					
		B	X	X	X		O			X					
		C	X	X	O	X	X		X	O	X	X	X		
	Tissue, bone, dentine	A	X	X	X	O									
		B	X	X	X	X	X	X	X	X					
		C	X	X	X	X	X	X	X	X		X	X		
	Circulating blood	A	X	X	X	X			O		X				
		B	X	X	X	X	X	X	X	X	X				
		C	X	X	X	X	X	X	X	X	X	X	X		
Adhesive used for implants	Tissue, bone	A	X	X	X	O									
		B	X	X	X	X	X	X	X	X					
		C	X	X	X	X	X	X	X	X		X	X		
Blood	A	X	X	X	X	X	X	X	X	X					
	B	X	X	X	X	X	X	X	X	X					
	C	X	X	X	X	X	X	X	X	X	X	X			

Note: X tests to be executed according to ISO 10993, O tests to be executed according to FDA "Blue Book Memorandum G95-1"

Table 8.20 Examples of Surgical and Medical Applications of Cyanoacrylate Adhesives[84, 95]

Procedure	Past, Present, and Potential Applications
General surgery	Surgical wound repair; control of hemorrhage; skin graft fixation
Emergency medical and general practice	Traumatic wound repair; fingernail repair
Endoscopy	Control of variceal bleeding and obliteration of oesophagogastric varices
Ophthalmology	Temporary repair of corneal perforations
Thoracic surgery	Closure of pulmonary leaks
Neurosurgery	Ossicular chain reconstruction
Otological surgery	Ossicular chain reconstruction
Interventional radiology and cardiology	Embolotherapy of various vascular abnormalities, including aneurysms
Pediatrics	Wound closure in children
Pharmacotherapeutics	Drug carriers

Although cyanoacrylate adhesives have been used, undergone trial, or suggested for use in many medical procedures, in practice few surgeons use cyanoacrylate adhesives except in unusual circumstances or in emergency cases. This is generally due to inexperience, toxicity issues, degradation rates, and to a lesser extent the adhesive's rigidity and low viscosity. Future desirable design features in a surgical grade cyanoacrylate would solve these issues as well as provide a set time that can be tailored to the needs of the surgeon and the procedure.

The discussion below provides a small sampling of the external and internal clinical uses of cyanoacrylate surgical adhesives that have been reported in the literature. A more comprehensive literature survey can be developed from MEDLINE and BIOSIS, two literature research facilities dedicated to the medical and biological sciences.

8.6.1 Closure of Skin Wounds and Superficial Incision Closure

The use of cyanoacrylate tissue adhesives for closing skin lacerations and surgical incisions is well documented in the scientific literature[79, 96]. The adhesive was first used during the Vietnam War to provide emergency battlefield treatment[97].

The adhesive is used in various situations to avoid using skin sutures in cosmetic surgery and by emergency room physicians to close smaller cuts or to provide support for deeper sutures. It is especially useful in minor pediatric surgery since cyanoacrylate adhesives avoid the use of needle and the resulting trauma[98]. Toriumi, et al., have published

an excellent paper on the use of 2-octyl-cyanoacrylate adhesives that underscores the need to reduce skin stresses at the site of laceration and the need to ensure that there is no dead-space present before sealing with the adhesive[86]. The FDA approved 2-octyl-cyanoacrylate (Dermabond) for topical application for the closure of incised skin and for the use as a barrier against common bacterial microbe[99, 100].

8.6.2 Other Surgical Procedures and Future Uses

Surgeons have begun to use cyanoacrylate tissue adhesives in the operating room for the closure of surgical skin incisions although there are fewer clinical trials to support this indication. Application beyond external use is considered to be unwise and could be dangerous to patients[101].

While the FDA has only approved the use of 2-octyl-cyanoacrylate in superficial closures, many European and off-label US clinical trials have been conducted illustrating the broad effectiveness of 2-octyl-cyanoacrylate in other applications. The following is a list of uses of 2-octyl-cyanoacrylate that have proven successful[102].

- Type I tympanoplasty (eardrum surgery)
- Repair of fractured teeth
- Total joint arthroplasty wounds
- Hemostasis and anastomoses of vessels in cardiac surgery
- Implanting pacemakers
- Direct application to visceral pleura to control air leaks
- Controlling bleeding from gastric varices
- As a wound barrier in clear corneal cataract surgery
- For patch fixation in a tension-free inguinal herniorrhaphy.

Use of the cyanoacrylate below the level of the skin can result in acute and chronic inflammation and tissue necrosis[39]. However, cyanoacrylates have been used for embolization[38, 40] and repair of endoleaks after conventional aortic surgery[41, 42]. Injection therapy with cyanoacrylates is now considered the first line endoscopic intervention of bleeding gastric varices as well as secondary prevention of gastric variceal bleeds outside of the US[43].

In an anatomical area that is difficult to reach, application of cyanoacrylate adhesive can be accomplished by using a long polyethylene catheter or needle. The tips of the instruments used for applying the cyanoacrylate should be siliconized or coated with Teflon or other low surface energy polymers so that the adhesive can flow freely and the application instrument does not adhere to the repaired wound.

8.6.3 Graft Fixation

Cyanoacrylate (2-octyl-cyanoacrylate) can be used for skin graft fixation among other grafting applications. A 2001 study[103] evaluated 2-octyl-cyanoacrylate for mechanical

fixation of an expanded polytetrafluoroethylene prosthesis in minimally invasive incisional hernias repair in rabbits. The mesh was successfully fixed to the abdominal wall musculature at 6 weeks. However, the force required to displace the mesh was lower than for mesh fixed with staples or sutures. Prosthesis fixed with 2-octyl-cyanoacrylate induced fewer intra-abdominal adhesions than those fixed with staples and sutures.

Kreamer discloses the use of an adhesive covering the entire outside of the graft to provide adherence of the luminal intima to the graft[104]. An example is given of a cyanoacrylate adhesive that can be sandwiched between Dacron or film-like materials that are relatively inactive to cyanoacrylate polymerization. During application this protective sheath is slid off, and the cyanoacrylate is allowed to attach the prosthesis to the vessel wall.

The restoration of receptors of the eye and the ear and oral applications represent delicate procedures that can also be aided by cyanoacrylate adhesives[1]. The adhesive can seal corneal or fistuls of the eye to prevent oozing of optical fluids. However, torn eye muscles cannot be fastened with these adhesives due to inadequate bond strength. Cyanoacrylate adhesives have also been used to rejoin bones in the middle ear during mastoid surgery. These adhesive have also been used to stop nose bleeding. In dental surgery, cyanoacrylates have been used as a hemostatic agent, protection for healing ulcers, and as a dental filling / adhesive material.

8.7 Future Potential

8.7.1 *Development Path*

The use of cyanoacrylates in surgery has been restricted over the years due to (1) application and physical properties not being suitable for specific procedures and (2) concerns about histotoxicity. The current commercially available cyanoacrylate surgical adhesives are only approved for external use in regions such as the US.

The development of surgical cyanoacrylate adhesives should aim at satisfying the unmet needs of both internal and external applications. Physicians need more advanced materials that are precisely deliverable, easily controlled, maintain a clear field of vision, and work reliably and promptly.

For external applications, increased viscosity to a gel form, antimicrobial properties, and greater strength and flexibility would be valued improvements. For internal procedures the development of adhesives with lower toxicity and faster degradation rates would be of significant benefit. In both external and internal applications, improvements may be possible in the easiness with which cyanoacrylate adhesives can be prepared and applied with a polymerization rate that can be controlled by the surgeon. Such improvements will be required before cyanoacrylate adhesives gain full surgeon acceptance and regulatory approval for the majority of surgical procedures.

Past research and more recent developments in the field indicate that such improvements may not be too far away. Meaningful accomplishments have been made especially in making the application and polymerization properties more convenient for complex surgical procedures. Several of these activities are described below.

8.7.1.1 Light Curing Cyanoacrylates

It is possible to formulate a light activated cyanoacrylate adhesive. These are now available commercially for the assembly of medical and electronic devices. However, the commercial products still cure on contact, and the "light activation" is used mainly to set cyanoacrylate material that is not sandwiched between two substrates (e.g., a coating used for wire tacking or the excess cyanoacrylate that exudes out from a joint).

Several light activated cyanoacrylates have been suggested for surgical adhesives. One is based on *n*-phenyl- α -cyanoacrylate that is stabilized by the types of additives mentioned in this review. Cyanoacrylate compositions with terminal vinyl groups have also been developed to be medical adhesives that can be activated by heat or light activated initiators and accelerators[105]. Free radical polymerization can then be initiated by irradiating the monomer with UV light or other radiation sources. This methodology may be superior to current cyanoacrylate surgical adhesives since one can "overdose" with an inhibitor and rely primarily on the radiation energy for crosslinking rather than the blood chemistry.

An interesting concept is contained in US Patent 6,718,212 that describes an implantable medical lead attached to the heart with a light activated adhesive[106]. The light activated adhesive comprises one of the more standard industrial light activated acrylic or cyanoacrylate adhesive (e.g., Loctite FlashCure, Henkel, Rocky Hill, CT, USA). An advantage of this method of delivery is that the speed of the cure can be adjusted by the intensity of the UV light. The patent also describes a method of adhesive delivery and of administering the light energy inside the body cavity.

8.7.1.2 Solid Cyanoacrylate

A solid cyanoacrylate adhesive composition is disclosed which can be applied to a substrate in solid form and which polymerizes into an adhesive upon liquefying[107]. The adhesive can be formulated so that it liquefies at temperatures slightly above room temperature and then polymerizes on wetting the substrate surface. ϵ -Caprolactones are used as the solidifying polymer with cyanoacrylate monomers and other additives to form the solid adhesive composition.

The solid cyanoacrylate is claimed to be easy to apply, non-polymerizing in solid form and capable of use in a variety of industrial, consumer, and medical applications. Furthermore, the formulation appears to be straightforward and not complex. A cyanoacrylate monomer is heated and maintained at 55°-70°C. The resin ϵ -caprolactone (Tone Polyol P-767-E, Dow Corporation, Midland, MI, USA) is mixed into the cyanoacrylate until completely dissolved. The solution is then cooled to a solid at room temperature. Melting temperature can be controlled by the concentration of the ϵ -caprolactone. A 70:30 ratio of cyanoacrylate to ϵ -caprolactone will provide a melt temperature of 40°C and a 50:50 mixture will provide a melt temperature of 43°C.

8.7.2 *Drivers for Increased Demand*

Over the past few decades, the wound closure market has seen the introduction of a number of new adhesive materials to hold tissues together or reinforce surgical sutures. According to MedMarket Diligence, LLC, approximately 114 million surgical and procedure-based wounds occur annually worldwide, including 36 million in the US, which can benefit from adhesives, sealants, or hemostatic agents[108].

Despite their high initial cost, coupled with reluctance on the part of some physicians to wholeheartedly adopt surgical adhesives, these products have gained increasing acceptance in recent years due to the advantages they provide over traditional suture- and staple-based closure methods. Trends that support the increasing demand in surgical adhesives include:

- Ambulatory same day surgery
- Laparoscopic procedure
- Operating room time reduction
- The shift over the past two decades to performing surgery in the less expensive outpatient setting
- Trend to less invasive procedures which produce shorter recovery times, faster discharges, less scarring, less pain and less need for pain medications
- The reclassification of tissue adhesives as Class II by the Food and Drug Administration (FDA).

The market for advanced wound closure processes including sealants and adhesives is growing and is expected to continue its expansion as new products and application devices are developed and regulatory approvals are achieved. The global market for these products is expected to grow to \$1.72 billion by 2017 (Figure 8.6). The cyanoacrylate tissue adhesive share of this global market was valued at \$35.7 million in 2009, and is expected to grow at a compounded annual growth rate of 5.4% to reach \$51.6 million by 2016[109].

8.8 Summary

A surgical adhesive is one that can join tissues without the complications of sutures or other mechanical fasteners. Cyanoacrylates were among the first synthetic organic compounds to be used as adhesives for human tissues. Cyanoacrylates for such medical purposes were originally developed and introduced in the 1960s under a cooperative agreement between Eastman Chemical and Ethicon, a subsidiary of Johnson & Johnson.

The first use of cyanoacrylate surgical adhesive came during the Vietnam War. Often seriously wounded soldiers would die from loss of blood before surgeons could make needed repairs. This was especially true for serious wounds of the chest or abdomen. Medical technicians found that a simple spray of cyanoacrylate stopped the bleeding almost immediately.

Early-on there were concerns about the compatibility of cyanoacrylate adhesives with the human system and possible toxicological effects of the adhesive. However, it was found

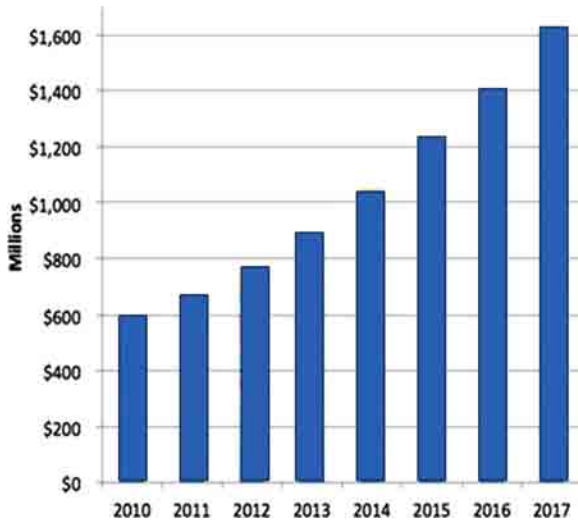


Figure 8.6 Worldwide estimated market, in million USD, for high strength medical adhesives, 2010-2017[108].

that the adhesive breaks down to relatively harmless by-products. More importantly, the rate of cyanoacrylate breakdown was about the same as the rate at which the wounds healed.

The full value of cyanoacrylate adhesives has been identified through many medical trials. Cyanoacrylate adhesives are valuable in many sutureless surgery procedures. They are also useful in sealing and reinforcing suture lines in more conventional surgery. In cosmetic surgery, the use of cyanoacrylate to replace or supplement sutures reduces scarring. Skin grafts using cyanoacrylate adhesives heal with much less scarring than those done with stitches.

Today, cyanoacrylate adhesives are approved by the U.S. Food and Drug Administration for specified surgical procedures in the United States. Cyanoacrylates are also more widely used by physicians in Canada, Europe and Japan. Continued development of cyanoacrylate adhesives and new operating procedures will insure that these “superglues” will continue to be a valuable part of the surgeon’s toolbox.

References

1. K.L. Shantha, S. Thennarasu, and N. Krishnamurti, Developments and applications of cyanoacrylate adhesives. *J. Adhesion Sci. Technol.* 3, 237–260 (1989).
2. W.D. Spotnitz, Tissue adhesives: Science, products and clinical use, in *Musculoskeletal Tissue Regeneration: Biological Materials and Methods*, W.S. Pietrzak and B.L. Eppley (Eds.), pp. 531–546, Humana Press, Totowa, NJ. (2008).

3. J. Blume and W. Schwotzer, Medical products and their application range, in *Biological Adhesive Systems: From Nature to Technical and Medical Application*, J. van Byern and I. Grunwald (Eds.), pp. 213–224, Springer, New York. (2010).
4. N. Nakabayashi, M. Nakamura, and N. Yasuda, Hybrid layer as a dentin-bonding mechanism. *European J. Esthetic Dentistry* 3(4), 133–138 (1991).
5. I. Webster and P.J. West, Adhesives for medical applications, in *Polymeric Biomaterials*, S. Dumitriu (Ed.), pp. 703–734, Marcel Dekker, New York. (2002).
6. D.C. Suh, K.S. Kim, S.M. Lim, H.B. Shi, C.G. Choi, H.K. Lee, and D.M. Seo, Technical feasibility of embolizing aneurysms with glue (n-butyl 2-cyanoacrylate): Experimental study in rabbits. *Amer. J. Neuroradiology* 24, 1532–1539 (2003).
7. H. Lee, B.P. Lee, and P.B. Messersmith, A reversible wet/dry adhesive inspired by mussels and geckos. *Nature* 448, 338–341 (2007).
8. K. Nishizaki, T. Seki, A. Fujii, Y. Nishida, M. Funabiki, and Y. Morikawa, Sutureless patch repair for small blowout rupture of the left ventricle after myocardial infarction. *Jpn J. Thorac Cardiovasc Surgery* 52, 268–271 (2002).
9. H.G. Borst, A. Haverich, G. Walterbusch, and W. Maatz, Fibrin adhesive: An important hemostatic adjunct in cardiovascular operations. *J. Thorac Cardiovascular Surgery* 84, 548–553 (1982).
10. J.R. Seguin, E. Picard, J. Frapier, and P. Chaptal, Aortic valve repair with fibrin glue for type A acute aortic dissection. *Annals Thorac Surgery* 58, 304–307 (1994).
11. A.J. Singer and H.C. Thode, A review of the literature on octyl-cyanoacrylate tissue adhesive. *Amer. J. Surgery* 187, 238–248 (2004).
12. D.E. Milkes, A novel method to control severe upper GI bleeding from metastatic cancer with a hemostatic sealant. *Gastrointestinal Endoscopy* 55, 735–740 (2002).
13. K.S. Black, Tissue restoration and repair: Applications of cutting edge technologies to surgical products, in *Business Briefing 2002: Medical Device Manufacturing and Technology*, E. Cooper (Ed.), pp. 1–3, Business Briefings Ltd., London. (2002).
14. J. Passage, H. Jalalix, R.K.W. Tamx, S. Harrocks, and M.F. O'Brien, BioGlue surgical adhesive – An appraisal of its indications in cardiac surgery. *Annals Thorac. Surgery*. 74, 432–437 (2002).
15. T.B. Reece, T.S. Maxey, and I.L. Kron, A prospectus on tissue adhesives. *Amer. J. Surgery* 182, 405–445 (2001).
16. F. Abuzaina and F. Munoz, Foam control for synthetic adhesive/sealant, US Patent Application 2009/005716 (January 1, 2009).
17. P. Vermette, *Biomedical Applications of Polyurethanes*, Landes Bioscience, Georgetown, TX. (2001).
18. L. Ninan, R.L. Stronshine, and R. Shi, Adhesive strength and curing rate of marine mussel protein extracts on porcine small intestinal submucosa. *Acta Biomater.* 3, 687–694 (2007).
19. Y. Otani, A new biological glue from gelatin and poly (l-glutamic acid). *J. Biomed. Mater. Res.* 31, 157–166 (1996).
20. J.W. Gooch, Tissue adhesives, in *Biocompatible Polymeric Materials and Tourniquets for Wounds*, J.W. Gooch (Ed.), pp. 73–89, Springer, New York. (2010).
21. R.A. Chivers and R.G. Wolowacz, The strength of adhesive-bonded tissue joints. *Int. J. Adhesion Adhesives* 17, 127–132 (1997).
22. A.E. Ardis, Preparation of monomeric alkyl alpha-cyanoacrylates, US Patent 2467926, assigned to B.F. Goodrich (April 19, 1949).
23. A.E. Ardis, Preparation of monomeric alkyl alpha-cyanoacrylates, US Patent 2467927, assigned to B.F. Goodrich (April 19, 1949).

24. F.B. Joyner and G.F. Hawkins, Method of making alpha-cyanoacrylates, US Patent 2721858, assigned to Eastman Kodak (October 25, 1955).
25. D.P. Melody, Advances in room temperature curing adhesives and sealants – A review. *British Polymer J.* 21, 175–179 (1989).
26. S.J. Harris, Additives for cyanoacrylate adhesives, US Patent 4450265, assigned to Loctite Corporation (May 22, 1984).
27. A.V. Pocius, *Adhesion and Adhesives Technology*, p. 211, Hanser Publications, New York. (1997).
28. G.H. Millet, Cyanoacrylate adhesives. *Adhesives Age* 24, 27 (October 1981).
29. P.J. Courtney and C. Verosky, Advances in cyanoacrylate technology for device assembly. *Medical Device & Diagnostic Industry* 21, 62–75 (1999).
30. P.J. Courtney, Light curing cyanoacrylates. *Adhesives Age* 44, 8–11 (May 2001).
31. H.W. Coover, F.B. Joyner, N.H. Shearer, and T.H. Wicker, Chemistry and performance of cyanoacrylate adhesives. *J Soc Plast Eng* 15, 413–417 (1959).
32. R.P. Pawar, S.R. Sardaa, R.M. Borade, A.E. Jadhav, S.A. Dake, and A.J. Domb, Cyanoacrylate polymers in medical applications. *Recent Patents Mater. Sci.* 1, 186–199 (2008).
33. P.I. Kosko, Upper lid blepharoplasty: Skin closure achieved with butyl-2-cyanoacrylate. *Ophthalmic Surgery.* 12, 424–425 (1981).
34. K.A. Galikl, I.D. Schofield, and G.Z. Wright, Effect of n-butyl-2-cyanoacrylate (Histoacryl Blue) on the healing of skin wounds. *J. Canadian Dental Assoc.* 50, 565–569 (1984).
35. J.M. Ayton, Polar hands: Spontaneous skin tissues closed with cyanoacrylate (Histoacryl Blue) tissue adhesive in Antarctica. *Arctic Med. Res.* 52, 127–130 (1993).
36. B. Braun Surgical SA, *Histoacryl: The Real Thing*, Brochure No. B01102, Rubí, Spain. (2011).
37. K. Kull, I. Martinelli, E. Briganti, P. Losi, D. Spiller, S. Tonlorenzi, and G. Soldani, Glubran 2 surgical glue: In vitro evaluation of adhesive and mechanical properties. *J. Surgery Res* 157, 15–21 (2009).
38. L. Finch, R.B. Heathcock, T. Quigley, G. Jiranek, and D. Robinson, Emergent treatment of a primary aortoenteric fistula with n-butyl 2-cyanoacrylate and endovascular stent. *J. Vascular Interventional Radiology* 13, 841–843 (2002).
39. D.M. Toriumi and K. O'Grady, Surgical tissue adhesives and otolaryngology-head and neck surgery. *Otolaryngol Clinical North America* 27, 2013–209 (1994).
40. B.S. Kim, H.M. Do, and M. Razavi, n-Butyl cyanoacrylate glue embolization of splenic artery aneurysms. *J. Vascular Interventional Radiology* 15, 91–94 (2004).
41. A. Garg, S. Banait, S. Babhad, N. Kanchankar, P.Nimade, and C. Panchal, Endovascular treatment of pseudoaneurysm of the common hepatic artery with intra-aneurysmal glue (n-butyl 2-cyanoacrylate) embolization. *Cardiovascular Interventional Radiology* 30, 999–1002 (2007).
42. T.S. Maldonado, Initial successful management of type I endoleak after endovascular aortic aneurysm repair with n-butyl cyanoacrylate adhesive. *J. Vascular Surgery* 38, 664–670 (2003).
43. B.M. Ryan, R.W. Stockbrugger, and J.M. Ryan, A pathophysiologic gastroenterologic and radiologic approach to the management of gastric varice. *Gastroenterology* 126, 1175–1189 (2004).
44. L.P. Bré, Y. Zheng, A.P. Pêgo, and W. Wang, Taking tissue adhesives to the future: From traditional synthetic to new biomimetic approaches. *Biomater. Sci.* 1, 239–253 (2013).
45. “SurgiSeal White Paper Summary”, www.adhezion.com.
46. N.H. Liversedge, Get stuck in!: Hands on experiences with surgical skin glue. *Obs & Gynae Product News* Issue 14, 24–28 (February 2007).
47. A.E. Schoenberg, Cyanoacrylates, in *Adhesives and Sealants, Vol. 3 Engineered Materials Handbook*, pp. 126–132, ASM International Materials Park, OH. (1990).

48. Anon. "How Super Glue is Made", www.madehow.com/Volume-1/Super-Glue.html.
49. K.C. Pani, The degradation of n-butyl alpha cyanoacrylate tissue adhesives. *Surgery* 63, 481–489 (1968).
50. S.C. Woodward, J.B. Herrman, and J.L. Cameron, Histotoxicity of cyanoacrylate tissue adhesive in the rat. *Annals Surgery* 162, 113 (1965).
51. R.J. Greff, P.J. Tighe, M.M. Byram, and L.V. Barley, Cyanoacrylate adhesive compositions, US Patent 6191202, assigned to Medlogic Global Corporation (February 20, 2001).
52. S. Kawamura, K. Kondo, K. Ito, H. Suzuki, E. Yasui, and T. Kobayashi, Stabilized α -cyanoacrylate adhesive compositions, US Patent 3652635, assigned to Toagosei Chemical Industry (March 28, 1972).
53. D.J. O'Sullivan, Cyanoacrylate adhesive composition, US Patent 3742018, assigned to Loctite Limited (June 26, 1973).
54. J.Y. Jonn and J. Quintero, Stabilized cyanoacrylate formulations, US Patent Application 2007/0078207 (April 5, 2007).
55. F. Stoesslein, G. Ditscherlein, and P.A. Romaniuk, Experimental studies on new liquid embolization mixtures. *Cardiovascular Interventional Radiology* 5, 264–267 (1982).
56. J.S. Pollack and R.I. White, The use of cyanoacrylate adhesives in peripheral embolization. *J. Vascular Interventional Radiology* 12, 907–913 (2001).
57. H. Oowaki, S. Matsuda, and N. Sakai, Non-adhesive cyanoacrylate as an embolic material for endovascular neurosurgery. *Biomaterials* 21, 1039–1046 (2000).
58. J.D. Barr, E.J. Hoffman, B.R. Davis, K.A. Edgar, and C.R. Jacobs, Microcatheter adhesion of cyanoacrylates: Comparison of normal butyl cyanoacrylate to 2-hexyl cyanoacrylate. *J. Vascular Interventional Radiology* 10, 165–168 (1999).
59. J. Comyn, Moisture cure of adhesives and sealants. *Intl. J. Adhesion Adhesives* 18, 247–253 (1998).
60. B.D. Cooke and K.W. Allen, Cyanoacrylates and their acid values. *Intl. J. Adhesion Adhesives* 13, 73–76 (1993).
61. J.C. Leung, Impregnated applicator tip, US Patent 5928611, assigned to Closure Medical Corp. (July 27, 1999); J.G. Clark and J.C. Leung, Monomeric compositions effective as wound closure devices, US Patent 5981621, assigned to Closure Medical Corp. (November 9, 1999); J.C. Leung, Impregnated applicator tip, US Patent 6099807, assigned to Closure Medical Corp. (December 29, 1998); and J.G. Clark and J.C. Leung, Methods of applying monomeric compositions effective as wound closure devices, US Patent 6217603, assigned to Closure Medical Corp. (April 17, 2001).
62. J.V. Quinn, *Tissue Adhesives in Clinical Medicine*, 2nd ed., p. 31, B.C. Decker, Hamilton, Ontario, Canada. (2005).
63. F.B. Joyner and H.W. Coover Jr., Plasticized monomeric adhesive compositions and articles prepared there-from, US Patent 2784127, assigned to Eastman Kodak Co. (March 5, 1957).
64. G. Whitaker, B.J. Kincaid, N.V. Hoof, F. Regan. M.R. Smyth, and R.G. Leonard, An investigation into the sample preparation procedure and analysis of cyanoacrylate adhesives using capillary electrophoresis. *Intl. J. Adhesion Adhesives* 7, 604–609 (2007).
65. C. Verosky and M. Shannahan, *Adhesive Performance Improvements with Next Generation Surface Insensitive Cyanoacrylates*, Technical Briefs Issue No. 12, Henkel Corporation. (2009).
66. W.R. Winter, Package containing 2-cyanoacrylate ester adhesives, US Patent 3524537, assigned to American Cyanamid Co. (August 18, 1970).
67. K.R. D'Alessio, A. Rivera, W.M. Cotter, and I.T. Badejo, Polymeric containers for 1,1-disubstituted monomer compositions, US Patent Application 2003/0039781, assigned to Closure Medical Corp. (February 27, 2003).

68. S.E. Schaefer and J.P. Eckstein, Dispensing tube package, US Patent 4685591, assigned to American Can Company (August 11, 1987).
69. R.D. Colvin, Container for cyanoacrylate adhesive, US Patent 3523628, assigned to Loctite Corp. (August 11, 1970).
70. K.R. D'Alessio, Halogenated polymeric containers for 1, 1-disubstituted monomer compositions, US Patent 6896838, assigned to Closure Medical Corp. (May 25, 2005).
71. R.E. Monteneri and G. Tremley, Squeezable multilayered container, US Patent 6506464, assigned to Loctite Corporation (January 14, 2003).
72. M. Azevedo and R. Zimmerman, Package for cyanoacrylate adhesive, WIPO Patent Application WO 2006/073922 assigned to Spartan Medical Products, LLC (December 29, 2005).
73. G.H. Millet, Properties of cyanoacrylate adhesive: An overview. *Adhesives Age* 24, 27–32 (October 1981).
74. G.H. Millet, Cyanoacrylates for fast, strong bonds. *Machine Design* 13, 66–69 (June 1986).
75. H.W. Coover, D.W. Dreifus, and J.T. O'Connor, Cyanoacrylate adhesives, in *Handbook of Adhesives*, I. Skeist, (Ed.), Van Nostrand Reinhold, New York. (1990).
76. J.L. Down, A literature review of cyanoacrylate adhesives. *Reviews in Conservation* 2, 35–38 (2001).
77. L.C. Perry, *An Evaluation of Acute Incisional Strength with Traumaseal Surgical Tissue Adhesive Wound Closure*, A report from Dimensional Analysis Systems Inc, Leonia, NJ. (1995).
78. J. Quinn, G. Wells, and T. Sutcliffe, A randomized trial comparing octylcyanoacrylate tissue adhesive and sutures in the management of lacerations. *J. Amer. Med. Assoc.* 277, 1527–1530 (1997).
79. J.P. Noordzij, P.A. Foresman, G.T. Rodeheaver, J.V. Quinn, and R.F. Edlich, Tissue adhesive wound repair revisited. *J. Emerg Med.* 12, 645–649 (1994).
80. K.A. Bresnahan, J.M. Howell, and J. Wizorek, Comparison of tensile strength of cyanoacrylate tissue adhesive closure of lacerations versus suture closure. *Annals Emerg Med.* 26, 575–578 (1995).
81. B.R. Taira, A.J. Singer, J. Rooney, N.T. Steinhaff, and T. Zimmerman, An in-vivo study of the wound-bursting strengths of octyl-cyanoacrylate, butyl-cyanoacrylate, and surgical tape in rats. *J. Emerg Med.* 38, 546–551 (2010).
82. A.J. Shapiro, R.C. Dinsmore, and J.H. North Jr., Tensile strength of wound closure with cyanoacrylate glue. *The American Surgeon* 67, 1113–1115 (2001).
83. P.A. Leggat, D.R. Smith, and U. Kedjarune, Surgical applications of cyanoacrylate adhesives: A review of toxicity. *ANZ J. Surgery (Royal Australasian College of Surgeons)* 77, 209–213 (2007).
84. M.H. Osmond, T.P. Klassen, and J.V. Quinn, Economic comparison of a tissue adhesive and suturing in the repair of pediatric facial lacerations. *J. Pediatrics* 126, 892–895 (1995).
85. C. Chu, J.A. Von Fraunhofer, and H.P. Greisler, *Wound Closure Biomaterials and Devices* (1st ed.). CRC Press, Boca Raton, FL. (1997).
86. D.M. Toriumi, W.F. Raslan, M. Friedman, and M.E. Tardy, Histotoxicity of cyanoacrylate tissue adhesives: A comparative study. *Archives Otolaryngology--Head Neck Surgery* 116, 546 (1990).
87. F. Leonard, Hemostatic applications of alpha cyanoacrylates: Bonding mechanism and physiological degradation of bonds, in *Adhesion in Biological Systems*, R.S. Manly (Ed.), p. 267, Academic Press, New York. (1970).
88. T. Matsumoto, Review of cyanoacrylate monomers in surgery, in *Adhesion in Biological Systems*, R.S. Manly (Ed.), pp. 209–214, Academic Press, New York. (1970).
89. C.A. Carton, L.A. Kessler, B. Seidenberg, and E.S. Hurwitt, Experimental studies in surgery of small blood vessels. II. Patching of arteriotomy using a plastic adhesive. *J. Neurosurgery* 18, 88–94 (1960).

90. M.S. Albin, A.N. Doagostino, R.J. White, and J.H. Grindlay, Nonsuture sealing of a dural substitute utilizing a plastic adhesive, methyl-2-cyanoacrylate. *J. Neurosurgery* 19, 545–550 (1960).
91. G.L. MacDonald, L. Tose, and R.A. Deterling Jr., A technique for reimplantation of the dog limb involving the use of a mechanical stapling device and a rapidly polymerizing adhesive. *Surgery Forum* 13, 88–90 (1962).
92. G.L. Mathes and J.W. Terry, Nonsuture closure of nephrotomy. *J. Urology* 89, 122–125 (1963).
93. J.E. Healey, K.S. Sheena, H.S. Gallagher, R.L. Clark, and P. O'Neill, The use of a plastic adhesive in the technique of bronchial closure. *Surgery Forum* 13, 153–154 (1962).
94. B. Bloch, Bonding of fractures by plastic adhesives - Preliminary report. *J. Bone Joint Surgery* 40B, 804–812 (1958).
95. G.G. Hallock, Expanded applications for octyl-2-cyanoacrylate as a tissue adhesive. *Annals Plastic Surgery* 46, 185–189 (2001).
96. P. Coulthard, M. Esposito, H.V. Worthington, M. van der Elst, O.J.F. van Waes, and J. Darcey, Tissue adhesives for closure of surgical incisions (review). *Cochrane Database Syst Rev.* 5, CD004287 (2010).
97. A.T. Trott, Cyanoacrylate tissue adhesives: An advance in wound care. *J Am Med Assoc* 277, 1559–1560 (1997).
98. G. Messi and A.G. Marchi, Evaluation of skin laceration repair by tissue adhesive in the pediatric emergency room. *Panminerva Medica* 34, 77–80 (1992).
99. P.M. Mertz, S.C. Davis, A.L. Cazzaniga, A. Drosou, and W.H. Eaglstein, Barrier and antibacterial properties of 2-octyl cyanoacrylate-derived wound treatment films. *J. Cutaneous Medical Surgery* 7, 1–6 (2003).
100. U. Narang, L. Mainwaring, G. Spath, and J. Barefoot, In-vitro analysis for microbial barrier properties of 2-octyl cyanoacrylate-derived wound treatment films. *J. Cutaneous Medical Surgery* 7, 13–19 (2003).
101. T.B. Reece, T.S. Maxey, and I.L. Kron, A prospectus on tissue adhesives. *Am. J. Surgery* 182, 40–44 (2001).
102. M.M. Gaffey, 2-Octyl cyanoacrylate (Dermabond) wound adhesives. Medscape, <http://emedicine.medscape.com/article/87407-overview>, accessed on 4/21/2014.
103. D.W. Burch and A. Park, Octylcyanoacrylate tissue adhesive as an alternative to mechanical fixation of expanded polytetrafluoroethylene prosthesis. *Am. J. Surgery* 67, 974–978 (2001).
104. J.W. Kremer, Aneurysm repair apparatus and method, US Patent 4577631 (March 25, 1986).
105. T. Hickey, Cyanoacrylate compositions with terminal vinyl group in the alcohol part, WIPO Patent Application WO/1999/042535, assigned to Closure Medical Corp. (August 26, 1999).
106. A.J. Parry and T.M. Williams, Implantable medical electrical lead with light-activated adhesive fixation, US Patent 6718212, assigned to Medtronic, Inc. (April 6, 2004).
107. D.L. Kotzey, Solid cyanoacrylate adhesive composition and method for its use, US Patent 6797107, assigned to Chemence, Inc. (May 2, 2003).
108. Report S190, *Worldwide Surgical Sealants, Glues, Wound Closure and Anti-Adhesion Markets, 2010–2017*, MedMarket Diligence, LLC, Foothill Ranch, CA, USA. (2012).
109. *Cyanoacrylates Tissue Adhesives - A Market Snapshot*, Report GDME0715VPT, GlobalData, London, UK. (April 2010).

Ways to Generate Monosort Functionalized Polyolefin Surfaces

J. Friedrich*, R. Mix and G. Hidde

*Bundesanstalt für Materialforschung und -prüfung
Berlin, Germany*

Abstract

Polyolefin surfaces are characterized by their chemical inertness. To create bio-sensitive surfaces by grafting brushes, dendrimers, proteins and other biomolecules with bio-sensor properties, the presence of anchoring points at the polyolefin surface for grafting these molecules is necessary. More precisely, the existence of only one sort of functional groups in sufficient concentration at polyolefin surfaces is a precondition for chemical grafting of such bio- or polymer molecules onto these monosort groups. Several routes for introduction of monotype functional groups are based on plasma treatment. Such plasma exposure has sufficient energy to modify the inert polyolefin surfaces and introduce plasma gas-specific functional groups. However, it is well-known that plasma treatment is not selective. Therefore, special plasma processes with high selectivity in producing monotype functional groups were developed, or alternatively combinations of plasma and chemical treatments were used, or the polyolefin substrates were coated with thin layers of functional-groups bearing polymer layers produced by plasma polymerization or electrospray ionization (ESI). Grafting was preferentially performed in a wet-chemical way by nucleophilic substitution of the graft molecules onto the monotype functional groups at polyolefin surfaces. Alternatively, radical initiated graft polymerization is possible onto plasma-produced radical sites in vacuum after switching-off the plasma and immediate introduction of vapors of vinyl and acrylic monomers. However, the life-time of most plasma-produced C radicals is very short ($<10^{-3}$ s), the graft yield is very low, non-anchored homopolymers are formed, and many side-reactions occur. If oxygen is present, these radicals are instantly transformed into peroxy and subsequently into hydroperoxy groups. The last ones can be decomposed by irradiation with UV light or by heating with formation of alkoxy radicals, which are able to initiate

* *corresponding author*: joerg.florian.friedrich@gmx.de

a graft polymerization. All radical graft processes have low yield and poor reproducibility. This review covers the energetic situation in plasmas, the dissociation energies in polyolefins, the oxidation of polyolefin surfaces, and the broad variety of produced O-containing groups, as well as side- and post-plasma reactions. The need for monotype functional groups for post-plasma wet-chemical grafting is explained. A few ways to introduce such monotype functional groups are explained in more detail.

Keywords: Hydroxyl groups, amino groups, azide groups, bromine groups, carboxylic groups, plasma modification, monosort functional groups

9.1 Introduction

9.1.1 General Principles

Polyolefins, such as polyethylene and polypropylene, are chemically inert and do not have any functional groups at their surfaces. To produce biocompatibility or to anchor sensor molecules, covalent grafting of brushes, dendrimers, proteins and other biomolecules is necessary. However, such grafting needs chemical anchoring points with monotype functional groups at the surface. Among chemical, photo-chemical, electro-chemical or radiation-chemical methods the plasma exposure of polyolefin surfaces is the most prominent approach to produce such functional groups [1]. Exposure to oxygen or air in low- or atmospheric-pressure plasmas oxidizes carbon atoms at the polyolefin surface to a broad variety of singly or multiple carbon-to-oxygen bonded species. To obtain only single (mono-) type of C-O species at the surface, chemical transformation of all different O-functional groups to a single type of C-O species is needed. At first glance two principal chemical routes allow such transformation to a single type of C-O functional groups. The first obvious way is the oxidation of all C-O species to carboxylic groups (COOH), which are most convenient for chemical graft reactions. The second possible way is the reduction of all O-species to hydroxyl groups (OH). Considering these two processes in detail, there does not exist a specific oxidation process to transform all C-O species into COOH groups [2]. Using a strong oxidizing agent, such as chromic sulfuric acid (Pickling), the oxidation does not stop at the carboxylic group formation. The oxidation proceeds to the formation of carbon dioxide and water, due to etching of the polymer [3]. Using a soft oxidizing reagent, such as selenium dioxide, the oxidation remains incomplete [2]. The low- or atmospheric pressure plasma oxidation of polyolefin surfaces has principally the same disadvantages. It is not selective and does not produce the desired monosort C-O functional groups [4,5]. However, the plasma oxidation is a dry process and can be controlled and adjusted by varying the plasma process parameters.

Similar oxidation results were found by irradiating with excimer lamps and excimer lasers with wavelengths $\lambda \leq 170$ nm. This vacuum UV (VUV) has an energy content of about 10 eV and is, therefore, also able to attack C-H and C-C bonds (bond dissociation energies ca. 3.5 eV) in polyolefins directly by exciting $\sigma \rightarrow \sigma^*$ transitions associated with bond scissions (cf. Figure 9.1) [6,7].

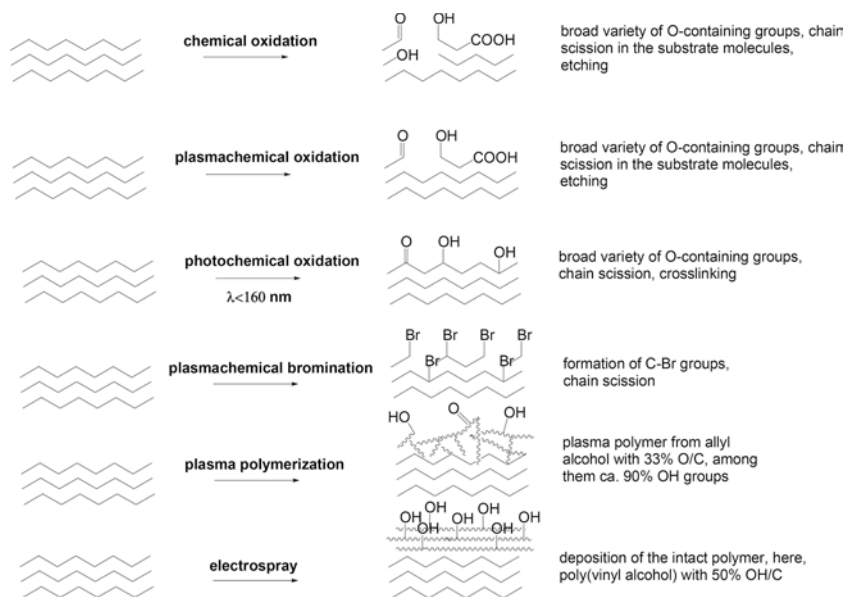


Figure 9.1 Overview of different variants of polyolefin surface modification

Reduction of O-containing groups is a more promising process. The final product of reduction would be the OH (hydroxyl) groups. Strong reducing agents, such as Zn/HCl or LiAlH_4 , remove oxygen-containing groups partially or nearly completely from the surface by their reduction to methyl or methylene groups. These agents also reduce C-O-C (ether) bonds. In case of polyethers, polyesters and polycarbonates such reduction cannot be used because of scissions of polymer backbones. However, weak reducing agents, such as diborane (B_2H_6) or sodium bis(2-methoxyethoxy)aluminum hydride (Vitride), are able to transform all types of carbonyl-containing functional groups to OH-groups as developed by H. C. Brown (Figure 9.2) [8]. This process was made popular for plasma-oxidized polymer surfaces in 1984 [9].

This (wet-) chemical post-plasma grafting was performed chemically by liquid-phase nucleophilic substitution of OH, NH_2 , N_3 , COOH or Br groups [10]. After formation of such monotype groups at the surface these groups can covalently bond organic molecules, oligomers and polymers to the polyolefin surface with high selectivity and in sufficient yield [11]. Thus, small and large graft molecules can be anchored to the polyolefin surface by a chemically well defined process (Figure 9.3). In contrast to this the gas-phase radical graft reaction of monomer molecules containing reactive double bonds with plasma-produced radicals at the polyolefin surface is of non-controllable selectivity and yield [12–17]. The kinetic chain-length of a radical-initiated graft co-polymerization is strongly limited under post-plasma vacuum conditions. Under such low-pressure conditions the density of monomer molecules is too low to maintain the chain growth process.

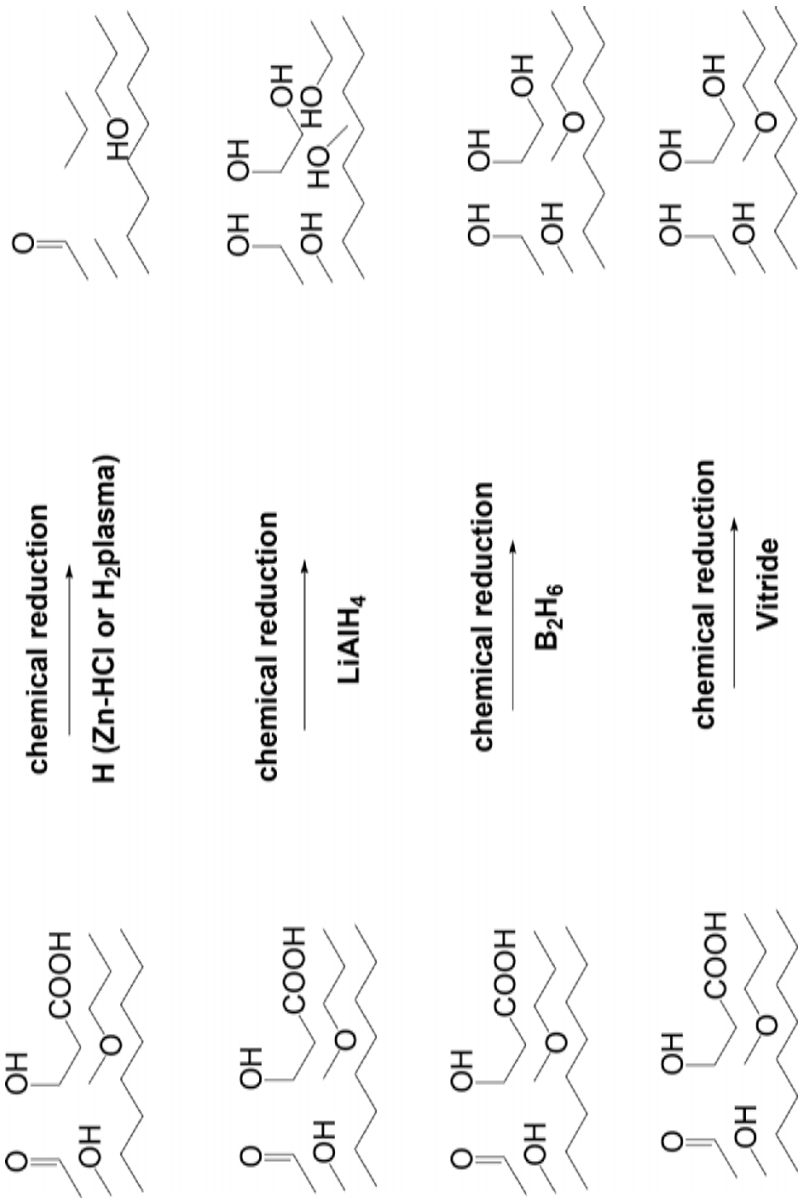


Figure 9.2 Variants of post-plasma chemical reduction of various O-functional groups at polyolefin surfaces

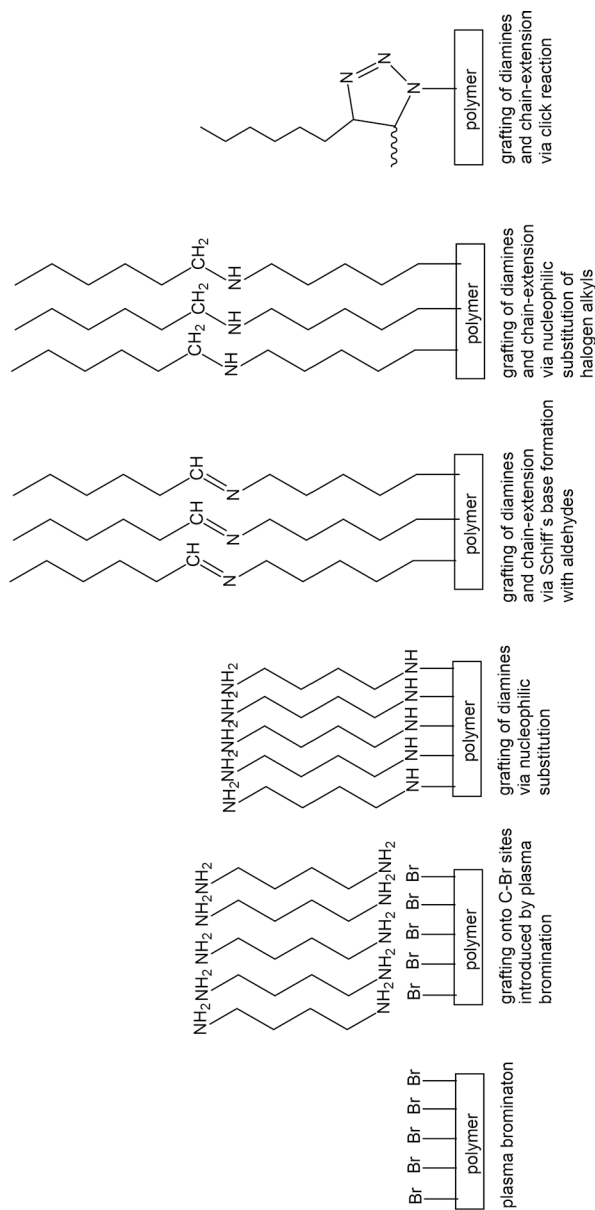


Figure 9.3 Chemical grafting onto C-Br groups and chain-extension

In contrast, chemical bonding of large and complex molecules onto functional groups at the surface of polyolefins is a well known reaction. It is performed by nucleophilic substitution and formation of stable bonds, such as Schiff's base ($-\text{CH}=\text{N}-$), ether formation ($\text{C}-\text{O}-\text{C}$), esterification ($-\text{CO}-\text{O}-$), silanization ($\text{C}-\text{O}-\text{Si}$), or by electrophilic/nucleophilic addition to double bonds [10,18]. Moreover, click chemistry is increasingly used for grafting of molecules (Figure 9.3) [19–20].

Radical bonding as a non-specific grafting method is achieved by irradiating the polyolefin and producing C radical sites, which can start a radical chain growth polymerization from the polyolefin surface with acrylic or vinyl monomers immediately after turning off the plasma and instantaneous addition of the monomer in the absence of oxygen (Figure 9.4) [12–16]. An alternative technique consists of post-plasma exposure of the plasma treated polyolefin surface to oxygen from the ambient air to produce peroxy radicals and subsequently hydroperoxides. The radiation induced decay of hydroperoxides to $\text{R}-\text{O}\cdot$ radicals can initiate the graft (co-) polymerization [16,21–23]. Kang and coworkers have developed this peroxy process for grafting vinyl monomers onto polymer surfaces (Figure 9.4) [17,24].

9.1.2 Formation of Functional Groups at Polyolefin Surfaces by Plasma Exposure

Any oxidation in plasma, thermally or by exposure to flame, oxidizing agents and acids generates different types of carbon-oxygen bonds at polyolefin surfaces. The lowest number of carbon-oxygen bonds is found for C-OH groups (+1). Higher C-O numbers for carbon-oxygen bonds are present in ketones and aldehydes (+2), in carboxylic or ester groups (+3) and in carbonate groups (+4). The problem is that within a single group of C-O bonds differently structured functional groups exist, such as for C(+1) hydroxyl, hydroperoxy, epoxy, phenol and ether groups.

The oxidation of polyolefin surfaces is accompanied by polymer etching leading to material ablation and formation of gaseous etching products such as CO_2 (+4), CO (+2) and H_2O [25].

Another problem is that most of O-containing functional groups cannot be formed directly by attachment of oxygen species from plasma. Hydrogen is also needed to form OH and COOH groups. It has to be removed from polymer chains to react with oxygen

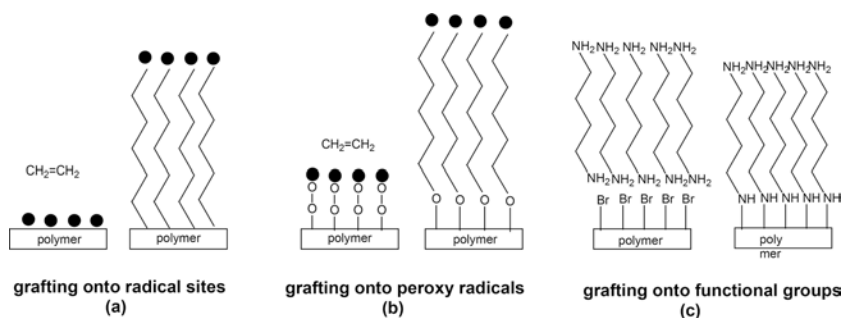


Figure 9.4 Three principal grafting modes (simplified scheme)

species to form hydroxyl and carboxylic groups [26]. These plasma-produced species then have to attach to the polymer surface as covalently bonded functional groups. It should be remembered at this point that on turning-off the oxygen plasma polyolefins can be oxidized further on exposure to the ambient air by “auto-oxidation”, also known from polyolefin ageing or weathering [27].

The removal of hydrogen from the polymer backbone (abstraction) is the desired starting reaction: $C-H + h\nu \rightarrow C\cdot + \cdot H$ ($0.5 H_2$) for forming an anchoring point for the covalent bonding of oxygen species from the plasma. For example, hydroxyl radicals can recombine with such C radical site and form the desired C-O group: $C\cdot + \cdot OH \rightarrow C-OH$. The most probable reaction is the reaction of molecular oxygen in the triplet ground state with C radicals. It is a chemical reaction and does not need plasma assistance: $C\cdot + \cdot O-O\cdot \rightarrow C-O-O\cdot$. The peroxy radical formed can then abstract hydrogen from neighboring C-H bonds of the polymer molecule to form hydroperoxides: $C-O-O\cdot + RH \rightarrow C-O-OH + \cdot R$. The newly formed $R\cdot$ is characteristic of chain reactions (auto-oxidation). The hydroperoxides can decompose in several ways, for example: $C-O-OH \rightarrow C-O\cdot + \cdot OH$ or $2 C-O-OH \rightarrow C-O-O\cdot + C-O\cdot + H_2O$. $C-O\cdot$ may pick up H: $C-O\cdot + RH \rightarrow C-OH + \cdot R$, thus forming hydroxyl, keto, aldehyde, carboxylic and other groups [27]. Figure 9.5 represents these complex reaction processes at polyethylene surfaces on exposure to the ammonia plasma as well as the deposition of a plasma polymer formed from allylamine ($CH_2=CH-CH_2-NH_2$). This plasma polymer carries primary amino groups formed by chain-growth and fragmentation-polyrecombination polymerization (Figure 9.5) [28].

Plasma particle bombardment of the topmost polymer surface as well as short-wavelength vacuum ultra-violet (VUV) irradiation produce C-radical sites on the topmost surface and within a near-surface layer of a thickness of a few or, in some cases, hundreds

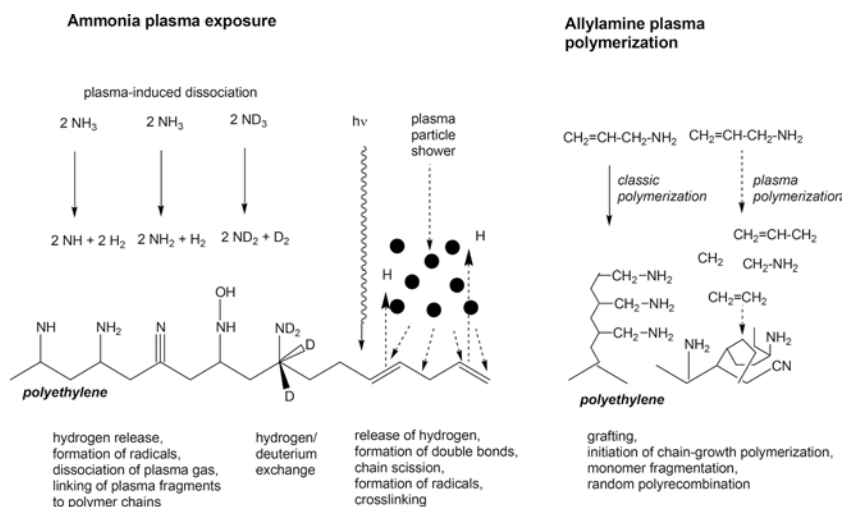
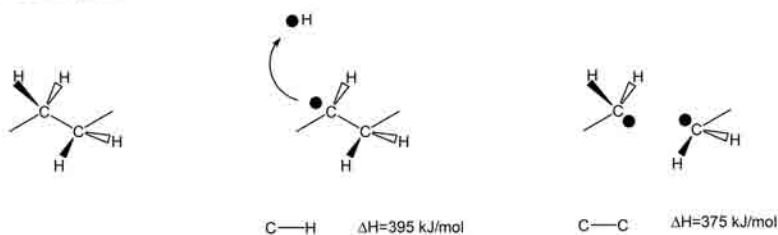


Figure 9.5 Schematic representation of processes on polyethylene surfaces on exposure to the ammonia or allylamine plasma

accompanied with the disadvantage of polymer degradation and formation of a mechanically unstable surface layer.

As stated before plasma particle bombardment as well as VUV irradiation do not act selectively. Filtering the species with lower energy from plasma (afterglow or remote plasma, downstream plasma) may be considered as an alternative [35]. However, the energy of such long-living species in the afterglow, such as metastable states of noble gases, is still going to be much higher than C-C bond energy (≈ 3.5 eV). Thus, the use of remote plasma did not improve the selectivity compared to the direct oxygen plasma exposure as derived from the resulting polymer surface functionalization characterized by XPS valence band spectra as well as angle-resolved XPS [36,37]. Another option was to filter the VUV radiation using LiF or MgF_2 windows from the plasma, cut-off the shortest and, therefore, energy-rich lines of the spectrum and to induce with a softer residual radiation the photo(co-)polymerization, for example ethylene with ammonia by VUV radiation of wavelength $\lambda < 120$ nm, which corresponds to $E \approx 12$ eV [38]. Excimer lamp and excimer laser ablations were used with the intent to achieve higher selectivity [6,7]. However, all these methods could not avoid sufficiently the undesired degradation, etching and side-reactions. The reduced

Bond dissociation energies in the polyethylene molecule and the respective probability of bond dissociation on exposure to the plasma



(Partial) shielding of polyethylene backbone from C-C chain scission by the surrounding hydrogen atoms

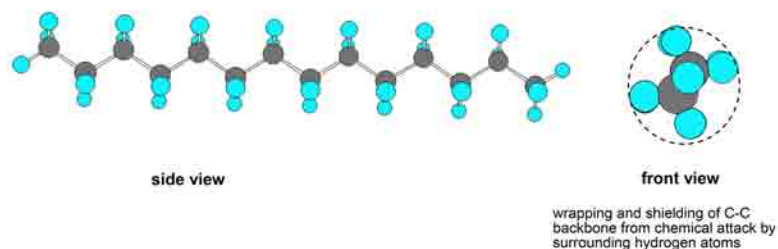


Figure 9.7 Bond dissociation energies in polyethylene and general possibilities of bond scissions

energy was still too high for initiating more selective reactions (Figure 9.8). The minimization of electron energies in the plasma, however, is limited because the plasma has to be sustained. However, this minimum kinetic energy of electrons still exceeds considerably the dissociation energies in polymers.

Another approach was the use of pulsed plasmas for reducing the effective power input into the plasma. Thus, only short plasma pulses would initiate chain reactions, which proceed in long plasma-less dark phases [19,39].

Plasma polymerization of functional groups carrying precursors and the deposition of a thin polymer layer is also an alternative way to produce a functionalized polyolefin surface. Thus, poly(acrylic acid) was deposited onto polypropylene and polyethylene to improve their adhesion to thermally evaporated aluminium layers [40]. However, monomer fragmentation dominates the process of continuous-wave plasma polymerization and the retention of carboxylic groups in the plasma polymer layer was no higher than 50%. Using the pulsed plasma mode the retention in carboxylic groups could be increased to about 75% [41]. It should be remembered that in pulsed plasma polymerization short plasma pulses (a few μs) were ignited followed by plasma-less (dark) phases (a few ms) (Figure 9.9). As mentioned before, the plasma phase should initiate the chain-growth polymerization, which proceeds in the dark phase because it is an exothermal process. This is a clever idea but under low-pressure conditions the chain-growth polymerization produces only very short kinetic chain length. As an alternative, plasma polymerization using pressure and power pulsing was developed to increase the monomer pressure in the dark phases. Thus, longer kinetic chain length was achieved and thus linear polymer products with a higher number of repeat units in the polymer backbone were produced [42,43].

Thus, the use of vinyl or allyl monomers, capable of undergoing classic chain growth polymerization in pulsed plasma polymerization, has shown that in comparison to the ordinary plasma induced fragmentation and recombination in the continuous-wave plasma,

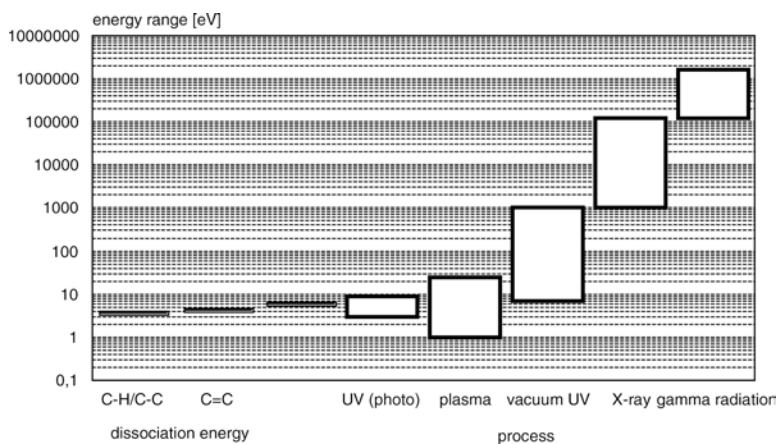


Figure 9.8 Dissociation energy in polymers compared with energy ranges found in various processes

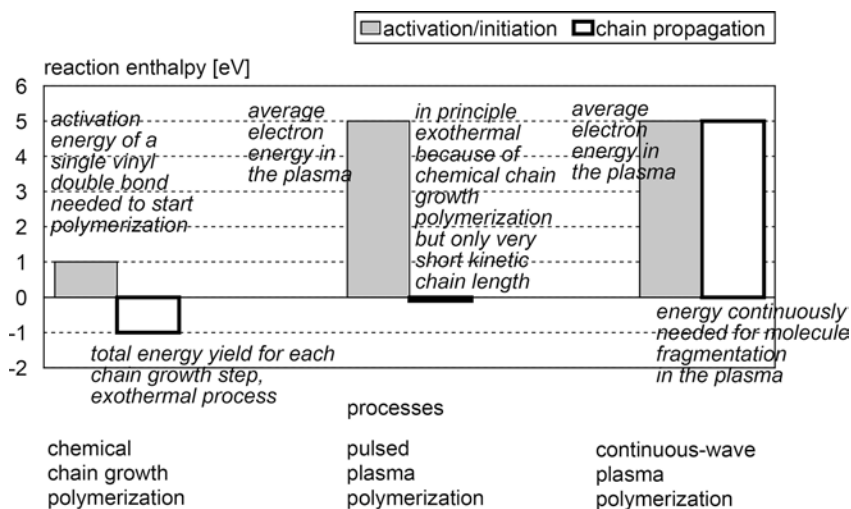


Figure 9.9 Simplified presentation of energies needed for chemical chain growth polymerization and plasma polymerization in comparison to energy present in low-pressure glow discharges (5 eV is the proposed average energy of electrons in the plasma)

the yield of retained monosort functional groups in the deposited layers can be slightly or, in some cases, significantly improved [44].

Plasma-initiated (quasi-) co-polymerization of ethylene with ammonia resulted in a plasma polymer with a certain concentration of primary amino groups [38]. This insertion of covalently bonded amino groups into the plasma polymer structure cannot be achieved by classic chemistry. This indicates that plasma chemistry does not follow classic chemistry. Nevertheless, surprisingly, the yield of amino groups was about 12–14% NH_2/C , because the formation of NH_2 groups in the ammonia plasma is thermodynamically unfavorable as shown later. Use of vinyl or allyl monomers and ammonia, water, carbon dioxide or bromine increased the number of (monotype) functional groups further [19]. The insertion of inorganic or non-polymerizable molecules into the polymer structure generally requires plasma fragmentation/recombination.

However, another situation is when using two vinyl, diene or allyl comonomers. The initiation of the classic chain-growth polymerization and, therefore, also the classic copolymerization is possible by use of a chemical initiator. Replacing the chemical initiator by plasma initiation, chemical chain-growth polymerization/copolymerization as well as fragmentation-recombination can be expected.

Styrene, ethylene or butadiene do not have functional groups in contrast to allyl alcohol (OH), allylamine (NH_2), allyl bromide (Br) or acrylic acid (COOH), which possess chemically reactive functional groups [39]. Varying the comonomer ratio of these two groups and considering the chemical copolymerization rules (copolymerization parameters) [46,47]

the concentration of OH, NH₂ or COOH groups could be varied over a large range in the deposited copolymer layer (Figure 9.10) [48–53].

Using the pulsed plasma mode with low duty cycle and low wattage, the retention of polymer structure and functional groups should be maximal and thus a single (dominating) kind of functional groups should be formed [54–62]. A detailed discussion of plasma polymerization is planned to be published in a separate review article.

9.1.3 Polymer Degradation Caused by Plasma Exposure

There have been many attempts to introduce switchable polymer combs and brushes, sensor and probe units as well as spacer molecules with several functions or flexible bonding of intact proteins, cells, etc. to polyolefin surfaces. A precondition is a well-defined modified polyolefin surface needed as the basis for grafting of molecules onto the polyolefin substrate. It was shown in Section 1.2 that these technical requirements cannot be fulfilled by a simple unspecific plasma treatment of polyolefin surface. Strong hindrance for such applications is caused by the broad variety of different types of O- or N-functional groups at the surface and other disadvantages such as formation of a weakly bonded layer of oxidized and degraded polyolefin material at the surface (Low-Molecular Weight Oxidized Material-LMWOM) [63] forming a Weak Boundary Layer (WBL) [64]. In case of non-specific oxidized polyolefin surfaces with a variety of O-functional groups different physical interactions dominate the adhesion to any material. Such physical interactions may be van der Waals type and hydrogen bonds but both types of interactions are sensitive to water. Additionally, the LMWOM is only loosely bonded to the polyolefin bulk. Although, strong adhesion between a coating (or a metal layer) and the oxidized polyolefin surface may exist but the LMWOM itself does not adhere well to the polymer substrate (bulk). At mechanical loading such polyolefin laminate fails within the LMWOM layer. Before coating, it is

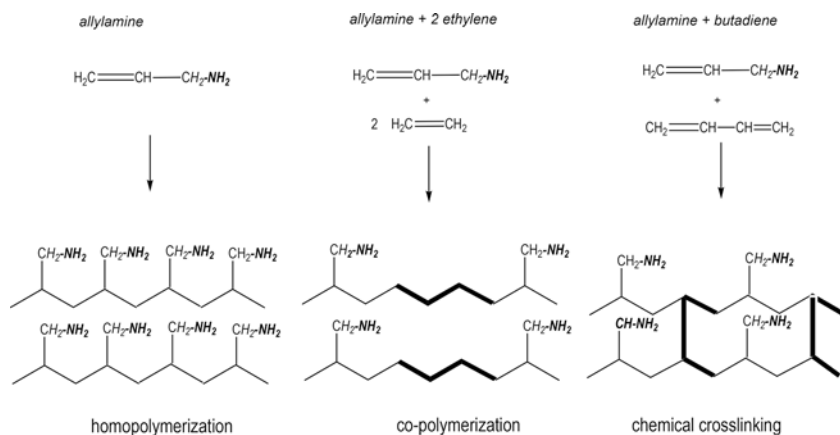
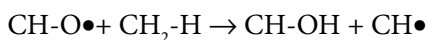
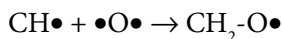
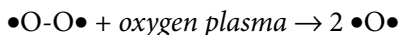


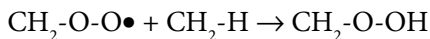
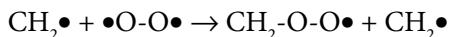
Figure 9.10 Schematic representation of plasma-induced homo- and co-polymerization as well as crosslinking of allylamine with ethylene or 1,3-butadiene [28]

recommended to remove the loosely bonded LMWOM from the topmost polyolefin surface by solvent extraction (washing) and thus to expose intact polymer chains. Unfortunately, these buried polymer molecules possess only a low concentration of adhesion-promoting polar groups. This is the general dilemma in polyolefin surface functionalization.

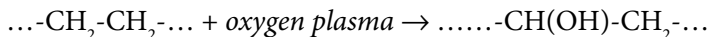
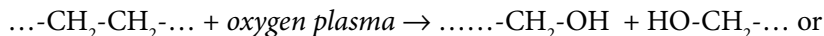
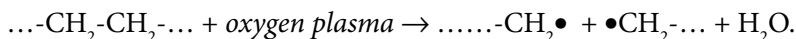
As mentioned in the beginning a further problem exists, i.e., the absence of hydrogen in the O₂ plasma. Attachment of hydroxyl and carboxyl groups onto polyolefin surfaces requires a prior release or abstraction of hydrogen from the polyolefin:



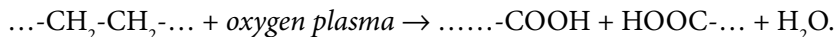
The other possibility is, as mentioned before, the peroxy-based auto-oxidation:



As mentioned before nearly identical dissociation energies of C-H and C-C bonds make chain scissions and formation of O-functional groups possible:



The formation of carboxylic groups at polyolefin surface needs also a hydrogen source. Moreover, COOH groups are terminal groups in polymers; therefore, their formation is associated with chain scissions of the polymer backbone (degradation):



9.1.4 Possible Strategies to Produce Monosort Functional Groups on Polyolefin Surfaces

The following routes to produce monosort functional groups can be considered:

1. Post-oxygen plasma wet-chemical reduction of O-functional groups to OH-groups
Accepting the unspecific oxygen plasma treatment with the formation of different types of O-functional groups, all the carbonyl unit-containing functional groups can

be chemically reduced to OH groups and also C=C double bonds can be transformed by addition of a OH group ($>C=C< + H_2O \rightarrow >CH-C(OH)<$).

2. Selective and high-yield plasma bromination

Selective plasma processes forming monosort functional groups in high density were not found in the older literature [25]. However, the newly introduced plasma bromination fulfils this requirement and produces exclusively C-Br bonds. These plasma-produced monotype C-Br groups are very reactive. As known from Organic Chemistry these bonds are ideally suited as anchoring points for molecules, oligomers and polymers via post-plasma wet-chemical nucleophilic substitution reactions. Additionally, C-Br bonds can also be converted to OH, NH_2 , NO_2 , CN, N_3 (N_3 precondition and, therefore, starting point for new “click” chemistry) etc. with high selectivity and yield by wet-chemical post-plasma conversion.

3. In situ-graft polymerization onto C-radical sites

Another possibility is, after turning off the plasma, the immediate grafting of vinyl or acrylic monomers carrying reactive functional groups (OH, COOH, NH_2 ,...) onto plasma produced C radical sites under vacuum conditions and starting a radical chain-growth polymerization.

Alternatively, post-plasma formed hydroperoxides can be radiatively or thermally decomposed to alkoxy radicals, which also can start a chain-growth polymerization.

4. Plasma polymerization of monomers carrying functional groups

A completely different alternative is the deposition of plasma polymer layers made from functional group carrying monomers (allyl alcohol, acrylic acid, allylamine,...) onto the polyolefin surface. Variation in the density of functional groups is possible by plasma-initiated co-polymerization of functional group bearing co-monomers and “chain-extending“ co-monomers, i.e. co-monomers without functional groups [41].

These possibilities of producing monosort-functionalized polymer surfaces and chemical grafting onto these functional groups or radicals are discussed using a few examples in Section 2.

The above listed variants of polyolefin surface modification with monotype functional groups are schematically presented in Figure 9.12.

The occurrence of various functional groups, double bonds and radical sites as well as crosslinking and oligomer inclusions are characteristics of the irregular structure of such plasma polymers, thus they are subject to rapid ageing. On the other hand, the high post-plasma reactivity of such layers can enhance the adhesion to other materials [61,65–79].

9.2 Production of Monotype Functional Groups

9.2.1 OH Group Formation by Exposure to Oxygen Plasma

As mentioned in Introduction, there is a good possibility to apply also an oxidative wet-chemical process for transforming all the C-O_x bonds to a single bonding state, for example, to COOH groups, which can serve as adhesion promoters because of their chemical reactivity

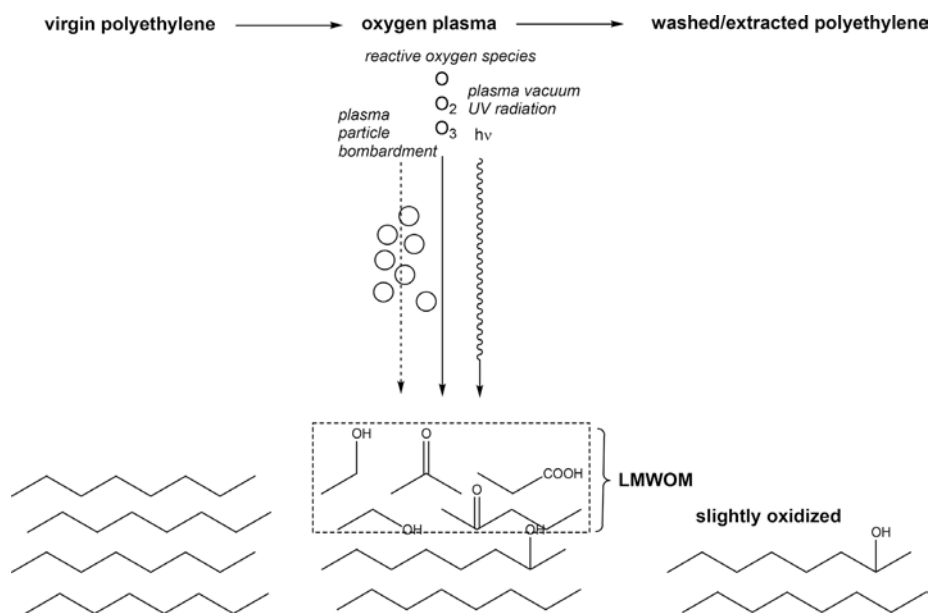


Figure 9.11 Schematics of the formation of Low-Molecular Weight Oxidized Material (LMWOM) in case of oxygen low-pressure plasma exposure of polyethylene and the situation after solvent extraction

and ability to form hydrogen bonds. An important disadvantage is that COOH groups are terminal groups. In case of polyethylene, they indicate scission of the polymer backbone. Moreover, certain known oxidation reactions can be initiated with selenium dioxide or potassium permanganate etc; however, they are not specifically suited for oxidation of all types of O-functional groups to COOH [12]. Moreover, COOH is not the highest oxidation level of carbon atoms. Therefore, the oxidation must be stopped at the level of 3 carbon-oxygen bonds. The highest oxidation ratio with 4 carbon-oxygen bonds is found in CO₂. However, formation of carbon dioxide is accompanied by polymer etching. The formation of organic carbonate structures by simple oxidation in plasma is unlikely but can occur [80].

The chemical reduction of carbonyl features introduced to the surface by exposure to the oxygen plasma to OH groups is a well-proven way to produce monotype hydroxy groups at polyethylene or polypropylene surface (Figure 9.13) [9]. Such reductions are based on investigations of H. C. Brown, who received the Nobel Prize in Chemistry in 1979 [81–85].

Following the Brown's route, carboxylic, ester, ketone and aldehyde functions can be transformed into OH groups by reduction with diborane as well as C=C double bonds can be hydroborated and hydrolyzed to OH groups (Figure 9.13) [18,86,87]. NaBH₄ is a gentler reducing agent and it reduces only ketones, aldehydes and acid chlorides [2].

Using strong reducing agents such as LiAlH₄ or Zn/HCl, C-O-C ether bonds were also broken and transferred to OH groups. However, a few polymers possess these ether bonds

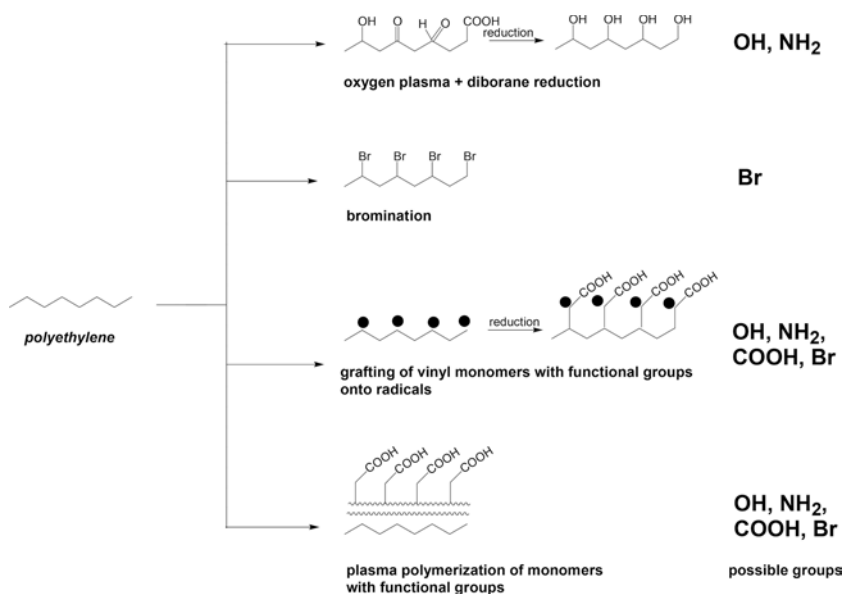
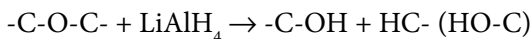
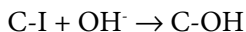
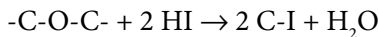


Figure 9.12 Processes to produce monotypic functional groups onto polyethylene surfaces

in their polymer backbone, such as polyethers (poly(oxymethylene)-POM, poly(ethylene glycol)-PEG, poly(phenylene oxide)-PPO), and may, therefore, be degraded during chemical reduction [86]:



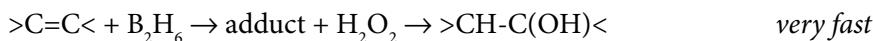
HI and HCl/Zn also attack C-O-C bonds quantitatively [2]:



The results of different reduction treatments are compared in Table 9.1.

Diborane (B₂H₆, dissolved in tetrahydrofuran-THF) reduces only carbonyl features occurring in different O-functional groups (C=O, CHO, COOH, COOR) and does not attack ether structures (C-O-C), therefore, chain scissions are minimized [9,88,89].

A similar reduction process of carbonyl features to OH groups can be performed using Vitride® (Na-bis (2-methoxyethoxy)aluminium hydride) or 9-BBN (9-borabicyclo[3.3.1]nonane) [18]. Using diborane in combination with hydrogen peroxide and hydrolyzing it, olefinic double bonds in the polymer can be additionally hydroborated, i.e. transformed to OH groups [90]:



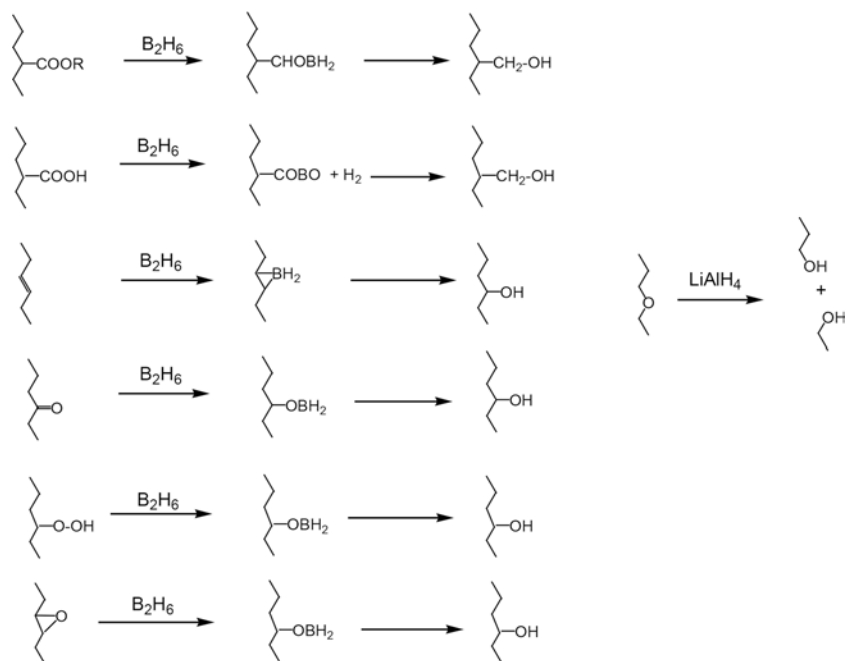


Figure 9.13 Reactions of carbonyl features and double bonds with diborane and ether groups with LiAlH_4 to hydroxyl groups

The hydroboration of double bonds also makes sense with polyethylene because double bonds are formed by oxygen plasma exposure. Using hexatriacontane (HTC, $\text{C}_{36}\text{H}_{74}$) as model molecule for polyethylene the formation of double bonds could be evidenced by Near-Edge X-ray Absorption Fine Structure (NEXAFS) and also in polypropylene exposed to oxygen plasma by Matrix-Assisted Laser Desorption/Ionization (MALDI) spectroscopy (Figure 9.14) [88].

Summarizing these different reduction routes, their relative efficiency for OH formation is reflected in Figure 9.15. However, it should be noted that use of strong reduction agents produces higher yields in OH groups but it is associated with some loss in total oxygen percentage ($\text{O}/\text{C}_{\text{total}}$) by reduction to C-H_x groups.

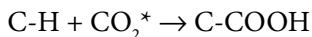
9.2.2 Formation of COOH Groups by Exposure to Carbon Dioxide Plasma

The choice of plasma gas essentially determines the type of functional groups introduced to the polymer surface. Therefore, it was observed that carbon dioxide plasma was able to bond this molecule to the polyolefin surface with formation of carboxylic groups [91,92]. Again, CO_2 attachment is not sufficient because hydrogen is needed to form COOH groups. However, the addition of water to the carbon dioxide plasma did not increase further the

Table 9.1 Overview of results of different chemical reduction processes of O-functional to OH groups

Reduction	Efficiency	Side-reactions
Chemical reduction		
Na/NH ₃	All O-functional groups were reduced	Reduction C-F bonds to carbon (PTFE)
Zn/HCl	All O-functional groups were reduced	Partial reduction to hydrocarbons
LiAlH ₄	All O-functional groups were reduced	Scission of ether groups in polymer backbones (polymer degradation)
NaBH ₄	All O-functional groups were reduced	Scission of ether groups in polymer backbones (polymer degradation)
B ₂ H ₆	O-functional groups were reduced except ether groups	
Vitride (Na-complex)	O-functional groups were reduced except ether groups	Reduction is not complete
Plasmachemical reduction		
H ₂ -plasma	All O-functional groups were reduced	Reduction to hydrocarbon, strong alteration of polymer structure, strong post-plasma oxidation
NH ₃ -plasma	All O-functional groups were reduced and N-functional groups introduced	Reduction to hydrocarbon, strong alteration of polymer structure, strong post-plasma oxidation

concentration of COOH groups at polyethylene surfaces [93]. Thus, the mechanism of COOH formation at polyolefin surfaces can be simplified to:



Detailed investigation of COOH formation and formation of other O-containing groups at polyethylene surfaces was already published in 1995 [94].

It was found that additional polar groups (oxidation) formation and ablation also occur on exposure of aromatic polyester surfaces (poly(ethylene terephthalate)-PET) to CO₂ plasma. The treatment results in the incorporation of carboxyl, carbonyl, and hydroxyl groups, together with a small percentage of carbonate species [95]. It should be stated that the COOH percentage among all plasma-produced O functional groups is low for modified polyolefins (max. 14% COOH/O) [94]) and also for carbon fibres [96]. Although CO₂ plasma treatment has low efficiency, plasma of 50 mol-% CO₂ and 50 mol-% acrylic acid produces almost twice as many COOH groups than without CO₂ addition [97].

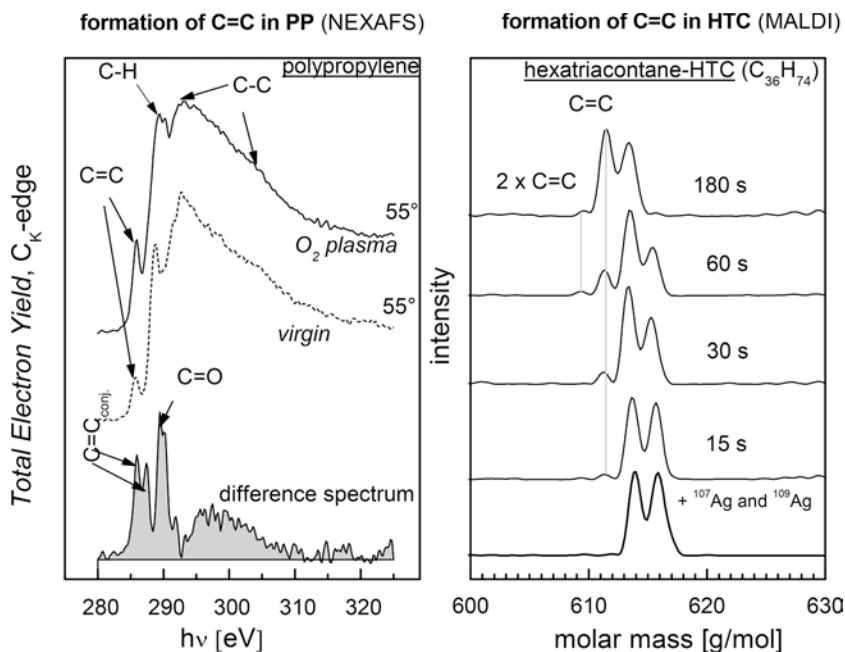
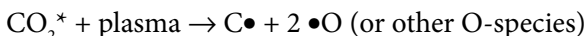


Figure 9.14 Near-Edge X-ray Absorption Fine Structure (NEXAFS) spectra of polypropylene and Matrix-Assisted Laser Desorption/Ionization (MALDI) spectra of hexatriacontane (HTC) with addition of silver ions (AgNO_3)

Hegemann et al. have found that the COOH formation by plasma polymerization of acrylic acid has different origin [98]. Many COOH groups in the acrylic acid monomer survived the plasma polymerization process. The other COOH groups are the product of monomer fragmentation, formation of CO_2 in the plasma and its insertion into the plasma polymer as newly formed COOH groups. CO_2 as intermediate is formed at moderate or high energy input. It can also copolymerize with C_2H_4 , which is also formed within the active plasma zone by monomer fragmentation [98]. Thus, polyolefin surface functionalization and plasma polymer deposition of COOH-containing monomers are characterized by some common fragmentation-recombination mechanism:



The multiple recombinations are strongly exothermal and the COOH group formed can dissociate again or etching can occur. It is assumed that stepwise recombination and flow of energy to the substrate material are needed. Intermediate rearrangements may also be responsible for the formation of other types of O-functional groups.

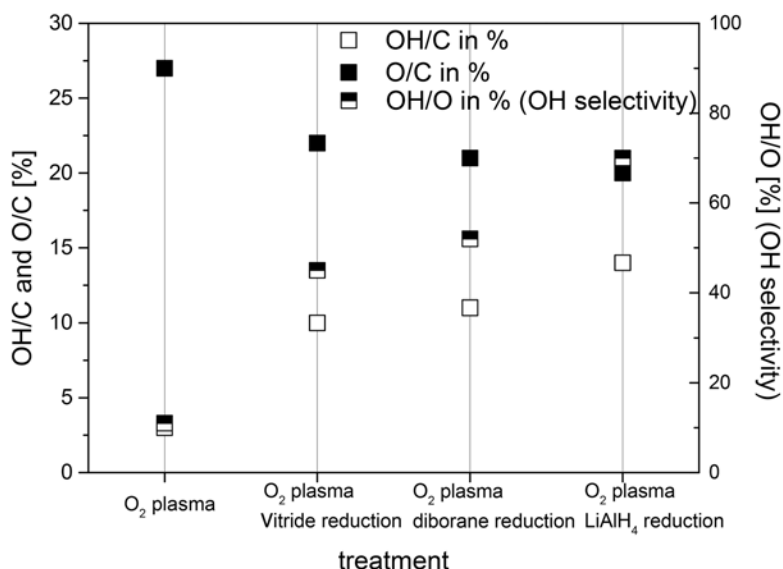
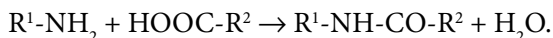


Figure 9.15 Efficiency of different wet-chemical processes in the reduction of oxygen plasma produced O-functional groups to OH groups

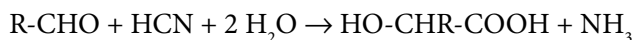
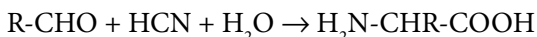
9.2.3 Formation of Amino Groups by Exposure to Ammonia or Nitrogen Plasmas

9.2.3.1 Significance of Primary Amino Groups in Life Sciences

Amino groups play an important role in biology and medicine, and are often found in vitamins, peptides and proteins. They are composed fully or partially of amino acids - the building blocks of all proteins. Amino groups react with carboxylic groups to form peptide (amide) bonds:



In 1953, ammonia plasma enriched with carbon monoxide or dioxide, water, hydrogen and so on were used to produce amino acids. S. L. Miller, under the guidance of H. C. Urey, who received the Nobel Prize in Chemistry in 1934, explained experimentally the genesis of life by exposure of a liquid-phase mixture of water, hydrogen, ammonia, methane and carbon monoxide to plasma. This mixture simulated the early earth atmosphere [99,100]. Initially hydrogen cyanide (HCN) and aldehydes (R-CHO) were formed followed by their reaction to form 28 amino acids:

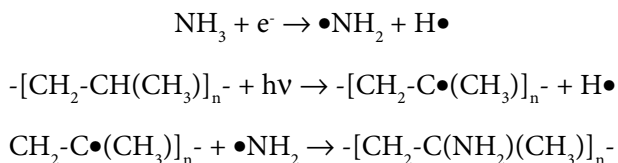


Because of their pronounced chemical reactivity amino groups are of special interest.

Hollahan *et al.* (1969) used an ammonia plasma for introduction of (primary) amino groups (-NH₂) onto polymer surfaces such as polypropylene, poly(vinyl chloride), poly(tetrafluoroethylene), polycarbonate, polyurethane and poly(methyl methacrylate) [101]. The primary amino group was well suited for anchoring of heparine and thus made the polymer surface biocompatible. Primary amino groups react easily with carbonyl groups to form Schiff's bases (azomethines) [102,103]. Secondary amino groups (-NH-) react with carbonyls to form enamines [2]. Carbon fibres [104], poly(ethylene terephthalate) [105], aromatic polyamide fibres (Kevlar) [106] and poly(tetrafluoroethylene) (PTFE) were also exposed to the ammonia plasma [107,108] with the intention to produce NH₂ groups at their surfaces.

9.2.3.2 Ammonia Plasma Treatment of Polymers and Graphitic Materials

Hollahan *et al.* had proposed that the ammonia molecule dissociated in the plasma phase by abstraction of hydrogen to the •NH₂ radical. Then, this radical can recombine with a plasma-produced C radical site at the polymer backbone [101]:



Later on it was shown that this assumption was too optimistic because of thermodynamic reasons and because of the general energy excess in the plasma. Therefore, the yield in primary amino groups at polymer surfaces exposed to plasmas of ammonia, nitrogen or nitrogen-hydrogen mixtures was lower than about 10% of all inserted N-containing groups as shown at carbon fibre surfaces [109]. ToF-SSIMS (Time-of-Flight Static Secondary Ion Mass Spectrometry) analysis identified 2 NH₂/100 C after exposure of polystyrene to the ammonia plasma [110]. Nitrogen [111,112], N₂/H₂-mixtures [101] and NH₃/H₂-mixtures [113–117] did not improve the yield in NH₂-groups compared to ammonia plasma exposure [118]. The dissociation energies of N-H bonds in the ammonia molecule prefer the formation of secondary amino (-NH-) and tertiary N (>N-) species [119]: N-H = 348 kJ/mol; NH-H = 381 kJ/mol; NH₂-H = 440 kJ/mol (for comparison CH-H_{PE} = 395 kJ/mol). Based on these values the formation of NH₂-species in ammonia plasma and their linking to the polyolefin surface is not favorable in terms of thermodynamics and also in light of energy excess in the plasma, as reflected by low yield of hydrazine in N₂/H₂ plasmas [120] due to the energetically preferred reaction: NH₃ → •NH + H₂ = 209 kJ/mol. The formation of desired NH₂-radicals needs more than twice the energy than is needed for NH formation. This fact explains the surprising low yield of NH₂ groups in contrast to the significant high percentage of nitrogen incorporation into polyolefin surfaces [120].

Nevertheless, to determine the functionalization process of polyolefin surfaces with primary amino groups in detail, polypropylene was exposed to ammonia, nitrogen or N₂ + H₂ plasmas (Figure 9.16) [117].

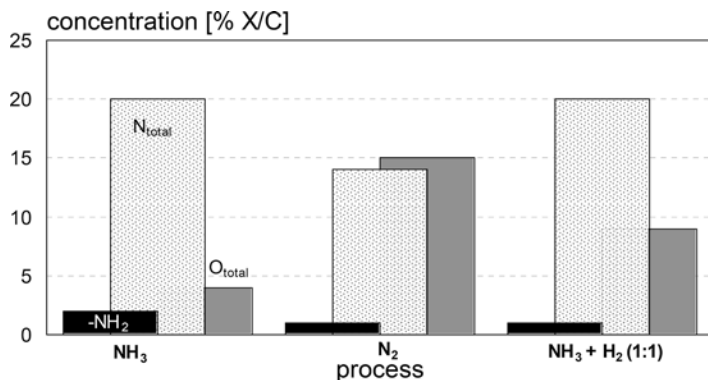


Figure 9.16 NH₃, N₂ and NH₃+H₂ pulsed-rf plasma exposure of polypropylene surfaces and XPS-measured N, O and NH₂ concentrations (X) (10 min, 6 Pa, 30 W, pulse frequency 1000 Hz, duty cycle 0.1)

The yields of NH₂ groups were in the same low range for all three N-containing gas plasmas ($\approx 2\%$ NH₂/C). It should be mentioned that the NH₂ groups concentration linked to polymer surfaces was estimated by their derivatization (labelling) using pentafluorobenzaldehyde [89] or trifluoromethylbenzaldehyde with Schiff's base formation [115]: (R-NH₂ + OHC-C₆F₅ (OHC-C₆H₄-CF₃) → R-N=CH-C₆F₅ (R-N=CH-C₆H₄-CF₃)) and XPS measurement of the resulting fluorine concentration.

The N introduction is also detectable by recording the XPS N1s peak. Here, Highly-Ordered Pyrolytic Graphite (HOPG) was exposed to ammonia plasma. A significant N1s peak position at a binding energy of 399 eV was observed (Figure 9.17) [121].

9.2.3.3 Undesired Oxygen Introduction on Exposure to Ammonia Plasma

Besides the desired introduction of N-functional groups on exposure to the ammonia plasma, high concentrations of undesired post-plasma attached oxygen were measured at the surface of polyolefins as well as carbonaceous materials [108,109]. The undesired introduction of oxygen into polymer surface layers or graphitic materials occurs during the plasma process with traces of oxygen in the reactor or sometimes from acetone from the ammonia bottles. However, it was shown clearly that post-plasma oxidation of radical sites on exposing the plasma-treated samples to ambient air was responsible for oxygen introduction and polymer ageing [108]. The same post-plasma oxidation was observed with carbon fibres after exposure to the ammonia plasma [109]. The detected oxygen concentration was very high and amounted to about 10% O/C for both carbonaceous materials as well as polyolefins on exposure to ammonia, nitrogen and nitrogen+hydrogen plasmas [25,117]. The addition of hydrogen to the ammonia plasma did not increase the yield of NH₂-groups as could be expected from chemical equilibrium processes following the Le Chatelier principle [117]. Replacing continuous-wave radio-frequency by pulsed radio-frequency plasma (pulse frequency 10³ Hz, duty cycle 0.1) the nitrogen introduction increases, the undesired

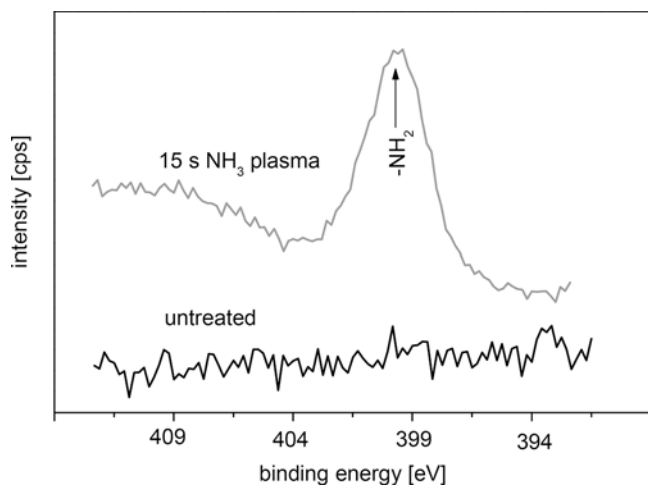


Figure 9.17 N1s XPS spectra of untreated and treated HOPG exposed to ammonia gas plasma (15 s, continuous-wave radio-frequency plasma, 100 W, 10 Pa)

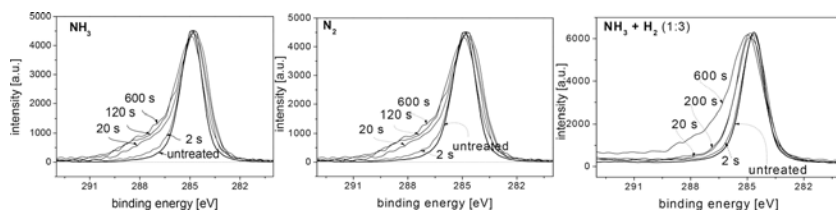


Figure 9.18 C1s XPS peaks of NH_3 , N_2 and $\text{NH}_3 + \text{H}_2$ (1:3) plasma treated polypropylene in dependence of treatment time (continuous wave radio-frequency plasma, 100 W, 6 Pa)

oxygen incorporation decreases but the desired NH_2 -group formation remains nearly constant and at a low level (cf. Figure 9.18).

In the C1s peak of polypropylene, peak broadening on the high energy side is observed in dependence on exposure time to the ammonia plasma. The peak broadening up to 286 eV can be attributed to the attached N-functional groups and at >286 eV to C-O, >C=O, O-C=O bonded functional groups.

The increasing concentrations of N and O incorporation into the PP surface are exemplified for the ammonia plasma and polypropylene in Figure 9.19.

It can be seen in Figure 9.19 that the undesired oxygen incorporation is significant also at short plasma exposure and is about 10% O/C [122,123].

Besides the undesired post-plasma incorporation, also oxygen attachment onto the various N-functional groups was observed. N-oxide (C-N...O), hydroxylamine (>N-OH), nitroso (-N=O) or amido (-CO-NH-) groups were assumed to be formed [125,126].

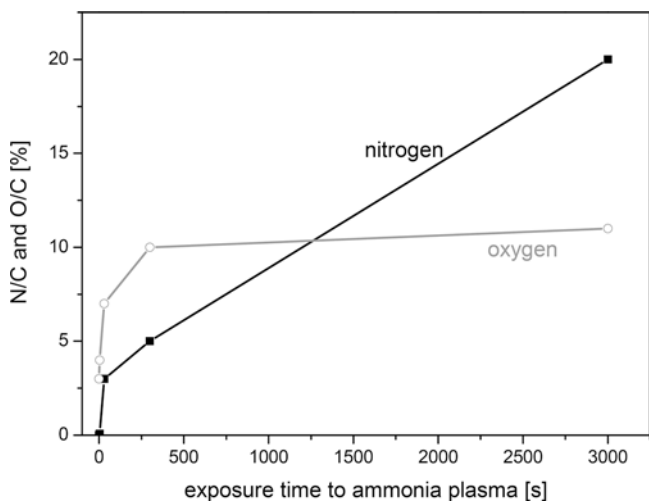


Figure 9.19 Time-dependence of oxygen and nitrogen incorporation into the polypropylene surface on exposure to the ammonia plasma (continuous wave radio-frequency plasma, 100 W, 6 Pa) as measured by XPS analysis after transport of samples from the plasma chamber to the spectrometer (exposure to air ca. 30 min)

9.2.3.4 Additional Side Reactions on Exposure to Ammonia Plasma

A number of newly formed additional groups were identified after ammonia plasma exposure using IR and XPS. Hydrogenation products are observed because the ammonia molecule is rich in hydrogen (1 N, 3 H). Thus, at carbon fibre surfaces the formation of hydrocarbon plasma polymers was observed by XPS and IR spectroscopy from the appearance of a new intense peak at 285.0 eV [109].

Exposure of polyethylene to the ammonia plasma also produced CH_3 groups. These were the consequence of polymer chain scissions by ammonia plasma exposure and respective hydrogenation of carbon atoms after scissioning (Figure 9.20) [117].

The completely deuterated (per-deuterated) hexatriacontane (d-HTC , $\text{C}_{36}\text{D}_{74}$) served as short-chain model for polyethylene. The formation of CH_3 bonds on exposure of d_4 -polyethylene to the NH_3 plasma confirmed the hydrogenation. It should be added that the same results were obtained if hexatriacontane (h-HTC , $\text{C}_{36}\text{H}_{74}$) or h_4 -polyethylene were exposed to the ND_3 plasma. Moreover, the hydrogenation covers a few micrometers from the surface because the C-H and C-D bands are intense considering the sampling depth of the ATR cell of about 2.5 μm [117]. Therefore, it can be concluded that the hydrogenation effect of ammonia plasma dominates strongly the nitrogen introduction and modifies μm thick layers. This is also evident by the appearance of strong D-related signals in ToF-SIMS and NMR (^1H , ^{13}C , ^2H MAS (Magic-Angle Spinning) using the ND_3 plasma [117].

It was assumed that short-wavelength vacuum UV radiation (VUV) of the ammonia plasma with its characteristic hydrogen lines produces dehydrogenation in analogy to

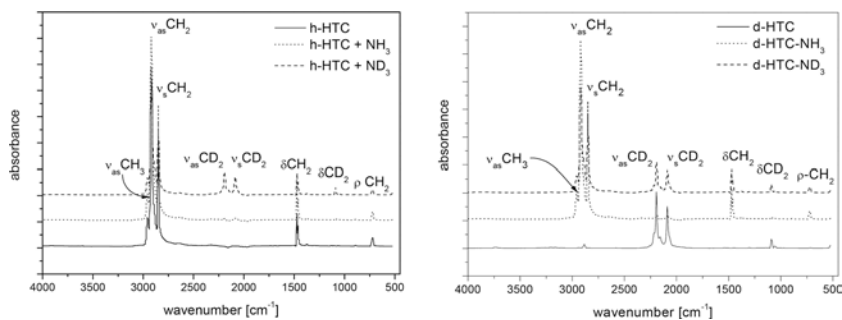
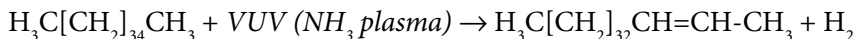


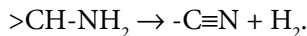
Figure 9.20 IR spectra of h-HTC and deuterated hexatriacontane (d-HTC) exposed to NH_3 or ND_3 plasma

observed dehydrogenation and formation of C=C double bonds on hydrogen plasma exposure of poly(vinyl chloride) [127] or polyethylene [128] or poly(tetrafluoroethylene) [129]. Considering HTC (or polyethylene) the following reaction is proposed:



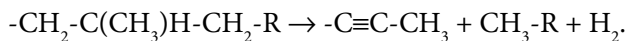
Moreover, in analogy to the observed di-, trimerization and crosslinking of h-HTC on exposure to the oxygen low-pressure plasma by means of Matrix-Assisted Laser Desorption/Ionization Time-of-Flight Mass Spectrometry (MALDI-ToF-MS) (cf. Figure 9.14) [130,131]. Ammonia plasma also produces crosslinking. Thus, ammonia plasma treated hexatriacontane (HTC) was not completely soluble and could not be analyzed using MALDI because of its partial crosslinking. A similar observation was made by Hudis, who has investigated the effect of hydrogen plasma on polyethylene, which may be acting in the same way as ammonia plasma [132]. The existence of low concentration of primary amino groups on polypropylene (cf. Figure 9.16) was evidenced by derivatization with pentafluorobenzaldehyde (PFBA) and quantified by measuring the F1s peak as described already (Figure 9.21).

Unexpected infrared absorptions were found between 2100 and 2200 cm^{-1} assigned to nitriles ($-\text{C}\equiv\text{N}$), isonitriles ($-\text{N}\equiv\text{C}$) and acetylenes ($\text{R}^1-\text{C}\equiv\text{C}-\text{R}^2$) indicating unexpected side-reactions (cf. Figure 9.22, $\nu=2127 \text{ cm}^{-1}$). The formation of nitrile (cyanide) groups requires an excess of energy because an energy-consuming dehydrogenation of amino groups is necessary. Moreover, it results in a chain scission:



Other reaction ways to formation of nitrile groups are also probable.

Moreover, the formation of acetylene bonds ($-\text{C}\equiv\text{C}-$) in polypropylene ($\nu_{\text{C}\equiv\text{C}} \approx 2100 \text{ cm}^{-1}$ and $\nu_{\text{C}\equiv\text{C}-\text{H}} \approx 3300 \text{ cm}^{-1}$) is found which may be produced by a similar process:



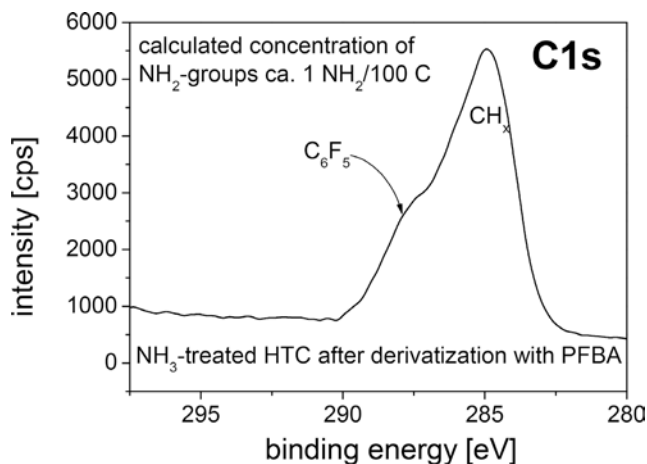


Figure 9.21 C1s XPS peak of hexatriacontane (HTC) exposed for 30 s to NH₃ plasma and reacted with pentafluorobenzaldehyde (PFBA) for 4 h

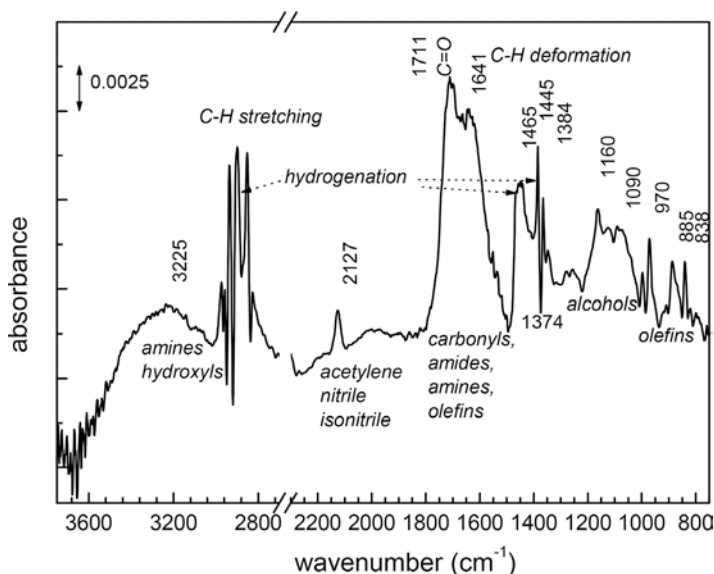
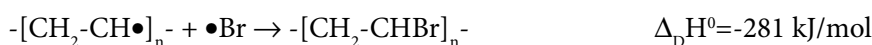


Figure 9.22 Polypropylene exposed to the ammonia plasma (cw-rf plasma, 100 W, 10 Pa, 300 s). The spectrum is the difference between treated-untreated. The spectra were recorded using the Surface-Enhanced Infra-Red Absorption (SEIRA) technique [14]

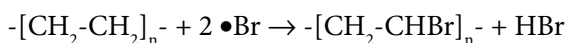
9.2.4 Surface Bromination

9.2.4.1 Kinetics, Thermodynamics and Mechanism

Using the bromoform or bromine plasma to functionalize polyolefin surfaces the exclusive formation of monotype C-Br groups was found [10,60,133]. Selectivity and yield of this process are extremely high. As a consequence, bromination is the only known plasma process for producing monosort functional groups. The presumed mechanism of plasma bromination should be a radical one given the standard (0) enthalpies (H) of dissociation ($_D$) ($\Delta_D H^0$):

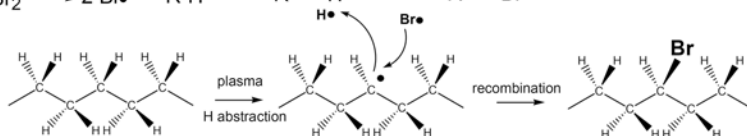
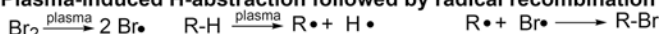


Bromine atoms are also capable for radical substitution and to initiate a chain reaction:

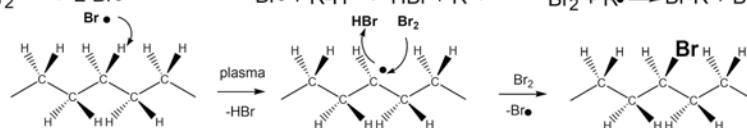
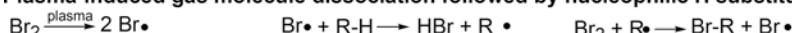


The proposed detailed bromination mechanisms are presented in Figure 9.23.

Plasma-induced H-abstraction followed by radical recombination



Plasma-induced gas molecule dissociation followed by nucleophilic H substitution



Plasma-induced chain scission and bromination but hindered by H shielding

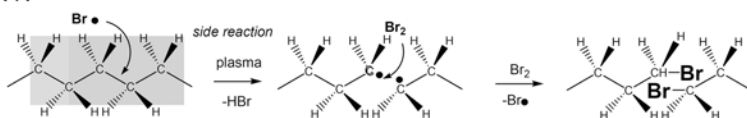
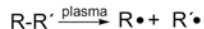


Figure 9.23 Proposed reaction mechanisms of plasma-activated bromine with a polyethylene chain

Under plasma conditions the bromoform molecule dissociates preferably by release of Br considering the different bond dissociation energies for the bromoform molecule:



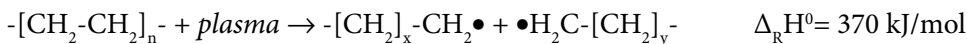
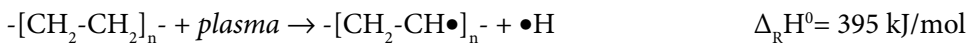
Using ethane as a model for polyethylene, the following thermodynamic calculation of the reaction heat is possible considering the Hess rule and disregarding entropy influences (see Gibbs equation $\Delta G = \Delta H - T\Delta S$) [2]:

$$\Delta_{\text{R}}\text{H}^0 = \Delta_{\text{D}}\text{H}^0_{\text{CH}_3\text{-CH}_2\text{-H}} - \Delta_{\text{D}}\text{H}^0_{\text{H-Br}} = (411 - 363) \text{ kJ/mol} = +48 \text{ kJ/mol.}$$

The positive reaction enthalpy shows that the bromination reaction needs additional activation enthalpy (vis or UV irradiation, plasma) in contrast to the strongly exothermal fluorination ($\Delta_{\text{R}}\text{H}^0 = -155 \text{ kJ/mol}$) with F_2 [26].

The monosort functionalization of polymers is expected because the Br atom has only one way to complete its outer electron shell, i.e., the formation of the C-Br bond and, thus, to achieve the noble electron configuration. The alternative completing of the outer electron shell by formation of Br⁻ anions was not found by analyzing the Br3d peak in the X-ray photoelectron spectrum. Also the formed HBr is volatile and, therefore, absent at the polyolefin surface. Side reactions with oxygen are only possible after transfer of the bromine plasma-treated polymer samples to the ambient air. However, the formation of oxygen-containing functional groups during and after the plasma process is not very probable because Br atoms are efficient radical scavengers and quench all C-radical sites before oxygen has a chance to attach. This effect is well known from flame retardation using Br containing additives, which quench radicals in the gas phase and also at the surface of solids.

In the order of $\text{CH}_2\text{-H}$, CH-H , C-H to C-C bonds the standard dissociation enthalpies ($\Delta_{\text{D}}\text{H}^0$) decrease from 411, 395, 389 to 370 kJ/mol, respectively, clearly showing that tertiary C-H (probability of Br-introduction into primary, secondary, tertiary C-H bonds = 1:250:6300) and also C-C bonds are more easily attacked by Br atoms than primary or secondary C-H bonds [2]. The conclusion is that the scission of polyethylene backbone should be much easier than that of C-H bonds in polyethylene:



As explained before, shielding of C-C bonded polyethylene backbone by its surrounding hydrogen atoms ("hydrogen jacket") suppressed extensive chain scissions, similar to the extra-chlorination of poly(vinyl chloride) (Figures 7,23) [2]. Thus, plasma bromination is a suitable way to produce monosort-functionalized polyolefin surfaces. To remove the low-molecular weight products of plasma bromination (LMWOM), because extensive chain-scissions still occur, it is recommended to wash the surfaces (cf. Figures 11,24) [19].

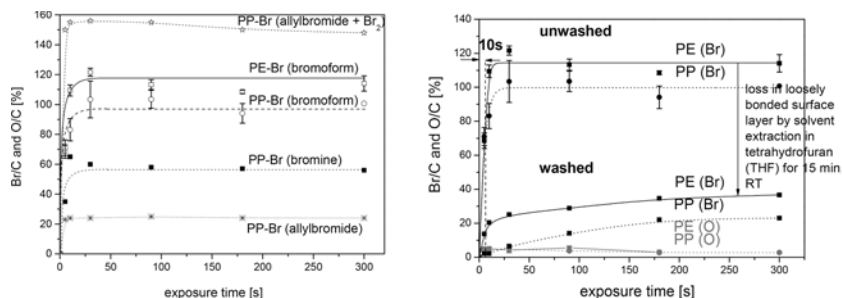


Figure 9.24 Time-dependent bromination of polyolefin surfaces using different types of bromine-releasing plasmas (left) and loss of bromination (right) by extracting the polyolefin with tetrahydrofuran for 15 min

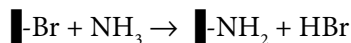
9.2.4.2 Parameter Dependence

The introduction of bromine on exposure to bromine-releasing plasmas is very fast. Within 10 s exposure the maximum bromination percentage is achieved [19]. The concentration of C-Br can be adjusted from a few percent Br/C to more than 100% Br/C (Figure 9.24).

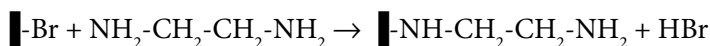
Bromoform (CHBr_3) plasma tends to substitute C-H in polymers by Br thus forming C-Br bonds and secondly to deposit of Br-containing plasma polymer layers. Allyl bromide ($\text{CH}_2=\text{CH}-\text{CH}_2-\text{Br}$) forms exclusively a plasma polymer but tends to trap plasma-produced C-radical sites in its structure, which then can undergo undesired post-plasma reactions on exposure to oxygen from the ambient air (auto-oxidation [27]).

9.2.4.3 Conversion of C-Br into Other Monotype Functional Groups

C-Br groups can be easily converted into other monotype functional groups in a post-plasma wet-chemical way (cf. Figure 9.25). An important process is the transformation of C-Br bonds into primary amino groups using pure ammonia under high pressure and elevated temperature [19]:



The yield of amino groups was 7% NH_2/C . Higher yields of NH_2 -groups were produced by grafting ethylenediamine via nucleophilic substitution (20–22% NH_2/C) [19,60,136]:



The reaction with NaNO_2 followed by reduction of nitrite groups to amino groups yielded about 4% NH_2/C ,

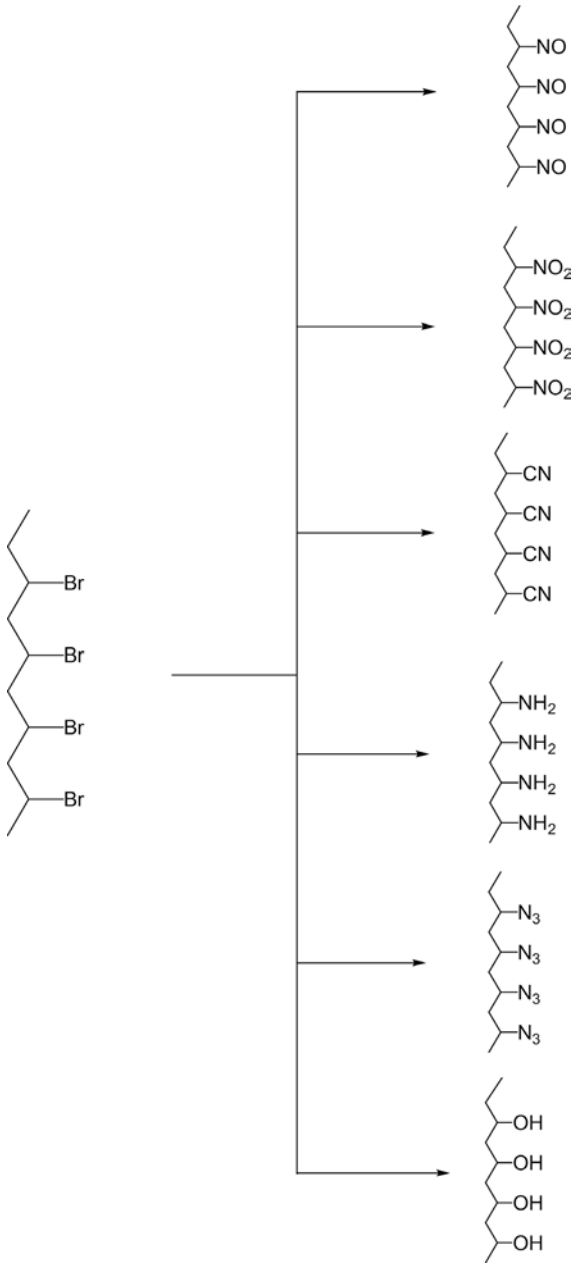
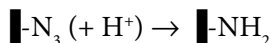


Figure 9.25 Post-plasma wet-chemical transformation of C-Br sites into different monotype functional groups

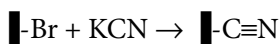


The reaction of brominated polymer surfaces with sodium azide (NaN_3) and the reduction of azides with LiAlH_4 or exposing it to low pH, amino groups are formed (4% NH_2/C):



$\blacksquare\text{-N}_3$ is the starting anchoring point for formation of 1,2,3 triazoles with differently substituted acetylenes known as Click Chemistry [19,20].

Another way is the incorporation of nitrile (cyanide) groups with potassium cyanide:



followed by reduction of the formed nitrile group with LiAlH_4 leading to about 3% NH_2/C :



Thus, plasma-produced monosort C-Br groups can be easily converted into other monosort functional groups in a chemical way.

Using the Williamson ether synthesis or other nucleophilic substitution reactions [2], bi- (or mono-) functional molecules (HO-R-OH , $\text{H}_2\text{N-R-NH}_2$) were covalently grafted onto C-Br functionalized polyolefin surfaces [19]. Br (halogen) atoms were consumed by OH (polymer-Br + HO-R-OH (Na) \rightarrow polymer-O-R-OH + HBr) with the assistance of sodium metal. NH_2 groups containing molecules are more reactive than OH group containing ones and react without assistance of Na (polymer-Br + $\text{H}_2\text{N-R-NH}_2 \rightarrow$ polymer-NH-R-NH₂ + HBr).

The graft yield of molecules ranges from 1–22 molecules/100 carbon atoms of the polyolefin. Large or voluminous oligomers could also be grafted such as poly(ethylene glycol) with a molecular weight 5000 g/mol, poly(amidoamine) (PAMAM) dendrimers or amino-phenylene group-substituted polyhedral oligomers of silsesquioxanes (POSS) in low concentrations (1–2 molecules/100 C) owing to the large space required by the POSS molecule at the polyolefin surfaces. Small molecules, such as ethylenediamine, were grafted in concentration up to 22 molecules per 100 C (Figure 9.26) [19].

9.3 Other Methods for Introduction of Monotype Functional Groups onto the Polyolefin Surface (Plasma Polymerization, Underwater Plasma, ElectroSpray Ionization Deposition, Atmospheric-Pressure Chemical Ionization, Chemical Pretreatment)

9.3.1 Plasma Polymerization

As suggested in the foregoing Section 1.4 plasma polymerization of monomers or precursors or their mixtures is also an often used variant in polyolefin surface functionalization

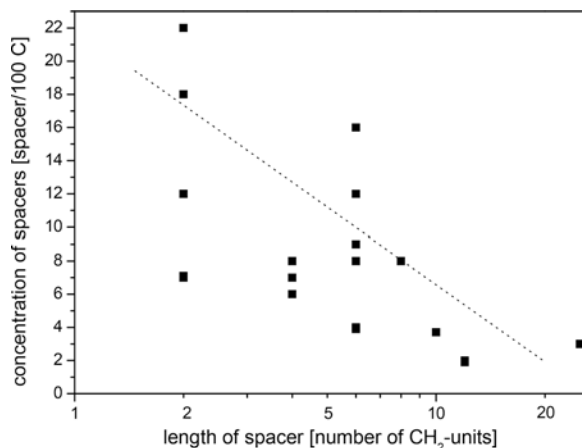


Figure 9.26 Dependence of grafted spacer molecules on length of spacer molecules (referenced to the number of CH₂ units in the grafted molecule)

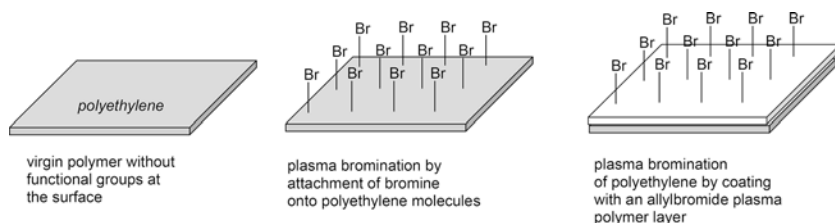


Figure 9.27 General possibilities to establish monotype functional groups at polyolefin surfaces, here exemplified by polyethylene and bromine groups

as an alternative to direct polyolefin surface functionalization in chemically reactive molecular plasmas and post-plasma chemical conversion. Thus, a few variants for production of monotype functional groups are available (Figure 9.27). Plasma polymerization as well as direct functionalization of polyolefin molecules (C-H) can be performed under low- or atmospheric-pressure conditions. Thin coating of polyolefins (C-H) by plasma polymers carrying functional groups (X) proceeds as follows: C-H + n CH₂=CH-X → C-H-[CH₂-CH-X]_n-

As known plasma polymers have several advantages such as good adhesion property, they are pinhole-free and their composition can be varied but they also have several disadvantages, such as irregular structure, post-plasma reactivity, and ageing sensitivity [137]. The use of such plasma polymer coatings for functionalization will be discussed in a separate review article.

9.3.2 Underwater Plasma

The process of liquid-based plasmas (“underwater plasma” – UWP) was established in the 1960s and termed as “glow-discharge electrolysis” (GDE) [137,138]. Gas-phase plasmas in contact with the surface of a liquid consisting of monomers or monomer solutions are also used for the production of polymers with ultra-high molar masses [139]. Waste water purification provided the stimulus to apply underwater plasmas to modify polymer surfaces, such as polyester yarns [140,141] or polyethylene [25,26]. Another traditional application of underwater plasmas is the passivation of magnesium (or other metals) components [142–144]. From the historical point of view the synthesis of amino acids in water by plasma exposure (lightning, arc) of the liquid surface in the presence of CO, CH₄, H₂ and NH₃ as inorganic precursors by Miller and Urey must be mentioned again [99,100].

As mentioned before several variations of underwater plasma arrangements and plasma types exist. The simplest arrangement consists of the liquid (water, solvent or liquid monomer) phase with a submerged electrode and an upper electrode in the gas (air) atmosphere, where the plasma glows in the gap between the upper electrode and the liquid [139] (Figure 9.28).

The real underwater plasma works in a water bath. The most popular capillary discharge variant consists of two chambers separated by a dielectric barrier. Only a quartz capillary within the barrier connects the two chambers. The two capillary-connected chambers are filled with the water (or other liquid) and each is equipped with submerged electrodes (cf. Figure 9.28). After applying the voltage water is vaporized and the plasma is established within the capillary and the bubbles. The plasma expands in the capillary, produces shock waves, and generates local supercritical conditions, UV-radiation and some plasma-filled bubbles in the liquid [146]. The plasma zone within and outside the capillary as well as plasma-illuminated water vapor bubbles contact the polymer surface and modify it by

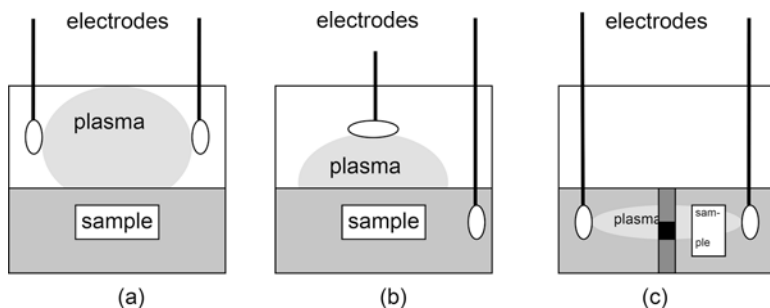


Figure 9.28 Different glow-discharge equipments for polymer surface modification and polymerization characterized by electrode arrangements, (a) gas phase-gas phase electrodes with plasma contact to liquid surface, (b) gas phase-liquid electrodes with plasma contact to liquid surface, (c) liquid-liquid electrodes, with capillary (black) through the barrier and plasma is underwater, in capillary and outside the capillary)

plasma-produced species from the liquid, by irradiation, shock-waves, electrochemical and chemical processes. Thus, water vapour plasma and chemically active water alternately contact the polymer surface. In this way, different oxygen functional groups were anchored at the polyolefin surface. The additionally formed hydrophilic polymer degradation products were continuously extracted from the polymer surface by the surrounding water. Moreover, plasma-produced C-radical sites are immediately quenched by water or OH and other radicals. It is obvious that OH radicals are the main product of plasma electrolysis of water [147]. Hydrogen, oxygen, ozone and hydroperoxide formation is also observed. Moreover, several types of anions were found, such as O_3^- , CO_3^{2-} , HCO_3^- , O_4^- , CO_4^- , $N_2O_2^-$, O_2^- and also solvated electrons e^-_{solv} [148].

Up to 40% of all UWP produced O-containing groups at polyolefin surface were identified as OH groups [149]. All efforts to increase the selectivity in OH group production by addition of hydrogen peroxide and Fenton's catalyst did not increase the yield of OH groups further [150,151].

Another general process in underwater plasma is the plasma polymerization. For example, underwater plasma polymerization of acrylic acid produced a water-soluble polymer. Copolymerization with N,N'-methylenebisacrylamide as crosslinker formed a transparent gel [152]. The outstanding, or may be exotic property of plasmas to polymerize monomers without polymerizable double bond, such as saturated carboxylic acids, e.g., acetic acid was also evidenced [153]. Mixtures of acrylic acid monomer, N,N'-methylenebisacrylamide crosslinker and poly(ethylene glycol) polymer without polymerizable double bonds were used to synthesize super-hydrogels by UWP plasma co-polymerization [152,154].

9.3.3 *ElectroSpray Ionization (ESI) Deposition*

ElectroSpray Ionization (ESI) deposition is a new method to coat substrates with ultrathin (10–30 nm) pinhole-free polymer layers of intact molecular structure and regular elemental composition under atmospheric-pressure conditions by spraying low concentration solutions of high molar mass polymers with functional groups or polar units in a high-strength electrical field between the capillary (anode) and the (grounded) counter electrode (cathode). The sample is deposited on the counter electrode (Figure 9.29) [26,155]. These high-molecular-weight polymers dissolved in polar liquids, such as methanol, could be sprayed without any polymer degradation because no plasma is present. Nearly all polymers can be sprayed, in particular, ionic polymers, biopolymers and polymers with polar groups. The absence of polar groups in the molecules and the need for high solution temperature, because of low solubility, make it difficult to spray polyolefins.

The ESI-deposited polymer films are pinhole-free for an average thickness of about 8 nm.

In the presence of atmospheric plasma, for example corona, the deposited polymer molecules were additionally activated and therefore partially degraded but adhere strongly to the substrate (Atmospheric-Pressure Chemical Ionization – APCI).

The third variant is the aerosol spraying into a dielectric barrier discharge (DBD). However, this causes significant polymer degradation (cf. Figure 9.30) [156].

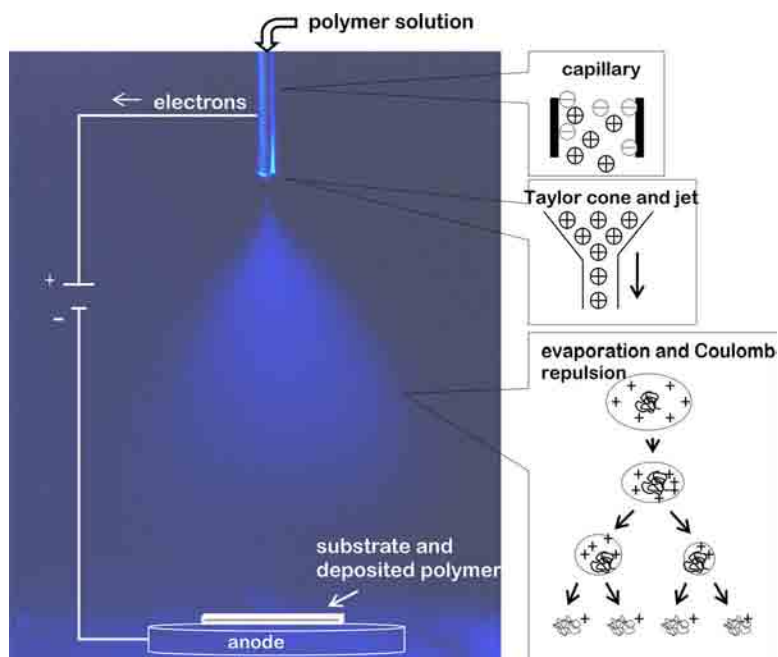


Figure 9.29 Schematic equipment and photograph of electrospray ionization (ESI). The powered capillary (cathode) is at the top. Taylor cone and liquid jet leave the capillary. The electro-spray region is visible (pale blue). The substrate is placed on the grounded counter electrode (anode). In case of electrically insulating polymer samples, the current polarity was alternated continuously to avoid surface charging of sample.

ESI retains the structure and composition of polymers completely, APCI deposits show significant loss in molar mass, and aerosol spray deposition via DBD is accompanied by strong polymer degradation.

In case of electrically conductive substrates used as (grounded) cathode, pinhole-free polymer layers were deposited as a consequence of the “electrophoretic (electrostatic) effect” of ESI. The reason is the surface charge on the deposited polymer film. Additional macromolecular ions were repelled and re-directed to non-coated areas of the cathode (conductive sample as cathode). This effect is responsible for polymer deposition of the shadowed backsides of samples as well as in buried gaps and voids in the sample. Thus, all carbon fibres of a bundle (roving) could be completely coated (wrapped) with poly(allylamine) or poly(acrylic acid) films within the roving to a distance of 100 μm from the surface [25].

9.3.4 Chemical Pretreatment

Wet-, gas-phase- and flame-chemical pretreatments of polyolefin foils were often performed in the past [157–162]. A number of oxidation variants were compared [3].

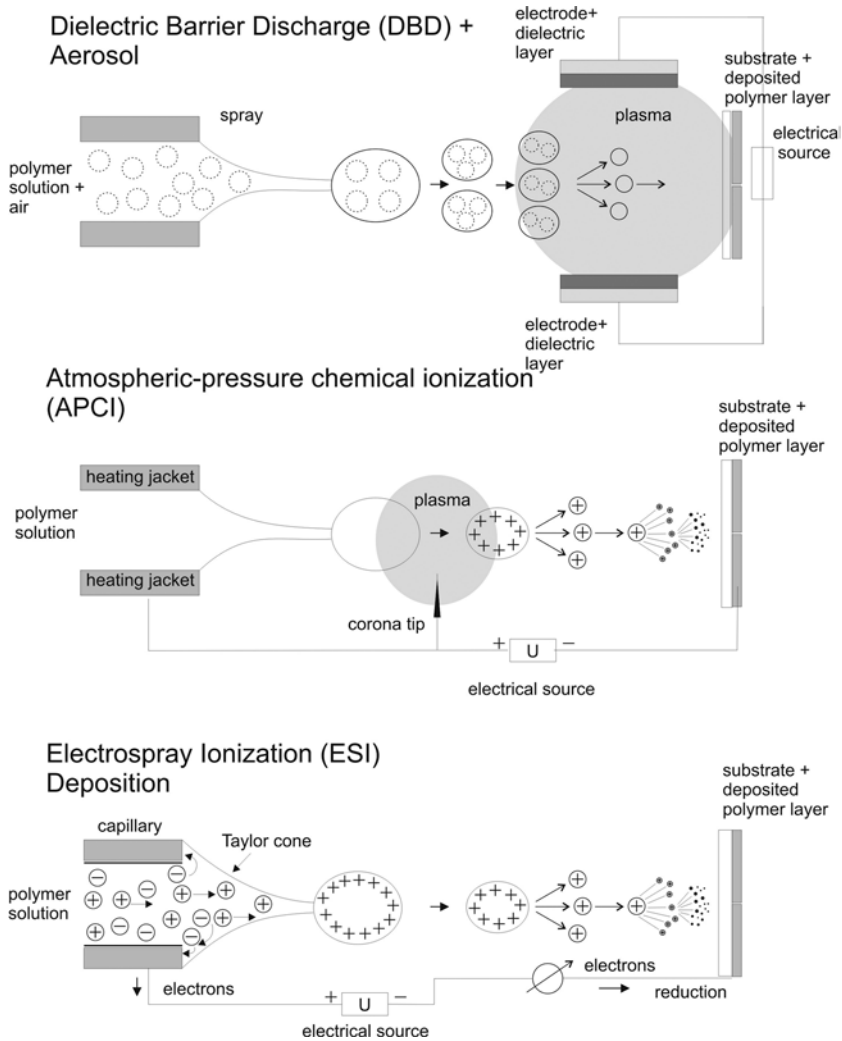


Figure 9.30 Schematics of aerosol-DBD, APCI and ESI processes for deposition of ultra-thin polymer films

Chromo-sulphuric acid is used for polyethylene and polypropylene etching, sodium in tetrahydrofuran for poly(tetrafluoroethylene), phosphoric acid for poly(oxyethylene) and formic acid for polyamide. Flame treatment has been used for many years to modify the surface of plastics. The effect of the treatment is to produce hydrophilic species on the surface of the plastic making it water-wettable. Flame treatment is ideal for functionalizing bi-axially oriented polypropylene (BOPP), poly(ethylene terephthalate) (PET), PE,

coextruded films, paperboard, metal foils, and foams for numerous product applications in the food, automotive, medical, industrial tape and textile industries.

9.4 Hydrophobic Recovery

Polymer surfaces generally are highly mobile (Figure 9.31) [163–167]. The mobility of polymer chain segments allows surface restructuring. This typically leads to a considerable decrease over time of the effects conferred on the surface by non-depositing plasma treatments [108]. Surface restructuring results from an energetically unfavourable situation that arises when polar groups are located at the surface in contact with air (extremely hydrophobic). Chain segments carrying polar groups migrate (diffuse) into the polymer. Thermodynamic driving force of diffusion is a chemical process in which molecules from an area of high concentration move to an area of low concentration as described by Fick's laws. The macromolecules or their segments equipped with functional groups by pretreatment of polymer surfaces tend to diffuse into the bulk for equilibration from all different concentrations to an average and uniform concentration in the polymer bulk and at its surface [38]. This diffusion is hindered by adjacent crosslinks.

Thus, functional groups can rotate around C-C single bonds and turn away from surface; segments with functional groups can slowly move and diffuse from the topmost layer into the bulk. Moreover, complete polymer chains equipped with functional groups diffuse into the bulk accelerated by temperature or flexibilizing additives. This mobility of functional groups and macromolecule segments is called "surface dynamics" or "hydrophobic recovery" [168–172]. The driving force is always the thermodynamics [38]. Dipping the samples

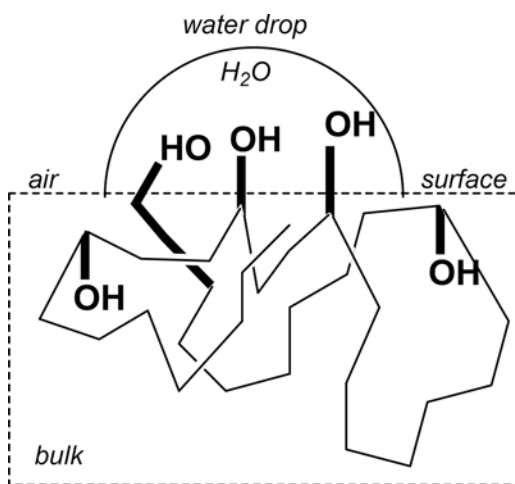


Figure 9.31 Schematics of surface dynamics with retention of functional groups permanently at surface by wetting with water and thus producing hydrogen bonds between functional groups and water as well as diffusion of hydroxyl groups without contact to water [163]

with polar groups in polar solvents, such as water, hydrogen bonds and physical interactions can be established between water and the polar groups at the surface. Thus, the polar groups remain at the surface of the polyolefin.

9.5 Grafting onto Functionalized Polyolefin Surfaces

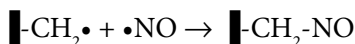
The most important aim to produce monotype functional groups is the creation of anchoring points at polyolefin surfaces for grafting of molecules, oligomers and polymers. In Figure 9.4 the three principal routes for grafting of molecules, oligomers and polymer molecules onto polyolefin surfaces are schematically shown,

- a) direct grafting onto C-radicals (radical route),
- b) formation of peroxides/hydroperoxides, their decay and the radical grafting (peroxy route) and
- c) the chemical grafting onto functional groups at the polyolefin surface (chemical route)

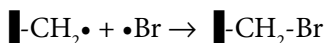
9.5.1 Direct Grafting onto Radical Sites

The term “radical” was introduced by A. L. Lavoisier and means atoms or molecules with one or two unpaired electrons [173]. Radicals are very reactive and short-lived [2].

Radical-radical recombination is a useful way for grafting. For example, NO is a permanent radical and can rapidly react with all C-radical sites in polymers by recombination and formation of a nitroso group, which can oxidize further on exposure to air [174]. This reaction was used for stabilizing the polymer against post-plasma oxidation by acting as a gaseous radical scavenger [174]:



or bromine:

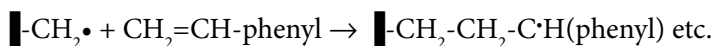


A prominent example for detection of C-radical sites in dissolved polymers is the reaction (recombination) with the stable radical 2,2-diphenyl-1-picrylhydrazyl radical (DPPH). Then, the DPPH solution becomes colorless or pale yellow as measured using photometry or Electron Paramagnetic Resonance (EPR) spectroscopy:



A different variant is the starting of a graft polymerization from plasma-produced radical sites at the polyolefin surface. The chain reaction is easily terminated by recombination,

disproportionation, chain-transfer or concurrent reaction with traces of oxygen or water. Grafting of easily polymerizable vinyl or acrylic monomers is possible such as styrene:



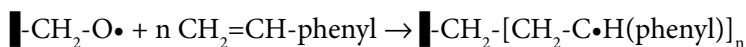
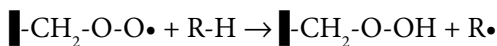
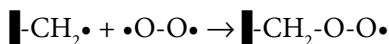
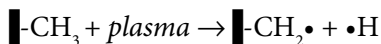
This reaction needs oxygen-free vacuum and no interruption between plasma switch-off and monomer addition (oxygen-free) [15,21], because the mentioned competing reaction with molecular oxygen ($\text{---CH}_2\cdot + \cdot\text{O-O}\cdot \rightarrow \text{---CH}_2\text{-O-O}\cdot$) is more rapid and would hinder the grafting of vinyl or acrylic monomers.

9.5.2 Grafting onto Peroxy Radicals/Hydroperoxides

In most cases carbon radicals are too unstable and too very short-lived ($<10^{-3}$ s [2]) for use in radical graft reactions. The radicals recombine, disproportionate or are annihilated before the reactive monomer gas or vapour can contact the initiator radicals. Longer-living trapped electrons may start homopolymerization at polyolefin surface but the formed polymer chains are not anchored to the polyolefin substrate [176]. Special radical initiators, such as azobisisobutyronitrile, dibenzoylperoxide, dicumylperoxide, were used to start chain-growth polymerization. However, such long-living radicals at polymer surface are not produced on plasma exposure.

Plasma-produced carbon radicals react rapidly with oxygen, e.g., on exposure to the ambient air, to form peroxide radicals. The peroxide radicals become stabilized by H-abstraction from neighboring chain segments with the formation of hydroperoxides (C-O-OH).

Grafting onto radiatively or thermally decomposed hydroperoxides is easy to realize but is not well controllable [21,24,177]. In this way all C-radical sites were converted into peroxy radicals at first on exposure to air, followed by reaction to hydroperoxides, which can be dissociated thermally or by irradiation. The alkoxy radicals formed can react with monomers, thus initiating a graft polymerization:



It is obvious that this reaction sequence cannot be controlled. Also the yield in radical formation depends on many factors and can vary strongly. In particular, adsorbed water layers on reactor walls, leak rate, incomplete degassing of monomer etc. have influence. This complete reaction route is schematically depicted in Figure 9.32.

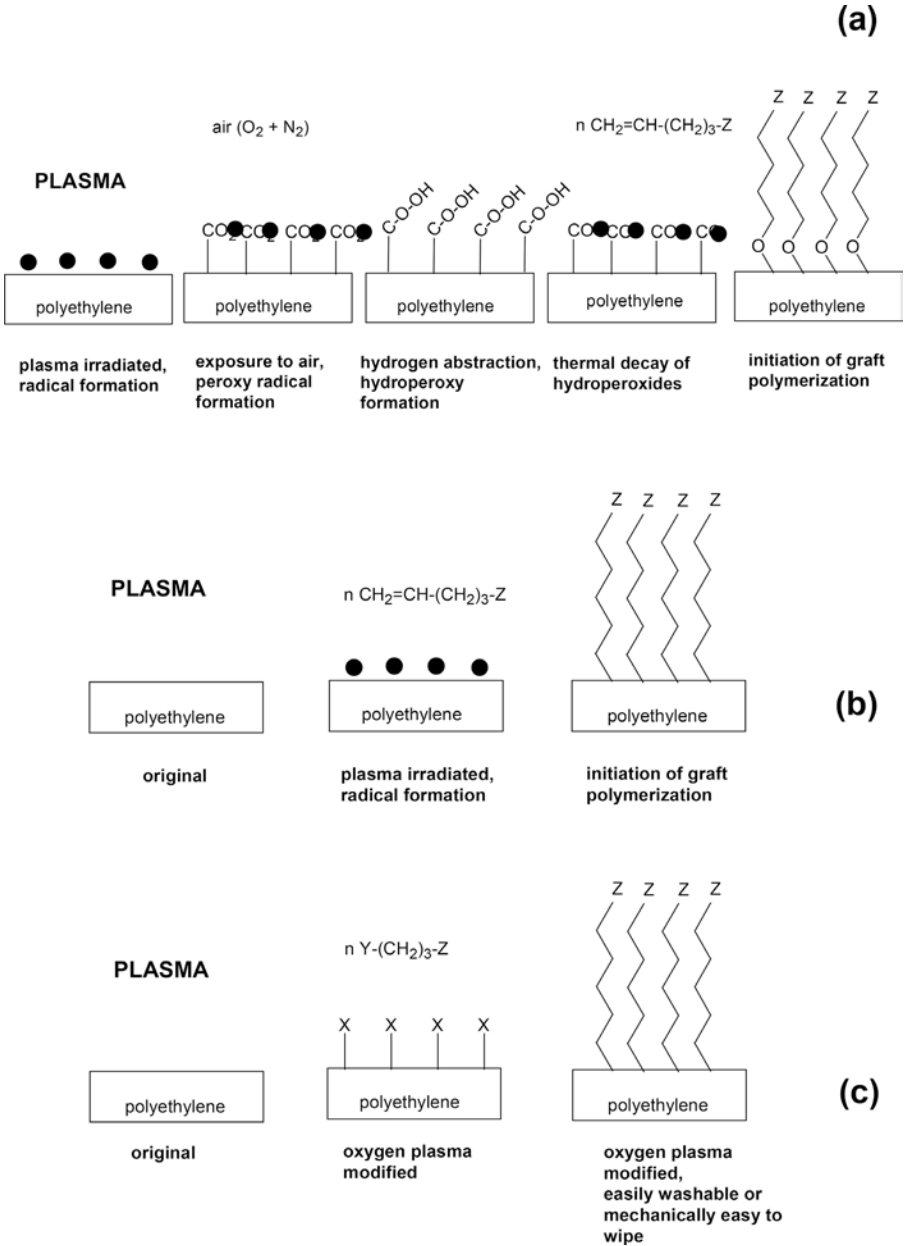
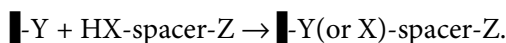


Figure 9.32 Schematic view on “Peroxy route” of graft polymerization starting from alkoxy radicals [24] (a), plasma-initiated graft polymerization starting from C radical sites (b), in comparison to chemical grafting via functional groups (c)

9.5.3 Grafting onto Monosort Functional Groups by Nucleophilic Substitution

The method of choice is the anchoring of spacer molecules onto monosort functional groups at the surface of polyolefins in a well-known and well-tested chemical way. It follows the general principle (Y, X, Z=functional groups, \blacksquare = polyolefin):



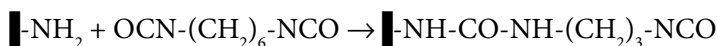
The grafted products were strongly bonded to the polyolefin by covalent bonds. Most often, these bonds are chemically and thermally stable and are not susceptible to hydrolysis.

9.5.3.1 Wet-Chemical Chain Extension at Amino Groups

One of the most prominent graft reactions is the attachment of glutaraldehyde onto amino groups at the polymer surface. This reaction is used for anchoring and chain-extension. The amino groups at substrate surface were produced by exposure to ammonia plasma or by plasma polymerization of allylamine and its deposition as thin polymer layer. Subsequently, the wet-chemical grafting of spacer molecules follows (plasma polymerized allylamine= \blacksquare):

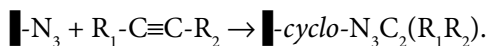
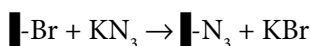
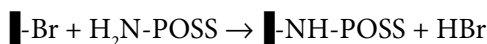
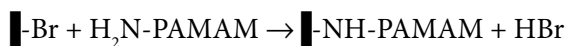


forming Schiff's base (azomethine) bond for anchoring onto the plasma polymerized allylamine. Reaction with isocyanates produces linkage via urea bonds [102,103], for example:



In principle, ammonia plasma exposure or aminolysis of C-Br bonds with ammonia or ethylenediamine is also possible showing about 2% NH_2/C , 6–8% NH_2/C or 18–22% NH_2/C , respectively [11,60]. The reaction of glutaraldehyde (GAH) with amino groups is selective but the yield depends on the availability of the anchoring groups and, therefore, it is no higher than about 50%. The density of surface-grafted GAH is about 6–10% GAH/C. The terminal aldehyde group is favored for reactions with amino groups, for example with aminopropyltriethoxysilane (APTES) [178].

In this way bi- or polyamino-functionalized molecules can be grafted onto the spacer aldehyde group, such as polyamidoamine (PAMAM) dendrimers, amino group-carrying polyhedral oligomers of silsesquioxanes (POSS) or cyclotriazine attachment at azide groups (click chemistry) is possible [19,20].



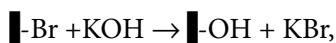
9.5.3.2 Spacer Grafting onto OH-Groups at Polymer Surface

Using OH groups for grafting of spacer molecules several routes were used in the past.

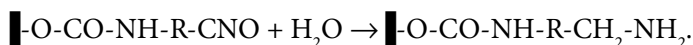
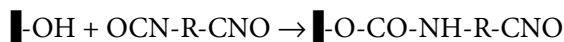
The first approach was the exposure of polyolefin surfaces to the oxygen plasma for maximum 2 s to prevent excessive polymer degradation at the surface [179] and followed by the post-plasma wet-chemical reduction of carbonyls to hydroxyl groups and the hydroxylation of double bonds. In this way a maximum of 11–14% OH/C were produced [18,87]:



The second way was the plasma bromination also used to produce OH groups by hydrolysis with 8–12% OH/C (—=polymer):



without other side products [60]. The hydroxyl groups can react with silanes, isocyanates or carboxylic acids. For example, OH groups at polyolefin surface react with diisocyanates (hexamethylene diisocyanate or toluene diisocyanate for example) [53,103,184]:

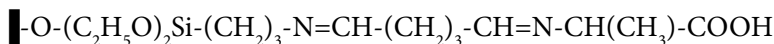
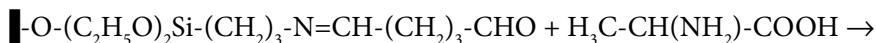
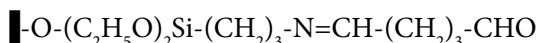


The third variant was the coverage of polyolefins with a thin layer of plasma polymerized allyl alcohol producing a maximum of 30% OH/C [181,182].

Wet-chemical post-plasma grafting onto OH groups was performed using aminosilane:



and subsequent chain-extension with glutaraldehyde as shown before and coupling of alanine (or cysteine) [18]:

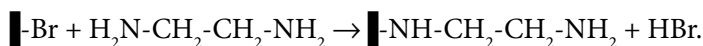


The concentration of such grafted bio-active spacer with terminal alanine (or cysteine) groups was about 2% alanine/C or 2% cysteine/C [86,87].

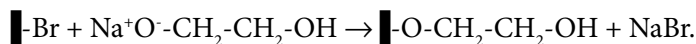
9.5.3.3 Spacer Anchoring onto C-Br Groups

C-Br groups on polyolefin surfaces were easily substituted by diols, glycols, poly(ethylene glycol)s (PEGs) and diamines or alcohols, thiols or amines [19,60,187–189]. Ethylenediamine

(EDA) was evaporated immediately after ending the plasma process and reacted with C-Br groups at the polymer surface as evidenced by the loss in Br:



The yield was 18–22% EDA/C as mentioned before. With growing chain length of the spacer (graft) molecule the graft density decreased, in particular if polymers were grafted, such as poly(ethylene glycol) 5000 (PEG) with a concentration of about 1–2 PEG per 100 C atoms at the surface of polyethylene. In case of glycols, diols and alcohols sodium is needed as a catalyst (Williamson's ether synthesis) as exemplified with ethylene glycol:



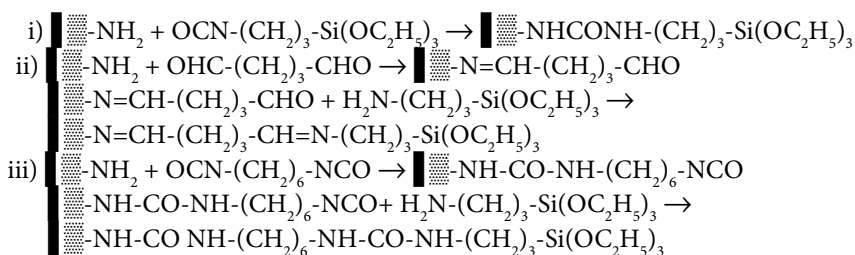
The graft density was found to depend on the chain length of the spacer molecule as shown before in Figure 9.26 [19]. The chain length was measured in terms of methylene units.

9.5.3.4 Silane Attachment

Three principal ways were adopted to anchor silanes onto the polymer surface.

The first way consists of deposition of allylamine plasma polymer (◻◻◻) onto the polyolefin substrate (here, polypropylene) substrate (◻) and then reacted:

- with isocyanatopropyltriethoxysilane or
- with glutaraldehyde and aminosilane (3-aminopropyltriethoxy (or trimethoxy) silane-APTES) or
- with hexamethylenediisocyanate and aminosilane (3-aminopropyltriethoxysilane-APTES):

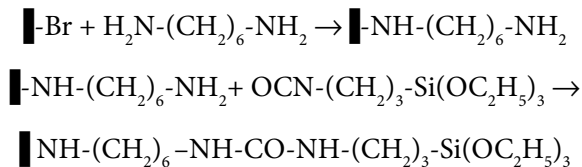


The second way was either bromination of the polyolefin substrate by exposure to the bromine plasma (◻-Br) or the deposition of a Br-containing plasma polymer (polyolefin substrate coated with plasma polymerized poly(allyl bromide)=◻◻◻-Br) onto the polyolefin.

The C-Br bonds were substituted by the amino groups of 3-aminopropyltriethoxysilane (APTES):



Chain extension was achieved using diamines and isocyanatosilane:



The Si-O-R groups at the spacer-modified polyolefin surface were then partially or fully hydrolyzed, thus producing Si-OH groups. After condensation of neighboring silanol groups siloxane bonds (Si-O-Si) are formed.

Aminosilane and isocyanatosilane were grafted onto brominated or aminated polyolefin surfaces with concentrations of about 6–10 silanes/100 C.

9.6 Summary and Conclusions

Introduction of O-functional groups onto polyolefin surfaces is a proven simple process. Chemical oxidation, plasma-chemical oxidation in low-pressure oxygen glow or atmospheric barrier discharges in air as well flaming are widely used. The maximum concentration of O-functional groups at polyethylene surfaces is limited to 25–28% O/C. All further oxygen attachment produces etching of polymers to gaseous degradation products, such as H₂O, CO₂, CO, etc. Thus, a steady-state of oxygen concentration is established. The etch front propagates linearly into the bulk of polyolefins with retention of the steady-state maximum oxygen concentration. Inorganic constituents remain at the surface as non-etchable oxides. The polyolefin surface becomes hydrophilic by the introduction of the polar oxygen-containing functional groups. The surface energy increases from 28–33 mJ/m² for the untreated polyolefins to 38–44 mJ/m² for the slightly oxidized ones. Now, the polyolefin foils are wettable by ink and thus can be printed. The adhesion of coatings and metal layers is also improved.

The propagation of the etch front into the polymer bulk proceeds with the formation of a thin layer of degraded and oxidized polymer molecules (LMWOM-Low-Molecular Weight Oxidized Material) [63]. This LMWOM layer is also etched by the oxygen plasma or other oxidation processes at its surface and is, therefore, further thinned. However, simultaneously, LMWOM formation propagates into the unmodified polymer bulk. In other words, LMWOM formation is also a steady-state phenomenon. LMWOM is highly oxidized, well wetting and partially soluble but mechanically unstable. This is important in case of adhesion improvement. Using coating processes with viscous resins, which harden later, such LMWOM can be dissolved and integrated within the coating resin by diffusion. Thus, it cannot form a mechanically unstable interlayer between polyolefin and resin coating. The

formation of a weak boundary layer [64] should be avoided. In case of hard coatings, such as metal layers, the LMWOM disturbs the mechanical and chemical anchoring between polyolefin and metal layer because the LMWOM is permanently present and acts as a release agent. The way out of this situation consists in washing or extracting the oxidized polyolefin surface; thus, LMWOM is removed. However, the non-degraded polymer structure is now exposed by solvent extraction. This new surface possesses only a few oxygen-containing polar groups. The effect of making the polyolefin surface wettable is partly lost. Therefore, oxidation of polyolefin surfaces has to be a compromise between maximum concentration of polar groups at the surface and the formation of a weak boundary layer.

LMWOM is produced by oxidizing species produced in the oxygen plasma and by irradiation with the vacuum-plasma UV radiation (and post-plasma reaction with oxygen from air) [132,190,191]. The plasma particle shower is limited to a few Angstroms at the surface but the UV radiation has penetration depths into the polymer bulk in the range of about 0.1–100 μm [87,192–196].

An important disadvantage for a number of applications is the broad variety of functional groups produced, which are not suitable for a post-plasma selective graft reaction. The co-existence of different functional groups would also affect or even inhibit the intended reaction.

Transformation of all oxygen-containing groups by post-plasma wet-chemical reduction with diborane to OH groups was necessary [8,9,197–199]. The thus produced 10–14% OH/C could be grafted with silanes, acids and isocyanates [10,18,86,87]. However, the whole process was expensive and consisted of two separate process steps.

For biological and medical purposes it would be advantageous if one could prepare monotype NH_2 groups [101,200]. However, the exposure to ammonia or nitrogen or ammonia-hydrogen and nitrogen-hydrogen mixtures in low- and atmospheric pressure plasmas could produce significant concentrations of primary amino groups [104,201,202]. Favia and coworkers reported tuning of amino group concentration by varying the ammonia-hydrogen feed gas composition [115]. A post-plasma reduction of the broad variety of N-containing groups using diborane to NH_2 groups, in analogy with the reduction of $\text{C}=\text{O}$ and $\text{C}=\text{C}$ to OH-groups with B_2H_6 , NaBH_4 , LiAlH_4 or sodium bis(2-methoxyethoxy)aluminum hydride (Vitrider), was not completely successful [89]. However, H. C. Brown and P. Heim demonstrated successfully the wet-chemical reduction of different amides [203]. Nevertheless, it has to be highlighted that the formation of monosort NH_2 groups is not used as well as is not completely possible yet. Partially, this problem can be solved by coating the polyolefin with a thin polymer film using the plasma polymerization process as shown [204].

A similar process is the electrospray ionization (ESI) deposition of commercial poly(allylamine), poly(acrylic acid), poly(vinylidene chloride), poly(styrene), poly(methyl methacrylate) etc. [155,156]. The adhesion of such sprayed polymer films to other materials was surprisingly high.

Plasma bromination is the most promising plasma process to produce chemically well-suited and highly reactive monotype functional groups at polyolefin surfaces with high selectivity and good yield [19,205]. The bromination of polyolefin surface achieves the maximum

Table 9.2 Yield in desired functional groups on polyethylene surfaces exposed to various treatments [25]

Treatment	Functional groups	Yield in all functional groups [%]	Desired functional group	Yield in desired monosort functional group [%]
Chemical oxidation	C-OH, C-O-OH, C-O-C, >C=O, CHO, COOH	28	OH	5
Oxygen plasma	C-OH, C-O-OH, C-O-C, >C=O, CHO, COOH	28	OH	2
Flaming	C-OH, C-O-OH, C-O-C, >C=O, CHO, COOH	28	OH	5
Ammonia plasma	-NH ₂ , -NH-, >N-, C≡N, >C=N-, >N-OH, -N=O, CO-NH-	20	-NH ₂	2
Bromine plasma	C-Br	65	C-Br	65

Br concentration within 10 s exposure to the bromine plasma. Covalently bonded 65% Br/C were found without side-reactions. The maximum yield in bromination of graphene amounts to 35% Br/C. The exposure to bromoform plasma allows increasing the C-Br yield to about 120% Br/C, originated from the bromination of polyolefin and partial covering with a Br-containing plasma polymer. Using the principle of plasma polymer deposition the yield in Br can be further improved by use of mixtures of bromoform with bromine or allyl bromide with bromine. Thus, concentrations up to 157% Br/C were achieved [19].

Other chemical and plasma-chemical processes do not produce similar results concerning monosort functionalization of polyolefin surfaces. Also the plasma polymerization and the ESI process may be considered as alternative processes to plasma bromination.

References

1. K. Rossmann, Improvement of bonding properties of polyethylene. *J. Polym. Sci.* 19, 141–144 (1956).
2. E. Fanghänel, *Organikum*, 22nd edition, Wiley-VCH, Weinheim. (2002).
3. G. Habenicht, *Kleben*, Springer, Heidelberg. (2009).
4. D.T. Clark and A. Dilks, ESCA applied to polymers. XXIII. RF glow discharge modification of polymers in pure oxygen and helium–oxygen mixtures. *J. Polym. Sci.: Polym. Chem. Ed.* 17, 957–976 (1979).

5. D.T. Clark and R. Wilson, Selective surface modification of polymers by means of hydrogen and oxygen plasmas. *J. Polym. Sci.: Polym. Chem. Ed.* **21**, 837–853 (1983).
6. U. Kogelschatz and J. Salge, High pressure plasmas: Dielectric-barrier and corona discharges, properties and technical applications, in *Low Temperature Plasma Physics, Fundamental Aspects and Applications*, R. Hippler, S. Pfau, M. Schmidt, and K.H. Schoenbach (Eds.), pp. 9–21, Wiley-VCH, Weinheim. (2001).
7. R. Srinivasan, Self-developing photoetching of poly(ethylene terephthalate) films by far-ultraviolet excimer laser radiation. *Appl. Phys. Lett.* **41**, 576–578 (1982).
8. H.C. Brown, From Little Acorns to Tall Oaks - From Boranes Through Organoboranes, Nobel Lecture (December 8, 1979).
9. R.G. Nuzzo and G. Smolinsky, Preparation and characterization of functionalized polyethylene surfaces. *Macromolecules* **17**, 1013–1019 (1984).
10. G. Kühn, A. Ghode, St. Weidner, I. Retzko, W.E.S. Unger, and J.F. Friedrich, Chemically well-defined polymer layers by grafting or pulsed plasma polymerization, in *Polymer Surface Modification: Relevance to Adhesion*, Vol. 2, K.L. Mittal (Ed.), pp. 45–64, CRC Press, Boca Raton, FL. (2000).
11. J. Friedrich, R. Mix, and S. Wettmarshausen, A new concept of adhesion promotion in metal-polymer composites by introduction of covalently bonded spacers at interface. *J. Adhesion Sci. Technol.* **22**, 1123–1143 (2008).
12. J.R. McCallum and C.T. Rankin, A novel method for modifying surfaces. *J. Polym. Sci. B* **9**, 751–752 (1971).
13. A. Bradley and J. Fales, Prospects for industrial applications of electrical discharge. *Chem. Technol.* 232–237 (April 1971).
14. H. Yasuda, Plasma for modification of polymers. *J. Macromol. Sci., Part A: Chem.* **10**, 383–420 (1992).
15. K.E. Geckeler, R. Gebhardt, and H. Grünwald, Surface modification of polyethylene by plasma grafting with styrene for enhanced biocompatibility. *Naturwissenschaften* **84**, 150–151 (1997).
16. C.I. Simionescu, F. Denes, M.M. Macoveanu, M. Totolin, and G. Cazakin, Polymerization of some potential “grafting-monomers” for natural and synthetic fibres in cold plasma conditions. *Acta Polymerica* **30**, 26–31 (1979).
17. K. Kato, E. Uchida, E.-T. Kang, Y. Uyama, and Y. Ikada, Polymer surface with graft chains. *Prog. Polym. Sci.* **28**, 209–259 (2003).
18. G. Kühn, St. Weidner, R. Decker, A. Ghode, and J. Friedrich, Selective surface functionalization of polyolefins by plasma treatment followed by chemical reduction. *Surface Coatings Technol.* **116–119**, 796–801 (1999).
19. J. Friedrich, S. Wettmarshausen, and M. Hennecke, Haloform plasmas applied to polymers. *Surface Coatings Technol.* **203**, 3647–3655 (2009).
20. R.T. Chen, B.W. Muir, G.K. Such, A. Postma, R.A. Evans, S.M. Pereira, K.M. McLean, and F. Caruso, Surface “click” chemistry on brominated plasma polymer thin films. *Langmuir* **26**, 3388–3393 (2010).
21. M. Suzuki, A. Kishida, H. Iwata, and Y. Ikada, Graft copolymerization of acrylamide onto polyethylene. *Macromolecules* **19**, 1804–1808 (1986).
22. J. Meichsner and H.-U. Poll, Plasmamodifizierung von Polymeroberflächen. *Acta Polymerica* **32**, 203–208 (1981).
23. E.M. Liston, L. Martinu, and M.R. Wertheimer, Plasma surface modification of polymers for improved adhesion: A critical review. *J. Adhesion Sci. Technol.* **7**, 1091–1127 (1993).

24. K.L. Tan, L.L. Woon, H.K. Wong, E.T. Kang, and K.G. Neoh, Surface modification of plasma-pretreated poly(tetrafluoroethylene) films by graft copolymerization. *Macromolecules* **26**, 2832–2836 (1993).
25. J. Friedrich, *The Plasma Chemistry of Polymer Surfaces, Advanced Techniques for Surface Design*, Wiley-VCH, Weinheim. (2012).
26. J.F. Friedrich, R. Mix, R.-D. Schulze, A. Meyer-Plath, R. Joshi, and S. Wettmarshausen, New plasma techniques for polymer surface modification with monotype functional groups. *Plasma Process. Polym.* **5**, 407–423 (2008).
27. J. Friedrich, G. Kühn, and J. Gähde, Untersuchungen zur Plasmaätzung von Polymeren. I. Strukturveränderungen von Polymeren nach Plasmaätzung. *Acta Polymerica* **30**, 470–477 (1979).
28. J. Friedrich, Mechanisms of plasma polymerization – A chemist's point of view. *Plasma Process. Polym.* **8**, 783–802 (2011).
29. R.H. Partridge, Exciton interpretation of the vacuum-ultraviolet absorption spectra of saturated organic polymers. *J. Chem. Phys.* **49**, 3656–3668 (1968).
30. L.J. Gerenser, XPS studies of in situ modified polymer surfaces, in *Plasma Surface Modification of Polymers: Relevance to Adhesion*, M. Strobel, C. Lyons, and K.L. Mittal (Eds.), pp. 43–64, CRC Press, Boca Raton, FL. (1994).
31. D.T. Clark and A. Dilks, ESCA applied to polymers. XV. RF glow-discharge modification of polymers, studied by means of ESCA in terms of a direct and radiative energy-transfer model. *J. Polym. Sci.: Polym. Chem. Ed.* **15**, 2321–2345 (1977).
32. J. Friedrich, R. Mix, and G. Kühn, Polymer surface modification with monotype functional groups of different type and density, in *Plasma Processing and Polymers*, R. d'Agostino, P. Favia, C. Oehr, and M.R. Wertheimer (Eds.), pp. 3–21, Wiley-VCH, Weinheim. (2005).
33. H. Germar, Die Mikrostruktur chlorierter Polyvinylchloride aus dem Ultrarotspektrum. *Makromolekulare Chemie* **86**, 89–97 (1965).
34. J.C.L. Hageman, G.A. de Wijs, R.A. de Groot, and R.J. Meier, Bond scission in a perfect polyethylene chain and the consequences for the ultimate strength. *Macromolecules* **33**, 9098–9108 (2000).
35. F.K. MacTaggart, *Plasma Chemistry in Electrical Discharges*, Elsevier, Amsterdam. (1967).
36. R. Foerch, G. Beamson, and D. Briggs, XPS valence band analysis of plasma-treated polymers. *Surf. Interf. Anal.* **17**, 842–846 (1991).
37. R. Förch, N.S. McIntyre, and D.H. Hunter, Oxidation of polyethylene surfaces by remote plasma discharge: A comparison study with alternative oxidation methods. *J. Polym. Sci.: Part A: Polym. Chem.* **28**, 193–204 (1990).
38. F. Truica-Marasescu and M.R. Wertheimer, Vacuum-ultraviolet photopolymerisation of amine-rich thin films. *Macromol. Chem. Phys.* **209**, 1043–1049 (2008).
39. J. Friedrich, G. Kühn, and R. Mix, Tailoring of polymer surfaces with different monotype functional groups of variable density using chemical and plasma chemical processes. *Progr. Colloid Polym. Sci.* **132**, 62–71 (2006).
40. J. Friedrich, I. Loeschke, and J. Gähde, Zur Adhäsion von Aluminium auf Polypropylen. *Acta Polymerica* **37**, 687–695 (1986).
41. J. Friedrich, R. Mix, R.-D. Schulze, and G. Kühn, Contribution of chemical interactions to the adhesion between metals and functional groups of different (mono-) type and density at polymer surfaces, in *Adhesion*, W. Possart (Ed.), pp. 265–288, Wiley-VCH, Weinheim. (2005).

42. J. Friedrich, G. Kühn, R. Mix, and W. Unger, Formation of plasmapolymer layers with functional groups of different type and density at polymer surfaces and their interaction to Al atoms. *Plasma Proc. Polym.* **1**, 28–50 (2004).
43. J. Friedrich, A. Meyer-Plath, I. Retzko, G. Kühn, and R. Mix, Comparison of different plasma-chemical processes for the formation of monotype functionalized polymer surfaces, in *Proceedings of International Symposium on Plasma Chemistry 16 (ISPC-16)*, Taormina, Italy (2003).
44. J.C. Calderon and R.B. Timmons, Surface molecular tailoring via pulsed plasma-generated acryloyl chloride polymers: Synthesis and reactivity. *Macromolecules* **31**, 3216–3224 (1998).
45. R. Mix, J.F. Friedrich, and G. Kühn, Adhesion between metal atoms and polymer surfaces fitted with different types and variable density of functional groups, in *Plasma Polymers and Related Materials*, M. Mutlu, G. Dinescu, R. Förch, J.M. Martin-Martinez, and J. Vyskocil (Eds.), pp. 107–114, Hacettepe University Press, Ankara. (2005).
46. S. Swaraj, U. Oran, J.F. Friedrich, A. Lippitz, and W.E.S. Unger, Surface analysis of plasma deposited polymer films, 6: Analysis of plasma deposited allyl alcohol films before and after aging in air. *Plasma Proc. Polym.* **2**, 572–580 (2005).
47. H.-G. Elias, *Macromolecules*, VCH, Weinheim. (1990).
48. R. Mix, J. Falkenhagen, R.-D. Schulze, V. Gerstung, and J.F. Friedrich, Plasma homo- and copolymerization of allyl alcohol and styrene, in *Polymer Surface Modification, Relevance to Adhesion*, Vol. 5, K.L. Mittal (Ed.), pp. 317–340, CRC Press, Boca Raton, FL. (2009).
49. A.J. Beck, F.R. Jones, and R.D. Short, Plasma copolymerization as a route to the fabrication of new surfaces with controlled amounts of specific chemical functionality. *Polymer* **37**, 5537–5539 (1996).
50. A.P. Kettle, A.J. Beck, L. O'Toole, F.R. Jones, and R.D. Short, Plasma polymerization for molecular engineering of carbon-fibre surfaces for optimized composites. *Composites Sci. Technol.* **57**, 1023–1032 (1997).
51. V. Jacobsen, B. Menges, A. Scheller, R. Förch, S. Mittler, and W. Knoll, In situ film diagnostics during plasma polymerisation using waveguide mode spectroscopy. *Surface Coatings Technol.* **142–144**, 1105–1108 (2001).
52. A. Fahmy, A. Schönhals, and J. Friedrich, Structure of plasma-deposited copolymer films prepared from acrylic acid and styrene, Part I Influence of duty cycle. *Plasma Process. Polym.* **9**, 273–284 (2012).
53. K. Hoffmann, R. Mix, J.F. Friedrich, and U. Resch-Genger, Spectroscopic characterization of plasma-chemically functionalized and fluorophor labeled polymer surfaces, in *Reviews in Fluorescence 2008*, C.D. Geddes (Ed.), pp. 139–160, Springer, New York. (2010).
54. B.M. Wickson and J.L. Brush, Surface hydroxylation of polyethylene by plasma polymerization of allyl alcohol and subsequent silylation. *Colloids Surfaces* **156**, 201–213 (1999).
55. A.P. Ameen, R.D. Short, and R.J. Ward, The formation of high surface concentrations of hydroxyl groups in the plasma polymerization of allyl alcohol. *Polymer* **35**, 4382–4391 (1994).
56. M.R. Alexander and T.M. Duc, The chemistry of deposits formed from acrylic acid plasmas. *J. Mater. Chem.* **8**, 937–943 (1998).
57. C.L. Rinsch, X. Chen, V. Panchalingam, R.C. Eberhart, J.-H. Wang, and R.B. Timmons, Pulsed radio frequency plasma polymerization of allyl alcohol: Controlled deposition of surface hydroxyl groups. *Langmuir* **12**, 2995–3002 (1996).
58. A.E. Lefohn, N.M. Mackie, and E.R. Fisher, Comparison of films deposited from pulsed and continuous wave acetonitrile and acrylonitrile plasmas. *Plasma Polymers* **3**, 197–209 (1998).

59. M.-Y. Teng, K.-R. Lee, D.-J. Liaw, Y.S. Lin, and J.-Y. Lai, Plasma deposition of acrylamide onto novel aromatic polyamide membrane for pervaporation. *Eur. Polym. J.* **36**, 663–672 (2000).
60. S. Wettmarshausen, H.-U. Mittmann, G. Kühn, G. Hidde, and J.F. Friedrich, Plasmabromination – The selective way to monotype functionalized polymer surfaces. *Plasma Proc. Polym.* **4**, 832–839 (2007).
61. A.R. Denaro, P.A. Owens, and A. Crawshaw, Glow discharge polymerization—III. Allyl alcohol and crotyl alcohol. *Eur. Polym. J.* **6**, 487–497 (1970).
62. J.C. Calderon, A. Harsch, G.W. Gross, and R.B. Timmons, Stability of plasma-polymerized allylamine films with sterilization by autoclaving. *J. Biomed. Mater. Res.* **42**, 597–603 (1998).
63. M. Strobel, C. Dunatov, J.M. Strobel, C.S. Lyons, S.J. Perron, and M.C. Morgan, Low-molecular-weight materials on corona-treated polypropylene. *J. Adhesion Sci. Technol.* **3**, 321–335 (1989).
64. J.J. Bikermann, *The Science of Adhesive Joints*, Academic Press, New York. (1968).
65. K. Jesch, J.E. Bloor, and P.L. Kronick, Structure and physical properties of glow discharge polymers. I. Polymers from hydrocarbons. *J. Polym. Sci.* **A1**, 1487–1497 (1966).
66. P.L. Kronick, K. Jesch, and J.E. Bloor, Spectra of glow-discharge polymers from aromatic compounds. *J. Polym. Sci.* **A1**, 767–727 (1969).
67. L.F. Thompson and K.G. Mayhan, The plasma polymerization of vinyl monomers. I. The design, construction, and operation of an inductively coupled plasma generator and preliminary studies with nine monomers. *J. Appl. Polym. Sci.* **16**, 2291–2315 (1972).
68. L.F. Thompson and K.G. Mayhan, The plasma polymerization of vinyl monomers. II. A detailed study of the plasma polymerization of styrene. *J. Appl. Polym. Sci.* **16**, 2317–2341 (1972).
69. A.R. Denaro, P.A. Owens, and A. Crawshaw, Glow discharge polymerization—II α -methylstyrene, ω -methylstyrene and allylbenzene. *Eur. Polym. J.* **5**, 471–482 (1969).
70. A.R. Denaro, P.A. Owens, and A. Crawshaw, Glow discharge polymerization—Styrene. *Eur. Polym. J.* **4**, 93–106 (1968).
71. A.R. Westwood, Glow discharge polymerization—I. Rates and mechanisms of polymer formation. *Eur. Polym. J.* **7**, 363–375 (1971).
72. J.M. Tibbitt, R. Jensen, A.T. Bell, and M. Shen, A model for the kinetics of plasma polymerization. *Macromolecules* **10**, 647–653 (1977).
73. J.M. Tibbitt, M. Shen, and A.T. Bell, Structural characterization of plasma-polymerized hydrocarbons. *J. Macromol. Sci., Chem.* **A10**, 1623–1648 (1976).
74. G. Rosskamp, Untersuchungen über Umlagerungen, Eliminierungen und Polymerisationen im Plasma einer Glimmentladung, PhD thesis, University of Tübingen, Germany (1972).
75. J. Friedrich, Untersuchungen zur Modifizierung von Feststoffoberflächen im nichtisothermen Plasma einer Hochfrequenzentladung, PhD thesis, German Academy of Sciences, Berlin (1974).
76. J. Friedrich, J. Gähde, H. Frommelt, and H. Wittrich, Modifizierung von Feststoffoberflächen in einer HF-Entladung. I. Polymerisation im geschlossenen und strömenden System, *Faserforsch. Textiltechn./Z. Polymerenforsch.* **27**, 517–522 (1976).
77. M. Shen and A.T. Bell, Review of recent advances in plasma polymerization, in *Plasma Polymerization*, M. Shen and A.T. Bell (Eds.), pp. 1–36, ACS Symposium Series 108, American Chemical Society, Washington D.C. (1979).
78. H.K. Yasuda, *Plasma Polymerization*, Academic Press, Orlando, FL. (1985).
79. E.J. Vastola and J.P. Wightman, The rearrangement of acetylene, benzene, ethane, ethylene, methane and naphthalene in a microwave discharge. *J. Appl. Chem.* **14**, 69–73 (1964).
80. R. d'Agostino (Ed.), *Plasma Deposition, Treatment, and Etching of Polymers*, Academic Press, San Diego, CA. (1999).

81. H.C. Brown, H.I. Schlesinger, and A.B. Burg, Hydrides of boron. XI. The reaction of diborane with organic compounds containing a carbonyl group. *J. Amer. Chem. Soc.* **61**, 673–680 (1939).
82. H.C. Brown and B.C. Subba Rao, Hydroboration. III. The reduction of organic compounds by diborane, an acid-type reducing agent. *J. Amer. Chem. Soc.* **82**, 681–686 (1960).
83. H.C. Brown and W. Korytnik, Hydroboration. IV. A study of the relative reactivities of representative functional groups toward diborane. *J. Amer. Chem. Soc.* **82**, 3866–3869 (1960).
84. H.C. Brown, K.-W. Kim, M. Srebnik, and S. Bakthan, Organoboranes for synthesis. 7. An improved general synthesis of primary amines from alkenes via hydroboration-organoborane chemistry. *Tetrahedron* **43**, 4071–4078 (1987).
85. H.C. Brown, *Hydroboration*, Benjamin, New York. (1962).
86. G. Kühn, I. Retzko, A. Lippitz, W. Unger, and J. Friedrich, Homofunctionalized polymer surfaces formed by selective plasma processes. *Surf. Coatings Technol.* **142–144**, 494–500 (2001).
87. J. Friedrich, W. Unger, A. Lippitz, I. Koprinarov, A. Ghode, Sh. Geng, and G. Kühn, Plasma-based introduction of monosort functional groups of different type and density onto polymer surfaces, Part I: Behaviour of polymers exposed to oxygen plasma. *Composite Interfaces* **10**, 139–172 (2003).
88. J.F. Friedrich, W.E.S. Unger, A. Lippitz, I. Koprinarov, S. Weidner, G. Kühn, and L. Vogel, Chemical reactions at polymer surfaces interacting with a gas plasma or with Cr atoms - Their relevance to adhesion, in *Metallized Plastics 5&6: Fundamental and Applied Aspects*, K.L. Mittal (Ed.), pp. 271–293, CRC Press, Boca Raton, FL. (1998).
89. D.S. Everhart and C.N. Reilley, Chemical derivatization in electron spectroscopy for chemical analysis of surface functional groups introduced on low-density polyethylene film. *Anal. Chem.* **53**, 665–676 (1981).
90. Sh. Geng, J. Friedrich, J. Gähde, and L. Guo, Surface-enhanced infrared absorption (SEIRA) and its use in analysis of plasma-modified surface. *J. Appl. Polym. Sci.* **71**, 1231–1237 (1999).
91. M. Aouinti, P. Bertrand, and F. Poncin-Epaillard, Characterization of polypropylene surface treated in a CO₂ plasma. *Plasmas Polymers* **8**, 225–235 (2003).
92. M.-J. Wang, Y.-I. Chang, and F. Poncin-Epaillard, Acid and basic functionalities of nitrogen and carbon dioxide plasma-treated polystyrene. *Surf. Interface Anal.* **37**, 348–355 (2005)
93. N. Medard, J.-C. Soutif, and F. Poncin-Epaillard, CO₂, H₂O, and CO₂/H₂O plasma chemistry for polyethylene surface modification. *Langmuir* **18**, 2246–2253 (2002).
94. J.A. Terlingen, H.F.C. Gerritsen, A.S. Hoffmann, and J. Feijen, Introduction of functional groups on polyethylene surfaces by a carbon dioxide plasma treatment. *J. Appl. Polym. Sci.* **57**, 969–982 (1995).
95. Q.T. Le, J.J. Pireaux, and R. Caudano, XPS study of the PET film surface modified by CO₂ plasma: Effects of the plasma parameters and ageing. *J. Adhesion Sci. Technol.* **11**, 735–751 (1997).
96. R.E. Allred and W.C. Schimpf, CO₂ plasma modification of high-modulus carbon fibres and their adhesion to epoxy resins. *J. Adhesion Sci. Technol.* **8**, 383–394 (1994).
97. N. Inagaki and M. Matsunaga, Preparation of carboxylate groups-containing thin films by plasma polymerization. *Polym. Bull.* **13**, 349–352 (1985).
98. D. Hegemann, E. Körner, and S. Guimond, Plasma polymerization of acrylic acid revisited. *Plasma Proc. Polym.* **6**, 246–254 (2009).
99. S.L. Miller, A production of amino acids under possible primitive earth conditions. *Science* **117**, 528–529 (1953).
100. S.L. Miller and H.C. Urey, Organic compound synthesis on the primitive earth. *Science* **130**, 245–250 (1959).

101. J.R. Hollahan, B.B. Stafford, R.D. Falb, and S.T. Payne, Attachment of amino groups to polymer surfaces by radiofrequency plasmas. *J. Appl. Polym. Sci.* **13**, 807–816 (1969).
102. U. Resch-Genger, K. Hoffmann, R. Mix, and J.F. Friedrich, Monitoring of amino-functionalities on plasma-chemically modified polypropylene supports with a chromogenic and fluorogenic pyrylium reporter. *Langmuir* **23**, 8411–8418 (2007).
103. R. Mix, K. Hoffmann, U. Resch-Genger, R. Decker, and J.F. Friedrich, Covalent coupling of fluorophores to surface-bonded functional groups, in *Polymer Surface Modification: Relevance to Adhesion*, Vol. 4, K.L. Mittal (Ed.), pp. 171–192, CRC Press, Boca Raton, FL. (2007).
104. J. Friedrich, J. Gähde, H. Frommelt, and H. Wittrich, Modifizierung von Feststoffoberflächen in einer HF-Entladung. III. Plasmachemisches Aufbringen funktioneller Gruppen und selektiver Abbau teilkristalliner Polymere, Faserforsch. *Textiltechn. / Z. Polymerenforsch.* **27**, 604–608 (1976).
105. J. Friedrich, I. Loeschke, J. Gähde, H. Frommelt, and H. Wittrich, Verfahren zur Herstellung von metallisierten Polyäthylenterephthalat-Formstoffen, patent DD-WP 115 708 (01.10.1974).
106. M.R. Wertheimer and H.P. Schreiber, Surface property modification of aromatic polyamides by microwave plasmas. *J. Appl. Polym. Sci.* **26**, 2087–2096 (1981).
107. H. Wittrich, J. Friedrich, J. Gähde, and I. Loeschke, Verfahren zur Herstellung von metallisierten nichtleitenden Stoffen, DD-patent 120 473 (17. July 1975).
108. T.R. Gengenbach, X. Xie, R.C. Chatelier, and H.J. Griesser, Evolution of the surface composition and topography of perfluorinated polymers following ammonia-plasma treatment. *J. Adhesion Sci. Technol.* **8**, 305–328 (1994).
109. J. Friedrich, V.G. Ivanova-Mumeva, J. Gähde, G.D. Andreevskaya, and I. Loeschke, Untersuchungen zum Einfluß einer Oberflächenmodifizierung von Fasermaterialien im nicht-thermischen Plasma einer Hochfrequenzentladung auf die Adhäsion zu Epoxidharz. III. Ergebnisse der Plasmabehandlung von Kohlenstoff-Fasern. *Acta Polymerica* **34**, 171–177 (1983).
110. J. Lub, F. van Vroonhoven, E. Bruninx, and A. Benninghoven, Interaction of nitrogen and ammonia plasmas with polystyrene and polycarbonate studied by X-ray photoelectron spectroscopy, neutron activation analysis and static secondary ion mass spectrometry. *Polymer* **30**, 40–44 (1989).
111. J. Behnisch, A. Holländer, and H. Zimmermann, Surface modification of polyethylene by remote dc discharge plasma treatment. *J. Appl. Polym. Sci.* **49**, 117–124 (1993).
112. H.J. Griesser, R.C. Chatelier, T.R. Gengenbach, G. Johnson, and J.G. Steele, Growth of human cells on plasma polymers: Putative role of amine and amide groups. *J. Biomater. Sci.* **5**, 531–554 (1994).
113. M.-J. Wang, Y.-I. Chang, and F. Poncin-Epaillard, Effects of the addition of hydrogen in the nitrogen cold plasma: The surface modification of polystyrene. *Langmuir* **19**, 8325–8330 (2003).
114. A. Meyer-Plath, R. Mix, and J. Friedrich, Aspects of amino functionalization for adhesion promotion of thermally evaporated copper films, in *Adhesion Aspects of Thin Films*, Vol. 3, K.L. Mittal (Ed.), pp. 177–198, CRC Press, Boca Raton, FL. (2007).
115. M.G. Buonomenna, L.C. Lopez, P. Favia, R. d'Agostino, A. Gordano, and E. Drioli, New PVDF membranes: The effect of plasma surface modification on retention in nanofiltration of aqueous solution containing organic compounds. *Water Res.* **41**, 4309–4316 (2007).
116. C. Oehr and M. Müller, Plasma amino functionalization of PVdF microfiltration membranes: comparison of the plasma modification with a grafting method using ESCA and an amino-selective fluorescence probe. *Surface Coatings Technol.* **116–119**, 802–807 (1999).

117. S. Wettmarshausen, H. Min, W. Unger, C. Jäger, G. Hidde, and J. Friedrich, Significance of hydrogen-deuterium exchange at polyolefin surfaces on exposure to ammonia low-pressure plasma. *Plasma Chem. Plasma Proc.* **31**, 551–572 (2011).
118. H. Min, S. Wettmarshausen, J. Friedrich, and W.E.S. Unger, A ToF-SIMS study of the deuterium - hydrogen exchange induced by ammonia plasma treatment of polyolefins. *J. Anal. Atomic Spectr.* **26**, 1157–1165 (2011).
119. W.J. Wedenjew, K.W. Gurwitsch, W.H. Kondratjew, W.A. Medwedjew, and E.L. Frankewitsch, *Energien chemischer Bindungen, Ionisationspotentiale und Elektronenaffinitäten*, VEB Deutscher Verlag für Grundstoffindustrie, Leipzig, (1971).
120. H.V. Boenig, *Fundamentals of Plasma Chemistry and Technology*, Technomic, Lancaster, PA, (1988).
121. J. Friedrich, E. Schulz, St. Weidner, and G. Kühn, Improvement in mechanical strength of fibre polymer composites by fibre pretreatment in low-pressure plasmas, Techtexil-Symposium '97 (14 May 1997), Frankfurt/Main, Section Plasma Finishing, Proceedings 5.22 (1977).
122. V.G. Ivanova-Mumeva, G.D. Andreevskaya, J. Friedrich, and J. Gähde, Untersuchungen zum Einfluß einer Oberflächenmodifizierung von Fasermaterialien im nicht-thermischen Plasma einer Hochfrequenzladung auf die Adhäsion zu Epoxidharz. I. Messung der Adhäsionsfestigkeit. *Acta Polymerica* **31**, 752–756 (1980).
123. J. Friedrich, I. Loeschke, J. Gähde, and Kh. Richter, Untersuchungen zur Plasmaätzung von Polymeren. VI. Veränderungen an der Oberfläche von Polypropylen. *Acta Polymerica* **32**, 337–343 (1981).
124. A. Holländer, S. Kröpcke, and F. Pippig, Chemical analysis of functionalized polymer surfaces. *Surf. Interf. Anal.* **40**, 379–385 (1998).
125. J. Friedrich, Sh. Geng, W. Unger, and A. Lippitz, Modelling the plasma-induced reactions on polymer surfaces by using aliphatic self-assembling and LB layers as substrates. *Surf. Coat. Technol.* **98**, 1132–1141 (1998).
126. K.S. Siow, L. Britcher, S. Kumar, and H.J. Griesser, Plasma methods for the generation of chemically reactive surfaces for biomolecule immobilization and cell colonization - A review. *Plasma Process. Polym.* **3**, 392–418 (2006).
127. J. Behnisch, H. Zimmermann, and J. Friedrich, Topokinetics of the polyene formation in PVC films during treatment with non-oxidative plasma. *Acta Polymerica* **42**, 51–53 (1991).
128. V.N. Vasilets, A.V. Kuznetsov, and V.I. Sevastianov, Vacuum ultraviolet treatment of polyethylene to change surface properties and characteristics of protein adsorption. *J. Biomed. Mater. Res. Part A* **69**, 428–435 (2004).
129. P. Chevallier, M. Castonguay, S. Turgeon, N. Dubrulle, D. Mantovani, P.H. McBreen, J.-C. Wittmann, and G. Laroche, Ammonia RF-plasma on PTFE surfaces: Chemical characterization of the species created on the surface by vapor-phase chemical derivatization. *J. Phys. Chem. B* **105**, 12490–12497 (2001).
130. St. Weidner, G. Kühn, J. Friedrich, W. Unger, and A. Lippitz, Plasmaoxidative degradation of polymers studied by matrix-assisted laser desorption/ionization mass spectrometry. *Rapid Comm. Mass Spectrom.* **10**, 727–737 (1996).
131. U. Oran, S. Swaraj, J. Friedrich, and W.E.S. Unger, Surface analysis of plasma-deposited polymer films by time-of-flight static secondary mass spectrometry (ToF-SSIMS) before and after exposure to ambient air. *Surf. Coatings Technol.* **200**, 463–467 (2005).
132. M.V. Hudis, Surface crosslinking of polyethylene using a hydrogen glow discharge. *J. Appl. Polym. Sci.* **16**, 2397–2415 (1972).

133. J. Friedrich, Plasma modification of polymers, in *Polymer-Solid Interfaces*, J.J. Pireaux, P. Bertrand, and J.L. Bredas (Eds.), pp. 443–454, Institute of Physics Publishing, Bristol, UK. (1991).
134. E. Kiss, J. Samu, A. Toth, and I. Bertoti, Novel ways of covalent attachment of poly(ethylene oxide) onto polyethylene: Surface modification and characterization by XPS and contact angle measurements. *Langmuir* **12**, 1651–1657 (1996).
135. J. Friedrich, Beschichtung und Modifizierung von Kunststoffoberflächen, in *Vakuum-Plasma-Technologien Beschichtung und Modifizierung von Oberflächen*, Teil I, G. Blasek, and G. Bräuer (Eds.), Eugen-G-Leuze-Verlag, Saulgau, Germany. (2010).
136. S. Wettmarshausen, R. Mix, A. Meyer-Plath, H.-U. Mittmann, and J. Friedrich, Plasmabromination – the selective way to monotype functionalized polymer surfaces, in *Polymer Surface Modification: Relevance to Adhesion*, Vol. 5, K.L. Mittal (Ed.), pp. 3–18, CRC Press, Boca Raton, FL. (2009).
137. A. Hickling and M.D. Ingram, Glow-discharge electrolysis. *J. Electroanalyt. Chem.* **8**, 65–81 (1964).
138. A.R. Denaro and K.O. Hough, Polymerisation by glow discharge electrolysis. *Electrochim. Acta* **18**, 863–868 (1973).
139. D.R. Johnson, Y. Osada, A.T. Bell, and M. Shen, Studies of the mechanism and kinetics of plasma-initiated polymerization of methyl methacrylate. *Macromolecules* **14**, 118–124 (1981).
140. M. Simor, H. Krump, I. Hudec, J. Rahel, A. Brablec, and M. Cernak, Atmospheric pressure H₂O plasma treatment of polyester cord threads. *Acta Physica Slovaca* **54**, 43–48 (2002).
141. F. de Baerdemaeker, M. Monte, and C. Leys, Capillary underwater discharges. *IEEE Trans. Plasma Sci.* **33**, 492–493 (2005).
142. P. Gupta, G. Tenhundfeld, E.O. Daigle, and D. Ryabkov, Electrolytic plasma technology: Science and engineering—An overview. *Surf. Coatings Technol.* **201**, 8746–8760 (2007).
143. H.H. Kellogg, Anode effect in aqueous electrolysis. *J. Electrochem. Soc.* **97**, 133–142 (1959).
144. A. Hickling, Glow discharge electrolysis, in *Modern Aspects of Electrochemistry*, Vol. 6, J.O' M. Bockris and B.E. Conway (Eds.), pp. 329–373, Butterworths, London. (1971).
145. Y. Osada, A.T. Bell, and M. Shen, Plasma-initiated polymerization of methyl methacrylate. *J. Polym. Sci., Polym. Lett.* **16**, 309–311 (1978).
146. B.R. Locke, M. Sato, P. Sunka, M.R. Hoffmann, and J.-S. Chang, Electrohydraulic discharge and nonthermal plasma for water treatment. *Ind. Eng. Chem. Res.* **45**, 882–888 (2006).
147. S.K. Sengupta and O.P. Singh, Contact glow discharge electrolysis: A study of its chemical yields in aqueous inert-type electrolytes. *J. Electroanal. Chem.* **369**, 113–120 (1994).
148. M. Lecuiller, R. Julien, and J. Pucheault, Simulation sur ordinateur de l'évolution temporelle des ions négatifs de l'air, Application au cas de la décharge couronne négative. *J. Chim. Phys.* **9**, 1353–1360 (1972).
149. R. Joshi, R.-D. Schulze, G. Hidde, and J.F. Friedrich, Selective surface modification of polypropylene with OH groups using the underwater capillary discharge. *Plasma Proc. Polym.* **5**, 695–707 (2008).
150. R. Joshi, R.-D. Schulze, A. Meyer-Plath and M. Wagner, and J. Friedrich, Selective surface modification of polypropylene using underwater plasma technique or underwater capillary discharge. *Plasma Proc. Polym.* **6**, S218–S222 (2009).
151. R.J. Joshi, M. Wagner, and J. Friedrich, Role of hydrogen peroxide in selective OH-group functionalization of PP surfaces using underwater capillary discharge. *J. Adhesion Sci. Technol.* **25**, 283–305 (2011).

152. R. Joshi, J. Friedrich, and S.K. Subramanian, Surface modification of ultra-high molecular weight polyethylene membranes using underwater plasma polymerization. *Plasma Chem. Plasma Proc.* **33**, 921–940 (2013).
153. R.S. Joshi, J.F. Friedrich, and M.H. Wagner, Study of carboxylic functionalization of polypropylene surface using the underwater plasma technique. *Eur. Phys. J. D* **54**, 1–10 (2009).
154. J. Yu, Y. Pan, Q. Lu, W. Yang, J. Gao, and Y. Li, Synthesis and swelling behaviors of P(AMPS-co-AAc) superabsorbent hydrogel produced by glow-discharge electrolysis plasma. *Plasma Chem. Plasma Proc.* **33**, 219–235 (2013).
155. K. Altmann, R.-D. Schulze, G. Hidde, and J. Friedrich, Electro spray-ionization deposition of polymers – Principle, electrophoretic effect and applications. *J. Adhesion Sci. Technol.* **27**, 988–1005 (2013).
156. J. Friedrich, R. Mix, R.-D. Schulze, and A. Rau, Ultra-thin polymer layer deposition by aerosol-barrier-discharge and electro spray at atmospheric pressure. *J. Adhesion Sci. Technol.* **24**, 1329–1350 (2010).
157. W. Goldie, *Metallic Coating of Plastics*, Electrochemical Publications Ltd., Middlesex, England. (1968).
158. R.C. Snogren, *Handbook of Surface Preparation*, Palmerton, New York. (1974). [159] K. Kato, Formation of 2,4-dinitrophenylhydrazones in polyethylene film treated with chromic acid mixture. *J. Appl. Polym. Sci.* **18**, 3087–3094 (1974).
159. R.H. Hansen and H. Schonhorn, A new technique for preparing low surface energy polymers for adhesive bonding. *J. Polym. Sci. B* **4**, 203–210 (1966).
160. W.H. Kreidl and F. Hartmann, The Kreidl process for better print adhesion on polyethylene. *Plastics Technology*. Issue 1, 31–35 (1955).
161. L. Mazzola and A. Cusma, Flame treatment of polymeric materials—Relevance to adhesion: A critical review. *Rev. Adhesion Adhesives*, to be published.
162. F.J. Holly and M.F. Refojo, Wettability of hydrogels I. Poly (2-hydroxyethyl methacrylate). *J. Biomed. Mater. Res.* **9**, 315–326 (1975).
163. J.D. Andrade (Ed.), *Polymer Surface Dynamics*, Plenum Press, New York. (1988).
164. H. Yasuda, A.K. Sharma, and T. Yasuda, Effect of orientation and mobility of polymer molecules at surfaces on contact angle and its hysteresis. *J. Polym. Sci., Polym. Phys. Ed.* **19**, 1285–1291 (1981).
165. F. Garbassi, M. Morra, E. Occhiello, L. Barino, and R. Scordamaglia, Dynamics of macromolecules: A challenge for surface analysis. *Surf. Interf. Anal.* **14**, 585–589 (1989).
166. M. Morra, E. Occhiello, and F. Garbassi, Contact angle hysteresis on oxygen plasma treated polypropylene surfaces. *J. Colloid Interface Sci.* **132**, 504–508 (1989).
167. J. Behnisch, A. Holländer, and H. Zimmermann, Factors influencing the hydrophobic recovery of oxygen-plasma-treated polyethylene. *Surf. Coat. Technol.* **59**, 356–358 (1993).
168. T. Yasuda, T. Okuno, K. Yoshida, and H. Yasuda, A study of surface dynamics of polymers. II. Investigation by plasma surface implantation of fluorine-containing moieties. *J. Polym. Sci., B: Polym. Phys.* **26**, 1761–1769 (1988).
169. F. Garbassi, M. Morra, and E. Occhiello, *Polymer Surfaces – From Physics to Technology*, J. Wiley&Sons, Chichester. (1994).
170. M. Morra, E. Occhiello, and F. Garbassi, Dynamics of plasma treated polymer surfaces: Mechanism and effects, in *Polymer-Solid Interfaces*, J.J. Pireaux, P. Bertrand, and J.L. Bredas (Eds.), pp. 407–428, IOP Publishing, Bristol, UK. (1992).

171. J. Behnisch, H. Zimmermann, and J. Friedrich, Topokinetics of the polyene formation in PVC films during treatment with non-oxidative plasma. *Intern. J. Mater. Sci.* **16**, 139–141 (1991).
172. C. Rüchardt, *Radikale - Eine chemische Theorie in historischer Sicht, Sitzungsberichte der Heidelberger Akademie der Wissenschaften*, pp. 319–345, Mathematisch-naturwissenschaftliche Klasse, Heidelberg. (1992).
173. M. Ramanujam, R. Mix, M. Wagner, and J.F. Friedrich, Investigation of C-radical production at polyolefins after Ar plasma treatment followed by bromine incorporation. *J. Adhesion Sci. Technol.* **27**, 1828–1839 (2013).
174. I. Retzko, J.F. Friedrich, A. Lippitz, and W.E.S. Unger, Chemical analysis of plasma-polymerized films: The application of X-ray photoelectron spectroscopy (XPS), X-ray absorption spectroscopy, (NEXAFS) and Fourier transform infrared spectroscopy (FTIR). *J. Electr. Spectr. Rel. Phenom.* **121**, 111–129 (2001).
175. W. Schnabel, *Polymer Degradation*, Hanser International, München. (1981).
176. U. König, M. Nitschke, A. Menning, G. Eberth, M. Pilz, C. Arnhold, F. Simon, G. Adam, and C. Werner, Durable surface modification of poly(tetrafluoroethylene) by low pressure H₂O plasma treatment followed by acrylic acid graft polymerization. *Colloids Surfaces B* **24**, 63–71 (2002).
177. J. Friedrich, Tailoring of interface/interphase to promote metal-polymer adhesion, in *Adhesion in Microelectronics*, K.L. Mittal and T. Ahsan (Eds.), Wiley-Scrivener, Beverly, MA. (2014).
178. J. Friedrich, W. Unger, A. Lippitz, I. Koprinarov, G. Kühn, St. Weidner, and L. Vogel, Chemical reactions at polymer surfaces interacting with a gas plasma or with Cr atoms - Their relevance to adhesion. *Surf. Coatings Technol.* **116–119**, 772–782 (1999).
179. G. Kühn, St. Weidner, R. Decker, A. Ghode, and J. Friedrich, Selective surface functionalization of polyolefins by plasma treatment followed by chemical reduction. *Surf. Coat. Technol.* **116–119**, 796–801 (1999).
180. J. Friedrich, G. Kühn, R. Mix, I. Retzko, V. Gerstung, St. Weidner, R.-D. Schulze, and W.E.S. Unger, Plasma polymer adhesion promoters to be used for metal-polymer systems, in *Polyimides and Other High Temperature Polymers: Synthesis, Characterization and Applications*, K.L. Mittal (Ed.), pp. 359–388, CRC Press, Boca Raton, FL. (2003).
181. J. Friedrich, G. Kühn, R. Mix, A. Fritz, and A. Schönhals, Polymer surface modification with monofunctional groups of variable types and densities. *J. Adhesion Sci. Technol.* **17**, 1591–1618 (2003).
182. C. Mühlhan, St. Weidner, J. Friedrich, and H. Nowack, Improvement of bonding properties of polypropylene by low-pressure plasma treatment. *Surface Coatings Technol.* **116–119**, 783–787 (1999).
183. K. Hoffmann, U. Resch-Genger, R. Mix, and J.F. Friedrich, Fluorescence spectroscopic studies on plasma-chemically modified polymer surfaces with fluorophore-labeled functionalities. *J. Fluorescence* **16**, 441–448 (2006).
184. K. Hoffmann, R. Mix, J.F. Friedrich, H.-J. Buschmann, and U. Resch-Genger, Anchoring of fluorophores to plasma-chemically modified polymer surfaces and the effect of cucurbit[6]uril on dye emission. *J. Fluorescence* **19**, 229–237 (2009).
185. R. Mix, K. Hoffmann, U. Resch-Genger, R. Decker, and J.F. Friedrich, Covalent coupling of fluorophores to surface-bonded functional groups, in *Polymer Surface Modification: Relevance to Adhesion*, Vol. 4, K.L. Mittal (Ed.), pp. 171–192, CRC Press, Boca Raton, FL. (2007).
186. R. Cuffe, G. Baud, M. Benmalek, J.P. Besse, J.R. Butruille, and M. Jacquet, X-ray photoelectron spectroscopy studies of plasma-modified PET surface and alumina/PET interface. *Appl. Surface Sci.* **115**, 292–298 (1997).

187. J.F. Friedrich, S. Wettmarshausen, S. Hanelt, R. Mach, R. Mix, E. Zeynalov, and A. Meyer-Plath, Plasma-chemical bromination of graphitic materials and its use for subsequent functionalization and grafting of organic molecules. *Carbon* **48**, 3884–3894 (2010).
188. S. Hanelt, J.F. Friedrich, G. Orts-Gil, and A. Meyer-Plath, Study of Lewis acid catalyzed chemical bromination and bromoalkylation of multi-walled carbon nanotubes. *Carbon* **50**, 1373–1385 (2012).
189. H. Schonhorn and R.H. Hansen, Surface treatment of polymers for adhesive bonding. *J. Appl. Polym. Sci.* **11**, 1461–1474 (1967).
190. M.V. Hudis, Plasma treatment of solid materials, in *Techniques and Applications of Plasma Chemistry*, J.R. Hollahan and A.T. Bell (Eds.), pp. 113–147, Wiley. (1973).
191. J. Friedrich, J. Gähde, and A. Nather, Auswirkung von nichtisothermen Plasmen auf ausgewählte mechanische Kennwerte und die chemische Struktur von schlagzähem Polystyren im Vergleich zur thermischen und UV-Alterungseinflüssen. *Plaste u. Kautsch.* **28**, 420–425 (1981).
192. J. Friedrich, M. Pohl, T. Elsner, and B. Altrichter, Visuelle und analytische Identifizierung und Lokalisierung gealterter Oberflächenschichten von bewitterten Polymeren. *Acta Polymerica* **39**, 544–549 (1988).
193. W. Stiller and J. Friedrich, Vergleich der Wirkprinzipien von Strahlen- und Plasmachemie. *Z. Chem.* **21**, 544–549 (1981).
194. J. Friedrich, Reaktionskinetische Vorgänge an der Grenzfläche zwischen nichtisothermen Plasma und Feststoff. *Contr. Plasma Phys.* **21**, 261–278 (1981).
195. J. Friedrich, R. Mix, G. Kühn, I. Retzko, A. Schönhals, and W. Unger, Plasma-based introduction of monosort functional groups of different type and density onto polymer surfaces, Part II: Pulsed plasma polymerization. *Composite Interfaces* **10**, 173–223 (2003).
196. J. Friedrich, Sh. Geng, W. Unger, A. Lippitz, J. Erdmann, H.-V. Gorsler, Ch. Wöll, A. Schertel, and Ch. Bierbaum, Plasma functionalization and reorientation of macromolecules at polymer surfaces. *Surface Coatings Technol.* **74–75**, 664–669 (1995).
197. J.F. Friedrich, W.E.S. Unger, A. Lippitz, St. Weidner, Sh. Geng, L. Wigant, Ch. Wöll, J. Erdmann, and H.-V. Gorsler, Characterization of plasma-modified organic surfaces by electron spectroscopy, SEIRA and MALDI-TOF, in *Applications of Surface and Interface Analysis*, H.J. Mathieu, B. Reihl, and D. Briggs (Eds.), pp. 803–807, John Wiley & Sons, Chichester, UK. (1996).
198. J. Friedrich, Sh. Geng, W. Unger, and A. Lippitz, Modelling the plasma-induced reactions on polymer surfaces by using aliphatic self-assembling and LB layers as substrates. *Surface Coatings Technol.* **98**, 1132–1141 (1998).
199. J.R. Hollahan and G.L. Carlson, Hydroxylation of polymethylsiloxane surfaces by oxidizing plasmas. *J. Appl. Polym. Sci.* **14**, 2499–2508 (1970).
200. G.C.S. Collins, A.C. Lowe, and D. Nicholas, An analysis of PTFE surfaces modified by exposure to glow discharges. *Europ. Polym. J.* **9**, 1173–1182 (1973).
201. C.P. Klages and A. Grishin, Plasma amination of low-density polyethylene by DBD afterglows at atmospheric pressure. *Plasma Process. Polym.* **5**, 368–375 (2008).
202. H.C. Brown and P. Heim, Selective reductions. XVIII. Fast reaction of primary, secondary, and tertiary amides with diborane. Simple, convenient procedure for the conversion of amides to the corresponding amines. *J. Org. Chem.* **38**, 912–916 (1973).
203. W.R. Gombotz and A.S. Hoffman, Functionalization of polymeric films by plasma polymerization of allyl alcohol and allylamine. *J. Appl. Polym. Sci.: Appl. Polym. Symp.* **42**, 285–303 (1988).
204. J.F. Friedrich, G. Hidde, A. Lippitz, and W.E.S. Unger, Plasma bromination of graphene for covalent bonding of organic molecules. *Plasma Chem. Plasma Process.* **34**, 621–645 (2013).

Nano-Enhanced Adhesives

Shahin Shadlou, Babak Ahmadi-Moghadam and Farid Taheri*

*Department of Civil and Resource Engineering, Dalhousie University,
Halifax, NS, Canada*

Abstract

This review aims at summarizing the recent advances made in the development of resilient adhesives reinforced with nanoparticles (NPs). Different aspects of nano-reinforced adhesives, including various types of NPs and their properties, various methods used for formulating and fabricating nanocomposites, their functioning mechanisms, as well as their advantages and disadvantages are discussed. In addition, the recent progresses made in improving the mechanical, electrical and thermal properties of adhesives reinforced by NPs are addressed. Moreover, the mechanisms that contribute to altering the properties of such adhesives are briefly discussed. Finally, a brief review of bio-adhesives and bio-inspired adhesives is also provided.

Keywords: Nanoparticles, adhesives, mechanical, electrical, thermal properties

10.1 Introduction

Adhesively bonded joints (ABJs) generally comprise of at least two joining components (adherends) with a layer of adhesive in between. The adhesive layer is considered to be an important part of a joint system, as it is the agent that accommodates the transfer of load from one adherend to another. ABJs are being widely used in industry owing to their many advantageous attributes compared to conventional mechanically fastened joints. Some of the advantages of adhesive bonding over alternative assembly techniques, especially when joining fiber-reinforced polymer (FRP) composites, are shown below [1]:

- Stresses are more evenly distributed over the entire bond region, thereby minimizing high localized stress concentrations.

*Corresponding author: farid.taheri@dal.ca

- More superior fatigue resistance than mechanically fastened joints.
- Excellent resistance to mechanical vibration.
- Better compliance to critical tolerances can be achieved compared to mechanical fastening methods.
- Produces leak-free joints.
- Provides weight and cost savings.

Moreover, briefly stated, the applications of composite materials in various industries (e.g., piping, aerospace, automotive, and infrastructures) have created demand for enhanced ABJ systems. Furthermore, in several industrial applications, FRP structural components have to be mated to other composite or metallic components. An ABJ is an efficient joining method for such purposes compared to mechanically fastened joints [2]. Last, but not least, the “smart adhesives”, which are another class of adhesives, have been recently introduced for further managing the stress concentration in ABJs [3, 4].

Altogether, the mentioned features are the key parameters that have made ABJs to gain significant interest in various industries. There are, however, some disadvantages to using adhesives as a joining agent; for instance, long curing time, relatively poor temperature/humidity resistance, requiring elaborate surface preparation in some cases, and difficulties in disassembly are some of the drawbacks of using adhesives for mating structural components. As a result, the attempts for modifying the properties of adhesives to overcome such drawbacks have been the focus of several studies [5-7]. One of the recent attempts opted by several researchers has been the use of nanostructured reinforcements as a promising means for enhancing the response of adhesives and combating some of the above-mentioned shortfalls.

10.2 Why Nanostructured Reinforcements?

A nanoparticle (NP) is defined as a particle with one of its dimensions being less than 100 nm . In fact, a NP is considered as a bridge between atomic and bulk scales. The key advantages of nano-size materials are as follows [8]: large specific surface area, high surface energy, reduced numbers of structural imperfections, and distinctively different physical properties from those of bulk materials. Unlike bulk materials, whose properties are fairly size independent, NPs exhibit size-dependency. This size-dependency is due to the significant increase in the ratio of the atoms on the surface of the particle to the total atoms forming the particle, as nanoparticle's dimension approaches zero.

Various types of NPs have been produced using a diverse range of materials. Each type of NP exhibits one or more unique physical properties, which cannot be achieved at macro scale. These unique properties have encouraged many scientists to devote their efforts in tailoring the desired properties of adhesives utilizing different types of NPs. In this vein, the following factors should be taken into consideration: the target properties of adhesive, the compatibility of adhesive and NPs, functionality of the NPs, and the service conditions, to name a few. Therefore, as the first step, one ought to acquire appropriate information in regard to the properties of each NP type, and how they would affect the properties of

the adhesive formed by inclusion of the NPs. The most common NPs used in reinforcing adhesives are classified based on their type; therefore, a brief description of each group is provided below.

10.2.1 Carbon-based NPs

Among the various types of NPs, the excellent capability of carbon NPs in ameliorating different properties of resins or matrices has persuaded researchers to perform extensive investigations into the behavior of carbon NP reinforced polymers. There are three common configurations of carbon nanofillers, including zero dimensional or spherical particles such as nano-diamond (ND) particles, one-dimensional or cylindrical fillers such as carbon nanotubes (CNTs) and carbon nanofibers (CNFs), and two-dimensional nanofillers such as graphene nanoplatelets (GNPs). The ND particles with their well-established superior tribological properties [9] have been widely used for surface modification of different materials [10, 11]. In addition, it has been shown that inclusion of CNTs and CNFs into polymers leads to notable increase in the mechanical properties [12, 13], electrical properties [14, 15], and thermal properties [16, 17] of the resulting nanocomposites. Besides, the nanocomposites reinforced with GNPs are postulated to offer remarkable thermal [18], mechanical [19], and electrical properties [20].

All these impressive features have encouraged the researchers to explore the reinforcing effect of nanomaterials when included in different polymer matrices. The main disadvantages of carbon nanomaterials are known to be: (a) the inconsistency in the quality of carbon NPs, especially in their mass-produced form, and (b) their cost.

10.2.2 Metal-based NPs

Metallic NPs have fascinated scientists for over a century, mainly due to their huge potential applications in nanotechnology, as well as the recent surge in their utilization in biomedical sciences and engineering [21]. Today, these materials can be synthesized and modified to obtain various chemical functionalities. Metallic nanomaterials can be formed from most metallic elements of the periodic table such as nano-gold, nano-silver and metal oxides (e.g., alumina (Al_2O_3) or zirconia (ZrO_2)) NPs. Although the metal based NPs have been mainly investigated for their electrical [22], optical [23] and magnetic properties [24], it has been shown that the mechanical properties can also be improved by inclusion of metallic NPs into polymers [25].

Although the interest in the optical and electrical properties of metallic NPs has had a long history [26], a number of recent experiments have renewed the interest in using metallic NPs for optical applications. This has also fostered better theoretical and experimental understandings of the key factors and mechanisms governing these properties [27]. Moreover, some metallic NPs have certain unique properties that are of clinical interest. For instance, nano-silver particles have antibacterial properties, which have made them one of the most commercialized metallic nanoparticles in healthcare [28]. This feature of nano-silver has also rendered it as a potential candidate for inclusion in adhesives used for biomedical applications.

10.2.3 POSS

Polyhedral oligomeric silsesquioxanes (POSS) are nanostructures with the empirical formula $\text{RSiO}_{1.5}$, where R may be a hydrogen atom or an organic functional group [29]. POSS nanostructures have diameters in the range 1–3 nm. In the last decade, POSS NPs have attracted considerable attention, mainly owing to their small dimensions, and easy incorporation into polymeric materials, thus providing excellent reinforcing attributes to polymers [30]. POSS is also being used as a facilitator for other NPs to improve their dispersion ability [31].

10.2.4 Other Nanomaterials

10.2.4.1 Nanoclays

Nanoclays are NPs of layered mineral silicates with platelet structure. Nanoclays are relatively inexpensive NPs, which have shown promising results as polymer reinforcements. Nanoclays have been incorporated into polymers to enhance their gas permeation barrier properties [32], mechanical properties [33], fire retardancy properties [34], rheological properties [35] and liquid infusion resistant properties [36]. Nanoclays modified with organic materials, referred to as organoclays, are an enticing class of hybrid organic-inorganic NPs with several applications, such as rheological modifiers, oil and gas absorbents, and drug delivery carriers.

10.2.4.2 Nanosilicas (SiO_2)

Nanosilicas have porous and relatively large surfaces that host a large number of hydroxyl groups and unsaturated residual bonds. Nanosilicas have proven to be an effective reinforcement for polymers for enhancing their strength [37], flexibility [38], and durability [39]. Moreover, nanosilicas have been used as an additive to improve workability and the strength of high-performance and self-compacting concrete [40].

10.3 Development of Polymer-based Nanocomposites

The last step in deployment of nanostructured materials is to devise a suitable strategy for the manufacturing process. Depending on the type of NP, a number of production methods could be used. For example, in selecting an effective and efficient dispersion technique, one should be concerned that the process would not damage the NPs, that the process would yield consistent results, and that it would be suitable for mass-production. In the next section, the manufacturing methods commonly used for generating nanocomposites are discussed.

Perhaps the prime challenge in manufacturing of polymer-based nanocomposites is the attainment of a uniform dispersion of NPs in the polymer matrix. Due to the small dimensions and relatively large surface area of NPs, the intermolecular forces attract individual particles to one another, and as a result, they tend to form large clumps or agglomerations. In order to promote the efficiency of nanocomposites, it is vital to minimize the formation

of such agglomerates and ensure a uniform dispersion of NPs. This task becomes more challenging as the volume content of the NPs in polymers increases, which, in turn, elevates the viscosity of the host polymer, thereby making it less workable. As an example, Figure 10.1 generated by Pinto et al. [41], reports the increase in the viscosity of poly(vinyl acetate) (PVAc) as a function of GNP content and shear rate.

An acceptable dispersion status can usually be achieved through two steps: (i) distribution of NPs within the matrix, and (ii) dispersion of NPs. A mechanical stirrer is usually used for distributing nanoparticles; however, depending on the selected method of dispersion, the distribution step may be avoided. For the second step (i.e. the dispersion), several methods have been developed. The selection of the most suitable method would depend on the type of NP, matrix and application. The most commonly used techniques for dispersion of nanomaterials are briefly discussed.

10.3.1 Sonication

Sonication is the act of applying high-energy sound waves to disperse NPs in a matrix. For this purpose, usually ultrasonic frequencies greater than 20 kHz are employed, which is referred to as ultrasonication. Dispersion by ultrasonication is accomplished by the ultrasonic cavitation developed at the end of the probe, which generates high speed liquid jets (with velocity as high as approximately 1000 km/h). The highly pressurized liquid is then forced between NPs agglomerates, thereby separating them from one another (see Figure 10.2). In addition, the NPs that are accelerated with the liquid jets may also crash into one another, resulting in a further dispersion [42].

Two types of sonication methods are generally used for the purpose of processing nanocomposites. These are: (i) the bath method, and (ii) the probe sonication method. In the bath method, the ultrasonic waves are propagated into the liquid through the bath walls. On the other hand, in the probe method, concentrated ultrasonic waves exit from a bar-shaped

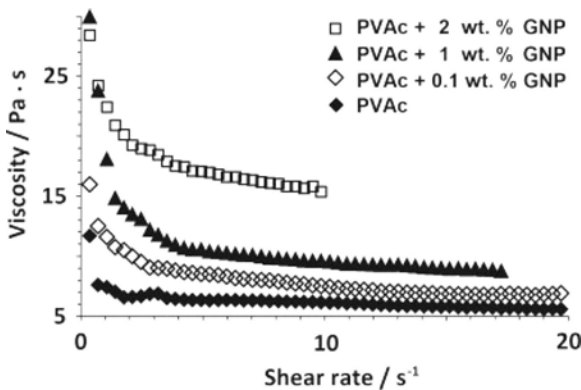


Figure 10.1 Variation in the Brookfield viscosity for PVAc hosting different contents of GNP as function of shear rate [41].



Figure 10.2 Cavitation phenomenon occurring during ultrasonication in two differently shaped probes [42]

probe. The resulting ultrasonic cavitation is usually powerful enough to break NPs agglomerates, especially when they are in relatively large volumes; thus, the probe method is more commonly used for this purpose. The shortfall of this method is that the material is not uniformly exposed to the entire sound waves energy. This issue can be addressed by continuous mechanical stirring of the liquid during sonication.

It is worth mentioning that the temperature of the liquid elevates and, as a result, the viscosity decreases during the process, thus further facilitating the dispersion process. However, the use of very high energies might result in overheating or burning of the polymer. Therefore, in some cases, one may place the mixing container in ice and water to keep the temperature in the desired range. An additional advantage and outcome of sonication is the degasification of the mixture. High speed mechanical stirring produces a large number of gas bubbles in the mixture, which in some cases could even cause brightening of the mixture's color. In such an event, the sound wave used in the ultrasonication would force the bubbles out of the liquid, thus degasifying the mixture.

Different factors are associated with an efficient sonication process, including the power, time and cycles of sonication. Montazeri and Chitsazzadeh [43] and Suave et al. [44] investigated the effects of these factors on the dispersion and structural damages of CNTs. They showed that whereas exposing the mixture to a little amount of ultrasonic energy would lead to residual agglomerations in the system, overusing sonication could cause severe damages to NPs. The scanning electron microscopy (SEM) micrographs shown in Figure 10.3, taken from the nanocomposites manufactured utilizing different time intervals of the sonication process, illustrate these phenomena. It can be seen that after 15 minutes of sonication (Figure 10.3 (a)) there are still large agglomerations in the system [45]. After 45 minutes, the desired state of dispersion is obtained and structural integrity of NPs is also maintained. However, after 135 minutes of sonication, NPs are severely damaged (I.e. broken into small pieces); as a result, they would not deliver any positive attributes to the host matrix.

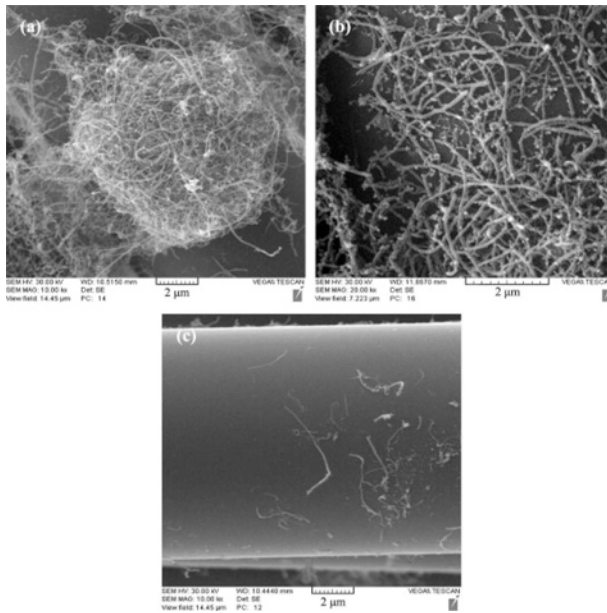


Figure 10.3 SEM micrographs of CNT/epoxy nanocomposites after the burn-off test, sonicated at 100 W, after: (a) 15 min (b) 45 min and (c) 135 min [43]

10.3.2 Three-roll Milling (Calendering)

The three-roll mill machine (calender) exerts shear forces to the matrix through three adjacent rollers, with a tiny gap in between them. The rollers rotate in opposite directions at progressively increasing speeds to break down NPs agglomerations, thus dispersing them into the matrix. Figure 10.4 shows the schematic of calendering mechanism. The material is loaded between the feed- and center-rollers. Because of the narrow gaps between the rollers, essentially all the material would remain in the feed region. The mixture makes its way through the rollers, experiencing very large shear force magnitudes, which in turn disperse NPs in the matrix. As the resin comes out the other side of the rollers, the material, which remains on the center roller (as a very thin layer), goes through the gap between the center roller and apron roller, experiencing even larger shear force resulting due to the higher rolling speed. The sharp knife-edge plate located immediately adjacent to the last roller collects the processed material from the apron roller. The three-roll milling process may be repeated for a number of cycles, until the material is perfectly dispersed. Calendering has proven to be a very effective means for dispersing different types of NPs, especially carbon-based NPs in resins [45, 46].

Although the damaging effect of calendering is much less than that exerted by sonication, an investigation recently carried out by Ahmadi-Moghadam and Taheri [47] demonstrated that depending on the type and dimension of NPs, very small roller gap distances could

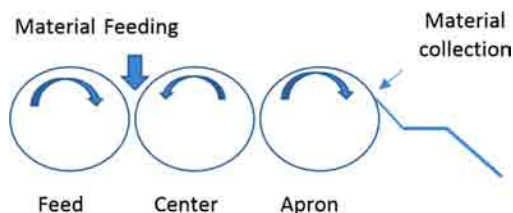


Figure 10.4 Schematic of calendaring mechanism

lead to breakage of NPs and reduce their effective length. Therefore, in order to obtain the desired results, the number of cycles and the gap distances should be carefully established. The duration of each cycle is significantly dependent on rollers gap distance. Consequently, depending on the rollers gap distance, calendaring could be accomplished faster or slower in comparison to the sonication. The other advantage of calendaring over sonication is that the entire resin/NP mixture is uniformly subjected to the applied energy, thus, leading to more consistent results.

10.3.3 High-Shear Mixing

A high-shear mixer, which has also been used for dispersing NPs within resins, consists of a driven vertical shaft together with a high-shear disk type blade. The blade rotates at up to 5000 rpm, which creates a radial flow pattern within a stationary vessel. As shown in Figure 10.5, the rotating blade creates a vortex that pulls in the material within the vessel toward the blades sharp edges. The blades surfaces then mechanically tear apart the particles, thereby reducing their size, and at the same time dispersing them throughout the resin [48]. Many researchers have used high shear mixing as a dispersion technique for processing nanocomposites [49].

10.4 Mechanical Properties of Nano-reinforced Adhesives

Essentially, two decades of research has been devoted to developing NP-reinforced adhesives. Achieving higher mechanical properties for ABJs is the goal of the majority of studies conducted in this field. The increase in the mechanical strength for ABJs can be more accurately described as the increase in their peel and shear strengths. Several researchers have studied the effects of inclusion of different types of NPs on the shear and peel strengths of adhesives. Table 10.1 and Table 10.2 have been prepared to provide a summary of some of the most notable studies, and to compare their findings related to the enhancement of peel and shear strengths, respectively. As can be seen, a wide range of results have been reported on the influence of NPs on the shear and peel strengths of adhesives. The reported results range from 757% improvement to 30% degradation in the properties. This enormous range stems from a large number of parameters that influence the final results, including the manufacturing-related factors, quality of NPs, particle size, and functionality of the NPs, to mention a few. However, more consistent results could be



Figure 10.5 The vortex created by rotating blades [48]

expected by elimination of the undesirable perturbations. The different mechanisms that influence the reinforcing efficacy of NPs in adhesives are reviewed in the next section.

The degradation of ABJs strength that has been reported in some of the studies as a result of inclusion of NPs can be attributed to different factors, including entrapped gasses in the adhesive mixture, NPs agglomeration, and damage in NPs structure. In addition, the presence of NPs may also affect the curing process of polymers. Dorigato et al. [50] reported reduction in the glass transition temperature of the host polymer at relatively high NP contents. This could be ascribed to contrasting effects of blocking the formation of polymeric chains and reducing the evolution of cross-linking.

10.4.1 *Effect of Adhesive Stiffness*

Adhesive stiffness is one of the important factors that significantly affect the performance of ABJs. Numerous researchers have reported enhancement in the stiffness of polymers by addition of NPs to various resins [77, 78]. It is believed that the increase in stiffness of polymers that include NPs is due to the constraint imposed on molecular mobility of the polymer chains. In fact, NPs which usually have much greater stiffness than their host polymers are nested within the spaces that exist among the polymer chains, thus reducing chains flexibility [79]. Shadlou et al. [80] studied the effect of graphene nanoplatelets content and loading rate on the tensile and compressive properties of epoxy nanocomposites. The values of tensile Young's modulus of their nanocomposites measured at various loading (strain) rates are shown in Figure 10.6. The results depict a noticeable increase in the Young's modulus of the nanocomposite as the loading rate increases. Moreover, comparison of the results at a given

Table 10.1 Influence of NPs on the peel strength of the host adhesives

Adhesive	NPs	Adherends	NP wt%	Strength Increase (%)	Reference
PVAc	CNT	Glass/Steel	0.1	7.9	[51]
			0.3	26.3	
			1	5.3	
Epoxy	CNT	White iron	1	29	[52]
Epoxy	SiO ₂	Steel/Aluminum	1	66	[53]
			8	30	
			23	-6	
Polyurethane	SiO ₂	Cast polypropylene	0.5	212	[54]
			1	462	
			1.5	375	
			2	337	
Epoxy	POSS (with various functionalities; see column 4)	Aluminum	0.3 (Aminoethyl)	100	[55]
			4 (Epoxycyclohexyl)	42	
			1 (Glycidoxypropyl)	68	
			5 (Isocyanatopropyl)	757	
			10 (Octaphenyl)	126	

Table 10.1 Influence of NIPs on the peel strength of the host adhesives cont.

Epoxy	Tungsten disulfide	Aluminum	0.3	6	[56]
			0.5	73	
			1	21	
Polystyrene	Fe ₂ O ₃	Iron	5	236	[57]
			10	276	
			25	260	
Epoxy	Al ₂ O ₃	Steel	1	75	[58]
			2	350	
			5	125	
Epoxy	Al ₂ O ₃	Steel	2	116	[59]
			5	23	
			10	49	
Polyurethane	Nanoclay	Aluminum	1	30	[60]
			3	10	
			5	10	
Epoxy	Aluminum/ composite	Aluminum/ composite	1	30	[61]
			3	10	
			5	10	

Table 10.2 Influence of NPs on the shear strength of the host adhesives

Adhesive	NPs	Adherends	NP wt%	Strength Increase (%)	Reference
Epoxy	CNT	Copper	0.8	-19	[62]
	MWNT	Steel	0.5	8	[63]
Polyimide			1	23	
			1.5	4	
Epoxy	MWNT	Carbon/epoxy	1	24	[64]
PVAc	Graphene	Wood	5	43	
			0.75	36	[65]
			1.5	136	
			3	309	
PVAc	Graphene	Beech veneer	0.1	41	[41]
			0.15	52	
			0.3	49	
			0.5	38	
			1	15	
			2	8	
Epoxy	Carbon black	Glass/epoxy	0.5	17	[66]
			1	40	
			1.5	46	
			2	38	
			3	9	

Table 10.2 Influence of NPs on the shear strength of the host adhesives cont.

Epoxy	Carbon black	Glass/epoxy composite,	0.5	14	[67]
			1	28	
			1.5	13	
			2	9	
			3	2	
Epoxy	CNF	Carbon fiber/epoxy	0.25	-3	[68]
			0.5	5	
			1	-6	
Epoxy	SiO ₂	Steel	2	15	[53]
			3	28	
			5	35	
			10	22	
			25	-28	
Silylated polyether	SiO ₂ (stem-ming from tetraethyl orthosilicate)	Glass	5	28	[69]
			8	72	
			10	109	
			13	83	
Epoxy	Nanoclay	Glass/epoxy	1	7	[70]
			3	-11	
			5	-18	
PVAc	Nanoclay	Wood	1	11	[71]
			2	20	
			4	25	

Table 10.2 Influence of NPs on the shear strength of the host adhesives cont.

Adhesive	NPs	Adherends	NP wt%	Strength Increase (%)	Reference
Polyurethane	Nanoclay	Aluminum	1	-6	[61]
			3	6	
			5	68	
Epoxy	Al ₂ O ₃	Epoxy-steel	1	8	[72]
			2	9	
			5	2	
			10	-1	
			50	-6	
PVAc	Al ₂ O ₃	Wood	1	4	[73]
			2	10	
			4	7	
Epoxy	Zirconia	Aluminum	0.5 (vol%)	30	[50]
			1 (vol%)	60	
			1.5 (vol%)	4	
Phenol-formaldehyde	CuO	Plywood	5.2	14	[74]
Soy protein	CaCO ₃	Plywood	1	194	[75]
			2	176	
			3	179	
			5	209	
			8	200	
			10	150	
	15	121			

Table 10.2 Influence of NPs on the shear strength of the host adhesives cont.

Epoxy	POSS (with various functionalities; see column 4)	Aluminum	0.3 (Aminoethyl)	-10	[55]
			4 (Epoxy-cyclohexyl)	-24	
			1 (Glycidoxypropyl)	-14	
			5 (Isocyanatopropyl)	14	
			10 (Octaphenyl)	14	
Epoxy	Nanoelastomeric copolymer	Aluminum	10	3	[76]
			20	91	
			30	32	
		Copper	10	26	
			20	94	
			30	31	
			Steel	10	
20	15				
30	11				
Epoxy	Tungsten disulfide	Aluminum	0.3	5	[56]
			0.5	9	
			1	5	
			3	1	
			5	14	

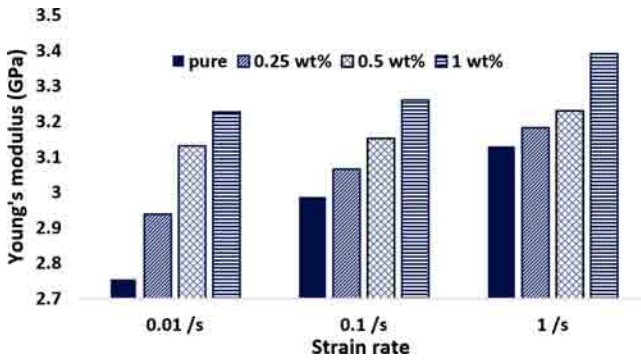


Figure 10.6 Comparison of the Young’s modulus for the neat epoxy and GNP nanocomposites evaluated at various strain rates [80]

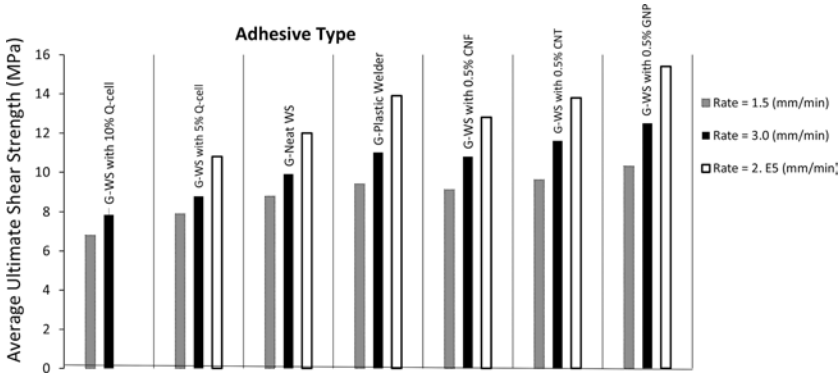


Figure 10.7 Effects of loading rate on nano-reinforced adhesively bonded single-lap joints with graphite/epoxy adherends [81]

loading rate indicates that the addition of GNPs improved the stiffness of their nanocomposites. The results also reveal the influence of loading rate on the efficiency gained through the use of GNPs; in other words, as seen, the efficiency of the GNP content decreases with increasing loading rate.

The effects of different NPs and loading rates on the ultimate strength of adhesively bonded single lap joints (SLJs) have also been reported by Soltannia and Taheri [81]. As illustrated in Figure 10.7, joints utilizing different types of NPs improved the resin’s stiffness and strength by significant margins. The average ultimate shear strength of SLJs with graphite adherends was increased as much as 32% (relative to the neat adhesive), when SLJs were subjected to high loading rates; the increase was also significant (on average of 26%), under the quasi-static loading rate. A large amount of information related to the change in the stiffness, and the entire response of an epoxy resin reinforced with various NPs, bonding

both glass- and carbon-reinforced epoxy adherends have also been reported by Soltannia and Taheri [81].

Considerable efforts have been expended by researchers with the aim to identify or develop accurate and reliable models for predicting the stiffness of nanocomposites. The Halpin-Tsai model is one of the most commonly used models for predicting the Young’s modulus of the composites. According to this model, the maximum attainable Young’s modulus of a composite with uniform fiber distribution and perfect fiber/matrix bond is given by:

$$E_C = \left(\frac{3}{8} \frac{1+2(\lambda)\eta_l V_f}{1-\eta_l V_f} + \frac{5}{8} \frac{1+2\eta_T V_f}{1-\eta_T V_f} \right) E_m \tag{10.1}$$

in which

$$\eta_l = \frac{E_f / E_m - 1}{E_f / E_m + 2(\lambda)}, \quad \eta_T = \frac{E_f / E_m - 1}{E_f / E_m + 2}, \quad \lambda = l_f / d_f \tag{10.2}$$

where E_C is the Young’s modulus of the composite, l_f , d_f and E_f are the length, average diameter and Young’s modulus of the reinforcement, E_m is the Young’s modulus of the matrix, and V_f is reinforcement volume content.

Ayatollahi *et al.* [82] evaluated the accuracy of Halpin-Tsai’s model against their experimental results for epoxy/CNT nanocomposites (see Figure 10.8) [80, 82-84].

As seen, there is a noticeable difference between the experimental and theoretically predicted results. This is mainly due to the underlying assumptions used in developing the model, i.e., uniformity in distribution of reinforcement, perfect bond between matrix and reinforcement, and the absence of any void in the matrix. As a result, various researchers

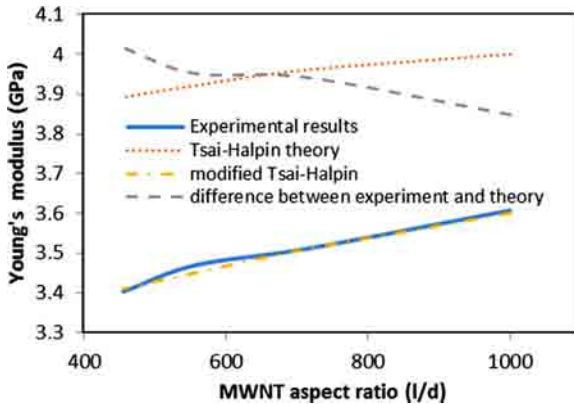


Figure 10.8 Comparison of the experimental results and theoretical predictions of the Young’s modulus of MWNT reinforced nanocomposites [82]

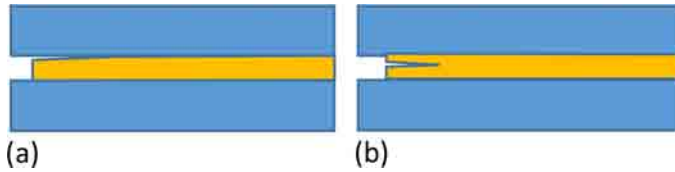


Figure 10.9 The failure mechanisms in ABJs (a) interfacial failure (b) cohesive failure (bulk adhesive failure)

have proposed modifications to the model in order to improve its predictive accuracy when applied to nanocomposites [80, 82-84].

Multi-scale modeling is another technique for prediction of the stiffness of nanocomposites, which is more complicated when compared to semi-empirical theories; however, such models usually lead to more accurate results [85, 86]. Multi-scale modeling refers to a modeling approach in which multiple models at different scales are used simultaneously to describe a system [87].

10.4.2 Effect of Fracture Toughness

In general, failure in ABJs is categorized as: (i) interfacial failure, in which a crack would initiate at the adhesive/adherend interface and subsequently propagate (see Figure 10.9(a)); (ii) cohesive failure, in which a crack would initiate and propagate within the bulk adhesive (see Figure 10.9 (b)). Either of these two scenarios could occur, depending on the interfacial bond strength, fracture toughness of the adhesive, and presence of probable voids and microcracks within the adhesive. In the case of cohesive failure, the fracture toughness of adhesive is the key factor that governs the mechanical strength and durability of ABJs, in particular, if a micro-crack is present within the adhesive.

The use of NPs for enhancement of the fracture toughness of adhesives has been reported by several researchers [77, 88]. Shadlou *et al.* [12] investigated the effect of inclusion of different carbon-based NPs on the fracture toughness of an epoxy resin under different fracture mode mixities. Figure 10.10 shows the experimental results obtained for pure epoxy and the three types of nanocomposites. It is seen that K_{eff} increases from mode-I to mode-II in pure epoxy and also for nano-diamond/epoxy nanocomposites. However, by adding the CNF and GNP reinforcements, the maximum value of K_{eff} occurs in a mixed-mode state, and then as the fracture state moves from the mixed-mode to the mode-II state, the enhancement of K_{eff} in nanocomposites reinforced with CNF and GNP decreases gradually.

Burkholder *et al.* [89] investigated the effectiveness of CNTs as an epoxy adhesive additive for bonding steel to composite and composite to composite materials. The results, shown in Figure 10.11, revealed that the additions of CNTs to epoxy adhesive enhanced the fracture toughness of their ABJs. However, higher contents of CNTs could decrease the properties by a significant margin (likely due to agglomeration).

Two principal mechanisms that contribute to enhancing the fracture toughness of polymers reinforced with NPs are: (i) crack deviation, and (ii) crack bridging. Either of these mechanisms may be dominant over the other one, depending on the geometry of NPs. For instance, in nanocomposites hosting CNTs of long cylindrical shapes, the main energy

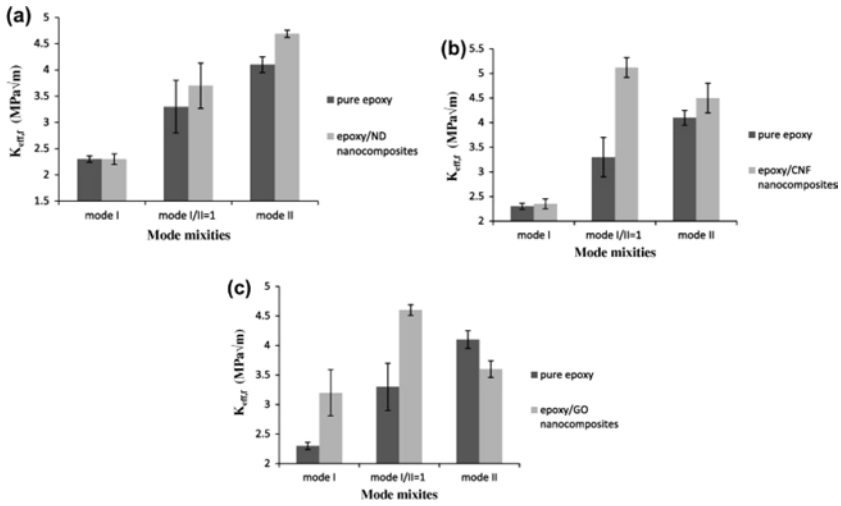


Figure 10.10 Effective fracture resistance, K_{eff} for pure epoxy and for nanocomposites reinforced with (a) ND, (b) CNF and (c) GO [12].

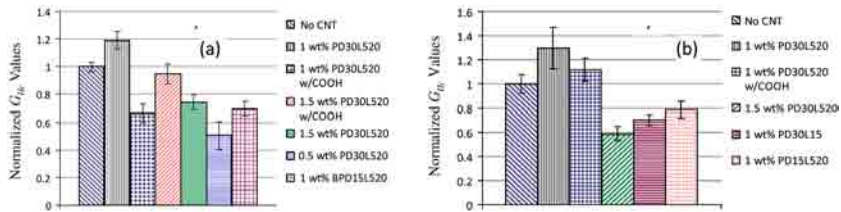


Figure 10.11 Normalized fracture energy G_{IIc} for (a) steel-composite (b) composite-composite adhesive joints (the codes in the legend relate to various dimensions and functionality of CNT as described in reference [89])

dissipating mechanism is the crack bridging. This is because CNTs have very small diameters compared to their lengths, and thus, the crack deviation might take a secondary role [79].

The crack deviation mechanism can be identified by investigation of the roughness of fracture surfaces of nanocomposites, i.e., the higher is the roughness of the fracture surface, the more the crack would be deviated from its original plane. Figure 10.12 shows the increase in fracture surface roughness as a function of CNT content. On the other hand, detection of crack bridging mechanism requires high magnification micrographs. The bridging mechanism plays an important role in improving the fracture toughness of composites [90]. When a NP bridges two fracture surfaces, depending on the embedded length, interfacial strength, angle to fracture surface and flexibility of the NP, it may either fracture or pull out from one of the surfaces. A micrograph illustrating the bridging mechanism in CNT/epoxy adhesive is shown in Figure 10.13.

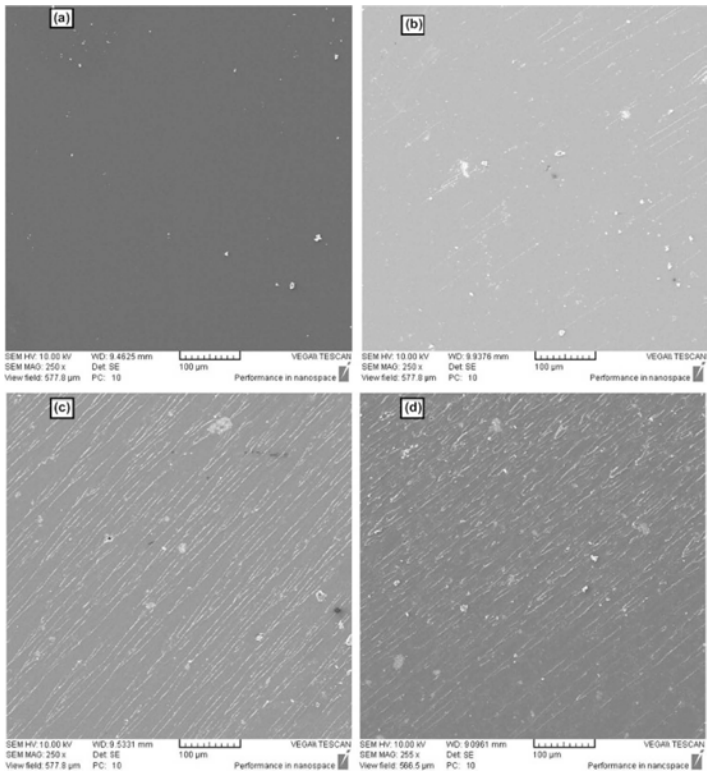


Figure 10.12 Mode-I fracture surfaces of (a) the neat epoxy (b) 0.1 wt.% CNT/epoxy (c) 0.5 wt.% CNT/epoxy (d) 1 wt.% CNT/epoxy near the pre-crack tip. The direction of crack propagation is from top right to bottom left [91]

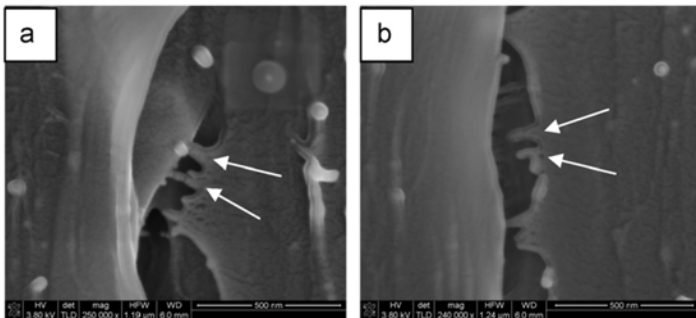


Figure 10.13 Micrographs showing the participation of CNTs, marked with white arrows, in bridging and (b) pull-out mechanisms [92]

10.4.3 Effect of Surface Wettability

As mentioned in Section 10.4.2, the interfacial strength is one of the key factors governing the performance of ABJs. A weak interfacial strength would lead to interfacial failure of ABJs (Figure 10.9(a)). The adhesive interfacial strength is largely related to the wettability of the adhered substrate by the adhesive, which can be quantified in terms of the interfacial tension. In other words, higher interfacial tension means poorer wettability [93]. The interfacial tension can be calculated using the following empirical formula [54]:

$$\gamma_{SL} = \frac{(\gamma_S^{0.5} - \gamma_L^{0.5})^2}{1 - 0.015(\gamma_S \gamma_L)^{0.5}} \quad (10.3)$$

where γ_S and γ_L are the surface free energy of substrate and the surface tension of nano-composite slurry, respectively and γ_{SL} represents the interfacial tension between the nano-composite slurry and the substrate. Figure 10.14 shows the variation in the surface tension of nano-SiO₂ reinforced nanocomposite slurry reported by Fu *et al.* [54]. The wettability can also be directly determined by measuring the static contact angle. In general, a smaller contact angle evidences better wettability of the adhesive. Dorigato *et al.* [50] measured the epoxy–water contact angle. Representative images of a water droplet on pure epoxy, on the epoxy filled with 0.5 vol% zirconia, and on the aluminum substrate, are illustrated in Figure 10.15. The measured values for all types of materials are shown in Figure 10.16. The results show that the presence of zirconia NPs led to a noticeable decrease of the equilibrium contact angle values. In fact, for the pure epoxy sample, an equilibrium contact angle of 82° was measured, while a mean angle of 71.5° was measured for the epoxy reinforced

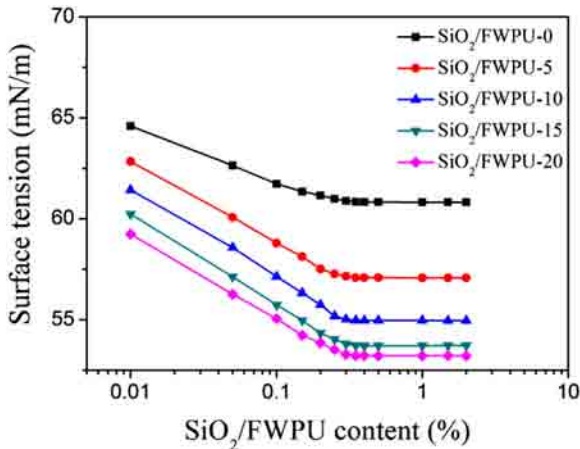


Figure 10.14 Surface tension of the SiO₂/FWPU nanocomposite slurry (FWPU: fluorinated waterborne polyurethane) [54]

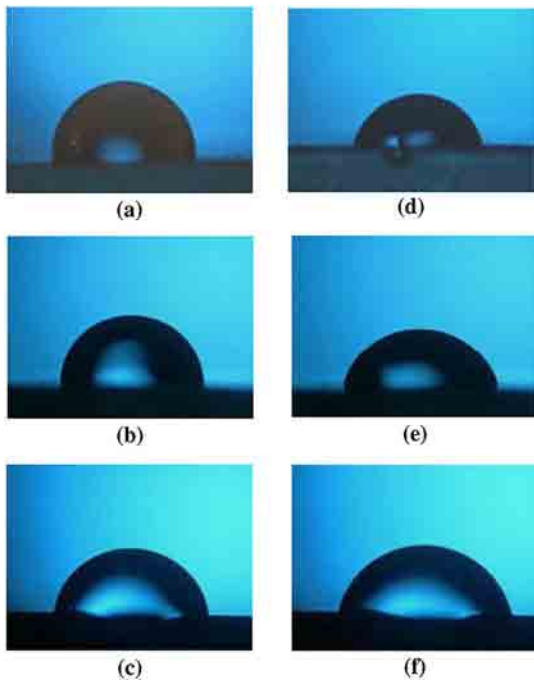


Figure 10.15 Images of epoxy–water contact angles; a, b and c are the static conditions, d, e and f represent the equilibrium (vibrated) conditions; a & d are epoxy, b & e are epoxy-B-0.5 (epoxy modified with calcined zirconia) and c & f are aluminum substrates [50].

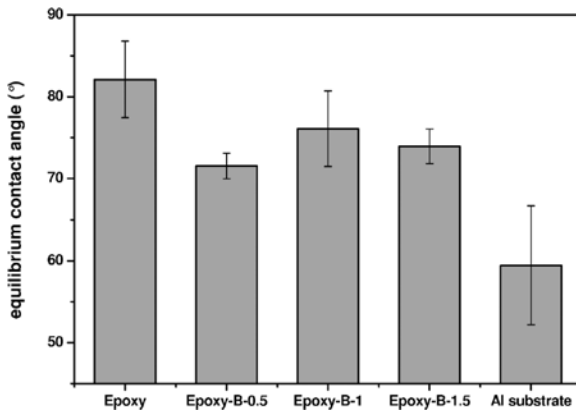


Figure 10.16 Substrate–water equilibrium contact angles for epoxy-B-x (epoxy-zirconia-vol%) nanocomposites and aluminum substrate [50].

with 0.5 vol% zirconia. These values indicate that the water contact angle values of the nanocomposite are closer to that displayed by the aluminum substrate (59.4°). Dorigato *et al.* [50] associated the subsequent increase of contact angle observed in specimens with relatively high NP contents to the degradation in dispersion uniformity of their NPs, possibly due to the formation of agglomerates.

Dorigato and co-workers concluded that the inclusion of zirconia NPs leads to a better wettability and chemical compatibility between the adhesive and substrate, positively contributing to the shear resistance of the joints.

Pinto *et al.* [41] also measured the equilibrium contact angle of ultra-pure water drops on PVAc films hosting various GNP weight contents (see Figure 10.17). As can be seen, the measured angle is approximately 43° on PVAc, while the angle increased to approximately 56° for PVAc specimens hosting 0.1 wt% GNPs. The higher hydrophobicity of the film has been attributed to the presence of partially exposed GNPs on the specimen surface.

Prolongo *et al.* [68] investigated the effect of different surface treatments and also different contents of CNFs on the contact angle of epoxy adhesive. The results are depicted in Figure 10.18. It should be noted that the plasma technique noted in the figure is another means for preparing the surface of composite adherends for bonding. In this technique, the adherend surfaces are bombarded by ionized gas(es) (typically oxygen and sometimes other gases such as nitrogen), generated by radio-frequency energy. The highest values of contact angle were measured on the as-received adherends (i.e. those without any surface treatment), and no notable differences were observed when a treatment was applied. They further observed that the contact angle for their neat epoxy adhesive decreased when CNF content increased. They ascribed this trend to the nano-scale size of CNF and the higher chemical compatibility between the carbon fiber-reinforced epoxy composite substrates and the nano-reinforced epoxy adhesive.

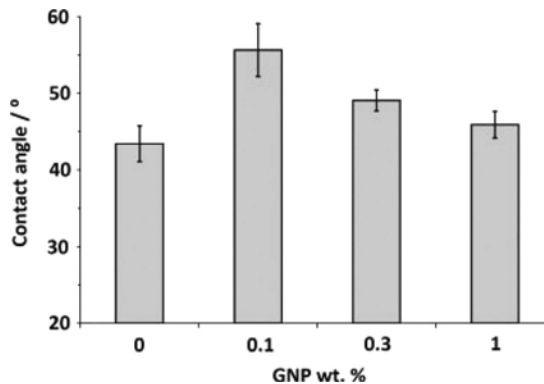


Figure 10.17 Equilibrium contact angle of ultra-pure water drops on PVAc films with different GNP loadings. Bars represent standard deviation [41].

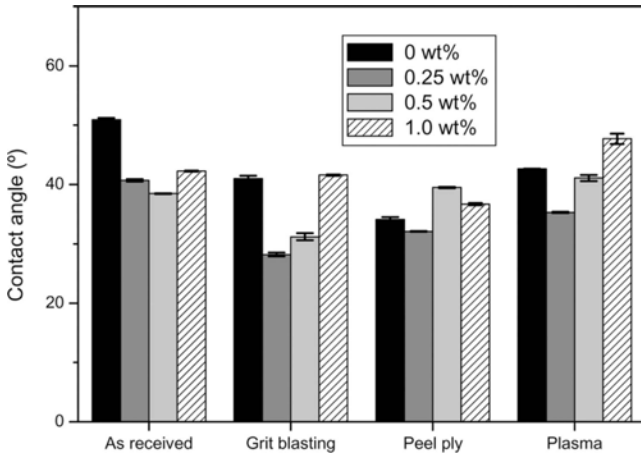


Figure 10.18 Contact angle of neat epoxy adhesive and modified adhesives reinforced with 0.25, 0.5, and 1 wt% CNF on carbon fiber/epoxy laminates (non-treated and treated with grit blasting, peel ply, and atmospheric plasma) [68].

It is worth mentioning that the interfacial tension can also be calculated by using the measured contact angles, for which different methods have been proposed [94-97]. For instance, γ_{SL} can be calculated using Young’s equation [98, 99]:

$$\gamma_S = \gamma_L \cos\theta + \gamma_{SL} \tag{10.4}$$

where θ is the contact angle of nanocomposite slurry on the nonpolar polyolefin films.

10.4.4 Effects of Residual Stresses

ABJs are generally constructed of different materials (i.e., adhesive and adherend, which could also be made of different materials). In cases where there is a large difference between the coefficient of thermal expansion (CTE) of the adhesive and adherend, the ABJs may suffer from thermal residual stresses. In ABJs formed by hot-cured adhesives, the residual stress would start developing during their fabrication process, which would remain throughout their service lives; on the other hand, ABJs made with cold-cured adhesives would not retain substantial level of residual stress. However, the thermal stress could be exasperated due to any applied thermal load to the ABJ during the service life.

The magnitude of the residual stress becomes more significant in ABJs with metallic adherends. This is because there is a larger mismatch in the CTE values of metals and adhesive, in comparison to that between fiber reinforced polymers (FRPs) and adhesives. For instance, the CTE of typical epoxies is approximately $60 \times 10^{-6} \text{ m/m K}$, while for aluminum it is $22 \times 10^{-6} \text{ m/m K}$, for steel it is around $13 \times 10^{-6} \text{ m/m K}$, and it would vary considerably

for FRPs, depending on the FRP's layout and fiber orientation (a typical value for epoxy reinforced with unidirectional E-glass fibers would be 0.66×10^{-5} m/m K, while values of -0.533×10^{-6} m/m K and 1.592×10^{-6} m/m K have been reported for cross-ply and quasi-isotropic graphite-epoxy laminates, (C6000/PMR-15, from the Celanese Corp., Irving, TX), respectively [100]).

A large number of NPs have a very small CTE compared to polymers. For instance, the CTE of a graphene sheet is about -0.5×10^{-6} m/m K (valid between 80°C and 197°C) [101]; thus, addition of small contents of NPs to polymer can reduce the polymer's CTE by a noticeable margin. Chow [102] proposed an equation for predicting the CTE of nanocomposites. He extended the "mean field theory", which was originally developed for evaluating the elastic modulus of composites, for evaluating the CTE of composite materials. He suggested the following equations for calculating the longitudinal and transversal CTE of a composite.

$$\theta_L = \theta_m + \frac{k_f (\gamma_f - \gamma_m) G_1 V_f}{k_m 2K_1 G_3 + K_3 G_1} \quad (10.5)$$

$$\theta_T = \theta_m + \frac{k_f (\gamma_f - \gamma_m) G_3 V_f}{k_m 2K_1 G_3 + K_3 G_1} \quad (10.6)$$

where θ_m is the matrix linear CTE, k_f and k_m are the bulk moduli of nanofiller and matrix, respectively, V_f is the filler volume fraction, γ_f and γ_m are the bulk thermal expansions of nanofiller and matrix, respectively, and finally, K_i and G_i are calculated by Eqs. (10.7) and (10.8).

$$K_i = 1 + \left(\frac{k_f}{k_m} - 1 \right) \left[(1 - V_f) \alpha_i + V_f \right] \quad (10.7)$$

$$G_i = 1 + \left(\frac{\mu_f}{\mu_m} - 1 \right) \left[(1 - V_f) \beta_i + V_f \right] \quad (10.8)$$

In the above equations, μ is the shear modulus, and α_i and β_i are functions of GNP characteristic ratio (i.e., t/D) and Poisson's ratio of the matrix, respectively [101].

The reduction in CTE of polymers using different types of NPs has been reported by many researchers [84, 103-105]. For example, Park *et al.* [66] investigated the effect of carbon black NPs on CTE of epoxy. Figure 10.19 shows CTE of the epoxy adhesive with respect to the carbon black content. As seen, the CTE decreases as the carbon black content is increased, this is because of the lower value of CTE of carbon black. The minimum CTE was reported as $48.4 \leftrightarrow 10^{-6}$ m/m °C, when the carbon black content was 3.0 wt%, which is 40% less than that of the neat epoxy. Park *et al.* also used the finite element method to investigate the influence of carbon black on the maximum principal strain in their ABJs (see Figure 10.20). As can be seen, the value of maximum principal strain decreases at higher contents of the carbon black.

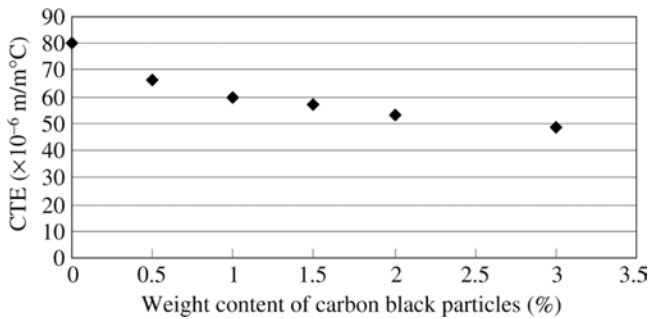


Figure 10.19 Coefficient of thermal expansion (CTE) of epoxy adhesive with respect to the weight content of carbon black particles [66].

10.4.5 Effect of Durability of Adhesives

The durability of ABJs could be significantly reduced by environmental stresses arising from the moisture and difference in temperature. The absorbed fluids may plasticize and induce relaxation of adhesives, as well as degrading adhesive's mechanical properties; the latter is considered to be one of the primary causes of failure of ABJs [106]. In this section, a summary of some of the notable investigations into the effect of NPs on the durability of ABJs is reported.

Yu *et al.* [107] studied the durability of a CNT reinforced epoxy adhesive bonded aluminum alloy joints utilizing the Boeing wedge test (see Figure 10.21), subjected to humid conditions [108]. They also studied the effect of the CNT content on the durability and failure mode of the joints. The wedge test creates a relatively high stress concentration at or near the interface, thus increasing joint's sensitivity to environmentally caused degradation. Therefore, the test is usually used to provide quantitative durability data for ABJs. The investigators used a tensometer to insert a wedge under a constant load (and also a constant speed) into the bond-line of the flat specimens. This process creates a tensile stress in the region surrounding the crack tip. After the specimens were allowed to equilibrate at the ambient conditions for several hours, the initial crack length was recorded. Subsequently, while the wedge was in each specimen, under the same applied constant load as used to initiate the crack, they immersed the specimens in 60°C water. They then measured the resulting crack propagation for a period of up to 90 h, in order to establish the relative bond durability performance in a humid environment. The results are depicted in Figure 10.22.

As can be seen, the initial crack length, which was measured immediately after the wedge specimen was immersed in water (i.e., at time 0 h), was very different from one specimen to another. For the specimens bonded with CNT-reinforced epoxy, the initial crack length depended highly on the CNT weight fraction. The initial crack length decreased when CNT weight fraction was increased from 0 to 1 wt%, but then it increased only slightly as the CNT weight fraction increased from 1 to 5 wt%. The initial crack length for the joint with epoxy filled with 0.5 wt% CNTs was about 70.3% lower in comparison to that of the joint made with neat epoxy. However, the best results were obtained for the joint made with

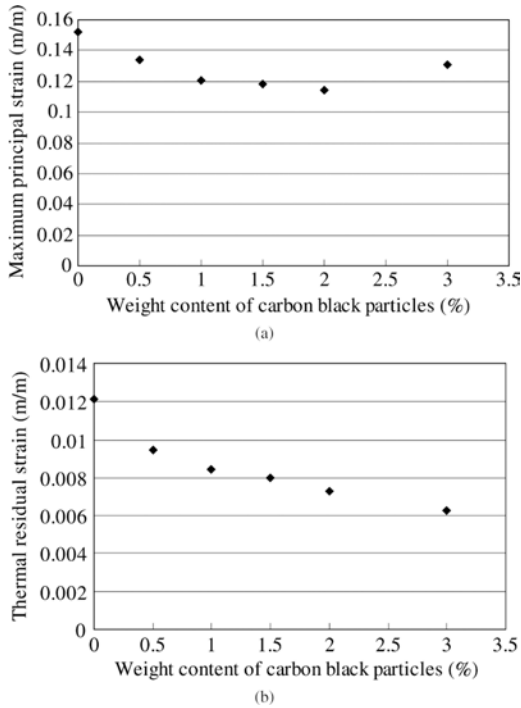


Figure 10.20 (a) Maximum principal strain in ABJ with respect to the weight content of the carbon black particles subjected to tensile load of 16 kN; (b) thermal residual strain [66].

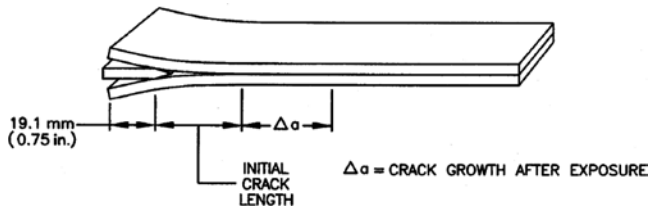


Figure 10.21 Configuration of the wedge-test specimen [108]

epoxy containing 1 w% CNT; obviously, the addition of CNTs into the epoxy significantly improved the bond strength of the ABJs.

10.5 Other Advantages of Nano-Reinforced Adhesives

The positive enhancing aspects of nano-reinforced adhesives discussed in section 10.4 were mainly those aspects that helped to improve the mechanical strength of ABJs. Although

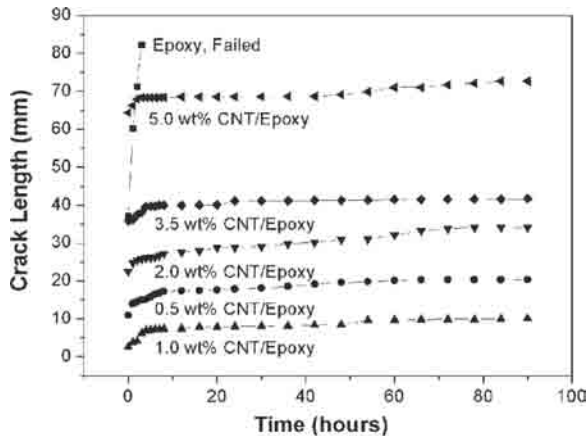


Figure 10.22 Crack length of the CNT-filled epoxy adhesive joints as a function of immersion time in 60°C water [107]

strength enhancement is the most important attribute that NPs could impart to ABJs, it is not the only positive attribute NPs offer. In this section, a brief description of other positive attributes of NPs in their role as a reinforcing agent in adhesives is discussed.

10.5.1 Electrical Properties

Common polymers used in structural application are not electrically conductive; however, some types of NPs, especially carbon NPs, are superconductive. Therefore, addition of an appropriate amount of such NPs to polymers could significantly decrease their electrical resistance (also referred to as the “percolation threshold”). Generally, there are two different types of thresholds, namely: static and kinetic thresholds. The static percolation threshold refers to a situation when randomly distributed filler particles form the percolating paths. In the kinetic percolation, the particles are free to move, thereby forming a conducting network at much lower particle concentrations [109]. Different parameters, however, could affect the resulting electrical conductivity, including the fabrication method, matrix wettability of filler, and filler dimensions. It is noteworthy to mention that while an effective method of NP dispersion would result in better mechanical properties, it may lower nanocomposites electrical conductivity [110].

Ayatollahi *et al.* [14] measured the DC electrical conductivity of CNT/epoxy for different NP contents. As seen in Figure 10.23, the resistivity decreases dramatically as the filler content approaches the value resulting into the electrical percolation threshold, and the conductive network of the CNTs is formed at about 0.25 wt%. Similar results have been reported by Yu *et al.* [111], and Wang *et al.* [51] for the surface electrical resistivity of epoxy adhesives. In addition, several analytical and semi-empirical models have been developed

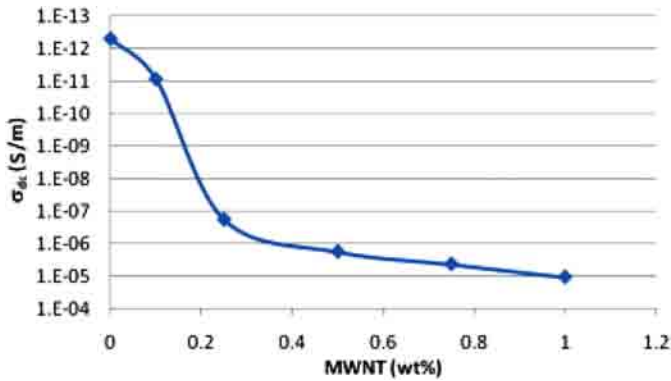


Figure 10.23 Electrical resistivity of epoxy/CNT nanocomposites [14]

for predicting the electrical conductivity of nanocomposites. Some examples of the predictive models are the “excluded volume model” [112], Lu and Mai’s model [113] and a more recently proposed model, which is based on the average inter-particle distance [114].

Electrically conductive adhesives could have a variety of applications, including magnetic painting, circuit boards, damage sensing and solar cells [115, 116]. In addition to the mentioned applications, the use of conductive adhesive for structural health monitoring purposes has recently attracted considerable attention. Lim *et al.* [117] used a conductive CNT modified adhesive (in addition to as an acoustic emission sensor) to monitor the effect of adherend surface treatments on the failure mechanism of an SLJ. The results are shown in Figure 10.24. For their untreated adherend, the electrical resistance increased in a step-like manner, which represents the sudden failure in adhesive. A potential weak interaction between the steel and adhesive could result in low overall shear strength of the ABJ, while the change in the resistance (i.e., jumps in the electrical resistance) can signify the onset of damage long before the specimen reaches its ultimate shear strength. On the other hand, in case of saline-treated adherend, the resistance increases gradually throughout the loading regime, which would indicate that a progressive damage event is occurring during the loading cycle, possibly due to presence of damage in the adhesive layer.

10.5.2 Thermal Properties

Inclusion of NPs in the adhesives could also alter the thermal properties of adhesives, including the thermal conductivity and thermal expansion coefficient (CTE), with the latter discussed in section 4.4. Some NPs have extraordinary thermal conductivity. For instance, the thermal conductivity of CNTs at room temperature can be as high as 6600 W/m K. Therefore, the thermal conductivity of the host polymer reinforced with these NPs would be significantly altered. The main applications of thermally conductive adhesives are in heat sink bonding, potting/encapsulating sensors and in fabrication of power semiconductors.

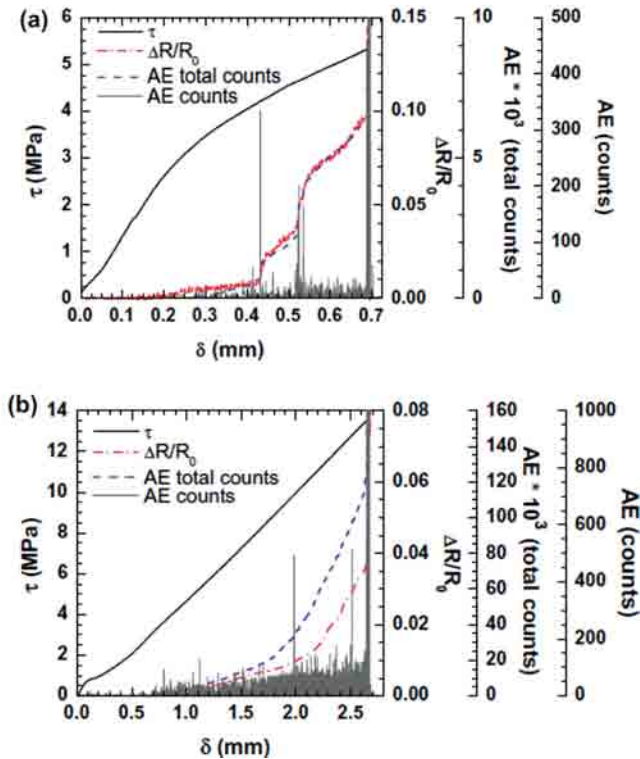


Figure 10.24 Mechanical, electrical and acoustic emission responses of (a) untreated specimens (b) saline-treated specimens (where τ is the shear stress and δ is the displacement)

Qiao *et al.* [118] investigated the effect of nano-silver particles on the thermal conductivity of an epoxy based adhesive, and the results are shown in Figure 10.25. An obvious increase in the thermal conductivity value is observed (i.e., an increase from 1.057 W/m K (70 wt%) to 1.70 W/m K (83 wt%). This indicates that the thermal conductivity would increase with the increase in the nano-silver content. The results further reveal that the thermal conductivity is not as sensitive to agglomeration of NPs as is the mechanical strength.

10.5.3 Gas Permeation Barrier Properties

In general, polymers, because of their large molecules, can act only as a relatively weak gas barrier. However, in some industries such as food packaging and fuel tank production, there is a high demand for materials with superior barrier properties. Plate-like NPs, because of their geometrical shape and high aspect ratio, have been found to be excellent candidates for enhancing the gas barrier properties of resins. In fact, effective improvements in the property could be obtained by inclusion of low volume fractions of such NPs, which enables the

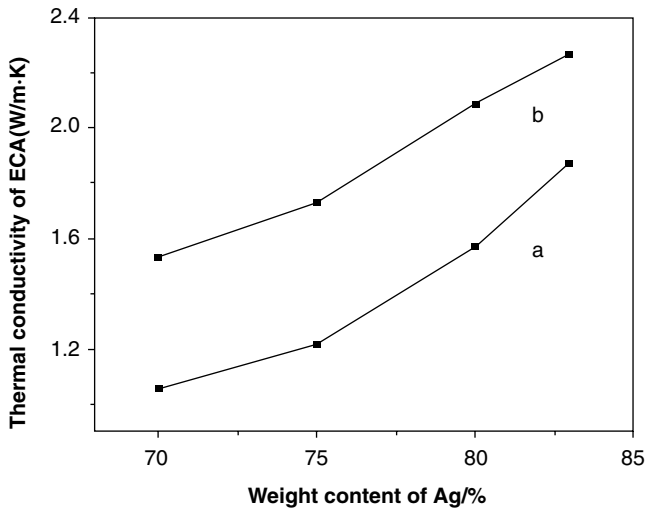


Figure 10.25 Relationship between thermal conductivity of epoxy and weight percent contents of nano-silver (a) spherical silver and (b) mixed spherical and flaky silver [118]

nanocomposite to retain the optical clarity of the neat resin, which is mostly desired in packaging applications [32, 119].

Osman *et al.* [120] investigated the gas permeation properties of polyurethane adhesives reinforced with three different types of nanoclays. The dependency of the water vapor transmission rate through the nanocomposites as a function of the volume fraction is illustrated in Figure 10.26. It can be seen that the transmission rate decreased asymptotically with increasing volume fraction of the nanoclays in all types of nanocomposites. It was also observed that the maximum efficiency could be obtained if the nanoclay particles were oriented parallel to one-another and perpendicular to the gas penetration direction.

10.5.4 Bio-Adhesives

Researchers have reported successful application of different types of bio-adhesives containing: POSS [30], SiO_2 [121], nanoclays [122, 123], silica [124], zirconia [125], nano-silver [126], to mention a few. In addition to increasing the mechanical strength of the base matrix, incorporation of various NPs could create other properties that could be of interest. For instance, Kassaei *et al.* [127] showed that the addition of silver NPs to an acrylic resin rendered a dental composite that exhibited strong antibacterial activity against *Escherichia coli*.

As another example, it is important for the adhesives used in dentistry to be easily distinguishable by X-raying teeth. The development of radiopaque adhesives using $\text{Ta}_2\text{O}_5/\text{SiO}_2$ NPs has been reported by Schulz *et al.* [121] and the improvement in the radiopacity is

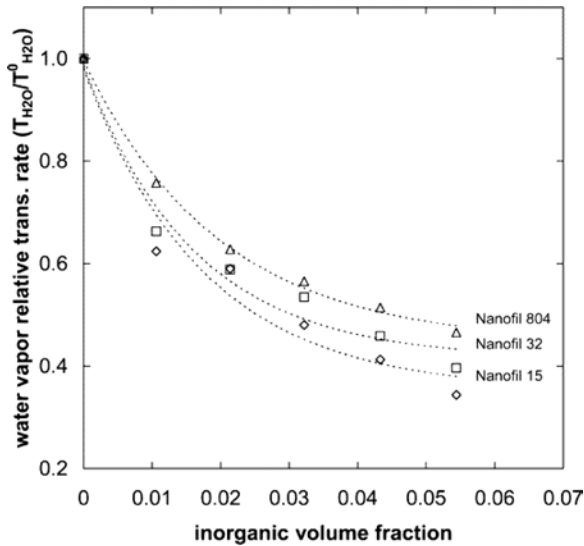


Figure 10.26 Dependence of the water vapor transmission rate through the PU–nanocomposites on the inorganic volume fraction. The dotted lines are guides for the eye (Nanofil 15, Nanofil 32, and Nanofil 804 are trade names for various types of organoclays by Sud-Chemie [Moosburg, Germany]) [120]

illustrated in Figure 10.27. As seen, the increase in Ta_2O_5 content increased the composite radiopacity by a notable margin. In fact, the nanocomposites containing 40 mol% (83 wt%) Ta_2O_5 exhibited higher radiopacity than dentin and enamel. However, the surface functionalized particles exhibited slightly lower radiopacity than the untreated ones.

The advances in nanotechnology have also led to the generation of a new class of adhesives called bio-inspired adhesives. As a result, a significant amount of efforts has been expended by various researchers to (i) characterize a broad array of adhesive mechanisms imparted by utilizing biological organisms in their natural environments; (ii) mimic such adhesives performance through synthetic platforms [128]. The efforts have thus far led to several interesting applications in various industries, such as [129]:

- In wood industry - Adhesives made of environmentally-friendly materials used in manufacturing plywood.
- For drug delivery - A bio-inspired adhesive system based on microspheres has been shown to significantly increase the systemic absorption of conventional drugs and polypeptides across the nasal membrane, without the need for use of absorption enhancing agents.
- In wound-healing dressing - A variety of bio-inspired surgical adhesives have been and are under development with applications in homeostasis, skin closure, and sealing of the colon and blood vessels.

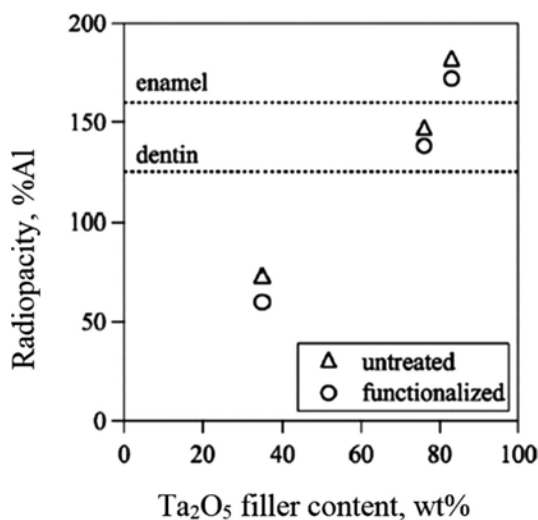


Figure 10.27 Radiopacity of nanocomposites containing 20 wt% filler with 35–83 wt% Ta_2O_5 content normalized with respect to that of equally thick aluminum (Particles were functionalized with γ -metacryloxypropyltrimethoxysilane [MPS])

- In military - Bio-inspired adhesives extracted from geckos are controllable, reversible, and adhere to surfaces with a strength that is approaching the strength of geckos toe pads.

10.6 Conclusion

The recent advances in adhesives reinforced with nanomaterials have been presented in this state-of-the-art review. It was also discussed that because nano-reinforced adhesives offer multifunctional properties, they have been used in a variety of applications. In comparison to the bulk materials, NPs possess relatively large specific surface areas, high surface energy, reduced number of structural imperfections, and distinctively different physical properties than in bulk form. Various types of NPs produced from a variety of materials and their attributes were discussed. As stated, each NP type exhibits one or more unique physical properties, which cannot be offered by the same material in its bulk form.

Extensive discussion demonstrated that one of the biggest challenges in manufacturing polymeric nanocomposites is the uniform dispersion of NPs within a given matrix. Due to their extremely small dimensions, NPs tend to form large bundles or agglomerations. The investigation of various dispersion methods, especially those suitable for mass production of nanocomposites, has been the objective of many ongoing investigations.

In addition, the achievement of higher mechanical properties for ABJs has been the main goal of most of the studies performed in this field. Therefore, a comprehensive review on

the effects of different types of NPs on the mechanical strength of ABJs was also presented. Moreover, the mechanisms that contribute in reinforcing ABJs were thoroughly discussed. Furthermore, a brief description of the positive attributes, other than those related to the mechanical properties, obtained by the inclusion of NPs in adhesives, was also presented.

10.7 Acknowledgements

The financial support of Auto21, which made this study possible, is gratefully appreciated. Auto21 is a multi-disciplinary, auto-related R&D initiative established by the Canadian Networks of Centres of Excellence (NCE) program.

References

1. <http://www.azom.com/>, Polymer adhesives – advantages of adhesive bonding over alternative assembly techniques by Master Bond. (2011).
2. R. Hosseinzadeh, Analysis and enhancement of tubular bonded joints subject to torsion, Ph.D. Thesis at Dalhousie University, Canada (2009).
3. J. Cheng and F. Taheri, A smart single-lap adhesive joint integrated with partially distributed piezoelectric patches. *Int J Solids Structures* 43, 1079–1092 (2006).
4. J. Cheng and F. Taheri, A novel smart adhesively bonded joint system. *Smart Materials Structures* 14, 971–981 (2005).
5. R. Hosseinzadeh and F. Taheri, Non-linear investigation of overlap length effect on torsional capacity of tubular adhesively bonded joints. *Composite Structures* 91, 186–195 (2009).
6. R.A. Esmaeel and F. Taheri, Stress analysis of tubular adhesive joints with delaminated adherend. *J Adhesion Sci Technol* 23, 1827–1844 (2009).
7. J. Cheng, F. Taheri, and H. Han, Strength improvement of a smart adhesive bonded joint system by partially integrated piezoelectric patches. *J Adhesion Sci Technol* 20, 503–518 (2006).
8. G. Korotcenkov, *Chemical Sensors: Fundamentals of Sensing Materials Volume 2: Nanostructured Materials*, Momentum Press, New York. (2010).
9. M.R. Ayatollahi, S. Doagou-Rad, and S. Shadlou, Nano-/microscale investigation of tribological and mechanical properties of epoxy/MWNT nanocomposites. *Macromol Mater Eng* 297, 689–701 (2012).
10. A.S. Artemov, Polishing nanodiamonds. *Physics of the Solid State* 46, 687–695 (2004).
11. M. Ayatollahi, E. Alishahi, S. Doagou-R, and S. Shadlou, Tribological and mechanical properties of low content nanodiamond/epoxy nanocomposites. *Composites Part B* 43, 3425–3430 (2012).
12. S. Shadlou, E. Alishahi, and M. Ayatollahi, Fracture behavior of epoxy nanocomposites reinforced with different carbon nano-reinforcements. *Composite Structures* 95, 577–581 (2013).
13. J. Gao, W. Li, H. Shi, M. Hu, and R.K. Li, Preparation, morphology, and mechanical properties of carbon nanotube anchored polymer nanofiber composite. *Composites Sci Technol* 92, 95–102 (2014).
14. M. Ayatollahi, S. Shadlou, M. Shokrieh, and M. Chitsazzadeh, Effect of multi-walled carbon nanotube aspect ratio on mechanical and electrical properties of epoxy-based nanocomposites. *Polymer Testing* 30, 548–556 (2011).
15. R.L. Poveda and N. Gupta, Electrical properties of carbon nanofiber reinforced multiscale polymer composites. *Materials & Design* 56, 416–422 (2014).

16. Y.K. Choi, K.I. Sugimoto, S.M. Song, and M. Endo, Mechanical and thermal properties of vapor-grown carbon nanofiber and polycarbonate composite sheets. *Mater Letters* **59**, 3514–3520 (2005).
17. J. Hone, M. Llaguno, M. Biercuk, A. Johnson, B. Batlogg, Z. Benes, and J. Fischer, Thermal properties of carbon nanotubes and nanotube-based materials. *Appl Phys A* **74**, 339–343 (2002).
18. C. Li, L. Miao, X. Tan, M. Han, and J. Jiang, Thermal conductivity of graphene nanoribbons with regular isotopic modification. *J Computational Theoretical Nanosci* **11**, 348–352 (2014).
19. E. Alishahi, S. Shadlou, S. Doagou-R, and M.R. Ayatollahi, Effects of carbon nanoreinforcements of different shapes on the mechanical properties of epoxy-based nanocomposites. *Macromol Mater Eng* **298**, 670–678 (2013).
20. H. Zhang, G. Lee, C. Gong, L. Colombo, and K. Cho, Grain boundary effect on electrical transport properties of graphene. *J Phys Chem C* **118**, 2338–2343 (2014).
21. V.V. Mody, R. Siwale, A. Singh, and H.R. Mody, Introduction to metallic nanoparticles. *J Pharmacy Bioallied Sci* **2**, 282–289 (2010).
22. S.K. Sardana, V.S. Chava, E. Thouti, N. Chander, S. Kumar, S. Reddy, and V.K. Komarala, Influence of surface plasmon resonances of silver nanoparticles on optical and electrical properties of textured silicon solar cell. *Appl Phys Letters* **104**, 073903 (2014).
23. A. Evlyukhin, A. Stepanov, A. Dmitriev, A. Akhmanov, V. Bagratashvili, and B. Chichkov, Influence of metal doping on optical properties of Si nanoparticles. *Optics Commun* **316**, 56–60 (2014).
24. P. Kucheryavy, J. He, V.T. John, P. Maharjan, L. Spinu, G.Z. Goloverda, and V.L. Kolesnichenko, Superparamagnetic iron oxide nanoparticles with variable size and an iron oxidation state as prospective imaging agents. *Langmuir* **29**, 710–716 (2013).
25. C.-W. Chou, S.-H. Hsu, H. Chang, S.-M. Tseng, and H.-R. Lin, Enhanced thermal and mechanical properties and biostability of polyurethane containing silver nanoparticles. *Polymer Degradation Stability* **91**, 1017–1024 (2006).
26. A.A. Lazarides, K. Lance Kelly, T.R. Jensen, and G.C. Schatz, Optical properties of metal nanoparticles and nanoparticle aggregates important in biosensors. *J Molecular Structure* **529**, 59–63 (2000).
27. A. Heber, M. Selmke, and F. Cichos, Metal nanoparticle based all-optical photothermal light modulator. *ACS Nano* **8**, 1893–1898 (2014).
28. G.A. Sotiriou and S.E. Pratsinis, Antibacterial activity of nanosilver ions and particles. *Environmental Sci Technol* **44**, 5649–5654 (2010).
29. E. Ayandele, B. Sarkar, and P. Alexandridis, Polyhedral oligomeric silsesquioxane (POSS)-containing polymer nanocomposites. *Nanomaterials* **2**, 445–475 (2012).
30. H. Dodiuk-Kenig, Y. Maoz, K. Lizenboim, I. Eppelbaum, B. Zalsman, and S. Kenig, The effect of grafted caged silica (polyhedral oligomeric silsesquioxanes) on the properties of dental composites and adhesives. *J Adhesion Sci Technol* **20**, 1401–1412 (2006).
31. W. Yu, J. Fu, X. Dong, L. Chen, and L. Shi, A graphene hybrid material functionalized with POSS: Synthesis and applications in low-dielectric epoxy composites. *Composites Sci Technol* **92**, 112–119 (2014).
32. G. Choudalakis and A.D. Gotsis, Permeability of polymer/clay nanocomposites: A review. *European Polym J* **45**, 967–984 (2009).
33. J.H. Park and S.C. Jana, The relationship between nano- and micro-structures and mechanical properties in PMMA–epoxy–nanoclay composites. *Polymer* **44**, 2091–2100 (2003).

34. G. Ji and G. Li, Effects of nanoclay morphology on the mechanical, thermal, and fire-retardant properties of vinyl ester based nanocomposite. *Mater Sci Eng A* **498**, 327–334 (2008).
35. V. Pistor and A.J. Zattera, Thermal and rheological properties of poly (ethylene-co-vinyl acetate) (EVA) nanoclay, in *Handbook of Polymer Nanocomposites Processing, Performance and Application*, J.K. Pandey, K.R. Reddy, A.K. Mohantyand, and M. Misra (Eds.), pp. 129–152, Springer. (2014).
36. T. Mohan and K. Kanny, Water barrier properties of nanoclay filled sisal fibre reinforced epoxy composites. *Composites Part A* **42**, 385–393 (2011).
37. M.Z. Rong, M.Q. Zhang, Y.X. Zheng, H.M. Zeng, and K. Friedrich, Improvement of tensile properties of nano-SiO₂/PP composites in relation to percolation mechanism. *Polymer* **42**, 3301–3304 (2001).
38. I. Javni, W. Zhang, V. Karajkov, Z. Petrovic, and V. Divjakovic, Effect of nano- and micro-silica fillers on polyurethane foam properties. *J Cellular Plastics* **38**, 229–239 (2002).
39. M.M. Jalili, S. Moradian, H. Dastmalchian, and A. Karbasi, Investigating the variations in properties of 2-pack polyurethane clear coat through separate incorporation of hydrophilic and hydrophobic nano-silica. *Prog Organic Coatings* **59**, 81–87 (2007).
40. B.B. Mukharjee and S.V. Barai, Influence of nano-silica on the properties of recycled aggregate concrete. *Construction Building Materials* **55**, 29–37 (2014).
41. A.M. Pinto, J. Martins, J.A. Moreira, A.M. Mendes, and F.D. Magalhães, Dispersion of graphene nanoplatelets in poly(vinyl acetate) latex and effect on adhesive bond strength. *Polymer Int* **62**, 928–935 (2013).
42. T. Hielscher, Ultrasonic Technology, Germany, Ultrasonic lab devices and industrial processors, www.hielscher.com (2014).
43. A. Montazeri and M. Chitsazzadeh, Effect of sonication parameters on the mechanical properties of multi-walled carbon nanotube/epoxy composites. *Materials & Design* **56**, 500–508 (2014).
44. J. Suave, L.A.F. Coelho, S.C. Amico, and S.H. Pezzin, Effect of sonication on thermo-mechanical properties of epoxy nanocomposites with carboxylated-SWNT. *Mater Sci Eng A* **509**, 57–62 (2009).
45. A. Yasmin, J.L. Abot, and I.M. Daniel, Processing of clay/epoxy nanocomposites by shear mixing. *Scripta Materialia* **49**, 81–86 (2003).
46. B. Ahmadi-Moghadam, B. Soltannia, and F. Taheri, Interlaminar crack detection in graphene nanoplatelet/CFRP composites using electric resistance change. in *Proc 19th International Conference on Composite Materials*, pp. 3597–3607 (2013).
47. B. Ahmadi-Moghadam and F. Taheri, Effect of processing parameters on the structure and multi-functional performance of epoxy/GNP nanocomposites. *J Mater Sci* **49**, 6180–6190 (2014).
48. H. Charles, Ross & Son Company, NY, High speed dispersers, <http://www.pharmaceuticalonline.com> (2014).
49. R. Andrews, D. Jacques, M. Minot, and T. Rantell, Fabrication of carbon multiwall nanotube/polymer composites by shear mixing. *Macromol Mater Eng* **287**, 395–403 (2002).
50. A. Dorigato, A. Pegoretti, F. Bondioli, and M. Messori, Improving epoxy adhesives with zirconia nanoparticles. *Composite Interfaces* **17**, 873–892 (2010).
51. T. Wang, C.H. Lei, A.B. Dalton, C. Creton, Y. Lin, K.A.S. Fernando, Y.P. Sun, M. Manea, J.M. Asua, and J.L. Keddie, Waterborne, nanocomposite pressure-sensitive adhesives with high tack energy, optical transparency, and electrical conductivity. *Adv Mater* **18**, 2730–2734 (2006).
52. H.S. Hedia, L. Allie, S. Ganguli, and H. Aglan, The influence of nanoadhesives on the tensile properties and Mode-I fracture toughness of bonded joints. *Eng Fracture Mech* **73**, 1826–1832 (2006).

53. S. Sprenger, C. Eger, A. Kinloch, J.H. Lee, A. Taylor, and D. Egan, Nano-modified ambient temperature curing epoxy adhesives. *Special Issue of Adhesion & Kleben and Dichten* (2004).
54. H. Fu, C. Yan, W. Zhou, and H. Huang, Nano-SiO₂/fluorinated waterborne polyurethane nanocomposite adhesive for laminated films. *J Ind Eng Chem* **20**, 1623–1632 (2013).
55. H. Dodiuk, S. Kenig, I. Blinsky, A. Dotan, and A. Buchman, Nanotailoring of epoxy adhesives by polyhedral-oligomeric-sil-sesquioxanes (POSS). *Int J Adhesion Adhesives* **25**, 211–218 (2005).
56. A. Buchman, H. Dodiuk-Kenig, A. Dotan, R. Tenne, and S. Kenig, Toughening of epoxy adhesives by nanoparticles. *J Adhesion Sci Technol* **23**, 753–768 (2009).
57. X.-r. He, R. Zhang, Q. Chen, Y.-q. Rong, and Z.-q. Yang, Different surface functionalized nano-Fe₃O₄ particles for EVA composite adhesives. *Int J Adhesion Adhesives* **50**, 128–135 (2014).
58. L.L. Zhai, G.P. Ling, and Y.W. Wang, Effect of nano-Al₂O₃ on adhesion strength of epoxy adhesive and steel. *Int J Adhesion Adhesives* **28**, 23–28 (2008).
59. L. Zhai, G. Ling, J. Li, and Y. Wang, The effect of nanoparticles on the adhesion of epoxy adhesive. *Mater Letters* **60**, 3031–3033 (2006).
60. E.N. Gilbert, B.S. Hayes, and J.C. Seferis, Nano-alumina modified epoxy based film adhesives. *Polym Eng Sci* **43**, 1096–1104 (2003).
61. H. Dodiuk, I. Belinski, A. Dotan, and S. Kenig, Polyurethane adhesives containing functionalized nanoclays. *J Adhesion Sci Technol* **20**, 1345–1355 (2006).
62. J. Li and J.K. Lumpp, Electrical and mechanical characterization of carbon nanotube filled conductive adhesive, in *Proc 2006 IEEE Aerospace Conference*, 6 pp. (2006).
63. M.B. Saeed and M.-S. Zhan, Adhesive strength of nano-size particles filled thermoplastic polyimides. Part-I: Multi-walled carbon nano-tubes (MWNT)–polyimide composite films. *Int J Adhesion Adhesives* **27**, 306–318 (2007).
64. K.-T. Hsiao, J. Alms, and S.G. Advani, Use of epoxy/multiwalled carbon nanotubes as adhesives to join graphite fibre reinforced polymer composites. *Nanotechnology* **14**, 791–793 (2003).
65. U. Khan, P. May, H. Porwal, K. Nawaz, and J.N. Coleman, Improved adhesive strength and toughness of polyvinyl acetate glue on addition of small quantities of graphene. *ACS Appl Mater Interfaces* **5**, 1423–1428 (2013).
66. S.W. Park, B.C. Kim, and D.G. Lee, Tensile strength of joints bonded with a nano-particle-reinforced adhesive. *J Adhesion Sci Technol* **23**, 95–113 (2009).
67. S.W. Park and D.G. Lee, Strength of double lap joints bonded with carbon black reinforced adhesive under cryogenic environment. *J Adhesion Sci Technol* **23**, 619–638 (2009).
68. S.G. Prolongo, M.R. Gude, J. Sanchez, and A. Ureña, Nanoreinforced epoxy adhesives for aerospace industry. *J Adhesion* **85**, 180–199 (2009).
69. Y. Zhang, B. You, H. Huang, S. Zhou, L. Wu, and A. Sharma, Preparation of nanosilica reinforced waterborne silylated polyether adhesive with high shear strength. *J Appl Polym Sci* **109**, 2434–2441 (2008).
70. S.M.R. Khalili, M. Tavakolian, and A. Sarabi, Mechanical properties of nanoclay reinforced epoxy adhesive bonded joints made with composite materials. *J Adhesion Sci Technol* **24**, 1917–1928 (2010).
71. A. Kaborani and B. Riedl, Effects of adding nano-clay on performance of polyvinyl acetate (PVA) as a wood adhesive. *Composites Part A* **42**, 1031–1039 (2011).
72. Y.A. Gorbakina, V.G. Ivanova-Mumzhieva, and T.M. Ufyanova, Adhesiveness of an epoxy oligomer filled with aluminum oxide powders. *Polym Sci C* **49**, 131–134 (2007).
73. A. Kaborani and B. Riedl, Nano-aluminum oxide as a reinforcing material for thermoplastic adhesives. *J Ind Eng Chem* **18**, 1076–1081 (2012).

74. W. Gao and G. Du, Curing kinetics of nano cupric oxide (CuO)-modified PF resin as wood adhesive: Effect of surfactant. *J Adhesion Sci Technol* **27**, 2421–2432 (2013).
75. D. Liu, H. Chen, P.R. Chang, Q. Wu, K. Li, and L. Guan, Biomimetic soy protein nanocomposites with calcium carbonate crystalline arrays for use as wood adhesive. *Bioresource Technol* **101**, 6235–6241 (2010).
76. S. Khoei and N. Hassani, Adhesion strength improvement of epoxy resin reinforced with nanoelastomeric copolymer. *Mater Sci Eng A* **527**, 6562–6567 (2010).
77. M.R. Ayatollahi, S. Shadlou, and M.M. Shokrieh, Mixed mode brittle fracture in epoxy/multi-walled carbon nanotube nanocomposites. *Eng Fracture Mech* **78**, 2620–2632 (2011).
78. M.M. Shokrieh, A.R. Kefayati, and M. Chitsazzadeh, Fabrication and mechanical properties of clay/epoxy nanocomposite and its polymer concrete. *Materials & Design* **40**, 443–452 (2012).
79. M.R. Ayatollahi, M.M. Shokrieh, S. Shadlou, A.R. Kefayati, and M. Chitsazzadeh, Mechanical and electrical properties of epoxy/multi-walled carbon nanotube/nanoclay nanocomposites. *Iran Polym J* **20**, 835–843 (2011).
80. S. Shadlou, B. Ahmadi-Moghadam, and F. Taheri, The effect of strain-rate on the tensile and compressive behavior of graphene reinforced epoxy/ nanocomposites. *Materials & Design* **59**, 439–447 (2014).
81. B. Soltannia and F. Taheri, Static, quasi-static and high loading rate effects on graphene nano-reinforced adhesively bonded single-lap joints. *Int J Composite Mater* **3**, 181–190 (2013).
82. M.R. Ayatollahi, S. Shadlou, M.M. Shokrieh, and M. Chitsazzadeh, Effect of multi-walled carbon nanotube aspect ratio on mechanical and electrical properties of epoxy-based nanocomposites. *Polymer Testing* **30**, 548–556 (2011).
83. A. Montazeri, J. Javadpour, A. Khavandi, A. Tcharkhtchi, and A. Mohajeri, Mechanical properties of multi-walled carbon nanotube/epoxy composites. *Materials & Design* **31**, 4202–4208 (2010).
84. B. Ahmadi-Moghadam and F. Taheri, Effect of processing parameters on the structure and multi-functional performance of epoxy/GNP nanocomposites. *J. Mater Sci* **49**, 6180–6190 (2014).
85. M.M. Shokrieh and R. Rafiee, Prediction of mechanical properties of an embedded carbon nanotube in polymer matrix based on developing an equivalent long fiber. *Mech Res Commun* **37**, 235–240 (2010).
86. M. Ayatollahi, S. Shadlou, and M. Shokrieh, Multiscale modeling for mechanical properties of carbon nanotube reinforced nanocomposites subjected to different types of loading. *Composite Structures* **93**, 2250–2259 (2011).
87. Multiscale modeling. *Scholarpedia* **6**, 11527 (2011).
88. R. Benzaid, J. Chevalier, M. Saâdaoui, G. Fantozzi, M. Nawa, L.A. Diaz, and R. Torrecillas, Fracture toughness, strength and slow crack growth in a ceria stabilized zirconia–alumina nanocomposite for medical applications. *Biomaterials* **29**, 3636–3641 (2008).
89. G.L. Burkholder, Y.W. Kwon, and R.D. Pollak, Effect of carbon nanotube reinforcement on fracture strength of composite adhesive joints. *J Mater Sci* **46**, 3370–3377 (2011).
90. F.H. Gojny, M.H.G. Wichmann, B. Fiedler, and K. Schulte, Influence of different carbon nanotubes on the mechanical properties of epoxy matrix composites – A comparative study. *Composites Sci Technol* **65**, 2300–2313 (2005).
91. M. Ayatollahi, S. Shadlou, and M. Shokrieh, Fracture toughness of epoxy/multi-walled carbon nanotube nano-composites under bending and shear loading conditions. *Materials & Design* **32**, 2115–2124 (2011).

92. M.R. Gude, S.G. Prolongo, T. Gómez-del Río, and A. Ureña, Mode-I adhesive fracture energy of carbon fibre composite joints with nanoreinforced epoxy adhesives. *Int J Adhesion Adhesives* **31**, 695–703 (2011).
93. K.L. Mittal, The role of the interface in adhesion phenomena. *Polym Eng Sci* **17**, 467–473 (1977).
94. P.J. Dynes and D.H. Kaelble, Surface energy analysis of carbon fibers and films. *J Adhesion* **6**, 195–206 (1974).
95. A.W. Neumann, R.J. Good, C.J. Hope, and M. Sejpal, An equation-of-state approach to determine surface tensions of low-energy solids from contact angles. *J Colloid Interface Sci* **49**, 291–304 (1974).
96. K. Johnson, K. Kendall, and A. Roberts, Surface energy and the contact of elastic solids. *Proc Royal Soc London A* **324**, 301–313 (1971).
97. F.M. Etzler, Determination of the surface free energy of solids. *Rev Adhesion Adhesives* **1**, 3–45 (2013).
98. P.R. Waghmare and S.K. Mitra, Contact angle hysteresis of microbead suspensions. *Langmuir* **26**, 17082–17089 (2010).
99. M.J. Geerken, R.G.H. Lammertink, and M. Wessling, Tailoring surface properties for controlling droplet formation at microsieve membranes. *Colloids Surfaces A* **292**, 224–235 (2007).
100. S.S. Tompkins, NASA Technical Memorandum 87572. NASA-TM-87572 19850023836 (1985).
101. J.W. Jiang, J.S. Wang, and B. Li, Thermal expansion in carbon nanotubes and graphene: Nonequilibrium Green's function approach. *Physical Review B* **80**, 205429, 7 pp., (2009).
102. T.S. Chow, The effect of particle shape on the mechanical properties of filled polymers. *J Mater Sci* **15**, 1873–1888 (1980).
103. L.-N. Tsai, Y.-T. Cheng, and W. Hsu, Nanocomposite effects on the coefficient of thermal expansion modification for high performance electro-thermal microactuator, in *Proc 18th IEEE International Conference on MEMS*, 467–470 (2005).
104. P. Yoon, T. Fornes, and D. Paul, Thermal expansion behavior of nylon 6 nanocomposites. *Polymer* **43**, 6727–6741 (2002).
105. Y. Rao and T.N. Blanton, Polymer nanocomposites with a low thermal expansion coefficient. *Macromolecules* **41**, 935–941 (2008).
106. G.D. Davis, Durability of adhesive joints, in *Handbook of Adhesive Technology*, second edition, A. Pizzi and K.L. Mittal (Eds.), pp. 273–291, CRC Press, Boca Raton, FL. (2003).
107. S. Yu, M.N. Tong, and G. Critchlow, Wedge test of carbon-nanotube-reinforced epoxy adhesive joints. *J Appl Polym Sci* **111**, 2957–2962 (2009).
108. ASTM-D3762-03. Standard test method for adhesive-bonded surface durability of aluminum (wedge test) (2010).
109. W. Bauhofer and J.Z. Kovacs, A review and analysis of electrical percolation in carbon nanotube polymer composites. *Composites Sci Technol* **69**, 1486–1498 (2009).
110. F.H. Gojny, M.H.G. Wichmann, B. Fiedler, I.A. Kinloch, W. Bauhofer, A.H. Windle, and K. Schulte, Evaluation and identification of electrical and thermal conduction mechanisms in carbon nanotube/epoxy composites. *Polymer* **47**, 2036–2045 (2006).
111. S. Yu, M.N. Tong, and G. Critchlow, Use of carbon nanotubes reinforced epoxy as adhesives to join aluminum plates. *Materials & Design* **31**, S126-S129 (2010).
112. A. Celzard, E. McRae, C. Deleuze, M. Dufort, G. Furdin, and J.F. Maréché, Critical concentration in percolating systems containing a high-aspect-ratio filler. *Phys Rev B* **53**, 6209–6214 (1996).
113. C. Lu and Y.W. Mai, Influence of aspect ratio on barrier properties of polymer-clay nanocomposites. *Phys Rev Lett* **95**, 088303 (2005).

114. J. Li and J.-K. Kim, Percolation threshold of conducting polymer composites containing 3D randomly distributed graphite nanoplatelets. *Composites Sci Technol* **67**, 2114–2120 (2007).
115. Y. Li and C.P. Wong, Recent advances of conductive adhesives as a lead-free alternative in electronic packaging: Materials, processing, reliability and applications. *Mater Sci Eng R* **51**, 1–35 (2006).
116. R. Gomatam and K.L. Mittal (Eds.), *Electrically Conductive Adhesives*, CRC Press, Boca Raton, FL. (2008).
117. A.S. Lim, Z.R. Melrose, E.T. Thostenson, and T.-W. Chou, Damage sensing of adhesively-bonded hybrid composite/steel joints using carbon nanotubes. *Composites Sci Technol* **71**, 1183–1189 (2011).
118. W. Qiao, H. Bao, X. Li, S. Jin, and Z. Gu, Research on electrical conductive adhesives filled with mixed filler. *Int J Adhesion Adhesives* **48**, 159–163 (2014).
119. H. Kim, Y. Miura, and C.W. Macosko, Graphene/polyurethane nanocomposites for improved gas barrier and electrical conductivity. *Chem Mater* **22**, 3441–3450 (2010).
120. M.A. Osman, V. Mittal, M. Morbidelli, and U.W. Suter, Polyurethane adhesive nanocomposites as gas permeation barrier. *Macromolecules* **36**, 9851–9858 (2003).
121. H. Schulz, B. Schimmoeller, S.E. Pratsinis, U. Salz, and T. Bock, Radiopaque dental adhesives: Dispersion of flame-made Ta₂O₅/SiO₂ nanoparticles in methacrylic matrices. *J Dentistry* **36**, 579–587 (2008).
122. M. Atai, L. Solhi, A. Nodehi, S.M. Mirabedini, S. Kasraei, K. Akbari, and S. Babanzadeh, PMMA-grafted nanoclay as novel filler for dental adhesives. *Dental Mater* **25**, 339–347 (2009).
123. L. Solhi, M. Atai, A. Nodehi, and M. Imani, A novel dentin bonding system containing poly (methacrylic acid) grafted nanoclay: Synthesis, characterization and properties. *Dental Mater* **28**, 1041–1050 (2012).
124. S. Kasraei, M. Atai, Z. Khamverdi, and S.K. Nejad, The effect of nanofiller addition to an experimental dentin adhesive on microtensile bond strength to human dentin. *J Dentistry of Tehran University of Medical Sciences* **6**, 36–41 (2009).
125. U. Lohbauer, A. Wagner, R. Belli, C. Stoetzel, A. Hilpert, H.D. Kurland, J. Grabow, and F.A. Muller, Zirconia nanoparticles prepared by laser vaporization as fillers for dental adhesives. *Acta Biomater* **6**, 4539–4546 (2010).
126. A. Akhavan, A. Sodagar, F. Mojtahedzadeh, and K. Sodagar, Investigating the effect of incorporating nanosilver/nanohydroxyapatite particles on the shear bond strength of orthodontic adhesives. *Acta Odontologica Scandinavica* **71**, 1038–1042 (2013).
127. M. Kassaei, A. Akhavan, N. Sheikh, and A. Sodagar, Antibacterial effects of a new dental acrylic resin containing silver nanoparticles. *J Appl Polym Sci* **110**, 1699–1703 (2008).
128. C.E. Brubaker and P.B. Messersmith, The present and future of biologically inspired adhesive interfaces and materials. *Langmuir* **28**, 2200–2205 (2012).
129. P.M. Favi, S. Yi, S.C. Lenaghan, L. Xia, and M. Zhang, Inspiration from the natural world: From bio-adhesives to bio-inspired adhesives. *J Adhesion Sci Technol* **28**, 290–319 (2014).

Bonding Dissimilar Materials in Dentistry

Muhammad Zakir¹, James Kit-Hon Tsoi¹, Chun Hung Chu²,
Christie Ying Kei Lung¹ and Jukka Pekka Matinlinna^{1,*}

¹*Dental Materials Science, Faculty of Dentistry, The University of Hong Kong, Hong Kong SAR, P.R. China*

²*Community and Family Dentistry, Faculty of Dentistry, The University of Hong Kong, Hong Kong SAR, P.R. China*

Abstract

Bonding of dental restorative materials to tooth tissues is one of the most important aspects in dentistry. Adhesion at the interface has been the topic of never-ending and growing discussion in the research field of adhesive dentistry for quite some time. Prosthetic materials have to be cemented in the moist oral cavity either to the remaining tooth structure or to another prosthetic dental material. The affinity of most of the dental materials to each other is inherently inadequate. Thus, to meet this harsh oral environment many so-called coupling agents are used after the surface modification to further enhance the adhesion between different materials. There has been considerable research on coupling agents, with most of it focusing on silane coupling agents as compared to studies on some other coupling agents. One of the main problems with silanes is their susceptibility to humidity, and thus other coupling agents have been investigated to provide a more hydrolytically stable bonding agent. Some phosphate, zirconium and titanium based inorganic-organic hybrid compounds are also actively being investigated for the purpose. This review is focused on the coupling agents used in the contemporary adhesive dentistry including silanes which have and are being extensively studied. This review starts briefly from the history of the coupling agents and finally moving on to the current trends in research on coupling agents. This review is aimed to give better view and understanding of the different coupling agents and how these can be used in adhesive dentistry in the future.

Keywords: Silane coupling agents, zirconates, phosphate coupling agents, sulfur-based coupling agents, adhesion, hydrolytic stability, titanate coupling agents, zircoaluminate coupling agents

*Corresponding author: jpmat@hku.hk

11.1 Introduction

One of the main clinical aspects in any field of dentistry is durable adhesion, and it is of critical importance in the fields of aesthetic, conservative, orthodontic and prosthetic dentistry. Modern adhesive dentistry is conservative, *i.e.*, it preserves tooth tissues as much as clinically possible. According to the Oxford Dictionary of Dentistry, "Adhesion is the sticking of two surfaces together" or according to ISO Dental Terminology, adhesion can be defined as "A state in which two surfaces are held together by chemical or physical attraction or both with or without the aid of a substance formulated for coating one or two surfaces for the purpose of holding or intend to be held by another body". In general, adhesion has been explained as coming together or sticking of two dissimilar surfaces together. It is simple to understand that two dissimilar surfaces may not have natural affinity for each other. Adhesion in dentistry can be described as connecting or joining of two dissimilar surfaces to obtain the optimal result for the particular purpose and it is different from cohesion which is the union of two similar surfaces. Adhesion can be broadly divided into two main categories: mechanical and chemical adhesion. Mechanical adhesion is the one in which the substrate surface is subjected to surface conditioners thus forming irregularities on the surface, and when the restorative material is placed on the substrate it penetrates into these irregularities. These small surface irregularities enable mechanical locking (interlocking) between the surfaces and provide good bonding as compared to the bodies without any irregularities. Dental silver amalgam restorations and resin composite restorations are good examples of mechanical adhesion. Chemical adhesion does not involve any surface treatment but only an adhesive which has affinity for both substrates when placed between them, thus increasing the bonding and giving good, adequate, and durable adhesion. Examples of this include adhesive resin bonded ceramic (porcelain).

Adhesion in dentistry is promoted by many factors such as clean surfaces, increased wettability (low contact angle) and absence of biofilms on the substrates. One of the main problems encountered and which is still of main concern is the adhesion property of dental materials when placed in the harsh and hostile oral environment. The materials in the oral cavity have to bear varying masticatory forces, changes in temperature (ca. + 5°C to + 55°C), varying pH, saliva, bacteria, fungi, proteins *etc.* [1, 2]. This limits the options for different types of adhesives which can be used in dentistry as compared to the adhesives being used in numerous industrial applications. In the 1950's acid etching technique was introduced to create mechanical retention on dental ceramics and thus giving birth to the concept of mechanical adhesion. In the 60's resin composite materials were developed with further modification of the composite material components to be used *e.g.*, with acid etching techniques to bond orthodontic brackets to the tooth structure. Since then acid etching of tooth tissues has been used in adhesive dentistry. In the 1970's the so-called polycarboxylate cements were introduced and subsequently followed by the introduction of glass ionomer cements (GICs) by Wilson and Kent [3, 4], thus giving rise to the concept of chemical adhesion.

In general, coupling agents are synthetic, functional compounds and conditioning agents used to increase the bond strength between *e.g.*, various oxide-based dental materials and

tooth structures with resin based composite luting cements. The coupling agents may be used for the bonding of resin composites to the tooth, bonding resin composites to surface-treated base or noble metal alloy frameworks or bonding resin composites to silanized silica and non-silanized non-silica based permanent ceramic crowns/inlays/onlays to be placed in the oral cavity. Coupling agents basically act as adhesives providing adhesion between dissimilar materials which without coupling agents would not bond or adhere to each other. Silane coupling agents were the first coupling agents to be introduced. The developments of other coupling agents such as zirconates, titanates and phosphates have been of increasing interest.

In this critical review we discuss all the currently used coupling agents or those which have a potential to be used and drawing the attention to their reactivity and molecular structure and the how they can be applied to benefit clinical dentistry.

11.2 Silane Coupling Agents

There has been a great deal of research in the field of silanes during the last six decades to promote adhesion between dissimilar materials, ranging from glass fiber lamination to building material coatings, mineral surface treatments, optical coatings, glass fillers in resin composites for high-tech applications, such as in dentistry. In dentistry silanes are also used in the bonding of porcelain with resin composites, repair of ceramics and metals, bonding of metals and ceramics to resin composites and a number of other applications [5-7].

Silanes are derivatives of silicon compounds and they contain Si-C and Si-H bond(s). Si and C are interestingly from the same periodic element group 14 (previously IV A) which includes carbon (C), silicon (Si), germanium (Ge), tin (Sn) and lead (Pb). Out of which carbon and silicon are the two most important elements for living things [8]. Silanes are, in general, synthetic organic-inorganic silicon compounds which have the synergic property of bi-functionality which enables promotion of adhesion between two chemically dissimilar materials [9-12]. Silanes are also of two main types, *viz.* functional and non-functional silanes. Functional silanes contain two functional end groups that can react with organic and inorganic surfaces, respectively. Silica-based ceramics are one of the most utilized (inorganic) substrates and resin composites are the (organic) material, which are unified to each other by the use of silanes, leading to the adhesion of two chemically different materials [8, 9]. Non-functional silanes have only reactive groups which react with the hydroxyl groups of the inorganic substrate. These types of silanes are used for special purposes, *e.g.*, coatings. Other types of silanes include the so-called bis-functional silanes (also known as bis-silanes) or cross-linking silanes. They can have *e.g.*, two Si atoms in the molecular backbone and with three hydrolysable alkoxy groups (usually ethoxy) as shown in Figure 11.1 [8, 9].

Such silanes are mainly used in steel and tire industry and also a few laboratory research studies have shown them to increase the adhesion of resin composites to titanium and zirconia substrates [9, 13, 14]. As most of the coupling agents are not completely reactive as such, they need to be activated by the process of hydrolysis before they can adsorb on the surface of the substrate. One of the most commonly used silane is

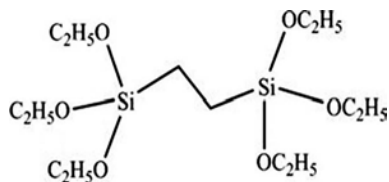


Figure 11.1 Example of bis-silane, bis-1, 2-(triethoxysilyl) ethane [1].

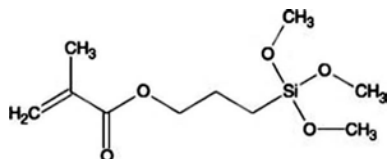


Figure 11.2 Molecular structure of 3-methacryloxypropyltrimethoxysilane [1].

3-methacryloxypropyltrimethoxysilane (MPS) and its structure is shown in Figure 11.2 [1]. This molecule has a very reactive methacrylate group at the end of the backbone, which provides good chemical reactivity in particular with other acrylic based dental materials [15-17].

MPS has to be pre-hydrolyzed before use. It should be noted that these silanes may have a relatively shorter shelf-life if they are kept in a pre-hydrolyzed form. But this pre-hydrolyzed form of silane has a very short shelf-life and should not be used after becoming milky, so now the silanes are also supplied as two-bottles systems commercially. When needed, the unhydrolyzed silane dissolved in ethanol is mixed with water and some acetic acid solution is added to hydrolyze it before its application (normally one coat) on the substrate (Figure 11.3) [8, 9]. Nevertheless, there is no international standard about the shelf-life after acid mixing or even after opening the bottle. Every company has its own indication of usage and thus should be followed accordingly by each user, be it in dental laboratories or at chair-side. Further research in this regard is necessary.

Silanes which intrinsically are nontoxic have a wide range of uses in dentistry, biomedicine and other fields. This said, the main function of silanes remains the promotion of union of dissimilar materials together.

In dentistry the silanes find their use in bonding the resin based composites to silica coated zirconia, acid-etched porcelain, other silica-coated substrates such as base metal and noble metal alloys, titanium and even Ag-amalgam [11, 12, 16, 17]. Another use in dentistry is the application of silanes for bonding glass-based fillers of various sizes to a resinous matrix to form the resin composites used in restorative dentistry

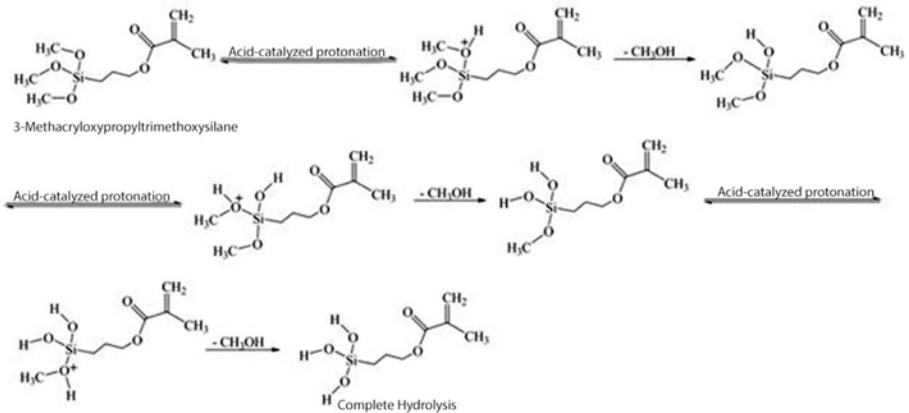


Figure 11.3 Silane hydrolysis reaction mechanism in an acidic medium, using 3-methacryloxypropyltrimethoxysilane as an example.

(filling materials) and luting cements. Thus, the mechanical properties, such as fracture toughness and hardness of the material are significantly enhanced. As a relatively new group of dental materials, silanized E-glass fibers are being used to increase the strength of fiber reinforced resin composites (FRCs), and are mainly used in removable prostheses, periodontal splinting and in some new filling materials [8, 18-21]. Silanes are also used in the intraoral repair of fractured/chipped ceramics, composite veneers, and Ag-amalgam [11, 12, 22, 23]. In another study, rebonding of resin cement to ceramic brackets (mainly zirconia) was found to have higher shear bond strength but high ceramic fracture rates after storage and thermocycling were observed because of the hydrolytic instability of silanes [24]. Using a new commercial silane primer containing three components, namely methacrylate silane, phosphoric acid methacrylate and sulfide methacrylate, the authors [24] tried to explain the higher adhesion between alumina brackets and adhesive, by the presence of lowly soluble phosphate layer on the bracket. This can be attributed to the phosphoric acid methacrylate present in the commercial silane. Despite silane being a conventional coupling agent used in dentistry, the nomenclature of silanes should not be confused with the new generation of coupling agents, in which [24] the "silane" should be referred to a coupling agent mixture that contains MPS and a phosphate monomer. Essentially the authors [24] are wrong and confusing the scientific community. Therefore, a generalized (re)definition about the terminologies is necessary.

A particular group of novel dental materials are E-glass fiber reinforced composites (FRCs). E-glass fibers are fibrous materials containing very thin silanized fibers embedded into a resinous matrix to form a composite material. These materials have a high fracture resistance because of the high amount of fibers present in them and thus it is difficult for the crack to propagate through them and these fibers act as reinforcing agents in the material. Such materials have a wide range of applications in dentistry especially the novel resin composite materials and also in prosthetic dentistry where they are used as denture base

polymers and the multi-directional fibers present in them can help eliminate fractures and these materials are also used to make dentures. In addition, E-glass fibers are hydrolytically stable because they do not practically dissolve in water in observable quantities. Various silane coupling agents have been screened and evaluated by Matinlinna and co-workers [25, 26] in FRCs to adhere the glass fibers to the polymer matrices and it was concluded that the mechanical properties of the materials weakened after aging in water storage, this may be because silanes are unstable in aqueous media. Some other coupling agents which are more hydrolytically stable might be incorporated into E-glass fibers to provide better mechanical properties and durable adhesion of dissimilar materials.

In the medical field, silanes can be used to provide longevity to the hip replacement prostheses, when the head and neck of the femur are formed from a base metal alloy (Co-Cr or TiAl_6V_4). The neck part can be silica-coated and can be silanized for adhesion to the socket of the hip bone by bone cement. These two parts are to be cemented by bone cement, but this raises an issue due to the hydrolytic environment. This can either be prevented by pre-coating the metal with *poly*(methyl methacrylate) as reported with various studies [8, 27, 28]. Another way of doing this is to first coat the metal with a silica layer and then silanize it as reported in [8]. Interestingly, silanes may also prevent the formation of biofilms which reduce the adhesion of the biomedical implants to the body tissues, and in addition, silanes have also been used as carriers in the field of drug delivery [8, 29-33]. Industrial uses of silanes include significantly enhanced mechanical properties of fiber reinforced resin composites by promoting adhesion. Such composites are used in the construction of spaceships, automobiles, aircraft, construction materials and different electronic products and even to prevent corrosion of certain metals and alloys [8, 25, 34]. The toxic hexa-valent chromium based coupling agents (*i.e.* chromates) were replaced by biocompatible and non-toxic silane coupling agents in the steel and tire industry as reported by van Ooij *et al.* [34]. Silanes are not only biocompatible in the oral environment but are also found to be non-toxic by different laboratory experiments [35]. Thus, silanes have a large application in the field of biomedicine and biomedical materials.

One of the main drawbacks when resin composites are bonded to prostheses is the loss of adhesion or degradation of bonding under aging. This indicates hydrolytic instability of commercial silanes (*e.g.*, MPS) [8, 36]. The silane coupling agents have been found to be very good for silica based (or hydroxyl groups containing surfaces) materials but the adhesion for non-silica based materials or some metals (*e.g.*, Mg, Ca) has not been found to be adequate at all. A solution to this has been found by conditioning the surface of the material by adding silica content, *e.g.*, by tribochemical silica coating after which the rough surface is wetted with the silane solution resulting in a more durable bonding of the materials by combined chemical and micro-mechanical adhesion [9].

Development of a hydrolytically stable silane material is the direction for the ongoing research and it may increase the durability of adhesion between dental materials in the oral environment.

Ceramic restorations are bonded to the tooth or other dental materials after surface treatments, such as either by the chemical action of hydrofluoric acid (HF) for silica-based ceramic materials and lately very commonly used method of tribochemical silica-coating

method for non-silica based ceramics like zirconia. As the next step, they are treated with silane for the bonding (cementation) step. However, the main shortcoming is the hydrolytic instability of silane-based bonding in the harsh oral environment [37]. Due to this the failure takes place at the interface and leads to clinical problems, such as marginal leakage and secondary caries. This is why the quest for more hydrolytically stable coupling agents is ongoing. Zirconate, phosphate, thiol, titanate based coupling agents which may have the potential to be more hydrolytically stable and thus they are being investigated to provide a durable bonding between the resin cements and the metal/ceramic indirect restorations.

11.3 Zirconate Coupling Agents

Zirconate coupling agents, *i.e.*, organozirconium compounds, have been studied extensively for coupling zirconium and ZrO_2 . They increase bonding between the zirconia substrate and resin composite in the same manner as silanes by bonding with their hydroxyl groups to ZrO_2 [37-40]. Zirconate coupling agents are considered to be more hydrolytically stable and have been used to increase the adhesion between the two dissimilar components in the composite material. Also, zirconates have been found to be non-toxic to the osteoblasts and, therefore, can be considered for bonding of zirconia to resin composite materials [38]. The chemical modifications of the ceramic surfaces are mainly focused on the application of zirconate coupling agents with resin composites, which give a good, stable bond by association of chemical bonding with mechanical bonding when compared with only chemical bonding [41]. Zirconate coupling agents along with phosphate adhesives are also said to have good chemical bonding property with metal oxides and react well with hydroxyls at the surfaces and thus can create durable adhesion with luting cements [41, 42]. Some of the pioneering studies using zirconate coupling agents were their use as a coupling agent between dental enamel and polymer filler [39] and between zirconia and resin cement by Cheng *et al.* [38]. Also, a very low weight percentage of zirconate in the resin composite material has shown to increase the adhesion between the inorganic and organic phases of dental composite material [40] and thereby reducing the amount of resin and being cost effective as well. Zirconates can be combined with polymers to obtain thereby materials with increased hydrolytic stability. Zirconates can be used for surface modification and thus can also be considered to not only increase the mechanical properties but also to reduce the moisture uptake [42].

Although zirconate coupling agents as shown in Figure 11.4 [38] increase the bond strength of the resin cements to zirconia, highly decreased bond strength was observed after thermo-cycling the test specimens [37]. Nevertheless, some studies have found that a mix of the acidic 10-methacryloxydecyl dihydrogen phosphate (MDP) and a zirconate coupling agent (2,2-di(allyloxymethyl) butyl trimethacryloyl zirconate) primer increased the bond strength between the resin cement and the zirconia substrate and was clinically found to be quite effective and durable [39, 40]. The ratio of such a mix is unknown, but the blend of various functional and non-functional coupling agents might be a good strategy for a synergistic effect and thus to improve the bonding performance.

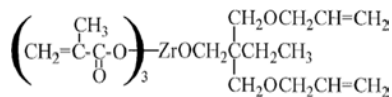


Figure 11.4 General structure of zirconate coupling agent [39].

In biomedicine, zirconate coupling agents have been found to increase adhesion in biodegradable implants by acting as an adhesive between hydroxyapatite crystals and the polymer matrix. During the last few years, hydroxyapatite incorporated into high density polyethylene has been used in the orthopedics. The incorporation of hydroxyapatite is obviously for biointegration and could also be used as a filler for improvement of mechanical properties. When the fillers were treated with a zirconate coupling agent at a particular weight ratio it increased the mechanical properties of the composite materials through better adhesion between the polyethylene matrix and the filler particles [43]. Hence, as in dental resin composites, if zirconia is used as a filler material, zirconate could be used as a coupling agent between the resin and zirconia which might possibly increase the strength of resin composites. More testing is necessary in this regard.

In industry, zirconate coupling agents find numerous applications such as in printing inks, lithographic printing plates, aluminum beverage cans, pigment coatings on titanium materials, and enhancement in the toughness of thermoplastics [42].

In dentistry, zirconate coupling agents have been studied and investigated only very sparingly so far. The zirconates can be modified according to their requirement in dentistry to increase the adhesion of organic and inorganic phases in the dental materials but can also help in increasing the adhesion of the ceramic prosthetic dental materials to metal prostheses. Zirconates possess the potential to provide the restorations a longer clinical service life by being hydrophobic under natural aging in the oral cavity.

11.4 Phosphate Coupling Agents

The first study in dentistry showing the durability of the shear bond strength between phosphate containing resin composites and ZrO_2 was done by Kern and Wegner [44]. 10-Methacryloxydecyl dihydrogen phosphate (MDP) shown in Figure 11.5 [45] has been widely studied and considered to be a very promising primer for the bonding of ceramic substrates to resin composites. The functional group of the MDP bonds with the metal oxide surfaces by chemical bonding mechanism along with secondary forces (or hydrogen bonds) at the interface between the ceramics and resins [46-48]. It was further established that the MDP-based resin cements could be used for the final cementation of the ZrO_2 -based restorations in clinical practice [49]. The recent research has focused on improving bonding with MDP-based monomers as they are very stable in hydrolytic environment over long periods [37].

With the good chemical bonding of 10-methacryloxydecyl dihydrogen phosphate coupling agent to zirconia substrate there have been a few studies which have shown adhesion

failure [22, 41, 49, 51]. It has been suggested that the possibility of using zirconate coupling agents instead of silanes and 10-methacryloxydecyl dihydrogen phosphate might be worth further studies [38, 42].

10-Methacryloxydecyl dihydrogen phosphate coupling agent has also been found to enhance the bonding of different alloys, such as chromium-titanium, nickel-chromium and cobalt-chromium alloys with resin composites. Thus, it can have a high potential in increasing the bonding between zirconia and resin composites [38]. Ikemura *et al.* explained the hypothetical bonding mechanism of phosphate monomers by stating that phosphonic acid monomer 6-methacryloxyhexyl phosphonoacetate (6-MHPA) (Figure 11.6) [51], and 6-methacryloxyhexyl 3-phosphonopropionate (6-MHPP) (Figure 11.6) [51] ionize by the water present on the surface of the ceramic and then penetrate into the micro-spaces in the substrate. Next, chemical bonds form first via hydrogen bonds and with the polymerization of resin composites with light irradiation, forming stronger bonds at the interface of resin composite and substrate [52]. Two primers were recently introduced in the dental market out of which one primer was methacrylate with a thiophosphoric acid moiety (MEPS) and the other primer was a combination of 10-methacryloxydecyl dihydrogen phosphate (MDP) and 6-(4-vinylbenzyl-n-propyl)-amino-1,-3,-5-triazine-2,-4-dithiol (VBATDT) which showed in the infrared spectroscopic studies that the phosphate groups of the MDP were adsorbed on the silver substrate thus giving quite a strong bonding. These types of coupling agents can provide good bonds between noble metal alloys and polymeric materials [53].

10-Methacryloxydecyl dihydrogen phosphate coupling agent even with high hydrolytic stability has been considered to be unstable under artificial aging [48, 54-56]. This is because its hydrolytic stability has been found to be less than the baseline which has been set up by silane coupling agents. Therefore, these bonding agents have to be looked into more detail and extensive study is necessary.

11.5 Thione/thiol Coupling Agents

Primers containing thione/thiol monomers form chemical bonds with precious (noble) metals and have the tendency to form a good bond to gold, gold alloys, silver alloys and gold-silver-palladium alloys. The methacrylate based monomers with sulfur atoms in the backbone are also used as primers for bonding noble metals and their alloys [52, 57]. When the sulfur based primers are combined with some other acidic monomers they impact positively the bonding efficacy of that substrate to resinous materials.

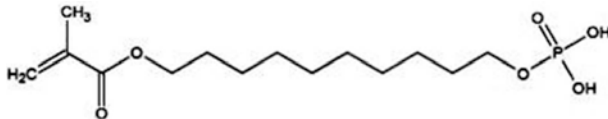


Figure 11.5 Chemical structure of 10-methacryloxydecyl dihydrogen phosphate (MDP) [45].

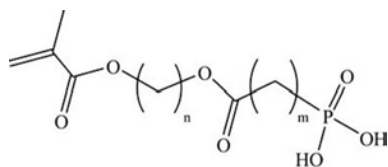


Figure 11.6 General structure for both MHPA and 6-MHPP molecules [51].

Bonding by sulfur containing primers to some noble metals may be due to the formation of a monolayer by self-assembly of thiol (-SH) groups. A recent study carried out on a thiol-based primer stated that the application of the mixture of 6-(4-vinylbenzyl-*n*-propyl)-amino-1,3,5-triazine-2,4-dithiol (VBATDT) as shown in Figure 11.7 [58] and 10-methacryloxydecyl dihydrogen phosphate even after thermocycling exhibited good bond strength between a gold-palladium-copper-silver alloy and titanium [52]. This observation was further confirmed by a study using a commercially available primer containing 6-(4-vinylbenzyl-*n*-propyl) amino-1,3,5-triazine-2,-4-dithiol and MDP which showed increased bond strength of not only precious metals but also non-precious metals [57, 59].

It has also been reported that the effect of sulfur-based primers on the enhancement of the bond strength to the metals is not as much as that of phosphates [56]. In addition, some studies have reported a high percent loss of bond strength after artificial aging and the increase in bond strength can vary depending on the substrate (adherend) [59-61]. Thus, further work is required on this topic as sulfur-based primers look favorable in the future to potentially act as good coupling agents.

11.6 Titanate Coupling Agents

Coupling agents form an interfacial unifying layer between two dissimilar materials. They promote the adhesion between the organic matrix and filler particles in dental resin composites. In addition, the biomechanical properties of the dental composites mainly depend on how the masticatory forces are transferred through the matrix to the reinforcing filler particles and thus, the bonding of the resin and filler particles is of primary importance and can be provided only by appropriate coupling agents [62]. As mentioned above, the coupling agents should be hydrolytically stable, should not deteriorate in an aqueous environment, and provide a waterproof bond at the interface of the two dissimilar materials [63]. In some commercial products, titanium dioxide has been incorporated as a filler material and it seems that titanate could bond dissimilar fillers and resins. However, very limited information is available about the titanates and more extensive investigations are needed.

The titanate coupling agents *i.e.*, tetravalent organo-titanium compounds, may form an organic reactive monomolecular layer on the inorganic surface of the substrate by reacting with the free protons of the hydroxyls at the inorganic interfacial surface. Ti at the molecular center undergoes reorganization and reshuffling enabling itself to act either as

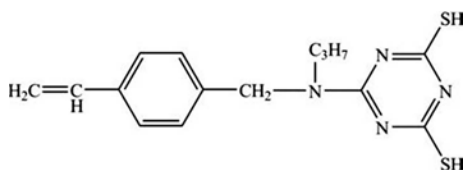


Figure 11. 7 Structural formula of VBATDT [58].

a proton donor or acceptor [64, 65], thus when introduced into a polymeric system it not only increases the bonding but also reduces the brittleness of the material [44]. The formation of -Ti-O-Ti-O- bonds leads to hydrophobicity of the substrate material. The chelate titanates, as the name implies, have a chelating function, attract filler protons more than water and are more hydrolytically stable than the alkoxide titanates which are more reactive in a moist environment and undergo hydrolysis quickly [63].

Titanates, the general formula of which is shown in Figure 11.8 [66], when used as a coupling agent in dental composites lead to an increase in their mechanical properties. This has been investigated [67-71], and it has been reported that mainly the increases in the tensile strength and the impact strength of the dental composites by using titanate coupling agents occur. Another study incorporated a titanate coupling agent into a composite which was a blend of polypropylene and two types of calcium carbonates. It was concluded that the titanate coupling agent increased the mechanical properties of the composite material due to the good adhesion between the filler and the matrix. The loading of the coupling agents should be properly investigated to obtain the desired effect of the coupling agent [65]. Different loading ratios of coupling agents can have different effects on the mechanical properties of the materials [62, 64] in that the Young's modulus of the composite increased when two materials were compared, out of which one was treated with the titanate coupling agent and the other not. Along with the increase in the modulus, the dispersion of fillers was better, which was another factor for an increase in the Young's modulus [62]. One more study on a talc-epoxy composite reported an increase in the flexural strength of the composite material when the talc was treated with a titanate as compared to the composite material in which talc was treated with a silane coupling agent [62].

Titanate coupling agents also changed the ferrite powder surface from hydrophilic to hydrophobic by the interaction of the Ti-O bond of the titanate with the Fe-OH bond forming a hydrophobic Ti-O-Fe layer on the surface and thereby increasing adhesion between the hydrophobic resin and ferrite powders [72]. Polybutadiene rubber/clay and nylon 6/mica composites showed superior mechanical properties when the fillers were treated with titanate coupling agents. This was because such titanates increased the adhesion of the matrix to the filler [65].

A definite conclusion has not yet been drawn as to what an optimum loading amount of a coupling agent should be, in order to bring about the required result in the material properties. Therefore, a more systematic approach should be taken for a final say regarding the use of titanates as coupling agents in modern dental applications.

11.7 Zircoaluminate Coupling Agents

Zircoaluminates are low molecular weight compounds and they are more hydrophobic than silanes and titanates [73]. Since their introduction in 1985 by Cohen [74, 75] who studied zircoaluminates as coupling agents and a surface modifier, zircoaluminates have been found to be applicable in different industrial applications as a coupling agent in plastics, rubbers, coatings, pigment and adhesives. They are also used as surface modifiers for certain metal surfaces and as corrosion resistant agents for materials which require a long exposure time to moisture [75-77]. Zircoaluminates are currently being used for enhancing the physical properties of paper and the treatment of TiO_2 with a zircoaluminate coupling agent results in improved optical properties and better print quality in the paper industry [73, 78].

These materials have not yet been studied extensively in the field of dentistry, although this type of coupling agent looks very promising. Nonetheless, nothing can be said until they have been studied thoroughly as to whether they fulfill all the criteria required by the coupling agents.

11.8 Other Coupling Agents

Lung *et al.* [54] carried out experiments with three different coupling agents, 2-hydroxyethyl methacrylate, oleic acid and itaconic acid (the latter two are carboxylic acids) and compared them with two different types of silane coupling agents. They concluded that even these types of coupling agents did not give better properties to the materials when compared with silane treated materials. However, these coupling agents were hydrolytically more stable, provided mechanical properties in the acceptable range prescribed by ISO standards, had a longer shelf-life and are much cheaper than the competitive silanes. These coupling agents have currently also been found to have a number of applications in different fields/industries. For example, they have been used as a surface modifier in oily wastewater treatment, in contact lenses, in paper industry, and in shampoos and detergents. Some of them are used in a drug delivery system for keloid and hypertrophic scarring, corrosion protection of steel and in many other applications [53]. These cost-effective coupling agents could be further investigated and optimized according to the required applications and modified accordingly for their use.

It cannot be stressed enough how important adhesion is in dentistry, but also in all aspects of life. Virtually all the adhesives or coupling agents which have been used are

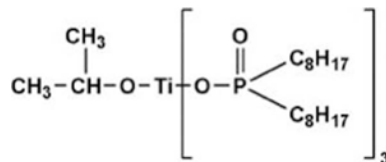


Figure 11.8 A general titanate structure [66].

synthetic. Interestingly, very recently natural marine mussels and their adhering ability are being studied as they have one of the best adhesive qualities and, more importantly, they are from an aquatic environment. This said, they are understood to be hydrolytically very stable and are not vulnerable in the aqueous environment. Hamming *et al.* [79] mimicked the marine mussel's foot protein and carried out the pull-out test between NiTi and Ti-6Al-4V wires and *poly*(methyl methacrylate) using this mussel adhesive. The results indicated an increase in the adhesive property [79]. In fact, the mussel adhesive property relies on the repeated 3, 4-dihydroxy-L-phenylalanine (L-DOPA) motif from food protein. Inspired by this, Zhou *et al.* [80] were successful in using the decarboxylated derivative 3, 4-dihydroxyphenethylamine (dopamine, DOPA) to remineralize the human teeth hydroxyapatite *in vitro*. Thus, this material has been found to be one of the best adhesives occurring naturally, also giving the remineralization of the natural tooth and can be further modified and used according to the requirements in dentistry.

Table 11.1 presents bond strength results obtained using various coupling agents in selected studies.

Table 11.1 Bond strength results obtained using various coupling agents from selected studies.

Coupling agents	Substrates	Reportedly bonded to	Shear bond strength (SBS) MPa with SD	References
Silane coupling agents				
3-isocyanatopropyl-trimethoxysilane	Zirconia	Resin composite	6.6 (2.6)	14
3-isocyanatopropyl-triethoxysilane	Zirconia	Resin composite	6.6 (2.2)	14
3-methacryloxypropyl-trimethoxysilane	Zirconia	Resin composite	12.1 (2.9)	54
3-acryloxypropyl-trimethoxysilane	Zirconia	Resin composite	14.6 (1.1)	54
3-trimethoxysilylpropyl-trimethoxysilane	Zirconia	Resin cement	16.6 (2.6)	46
3-acryloxypropyl-trimethoxysilane + cross-linking silane	Titanium	Resin composite	14.6 (2.9)	36
3-isocyanatopropyl-triethoxysilane	Titanium	Resin composite	12.5 (5.8)	81

(Continued)

Table 11.1 cont.

Phosphate coupling agents				
10-methacryloxydecyl dihydrogen phosphate (MDP)	Pure zirconium	Resin luting cement	52.7 (2.7)	39
10-methacryloxydecyl dihydrogen phosphate (MDP)	Zirconia	Resin luting cement	49.2 (4.0)	39
Coupling agents	Substrates	Reportedly bonded to	Shear bond strength (SBS) MPa with SD	References
Thiol coupling agents				
6-(4-vinylbenzyl-n-propyl)amino-1,3,5-triazine-2,4-dithione tautomer	Ag-Pd-Cu-Au alloy	Resin composite	13.0 (1.4)	59
6-(4-vinylbenzyl-n-propyl)amino-1,3,5-triazine-2,4-dithione tautomer	Stainless steel	Luting cement	33.4 (3.6)	82
Zirconate coupling agents				
2,2-Di(allyloxymethyl) butyl trimethacryloyl zirconate	Zirconia	Resin luting cement	30.7 (3.2)	39
2,2-Di(allyloxymethyl) butyl trimethacryloyl zirconate	Pure zirconium	Resin luting cement	37.4 (3.8)	39

11.9 Conclusion

It is fair enough to say that many different coupling agents, especially silanes, have been studied extensively but still at this point we do not have a single coupling agent which can be universally used on all substrates and which fulfills all the criteria which are necessary for a coupling agent to function properly. This can be difficult, so more focus should be on at least finding one coupling agent which is good enough for a single substrate to be used either in restorative, prosthetic or other branches of dentistry but which is hydrolytically stable. A lot has been done but as it is said nothing is ever enough. Therefore, still a lot can be done and should be done to develop much better performing coupling agents. The question may be: How to overcome the detrimental and inevitable effects of water aging?

References

1. J.P. Matinlinna, J.R. Dahl, S. Karlsson, L.V.J. Lassila, and P.K. Vallittu, The effect of the novel silane system on the flexural properties of E-glass fiber-reinforced composites for dental use, in *Silanes and Other Coupling Agents*, Vol. 5, K.L. Mittal (Ed.), pp. 107–121, CRC Press, Boca Raton, FL. (2009).
2. B.W. Darvell, *Materials Science for Dentistry*, 9th edition, pp. 115–146, Woodhead Publishing Limited, Cambridge, U.K. (2009).
3. A.D. Wilson and B.E Kent, The glass-ionomer cement: A new translucent dental filling material. *J. Appl. Chem. Biotechnol.* 21, 313–318 (1971).
4. A.D. Wilson and B.E Kent, A new translucent cement for dentistry: The glass ionomer cement. *Brit. Dental J.* 132, 133–135 (1972).
5. J.P. Matinlinna, M. Özcan, L.V.J. Lassila, and P.K. Vallittu, Applications of trialkoxysilanes in dental biomaterials: A review, in *Silanes and Other Coupling Agents*, Vol. 4, K.L. Mittal (Ed.), pp. 199–215, CRC Press, Boca Raton, FL. (2007).
6. J.G. Marsden, in *Handbook of Adhesives*, I. Skeist (Ed.), pp. 536–548. Van Nostrand-Reinhold, New York (1990).
7. B. Arkles, Silane esters, in *Kirk-Othmer Encyclopedia of Chemical Technology*, K. Othmer (Ed.), pp. 69–81. Wiley, London (1997).
8. C.Y.K. Lung and J.P. Matinlinna, Silanes for adhesion promotion and surface modification, in *Silane Chemistry, Applications and Performance*, K. Moriguchi and S. Utagawa (Eds.), pp. 87–109, Nova Science Publisher, Hauppauge, NY. (2013).
9. C.Y.K. Lung and J.P. Matinlinna, Aspects of silane coupling agents and surface conditioning in dentistry: An overview. *Dental Mater.* 28, 467–477 (2012).
10. E.P. Plueddemann, *Silane Coupling Agents*, 2nd edition, Plenum Press, New York (1991).
11. G.W. Ho and J.P. Matinlinna, Insights into ceramics as dental materials. Part I: Ceramic material types in dentistry. *Silicon* 3, 109–115 (2011).
12. G.W. Ho and J.P. Matinlinna, Insights into ceramics as dental materials. Part II: Chemical surface treatments. *Silicon* 3, 117–123 (2011).
13. U. Gbureck, A. Masten, J. Probst, and R. Thull, Tribochemical structuring and coating of implant metal surfaces with titanium oxide and hydroxyapatite layers. *Mater. Sci. Eng. C* 23, 461–465 (2003).
14. C.Y.K. Lung and J.P. Matinlinna, Resin bonding to silicized zirconia with two isocyanatosilanes and a cross-linking silane. Part I. Experimental. *Silicon* 2, 153–161 (2010).
15. J.P. Matinlinna, J.K.-H. Tsoi, J. de Vries, and H.J. Busscher, Characterization of novel silane coatings on titanium implant surfaces. *Clin. Oral Implant Res.* 24, 688–697 (2013).
16. C.Y.K. Lung, E. Kukk, T. Hägerth, and J.P. Matinlinna, Surface hydroxylation of silica-coated zirconia by various chemical treatments. *Appl. Surface Sci.* 257, 1228–1235 (2010).
17. J.P. Matinlinna, L.V.J. Lassila, M. Özcan, A. Yli-Urpo, and P.K. Vallittu, An introduction to silanes and their clinical applications in dentistry. *Int. J. Prosthodont.* 17, 155–164 (2004).
18. F.C. Eichmiller, Titanium applications in dentistry. *J. Am. Dental Assoc.* 134, 347–349 (2003).
19. M. Sharma, A.V.R. Kumar, N. Singh, N. Adya, and B. Saluja, Electrochemical corrosion behavior of dental/implant alloys in artificial saliva. *J. Mater. Eng. Performance* 17, 695–701 (2008).
20. J.H. Lee, C.M. Um, and I.B. Lee, Rheological properties of resin composites according to variations in monomer and filler composition. *Dental Mater.* 22, 515–526 (2006).
21. M. Zhang and J.P. Matinlinna, The effect of resin matrix composition on mechanical properties of E-glass fiber reinforced composite for dental use. *J. Adhesion Sci. Technol.* 25, 2687–2701 (2011).

22. M.B. Blatz, A. Sadan, J. Martin, and B. Lang, In vitro evaluation of shear bond strengths of resin to densely sintered high-purity zirconium-oxide ceramic after long-term storage and thermal cycling. *J. Prosthetic Dentistry* 91, 356–362 (2004).
23. J.P. Matinlinna and P.K. Vallittu, Silane based concepts on bonding resin composite to metals. *J. Contemp. Dental Pract.* 8, 1–8 (2007).
24. F. Falkensammer, E. Jonke, M. Bertl, J. Freudenthaler, and H.P. Bantleon, Rebonding performance of different ceramic brackets conditioned with a new silane coupling agent. *European J. Orthodontics* 35, 103–109 (2013).
25. M. Zhang and J.P. Matinlinna, E-glass fiber reinforced composites in dental applications. *Silicon* 4, 73–78 (2012).
26. J.P. Matinlinna, J.E. Dahl, L.V.J. Lassila, and P.K. Vallittu, The effect of trialkoxysilane coupling agent coatings on E-glass fibers on the flexural properties of fiber-reinforced composites, in *Silanes and Other Coupling Agents*, Vol. 4, K.L. Mittal, (Ed), pp. 83–97, CRC Press, Boca Raton, FL. (2007).
27. R.T. Muller and N. Schurmann, Shear strength of the cement metal interface: An experimental study. *Arch. Orthopaedic Trauma Surgery* 119, 133–138 (1999).
28. S. Raab, A.M. Ahmed, and J.W. Provan, Thin film PMMA precoating for improved implant bone-cement fixation. *J. Biomed. Mater. Res.* 16, 679–704 (1982).
29. H.J. Erli, R. Marx, O. Paar, F.U. Niethard, M. Weber, and D.C. Wirtz, Surface pretreatments for medical application of adhesion. *BioMedical Engineering OnLine* 2, 15–33 (2003).
30. T. Mumme, R. Marx, R. Müller-Rath, C.H. Siebert, and D.C. Wirtz, Surface coating to improve the metal-cement bonding in cemented femur stems. *Arch. Orthopaed Trauma Surgery* 128, 773–781 (2008).
31. J.W. Costerton, P.S. Stewart, and E.P. Greenberg, Bacterial biofilms: A common cause of persistent infections. *Science* 284, 1318–1322 (1999).
32. P.S. Stewart and J.W. Costerton, Antibiotic resistance of bacteria in biofilms. *Lancet* 358, 135–138 (2001).
33. E. Allemann, R. Gurny, and E. Doelke, Drug-loaded nanoparticles – Preparation methods and drug targeting issues. *Eur. J. Pharm.* 39, 173–191 (1993).
34. W.J. van Ooij, D. Zhu, S. Prasad, S. Jayaseelan, Y. Fu, and N. Teredesai, Silane based chromate replacements for corrosion control, paint adhesion and rubber bonding. *Surface Eng.* 16, 386–396 (2000).
35. B. Arkles, Look what you can make out of silicones. *Chemtech* 13, 542–555 (1983).
36. J.P. Matinlinna and L.V. Lassila, Experimental novel silane system in adhesion promotion between dental resin and pretreated titanium. Part II: Effect of long term water storage. *Silicon* 2, 79–85 (2010).
37. J.Y. Thompson, R.B. Stoner, J.R. Piascik, and R. Smith, Adhesion/cementation to zirconia and other non-silicate ceramics: Where are we now? *Dental Mater* 27, 71–82 (2011).
38. H.C.K. Cheng, J.K.-H. Tsoi, R.A. Zwahlen, and J.P. Matinlinna, Effect of silica-coating and a zirconate coupling agent on shear bond strength of flowable resin–zirconia bonding. *Intl. J. Adhesion Adhesives* 50, 11–16 (2014).
39. K. Yoshida, Y. Tsuo, and M. Atsuta, Bonding of dual-cured resin cement to zirconia ceramic using phosphate acid ester monomer and zirconate coupler. *J. Biomed. Mater. Res. Part B* 77, 28–33 (2006).
40. A.N. Cavalcanti, R.M. Foxton, T.F. Watson, M.T. Oliveira, M. Giannini, and G.M. Marchi, Y-TZP ceramics: Key concepts for clinical application. *Operative Dentistry* 34, 344–351 (2009).

41. J.R. Piascik, S.D. Wolter, and B.R. Stoner, Enhanced bonding between YSZ surfaces using a gas-phase fluorination pretreatment. *J. Biomed. Mater. Res. B* 98, 114–119 (2011).
42. J.D.C. Wong, C.Y.K. Lung, J.K.-H. Tsoi, and J.P. Matinlinna, Effects of a zirconate coupling agent incorporated into an experimental resin composite on its compressive strength and bonding to zirconia. *J. Mechanical Behavior of Biomedical Materials* 29, 171–176 (2014).
43. A. Carmen, P. Rosestela, K. Arquimedes, G. Gema, D. Nohemy, S. Yanixia, and B.J. Luis, Characterization of HDPE/HA composites treated with titanate and zirconate coupling agents. *Macromol. Symp.* 247, 190–198 (2007).
44. M. Kern and S.M. Wegner, Bonding to zirconia ceramic: Adhesion methods and their durability. *Dental Mater.* 14, 64–71 (1998).
45. N. Moszner, U. Salz, and J. Zimmermann, Chemical aspects of self-etching enamel-dentine adhesives: A systemic review. *Dental Mater.* 21, 895–890 (2005).
46. S. Sanohkan, B. Kukiattrakoon, N. Larpboonphol, T. Sae-Yib, T. Jampa, and S. Manoppa, The effect of various primers on shear bond strength of zirconia ceramic and resin composite. *J. Conservative Dentistry* 16, 499–502 (2013).
47. M. Kern, A. Barloi, and B. Yang, Surface conditioning influences zirconia ceramic bonding. *J. Dental Res.* 88, 817–822 (2009).
48. R. Tanaka, A. Fujishima, Y. Shibata, A. Manabe, and T. Miyazaki, Cooperation of phosphate monomer and silica modification on zirconia. *J. Dental Res.* 87, 666–670 (2008).
49. S.M. Wegner and M. Kern, Long-term resin bond strength to zirconia ceramic. *J. Adhesive Dentistry* 2, 139–147 (2000).
50. H. Matsumura, H. Shimizu, N. Tanoue, and H. Koizumi, Current bonding systems for resin-bonded restorations and fixed-partial dentures made of silver-palladium-copper-gold alloy. *Japanese Dental Sci. Review* 47, 82–87 (2011).
51. K. Ikemura, T. Fujii, N. Negoro, T. Endo, and Y. Kadoma, Design of a metal primer containing a dithiooctanoate monomer and phosphonic acid monomer for bonding of prosthetic light-curing resin composite to gold, dental precious and non-precious metal alloys. *Dental Mater. J.* 30, 300–307 (2011).
52. K. Ikemura, H. Tanaka, T. Fujii, M. Deguchi, N. Negoro, T. Endo, and Y. Kadoma, Design of a new, multi-purpose, light-curing adhesive comprising a silane coupling agent, acidic adhesive monomers and dithiooctanoate monomers for bonding to varied metal and dental ceramic materials. *Dental Mater. J.* 30, 493–500 (2011).
53. Y. Taira, H. Yanagida, H. Matsumura, K. Yoshida, M. Atsuta, and S. Suzuki, Adhesive bonding of titanium with a thione-phosphate dual functional primer and self-curing luting agents. *Eur. J. Oral Sci.* 108, 456–460 (2000).
54. C.Y.K. Lung, M.G. Botelho, M. Heinonen, and J.P. Matinlinna, Resin zirconia bonding promotion with some novel coupling agents. *Dental Mater.* 28, 863–872 (2012).
55. M. Özcan, H. Nijhuis, and L.F. Valandro, Effect of various surface conditioning methods on the adhesion of dual-cure resin cement with MDP functional monomer to zirconia after thermal aging. *Dental Mater. J.* 27, 99–104 (2008).
56. Y. Taira and K. Kamada, Effect of primers containing sulfur and phosphate monomers on bonding type IV gold alloy. *J. Dentistry* 36, 595–599 (2008).
57. H. Koizumi, T. Ishii, K. Naito, T. Yoneyama, N. Tanoue, and H. Matsumura, Effects of triazine dithione and hydrophobic phosphate monomers on bonding to Ag-Pd-Cu-Au alloy and titanium with a methacrylic resin-based luting agent. *J. Adhesive Dentistry* 12, 215–222 (2010).
58. Y. Kadoma, Chemical structures of adhesion promoting monomers for precious metals and their bond strengths to dental metals. *Dental Mater. J.* 22, 343–358 (2003).

59. H. Matsumura, K. Kamada, N. Tanoue, and M. Atsuta, Effect of thione primers on bonding of noble metal alloys with an adhesive resin. *J. Dentistry* 28, 287–293 (2000).
60. H. Matsumura, T. Tanaka, and M. Atsuta, Bonding of silver–palladium–copper–gold alloy with thiol derivative primers and tri-n-butylborane initiated luting agents. *J. Oral Rehabilitation* 24, 291–296 (1997).
61. A.J. Ireland and M. Sherriff, The influence of alloy copper content on the polymerisation of anaerobic adhesives. *J. Dentistry* 27, 155–161 (1999).
62. M. Hussain, A. Nakahira, S. Nishijima, and K. Niihara, Effects of coupling agents on the mechanical properties improvement of the TiO₂ reinforced epoxy system. *Mater. Letters* 26, 299–303 (1996).
63. N. Menon, F.D. Blum, and L.R. Dharani, Use of titanate coupling agents in Kevlar/phenolic composites. *J. Appl. Polym. Sci.* 54, 113–123 (1994).
64. J. Gonzalez, C. Albano, M. Ichazo, and B. Diaz, Effects of coupling agents on mechanical and morphological behavior of the PP/HDPE blend with two different CaCO₃. *European Polymer J.* 38, 2465–2475 (2002).
65. W.L. Tham, W.S. Chow, and Z.A.M. Ishak, Effects of titanate coupling agent on the mechanical, thermal, and morphological properties of poly(methyl methacrylate)/ hydroxyapatite denture base composites. *J. Composite Mater.* 45, 2335–2345 (2011).
66. S.J. Monte. Titanates and zirconates in thermoplastic and elastomer compounds, Kenrich Petrochemicals, Inc., Bayonne, NJ (USA), <http://www.4kenrich.com/mediashare/5c/igxauf-c6j5ms5r2jci0xliywxylhc-org.pdf>.
67. C.D. Han and R. Shetty, Studies on multilayer film coextrusion II. Interfacial instability in flat film coextrusion, *Polym. Eng. Sci.* 18, 180–186 (1978).
68. C.D. Han, T. Van Den Weghe, P. Shete, and J.R. Hav, Effects of coupling agents on the rheological properties, processability, and mechanical properties of filled polypropylene. *Polym. Preprints* 21, 241–242 (1981).
69. P. Bajaj, N.K. Jha, and R.K. Jha, Effect of titanate coupling agent on mechanical properties of mica-filled polypropylene. *Polym. Eng. Sci.* 29, 557–563 (1989).
70. S.N. Maiti and P.K. Mahapatro, Mechanical properties of i-PP/ CaCO₃ composites. *J. Appl. Polym. Sci.* 42, 3101–3110 (1991).
71. Z.A.M. Ishak, H. Aminullah, H. Ismail, and H.D. Rozman, Effect of silane-based coupling agents and acrylic acid based compatibilizers on mechanical properties of oil palm empty fruit bunch filled high-density polyethylene composites. *J. Appl. Polym. Sci.* 68, 2189–2203 (1998).
72. W-S. Chen, Y-L. Chang, H-I. Hsiang, F-C. Hsu, and F-S. Yen, Effects of titanate coupling agent on the dielectric properties of Ni-Zn ferrite powders–epoxy resin coatings. *Ceramics Intl.* 37, 2347–2352 (2011).
73. B. Li, H. Mou, Y. Li, and Y. Ni, Synthesis and thermal decomposition behavior of zircoaluminate coupling agents. *Ind. Eng. Chem. Res.* 52, 11980–11987 (2013).
74. L.B. Cohen, Aluminum zirconium metallo-organic complexes useful as coupling agents. U.S. Patent 4,539,048, assigned to Jos. Cavedon Company Inc. (1985).
75. L.B. Cohen, Zircoaluminate adhesion promoters. *J. Adhesion Sci. Technol.* 5, 439–448 (1991).
76. A.R. Marrion, *The Chemistry and Physics of Coatings*, 2nd edition, Royal Society of Chemistry, Tyne and Wear, U.K. (2004).
77. J.I. Melzer and B.P. Gunagan, Process for enhanced drainage of residual aqueous rinse on the external surface of plastic parts. U.S. Patent 5,314,546 (May 24, 1994).

78. B. Li, Y-M. Li, and R-J. Lu, Effect of modified nanoTiO₂ on properties of coating and coated paper. *Chemical Industry and Engineering Society of China Journal* 61, 228–234 (2010).
79. L.M. Hamming, X.W. Fan, P.B. Messersmith, and L.C. Brinson, Mimicking mussel adhesion to improve interfacial properties in composites. *Composites Sci. Technol.* 68, 2042–2048 (2008).
80. Y-Z. Zhou, Y. Cao, W. Liu, C.H. Chu, and Q-L. Li, Polydopamine-induced tooth remineralization. *ACS Appl. Mater. Interfaces* 4, 6901–6910 (2012).
81. J.P. Matinlinna, L.V.J. Lassila, I. Kangasniemi, and P.K. Vallittu, Isocyanato- and methacryloxysilanes promote Bis-GMA adhesion to titanium. *Dental Res.* 84, 360–364 (2005).
82. Y. Ishikawa, Y. Kawamoto, H. Koizumi, M. Furuchi, H. Matsumura, and N. Tanoue, Effect of metal priming agents on bonding characteristics of an acrylic resin joined to SUS XM27 steel. *Oral Sci.* 48, 215–218 (2006).

Flame Treatment of Polymeric Materials: Relevance to Adhesion

L. Mazzola^{1,*} and A. Cusma²

¹CIRA – Italian Aerospace Research Centre, Capua, Italy

²National Research Council of Italy, Department of Chemistry and Materials Technology,
Rome, Italy

Abstract

Flame treatment was initially developed in the 1950s to improve the adhesion properties of polyolefin films. Flame treatment typically creates oxidized species on the surface of films, by the formation of hydroxyl, carboxyl and carbonyl functionalities. Treatment (oxidation) depth varies with the substrate type, as does the generation of low molecular weight oxidized material at the surface.

Surface exposure to flame treatment directly modifies the electron distributions and densities of molecules, resulting in oxidation at the polymer surface up to several nanometers deep.

This review aims to provide a summary of developments regarding flame treatment as a valuable technique for improving the surface properties of polymers. In particular, in the first part special focus is on the combustion process and the main process parameters of flame treatments. In the second part, effects due to flame activation processes on polymers are discussed from different points of view (chemical, physical, morphological).

Although the flame treatment represents the oldest activation treatment, the optimization of process parameters and the changes in chemistry and morphology of the polymeric materials were investigated in detail only recently.

Keywords: Flame treatment, oxidation, wettability, surface free energy, surface activation, polypropylene, polyethylene

*Corresponding author: l.mazzola@cira.it

12.1 Introduction

Polymers usually do not possess the surface properties necessary for their successful applications in fields requiring adhesion (of coatings, paints and varnishes), printability, biocompatibility. Such surface properties depend on very short-range forces so only chemical groups close to the surface are involved. Thus, new functional groups must be created to enhance the surface properties, and surface treatments have proved to be very effective in providing new functional groups.

Numerous techniques have been developed to modify the surface properties of polymeric materials in order to yield valuable finished products. Examples of such techniques include plasma, chemical, corona, flame, and ion implantation treatments [1–13]. These techniques affect only the chemical and physical properties of the outermost surface layer depending on the type of treatment and treatment conditions and thus, they do not alter the bulk properties [9–14]. It is well known that plasma treatment has become increasingly important in the last 20 years and it is possible to treat even substrates with complex shapes. The different high energy species present in the plasmas (both low-pressure and atmospheric pressure) induce the formation of free radicals in the polymer chains and this permits the formation of certain polar functional groups on the polymeric surface which enhance the surface adhesion. In addition, the treatment is fast, clean, environmentally safe, uniform and precisely controllable [8,15–24]. On the other hand, clear disadvantages of the plasma treatment include the fact that it is a complex process and that the adjustment of the plasma discharge parameters is a complicated task [9,10,18]. Moreover, changes in the surface chemistry obtained by plasma treatment are not permanent and this may affect industrial applications [22].

In the last 50 years, corona discharges and flames have been the most widely used industrial pre-treatment methods for polymer films. Corona discharge treatment is generally used for the pre-treatment of polyolefin films, whereas flame treatment is used for thicker components. Corona discharge treatment produces significant changes in the surface topography of polymers, and a flame is probably the oldest type of plasma known to mankind. Compared with corona, a flame treatment offers a number of practical advantages, including the ability to achieve extensive surface oxidation and excellent wettability at extremely short processing times. In addition, this method does not generate toxic corrosive ozone and displays no significant loss of treatment upon aging [24]. Though a straightforward set-up is required for this technique, a certain craftsmanship is still needed to obtain consistent results [25].

Currently, flame treatment is receiving a renewed industrial interest as a technique for modifying films because of major improvements in its safety, reliability and ease of operation [26]. An in-depth understanding and a close look at the physical and chemical properties of flame treated polymer surfaces are required to gain an understanding and be able to optimize the process [27].

12.2 Flame Treatment Equipment

Although conceptually similar, flame treaters show obvious differences depending on whether the sample to be treated has a two or three-dimensional geometry. In both cases, the main components of a flame treatment equipment are:

- The premixing chamber, in which fuel and oxidant are mixed;
- The burner, from which the flame starts and which should produce a suitable flame for treating the surface;
- The holder, which supports the plastic component to be treated.

Many different configurations have been developed in order to accommodate the different materials and shapes to be treated (webs, films, sheets, 3D complex shapes). In Figures 12.1 to 12.4 some of the main configurations are shown:



Figure 12.1 Flame treatment equipment developed to activate webs or polymeric films. The common configuration for this type of activation is roll to roll.

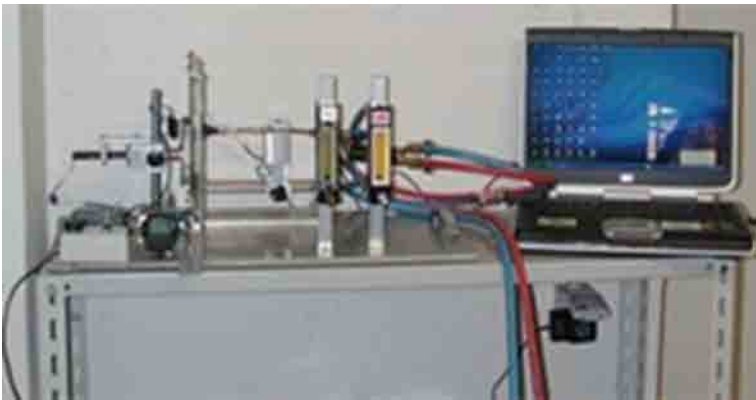


Figure 12.2 Flame treatment equipment for laboratory testing.

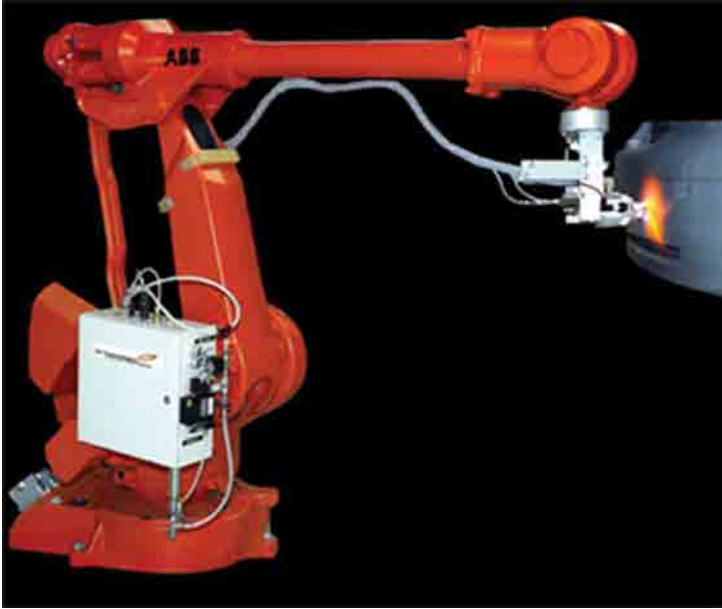


Figure 12.3 Flame treatment equipment for 3D plastic parts. The gas burner is mounted on the end of a robot arm.



Figure 12.4 Flame treatment equipment able to activate 2D plastic parts. The components slide under the flame and only one side of the component is surface activated.

Certainly, the core of a typical flaming system is the burner. Nowadays, burners are complex parts affecting strongly the outcome of the whole process. Despite the wide range of burners available on the market, a common feature is the system that delivers the gas/air mixture to the burner nozzle (head) by exploiting the still valid principles developed by Venturi and Bunsen. Such a system, generally known as Venturi mixer, is located a few meters upstream of the burner.

Burners fall into two main groups:

1. Atmospheric burners take part of the air necessary to generate the premixed fuel/air laminar flame from the surrounding atmosphere, which is at atmospheric pressure. This is because the gas entering the orifice at the base of the mixing tube is at a low pressure (only a few centimeters of water column), providing only approximately 50% of the required air for the combustion. Consequently, the remainder is drawn from the environment around the nozzle, where the air is usually conveyed through openings near the burner. An example of atmospheric air burner is the Bunsen burner.
2. Power burners provide a powerful source of combustion air, making it possible to achieve higher energy output compared with atmospheric burners. In an attempt to fulfill different requirements, different burners have been designed and developed over time, and a large variety of configurations are currently available. Gun-type nozzles were developed for flame treatment of three-dimensional objects, where part of the gas/air mixture is directed into small holes at a speed that is gradually reduced until continuous ignition is provided to the main gas/air flux coming out of the central orifice. This makes it possible to increase the velocity of the laminar flame coming out of the head of the burner, thereby achieving the targeted heat output.

12.2.1 Process Parameters

12.2.1.1 Combustion Conditions – Air/Gas Ratio

Flame treatment requires a slightly air-rich flame that uses all the combustibles in the combustion process. An excess of oxygen is crucial to activate the surface of the substrate.

The molar ratio of the fuel to the oxidizer is probably the most important parameter in the flame treatment process. For this reason, particular care must be paid to setting it properly before the flame treatment is started. For each gas there is a specific and well-defined amount of oxidizer mass at which the fuel is completely burnt. This precise ratio is known as the stoichiometric ratio, which depends on the chemical structure of the gas. For example, the stoichiometric ratio for methane/air is equal to 1:17.2, whereas for a propane/air flame it is 1:15.5. However, in practical applications it is unlikely to obtain the exact stoichiometric ratio. Most commonly, the flame obtained will have a ratio that is below or above this value.

Therefore, the concept of the equivalence ratio (Φ), defined as the actual gas/air ratio used during treatment divided the stoichiometric fuel-to-oxidizer ratio [28], is widely accepted:

$$\phi = \frac{\frac{m_{\text{fuel}}}{m_{\text{oxidizer}}}}{\left(\frac{m_{\text{fuel}}}{m_{\text{oxidizer}}}\right)_{\text{stoichiometric}}}$$

Another common parameter is the reciprocal of the equivalence ratio, which is called “lambda factor”:

$$l = \phi^{-1}$$

As a consequence, oxidizing flames will have $\phi < 1$ and fuel-rich flames $f > 1$ (and the opposite applies if one refers to the l factor). Both l and f will be equal at the stoichiometric ratio.

12.2.1.2 Flame Energy

The latest technological innovations in the flame treatment field are refining the way that the flame is produced, both optimizing the flame control and the overall gas consumption in the system. Most recent combustion generators are equipped with all the controls needed, including oxygen analyzers, flowmeters and regulators. They also have burner position controls to ensure an accurate positioning of the flame with respect to the component to be treated and thus the burner output is optimized.

12.2.1.3 Burner to Substrate Gap

There is an optimum area just off the inner cones of the flame that must come into contact with the substrate. This is known as the active zone of the flame. Different flame profiles can be used which are tailored to the different substrates.

The flame size is modulated in accordance with the line speed in order to avoid over-treatment and overheating of the substrate.

12.2.1.4 System Layout

Depending on the production requirements, the flame treatment systems can be used in a single or double burner configuration.

12.2.1.5 Valve Train

In order to maintain an accurate control of the flame, the gas valve train is automatically controlled and monitored by an integral programmable logic controller (PLC). The flame energy is modulated via either the speed of the combustion fan on a single burner system or by a “capacity valve” on a double burner unit. The flame energy is automatically tuned to give the optimum treatment for any given line speed. A crucial part of the mixture generator is the oxygen analyser. This allows automatic monitoring of the air/gas ratio of the flame.

The signal from this unit is used to fine-tune the gas supply to the flame: this ensures that the same flame condition is maintained and even if the composition of the gas changes, as it often happens, the treatment is not affected. The oxygen analyzer measures directly the composition of the flame and the concentration of the oxygen, which cannot be achieved using flowmeters. Flowmeters are installed in the system with the aim to monitor the gas flow in the burners.

12.2.1.6 Control Instrumentation

Digital controls allow to easily operate a flame treatment equipment. Flame controls such as the oxygen analyzer are also integrated with PLC.

12.2.1.7 Gas Saving

All the above controls have been designed with the main aim to optimize the adhesion property of the treated substrates, which is the main reason to perform a flame treatment. However, the controls also have the great benefit of reducing gas consumption. Automatic flame controllers, burner positioning relative to web and the use of the oxygen analyzer all reduce the gas consumption to a minimum.

12.2.2 Flame Chemistry

Farris *et al.* [28] describe in detail the complexity of the combustion process. Combustion is a complex process involving many chemical reactions between a fuel (generally a hydrocarbon) and an oxidant (e.g., the oxygen in the air) with the production of heat and (although not always) light, in the form of a flame. Migration of chemical species within the flame results in a subsonic wave (40–45 cm s⁻¹ in air/hydrocarbon systems) supported by combustion [29]. Although a huge variety of chemical reactions take place during combustion, leading to many active radical species, it is generally acknowledged that the overall process can be summarized in few main steps, as schematically displayed in Figure 12.5.

Flame treaters ordinarily employ a laminar flame which is defined as a mixture of a fuel and an oxidiser, thoroughly premixed before combustion. The term "premixed laminar flame" is interchangeable with the term "deflagration" to indicate the propagation of the combustion process accompanied by a decrease in both density and pressure together with an increase in velocity (contrary to the propagation known as "detonation"). Within a laminar flame profile, three main zones can be observed (Figure 12.6), which lead to specific reactions.

As a consequence, different thermal gradients and reactive species can be achieved.

12.2.2.1 Pre-reaction Zone

This region, also called the 'dark zone', has a typical dark bluish colour. It is the coldest region of a flame because even though some of the hydrogen formed is oxidised to water, the combustion process has not yet reached the explosion condition, and thereby the amount

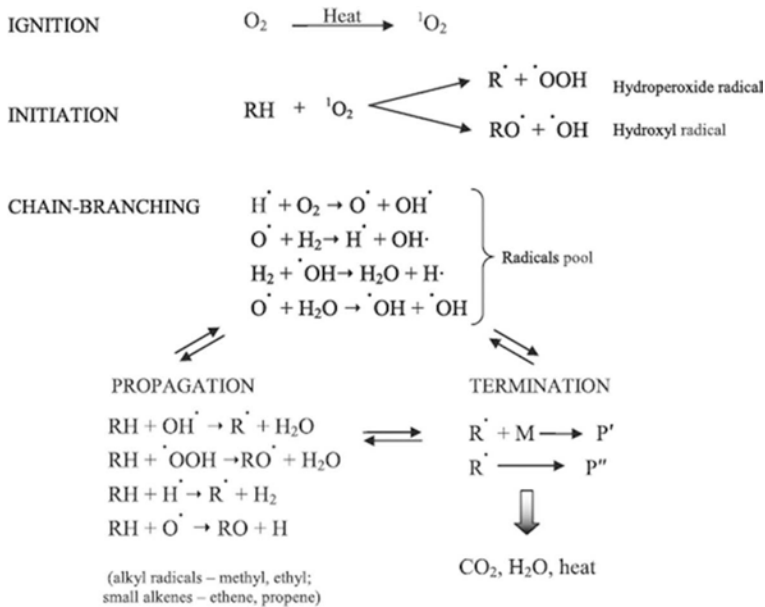


Figure 12.5 Overview of the combustion process.

of net energy released is negligible. In this zone, the free radicals are mainly composed of hydrogen atoms, which quickly react with hydrocarbons and oxygen, thereby avoiding the formation of the radical pool. For this reason, this zone is also known as the 'reducing zone'. This is an ineffective and not important region for surface activation purposes, since in no way it contributes to the oxidation of the plastic substrate.

12.2.2.2 Main Reaction Zone

Also called the 'luminous zone', this zone is characterized by the highest temperature of the combustion system (for propane-based mixtures the temperature reaches 1900–2000°C). In this zone, radical content increases dramatically to the detriment of the reactant concentration. The high concentration of the radical species makes this region strongly oxidizing, in contrast to the reducing zone mentioned above. Such an oxidizing region is valuable for an effective flame treatment of polyolefins. The color of this zone depends on the fuel/air ratio: a deep bluish violet radiation, with the flame becoming almost transparent if the quantity of gas is increasingly reduced, is produced when the mixture is gas-lean (due to excited CH radicals); conversely, a green radiation appears when the mixture is gas-rich. The observation of the colour of the flame is an empirical tool widely used by operators in order to maintain the right mixture composition throughout the process.

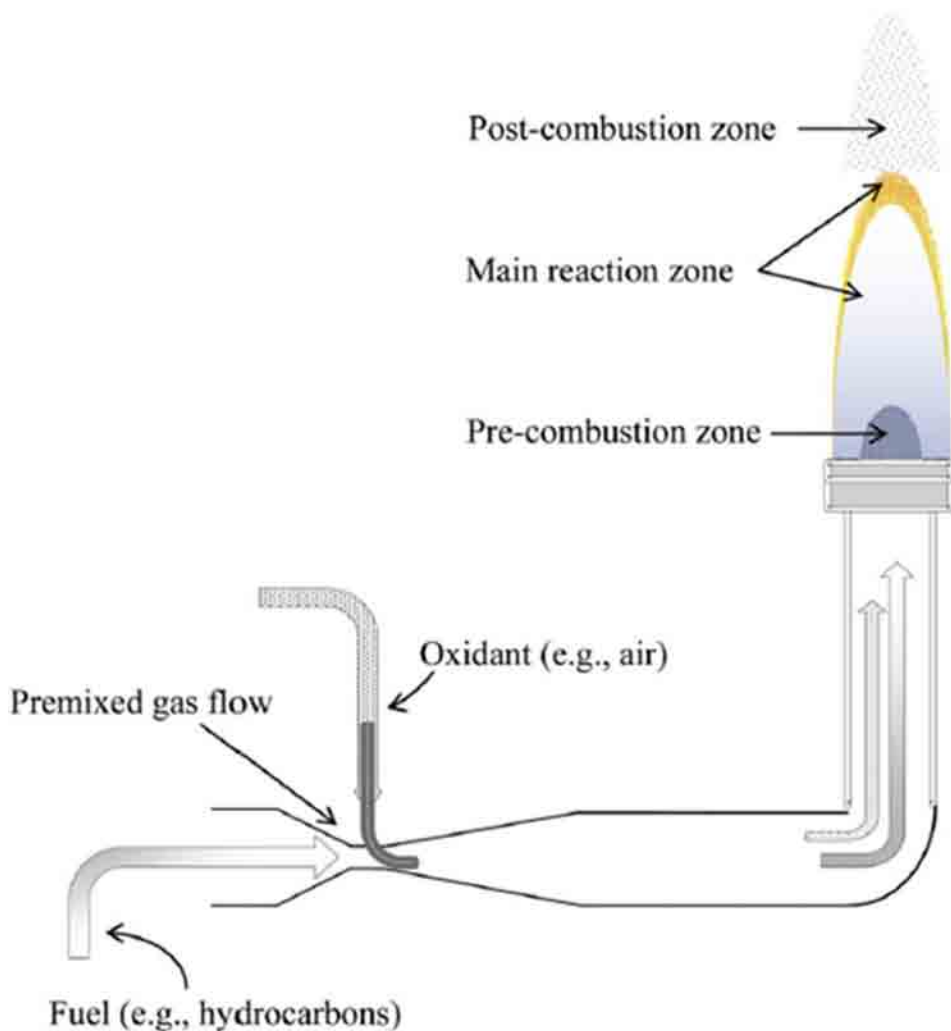


Figure 12.6 Main zones in a laminar flame profile.

12.2.2.3 Post-combustion Zone

This is the largest of the three regions found in a typical laminar flame profile. The temperature here remains high due to the exothermic oxidation reaction (partial or complete) of CO into CO_2 , with a release of heat. Although intermediate species such as CH_3 , C_2H_2 , and CH_2O are typical in the luminous region, radicals such as H^\cdot , OH^\cdot , and O^\cdot can also be

detected in the post-combustion zone [30]. Generally speaking, the concentration of radicals in a laminar flame profile amounts to approximately 10^{-3} times the concentration of the reactants, whereas ion species (among which the H_3O^+ is the most abundant) are definitely less (10^{-6} relative to the reactants). Normally, ion species exist slightly beyond the luminous portion of the flame [24].

The presence of a profile of compositional differences over a laminar flame can be explained in terms of the convective flows of unburned gases from the dark zone to the luminous zone and the diffusion of radical species from the high temperature zone to the pre-heating region i.e., in the opposite direction to the convective flow.

In particular, the diffusion of radical species is due to the presence of hydrogen atoms, which do not participate in the chain branching step because of the lower temperature in the dark region. Instead, H atoms combine with oxygen radicals in the pre-heating zone to yield a large amount of HOO^{\cdot} radicals. These form hydrogen peroxide (H_2O_2), which does not dissociate because of the low temperature in the dark zone. H_2O_2 is then conveyed to the luminous zone by convective flows, where the high temperature conditions make the formation of OH^{\cdot} radicals possible. This explains the high concentration of OH^{\cdot} radicals relative to O^{\cdot} and H^{\cdot} in the early part of the luminous zone and the very high temperature reached there, with the OH^{\cdot} radicals forming reaction being highly exothermic ($\approx 85 \text{ kcal mol}^{-1}$). In addition, it explains why the OH^{\cdot} attack on the fuel is the primary route for fuel degradation. Finally, it is worth noting that combustion processes are never complete. In the combustion of hydrocarbons, both unburned carbon and carbon compounds (such as CO and others) are always present. In addition, when air is the oxidant, like in a typical flame treater plant, some nitrogen can be oxidized to various nitrogen oxides (NOx) [31].

12.3 Effects of Flame Treatment on Plastics

12.3.1 Flame Treatment of Polypropylene

Polypropylene (PP) films generally require some kind of surface modification before they can be used, with the aim to improve their wetting and adhesion properties.

A large number of polypropylene grades are available, each specifically developed for a specific need and intensively tested for each specific application. The starting ingredient may be Polypropylene (PP) homopolymer or copolymer and Polyethylene (PE) and Ethylene propylene rubber (EPR). A number of additives which might be used for the processing and for the application are, for example, heat stabilizers, release agents, antistatics and UV stabilizers. Several fillers may be used, such as glass fibers, lime, talc, carbon black, pigments. Different PP grades have their specific properties such as E-modulus, Izod strength, density, etc...

Due to the complexity of the PP grades, the surface composition might be influenced in each step of the production process, from injection molding condition to flame treatment and painting. It will be clear that controlling the surface composition and modification process of PP grades is essential in the production process where good adhesion is required [32].

Most commonly, surface oxidation techniques are used to improve wetting and adhesion properties of PP films.

Strobel *et al.* [26] have compared the two most commonly used industrial surface oxidation techniques on polypropylene films. In their study, the authors used atomic force microscopy (AFM), X-ray photoelectron spectroscopy (XPS or ESCA), and contact angle measurements to investigate the surface properties of PP modified by corona and flame processes.

AFM analysis was used to directly examine the surface topography of flame-treated PP and it was found that flame treatment creates a “nodular” surface topography that is caused by the oxidation of the PP rather than by any heating of the PP surface that might occur in the flame. The surface topography, wettability, and extent of oxidation of flame-treated PP were not affected by washing with any type of solvent, so it was supposed that no water-soluble low-molecular-weight oxidized material was formed. The authors concluded that the nodular topography of flame-treated PP was formed by the agglomeration and rearrangement of intermediate-molecular-weight oxidized products.

Compared to plasma treated polymers, the flame treated films were not affected by water washing and their wettability and O/C ratio do not change when materials are washed in water, as shown in Table 12.1, in which the surface properties of a number of corona- and flame-treated PP films are reported. The corona and flame treatment conditions were varied to generate a series of PP samples with varying levels of oxidation. The most interesting difference between the two types of treated surfaces is the effect of water washing. In the case of flame-treated PP, washing with water has no effect on the wettability or on the O/C atomic ratio.

Figure 12.7 is a representative AFM image of flame-treated PP having an XPS O/C atomic ratio of 0.18. Flame treatment alters the fibrils by forming small nodules, which have the appearance of a “bead-like” structure. This structure is much less distinct and is of larger characteristic dimensions than the fibrils of the untreated PP. The characteristic size of the nodules is in the sub-micrometer range. The formation of the bead-like structure is not a result of surface heating but is directly associated with the oxidation of the PP by the flame. The nodular topography of the flame-treated materials used in this study is neither removed nor visibly altered by vigorous extraction with water, methanol, acetone, or xylene. The combined contact angle, XPS, and AFM results showed that no water-soluble material was formed on PP as a result of exposure to the flames.

As for the stability, long-term aging of flame treated PP does not cause a significant loss in wettability or in the extent of oxidation. Only the receding contact angle of water decreases over a 180-day period, and this by only 3%. In contrast, corona-treated PP exhibited more significant changes upon aging. The authors concluded that while both treated surfaces are quite stable, flame-treated PP is definitely more stable than corona-treated PP.

Pijpers and Meier [32] showed by XPS the changes in the surface chemistry of PP, with varying flame process parameters. In particular they studied the oxygen concentration of the PP surface because oxygen concentration is an important parameter to promote adhesion of paints and varnishes. In particular, H-bonding through enolic –OH is involved in adhesion. The presence of enolic –OH enhances auto-adhesion as well as ink adhesion to

Table 12.1 Surface properties of modified polypropylene films before and after washing with water [32]. Properties were measured within a few hours of surface treatment. θ_a and θ_r are the advancing and receding contact angles of water in air, respectively.

Treatment	XPS O/C atomic ratio		θ_a (°)		θ_r (°)	
	Unwashed	Washed	Unwashed	Washed	Unwashed	Washed
None	0.0	0.0	110	109	83	83
Flame (0.03 s)	0.07	0.07	97	96	41	42
Flame (0.06 s)	0.12	0.12	94	94	29	29
Flame (0.09 s)	0.18	0.18	84	85	21	21
For RH = 2–5%						
Corona (0.17 J/cm ²)	0.07	0.04	93	97	56	58
Corona (1.7 J/cm ²)	0.12	0.06	76	96	51	53
Corona (17 J/cm ²)	0.23	0.08	59	88	35	36
For RH = 95–100%						
Corona (0.17 J/cm ²)	0.08	0.06	91	97	54	54
Corona (1.7 J/cm ²)	0.12	0.07	75	96	50	51
Corona (17 J/cm ²)	0.23	0.09	54	90	31	30

treated PP. The bonding is between the carbonyl group and its enol tautomer across the surface. Keto and/or aldehyde ($-C=O$) groups are essential for auto-adhesion. The minimum requirement is that one surface should contain enol (or potential enol) and the other carbonyl (keto or aldehyde) groups.

The authors analyzed the effect of flame treatment on the surface chemistry of PP and the samples were treated under constant speed and distance but air/propane ratio was varied. The results obtained from XPS measurements of these modified PP samples are shown in Figure 12.8. The total oxygen concentration at the surface of the flame treated samples changes under these treatment conditions and it is plotted as a function of the gas composition (upper curve). Clearly a maximum is observed in this curve.

From practical experience and from adhesion tests, an oxygen concentration of 10–12 at.% is required for an acceptable adhesion behavior. As can be seen, this is obtained in a relatively large air/propane window. This change in oxygen concentration is reported to correlate well with wetting properties (the ASTM wetting test) and with contact angle

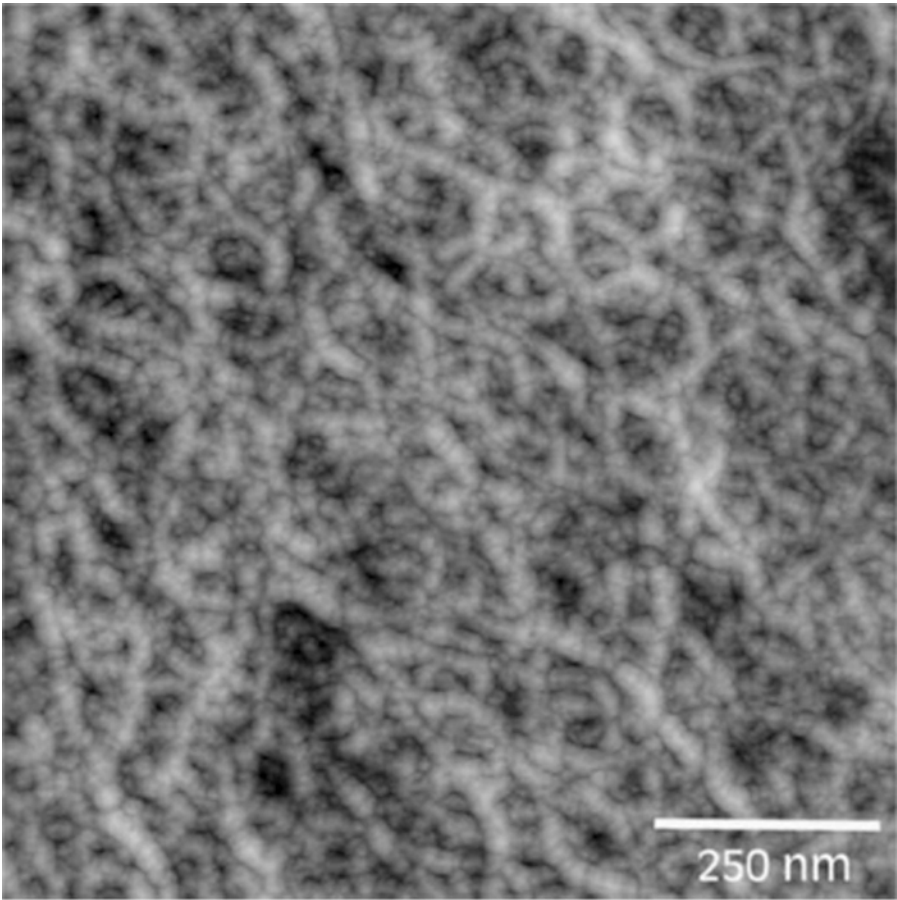


Figure 12.7 Tapping-mode AFM topographic image of a flame treated polypropylene film having an XPS O/C atomic ratio of 0.18. From the darkest to the lightest tone represents 50 nm of height in the z-direction. The mean roughness of this sample is 0.35 nm.

measurements. The maximum oxygen concentration observed was obtained at an air/propane ratio of 24.8.

To obtain information about the influence of the flame distance on the surface modification, PP plates were flame treated under the following conditions: air 229 l/min, propane 9.9 l/min, ratio 23.1, velocity 30 m/min and flame distance varying from 2 to 24 cm. The results obtained are shown in Figure 12.9. The value of about 12 at.% O at a distance of 7 cm is as expected (as seen in Figure 12.8). At an air/propane ratio of 24.8, much higher values for O can be expected.

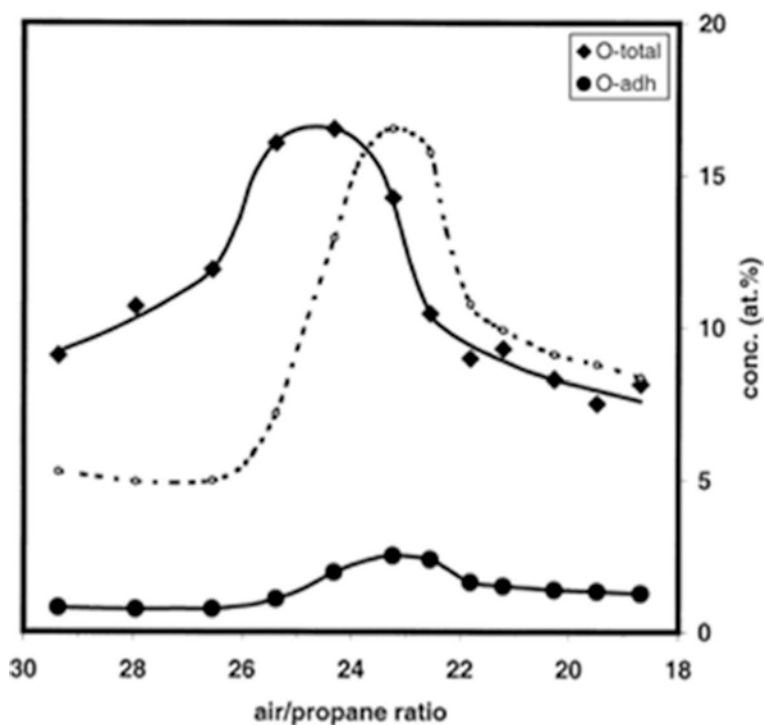


Figure 12.8 XPS results on the determination of the total oxygen concentration (O-total) and enolic oxygen concentration responsible for promoting adhesion (O-adh, from enolic group -OH) on the surface of flame treated PP as a function of the gas composition. The dashed line represents the O-adh concentration scaled to the level of O-total, to emphasize the difference in concentration as a function of the gas composition.

The oxygen concentration remains relatively high in a wide range and it decreases only slowly. This suggests an acceptable adhesion over a broad distance range. In comparison, the observed O-adhesion, related to the enol, and displayed in Figure 12.9, is stable in a much narrower region, i.e. between 4 and 12 cm, which of course is still a relatively broad experimental window. This window is considered as the region in which good adhesion after ageing tests is obtained.

From the experiments, it is clear that the chemical effects of the flame treatment are influenced by gas composition (see Figure 12.8) and by flame distance (see Figure 12.9).

For a stable and fixed flame, changing the conveyor belt speed changes the contact time of the polymer sample and the flame. To obtain information about the influence of the flame contact time on the surface modification and therefore on the adhesion behavior, the PP copolymer plates were flame treated under the following conditions: air 229 l/min, propane 9.9 l/min, ratio 23.1, distance 7 cm and a varying conveyor belt speed from 5 to 55 m/min.

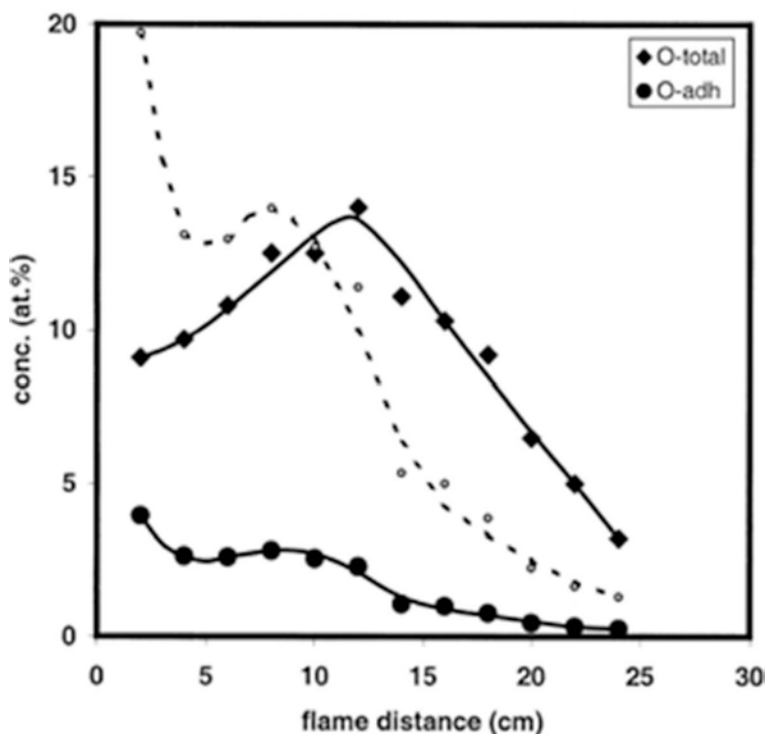


Figure 12.9 XPS results on the determination of the total oxygen concentration (O-total) and the enolic oxygen concentration (O-adh) on the surface of flame treated PP as a function of the flame distance. The dashed line represents the O-adh concentration scaled to the level of O-total to emphasize the difference in concentration as a function of the flame distance.

Figure 12.10 shows the results obtained for the total O concentration and the relative O-adh concentration. The O-total concentration remains relatively high from 10 to 25 m/min and then gradually decreases. The O-adh concentration is stable in the region from about 15 to 35 m/min. The latter values, combined with an estimate of the actual flame dimensions, leads to calculated flame contact times varying from about 50 to 20 ms in which stable results are obtained. Clearly overtreatment occurred at a speed of 5 m/min: the lower limit, for an acceptable treatment, seems to be 10 m/min. At higher speeds, i.e. shorter flame contact times, the O-adh concentration is expected to go down proportionally. The effect of lowering the flame contact times can be observed from 35 m/min on, when a gradual decrease in the O concentration is observed.

The main problem of flame treatment is to identify optimum process parameters in order to attain the best results in terms of improvement of surface free energy. Usually a monovariate analysis is carried out; however, this kind of analysis does not take into account the interaction among factors; consequently, there is a lack of information and thus the results

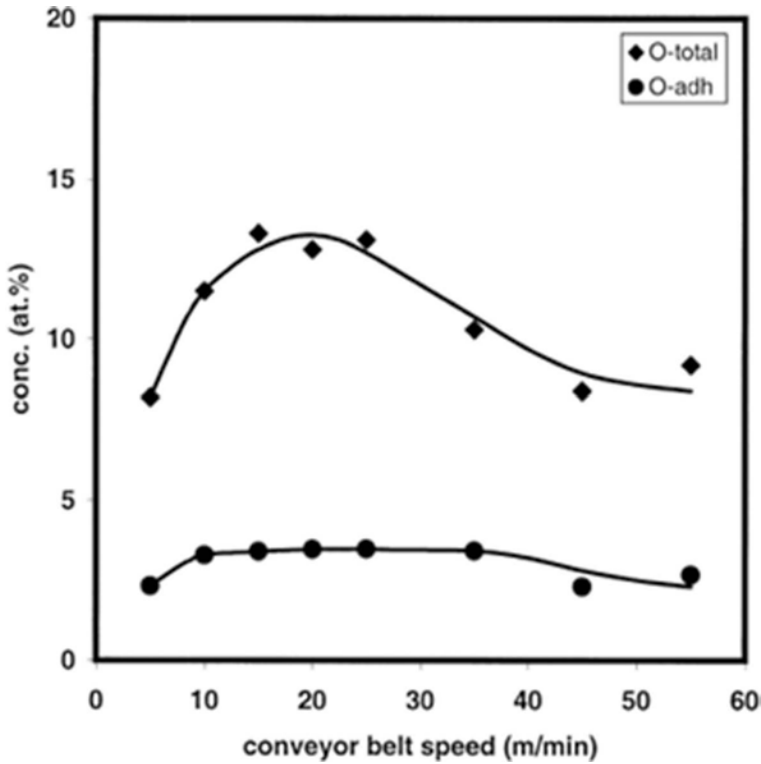


Figure 12.10 The total oxygen concentration (O-total) and the enolic oxygen concentration (O-adh) on the surface of flame treated PP as a function of the conveyor belt speed.

obtained are unsatisfactory. A multivariate analysis represents a useful method to correlate adequately the process parameters with the performance indexes such as the wettability and surface free energy.

Mazzola *et al.* [33] have shown the benefits obtained using this approach. They took into account the main process parameters of flame treatment discussed before and performed a Design of Experiments (DoE) from which a multivariate analysis was carried out. This was addressed to identify an optimal set of process parameters necessary to achieve the above mentioned goal.

In their work, the authors used a flame obtained by propane as fuel and oxygen as oxidant.

In the first step a factorial design is usually used in order to define which process parameters influence the responses. In general, two levels are used for each factor (two-level factorial design). In this case, to overcome the problem due to possible curvatures, the inclusion of a central point in factorial plan 2^k was taken into account. The central point was replicated

four times in order to obtain a robust estimation of the experimental error. In Table 12.2, the levels taken into consideration for each factor (that identify different factorial plans) are summarized. The second step was to use the surface response method (RSM). The RSM was realized including a star point that improves factorial plans. So the factorial plans (surfaces of experiments obtained by the ranges of the process parameters) were enlarged in order to optimize the solution and to understand what the real trend was [34]. In order to improve the reliability of the model with respect to factorial design, all points are repeated twice and the central point for the seventh time.

The experimental results were examined by the ANalysis Of VAriance (ANOVA) to estimate the significance of the principal effects and interactions of the operating factors.

Tables 12.3 and 12.4 report the ANOVA results and regression information about surface free energy, using the response surface method; also in this case, the significance of the main factors and their interactions are assessed by the F-test method. The model obtained fits more than 70% of the experimental data; the analysis of variance highlights the fact that the response is influenced by linear effect, interaction effect and quadratic effect; in particular from regression information, it results that the estimate response is due in order of importance to the following parameters: distance, distance \times O/C ratio, distance \times distance, speed. This was obtained with a risk level 0.02.

In Figure 12.11 four possible response surfaces relative to four possible combinations of factors are shown. The reported three-dimensional surface is the most useful approach in terms of visualization of the response (in this case SFE) because it shows the simultaneous dependence on two out of four most significant parameters which affect the surface free energy value. The statistical model used to predict SFE is valid over the large range investigated.

Through this approach it is possible to develop a model which correlates the variation of surface free energy with the main process parameters that influence the flame treatment process.

In fact from the regression analysis results (Table 12.4) it is possible to make an SFE quantitative statistical model, in which only the significant factors are taken into account. Below the two empirical-statistical models of surface free energy (SFE) and the polar component are reported:

$$\text{SFE}_{\text{total}} = 40.7229 - (1.974 \times \text{distance}) - (1.3581 \times \text{speed}) - (2.0259 \times \text{distance} \times \text{O/C ratio}) + (1.607 \times \text{distance})^2$$

$$\text{SFE}_{\text{polar component}} = 2.4329 - (1.9656 \times \text{distance}) - (1.5509 \times \text{distance} \times \text{O/C ratio}) + (1.2967 \times \text{distance})^2$$

In all of these equations, the presence of a curvature (or interaction amongst factors) is evident. This confirms that the multivariate analysis represents the best method to optimize the flame treatment process.

Knowing the evolution on 3D space of process parameters versus the main performance indexes, it is possible to identify also the best process parameters that maximize the responses (Figure 12.12).

Table 12.2 Operating conditions of the factorial design: Investigated factors, levels and central point.

Factor ID	Investigated factors	Low level “_”	Low level “+”	Central point
A	Distance [mm]	115	205	160
B	Time [s]	7	17	12
C	Speed [rpm]	130	310	220
D	O/C ratio	4	6	5

Table 12.3 Analysis Of Variance of surface free energy in the Response Surface Method. It is possible to evaluate the interaction effects and quadratic effects in addition to linear effects.

Source of variation	Degrees of freedom	Sum of squares [partial]	Mean squares [partial]	F ratio	P value
Model	14	618.716	44.194		
Linear effects	4	283.485	70.8713	8.9254	3.00E-05
Interaction effects	6	192.685	32.1141	4.0444	0.0029
Quadratic effects	4	142.546	35.6365	4488	0.0043
Residual	40	317.616	7.9404		
Lack or fit	10	23.215	23.2151	8149	3.41E-06
Pure error	30	85.465	2.8488		
Total	54	936.332			

Once parameters range limits are imposed, by means of a DoE software, it is possible to calculate the maximum values of surface free energy and its polar part, using the models developed.

The optimal solution for these two responses is shown in Figure 12.12, in particular the maximum values predicted are $\gamma_{\text{tot}} = 58.9 \text{ mJ/m}^2$, $\gamma_{\text{pol}} = 17.5 \text{ mJ/m}^2$, when the optimal process parameters are flame distance = 87mm, speed sample = 125 rpm (revolution per minute), time = 17 s, O/C ratio = 6.5. Before checking the theoretical maximum values of SFE and its polar part, the SFE value and polar component of an untreated PP sample were determined; the experimental result of SFE (39.75 mJ/m^2) is in accord with the literature values ($35\text{--}40 \text{ mJ/m}^2$); the variation of SFE is due to many factors, such as environmental conditions (temperature, moisture) under which tests are conducted or different roughnesses of samples.

Table 12.4 Regression information on surface free energy in the Response Surface Method. The combination is evident amongst the factors (i.e. the combination AD = distance \times O/C ratio).

Term	Coefficient	Standard error	Low CI	High CI	T value	P value
Intercept	40.7229	1.0651	38.142	43.3038	38.2354	0
A: distance	-1.974	0.4067	-2.9596	-0.9884	-4.8533	1.89E-05
B: time	-0.2185	0.4067	-1.2041	0.7671	-0.5373	0.594
C: speed	-1.3581	0.4067	-2.3437	-0.3275	-3.3392	0.0018
D: O/C ratio	0.3423	0.4067	-0.6433	1.3279	0.8416	0.405
AB	-0.6241	0.4981	-1.8312	0.583	-1.2528	0.2176
AC	0.5972	0.4981	-0.6099	1.8043	1.1988	0.2376
AD	-2.0259	0.4981	-3.233	-0.8188	-4.0671	0.0002
BC	-0.8684	0.4981	-2.0755	0.3387	-1.7434	0.0889
BD	0.5772	0.4981	-0.6299	1.7843	1.1587	0.2534
CD	-0.2891	0.4981	-1.4962	0.918	-0.5803	0.565
AA	1.607	0.4175	0.5954	2.6187	3.8494	0.0004
BB	-0.0917	0.4175	-1.1034	0.92	-0.2197	0.8273
CC	-0.0673	0.4175	-1.079	0.9443	-0.1613	0.8727
DD	0.1314	0.4175	-0.8802	1.1431	0.3148	0.7546

In order to verify the predicted maximum values of SFE and its polar part, the contact angle measurements were performed on treated samples (activated through optimized process parameters). The results are summarized in Table 12.5: the percentage errors between the predicted value and the observed value is less than 2% in the case of SFE, less than 1% in its polar part.

Using optimized process parameters, flame treatment improved the SFE more than 48% with respect to the untreated sample of PP; in addition the SFE polar component of the flame treated sample increased about 20 times with respect to the untreated sample (from 0.76 mJ/m² to 17.55 mJ/m²).

The improvement in polarity was confirmed also by XPS analysis, which showed an increase in single-bonded carbon (alcohol and/or ether group). In addition, in the treated sample (Figure 12.13b) two new components are present at high binding energies; in particular at 287.97 eV double-bonded carbons (carbonyl groups C=O) and at 289.52 eV carboxyl groups O=C=O are present. These data are summarized in Table 12.6. The optimization of the flame process parameters is also supported by an increase of more than 14% in oxygen concentration than the O concentration reported by Pijpers and Meier [32]. The XPS results corroborate the increase in polarity, shown also through contact angle measurements and SFE value. In fact, it has been demonstrated [35, 36] that the polar functional group (in

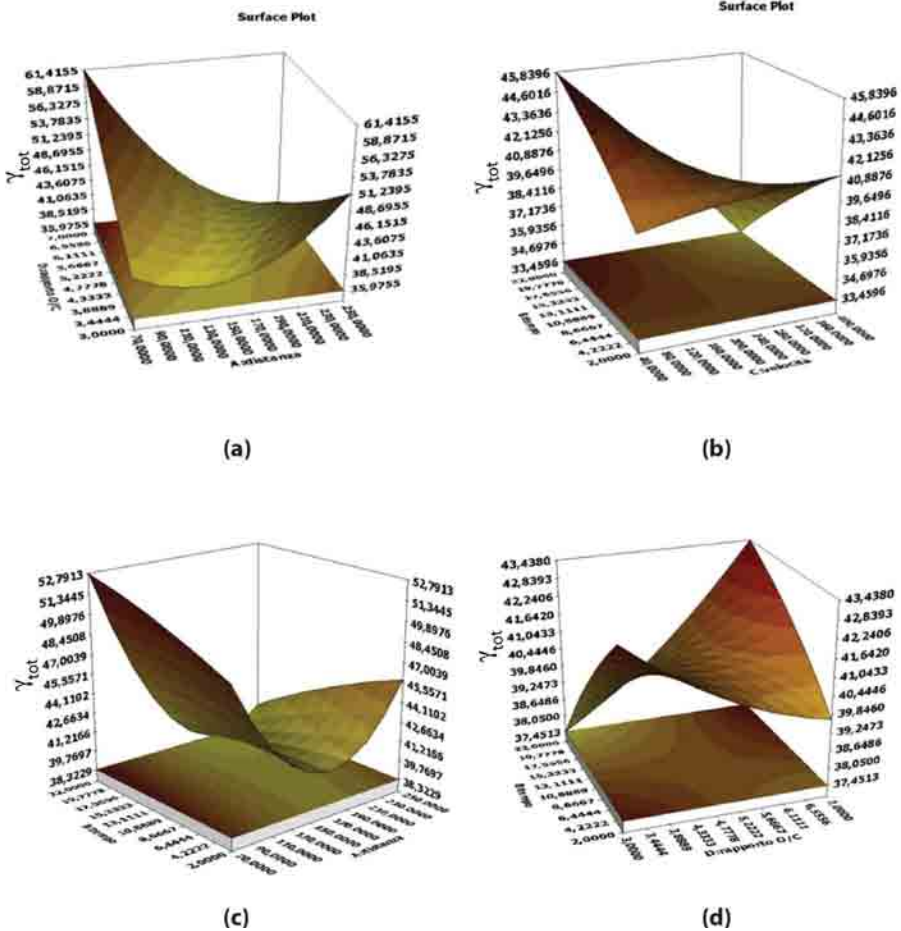


Figure 12.11 Surface free energy (SFE) as function of distance and O/C ratio (a), speed and distance (b), time and distance (c) and time and O/C ratio (d).

particular C=O) significantly increases surface free energy. The C=O bond, which has the largest dipole moment (2.3–2.7 D), is the most effective in increasing the SFE.

The main problem with this type of treatment is to know the exact treatment depth of the material involved in flame treatment process.

The authors [33] used a Focused Ion Beam (FIB) and Transmission Electron Microscopy to determine the exact depth of the polymeric material affected by flame treatment.

At the beginning, FIB analysis was carried out in order to observe the topography changes of flame treated sample versus the untreated one. As a matter of fact, the untreated sample has a rougher surface than the treated one. The surface of the treated sample appears melted and somewhat smoother and exhibits round-shaped features. It is known that wettability is

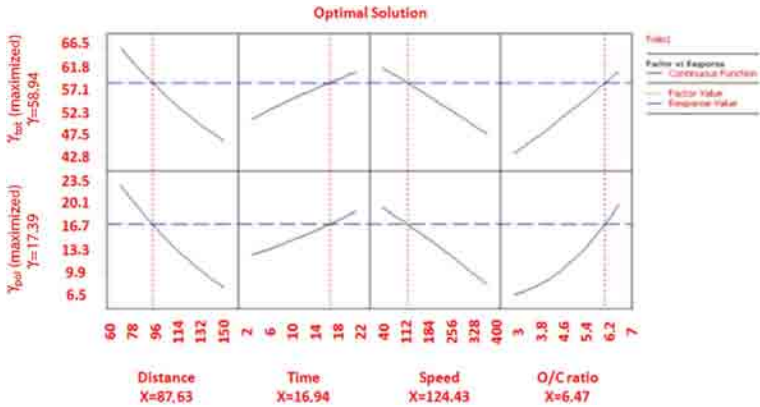


Figure 12.12 Best responses (surface free energy and its polar component) as a function of optimal process parameters of flame treatment. Horizontal dotted line indicates the best solution of the model, vertical dotted lines identify the optimal process parameters

Table 12.5 Surface free energy (γ_{tot}) and polar component of SFE (γ_{pol}) results of untreated PP sample and predicted empirical-statistical model value and observed experimental value for treated sample.

	γ_{tot} [mJ/m ²]	γ_{pol} [mJ/m ²]
Untreated	39.75	0.76
Predicted value	58.9	17.5
Observed value	58.16	17.55

improved for smoother surfaces and this is confirmed by the contact angle results, shown previously.

Cross sections of both treated and untreated PP samples were examined by FIB up to a depth of 17 μm (beneath the surface). The treated sample (Figure 12.14c) exhibited a porous region of 6.5 μm in depth with respect to the untreated sample (Figure 12.14a); this is the region affected by the flame treatment, where the gas bubbles are trapped within the polymer. In this zone, during exposure to the flame, the polypropylene is melted and the polymeric chains are free to move. The gas produced by the flame remains within the polymer when it hardens. Magnified picture of the treated sample near the surface shows a narrow region of about 300–450 nm, which represents the effective activated zone (Figure 12.14d), in the untreated sample such a zone was not present (Figure 12.14b).

A further TEM characterization of this oxidized zone shows a detailed structure of the activated zone: the real oxidized zone of 290 nm thickness near the surface, a small transition zone of 130 nm thickness in which the diffusion effect is present (diffusion zone) and the remaining zone where the material stays unoxidized.

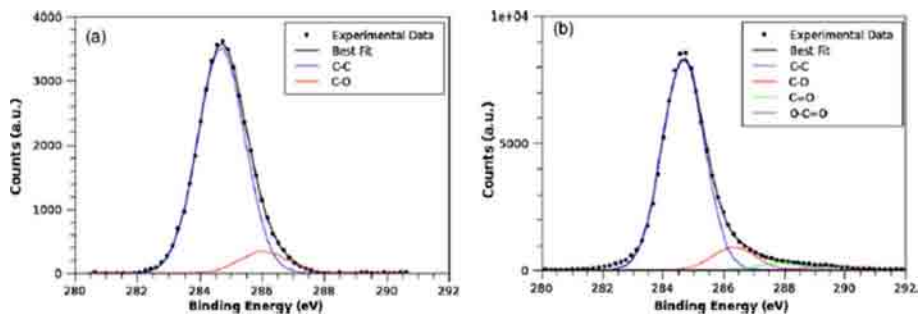


Figure 12.13 XPS C 1s peaks of untreated (a) and treated PP samples (b).

Table 12.6 Quantitative XPS results on untreated and treated PP samples. Note the increase in O-radicals in treated sample.

Sample	Signal	BE (eV)	Assignment	%
Untreated	C 1s	284.7	C-C	91.2
		286.05	C-O	8.8
		284.7	C-C	77.5
Treated	C 1s	286.34	C-O	14.9
		287.97	C=O	5
		289.52	O-C=O	2.6

Note that the unoxidized bulk polymer (Figure 12.15b) is formed of amorphous domains (macromolecular chains that are disordered), as a matter of fact lamellar or spherulitic crystals are absent. There are fewer amorphous domains in the diffusion zone and they completely disappear in the oxidized zone.

Energy Dispersive Spectroscopy (EDS) was performed for a semi-quantitative analysis of the elements in three zones A, B, and C (Figure 12.15); results showed an increase in oxygen from bulk to surface: 13 wt.% in the unoxidized zone, 85 wt.% in the diffusion zone and 93 wt.% in the oxidized zone. On the contrary, the wt.% of carbon decreased from the oxidized zone to the surface (Table 12.7).

Finally, a selected area electron diffraction (SAED) was performed on oxidized and unoxidized locations and, as shown in the insets of Figure 12.15a and b, both are in the amorphous phase; this corroborated the absence of periodic, ordered, and oriented structures in Figure 12.15.

The PP treated by the flame is subjected to a non-uniform environment, because of the conical shape of the flame. This translates into a non-uniform wettability property of the film.

The influence of the treatment conditions on the spatial non-uniformity of the film as well as the quantification of such non-uniformity have been performed by Park and co-authors [37].

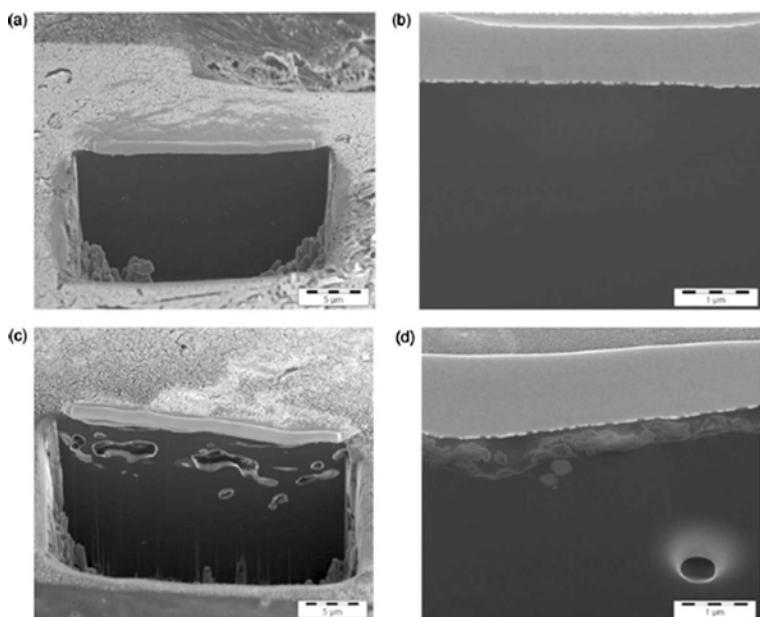


Figure 12.14 FIB cross sections of an untreated PP sample (8000x, (a) and 50000x (b)) and a treated PP sample (8000x (c) and 50000x (d)).

Park and co-authors [37] used contact angle measurements, XPS and AFM to characterize the films after flame treatment under several conditions. They used the Wilhelmy plate technique to obtain force and contact angle data as a function of position on the PP film. This type of information allows to identify and quantify non-uniformity in the wetting property of the flame-treated film, as a function of position. The force on the film is given by the Wilhelmy equation:

$$F(x) = \frac{\gamma P}{g} \cos \theta(x) + bx$$

in which $F(x)$ is the total measured force, g is the measured surface tension of water, P is the measured perimeter of the sample, g is gravitational acceleration, $q(x)$ is the contact angle, b is the buoyancy factor, and x is the position of the sample in the water [37].

The authors [37] prepared a PP laminate consisting of a flame-treated surface on one of the outward-facing sides of the laminate and an untreated surface on the other outward-facing side which allowed them to isolate the surface of interest, which they refer to as “dissimilar laminate”. The dissimilar laminate was prepared so that the lanes on the flame-treated surface were parallel to the surface of the water. This is critical because as the sample is lowered into the water, the lanes need to be aligned to accurately measure the variation

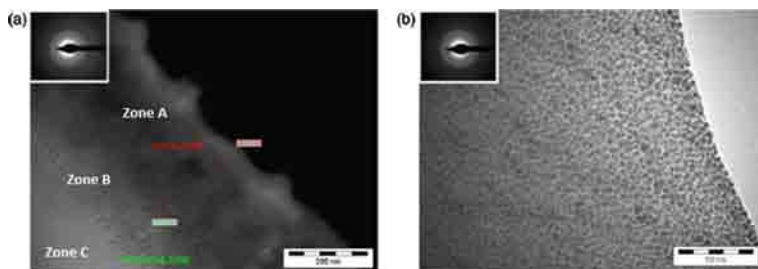


Figure 12.15 TEM micrographs of oxidized PP layer (a) and polymeric bulk (b).

Table 12.7 EDS semiquantitative analysis on TEM lamella of treated PP sample (EDS parameters: count = 3,000, nanoprobe 10 nm, 80 kV).

Element	wt. %	at. %
Zone A		
C K	93	94.6
O K	7	5.4
Total	100	100
Zone B		
C K	85.4	88.6
O K	14.6	11.4
Total	100	100
Zone C		
C K	13	16.6
O K	87	83.4
Total	100	100

in wettability. When the data of Figure 12.16, which shows the Wilhelmy force traces for untreated and treated dissimilar laminates, are examined closely, the periodic variations in the force as a function of position in both the advancing and receding modes are apparent. This type of variation, which is a result of the flame treatment process, is not present in untreated PP. Having previously calculated the force contribution from the untreated side of the laminate, it was possible to subtract this force from the total force and correct for buoyancy.

This calculation gives the force on the flame-treated surface only, as a function of position in water. Figure 12.17 shows the advancing-cycle force for the flame-treated surface only. This allowed the authors to calculate the advancing contact angle as a function of position for the flame-treated surface (Figure 12.18). Using the data of both figures it was

observed that the period of variation of the surface modification was about 2.5 mm. The final step was to quantify the periodic variation seen in the data, by calculating the difference between any given data points and the corresponding linear trendline at the same position. The trendline was a 'best-fit' linear regression through the advancing-cycle force data as shown in Figure 12.17. Similar results were obtained for the receding-cycle force.

The mean of the absolute values of these differences provides an indication of the magnitude of the variation. This mean deviation was called the 'laning value', and it was found that for untreated PP this value was about 1.5 mg in both the advancing and receding modes. This deviation represents random variations in the data about the mean; as discussed previously, there is no periodic variation in the Wilhelmy force data for untreated PP. This laning value represents the most uniform wettability that can be achieved on the specific type of PP film used in this study. On the other hand, the laning value for the flame-treated side of the laminate was 3.9 mg.

The authors also performed AFM and XPS analyses to evaluate whether the periodic variation in surface wettability was a result of variations in surface topography or surface oxidation or both. While AFM showed that no variation in surface topography occurred, XPS data (Figure 12.18) indicate that the periodicity observed in the Wilhelmy force trace is the result of the periodic variation in surface oxidation.

12.3.2 Flame Treatment on Polyethylene

Polyethylene (PE) is a material widely used for many applications owing to its unique combination of easy processability, barrier behavior, low cost, etc. When PE is used as a film, good adhesion is required, which in PE is intrinsically low because of low surface free energy of hydrocarbons. Adhesion can be improved by flame treatment and the relationship between the surface chemistry and morphology of flame-treated low-density polyethylene (LDPE) has been investigated by various authors.

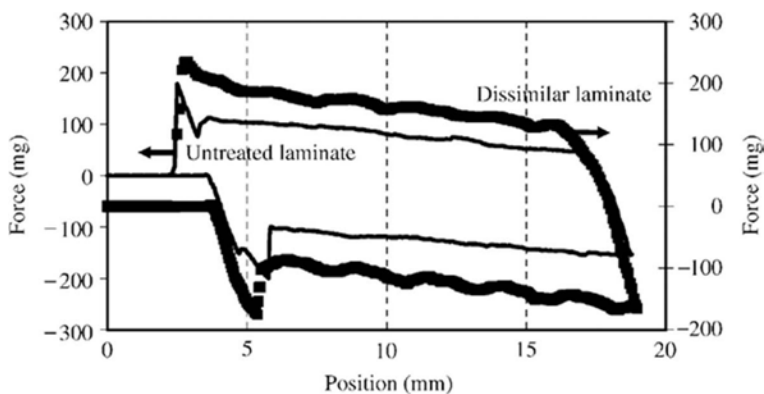


Figure 12.16 Wilhelmy force data for the untreated PP laminate and for the dissimilar laminate. The force data for the dissimilar laminate show spatially periodic non-uniformities.

Significant results were obtained by Song *et al.* [27]. The LDPE films were repeatedly pulled across the tip of the flame at a distance of 1 mm at a speed of 0.5 m/s. The flame cone was of approximately 1 cm length, i.e. the exposure time of the film to the flame was about 0.02 s. The frequency of repetitions was defined as the treatment number, which was proportional to the total treatment time. Thus the total treatment time varied from 0 to 4 s. For all experiments, the flame treatment number had to be lower than 200 or else the LDPE films became deformed.

Results of the wetting properties presented in Figure 12.19 show the variation of the water contact angle with the flame treatment as a function of treatment number.

The observed advancing angle was found to change from 100° for the untreated sample to 47.5° for the sample treated 200 times. The receding angle changed from 72° to 12°. This reduction in contact angle demonstrated an increase in the surface wettability and surface free energy following the flame treatment. This behavior indicated that the amount of polar functional groups at the LDPE surface increased for an increasing number of flame treatments up to 100 after which the surface became saturated.

XPS was used to probe the chemical composition and to identify the functional groups that were present within the outermost layer of the surface. Analyses revealed that the oxygen concentration increased with an increasing number of treatments. The surface concentration of oxygen was found to be 10.71% (take-off angle was 60°) whereas 12% was determined by Briggs *et al.* in an independent study (take-off angle was 90°) [39].

In addition, Song *et al.* [27] determined that the suggested depth of oxidation was in the 20–50 nm range.

It is evident that using imaging techniques, such as those used by Mazzola *et al.* [33], could give more detailed information on the depth of oxidation. It is also evident that

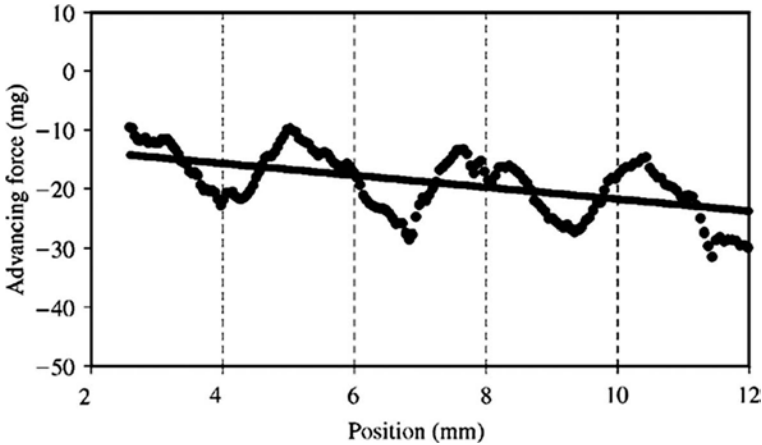


Figure 12.17 Advancing force as a function of position for the dissimilar laminate of this study. These are buoyancy-corrected data from Figure 12.16.

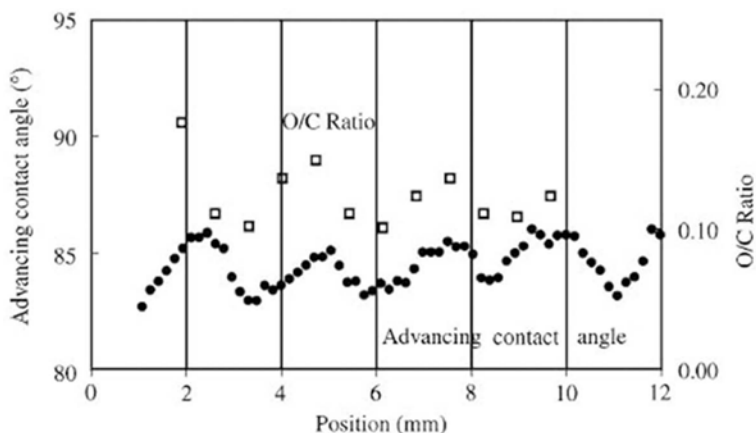


Figure 12.18 Advancing contact angle and XPS O/C atomic ratio as a function of position on flame-treated PP.

combining imaging techniques (such as FIB-SEM analysis) with elemental analysis (such as XPS analysis), a complete description of flame treatment effect could be carried out.

It has been proposed by Briggs and coworkers [38,39] that flame treatment introduces hydroxyl, carbonyl, and carboxyl groups on the surface of PE.

Analyzing the C1 spectra of the untreated LDPE, a symmetric C-C peak and no chemical shift was observed for this signal (Figure 12.20a). This result indicates the presence of a single carbon valence state which corresponds to C_xH_y functionalities (i.e. $-CH$, $-CH_2$, $-CH_3$). In contrast, flame modification led to the appearance of a shoulder at higher binding energy, which was taken as an indication of the buildup of carbon-oxygen groups. This result was also consistent with the observed variation in the O concentration. A simple deconvolution of the C 1s spectrum for the LDPE flame treated 200 times showed three peaks at higher binding energies (BE) relative to the primary hydrocarbon peak. These peaks were assigned to alcohol and/or ether (C-O), and to carbonyl (C=O) and carboxyl (HO-C=O) groups (Figure 12.20b).

The deconvoluted O 1s spectrum for the flame treated LDPE was not particularly informative due to contributions of every possible chemical environment for O except O-C=O which has a binding energy 1.5 eV higher. The relative concentrations of functional groups were obtained by normalizing the integrated peak areas. It was also observed that the relative concentration remained constant with the number of flame treatments i.e. the ratio among C-O:C=O:O-C=O groups was found to be 46:44:10.

Song and coworkers [27] also analyzed the treated and untreated LDPE with SIMS. However, SIMS has a shallower observation depth than XPS, so the observed fragments are emitted from the first 1–3 top monolayers of the surface, as compared to ca. 1–10 nm layer in XPS analysis. Therefore, ToF-SIMS measurements were also carried out in order to quantitatively study the surface composition of flame treated LDPE as a function of the number

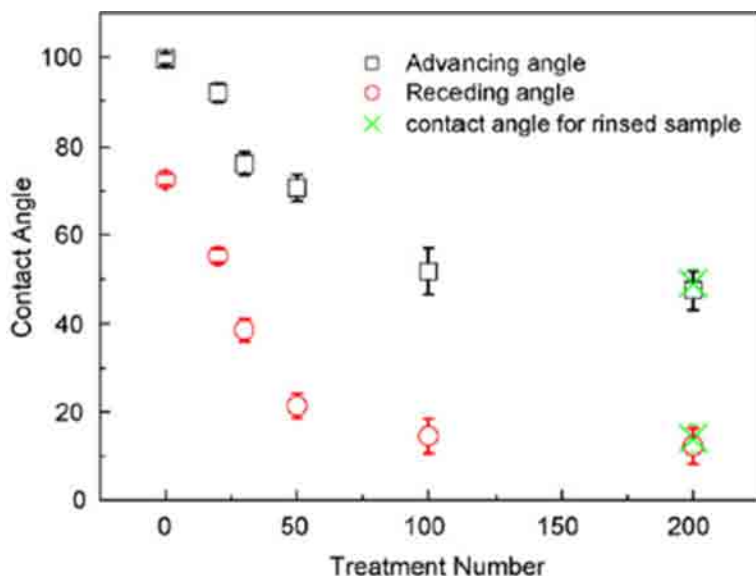


Figure 12.19 Variation of contact angles, measured with water, as a function of the flame treatment number of LDPE.

of treatments. As mentioned above, by analyzing and deconvoluting, the XPS results concerning the C 1s peak could provide information about the chemical species formed as a result of the surface modification. A direct indication of the compositions of these species can be obtained by analyzing the ToF-SIMS data, but the difference in the sampling depths must be kept in mind.

Figure 12.21 shows typical ToF-SIMS spectra of untreated LDPE and the LDPE sample treated 200 times. Besides the presence of hydrocarbon peaks, i.e. $C_nH_m^+$, due to fragmentation of the polymer, the formation of oxygen-containing functional species was directly observed.

LDPE is one of the most widely used material in extrusion coating of fibre-based packaging materials because of its low cost and easy processability. It also exhibits excellent barrier against water vapour and good heat sealing properties. The correlation between the surface properties and heat sealability of flame-treated low-density polyethylene coating was studied by Tuominen *et al.* [40] with the aim to find out how to modify the surface properties of LDPE coating without losing its heat sealing properties.

The authors [40] evaluated the heat sealability of flame-treated LDPE-coated paper by measuring the heat sealing and hot tack temperature and hot tack strength. It was found that flame treatment using the equivalence ratios of 0.86–0.80 enhanced the heat sealability of LDPE-coated paper by decreasing the heat sealing temperature by approximately 20°C.

As for the hot tack strength (i.e. the force required to separate substrates while the seal is still in semi-molten state), a correspondence between the hot tack strength and the heat

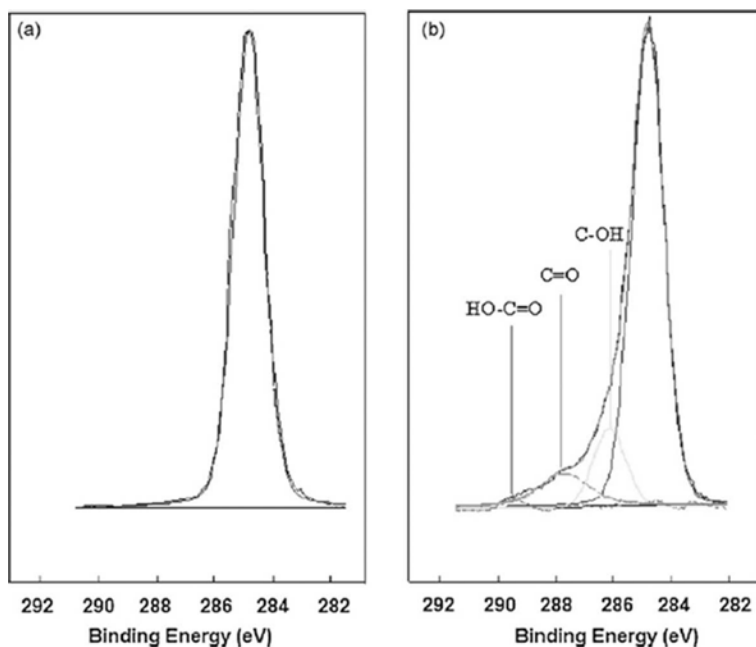


Figure 12.20 High resolution C 1s XPS spectra of untreated LDPE (a) and LDPE treated 200 times (b).

sealing property of flame-treated LDPE coating was observed. Flame treatment using the equivalence ratios between 0.92 and 1.2 reduces the seal strength significantly and thus impairs the heat sealability of LDPE-coated paper, but the change in equivalence ratio to 0.86 – 0.8 increases the seal strength, especially at lower hot tack temperatures.

Thus, depending on the equivalence air–propane ratio in flame treatment, the gas-rich flame treatment increases the heat sealing and hot tack temperatures. On the other hand, flame treatment using oxygen-rich flame decreases the heat sealing and hot tack temperatures and increases the hot tack strength. The poor heat sealing performance of LDPE coating in gas-rich conditions was believed to be the result of the cross-linking of top molecular layers due to the high surface temperature and the lack of oxygen during flame treatment.

The change of equivalence ratio to oxygen-rich flame ($\Phi \leq 0.86$) decreases the surface temperature of LDPE coating and increases the surface oxygen content significantly. Consequently, surface molecular weight decreases, which leads to increased mobility and chain interdiffusion across the seal interface and finally to the enhanced heat sealability.

12.4 Conclusion

Flame treatment is a powerful technique for enhancing the surface attributes of plastic materials.

Although it has not been possible to address all the topics related to the flame phenomenon, this review has attempted to provide the basic knowledge about flame treatment. In particular, the influences of the several process parameters and their interactions on the changes in wettability and surface free energy due to the chemistry and morphology changes were highlighted. Several applications of flame treatment on plastics were shown in order to show the effects and advantages of this activation process.

Our discussion was based on some major guiding principles. First, without knowing the underlying fundamentals of flame chemistry it is difficult to manage the flame phenomena in any application. Second, knowing the most important controlling factors of the overall process and being aware of how these parameters can affect the final outcome is of utmost importance to gain the maximum benefit from the treatment. Finally, it is essential to understand how to control the process variables in order to obtain the most efficient and repeatable activation process by flame treatment, because even minimal changes can cause huge deviations in the expected results, i.e., a low surface activation of treated surfaces.

In addition, the importance of optimizing the process, determining the best process parameters that maximize the surface free energy, wettability and adhesion was also shown. This is possible through Design of Experiments and multivariate analysis. It is evident that for each flame treatment and for each plastic material it is necessary to determine the optimum process parameters.

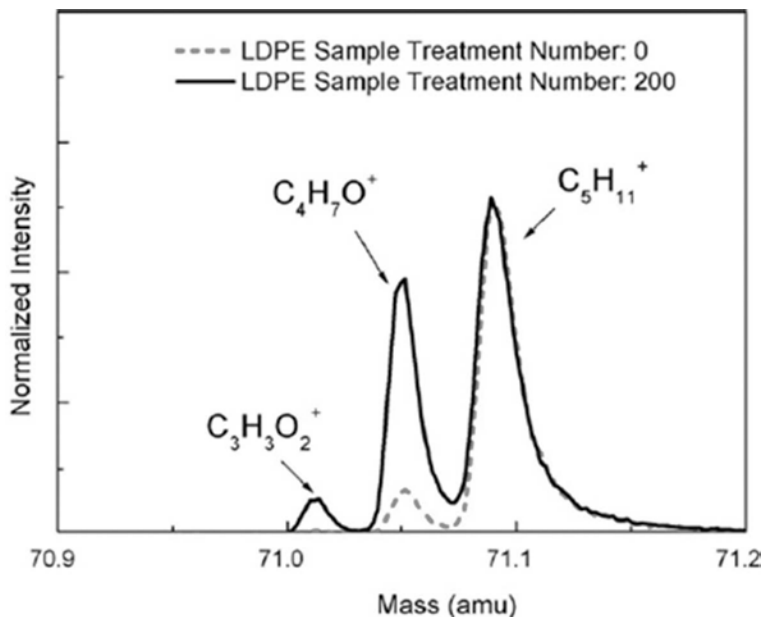


Figure 12.21 Positive ToF-SIMS spectra of untreated and flame treated LDPE.

A systematic approach to the use of flame as a surface activation technique is necessary for obtaining reproducible results.

Recent improvements in the coatings field have provided the opportunity of fabricating composite structures by covering plastic substrates with water-based coatings. Among other benefits, this would allow a cleaner process, since the use of organic solvents is avoided. However, the deposition of totally waterborne coatings onto plastic surfaces is a difficult task because of the higher surface tension of water-based coatings compared to current formulations. With this scenario in mind, flame treatment would become a leading technique for the surface activation of inherently hydrophobic polymers. This can be accomplished not only by appropriately using this technique but also finding out new operative conditions and technical advancements that would achieve very high surface free energy values on treated surfaces.

References

1. E.M. Liston, L. Martinu, and M.R. Wertheimer, Plasma surface modification of polymers for improved adhesion: A critical review. *Adhesion Sci. Technol.* 7, 1091–1127 (1993).
2. J.S. Chen, Z. Sun, P.S. Guo, Z.B. Zhang, D.Z. Zhu, and H.J. Xu, Effect of ion implantation on surface energy of ultrahigh molecular weight polyethylene. *J. Appl. Phys.* 93, 5103–5108 (2003).
3. H. Iwata, A. Kishida, M. Suzuki, Y. Hata, and Y. Ikada, Oxidation of polyethylene surface by corona discharge and the subsequent graft polymerization. *J. Polym. Sci., Part A, Polym. Chem.* 26, 3309–3322 (1988).
4. F. Severini, L. Di Landro, L. Galfetti, L. Meda, G. Ricca, and G. Zenere, Flame surface modification of polyethylene sheets. *Macromol. Symp.* 225, 225–244 (2002).
5. M. Strobel, V. Jones, C.S. Lyons, M. Ulsh, M.J. Kushner, R. Dorai, and M.C. Branch, A comparison of corona-treated and flame-treated polypropylene films. *Plasmas Polymers* 8, 61–95 (2003).
6. S.M. Desai and R.P. Singh, Surface modification of polyethylene: Long-term properties of polyolefins. *Adv. Polym. Sci.* 169, 231–293 (2004).
7. M.L. Salleo, M.S. Chabinyk, Yang, and R.A. Street, Polymer thin-film transistors with chemically modified dielectric interfaces. *Appl. Phys. Lett.* 81, 4383–4385 (2002).
8. K. Kim, K.S. Kim, K. Cho, and C.E. Park, Retardation of the surface rearrangement of O₂ plasma-treated LDPE by a two-step temperature control. *J. Adhesion Sci. Technol.* 15, 1805, (2001).
9. M. Chan, *Polymer Surface Modification and Characterization*, pp. 225–261, Hanser Publications, Munich (1994).
10. M. Chan, *Polymer Surface Modification and Characterization*, pp. 265–279, Hanser Publications, Munich (1994).
11. K.L. Mittal (Ed.), *Polymer Surface Modification: Relevance to Adhesion*, Volumes 2–5, CRC Press, Boca Raton, FL (2000–2009).
12. M. Strobel, C.S. Lyons, and K.L. Mittal (Eds.), *Plasma Surface Modification of Polymers: Relevance to Adhesion*, CRC Press, Boca Raton, FL (1994).
13. M. Thomas and K.L. Mittal (Eds.), *Atmospheric Pressure Plasma Treatment of Polymers: Relevance to Adhesion*, Wiley-Scrivener, Beverly, MA (2013).
14. D.M. Brewis and D. Briggs, Adhesion to polyethylene and polypropylene. *Polymer* 22, 7–16 (1981).

15. Y. Momose, Y. Tamura, M. Ogino, S. Okazaki, and M. Hirayama, Chemical reactivity between Teflon surfaces subjected to argon plasma treatment and atmospheric oxygen. *J. Vac. Sci. Technol. A* 10, 229–235 (1992).
16. F. Clouet and M.K. Shi, Interactions of polymer model surfaces with cold plasmas: Hexatriacontane as a model molecule of high-density polyethylene and octadecyl octadecanoate as a model of polyester. I. Degradation rate versus time and power. *J. Appl. Polym. Sci.* 46, 1955–1966 (1992).
17. R.H. Hansen, J.V. Pascale, T. De Benedictis, and P.M. Rentzepis, Effect of atomic oxygen on polymers. *J. Polym. Sci. A* 10, 2205–2214 (1965).
18. M. Strobel, S. Corn, C.S. Lyons, and G.A. Korba, Surface modification of polypropylene with CF_4 , CF_3H , CF_3Cl , and CF_3Br plasmas. *J. Polym. Sci. Polym. Chem.* 23, 1125–1135 (1985).
19. J.R. Hollahan and A.T. Bell (Eds.), *Techniques and Applications of Plasma Chemistry*. John Wiley & Sons, New York (1974).
20. T.G. Shikova, V.V. Rybkin, V.A. Titov, D.A. Shutov, and E.V. Kuvaldina, Modification and degradation of polyethylene under the action of oxygen plasma. *High Energy Chemistry* 39, 337–341 (2005).
21. B. Olander, A. Wirsén, and A. Albertsson, Oxygen microwave plasma treatment of silicone elastomer: Kinetic behavior and surface composition. *J. Appl. Polym. Sci.* 91, 4098–4104 (2004).
22. F. Truina-Marasescu and M.R. Wertheimer, Nitrogen-rich plasma-polymer films for biomedical applications. *Plasma Process. Polym.* 1, 44–57 (2004).
23. C. Klapperich, L. Pruitt, and K. Komvopoulos, Chemical and biological characteristics of low-temperature plasma treated ultra-high molecular weight polyethylene for biomedical applications. *J. Mater. Sci.: Mater. In Medicine* 12, 549–564 (2001).
24. M. Strobel, M.C. Branch, M. Ulsh, R.S. Kapaun, S. Kirk, and C.S. Lyons, Flame surface modifications of polypropylene film. *J. Adhesion Sci. Technol.* 10, 515–539 (1996).
25. F. Garbassi, M. Morra, and E. Occhiello, *Polymer Surfaces: From Physics to Technology*. John Wiley & Sons, Chichester, UK (1994).
26. M. Strobel, N. Sullivan, M.C. Branch, J. Park, M. Ulsh, R.S. Kapaun, and B. Leys, Surface modification of polypropylene film using N_2O -containing flames. *J. Adhesion Sci. Technol.* 14, 1243–1264 (2000).
27. J. Song, U. Gunst, H.F. Arlinghaus, and G.J. Vancso, Flame treatment of low-density polyethylene: Surface chemistry across the length scales. *Appl. Surface Sci.* 253, 9489–9499 (2007).
28. S. Farris, S. Pozzoli, P. Biagioni, L. Duò, S. Mancinelli, and L. Piergiovanni, The fundamentals of flame treatment for the surface activation of polyolefin polymers – A review. *Polymer* 51, 3591–3605 (2010).
29. L. Glassman and R. Yetter, *Combustion*, 4th Edition, Academic Press, San Diego, CA, USA (2008).
30. J. Vandoooren, M.C. Branch, and P.J. Van Tiggelen, Comparisons of the structure of stoichiometric CH_4-N_2O-Ar and CH_4-O_2-Ar flames by molecular beam sampling and mass spectrometric analysis. *Combustion and Flame* 90, 247–258 (1992).
31. J.N. Galloway, F.J. Dentener, D.G. Capone, E.W. Boyer, R.W. Howarth, S.P. Seitzinger, G.P. Asner, C.C. Cleveland, P.A. Green, E.A. Holland, D.M. Karl, A.F. Michaels, J.H. Porter, A.R. Townsend, and C.J. Vorosmarty, Nitrogen cycles: Past, present, and future. *Biogeochemistry* 70, 153–226 (2004).
32. A.P. Pijpers and R.J. Meier, Adhesion behavior of polypropylenes after flame treatment determined by XPS (ESCA) spectral analysis. *J. Electr. Spectr. Rel. Phenom.* 121, 299–313 (2001).

33. L. Mazzola, E. Bemporad, and F. Carassiti, Flame treatment on plastic: A new surface free energy statistical prediction model and characterization of the treated surfaces. *Appl. Surface Sci.* 257, 2148–2158 (2011).
34. D.C. Montgomery, *Statistical Quality Control*, Mc Graw Hill (2000).
35. K.L. Mittal, The role of the interface in adhesion phenomena. *Polym. Eng. Sci.* 17, 467–473 (1977).
36. R. Sharma, S.A. Sims, and M.K. Mazumder, Charge decay enhancement in polymer powders using plasma treatment, in: *Record of the 2002 IEEE Industry Application Conference* 1, 610–613 (2002).
37. J. Park, C.S. Lyons, M. Strobel, M. Ulsh, M.I. Kinsinger, and M.J. Prokosch, Characterization of non-uniform wettability on flame-treated polypropylene-film surfaces. *J. Adhesion Sci. Technol.* 17, 643–653 (2003).
38. D. Briggs, D.M. Brewis, R.H. Dahm, and L.W. Fletcher, Analysis of the surface chemistry of oxidized polyethylene: Comparison of XPS and ToF-SIMS. *Surf. Interface Anal.* 35, 156–167 (2003).
39. D. Briggs, C.R. Kendall, A.R. Blythe, and A.B. Wootton, Electrical discharge treatment of polypropylene film. *Polymer* 24, 47–52 (1983).
40. M. Tuominen, M. Ek, P. Saloranta, M. Toivakka, and J. Kuusipalo, The effect of flame treatment on surface properties and heat sealability of low-density polyethylene coating. *Packaging Sci. Technol.* 26, 201–214 (2013).

Mucoadhesive Polymers for Enhancing Retention in Ocular Drug Delivery

Anubha Khare, Kanchan Grover, Pravin Pawar and Inderbir Singh*

Chitkara College of Pharmacy, Chitkara University, Patiala, Punjab, India

Abstract

Ocular drug delivery is a very challenging task faced by pharmaceutical scientists, inspite of the fact that eye is the most sensitive and accessible organ for the delivery of drugs. A major disadvantage associated with conventional dosage form is its low bioavailability, i.e., less than 10%. To improve the bioavailability, viscosity-enhancing agents or mucoadhesive polymers are used for treating severe ocular diseases. These polymers play an important role in increasing the precorneal residence of drug at ocular site. Chitosan was initially endorsed to open up the tight junction of epithelium which increases the viscosity and penetration ability of drug solution. Alginate is an anionic polymer which acts as a good penetration enhancer and has high mucoadhesive strength. This review gives an overview of various mucoadhesive polymers such as chitosan, alginate, gellan gum, guar gum, Carbomer, Eudragit, etc. used to increase the bioavailability, precorneal residence time and controlled release with reduced dosing frequency without causing any visual disturbances. Ocular delivery formulations can be made more acceptable and excellent drug delivery systems by using both natural and synthetic polymers. Polymeric materials have a vast potential for exciting new applications in the foreseeable future and will have a great future in ocular drug delivery research.

Keywords: Gene delivery, human mucin genes, mucoadhesive polymers, ocular drug delivery

13.1 Introduction

Eye is a complex organ with unique anatomy and physiology having various protective barriers that prevent the administered drugs from penetrating into the target tissues [1]. The main problem for the formulator is to cross the protective barriers of eye without causing

*Corresponding author: inderbir.singh@chitkara.edu.in

any tissue damage. Cornea is the most anterior portion of the outer part of the eye which forms the strongest refractive medium of the eye due to the presence of layers: hydrophobic epithelium, the hydrophilic stroma and a hydrophobic endothelium, so it offers resistance to the passage of most drugs [2]. Corneal barrier causes low ocular bioavailability due to which only <5% of the applied drugs is able to penetrate through the cornea into the intra-ocular tissues [3].

The normal volume of tears has been estimated to be 7 μl and without blinking, the eyeball can hold 30 μl without spillage. Instillation of eye drops from the dropper (50 μl) causes reflex blinking of the eyelids. Another serious problem for the precorneal surface is drainage from the nasolacrimal duct to the nasal cavity [4]. The most popular and well accepted route of administration for treatment of eye disorders is the topical route, but the protective mechanisms of the eye and the barrier function of cornea lead to drainage of the drug which results in very small corneal contact times for instilled solution [5]. In order to optimize ophthalmic drug delivery, numerous strategies were developed in order to increase the bioavailability of drugs. For increasing the residence time, various formulations such as gels and ointments, matrix system such as inserts, collagen shields [6], nanoparticles [7] and nanocapsules [8,9] have been used. However, these dosage forms also suffer from some disadvantages such as they cause a sticky sensation, blurred vision, discomfort especially in elderly patients, loss of device during sleep or rubbing eye, and poor patient compliance [10].

Mucoadhesion may be defined as adhesion of a delivery system to the mucosal surface for releasing the drug at the site in a controlled fashion. Mucoadhesive polymers are responsible for the mucoadhesion phenomenon. The advantages of mucoadhesive drug delivery systems include the prolongation of residence time of the dosage form at the site of absorption leading to enhanced absorption and hence the therapeutic efficacy of the drug. Mucoadhesion approach can be advantageous in improving bioavailability of ocular drugs by increasing the residence time of the drug in the eye. Mucus coats many biological surfaces as it is a viscous and heterogeneous biological product [11]. On hydration, certain water soluble polymers become adhesive to mucous membrane and hence increase the residence time of drugs to the surface. The type and properties of the mucoadhesive polymers are responsible for the development of mucoadhesive bonds and controlling the release of the drug from the delivery system. In general, the mucoadhesion phenomenon involves wetting and swelling of the polymer followed by interpenetration and/or entanglement of the polymer and the mucin chains and formation of chemical bond responsible for mucoadhesion. Mucoadhesion phenomenon could be explained by diffusion theory (physical entanglement and/or interpenetration of polymer chains and mucus chains), wetting theory (ability of mucoadhesive polymer to spread and develop intimate contact with the mucous layer), adsorption theory (surface forces resulting in chemical bonding), electronic theory (attractive electrostatic forces between glycoprotein mucin network and the mucoadhesive polymer) [12]. Commonly used *in vitro/ex vivo* methods for the evaluation of mucoadhesion phenomenon in drug delivery systems include tensile strength measurement, shear strength measurement and chip based systems, whereas various imaging techniques are used for the evaluation of the delivery systems under *in vivo* conditions.

For studying the mechanism of mucoadhesion, texture analysis, rheological measurements, atomic force microscopy, wetting measurements, and zeta potential measurements have been used [13].

Mucus is the tissue layer responsible for the formation of the adhesive interface which forms continuous gel blanket adhering to the mucosal epithelial surface and also constitutes the innermost layer of the tear film [14]. Generally, the mucins on the ocular surface are derived from the goblet cell which is closely associated with the glycocalyx of the corneal/conjunctival epithelial cells [15]. Mucus protects the epithelia from damage and facilitates the movements of the eyelids. The mucus gel entraps bacteria, cell debris, and foreign bodies forming “mucous threads” consisting of thick fibers arranged in bundles. Mucins improve the spreading of the tear film and enhance its stability and cohesion [16,17].

13.2 Composition of Mucus Layer

Mucus layers are very high molecular weight glycoproteins, with up to 80% of their mass as O-linked glycan chains. Mucus consists of 95% water, 0.5–5% glycoproteins and lipids, 0.5–1% free proteins, enzymes, and mucopolysaccharides [18,19]. Mucin is the primary component of mucus which is a high-molecular-mass glycoprotein with subunits containing a protein core, approximately 800 amino acids long, of which about 200 bear polysaccharide side-chains.

13.2.1 Expression of Human Mucin Genes

Out of several human mucin genes (depicted in Figure 13.1), the ocular surface expresses at least nine mucin genes: MUC1, MUC2, MUC4, MUC5AC, MUC7, MUC13, MUC15, MUC16, and MUC17 [20-27]. The corneal and conjunctival epithelia produce transmembrane mucins such as MUC1, MUC2 and MUC4. In contrast, goblet cells produce the gel-forming secretory mucin, MUC5AC. The lacrimal gland produces MUC7. Table 13.1 describes the role of mucins and various mucin genes expressed on ocular surface.

Due to its prospective importance in drug delivery, mucoadhesion has recently received considerable attention from pharmaceutical scientists. For mucoadhesion the charge of the polymer has also great influence. It is found that mucin resistance to negatively charged compounds is higher as compared to positively charged compounds to the cornea as revealed in Figure 13.2. Thus, the strength of mucoadhesive polymers with carboxyl groups is much stronger than of those with neutral groups because uncharged groups, rather than ionized carboxyl groups, react with mucin molecules, apparently only through hydrogen bonds [28,29].

Mucoadhesive polymers are capable of retaining the medication in the precorneal area by establishing physico-chemical interactions with the mucin layer covering the corneal epithelium. Mucoadhesive polymers with numerous hydrophilic functional groups e.g., carboxyl, hydroxyl, amide and sulfate groups can form hydrogen bonds. These hydrophilic groups also cause polymers to swell in water and thus expose the maximum number of adhesive sites [30]. Mucoadhesive polymers are classified into natural and synthetic

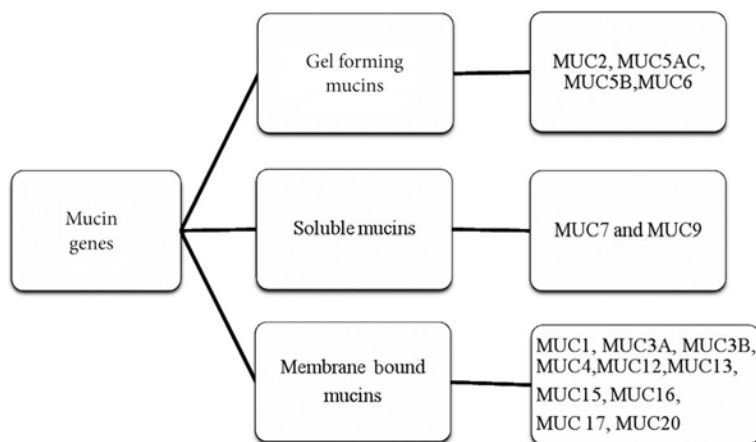


Figure 13.1 Schematic diagram of various human mucin genes based on their amino acid sequences.

polymers. The physical and physicochemical characteristics of various mucoadhesive polymers used in ocular drug delivery have been summarized in Table 13.2.

13.3 Natural Mucoadhesive Polymers

Natural gums and their derivatives are used widely in pharmaceutical dosage forms due to their inert, biodegradable, and biocompatible properties and lack of immunogenicity. These natural polymers do hold advantages over the synthetic polymers, generally because they are nontoxic, less expensive, and freely available.

13.3.1 Chitosan

Chitosan is a cationic polysaccharide bipolymer with mucoadhesive property and is a copolymer of glucosamine and N-acetylglucosamine. Chitosan [poly (β -(1 \rightarrow 4)-2-amino-2-deoxy-D-glucose)] is a deacetylated derivative of chitin, a naturally occurring polysaccharide. It is a linear polyamine containing free amine groups that are readily available for crosslinking and shows strong mucoadhesion due to its cationic nature which allows chitosan to combine with negatively charged sialic acid residues present in mucus or with multivalent anions [31,32]. Chitosan plays an important role in improving corneal healing by a process in which kerocyte migration increases, therefore leading to rapid production of collagen and improves wound healing [33]. The effective concentration of chitosan in topical ophthalmology is considered to be 1.5% [34-36]. Chitosan having high molecular weight, approximately 1400 kDa, shows better penetration property as compared to low molecular weight chitosan, i.e., 500-800 kDa [37]. Chitosan is a mucoadhesive polymer, but also has bioadhesive capability. At neutral pH or slightly alkaline pH, its mucoadhesive performance

Table 13.1 Mucin gene expression on ocular surface.

Mucin gene	Type of mucin	Ocular surface for expression	Role of mucin	References
MUC1	Transmembrane mucin	Corneal/conjunctival epithelial cell	To prevent cellular adhesion to ocular surface	20,160,161
MUC2	Gel forming mucin	Conjunctival cell	To control rheological properties	162,163
MUC4	Transmembrane mucin	Corneal epithelial/conjunctival stratified epithelium cells	To maintain and stabilize tear film structure	20,164,22
MUC5AC	Gel forming mucin	Conjunctival goblet cell	To control rheological properties	165
MUC7	Soluble mucin	Conjunctival/lacrimal gland	To provide protection against fungi, pathogens and bacteria	20,166
MUC16	Transmembrane mucin	Corneal apical cell layers/suprabasal region of conjunctiva	Function not determined yet	167,168

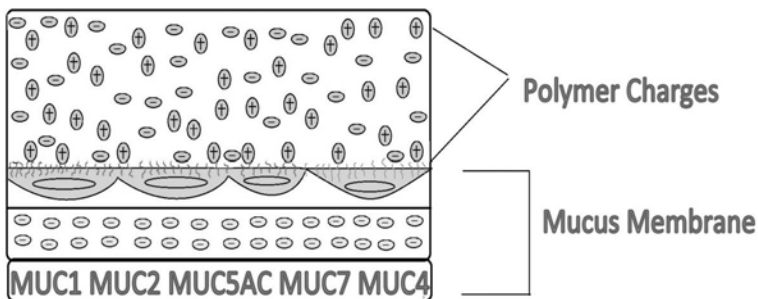
**Figure 13.2** Schematic diagram showing the mucoadhesive property of polymers based on their charge bound to the mucus surface.

Table 13.2 Summary of physical and physicochemical characteristics of mucoadhesive polymers used in ocular drug delivery.

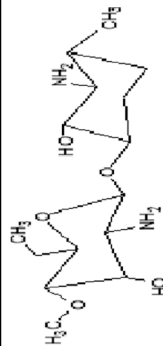
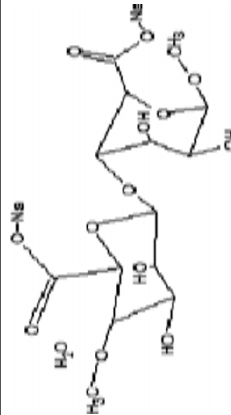
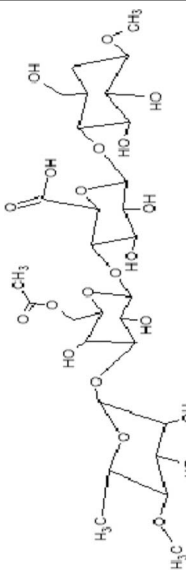
Polymer	Molecular weight	Solubility	Corneal Mucoadhesiveness	Charge	Structure	Refs.
Chitosan	3800-2800 Da	Sparingly soluble in water Soluble in acetic acid & formic acid Practically insoluble in ethanol	++	Negative		105
Human serum albumin (HSA)	67 kDa	Freely soluble in water & salt solutions	+	Negative		105
Alginate	20000-2,40,000 Da	Dissolves slowly in water Insoluble in ethanol & ether	+++	Negative		105
Gellan gum	70000-5*10 ⁵ Da	Soluble in water	+++	Negative		105

Table 13.2. Cont.

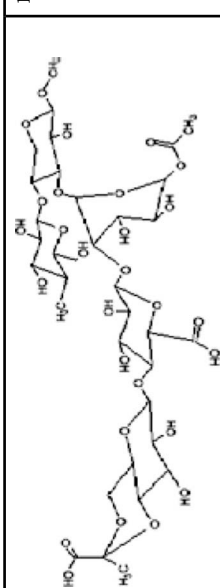
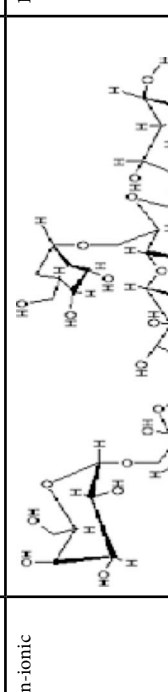
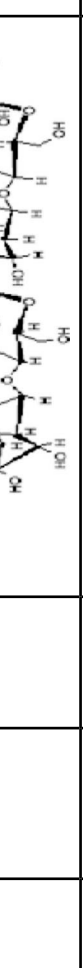
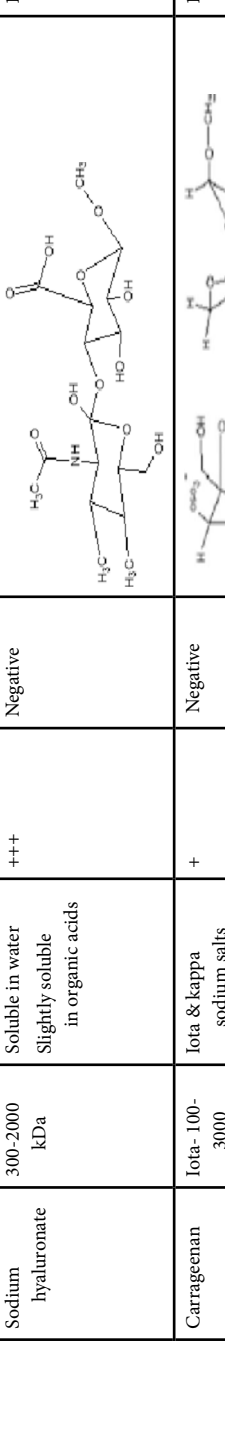
Xanthan gum	4 to 12×10^6 g/mol	Soluble in both cold and hot water Insoluble in most organic solvents	+	Negative		105
Guar gum	1000-5000 kDa	Disperses in hot & cold water Practically insoluble in organic solvents	+	Non-ionic		105, 174
Sodium hyaluronate	300-2000 kDa	Soluble in water Slightly soluble in organic acids	+++	Negative		105
Carrageenan	Iota- 100- 3000 kDa Kappa-25- 900 kDa	Iota & kappa sodium salts of carrageenan are soluble in water at 20°C	+	Negative		105, 175

Table 13.2. Cont.

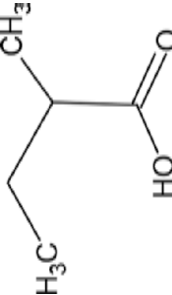
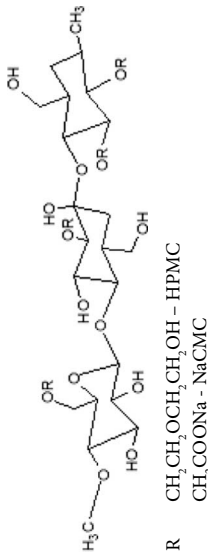
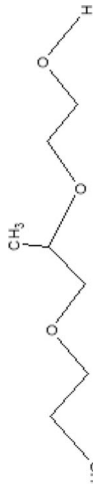
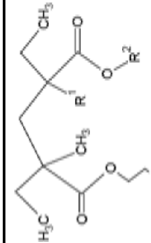
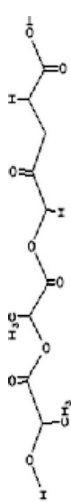
Xyloglucan	620,000 Da	Disperses quickly in cold water and forms viscous solution on heating	+	Non-ionic		176
Arabinogalactan	10000-120,000 Da	Soluble in water	++	Negative		105, 177
Carbomer	4,50,000 Da	Soluble in water & alcohol Freely soluble in chloroform	+++	Negative		178

Table 13.2. Cont.

Cellulose derivatives	HPMC- 86 kDa NaCMC-90 kDa	Soluble in water & some organic solvents	+++	HPMC-non-ionic NaCMC-negative	 <p> $\text{H}_3\text{C}-\text{CH}_2-\text{O}-\text{CH}_2-\text{CH}_2-\text{OH} - \text{HPMC}$ $\text{CH}_2-\text{COONa} - \text{NaCMC}$ </p>	178
Poloxamer	4000 g/mol	Soluble in water & alcohol Insoluble in light petroleum	++	Non-ionic		178
Eudragit	32000 g/mol	Soluble in ethanol, methanol, acetone Insoluble in water	+	Negative	 <p> $\text{R}1-\text{H}_2\text{CCH}_3$ $\text{R}2-\text{CH}_3, \text{C}_2\text{H}_5$ </p>	178
Poly (D,L-lactide-co-glycolide)	50,000-75000 Da	Soluble in ethyl acetate, acetone, THF	+	Amphoteric		151, 178

+ low, ++ moderate, +++ adequate mucoadhesiveness.

is considerably high as in tear film and increase of the mucoadhesiveness occurs only in the presence of an excess of mucin [38]. In comparison to normal formulations, these mucoadhesive particulate systems demonstrated significantly increased ocular bioavailability [9]. Chitosan is a nontoxic, biocompatible and biodegradable polymer. Chitosan is soluble in most organic acids including formic, acetic, tartaric, and citric acids [39,40]. It is insoluble in phosphoric and sulfuric acids [41,42]. The reason for its high solubility in organic acids is due to its pH being less than 6; it forms protonated amines and shows polycationic behaviour. But its solubility in neutral and basic pH can be improved by quaternization of chitosan to form trimethyl chitosan derivative. In solutions of pH >6.5, chitosan amines are deprotonated and are reactive and thus can undergo interpolymer associations leading to fibre and network (i.e., film and gel) formation [43-45].

13.3.1.1 Chitosan-based Formulations

Chitosan nanoparticles are reported to have a higher affinity towards corneal epithelium due to their small size and thus also have a higher precorneal retention than chitosan solutions [46]. Cyclosporine A-loaded chitosan solid lipid nanoparticles demonstrated higher permeation of drug across the rabbit corneal epithelium in the *in vitro* and through excised pig cornea in the *ex vivo* studies as compared with Cyclosporine alone [47]. Cyclosporine-loaded chitosan microspheres in rabbits showed their ability to be retained in corneal/conjunctival epithelium for longer time and therefore increased delivery to external ocular tissues without compromising inner ocular structure [37]. The minitables of Acyclovir with chitosan gave the highest C_{\max} (maximum serum concentration that a drug achieves in a specific compartment) and AUC (area under curve, which represents the total exposure of drug over time) when compared with the marketed ointment [48]. Chitosan alginate polyionic complexes are formed through ionic gelation via interactions between the carboxyl groups of alginate and the amine groups of chitosan. The nano-reservoir system of chitosan-alginate-loaded gatifloxacin against ocular infections demonstrated that the drug released in a sustained manner from the optimised formulation over a period of 24 h, primarily by non-Fickian diffusion [49]. 5-Fluorouracil (5-FU) loaded in chitosan coated sodium alginate-chitosan nanoparticles were prepared by ionic gelation technique and then suspended in chitosan solution which is responsible for the enhanced viscosity as nanoparticles did not show any interaction with mucin. *In vivo* study on rabbit eye showed significantly greater level of 5-FU in aqueous humor compared to 5-FU solution and enhanced mucoadhesiveness of CH-SA-CH-loaded 5-FU nanoparticles [50]. For delivery to the ocular surface, cationic chitosan, and anionic dextran sulfate are introduced to overcome the short residence time of topical drugs through their sustained release from mucoadhesive nanoparticles. Chitosan-dextran nanoparticles were stable to lysozyme and showed prolonged adhesion to the corneal surface [51]. The potential of carboplatin-loaded chitosan-alginate nanoparticles for the treatment of retinoblastoma was investigated. These nanoparticles demonstrated greater cellular drug uptake and sustained antiproliferative activity of the drug as well as an enhanced apoptotic effect as compared to the drug solution in a retinoblastoma cell line [52].

In vivo studies in rabbit eye showed a marked improvement in the anti-inflammatory activity of eye treated with dexamethasone-chitosan coated cationic microemulsions compared with a marketed suspension formulation in a uveitis-induced rabbit eye model. Therefore, chitosan microemulsions have the ability to prolong their precorneal residence time and sustain the release of the drug [53]. Pluronic surfaces are modified with chitosan to enhance their residence time in ocular delivery. Pluronic-chitosan micelle system in *in vitro* and *in vivo* studies demonstrated that surface modification of Pluronic by chitosan provides sustained release behavior and good pharmacological response [54]. Modification of chitosan with thiolated polymers provides much better mucoadhesive property than chitosan by itself which can be explained by the formation of covalent disulfide bonds between the thiol groups and the mucus glycoproteins, which are much stronger than non-covalent bonds. Thiolated chitosan-sodium alginate for ocular delivery is more stable and effective than chitosan-sodium alginate nanoparticles. The results demonstrated that nanoparticles have higher mucoadhesive property and could deliver greater amounts of drugs into HCE cells *in vitro* and cornea *in vivo* [55]. Chitosan/SBE- β -CD nanoparticles of Econazole are promising carriers for controlled delivery of drug to the eye and *in vivo* studies revealed that mucoadhesive nanoparticles had better ability in sustaining the antifungal effect of Econazole than Econazole solution [56].

13.3.2 Human Serum Albumin (HSA)

Albumin is a nonglycosylated protein naturally found in blood, consisting of a single polypeptide chain of 585 amino acids with 33 cystine residues with a molecular weight of 66 kDa. HSA is a major plasma protein constituent, accounting for 35% of the total protein in human plasma. Albumin is an acidic protein and remains stable between pH range 4–9 and temperature up to 60°C. HSA has the unique ability to reversibly or covalently bind to a variety of endogenous or exogenous ligands such as long chain fatty acids, vitamins, hormones, and metal ions with high affinity [57,58].

Pilocarpine-loaded egg albumin microspheres were prepared by simple emulsion technique and heat denaturation process. Comparative studies of 1% w/v pilocarpine nitrate-loaded albumin (PN) microsphere suspensions were done with eye drops of Pilocar (marketed preparations) 1%, 2% and 4% w/v. Marked increase in miotic response, duration and AUC (area under curve, which represents the total exposure of drug over time) of 1% PN microsphere suspension was observed as compared to the solutions [59]. To overcome several barriers with the conventional nonviral gene delivery, human serum albumin nanoparticles (HSA NP) of Cu, Zn superoxide dismutase (SOD1) were formulated by a desolvation-crosslinking method. HSA NP offers a very promising approach for nonviral gene delivery to the retina and shows great potential as a gene delivery vector for successful gene therapy applications [60].

In another study, importance of refractive index was investigated by considering the variations between human cornea and bovine cornea. It was reported that there were small local differences in the refractive index of the bovine and human corneal epithelia and the

refractive index of the epithelium is higher than that of the anterior and posterior stroma of the bovine cornea [61].

The influence of nanoparticles surface charge on retinal injury was determined by checking the movement of intravitreally injected human serum albumin nanoparticles. The cationization of HSA is done by covalent coupling hexamethylenediamine on the particle surface. Anionic particles diffused more easily through the 3-dimensional vitreal network of collagen fibrils than did their cationic counterparts. These results suggested that the anionic HSA-NP is a promising drug to the sub-retinal space and RPE (Retinal Pigment Epithelium) [62]. The anesthetic drug tetracaine is used during ocular surgery and its lasts approximately for 10-15 minutes. Most ocular surgical procedures take approximately 60 minutes to complete them. Therefore, tetracaine hydrochloride-loaded albumin-chitosan microparticles are formulated so as to sustain the effect of anesthetic drug during surgical procedure for longer times in case of ocular drug delivery system [63].

13.3.3 Alginate

Alginate is a naturally occurring polysaccharide which is a copolymer of (1,4) linked β -D-mannuronic (M) acid and α -1,4-linked-L-gulucronic acid (G) residues and is also quite abundant in nature as structural component in marine brown algae (*Phaeophyceae*) and as capsular polysaccharides in soil bacteria. Alginic acid is insoluble in water, but sodium alginate produces clear gels. The pKa value of alginic acid ranges from 3.4 to 4.4 due to the presence of carboxyl groups on the constituent uronic acid residues and if M and G residues are present pKa values are 3.38 and 3.65 respectively [64]. Alginate with G content more than 65% forms gel instantaneously while that with low G content forms a weak gel at relatively slow rate. Alginate instantaneously forms gel-spheres at pH > 6 by ionotropic gelation with divalent cations such as Ca, Ba, or Zn and leads to *in situ* gelling. On the other hand, at low pH, hydration of alginic acid leads to the formation of a high-viscosity "acid gel" [65].

Sodium alginate forms low-viscosity solutions even at high concentrations without causing any blurring effect. Increase in charge density of the polymer leads to better adhesion. Alginate is an anionic polymer with carboxyl end groups, so it acts as a good penetration enhancer as compared to other polymers such as polystyrene, and CMC (Carboxy methyl cellulose). Gatifloxacin based mucoadhesive systems showed significantly improved mucoadhesion strength with increase in the concentration of sodium alginate and sodium CMC. Sodium alginate has better mucoadhesive capability compared to other mucoadhesive polymers like poly (acrylic acid) and polycarbophils and also exhibits better bioadhesive property than hydroxyethyl cellulose [66]. Alginate is also responsible for sustained release of *in situ* gel as shown by carteolol which diffuses slowly from alginic acid as compared to hydroxyethylcellulose gel. The alginate surface tension (31.5 mN/m) is lower than the critical surface tension of the mucin coated cornea (38 mN/m) which is responsible for the good adhesion and spreading [67]. The sustained drug release obtained from the *in situ* gel formulation is directly proportional to the sodium alginate concentration. Diclofenac sodium gels prepared using sodium alginate at 5%, 4% and 3% w/v concentrations give a prolonged release for 9, 8 and 6 hours respectively [68]. In ocular infections, moxifloxacin

hydrochloride was successfully formulated as *in situ* gel-forming eye drops using sodium alginate as a gelling agent in combination with HPMC (Hydroxy propyl methyl cellulose) as a viscosity enhancing agent. *In vivo* testing on albino rabbit (male) suggested no abnormal clinical signs to the cornea. The developed formulations exhibited sustained release of drug from formulations over a period of 10 hours, thus increasing residence time [69].

13.3.4 Gellan gum

Gellan gum is a high molecular weight bacterial exopolysaccharide secreted by aerobic, well-characterized, non-pathogenic, Gram-negative strains of *Pseudomonas and Auromonas elodea* [70,71]. It is a linear anionic heteropolysaccharide composed of tetrasaccharide (1/4)-L-rhamnose- α (1/3)-D-glucose- β (1/4)-D-glucuronic acid- β (1/4)-D-glucose as a repeat unit [72]. Gellan gum possesses bioadhesive property, disperses and hydrates easily in both hot and cold deionized water, forming a viscous solution in cold distilled water [73].

Gelrite[®] (Kelco Div., Merck & Co., Inc., San Diego, California, USA) solution, a novel ophthalmic vehicle, gels in the presence of mono or divalent cations. It is available in two forms: high acyl form produces soft elastic and non-brittle gels while low acyl form produces non-elastic and brittle gels [74]. To improve the bioavailability of drugs such as Timolol maleate, Moxifloxacin, Flurbiprofen axetil and a carbonic anhydrase inhibitor, numerous studies were done using Gelrite[®] [75-77]. Gelrite[®] (0.2% w/v) has been reported to have a good gel strength property and showed higher bioavailability in simulated tear fluid with a combination of alginate (0.6% w/v) [78]. The Gatifloxacin *in situ* gel prepared by using gellan gum in combination with sodium carboxymethylcellulose or sodium alginate showed enhanced mucoadhesion strength. With increase in the concentration of mucoadhesive polymers, drug release seemed to slow down significantly [67].

Timoptol XE[®] (Merck & Co., Inc Whitehouse Station, N.J, USA) is the commercial product of Timolol maleate (0.5% and 0.2%), gel forming solution containing Gelrite[®], used to treat glaucoma and increased pressure in the eye. Timoptol XE[®] remains for a longer period of time on the eye surface compared to conventional timolol maleate eye drops [79]. A comparative study suggests that there is less systemic exposure to once-daily therapy with Timolol GS 0.5% (Timoptol-XE[®]) compared with twice-daily therapy with timolol maleate ophthalmic solution 0.5% [80].

13.3.5 Xanthan gum

Xanthan gum is a high molecular weight anionic polysaccharide produced by the fermentation process of microorganism (*Xanthomonas campestris*). It has a linear (1 to 4) linked β -D-glucose backbone with a trisaccharide side chain on every other glucose at C-3, containing a glucuronic acid residue linked (1 to 4) to a terminal mannose unit and (1 to 2) to a second mannose that connects to the backbone. The properties of xanthan gum led to increase in its use for sustained release of drugs due to its mucoadhesive and bioadhesive abilities. The viscosity of the xanthan gum solution is nearly independent of pH and temperature. Xanthan gum exhibits a synergistic interaction with the galactomannans guar

gum, locust bean gum (LBG) and the glucomannan konjac mannan resulting in enhanced viscosity [81]. Solutions of xanthan gum at 1% or higher concentration appear almost gel-like at rest yet these same solutions pour readily and have low resistance to mixing and pumping. These qualities are observed at levels of about 0.1–0.3%. The high viscosity of xanthan gum solutions at low shear rates is responsible for their ability to provide long-term stability to colloidal systems. The reduction in viscosity in response to increasing shear is important due to better pouring property of suspensions and emulsions and to the efficacy of xanthan gum as a processing aid. At low shear rates, solutions of xanthan gum show approximately 15-fold higher viscosity than guar gum and carboxymethylcellulose (CMC) and sodium alginate which accounts for its superior performance in stabilising suspensions [82,83]. The mucoadhesive effect of xanthan gum is dictated by its physicochemical properties. Increase in the polymer concentration results in an increase in viscosity and elasticity of the dispersion because of the secondary bond formation between the double stranded helices. Various grades of xanthan gum are available such as Keltrol' RHD and Keltrol' RD (CP Kelco, USA) xanthan gums. Where dispersion and mixing conditions are good, fine particle size food grades of xanthan gums such as Keltrol' F and Keltrol' TF (CP Kelco, USA) are available. Special grades of xanthan gum such as Keltrol' BT (CP Kelco, USA) are commercially available that are suitable for the preparation of ophthalmic solutions [84]. The results of *in vivo* study in healthy volunteers showed increase in viscosity of ophthalmic solution by xanthan gum to be responsible for delaying the clearance of the instilled solution. Xanthan gum is, therefore, more suitable as a viscosifying agent compared to poly (vinyl alcohol), hydroxyethylcellulose and hydroxypropylmethyl cellulose [85].

13.3.6 Guar gum

Guar gum consists of a linear chain of β -(1 \rightarrow 4)-linked D-mannose units with D-galactose attached by α -(1 \rightarrow 6) linkages to every other mannose unit to form short side chains [86]. Guar gum is a natural water-soluble non-ionic galactomannan polysaccharide, obtained from the ground endosperms of Indian cluster bean, *Cyamopsis tetragonolobus* (Leguminosae). Strong acids cause its hydrolysis and loss of viscosity, and alkalis in high concentration also tend to reduce its viscosity. Guar gum has a high shear viscosity. Because it is non-ionic, it is not affected by ionic strength. It has the ability to produce highly viscous, pseudoplastic aqueous solutions even at low concentrations due to its high molecular weight (up to 2 MDa). The therapeutic effect of guar gum is due to its ability to swell rapidly in aqueous media to form viscous dispersion or gel. Guar gum is also used as a controlled-release agent for drugs due to its high hydration rate [87-90]. Guar gum is the main ingredient in Systane eye drops, used in dry eye disease, and guar gum with borax cross-linking is used in ophthalmic compositions; therefore, it can also be used as a polymer in ocular inserts. Guar gum contains about 80% galactomannan, 12% water, 5% protein, 2% acid soluble ash, and 0.7% fat. Guar gum is rapidly soluble in both cold and hot water but is insoluble in many organic solvents. However, guar gum is susceptible to microbial degradation in the large intestine [91]. Foulks studied the role of HP-Guar as a gelling agent in poly

(ethylene glycol) (PEG) 400/propylene glycol 9 eye drops used for the treatment of dry eye disease [92].

13.3.7 Sodium Hyaluronate

Hyaluronan is a polysaccharide found in all tissues and body fluids of vertebrates as well as in some bacteria and is composed of alternating units of D-glucuronic acid and N-acetyl-D-glucosamine, linked together via alternating β -1,4 and β -1,3 glycosidic bonds. It has a high molecular mass and viscoelastic property due to its polymeric and polyelectrolyte characteristics. In the human body, hyaluronic acid is found in synovial fluid, umbilical cord, and in vitreous humour of eye [93,94].

Hyaluronic acid (HA) in aqueous solution has been reported to undergo transition from Newtonian to non-Newtonian characteristics with increasing molecular weight, concentration or shear rate. In addition, the higher the molecular weight and concentration of HA, the higher is the viscoelasticity of solutions [95]. Hyaluronan rheological properties, which are similar to those of mucus, are beneficial to dry eye patients due to its water retention capacity and its protective role at corneal/conjunctival epithelium [96]. Sodium hyaluronate has been shown to confer both subjective and objective improvements in patients with dry eye syndrome or keratoconjunctivitis sicca as it possesses both mucoadhesive and bioadhesive abilities [97]. The patients with moderate dry eye and superficial keratitis have increased expression of the CD44 receptors and sodium hyaluronate given for a period of 2 months causes decreased expression of the adhesion receptor i.e., CD44 [98]. Vismed[®] (TRB Chemedica, UK) and Rejena[™] (River Plate Biotechnology, Inc., USA) are marketed ophthalmic solutions available in the market for dry eye syndrome and blepharitis [99].

Tropicamide solutions, gels and matrices prepared with hyaluronic acid showed good to excellent mucoadhesive property than poly (acrylic acid) [100]. Pilocarpine (0.5%) combined with sodium hyaluronate increased 1.75 times the bioavailability than the 1% Pilocarpine marketed solution [101]. Sodium hyaluronate at a concentration of 0.25% provides higher bioavailability of gentamicin sulfate than phosphate buffer solution of gentamicin [102].

13.3.8 Carrageenan

Carrageenans are anionic, linear sulphated polysaccharides extracted from edible red seaweeds. These are widely used in the food industry, for their gelling, thickening, and stabilizing properties.

The alternate linkages α -1,3 and β -1,4 in the polymer differ from one another in the content of 3,6-anhydro-D-galactose and the number and position of the ester sulfate groups [103].

Three major carrageenans are *kappa*-, *lambda*-, and *iota* carrageenans. Iota- and *kappa*-carrageenans are gel forming carrageenans, whereas *lambda*-carrageenan is a thickener/viscosity builder [104]. *Lambda*-carrageenan interacts both with an alkaline anti-glaucoma drug, Timolol maleate and a mucoadhesive polymer such as gelatin. The combinations of

carrageenan and gelatin in different ratios proved to be useful in modulating their mucoadhesive property, drug release profiles and their rheological properties. Timolol maleate incorporated lambda-carrageenan microspheres showed four-fold increase in drug concentration and bioavailability in the aqueous humour in comparison with commercial formulations [105]. Ion activated *in situ* gel formulations based on gellan gum and carrageenan lead to a significant increase in viscosity, pseudoplasticity and hardness upon the addition of Ca^{2+} and K^{+} . Once in contact with the cations in the tear fluid, gellan gum and carragenen cause gelation, thus reducing nasolacrimal drainage, which renders them favorable for ocular use [106]. Pilocarpine demonstrated 2.5-fold increase in the *in vivo* miotic response in comparison to an aqueous solution, after administering gellan gum, xanthan gum and carrageenan formulations [106].

13.3.9 Tamarind Gum Polysaccharide (TGP)

Tamarind gum, a product of natural origin obtained from the seeds of *Tamarindus indica*, has been described as a viscosity enhancer showing mucomimetic property and bioadhesive activity. Purified TGP is a high molecular weight, branched polysaccharide consisting of xylose and galactoxylose and glucose substituents in the ratio 2.25:1.0:2.8 [107]. The arrangement of TGP gives the product a 'mucin-like' molecular structure [108], with particular similarity to MUC1, and thus confers most favorable mucoadhesive property. The concentration of tamarind polysaccharide ranges between 1 to 4% [109]. In the treatment of dry eye syndrome the activity of TGP and hyaluronic acid was compared and the results suggested that both 0.5% and 1% TGP concentrations were equivalent to 0.2% hyaluronic acid in relieving dry eye symptoms. TGP is a better alternative than hyaluronic acid in the treatment of dry eyes due to a significant attribute that makes it similar to natural tears [110].

Xiloyal' (Farmigea, Pisa, Italy) eyedrops (0.2% hyaluronic acid and 0.2% TGP) two-month treatment showed good tolerance and appeared to reduce ocular surface damage and symptoms of discomfort [111]. The synergistic effect of TGP and hyaluronic acid stabilizes the tear film, thereby prolonging the residence of ketotifen fumarate and diclofenac sodium in the tear fluid, but is unable to permeate the cornea [112]. Interaction between internal glucose and galactose units of TGP and acetyl groups of hyaluronic acid occurred in the solution which indicated the potential of these polymers for use as a tear substitute [113].

To overcome the drawbacks of TGP and to enhance its applicability it has been modified by chemical treatment with various groups like acetyl, hydroxyalkyl and carboxymethyl. Tropicamide-loaded carboxymethyl tamarind kernel polysaccharide (CMTKP) interacts with cationic moieties of mucin to form a gel. The mucoadhesive and non-irritant nature of CMTKP nanoparticles indicate its suitability as an ocular delivery system [114]. TGP mucoadhesive property was confirmed by NMR spectroscopy which is two to three times higher than that of arabinogalactan [115]. NMR spectroscopy ascertained the effect of TGP, HA or TGP/HA mixtures and the formation of stable aggregates with enhanced mucoadhesive property over those of the separate polysaccharides [116].

13.3.10 *Arabinogalactan*

Arabinogalactan (AG) a highly branched natural polysaccharide derived from the trees of the genus *Larix* (Larch) is a unique hemicellulosic product and is easily extractable by water in a pure form from non-delignified plant tissues. Its high water solubility, biocompatibility and ease of drug conjugation in an aqueous medium makes AG attractive as a potential drug carrier. It is a non-ionic highly branched polysaccharide of the 3,6- β -D galactan type, the side chains of which consist of β -galactose and β arabinose residues. AG dispersions showed a non-Newtonian viscous behaviour (viscosity = 1.6 mPa.s at 10% w/w concentration) along with good mucoadhesive property, useful for retention on the eye surface. In fact, a prolonged time of residence in rabbit eyes was ascertained by using fluorescein-labeled AG. Five percent w/w AG provided a good protective effect against the appearance of corneal dry spots. It also reduced significantly the healing time of an experimental corneal lesion. These findings suggest that AG is potentially effective for dry eye protection and in the treatment of corneal wounds [117].

13.4 Synthetic Polymers

Synthetic polymers offer tremendous advantages over natural polymers. Due to their synthesis flexibility it is possible to develop polymers having a wide spectrum of properties with excellent reproducibility.

13.4.1 *Poly (acrylic acid) PAA or Carbomer*

Polyacrylates are anionic polyelectrolytes, which consist of a vinyl group and a carboxylic acid terminus. These have been widely used for designing mucoadhesive delivery systems due to their ability to form strong hydrogen bonding with the mucin present in the mucosal layer [118]. Hydrogen bonding between mucus glycoprotein and mucoadhesive poly (carboxylic acid) occurs at low pH, the maximum adhesion strength is obtained at pH 4 due to presence of carboxylic acid groups which are responsible for forming conventional head-to-head dimers; whereas at pH >4, the majority of the carboxylic acid groups of both poly (acrylic acid) and the mucus glycoprotein are ionizable [119,120].

Carbomers have inherent mucus-like lubricating properties. Therefore, these have been used as artificial tears in the treatment of dry eye syndrome. However, blurred vision was reported in 23 patients while using Carbomer gel in artificial tears [121,122]. In the treatment of moderate dry eye syndrome, the study compared two commercially available ocular lubricants: 0.3% Carbomer 934 or 0.18% sodium hyaluronate (SH). After a month of use both Carbomer and SH reduced the severity of symptoms and ocular staining. The effectiveness of both treatments is similar but neither has a lasting effect on NTBUT (tear break up time without fluorescein) and TBUT (tear break up time with fluorescein) [123]. In another study it was reported that Carbomer gel had longer precorneal residence time and was more effective than 1% carboxymethylcellulose in the treatment of patients with dry eye [124].

Carbopol is a widely used in *in situ* gel forming system, owing to its property to transform from solution to gel when the pH is raised. *In situ* gel of puerarin was formulated by using Carbomer as gelling agent and HPMC (hydroxypropyl methyl cellulose) as viscosity enhancer. *In vitro* and *in vivo* results demonstrated higher bioavailability of puerarin gel as compared to conventional puerarin eye drops. Thus, it also prolongs the residence time and decreases the systemic side effects [125].

Baicalin *in situ* gel (a pH-triggered gelling system) is composed of Carbopol 974P (0.3%w/v) and HPMC E4M (0.6% w/v). The results of baicalin *in situ* gel were compared with marketed baicalin eye drops which demonstrated that *in situ* gelling system has a better ability to keep baicalin stable and also has the ability to enhance ocular bioavailability. The AUC and C_{\max} values were 6.1-fold and 3.6-fold higher than those of the control solution [126].

To enable a controlled release of a drug with low aqueous solubility, HP- β -CD is used as a solubilizer and a permeation enhancer for dexamethasone (DXN). To treat uveitis, HP- β -CD based pH-induced mucoadhesive hydrogel for ophthalmic delivery was formulated. Carbopol 980 NF with sodium carboxy methyl cellulose was added in the formulation as phase transition and mucoadhesive agents. Rheological study demonstrated pseudoplastic behavior of all formulations and both *in vitro* and *in vivo* results indicated that DXN mucoadhesive hydrogel systems were viable alternative to marketed solution [127]. A novel pH-triggered nanoemulsified *in situ* gelling system (NE-ISG) of fluconazole (FLZ) was prepared using Carbopol 934 as a vehicle for ophthalmic delivery. The *in-situ* gelling system was prepared by dispersing optimized nanoemulsion (NE) into the gelling solution of Carbopol. The optimized nanoemulsified *in situ* ophthalmic gel of FLZ showed higher permeation along with sustained drug release and moreover, the presence of *in situ* gelling polymer leads to longer residence of the drug on the ocular surface [128]. Combination of two gelling polymers i.e. poly(acrylic acid) (Carbopol 934P) and xanthan gum was responsible for enhancing the retention time of drug at precorneal surface and also for sustained drug release [129]. Poly (acrylic acid) forms hydrogen bonds between its -COOH groups and sialic acid -COOH groups of the mucin glycoprotein. Its commercial products polycarbophil and carbophil exhibit a strong mucoadhesion. To reduce the intraocular pressure, sustained release ocular inserts were formulated using poly (2-hydroxyethyl methacrylate). The results from ocular inserts confirmed the sustained release of pilocarpine for a 24-hour period and the pressure decrease was significant for a period longer than 48 hours [130]. Polycarbophil is insoluble in water, but due to its swelling property it forms a network with mucus layer. Polycarbophil-based formulation showed no adverse effects in intact eyes of albino rabbits. AzaSite[®] (Inspire Pharmaceuticals, Inc, Durham, NC) is an azithromycin ophthalmic solution containing 1% polycarbophil which is a commercially product available in the market. Due to the combination of polycarbophil with an anti-inflammatory drug, it enhances the azithromycin concentration in a variety of ocular tissues, including the conjunctiva, cornea and particularly the eyelid [131].

13.4.2 Eudragit

Eudragit RL 100 and Eudragit RS 100 are copolymers of poly (ethyl acrylate), poly (methyl methacrylate) and a low content of methacrylic acid ester with quaternary ammonium

groups (trimethylammonioethyl methacrylate chloride). The presence of ammonium groups makes the polymer permeable. Eudragit is a cationic polymer and it facilitates an effective adhesion with the ocular site, since the former has a negative surface [132]. *In vitro* release studies of azelastine hydrochloride loaded Eudragit RL100 microspheres demonstrated prolonged release of the drug over a period of 6 hours. The polymeric microspheres for treatment of allergic conjunctivitis demonstrate a longer residence time in rat model as compared to the marketed formulation, Azelast[®] (Sun Pharmaceuticals, India) [133].

Eudragit RS 100 and Eudragit RL 100 have been used as inert carriers for the preparation of nanosuspensions for ophthalmic drug delivery. Drug loaded Eudragit nanosuspension prolonged the residence time and also improved the ocular availability of the drugs [132]. For the treatment of bacterial keratitis, sustained drug delivery is required. For prolonged release of drug, gatifloxacin/prednisolone-loaded nanoparticles were prepared using Eudragit RS 100 and Eudragit RL 100 and coated with hyaluronic acid for providing bioadhesion. When compared to the commercial eye drops, gatifloxacin nanosuspensions showed improved patient compliance and sustained release in aqueous humour and corneal tissue [134]. Cloricromene (AD6) is a very unstable compound in aqueous solution and is used in the treatment of uveitis for ocular application. To improve the stability of cloricromene (AD6) in ophthalmic formulations, its polymeric nanoparticle suspensions were made using inert polymer resins (Eudragit RS100 and RL100). In ophthalmic drug delivery, AD6-loaded Eudragit nanoparticle suspensions showed higher drug availability in the rabbit aqueous humour, improved corneal adhesion, and also enhanced stability on storage [135].

Ocular inserts of gatifloxacin were fabricated in order to reduce the dosing frequency of drug and to increase corneal residence time. By using the polymers sodium alginate, poly (vinyl alcohol) (PVA) and glycerin, ocular inserts of gatifloxacin sesquihydrate were prepared. It can be concluded that the formulation based on PVA and sodium alginate, cross-linked by CaCl_2 , and coated with Eudragit RL-100, was well tolerated by the rabbit eye. The coating of formulations with Eudragit RL-100 was able to sustain the *in vitro* drug release up to 11 hour [136]. In another study, a cross-linked ocular insert coated with Eudragit RL-100 showed higher drug permeation compared to other formulations. Moxifloxacin concentration and mucoadhesive strength of the ocular insert were found to be satisfactory [137].

13.4.3 Cellulose Derivatives

Cellulose is a linear and fairly rigid homopolymer consisting of D-anhydroglucopyranose units (AGU). These units are linked together by β -(1 \rightarrow 4) glucosidic bonds formed between C-1 and C-4 of adjacent glucose moieties [138]. Cellulose ethers like hydroxypropylmethylcellulose (HPMC) and hydroxypropylcellulose act as a viscosity enhancing ophthalmic vehicle. *In situ* gel forming eye drops of moxifloxacin hydrochloride were formulated using sodium alginate as a gelling agent and HPMC as a viscosity enhancing agent [139]. To enhance the ocular bioavailability and patient compliance, ion activated gatifloxacin *in situ* gelling formulations were designed. Alginate was combined with HPMC and incorporated into formulations. The results indicated that the alginate/HPMC solution retained the drug for a longer time than the alginate or HPMC E50LV solution alone [140].

The efficacy of HPMC and hyaluronic acid (HA) in maintaining corneal hydration and optical clarity suggested that HA maintained corneal hydration significantly longer than 2% HPMC [141]. During cataract surgery, 2% HPMC provided significantly better optical clarity than the balanced salt solution. HPMC is a viscous eye lubricant and thus it provides an increased comfort for the patient, especially under topical anesthesia, and a simpler and possibly safer surgical procedure [142]. Ion activated *in situ* gel of azithromycin was formulated using pectins, which becomes gel in the presence of divalent cations. To achieve the desired rheological behaviour, viscosity enhancing polymers such as HPMC or SMC (sodium carboxymethyl cellulose) were included in the formulations. The results suggested that the formulations developed containing 3% w/w pectin, and 0.5% w/v SMC showed more promising results in prolonging the release and efficacy of azithromycin [143]. Thermo-sensitive *in-situ* gels for the ophthalmic delivery of ketorolac using methylcellulose in combination with hydroxypropylmethyl cellulose have been reported. Methylcellulose solution is known to undergo thermoreversible sol-to-gel transition. From *in vitro* release studies, it was concluded that a sustained release of the drug over a 4-hour period was achieved by addition of HPMC. The results indicated that the developed systems were thus a better alternative to conventional eye drops [144].

Cellufresh[®], Celluvisc[®], and Refresh[®] (Allergan Inc., Australia) are commercial products of cellulose ethers available in the market as a lachrymal substitute for the treatment of dry eye conditions. To examine the effects of artificial tears on visual performance, Refresh Celluvisc (Allergan, Irvine, CA, 1.0% high-viscosity CMC) with Refresh Liquefil (Allergan, 1.0% total CMC made by blending 0.35% high-viscosity with 0.65% medium viscosity CMC) were compared on twenty normal subjects. The results showed that both products, Liquefil[®] and Celluvisc[®] led to an alteration of the tear layer. Patients observed a moderate amount of blur with Celluvisc, which gradually subsided and a shorter duration of blur with Liquefil (about half that of Celluvisc). Thus, it was concluded that total 0.1% concentration of CMC may be valuable in dry eye therapy without causing too much blurring to patients [145].

13.4.4 Poly (D, L-Lactic acid) and poly (D, L-Lactide-co-glycolide)

Poly (lactic-co-glycolic acid) (PLGA) is a copolymer synthesized by means of random ring-opening copolymerization of the monomers: the cyclic dimers (1, 4-dioxane-2, 5-diones) of glycolic acid and lactic acid [146,147]. PLGA is approved by FDA for therapeutic use in humans and is also a suitable candidate for nanoparticles formation because of ease of formulation for use in drug delivery. PLGA nanoparticles were frequently used for target delivery of various drugs like flubiprofen, sparfloxacin, diclofenac and chloramphenicol and it was reported that the polymer was safe for ocular delivery [148-150].

In case of retinoblastoma (RB) primary tumors, a transmembrane protein, epithelial cell adhesion molecule (EpCAM) is highly expressed on the eye surface which leads to epithelial cancer. Paclitaxel-loaded PLGA nanoparticles were prepared for use against RB tumors and their surfaces were functionalized with EpCAM monoclonal antibody for targeted delivery of the chemotherapy drug paclitaxel. It was concluded that the EpCAM antibody-functionalized biodegradable NPs for tumor-selective drug delivery and the prepared

PLGA NPs accumulated at the solid tumor site by an “enhanced permeation and retention” effect which was an alternative strategy against retinoblastoma tumor [151]. The *in vitro* release of voriconazole from PLGA microspheres had an initial burst release on the first day followed by a long, steady release phase. In the initial 7 days, voriconazole released 10% drug per day and about 85% of the drug was released at day 21. Histopathological examination showed no necrotic foci in the retina, and each layer could be identified clearly. Thus a strong burst effect is beneficial for decreasing fungal growth in the tissues, and thus eliminating reoccurrences [152].

PEGylation of the PLGA nanosuspension can modulate the surface properties of the system, and thus influence mucoadhesion to prolong the residence time of the particles in the precorneal area. Flubiprofen (FB) is a nonsteroidal anti-inflammatory drug for the management of ocular inflammatory diseases. It was encapsulated in PLGA and PLGA-PEG nanosuspensions. The effects of freeze-drying with various cryoprotectants and the effect of γ -irradiation sterilization on the properties of FB-loaded PLGA and PLGA-PEG NSs were evaluated. HP- β -CD was found to be an effective system for increasing the bioavailability of FB and also a suitable cryoprotectant in order to maintain the properties of nanosuspension. The presence of HP- β -CD resulted in a reduction of burst effect, providing a more sustained release of the drug and long term stability was achieved by γ -irradiation [153].

13.4.5 Poloxamers

A Poloxamer (Pluronic) is a triblock copolymer made of poly(ethylene oxide) and poly(propylene oxide) units. Poloxamers are composed of white, waxy, free-flowing granules that are almost odorless and tasteless. In the presence of acid, alkalis, and metal ions, aqueous solutions of Poloxamers remain stable. Poloxamers which are freely soluble in water include the 188 (F-68 grade), 237 (F-87 grade), 338 (F-108 grade) and 407 (F-127 grade) types. Pluronics exhibit the phenomenon of reverse thermal gelation or sol-to-gel transition in the 25–30°C [154,155] range. Poloxamers possess mucoadhesive property due to their hydrophobic and hydrophilic sequences simulating mucin action by adsorption of the aqueous layer of tears through the hydrophobic epithelium. This makes them suitable for use as a drug delivery system [156]. To overcome the problems of poor bioavailability and to prolong the precorneal time at the ocular surface, a novel approach of forming mucoadhesive dual-drug delivery system based on *in situ* gel forming nanosuspension of forskolin was reported. A physical admixture of two different polymers (Noveon[®] AA-1 polycarbophil/ Poloxamer 407) was used to form new pH and thermoreversible *in situ* gel formulations with nanosize forskolin crystals. Noveon[®] (The Lubrizol Corporation, USA) AA-1 polycarbophil exhibits a definite sol-to-gel transition in aqueous solutions as the pH is raised above its pKa of about 6.0±0.5. The formulation is liquid at room temperature (20 ± 10°C) which undergoes rapid gelation at pH 7.4 and temperature (35°C). The *in vitro* results showed prolonged and controlled forskolin release for more than 5 h, thus maintaining concentrations for a longer period of time [157].

Blephagel[®] (Spectrum Thea Pharmaceuticals, UK) a hypoallergenic gel is a colorless aqueous gel which contains Carbomer, Poloxamer 188, Macrogol 4000, sodium hydroxy

methyl glycinate, 1 N sodium hydroxyde, and purified water. It is a highly effective treatment for blepharitis which is commonly associated with dry eye. *In vitro* and *in vivo* studies indicated it to be safe and nontoxic in the subjects and also found it effective for cleansing the eyelids of mucus and squama around eyelash root [158].

13.5 Gene Delivery

Ocular gene delivery is a sophisticated approach and offers new hope for treating severe eye diseases. Ocular diseases mainly occur due to gene defects in the eye [179]. Ocular gene therapy offers many advantages for ocular drug delivery systems [180]. For the gene delivery to eye, some advanced bio- and nanotechnology systems are used such as mucoadhesive systems, liposomes, ocular inserts, and nanoparticles [182]. Tandon *et al.*, demonstrated that PEI2-GNPs (polyethylimine-conjugated gold nanoparticles) mediated BMP7 gene delivery causes minimum toxicity and inhibits corneal fibrosis *in vivo* using rabbit eye model. PEI2-GNPs are potent vectors for corneal wound healing [183]. Puras *et al.*, worked on low molecular weight oligochitosans for delivery of nucleic acid. As polyplexes are positively charged, they protect and release the plasmid safely. The *in vitro* studies showed that when pH decreased from 7.4 to 7.1, the transfection efficiency increased drastically [181]. Jiang *et al.*, designed cationic core shell liponanoparticles and chitosan nanoparticles (CS-NPs) for ocular gene delivery. In this study DLCS (DNA Laden Chitosan) nanoparticles showed high cellular uptake, protection of DNA, endolysosomal escaping ability and other functions. DLCS nanoparticles revealed 2.52-fold increase in transfection efficiency *in vivo* and 1.25-fold increase in cellular uptake than CS-NPs [184].

13.6 Patented Formulations

Patented *in-situ* gel of estrogen was formulated using gellan gum (0.1%–0.3% w/v) as the gelling agent. The drug is hydrophobic in nature so complexation with 0.06%–0.6% cyclodextrin was carried out. Gellan gum forms a gel which helps in holding estrogen in the cornea for reducing the risks of cataract [185]. Ophthalmic compositions containing alginic acid and hyaluronic acid could be employed for increasing the retention time of the system on ocular mucosa. The combination of these two polymers is useful for dry eye syndrome sufferers. This invention improves the sense of use and also reduces stickiness and blurred vision [186]. Eye drops of TGP and hyaluronic acid could be used in the treatment of dry eye syndrome by inducing a significant enhancement in the morphology of conjunctival microvilli and could be employed as a tear substitute [187].

13.7 Future Prospects

During the past 20 years, considerable advances have been made in ocular drug delivery starting from the use of conventional solutions, suspensions and ointments, *in situ* gels, nanoparticles, microspheres which provide the mucoadhesive property for the delivery of drug to the eye. So, ocular drug delivery offers a unique undertaking in ophthalmology.

Various advances have been made in order to maintain therapeutic levels over an extended period of time in the tear film and anterior chamber. Treatment and management of the eye diseases such as uveitis, fungal infection, dry eye syndrome is a challenging work for the researchers due to the anatomy and physiology of ocular barriers. There is a need for a delivery system that can provide controlled release to treat chronic ocular diseases with a reduced dosing frequency without causing any visual disturbances. Mucoadhesion is one of these advances, which is based on the entanglement of non-covalent bonds between the polymer and mucus. The use of mucoadhesive polymers in various dosage forms has created a major interest among the research scientists due to their tendency to interact with the mucosal surface. Many clinical studies have also been performed on mucoadhesive ocular dosage forms. Mucoadhesive polymers usage in ophthalmic drug delivery has been reported in various dosage forms such as viscous solutions [159,160], suspensions, ointments [161,162], *in situ* gelling systems, particulate systems [163-165], ocular films [166,167], ocular inserts, and nanoparticles [168-170]. Such systems provide high adhesion, prolonged residence time, low irritation, increased bioavailability and acceptance by the patients. Commercialization of newer dosage forms with the help of these mucoadhesive polymers is in progress and many products are also available in the market for use for various ocular diseases.

Mucoadhesive property of nanoparticles containing thiolated non-ionic surfactant cysteine-poly(ethylene glycol) stearate (Cys-PEG-SA) was evaluated and it was found that thiolated formulations were better as compared to non-thiolated formulations as free thiol group was found to have direct influence on mucoadhesive property [165].

Patented eye drops of N- acetylcarnosine were designed as 1% N-acetylcarnosine pro-drug of L-carnosine containing a cellulose-based mucoadhesive compound with a corneal absorption promoter in a drug delivery system. It is used in the management of age related serious eye disease, macular dystrophy, and also in ocular manifestation of diabetics. The mucoadhesive cellulose polymer entangles with mucin on the eye surface, and thus provides a prolonged release of the drug [171].

For topical ophthalmic gene therapy, De la Fuente *et al.* investigated the efficacy and mechanism of action of a bioadhesive DNA nanocarrier made of hyaluronan and chitosan. The authors found that on topical administration the nanoparticles entered the corneal and conjunctival epithelial cells and were assimilated by the cells. More importantly, the nanoparticles provided an efficient delivery of the associated plasmid DNA into the cells, reaching significant transfection levels [172].

Despite the pre-eminence of mucoadhesive polymers in ocular drug delivery in conventional as well as novel ophthalmic formulations, the utility of these formulations is inadequate due to the lack of proficient scale-up technologies and sterility problems of ophthalmic dosage forms.

13.8 Conclusion

Ocular drug delivery formulations using mucoadhesive polymers could be employed for increasing the precorneal residence time and to resolve the bioavailability issues associated

with ophthalmic drug delivery systems; both natural and synthetic polymeric materials play a significant role in the controlled drug delivery. The main purpose of these agents is to increase the viscosity and mucoadhesiveness so as to remain at the ocular site for longer time. These mucoadhesive polymers have mobile and flexible chains which interdiffuse into the mucus and penetrate to a sufficient depth to create a network. Charged polymers, both anionic and cationic, demonstrate a higher mucoadhesive capability in comparison to non-ionic. The main effect of viscosity enhancers is to reduce surface tension, to increase the corneal contact time and to decrease the drainage rate. It has been observed that a viscosity enhancer is effective in the treatment of aqueous tear-deficient dry eye symptoms. It has been demonstrated that these polymers also act by increasing corneal uptake by modifying the integrity of corneal epithelium. Also, ocular gene delivery is a very vast and promising area of research to deliver the genes to host cells for treating severe eye diseases.

Acknowledgement

The authors are grateful to Dr. Madhu Chitkara, Vice Chancellor, Chitkara University, Punjab, India and Dr. Sandeep Arora, Director, Chitkara College of Pharmacy, Chitkara University, Punjab, India for support and institutional facilities.

Disclaimer

The authors state no conflict of interest and have received no payment in preparation of this manuscript.

References

1. Y. Sultane, R. Jain, and M. Aqil, Review of ocular drug delivery. *Curr. Drug Deliv.* 3, 207-217 (2006).
2. J.D. Henderer and C.J. Rapprano, Ocular pharmacology, in: *Goodman & Gilman's the Pharmacological Basis of Therapeutics*, 11th edition, L.L. Brunton, J.S. Lazo, and K.L. Parker, (Eds.), pp. 1707-1737, McGraw-Hill, New York (2005).
3. U. Arto, Challenges and obstacles of ocular pharmacokinetics and drug delivery. *Adv. Drug Deliv. Rev.* 58, 1131-1135 (2006).
4. N.M. Davies, Biopharmaceutical considerations in topical ocular drug delivery. *Clin. Expl. Pharmacol. Physiol.* 27, 558-562 (2000).
5. J.W. Shell, Ocular drug delivery systems-A review. *Cutaneous Ocular Toxicol.* 1, 49-63 (1982).
6. S. Ding, Recent developments in ophthalmic drug delivery. *Pharm. Sci. Technol Today* 1, 328-335 (1998).
7. C. Losa, P. Calvo, E. Castro, J.L. Vila-Jato, and M.J. Alonso, Improvement of ocular penetration of amikacin sulphate by association to poly (butylcyanoacrylate) nanoparticles. *J. Pharm. Pharmacol.* 43, 548-552 (1991).
8. C. Losa, L. Marchal-Heussler, F. Orallo, J.L. Vila-Jato, and M.J. Alonso, Design of new formulations for topical ocular administration: Polymeric nanocapsules containing metipranolol. *Pharm. Res.* 10, 80-87 (1993).

9. A.M. De Campos, A. Sanchez, R. Gref, P. Calvo, and M.J. Alonso, The effect of a PEG versus a chitosan coating on the interaction of drug colloidal carriers with the ocular mucosa. *Eur. J. Pharm. Sci.* 20, 73–81 (2003).
10. O. Dudinski, B.C. Finnin, and B.L. Reed, Acceptability of thickened eye drops to human subjects. *Curr. Ther. Res.* 33, 322–337 (1983).
11. C. Marriott and N.P. Gregory, Mucus physiology and pathology, in: *Bioadhesive Drug Delivery Systems*, V. Gurny (Ed.), pp. 1–24, CRC Press, Boca Raton, FL (1990).
12. S. Roy, K. Pal, A. Anis, K. Pramanik, and B. Prabhakar, Polymers in mucoadhesive drug delivery system: A brief note. *Designed Monomers Polymers* 12, 483–495 (2009).
13. I. Singh and V. Rana, Enhancement of mucoadhesive property of polymers for drug delivery applications: A critical review. *Rev. Adhesion Adhesives* 1, 271–290 (2013).
14. B.A. Nichols, M.L. Chiappino, and C.R. Dawson, Demonstration of the mucous layer of the tear film by electron microscopy. *Invest. Ophthalmol. Visual Sci.* 26, 464–473 (1985).
15. I.K. Gipson, M. Yankauckas, S.J. Spurr-Michaud, A.S. Tisdale, and W. Rinehar, Characteristics of a glycoprotein in the ocular surface glycocalyx. *Invest. Ophthalmol. Visual Sci.* 33, 218–227 (1992).
16. J.L. Greaves and C.G. Wilson, Treatment of diseases of the eye with mucoadhesive delivery systems. *Adv. Drug Deliv. Rev.* 11, 349–383 (1993).
17. J.C. Robinson, Ocular anatomy and physiology relevant to ocular drug delivery, in: *Ophthalmic Drug Delivery Systems*, A.K. Mitra (Ed.), pp. 29–57, Marcel Dekker, New York (1993).
18. C.M. Lehr, Lectin-mediated drug delivery: The second generation of bioadhesives. *J. Controlled Release.* 65, 19–29 (2000).
19. G.P. Andrew, T.P. Laverty, and D.S. Jones, Mucoadhesive polymeric platforms for controlled drug delivery. *Eur. J. Pharm. Biopharm.* 71, 505–518 (2009).
20. T. Inatomi, S. Spurr-Michaud, A.S. Tisdale, and I.K. Gipson, Human corneal and conjunctival epithelia express MUC1 mucin. *Invest. Ophthalmol. Visual Sci.* 36, 1818–1827 (1995).
21. T. Inatomi, S. Spurr-Michaud, A.S. Tisdale, and I.K. Gipson, Expression of secretory mucin genes by human conjunctival epithelia. *Invest. Ophthalmol. Visual Sci.* 37, 1684–1692 (1996).
22. M. Berry, R.B. Ellingham, and A.P. Corfield, Polydispersity of normal human conjunctival mucins. *Invest. Ophthalmol. Visual Sci.* 37, 2559–2571 (1996).
23. M.M. Jumblatt, R.W. McKenzie, and J.E. Jumblatt, MUC5AC mucin is a component of the human precorneal tear film. *Invest. Ophthalmol. Visual Sci.* 40, 43–49 (1999).
24. R.W. McKenzie, J.E. Jumblatt, and M.M. Jumblatt, Quantification of MUC2 and MUC5AC transcripts in human conjunctiva. *Invest. Ophthalmol. Visual Sci.* 41, 703–708 (2000).
25. M.M. Jumblatt, R.W. McKenzie, P.S. Steele, C.G. Emberts, and J.E. Jumblatt, MUC7 expression in the human lacrimal gland and conjunctiva. *Cornea.* 22, 41–45 (2003).
26. P. Argueso, M. Balam, S. Spurr-Michaud, H.T. Keutmann, M.R. Dana, and I.K. Gipson. Decreased levels of the goblet cell mucin MUC5AC in tears of patients with Sjogren syndrome. *Invest. Ophthalmol. Visual Sci.* 43, 1004–1011 (2002).
27. P. Argueso, S. Spurr-Michaud, C.L. Russo, H.T. Keutmann, M.R. Dana, and I.K. Gipson. MUC16 mucin is expressed by the human ocular surface epithelia and carries the H185 carbohydrate epitope. *Invest. Ophthalmol. Visual Sci.* 44, 2487–2495 (2003).
28. H.S. Ching, H. Park, P. Kelly, and J.R. Robinson, Bioadhesive polymers as platforms for oral-controlled drug delivery. II. Synthesis and evaluation of some swelling, water-insoluble bioadhesive polymers. *J. Pharm. Sci.* 74, 399–405 (1985).
29. J.W. Lee, J.H. Park, and J.R. Robinson, Bioadhesive-based dosage forms: The next generation systems. *J. Pharm. Sci.* 89, 850–866 (2000).

30. X. Yang and J.R. Robinson, Bioadhesion in mucosal drug delivery, in: *Biorelated Polymers and Gels*, T. Okano (Ed.), Academic Press, London. (1998).
31. M.N. Kumar, R.A. Muzzarelli, C. Muzzarelli, H. Sashiwa, and A.J. Domb. Chitosan chemistry and pharmaceutical perspectives. *Chem. Rev.* 104, 6017–6084 (2004).
32. S.A. Agnihotri, N.N. Mallikarjuna, and T.M. Aminabhavi, Recent advances on chitosan-based micro and nanoparticles in drug delivery. *J. Controlled Release.* 100, 5–28 (2004).
33. O. Felt, P. Furrer, J.M. Mayer, B. Plazonnet, P. Buri, and R. Gurny, Topical use of chitosan in ophthalmology: Tolerance assessment and evaluation of precorneal retention. *Int. J. Pharm.* 180, 185–193 (1999).
34. P.K. Pawar and D.K. Majumdar, Effect of formulation factors on in vitro permeation of moxifloxacin from aqueous drops through excised goat, sheep, and buffalo corneas. *AAPS Pharm. Sci. Technol.* 7, 13 (2006).
35. M.S. Rathore and D.K. Majumdar, Effect of formulation factors on in vitro transcorneal permeation of gatifloxacin from aqueous drops. *AAPS. Pharm. Sci. Technol.* 7, 57 (2006).
36. V. Dodane and V.D. Vilivalam, Pharmaceutical applications of chitosan. *Pharm. Sci. Technol. Today* 1, 246–253 (1998).
37. A.M. De Campos, A. Sanchez, and M.J. Alonso, Chitosan nanoparticles: A new vehicle for the improvement of the delivery of drugs to the ocular surface. *Int. J. Pharm.* 224, 159–168 (2001).
38. C.M. Lehr, J.A. Bouwstra, E.H. Schacht, and H.E. Junginger, In vitro evaluation of mucoadhesive properties of chitosan and other natural polymers. *Int. J. Pharm.* 78, 43–48 (1992).
39. J.G. LeHoux and F. Grondin, Some effects of chitosan on liver function in the rat. *Endocrinology.* 132, 1078–1084 (1993).
40. S.R. Jameela, T.V. Kumary, A.V. Lal, and A. Jayakrishna, Progesterone-loaded chitosan microspheres: A long acting biodegradable controlled delivery system. *J. Controlled Release.* 52, 17–24 (1998).
41. K. Bowman and W. Leong, Chitosan nanoparticles for oral drug and gene delivery. *Int. J. Nanomedicine.* 1, 117–128 (2006).
42. A.K. Singla and M. Chawla, Chitosan: Some pharmaceutical and biological aspects- an update. *J. Pharm. Pharmacol.* 53, 1047–1067(2001).
43. K. Nagpal, S.K. Singh, and D.N. Mishra, Chitosan nanoparticles: A promising system in novel drug delivery. *Chem. Pharm Bull (Tokyo).* 58, 1423–1430 (2010).
44. H. Yi, L.Q. Wu, W.E. Bentley, R. Ghodssi, G.W. Rubloff, J.N. Culver, and G.F. Payne, Biofabrication with chitosan. *Biomacromolecules.* 6, 2882–2894 (2005).
45. A. Bernkop-Schnürch, D. Guggi, and Y. Pinter, Thiolated chitosans: Development and in vitro evaluation of a mucoadhesive, permeation enhancing oral drug delivery system. *J. Controlled Release.* 94, 177–186 (2004).
46. M.J. Alonso and A. Sanchez, The potential of chitosan in ocular drug delivery. *J. Pharm. Pharmacol.* 55, 1451–1463 (2003).
47. G. Sandri, M.C. Bonferoni, E.H. Gokce, F. Ferrari, S. Rossi. M. Patrini, and C. Caramella, Chitosan-associated SLN: In vitro and ex vivo characterization of cyclosporine A loaded ophthalmic systems. *J. Microencapsulation.* 27, 735–476 (2010).
48. H. Refai and R. Tag, Development and characterization of sponge like acyclovir ocular minitab-lets. *Drug. Deliv.* 18, 38–45 (2011).
49. K.M. Sanjay, S. Chopra, S. Talegoankar, and K. Kohli, Chitosan-sodium alginate nanoparticles as submicroscopic reservoirs for ocular delivery: Formulation, optimization and in vitro characterization. *Eur. J. Pharm. Biopharm.* 68, 513–525 (2008).

50. R.C. Nagarwal, R. Kumar, and J.K. Pandit, Chitosan coated sodium alginate-chitosan nanoparticles loaded with 5-FU for ocular delivery: In vitro characterization and in vivo study in rabbit eye. *Eur. J. Pharm. Sci.* 47, 678–685 (2012).
51. W. Chaiyasan, S.P. Srinivas, and W. Tivaboonchai, Mucoadhesive chitosan-dextran sulfate nanoparticles for sustained drug delivery to the ocular surface. *J. Ocular. Pharmacol. Therapy.* 29, 200–207 (2013).
52. P. Suphiya, M. Moutushy, S. Krishnakumar, and S.K. Sahoo, Enhanced antiproliferative activity of carboplatin-loaded chitosan-alginate nanoparticles in a retinoblastoma cell line. *Acta. Biomaterialia.* 6, 3120–3131 (2010).
53. K. Kesvan, S. Kant, P.N. Singh, and J.K. Pandit, Mucoadhesive chitosan-coated cationic microemulsion of dexamethasone for ocular delivery: In vitro and in vivo evaluation. *Curr. Eye. Res.* 38, 342–352 (2013).
54. H.R. Lin and P.C. Chang, Novel Pluronic-chitosan micelle as an ocular delivery system. *J. Biomed. Mater. Res. B.* 101, 689–699 (2013).
55. Z. Xuan, S. Meiqin, T. Shaoheng, L. Wang, and X. Liang, Synthesis of thiolated chitosan and preparation of nanoparticles with sodium alginate for ocular drug delivery. *Mol. Vision.* 18, 1973–1982 (2012).
56. A.A. Mahmoud, G.S. El-Feky, R. Kamel, and G. E. A. Awad, Chitosan/sulfobutylether- β -cyclodextrin nanoparticles as a potential approach for ocular drug delivery. *Int. J. Pharm.* 413, 229–236 (2011).
57. F. Kratz, Albumin as a drug carrier: Design of prodrug conjugates and nanoparticles. *J. Controlled Release.* 132, 171–183 (2008).
58. U. Kragh-Hansen, Structure and ligand binding properties of human serum albumin. *Danish. Med. Bull.* 37, 57–84 (1990).
59. R.S. Sudha and G. Deshpande, Albumin microspheres as an ocular delivery system for Pilocarpine nitrate. *Ind. J. Pharm. Sci.* 70, 193–197 (2008).
60. M. Yun, E.B. Michael, and T. Dolores, Human serum albumin nanoparticles for efficient delivery of Cu, Zn superoxide dismutase gene. *Mol. Vision.* 13, 746–757 (2007).
61. B. Vasudevan, T.L. Simpson, and J.G. Sivak, Regional variation in the refractive-index of the bovine and human cornea. *Optometry Visual Sci.* 85, 977–981 (2008).
62. H. Kim, S.B. Robinson, and K.G. Csaky, Investigating the movement of intravitreal human serum albumin nanoparticles in the vitreous and retina. *Pharm. Res.* 26, 329–337 (2009).
63. R.T. Addo, A. Siddig, and R. Siwale, Formulation, characterization and testing of tetracaine hydrochloride loaded albumin-chitosan microparticles for ocular drug delivery. *J. Microencapsulation.* 27, 95–104 (2010).
64. O. Smidsrod and G. Skjak-Braek, Alginate as immobilization matrix for cells. *Trends in Biotechnology.* 8, 71–78 (1990).
65. R. Russo, M. Malinconico, and G. Santagata, Effect of cross-linking with calcium ions on the physical properties of alginate films. *Biomacromolecules.* 8, 3193–3197 (2007).
66. K. Kesvan, G. Nath, and J.K. Pandit, Preparation and in vitro antibacterial evaluation of gatifloxacin mucoadhesive gellan system. *Daru.* 18, 237–246 (2010).
67. K.L. Mittal, The role of the interface in adhesion phenomena, *Polym. Eng. Sci.*, 17, 467–473 (1977).
68. N. Ahuja, V. Saini, V.K. Bishnoi, A. Garg, M. Hisoria, and J. Sharma, Formulation and evaluation of diclofenac sodium gel by using natural polymer. *Rasayan. J. Chem.* 1, 564–66 (2008).

69. C. Trinquand, J.P. Romanet, J.P. Nordmann, J.C. Dascotte, J.L. George, P. Lesure, R.C. Allen, A.L. Robin, D. Long, G.D. Novack, J.C. Lue, and G. Kaplan, Efficacy et tolerance du carteolol 1% liberation prolongee une fois par jour. *J. Fr. Ophthalmol.* 26, 131–136 (2003).
70. P.E. Jansson and B. Lindberg, Structural studies of gellan gum, an extracellular polysaccharide elaborated by *Pseudomonas elodea*. *Carbohydrate. Res.* 124, 135–139 (1983).
71. M.S. Kuo, A.J. Mort, and A. Dell, Identification and location of L-glycerate, an unusual acyl substituent in gellan gum. *Carbohydrate. Res.* 156, 173–187 (1986).
72. D. Lobas, S. Schumpe, and W.D. Deckwer, The production of gellan exopolysaccharide with *Sphingomonas paucimobilis* E2 (DSM 6314). *Appl. Microbiol. Biotechnol.* 37, 411–415 (1992).
73. D.E. Pszczola, Gellan gum wins IFT's food technology industrial achievement award. *Food. Technol.* 47, 94–96 (1993).
74. J. Balasubramaniam, S. Kant, and J.K. Pandit, In vitro and in vivo evaluation of the Gelrite gellan gum-based ocular delivery system for indomethacin. *Acta. Pharm.* 53, 251–261 (2003).
75. H.M. El-Laithy, D.I. Nesseem, A.A. El-Adly, and M. Shoukry, Moxifloxacin-Gelrite in situ ophthalmic gelling system against photodynamic therapy for treatment of bacterial corneal inflammation. *Arch. Pharm. Res.* 34, 1663–1678 (2011).
76. J.Q. Shen, Y. Gan, L. Gan, C.L. Zhu, and J.B. Zhu, Ion-sensitive nanoemulsion-in situ gel system for ophthalmic delivery of flurbiprofen axetil. *Yao Xue Xue Bao.* 45, 120–125 (2010).
77. Y.D. Sanzgiri, S. Maschi, V. Crescenzi, L. Callegaro, E.M. Topp, and V.J. Stella, Gellan-based systems for ophthalmic sustained delivery of methylprednisolone. *J. Controlled Release.* 26, 195–201 (1993).
78. Y. Liu, J. Liu, X. Zhang, and R. Zhang, In situ gelling Gelrite/alginate formulations as vehicles for ophthalmic drug delivery. *AAPS. Pharm. Sci. Technol.* 11, 610–620 (2010).
79. E.F. Rosenlund, The intraocular pressure-lowering effect of timolol in gel-forming solution. *Acta. Ophthalmol. Scand.* 74, 160–162 (1996).
80. A.H. Shedden, J. Laurence, A. Barrish, and T.V. Olah, Plasma timolol concentrations of timolol maleate: Timolol gel-forming solution (TIMOPTIC-XE) once daily versus timolol maleate ophthalmic solution twice daily. *Doc. Ophthalmol.* 103, 73–79 (2001).
81. S.A. Altaf, K. Yu, J. Parasrampur, and D.R. Friend, Guar gum-based sustained release. *Diltiazem. Pharm. Res.* 15, 1196–1201 (1998).
82. M.A. Zirnsak, D.V. Boger, and V. Tirtaatmadja, Study of shear and dynamic rheological properties of xanthan gum solution in viscous solvents. *J. Rheology.* 43, 627–650 (1999).
83. J.L. Zatz and S. Knapp, Viscosity of xanthan gum solution at low shear rates. *J. Pharm. Sci.* 73, 468–471 (1984).
84. J. Ceulemans, I. Vinckier, and A. Ludwig, The use of xanthan gum in ophthalmic dosage form: Rheological characterisation of the interaction with mucin. *J. Pharm. Sci.* 91, 1117–1127 (2002).
85. G. Meseguer, P. Buri, B. Plazonnet, A. Rozier, and R. Gurny, Gamma scintigraphic comparison of eye drops containing pilocarpine in healthy volunteers. *J. Ocul. Pharmacol. Therapy.* 12, 481–488 (1996).
86. S.M. Al-Saidan, Y.S.R. Krishnaiah, S.S. Patro, and V. Satyanaryana, In vitro and in vivo evaluation of guar gum matrix tablets for oral controlled release of water-soluble diltiazem hydrochloride. *AAPS. Pharm. Sci. Technol.* 6, 14–21 (2005).
87. N.I. Dure and A.H. Erum, Physiological and pharmaceutical properties of guar gum derivatives. *Rep. Opin.* 2, 77–83 (2010).
88. P. Khullar, R.K. Khar, and S.P. Agarwal, Evaluation of guar gum in the release of sustained release matrix tablets. *Drug. Dev. Ind. Pharm.* 24, 1095–1099 (1998).

89. T.R. Bhardwaj, M. Kanwar, R. Lal, and A. Gupta, Natural gums and modified natural gums as sustained release carriers. *Drug. Dev. Ind. Pharm.* 26, 1025–1038 (2000).
90. J.H. Guo, G.W. Skinner, W.W. Harcum, and P.E. Barnum, Pharmaceutical applications of naturally occurring water soluble polymers. *Pharm. Sci. Technol. Today.* 1, 254–261 (1988).
91. A. Matheson, Your patient has dry eye: What treatments are available. <http://www.ocularsolutions.com>
92. G.N. Foulks, Clinical evaluation of the efficacy of PEG/PG lubricant eye drops with gelling agent (HP-Guar) for the relief of the signs and symptoms of dry eye disease: A review. *Drugs Today. (Barcelona)* 43, 887–896 (2007).
93. H.G. Garg and C.A. Hales, *Chemistry and Biology of Hyaluronan*. 1st edition., pp. 1–21, Elsevier, Oxford (2004).
94. G. Kogan, L. Soltes, R. Stern, and P. Gemeiner, Hyaluronic acid: A natural biopolymer with a broad range of biomedical and industrial applications. *Biotechnol. Lett.* 29, 17–25 (2006).
95. P. Gribbon, B.C. Heng, and T.E. Hardingham, The analysis of intermolecular interactions in concentrated hyaluronan solutions suggests no evidence for chain–chain association. *Biochem. J.* 350, 329–335 (2000).
96. F. Guillaumi, P. Furrer, O. Felt-Baeyens, B.L. Fuhlendorff, and S. Nymand, Comparative studies of various hyaluronic acids produced by microbial fermentation for potential topical ophthalmic applications. *Invest. Ophthalmol. Visual Sci.* 43, 3409–3415(2002).
97. V.P. De Luise and S.W. Peterson, The use of topical Healon tears in the management of refractory dry-eye syndrome. *Ann. Ophthalmol.* 16, 823–824 (1984).
98. F. Baudouin, F. Brignole, and B. Dupas, Reduction in keratitis and CD44 expression in dry eye patients treated with a unique 0.18% sodium hyaluronate solution. *Invest Ophthalmol Visual Sci.* 42, S32 (2001).
99. R. Vogel, R.S. Crockett, N. Oden, T.W. Laliberte, and L. Molina, Demonstration of efficacy in the treatment of dry eye disease with 0.18% sodium hyaluronate ophthalmic solution. *Am. J. Ophthalmol.* 149, 594–601 (2010).
100. M.F. Saettone, P. Chetoni, M.T. Torracca, S. Buralassi, and B. Giannaccini, Evaluation of muco-adhesive properties and in vivo activity of ophthalmic vehicles based on hyaluronic acid. *Int J Pharm.* 51, 203–212 (1989).
101. Y. Xu, J.Z. Song, G.R. Pang, Z.J. Chen, J.J. Zhang, and X.F. Lu, Ocular pharmacokinetics of 0.5% pilocarpine with sodium hyaluronate in rabbits. *Zhonghua. Yan. Ke. Za. Zhi.* 40, 87–89 (2004).
102. S.F. Bernatchez, C. Tabatabay, and R. Gurny, Sodium hyaluronate 0.25% used as a vehicle increases the bioavailability of topically administered gentamicin. *Graefes Arch. Clin. Expl. Ophthalmol.* 231, 157–161 (1993).
103. R.C. Rowe, P.J. Sheskey, and S.C. Owen, (Eds), *Handbook of Pharmaceutical Excipients*, 5th edition, Pharmaceutical Press, London, UK (2006).
104. Remington: *The Science and Practice of Pharmacy*, 21st edition, P.P. Gerbino (Ed), pp. 1318–1349, Lippincott, Williams & Wilkins, Philadelphia (2005).
105. C. Rochas and M. Rinaudo, Activity coefficients of counterions and conformation in kappa-Carrageenan systems. *Biopolymers.* 19, 1675–1687 (1980).
106. I.D. Rupenthal, C.R. Green, and R.G. Alany, Comparison of ion-activated in situ gelling systems for ocular drug delivery. Part 1: physicochemical characterization and in vitro release. *Int J Pharm.* 411, 69–77 (2011).
107. M. Saettone, E. Buralassi, P. Boldrini, P. Bianchini, and G. Luciani, Ophthalmic solutions viscosified with tamarind seed polysaccharide, US Patent 6056950A, assigned to. Farmigea SPA (May 2. 2000).

108. L.L. Mannucci, I. Fregona, and D. Gennaro, Use of a new lachrymal substitute (TS polysaccharide) in contactology. *J. Med. Contacology. Low. Vision.* 1, 6–9 (2000).
109. E. Ghelardi, A. Tavanti, P. Davini, and F. Celandroni, A mucoadhesive polymer extracted from tamarind seed improves the intraocular penetration and efficacy of Rufloxacin in topical treatment of experimental bacterial keratitis. *Antimicrobial Agents. Chemother.* 48, 3396–3401 (2004).
110. M. Rolando and C. Valente, Establishing the tolerability and performance of tamarind seed polysaccharide (TSP) in treating dry eye syndrome: Results of a clinical study. *BMC Ophthalmol.* 7, 5:1–8 (2007).
111. P. Versura, V. Profazio, N. Balducci, and E.C. Campos, Efficacy of two-month treatment with Xilolal eyedrops for discomfort from disposable soft contact lenses. *Clin. Ophthalmol.* 4, 1035–1041 (2010).
112. G. Uccello-Barretta, S. Nazzi, Y. Zambito, G. Di Colo, F. Balzano, and M. Sansò, Synergistic interaction between TS-polysaccharide and hyaluronic acid: Implications in the formulation of eye drops. *Int. J. Pharm.* 395, 122–131 (2010).
113. A.D. Prete and M. Sanso, Ophthalmic compositions based on tamarind seed polysaccharide and hyaluronic acid. EP2197456B1 (February 23, 2010).
114. H. Kaura, M. Ahuja, S. Kumar, and N. Dilbaghia, Carboxymethyl tamarind kernel polysaccharide nanoparticles for ophthalmic drug delivery. *Int. J. Biol. Macromol.* 50, 833–839 (2012).
115. G. Uccello-Barretta, S. Nazzi, F. Balzano, and M. Sansò, A nuclear magnetic resonance approach to the comparison of mucoadhesive properties of polysaccharides for ophthalmic uses. *Int. J. Pharm.* 406, 78–83 (2011).
116. G. Uccello-Barretta, F. Balzano, L. Vanni, and M. Sanso, Mucoadhesive properties of tamarind-seed polysaccharide/hyaluronic acid mixtures: A nuclear magnetic resonance spectroscopy investigation. *Carbohydrate Polym.* 91, 568–72 (2013).
117. S. Burgalassi, N. Nicosia, D. Monti, and G. Falcone, Larch arabinogalactan for dry eye protection and treatment of corneal lesions: Investigation on rabbits. *J. Ocular Pharmacol. Therapy.* 23, 541–550 (2007).
118. S.S. Leung and J.R. Robinson The contribution of anionic polymer structural features to mucoadhesion. *J. Controlled Release.* 5, 223–231 (1988).
119. M.M. Patel, J.D. Smart, T. G. Nevell, R.J. Ewen and P J. Eaton, Mucin/poly (acrylic acid) interactions: A spectroscopic investigation of mucoadhesion. *Biomacromolecules.* 4, 1184–1190 (2003).
120. Z. Degim and I.W. Kellaway, An investigation of the interfacial interaction between poly (acrylic acid) and glycoprotein. *Int. J. Pharm.* 175, 9–16 (1998).
121. M. Oescher and S. Keipert, Polyacrylic acid/polyvinylpyrrolidone biopolymeric systems: I. Rheological and mucoadhesive properties of formulations potentially useful for the treatment of dry-eye-syndrome. *Eur. J. Pharm. Biopharm.* 47, 113–118 (1999).
122. K. Marner, P.M. Moller, M. Dillon, E.R. Pedersen, P. Armitage, and M. Hills, Viscous Carbomer eye drops in patients with dry eye. *Acta. Ophthalmol. Scand.* 74, 249–252 (1996).
123. E.J. Michael, J.M. Paul, and B. Mike, Carbomer and sodium hyaluronate eyedrops for moderate dry eye treatment. *Optometry. Visual Sci.* 85, 750–757 (2008).
124. Q. Xiao, Y. Hu, F. Chen, and X. Chen, A comparative assessment of the efficacy of Carbomer gel and carboxymethyl cellulose containing artificial tears in dry eyes. *J. Huazhong. Univ. Sci. Technol.* 28, 592–595 (2008).
125. C. Wu, H. Qi, and W. Chen, Preparation and evaluation of a Carbopol/ HPMC based in situ gelling ophthalmic system for puerarin. *Yakugaku Zasshi.* 127, 183–191 (2007).

126. H. Wu, Z. Liu, J. Peng, L. Li, N. Li, J. Li, and H. Pan, Design and evaluation of baicalin-containing in situ pH-triggered gelling system for sustained ophthalmic drug delivery. *Int. J. Pharm.* 410, 31–40 (2011).
127. K. Kesavan, S. Kant, P.N. Singh, and J.K. Pandit, Effect of hydroxypropyl- β -cyclodextrin on the ocular bioavailability of dexamethasone from a pH-induced mucoadhesive hydrogel. *Curr. Eye. Res.* 36, 918–929 (2011).
128. K. P. Mukesh, C. Gulshan, and P. Kamla, Design and development of a novel pH triggered nanoemulsified in-situ ophthalmic gel of fluconazole: Ex-vivo transcorneal permeation, corneal toxicity and irritation testing. *Drug. Dev. Ind. Pharm.* 39, 780–790 (2013).
129. P.K. Deshmukh and S.G. Gattani, In vitro and in vivo consideration of novel environmentally responsive ophthalmic drug delivery system. *Pharm. Dev. Technol.* 18, 950–956 (2013).
130. G.H. Hsiue, J.A. Guu, and C.C. Cheng, Poly (2-hydroxyethyl methacrylate) film as a drug delivery system for pilocarpine. *Biomaterials.* 22, 1763–1769 (2001).
131. A.U. Canan, Update and critical appraisal of the use of topical azithromycin ophthalmic 1% (Azasite[®]) solution in the treatment of ocular infections. *Clin. Ophthalmol.* 5, 801–809 (2011).
132. R. Pignatello, C. Bucolo, and G. Puglisi, Ocular tolerability of Eudragit RS 100R and RL 100R nanosuspensions as carriers for ophthalmic controlled drug delivery. *J. Pharm. Sci.* 91, 2636–2641 (2002).
133. U.A. Shinde, J.N. Shete, H.A. Nair, and K.H. Singh, Eudragit RL100 based microspheres for ocular administration of azelastine hydrochloride. *J. Microencapsulation.* 29, 511–519 (2012).
134. H.K. Ibrahim, I.S. El-Leithy, and A.A. Makky, Mucoadhesive nanoparticles as carrier systems for prolonged ocular delivery of gatifloxacin/prednisolone biotherapy. *Mol. Pharmaceutics.* 7, 576–585 (2010).
135. R. Pignatello, N.K. Ricupero, C. Bucolo, F. Maugeri, A. Maltese, and G. Puglisi, Preparation and characterization of Eudragit Retard nanosuspensions for the ocular delivery of Cloricromene. *AAPS. Pharm. Sci. Technol.* 7, E27 (2006).
136. G. Khurana, S. Arora, and P.K. Pawar, Ocular insert for sustained delivery of gatifloxacin sesquihydrate: Preparation and evaluations. *Int. J. Pharm. Investig.* 2, 70–77 (2012).
137. P.K. Pawar, R. Katara, and D.K. Majumdar, Design and evaluation of moxifloxacin hydrochloride ocular inserts. *Acta Pharm.* 62, 93–104 (2012).
138. K.P.R. Chowdary, and Y. Shrinivasrao, Mucoadhesive drug delivery systems: A review of current status. *Indian Drugs.* 37, 400–406 (2000).
139. Z. Liu, J. Li, S. Nie, H. Liu, P. Ding, and W. Pan, Study of an alginate/HPMC-based in situ gelling ophthalmic delivery system for gatifloxacin. *Int. J. Pharm.* 315, 12–17 (2006).
140. S. Mandal, M.K. Thimmasetty, G. Prabhushankar, and M. Geetha, Formulation and evaluation of an in situ gel-forming ophthalmic formulation of moxifloxacin hydrochloride. *Int. J. Pharm. Investig.* 2, 78–82 (2012).
141. A. Prinz, C. Fennes, W. Buehl, and O. Findl, Efficacy of ophthalmic viscosurgical devices in maintaining corneal epithelial hydration and clarity: In vitro assessment. *J. Cataract. Refract. Surgery.* 38, 2154–2159 (2012).
142. Y.A. Chen, N. Hirschschall, and O. Findl, Comparison of corneal wetting properties of viscous eye lubricant and balanced salt solution to maintain optical clarity during cataract surgery. *J. Cataract. Refract. Surgery.* 37, 1806–1808 (2011).
143. C. Vijaya and G.K. Swetha, Ion-activated in situ gelling ophthalmic delivery systems of Azithromycin. *Indian J. Pharm. Sci.* 73, 615–620 (2011).

144. M. Bhowmik, S. Das, D. Chattopadhyay, and L. Ghosh, Study of thermo-sensitive in-situ gels for ocular delivery. *Sci. Pharm.* 79, 351–358 (2011).
145. W.H. Ridder, J.O. Lamotte, L. Ngo, and J. Fermin, Short-term effects of artificial tears on visual performance in normal subjects. *Optometry Visual Sci.* 82, 370–377 (2005).
146. A. Kumari, S.K. Yadav, and S.C. Yadav, Biodegradable polymeric nanoparticles based drug delivery systems. *Colloids Surfaces B.* 75, 1–18 (2010).
147. J.M. Barichello, M. Morishita, K. Takayama, and T. Nagai, Encapsulation of hydrophilic and lipophilic drugs in PLGA nanoparticles by the nanoprecipitation method. *Drug. Dev. Ind. Pharm.* 25, 471–476 (1999).
148. J. Araujo, E. Vega, C. Lopes, M.A. Egea, M.L. Garcia, and E.B. Souto, Effect of polymer viscosity on physicochemical properties and ocular tolerance of FB-loaded PLGA nanospheres. *Colloids Surfaces B.* 72, 48–56 (2009).
149. S.M. Agnihotri and P.R. Vavia, Diclofenac-loaded biopolymeric nanosuspensions for ophthalmic application. *Nanomedicine.* 5, 90–95 (2009).
150. B. Mandal, K.K. Halder, S.K. Dev, M. Bhowmik, M.C. Debnath, and L.K. Ghosh, Development and physical characterization of chloramphenicol loaded biodegradable nanoparticles for prolonged release. *Pharmazie.* 64, 445–449 (2009).
151. M. Mitra, R. Misra, A. Harilal, S.K. Sahoo, and S. Krishnakumar, Enhanced in vitro antiproliferative effects of EpCAM antibody-functionalized paclitaxel-loaded PLGA nanoparticles in retinoblastoma cells. *Mol. Vision.* 17, 2724–2737 (2011).
152. W. Xiang-Gen, Y. Li-Na, X. Meng, and J. Hao-Ran, Anti-infectious activity of intravitreal injectable voriconazole microspheres on experimental rabbit fungal endophthalmitis caused by *aspergillus fumigatus*. *J. Pharm. Sci.* 100, 1745–1759 (2011).
153. E. Vega, M. A. Egea, A. C. Calpena, M. Espina, and M. L. Garcia, Role of hydroxypropyl- β -cyclodextrin on freeze-dried and gamma-irradiated PLGA and PLGA-PEG diblock copolymer nanospheres for ophthalmic flurbiprofen delivery. *Int. J. Nanomedicine.* 7, 1357–1371 (2012).
154. K. Edsman, J. Carlfors, and R. Peterson, Rheological evaluation of Poloxamer as an in situ gel for ophthalmic use. *Eur. J. Pharm. Sci.* 6, 105–12 (1998).
155. L. Bromberg, Properties of aqueous solutions and gels of poly(ethylene oxide)-*b*-poly(propylene oxide)-*b*-poly(ethylene oxide)-*g* poly(acrylic acid). *J. Phys. Chem. B.* 102, 10736–10744 (1998).
156. Q. Zhang, N.R. Ko, and J.K. Oh, Recent advances in stimuli-responsive degradable block copolymer micelles: Synthesis and controlled drug delivery applications. *Chem. Commun.* 48, 7542–7552 (2012).
157. S. Gupta, M.K. Samanta, and A.M. Raichur, Dual-drug system based on in situ gel-forming nanosuspension of forskolin to enhance antiglaucoma efficacy. *AAPS. PharmSci. Technol.* 11, 322–335 (2010).
158. D.I. Nesseem, Ophthalmic delivery of sparfloxacin from in situ gel formulation for treatment of experimentally induced bacterial keratitis. *Drug. Test. Anal.* 3, 106–115 (2011).
159. D. Serge, Tolerability and acceptability of Blephagel: A novel eyelid hygiene aqueous gel. *Clin. Ophthalmol.* 6, 71–77 (2012).
160. N.M. Davis, S.J. Farr, J. Hadgraft, and I.W. Kellaway, Evaluation of mucoadhesive polymers in ocular drug delivery. I. Viscous solutions. *Pharm. Res.* 8, 1039–43 (1991).
161. H. Sasaki, K. Yamamura, T. Mukai, K. Nishida, J. Nakamura, M. Nakashima, and M. Ichikawa, Enhancement of ocular drug penetration. *Crit. Rev. Therapy. Drug. Carrier. Syst.* 16, 85–146 (1999).
162. A.R. Bary, I.G. Tucker, and N.M. Davies, Considerations in the use of hydroxypropyl-beta-cyclodextrin in the formulation of aqueous ophthalmic solutions of hydrocortisone. *Eur. J. Pharm. Biopharm.* 2, 237–244 (2000).

163. G. Abdelbary, Ocular ciprofloxacin hydrochloride mucoadhesive chitosan-coated liposomes. *Pharm. Dev. Technol.* 1, 44–56 (2011).
164. M.M. Mehanna, H.A. Elmaradny, and M.W. Samaha, Mucoadhesive liposomes as ocular delivery system: Physical, microbiological, and in vivo assessment. *Drug. Dev. Ind. Pharm.* 1, 108–118 (2010).
165. J. Shen, Y. Wang, Q. Ping, Y. Xiao, and X. Huang, Mucoadhesive effect of thiolated PEG stearate and its modified NLC for ocular drug delivery. *J. Controlled Release.* 137, 217–223 (2009).
166. R.M. Byrro, G.D.O. Fulgenico, and A.J. Da Silva- Cunha, Determination of ofloxacin in tear by HPLC-ESI-MS/MS method: Comparison of ophthalmic drug release between a new mucoadhesive chitosan film and a conventional eye drop formulation in rabbit model. *J. Pharm. Biomed. Anal.* 70, 544–548 (2012).
167. G.O. Fulgêncio, F.A. Viana, R.R. Ribeiro, M.I. Yoshida, A.G. Faraco, A.S. Cunha-Júnior, New mucoadhesive chitosan film for ophthalmic drug delivery of timolol maleate: In vivo evaluation. *J. Ocular Pharmacol. Therapy.* 4, 350–358 (2012).
168. G. Di Colo, S. Buralassi, P. Chetoni, M.P. Fiaschi, Y. Zambito, and M.F. Saettone, Gel-forming erodible inserts for ocular controlled delivery of ofloxacin. *Int. J. Pharm.* 215, 101–111 (2001).
169. P.A. Campochiaro, Q.D. Nguyen, G. Hafiz, S.M. Shah, S. Bloom, D.M. Brown, M. Busquets, and T. Ciulla, Aqueous levels of fluocinolone acetonide after administration of fluocinolone acetonide inserts or fluocinolone acetonide implants. *Ophthalmology.* 120, 583–587 (2013).
170. T. Nguyen and R. Latkany, Review of hydroxypropyl cellulose ophthalmic inserts for treatment of dry eye. *Clin. Ophthalmol.* 5, 587–591 (2011).
171. M.A. Babizhayev, Current ocular drug delivery challenges for *N*-acetylcarnosine: Novel routes and modes of delivery, design for enhancement of therapeutic activity and drug delivery relationships. *Recent. Patent Drug. Deliv. Formul.* 3, 229–265 (2009).
172. M. De la Fuente, B. Seijo, and M.J. Alonso, Bioadhesive hyaluronan-chitosan nanoparticles can transport genes across the ocular mucosa and transfect ocular tissue. *Gene Therapy.* 15, 668–676 (2008).
173. S. Suri and R. Banerjee, In vitro evaluation of in situ gels as short term vitreous substitutes. *J. Biomed. Mater. Res. A.* 79, 650–664 (2006).
174. J.L. Ubels, D.P. Clousing, T.A. Van Hantsma, B.S. Hong, P. Stauffer, B. Asgharian, and D. Meadows, Pre-clinical investigation of the efficacy of an artificial tear solution containing hydroxypropyl-guar as a gelling agent. *Curr. Eye. Res.* 28, 437–444 (2004).
175. M. Karakelle and M.R. Brunstedt, Carrageenan viscoelastics for ocular surgery. US Patent, No. 7060297B2 (2006).
176. S. Buralassi, P. Chetoni, L. Panichi, E. Boldrini, and M.F. Saettone, Xyloglucan as a novel vehicle for timolol: Pharmacokinetics and pressure lowering activity in rabbits. *J. Ocular. Pharmacol. Therapy.* 16, 497–509 (2000).
177. T. Tammelín, A. Paananen, and M. Osterberg, Hemicelluloses at interfaces: Some aspects of the interactions, in: *The Nanoscience and Technology of Renewable Biomaterials*, 1st edition, O.J. Rojas and L.A. Lucia (Eds.), pp. 149–172, Wiley Publishing (2009).
178. A. Ludwig, The use of mucoadhesive polymers in ocular drug delivery. *Adv. Drug. Dev. Rev.* 57, 1595–1639 (2005).
179. N. Sanders, L. Peeters, I. Lentacker, I. Demeester, and S.C. De Smedt, Wanted and unwanted properties of surface PEGylated nucleic acid nanoparticles in ocular gene transfer. *J. Controlled Release.* 122, 226–235 (2007).
180. A. Venkatesh, M. Shan, F. Langellotto, and G. Gao, Retinal gene delivery by rAAV and DNA electroporation. *Curr Protocol in Microbiol.* 28, 14D.4.1–14D.4.32 (2013).

181. G. Puras, J. Zarate, M. Aceves, A. Murua, and A.R. Dhaz, Low molecular weight oligochitosans for non-viral retinal gene therapy. *Euro. J. Pharm. Biopharm.* 83, 131–140 (2013).
182. S. Alqawlaq, J.T. Huzil, M. V. Ivanova, and M. Foldvari, Challenges in neuroprotective nanomedicine development: Progress towards noninvasive gene therapy of glaucoma. *Nanomedicine.* 7, 1067–1083 (2012).
183. A. Tandon, A. Sharma, J.T. Rodier, A.M. Klibanov, and F.G. Rieger, BMP7 Gene transfer via gold nanoparticles into stroma inhibits corneal fibrosis in vivo. *Plos One.* 8, 434 (2013).
184. M. Jiang, Li Gan, C. Zhu, Y. Dong, J. Liu, and Y. Gan, Cationic core shell liponanoparticles for ocular gene delivery. *Biomaterials.* 33, 7621–7630 (2012).
185. C.M. Adeyeye, L.V. Davis, and K.U. Kotreka, In-situ gel ophthalmic drug delivery system of estradiol for prevention of cataracts. US Patent, No. 20110082128 A1 (2011).
186. E. Matsumoto, Y. Nishina, and K. Haruna, Ophthalmic composition containing alginate acid and salt thereof. US Patent, No. 8501822 B2 (2013).
187. A.D. Prete and M. Sanso, Ophthalmic compositions based on tamarind seed polysaccharide and hyaluronic acid. US Patent, No.20100279981A1 (2010).

Index

- ABJs. *See* Adhesively bonded joints
- Acid-base theory, 149–150
- Acid-hardening of resin, 93
- Active pharmaceutical ingredient (API), 232
- Adhesive-adherend interfaces, 59, 60
- Adhesive joints
- and composite material problems, 61
 - thermal stresses, 60
- Adhesive joints exhibit interfacial failure, 59
- Adhesive joint strength, 130
- Adhesively bonded joints (ABJs), 357
- Adhesively bonded single lap joint, 67
- Adhesive stiffness, 365–374
- AFM. *See* Atomic force microscopy
- AG. *See* Arabinogalactan
- Albumin, 256
- Alginate, 462–463
- Amino groups, wet-chemical chain extension, 339
- Amino-terminated L-Arginyl-Glycyl-L-Aspartic acid, 48
- Ammonia plasma, 319–322, 322–324
- Amphiphilic block copolymers, 46–47
- ANALYSIS OF VARIANCE (ANOVA), 433–434
- Analytical ultracentrifugation (AUC), 231
- ANOVA. *See* ANALYSIS OF VARIANCE
- API. *See* Active pharmaceutical ingredient
- AP-PECVD. *See* Atmospheric-pressure plasma-enhanced chemical vapor deposition
- Arabinogalactan (AG), 467
- Artificial neural networks, 73
- Atmospheric-pressure plasma-enhanced chemical vapor deposition (AP-PECVD), 38
- Atomic force microscopy (AFM), 132–135, 194–195
- advantages of, 234–236
 - and pharmaceutical formulations, 233–234
 - prospects, 236–237
- ATR-IR. *See* Attenuated total reflectance infrared spectroscopy
- Attenuated total reflectance infrared spectroscopy (ATR-IR), 205–206
- AUC. *See* Analytical ultracentrifugation
- Balanced joints, 58
- BEM. *See* Boundary element method
- Bi-material interface, 61
- Bio-adhesives, 387–388
- Bio-based matrices
- cellulose, 179–180
 - chitosan (CH), 180–181

- natural rubber, 182–183
- poly(lactic acid) (PLA), 177–178
- polyhydroxybutyrate (PHB), 178–179
- starch, 181–182
- Biocompatibility, cyanoacrylate adhesives, 284–285
- Biocomposites and bionanocomposites
 - bio-based matrices, 177–183
 - biopolymers, 170–174
 - interface characterization techniques, 189–206
 - interfacial adhesion issues, 185–189
 - processing techniques, 184
- Biopolymers
 - cellulose, 170–171
 - chemical modification, 174–177
 - chitin, 171–173
 - starch, 173–174
- Bond strength, cyanoacrylate adhesives, 282–283
- Boundary conditions, 59
- Boundary element method (BEM), 70
- Bulk modulus, 66
- n-Butyl-2-cyanoacrylate
 - glubran 2, 264
 - histoacryl blue, 264
 - truffill, 267
- Carbomer, 467–468
- Carbon-based NP, 359
- Carbon dioxide plasma, 315–318
- Carbon nanotubes (CNTs), 2–3
 - adhesion, 17–20
 - deformation, 2
 - elastica model of, 17–20
 - elastic system, 24
- Carrageenan, 465–466
- Cassie-Baxter equation, 14
- C-Br groups, 340–342
- C-C covalent bonding, 2
- Cell adhesion, 3, 20–23
- Cellulose, 170–171, 174–177, 179–180, 469–470
- Ceramic-metal-adhesive-metal-ceramic plate configuration, 71
- CH. *See* Chitosan
- Chemical (covalent) bonding theory, 148–149
- Chitin, 171–173, 174–177
- Chitosan (CH), 180–181, 454
- Chitosan-based formulations, 460–461
- Clinical history, cyanoacrylate adhesives
 - biocompatibility tests for, 286–287
 - graft fixation, 289–290
 - skin wounds, closure of, 288–289
 - superficial incision closure, 288–289
 - surgical and medical applications of, 288
 - surgical procedures and future uses, 289
- CNTs. *See* Carbon nanotubes
- Cohesive failure, 59
- Cohesive zone model, 59
- Collagen-based adhesives, 255
- Condensation curing, 33–34
- Corona treatment, 39–40
- Covalent surface grafting, 44–46
- Curing mechanism, cyanoacrylate adhesives
 - chemical reaction of, 278
 - comparative shelf-life, 279
 - packaging, container materials for, 279–282
- Curing reactions, 32–36
- Cyanoacrylate adhesives
 - biocompatibility, 284–285
 - bond strength, 282–283
 - clinical history, 285–290
 - curing mechanism, 278–282
 - development path, 290–291
 - formulation development, 269–278
 - increased demand, drivers for, 292
 - industrial adhesives, 257–263
 - properties, 278–285
 - tissue adhesives, 263–269
 - toxicity, 283–284

- Cys-PEG-SA. *See* Cysteine-poly(ethylene glycol) stearate
- Cysteine-poly(ethylene glycol) stearate (Cys-PEG-SA), 473
- Deformation states, 71
- Dentistry, bonding dissimilar materials in
- 2-hydroxyethyl methacrylate, 408–410
 - itaconic acid, 408–410
 - oleic acid, 408–410
 - phosphate coupling agents, 404–405
 - silane coupling agents, 399–403
 - thione/thiol coupling agents, 405–406
 - titanate coupling agents, 406–407
 - zircoaluminate coupling agents, 408
 - zirconate coupling agents, 403–404
- Derjaguin, Landau, Verwey and Overbeek (DLVO), 220
- Derjaguin, Muller and Toporov (DMT) theory, 132–134, 220
- Design of experiments (DoE), 432
- Differential scanning calorimetry (DSC), 199
- Diffusion theory of adhesion, 145–148
- 3, 4-Dihydroxy-L-phenylalanine (L-DOPA), 409
- 4,4' Diphenylmethane diisocyanate (MDI), 109
- DLVO. *See* Derjaguin, Landau, Verwey and Overbeek
- DMT. *See* Derjaguin, Muller and Toporov theory
- DMTA. *See* Dynamic mechanical thermal analysis
- DoE. *See* Design of experiments
- DPIs. *See* Dry powder inhalers
- Droplet adhesion, 12–17
- Dry powder inhalers (DPIs), 221, 223
- DSC. *See* Differential scanning calorimetry
- Durability of adhesives, 382–383
- Dynamic fracture, 63
- Dynamic mechanical thermal analysis (DMTA), 199–203
- EDL. *See* Electrostatic double layer
- EDS. *See* Energy Dispersive Spectroscopy ()
- Elastic deformation, 3
- Elastic energy, 4
- Electronic or electrostatic theory, 135–137
- Electrospray ionization (ESI) deposition, 332–333
- Electrostatic double layer (EDL), 220
- Energy Dispersive Spectroscopy (EDS), 438
- EPR. *See* Ethylene propylene rubber
- EPS. *See* Extracellular polymeric substances
- ESI. *See* Electrospray ionization deposition
- Ethylene propylene rubber (EPR), 426
- Eudragit, 468–469
- Extracellular polymeric substances (EPS), 221
- FBRM. *See* Focused beam reflectance measurements ()
- FGMs. *See* Functionally graded materials
- FIB. *See* Focused Ion Beam
- Fiber placement, 67
- Fiber reinforced resin composites (FRCs), 401
- Fiber-tear, 59
- Fibrin sealants, 252–254
- Finite element discretization approach, 62
- Flame energy, 422
- Flame treatment equipment, 418–421
- burner to substrate gap, 422
 - combustion conditions - air/gas ratio, 421–422
 - control instrumentation, 423
 - flame chemistry, 423–426
 - flame energy, 422
 - gas saving, 423

- main reaction zone, 424–425
- on plastics, 426–441
- of polypropylene (PP), 426–441
- post-combustion zone, 425–426
- pre-reaction zone, 423–424
- process parameters, 421–423
- system layout, 422
- valve train, 422–423
- Focused beam reflectance
 - measurements (FBRM), 231
- Focused ion beam (FIB), 436
- Formaldehyde-based
 - thermosetting resins, 85
- Formaldehyde emission, 91
- Formulation development
 - monomeric derivatives, 270–272
 - optimal formulation development, 272–278
- Fouling release coatings, 37
- Fourier series, 59
- Fourier transform infrared (FTIR)
 - spectroscopy, 203–205
- Fracture mechanics, 59
- FRCs. *See* Fiber reinforced resin composites
- Free-radical curing, 33
- FTIR. *See* Fourier transform infrared spectroscopy
- Functionally graded adherends, 67–73
- Functionally graded adhesives, 73–77
- Functionally graded materials (FGMs), 61–63
 - constitutive relations, 63–67
 - mechanical behaviour of, 64
- Gas saving, flame treatment
 - equipment, 423
- Gellan gum, 463
- Gel permeation chromatography (GPC), 91
- Gene delivery, 472
- Geometrical nonlinear effects, 59
- Geometrical non-linearity, 58
- Gibbs free energy, 15
- GICs. *See* Glass ionomer cements
- Glass ionomer cements (GICs), 398
- Glutaraldehyde products, 256
- Golden-section methods, 62
- GPC. *See* Gel permeation chromatography
- Grafting, functionalized polyolefin surfaces
 - nucleophilic substitution, monosort functional groups by, 339–342
 - peroxy radicals/hydroperoxides, 337–338
 - radical sites, direct grafting, 336–337
- Green functions, 59
- Guar gum, 464–465
- Gurtin's theory, 10
- Hardboard, 87
- Hertz, 132–134
- High performance liquid chromatography (HPLC), 232
- High-temperature adhesive (HTA), 74
- HMR. *See* Hydroxymethyl resorcinol
- HPLC. *See* High performance liquid chromatography
- HSA. *See* Human serum albumin
- HTA. *See* High-temperature adhesive
- Human mucin genes, 453–455
- Human serum albumin (HSA), 461–462
- Hydrophilic acrylate, 132
- Hydrosilylation (addition)
 - curing, 35–36
- Hydrosilylation-induced grafting, 46
- 2-Hydroxyethyl methacrylate, 408–410
- Hydroxymethyl resorcinol (HMR), 143
- IGC. *See* Inverse gas chromatography
- Interface characterization techniques
 - atomic force microscopy (AFM), 194–195
 - differential scanning calorimetry (DSC), 199
 - dynamic mechanical thermal analysis (DMTA), 199–203

- morphological characterization, 189–195
- scanning electron microscopy (SEM), 190–194
- spectroscopic techniques, 203–206
- thermal analysis, 196–203
- thermogravimetric analysis (TGA), 196–199
- Interfacial adhesion issues
 - fibre/matrix interfacial adhesion, 188–189
 - improving strategies, 186–188
 - natural fibres, interfacial adhesion of, 185–186
- Interfacial energy, 4
- Inverse gas chromatography (IGC), 231
- Isocyanate, 106–116
- Isocyanate wood adhesives
 - chemistry of, 107–109
 - conditions for application, 114–116
 - emulsified/emulsifiable water-dispersed PMDI, 112
 - PF/pMDI and UF/pMDI hybrid adhesives, 112–114
 - technology of, 109–112
- Isothermal calorimetry (ITC), 232
- Itaconic acid, 408–410
- ITC. *See* Isothermal calorimetry
- JKR theory. *See* Johnson, Kendall, and Roberts theory
- Johnson, Kendall, and Roberts (JKR) theory, 132–134, 220
- Joint configuration, strength of, 60
- Joint geometry, 60
- Jurin's law, 11
- Kinematics, 3–9
- Laminated veneer lumber (LVL), 87, 142
- Laplace equation, 14, 17
- Laplace transforms, 59
- Layer-by-layer (LbL) deposition, 42–43
- LbL. *See* Layer-by-layer deposition
- L-DOPA. *See* 3, 4-Dihydroxy-L-phenylalanine
- Lead zirconate titanate (PZT), 73
- Light-fiber-tear, 59
- Lotus effect, 2
- Low temperature adhesive (LTA), 74
- LTA. *See* Low temperature adhesive
- LVL. *See* Laminated veneer lumber
- Material non-linearity, 58
- MDF. *See* Medium Density Fibreboard
- MDI. *See* 4,4' Diphenylmethane diisocyanate
- MDP. *See* 10-methacryloxydecyl dihydrogen phosphate
- Mechanical interlocking theory, 129–135
- Medium Density Fibreboard (MDF), 86
- Melamine, 93, 96
- Melamine-formaldehyde (MF) adhesives, 85, 93–99
- Melamine-urea-formaldehyde (MUF) adhesives, 85, 93–99
- MEMS. *See* Microelectromechanical systems
- Metal-based NP, 359
- 10-methacryloxydecyl dihydrogen phosphate (MDP), 403, 404
- 3-Methacryloxypropyl-trimethoxysilane (MPS), 400
- Methods of Mathematical Physics (Courant and Hilbert), 8
- Methylenebisurea, 90
- Methylolureas, 88–90
- MF. *See* Melamine-formaldehyde adhesives
- Microbeam, 9–13
- Microbeam adhesion, 9
- Micro-contact printing technology, 2
- Microelectromechanical systems (MEMS), 221
- Micro/nano-electro-mechanical systems (M/NEMS), 2

- M/NEMS. *See* Micro/nano-electro-mechanical systems
- Modulus of elasticity, 65
- Monomethylolurea, 89
- Monotype functional groups
- amino groups, 318–319
 - ammonia plasma, additional side reactions, 322–324
 - ammonia plasma treatment, 319–322
 - carbon dioxide plasma, 315–318
 - C-Br groups, 327–329
 - chemical pretreatment, 333–335
 - electrospray ionization (ESI) deposition, 332–333
 - general principles, 300–304
 - grafting, 336–342
 - hydrophobic recovery, 335–336
 - kinetics, 325–327
 - oxygen plasma, 312–315
 - parameter dependence, 327
 - plasma polymerization, 329–330
 - polymer degradation, 310–311
 - polyolefin surfaces, 304–310
 - polyolefin surfaces, monosort functional groups on, 311–312
 - production of, 312–318
 - surface bromination, 324–329
 - thermodynamics and mechanism, 325–327
 - underwater plasma, 331–332
- Morphological characterization
- atomic force microscopy (AFM), 194–195
 - scanning electron microscopy (SEM), 190–194
- Movable boundary conditions
- energy variation with, 3–9
- MPS. *See* 3-Methacryloxypropyl-trimethoxysilane
- Mucoadhesive polymers
- alginate, 462–463
 - arabinogalactan (AG), 467
 - carbomer, 467–468
 - carrageenan, 465–466
 - cellulose derivatives, 469–470
 - chitosan, 454
 - chitosan-based formulations, 460–461
 - cysteine-poly(ethylene glycol) stearate (Cys-PEG-SA), 473
 - eudragit, 468–469
 - gellan gum, 463
 - gene delivery, 472
 - guar gum, 464–465
 - human mucin genes, 453–455
 - human serum albumin (HSA), 461–462
 - mucus layer, composition of, 453–454
 - natural mucoadhesive polymers, 454–461
 - ocular drug delivery, 472–473
 - patented formulations, 472
 - physical and physicochemical characteristics of, 456–460
 - poloxamer, 471–472
 - poly (acrylic acid) (PAA), 467–468
 - poly (D, L-lactic acid), 470–471
 - poly (D, L-lactide-co-glycolide), 470–471
 - sodium hyaluronate, 465
 - synthetic polymers, 467–472
 - tamarind gum polysaccharide (TGP), 466
 - xanthan gum, 463–464
- MUF. *See* Melamine-urea-formaldehyde adhesives
- Nanobeam adhesion, 10
- Nanoclays, 360
- Nanocomposites, processing techniques, 184
- Nano-enhanced adhesives
- nanoparticle (NP), 458
 - nano-reinforced adhesives, 364–365
 - polymer-based nanocomposites, 360–361

- Nanoindentation, 132–135
- Nanoparticle (NP)
 carbon-based, 359
 metal-based, 359
 nanoclays, 360
 nanosilicas (SiO₂), 360
 polyhedral oligomeric silsesquioxanes (POSS), 359–360
- Nano-reinforced adhesives
 adhesive stiffness, 365–374
 advantages of, 383–384
 bio-adhesives, 387–388
 durability of adhesives, 382–383
 electrical properties, 384–385
 fracture toughness, 374–376
 gas permeation barrier properties, 386–387
 residual stresses, 380–382
 surface wettability, 377–380
 thermal properties, 385–386
- Nanosilicas (SiO₂), 360
- Natural mucoadhesive polymers, 454–461
- Natural rubber, 182–183
- Navier equations, 71
- Near-infrared (NIR) spectroscopy, 231–232
- Newton-Raphson and arc-length methods, 59
- NIR. *See* Near-infrared spectroscopy
- NMR. *See* Nuclear magnetic resonance spectroscopy
- Nonlinear aero-thermo-elasticity, 63
- NP. *See* Nanoparticle
- Nuclear magnetic resonance (NMR) spectroscopy, 206
- 2-Octyl-cyanoacrylate, 267–268
 dermabond, 268
 SurgiSeal, 268
- Ocular drug delivery, 472–473
- Oleic acid, 408–410
- One fixed joint-edge, 70
- Optimal formulation development
 accelerators, 276–277
 inhibitors, 273–274
 plasticizers, 277–278
 stabilizers, 274–276
 thickeners, 277
- Oriented Strand Board (OSB), 87
- OSB. *See* Oriented Strand Board
- Oxygen plasma, 312–315
- PAA. *See* Poly (acrylic acid)
- PDMS. *See* Poly(dimethylsiloxane)
- PEG. *See* Poly(ethylene glycol) polymers
- Penalty-function, 62
- PF. *See* Phenol-formaldehyde
- Pharmaceutical industry
 active pharmaceutical ingredient (API), 222–223
 adhesion interactions, 223
 colloidal system, 222
 drug-device/package interactions, 224–225
 drug-drug/carrier interactions, 223–224
 factors influencing adhesion, 225–229
 monitoring and controlling influential factors, 229–232
- PHB. *See* Polyhydroxybutyrate
- Phenol-formaldehyde (PF), 85, 99–106
- Phenol-formaldehyde thermosetting adhesives, 99
- Phenolic resins, modification of
 co-condensation, phenol vs. urea, 105
 isocyanates, 105–106
 lignins, 105–106
 tannins, 105–106
 urea, post-addition of, 104–105
- Phosphate coupling agents, 404–405
- Piezoelectric patches, 73
- PLA. *See* Poly(lactic acid)
- Plasma-induced grafting, 44–46

- Plasma treatment, 37–39
Plate Adhesion, 9–13
Plywood, 87
PMDIs. *See* pressurised metered dose inhalers
PMMA. *See* Poly(methyl methacrylate)
Poisson's ratio, 66, 70, 72
Poloxamer, 471–472
Poly (acrylic acid) (PAA), 467–468
Poly(dimethylsiloxane) (PDMS)
adhesion property, 37
amino-terminated L-Arginyl-Glycyl-L-Aspartic acid, 48
amphiphilic block copolymers, 46–47
condensation curing, 33–34
corona treatment, 39–40
covalent surface grafting, 44–46
curing reactions, 32–36
free-radical curing, 33
hydrosilylation (addition) curing, 35–36
hydrosilylation-induced grafting, 46
laser, 46
laser treatment, 41
layer-by-layer (LbL) deposition, 42–43
physical adsorption, 41–42
physical techniques, 37–42
piranha and KOH solution treatments, 43
plasma-induced grafting, 44–46
plasma treatment, 37–39
sol-gel method, 43
Sum Frequency Generation (SFG), 36
surface properties, 36
UV irradiation-induced grafting, 46
UV-ozone (UV/O₃) treatment, 40–41
wet chemical techniques, 42–48
Poly(lactic acid) (PLA), 177–178
Poly(methyl methacrylate) (PMMA), 132
Poly (D, L-lactic acid), 470–471
Poly (D, L-lactide-co-glycolide), 470–471
Poly (vinyl acetate) (PVAc) adhesive, 132
Polychlorinated biphenyls (PCBs), 33
Polyhedral oligomeric silsesquioxanes (POSS), 359–360
Polyhydroxybutyrate (PHB), 178–179
Polymer-based nanocomposites
high-shear mixing, 364
sonication, 361–363
three-roll milling (calendering), 363–364
Polymer surface, spacer grafting, 340
Poly(ethylene glycol) (PEG) polymers, 255–256
Polypropylene (PP)-wood powder (WP) composites, 131
POSS. *See* Polyhedral oligomeric silsesquioxanes
Pressurised metered dose inhalers (pMDIs), 223
PZT. *See* Lead zirconate titanate
Raman spectroscopies, 203–205
RCF. *See* Relative centrifugal force
Relative centrifugal force (RCF), 231
Resins
alkaline phenolic, 104
penetration behaviour, 103
phenolic resins, 104–106
production process, 103
of two-phase system, 104
ultimate strength of, 104
Resin solids, 86
Resorcinol-formaldehyde, 85
SAED. *See* Selected area electron diffraction
Scanning electron microscopy (SEM), 190–194
Selected area electron diffraction (SAED), 438
Self-folding, 2

- SEM. *See* Scanning electron microscopy
- Shear modulus, 66
- Shear stresses, 60
- Silane coupling agents, 399–403
- Sodium hyaluronate, 465
- Sol-gel method, 43
- Spectroscopic techniques
- attenuated total reflectance infrared spectroscopy (ATR-IR), 205–206
 - Fourier transform infrared (FTIR) spectroscopy, 203–205
 - nuclear magnetic resonance (NMR) spectroscopy, 206
 - Raman spectroscopy, 203–205
- Starch, 173–174, 174–177, 185–182
- State-of-the-art in linear, 63
- Stock-break failure, 59
- Stress and strain levels, 61
- Stress distribution, 60
- Stress-strain transfer ratio, 65
- Structural stress concentrations, 62
- Surface wettability, 377–380
- Surgeon's toolbox
- albumin, 256
 - collagen-based adhesives, 255
 - cyanoacrylates, 254
 - fibrin sealants, 252–254
 - glutaraldehyde products, 256
 - poly(ethylene glycol) (PEG) polymers, 255–256
- Surgical adhesives
- basic requirements of, 246–248
 - comparison of, 257
 - full scope of, 249–252
 - general requirements of, 247
 - scope and objectives of, 249
 - surgeon's toolbox, 252–257
 - surgical substrates, 248–249
 - tissue substrates, 248
 - types of, 249
- Synthetic polymers, 467–472
- Tamarind gum polysaccharide (TGP), 466
- TGA. *See* Thermogravimetric analysis
- TGP. *See* Tamarind gum polysaccharide
- Thermal analysis
- differential scanning calorimetry (DSC), 199
 - dynamic mechanical thermal analysis (DMTA), 199–203
 - thermogravimetric analysis (TGA), 196–199
- Thermal expansion coefficient, 65
- Thermal residual stress, 71
- Thermodynamic interfacial interactions, 130
- Thermogravimetric analysis (TGA), 196–199
- Thin-layer cohesive failure, 59
- Thione/thiol coupling agents, 405–406
- Third-order shear deformation plate theory, 62
- Three-dimensional elastic flexural behaviour, 68
- Three-dimensional elastic stress state, 67
- Three-dimensional stress analyses, 68
- Three-dimensional stress state, 69
- Through-thickness composition variation, 64
- Titanate coupling agents, 406–407
- Toxicity, cyanoacrylate adhesives, 283–284
- Transmission Electron Microscopy, 436
- Transversality condition, 3
- Two fixed joint edges, 70
- UF adhesives. *See* Urea-formaldehyde adhesives
- Unbalanced joints, 58
- Underwater plasma, 331–332
- Urea-formaldehyde (UF) adhesives, 85, 87–93
- Uron structures, 91

- UV irradiation-induced grafting, 46
- UV-ozone (UV/O₃) treatment, 40–41
- Van der Waals force, 2, 137, 220, 223
- Variational theory, 24
- VBATDT. *See* 6-(4-Vinylbenzyl-n-propyl)-amino-1,-3, 5-triazine-2,4-dithiol
- Vesicle adhesion, 3
- 6-(4-Vinylbenzyl-n-propyl)-amino-1,-3, 5-triazine-2,4-dithiol (VBATDT), 406–407
- von Mises stress, 68
- Water contact angle (WCA), 37
- WCA. *See* Water contact angle
- Weak boundary layers, theory of
 - extractives, 151
 - heat treatment, 152–153
 - machining processes, 153–154
 - surface activation, 154–155
 - surface degradation, 154
 - wood impregnation and densification, 153
- Wenzel and Cassie models, 16
- Wenzel equation, 14
- Wet chemical techniques, 42–48
- Wettability
 - acetylation, 142
 - adhesive wettability, 141
 - extractives, 141
 - fire retardants, 142–143
 - grafting, 142
 - preservatives and adhesion promotion, 142–143
 - test methods, 143–145
 - wood anatomy impact, 140–141
 - wood modification, 141–143
- Wood
 - cell wall structure, 127
 - chemical composition of, 127
 - elements, 128
 - mutually-orthogonal planes, 126
 - surface property issues, 127
 - warty layer, 127
 - wood-adhesive interactions, 128–129
- Wood adhesive bonding
 - acid-base theory, 149–150
 - covalent bonding, 148–149
 - diffusion theory of adhesion, 145–148
 - electrostatic adhesion, 135–137
 - mechanical interlocking, 129–135
 - mechanics of adhesive-wood interactions, 129–135
 - surface energy, 137–145
 - thermodynamic adhesion, 137–145
 - weak boundary layer, 150–155
 - wettability, 137–145
- Wood adhesives
 - formaldehyde-based thermosetting resins, 85
 - formulation of, 101
 - isocyanate, 106–116
 - main application, 86
 - melamine-formaldehyde (MF) adhesives, 85, 93–99
 - melamine-urea-formaldehyde (MUF) adhesives, 85, 93–99
 - phenol-formaldehyde (PF), 85, 99–106
 - resin solids, 86
 - resorcinol-formaldehyde, 85
 - technical point of, 86
 - urea-formaldehyde (UF) adhesives, 85, 87–93
- Wood material properties, 126–129
- Xanthan gum, 463–464
- Young's equation, 15, 17
- Young's modulus, 9
- Zircoaluminate coupling agents, 408
- Zirconate coupling agents, 403–404

Also of Interest

Check out these published and forthcoming related titles from Scrivener Publishing

Reviews of Adhesion and Adhesives

Editor: K.L. Mittal

Quarterly publication. ISSN 2168-0965

www.scrivenerpublishng.com

Adhesion in Polymer Nanocomposites

Edited by Anil Netravali and K.L. Mittal

Forthcoming summer 2015.

Advances in Contact Angle, Wettability and Adhesion Volume 2

Edited by K.L. Mittal

Forthcoming summer 2015. ISBN 978-1-119-11698-1

Particle Adhesion and Removal

Edited by K.L. Mittal and Ravi Jaiswal

Published 2014. ISBN 978-1118-83153-3

Laser Surface Modification and Adhesion

Edited by K.L. Mittal and Thomas Bahners

Published 2014. ISBN 978-1-118-83163-2

Adhesion in Microelectronics

Edited by K.L. Mittal and Tanweer Ahsan

Published 2014. ISBN 978-1-118-83133-5

Advances in Contact Angle, Wettability and Adhesion Volume 1

Edited by K.L. Mittal

Published 2013. ISBN 978-1-118-47292-7

Advances in Modeling and Design of Adhesively Bonded Systems

Edited by S. Kumar and K.L. Mittal

Published 2013. ISBN 978-1-118-68637-9

Atmospheric Pressure Plasma Treatment of Polymers

Edited by Michael Thomas and K.L. Mittal

Published 2013. ISBN 978-1-118-59621-0

Atomic Layer Deposition

Principles, Characteristics, and Nanotechnology Applications

By Tommi Kääriäinen, David Cameron, Marja-Leena Kääriäinen and Arthur Sherman

Published 2013. ISBN 978-1-118-06277-7

Encapsulation Nanotechnologies

Edited by Vikas Mittal

Published 2013. ISBN 978-1-118-34455-2

Atmospheric Pressure Plasma for Surface Modification

By Rory A. Wolf

Published 2012. ISBN 9781118016237

Introduction to Surface Engineering and Functionally Engineered Materials

By Peter Martin

Published 2011. ISBN 978-0-470-63927-6

WILEY END USER LICENSE AGREEMENT

Go to www.wiley.com/go/eula to access Wiley's ebook EULA.